Università degli Studi di Ferrara

Uniwersytet Wrocławski

DOCTORAL COURSE IN "CHEMISTRY"

CYCLE XXXIII

International Joint Doctoral Study Programme in Chemistry with University of Wrocław (Poland)

COORDINATOR Prof. Cavazzini Alberto

Study of the metal ions transport phenomena involved in the expression of pathogenic virulence

Scientific/Disciplinary Sector (SDS) CHIM/01

Candidate
Dott. Bellotti Denise

(signature)

Supervisor
Prof. Remelli Maurizio

(signature)

Co-Supervisor
Prof. Rowińska-Żyrek Magdalena

(signature)

Years 2017/2020

Perché la ruota giri, perché la vita viva, ci vogliono le impurezze
e le impurezze delle impurezze: anche nel terreno, come è noto, se ha da essere fertile.
Ci vuole il dissenso, il diverso, il grano di sale e di senape.

"Zinco - Il sistema periodico" Primo Levi

Contents

Abstract

The necessity of new antimicrobial agents is unarguable, since current therapeutic treatments are not always effective: drug-resistant pathogenic microorganisms have significantly increased over the last decades and their associated mortality rate still remains a global concern. Several studies have shown that metal acquisition and regulation greatly contribute to virulence and physiology of pathogens. In particular, to prevent infections, humans restrict the access to essential micronutrients by means of an innate immune response termed "nutritional immunity"; on the contrary, pathogens rely on sophisticated systems (e.g. siderophores) to overcome the scarce metal bioavailability. From this perspective, a deeper insight into the mechanism of metal trafficking in pathogens and host nutritional immune response can provide crucial information to design new effective antibiotic therapies, e.g. by developing species-selective transport or imaging drugs which can be recognized only by specialized metal transport proteins ("Trojan Horse" approach). Furthermore, metal complexes are not only a promising tool in antimicrobial treatments, but they can also find application against pathologies which, in general, involve metal ions (e.g. neurodegenerative diseases or cancer). The first essential step to develop novel metal-based antimicrobials is the elucidation of thermodynamics and coordination chemistry of the metal chelators involved in pathogenic events.

The main aim of this work is to provide insight into the correlation between metal transport, homeostasis and virulence in pathogens. The research work is mostly focused on Zn(II), which is crucial for the survival of human and pathogen cells. Its assimilation by pathogens is extremely challenging: free zinc concentration is normally subnanomolar, and many other divalent endogenous metal ions, such as Cu(II) (or Ni(II) in some organisms), can compete for the same protein binding sites, thus requiring a more extensive study of the phenomenon. For this purpose, the interaction of metal ions with human antimicrobial peptides, metal transporters, natural metallophores and biomimetic molecular systems are investigated, with particular emphasis on the thermodynamic properties of the obtained complexes and the elucidation of their speciation in solution.

The choice of the unstructured peptide fragments as protein models, that simulate the coordination and transport of metals, is the first essential step of this research. Consultation of specific databases and scientific literature provides information about evolutionarily conserved sequences with metal binding function. The further characterization of the metal complexes required several experimental techniques. Mass spectrometry and potentiometric titrations allow to evaluate the stoichiometry, coordination modes and stability of the formed complexes in aqueous solution, varying the experimental conditions like metal/ligand ratio and the pH value. Furthermore, competition diagrams obtained from calculated partial and overall stability constants provide a deeper understanding of the metal binding affinity. Spectroscopic techniques, such as UV-Vis spectrophotometry, circular dichroism (CD), electron paramagnetic resonance and nuclear magnetic resonance ensure a complementary study to understand the coordination geometries and to identify the precise binding sites. CD measurements in the far-UV region also give indications on the presence of specific conformations (α-helices, random coils, etc.). Biological studies in vitro of potential antimicrobial agents involved in the process of nutritional immunity can complete the information about the way of action of some systems and the role of metal ions. Moreover, the comparison between different peptide analogues helps clarifying the role of some residues of the sequence, not always directly involved in complexation but rather influencing the complex geometry and contributing to its stability.

Acknowledgements

Thank you. Grazie. Dziękuję.

It is the simplest and most complete, neither stilted, nor poor, but rich and heartfelt thanks for all of you.

An unfading thanks to my supervisors, who are indeed *super* in all respects. Not only great scientists, but great teachers and great persons. Therefore, I must express my gratitude to prof. Maurizio Remelli and prof. Magdalena Rowińska-Żyrek for their valuable guidance and their continuous support, for their patience and priceless motivation, for welcoming me in their research groups and for all the opportunities I was given during the past years.

A carefree *dziękuję bardzo* to the colleagues from the University of Wrocław. It is carefree like my favourite sentence in Polish. I thank all the professors, researchers and students of the group of Biological Inorganic Chemistry of Wrocław University for the amazing time spent together, for the help in any circumstance, the hospitality and the kindness.

A steady, resolute and necessary thanks to the colleagues from the University of Ferrara, because steady, resolute and necessary are the bonds we formed in these years. I thank them and the group of Analytical Chemistry of Ferrara University for the precious support, excellent cooperation and for the creation of a brilliant and stimulating scientific environment.

Merci beaucoup to prof. Michel Meyer for giving me the chance to visit his laboratory in Dijon and for the truly formative research experience at the Institute of Molecular Chemistry of the University of Burgundy.

An uncountable thanks to all my friends and relatives, who are indeed inestimable in numbers and values, and even if unknowingly, who contributed to this accomplishment.

Finally, a never-ending thanks to my family. Never-ending like the story, or like the time I use to spend talking about my scientific adventures. They always listen to me with unwavering enthusiasm, and never stop believing in me. I thank my family for the unfailing support and continuous encouragement.

List of publications

This research work includes the following publications:

Journal articles

1. D. Bellotti, A. Sinigaglia, R. Guerrini, E. Marzola, M. Rowińska-Żyrek, M. Remelli, *J. Inorg. Biochem*. **2021**, 214, 111304.

2. D. Bellotti, M. Rowińska-Żyrek, M. Remelli, *Dalton Trans.*, **2020**, 49(27), 9393–9403.

3. D. Bellotti, C. Tocchio, M. Rowinska-Zyrek, M. Remelli, *Metallomics* **2019**, 11(12), 1988–1998.

4. M. Perinelli, R. Guerrini, V. Albanese, N. Marchetti, D. Bellotti, S. Gentili, M. Tegoni, M. Remelli, *J. Inorg. Biochem*., **2020**, 205, 110980-110993.

5. C. Bacchella, S. Gentili, D. Bellotti, E. Quartieri, S. Draghi, M. C. Baratto, M. Remelli, D. Valensin, E. Monzani, S. Nicolis, L. Casella, M. Tegoni, S. Dell'Acqua, *Inorg. Chem*., **2020**, 59(1), 274-286.

6. D. Bellotti, M. Toniolo, D. Dudek, A. Mikolajczyk, R. Guerrini, A. Matera-Witkiewicz, M. Remelli, M. Rowinska-Zyrek, *Dalton Trans*. **2019**, 48(36), 13740-13752.

7. D. Bellotti, D. Łoboda, M. Rowińska-Żyrek, M. Remelli, *New J. Chem*. **2018**, 42(10), 8123-8130.

Conference proceedings - Oral presentations

8. D. Bellotti, M. Rowińska-Żyrek, M. Remelli, "Study of Cu(II) and Zn(II) interaction with the metal binding domain of ZinT protein" in "Proceedings of the Merck Young Chemists' Symposium 2019", Ed. G. Annunziato, M. Atzori, F. Bella, C. Bonfio, S. Cinti, M. Da Pian, V. Lazazzara, E. Lenci, E. Paone, F. Ponte, L. Rivoira, M. Schlich, and L. Triggiani, ISBN: 978-88-94952-15-5, 2019, Rome (Italy), p. 61.

9. D. Bellotti, M. Rowińska-Żyrek, M. Remelli, "Zn(II) and Cu(II) binding ability of ZinT – a highly conserved periplasmic protein expressed by different bacterial species", ICBIC 2019 - 19th International Conference on Biological Inorganic Chemistry, August 11th–16th 2019, Interlaken (Switzerland), p. 342.

10. D. Bellotti, M. Toniolo, D. Dudek, M. Rowińska-Żyrek, M. Remelli, "Zn(II) and Cu(II) binding sites of Calcitermin, an antimicrobial peptide found in human airways", Acta of the International Symposia on Metal Complexes, ISMEC GROUP SERIES, Vol. 9, (2019), ISSN: 2239-2459, Symposium Edition: XXX, ISMEC 2019, June 11th–14th 2019, Debrecen (Hungary), pp. 83-84.

11. D. Bellotti, C. Tocchio, M. Rowińska-Żyrek, M. Remelli, "Investigation on Zn(II) and Cu(II) binding sites in C4YJH2, a putative metal transporter of Candida albicans", in "Proceedings of the Merck & Elsevier Young Chemists Symposium (MEYCS 2018)", Ed. F. Bella, L. Botta, R. Cucciniello, A. D'Urso, P. Franco, E.

Lenci, G. Mazzone, M. Schlich, A. Soldà, R. Spezzano, S. Staderini and L. Triggiani, ISBN: 978-88-94952-03-2, 2018, Rome (Italy), p. 46.

12. D. Bellotti, C. Tocchio, M. Rowińska-Żyrek, M. Remelli, "Does protein sequence C4YJH2 participate in Candida albicans metal homeostasis? A focus on Zn(II) and Cu(II) binding behaviour", in "XIV International Symposium on Inorganic Biochemistry", Ed. E. Gumienna-Kontecka, K. Krzywoszyńska, S. Potocki, ISBN: 978-83-60043-35-6, 2018, Wrocław (Poland), pp. 84-85.

13. D. Bellotti, C. Tocchio, M. Rowińska-Żyrek, M. Remelli, "An in-depth analysis of the metal binding domain in a putative Zn(II) transporter of Candida albicans", Acta of the International Symposia on Metal Complexes, ISMEC GROUP SERIES, Vol. 8, (2018), ISSN: 2239-2459, Symposium Edition: XXIX, ISMEC 2018, June 3rd–7th 2018, Florence (Italy), pp. 65-66.

Conference proceedings – Other contributions

14. M. Rowińska-Żyrek, D. Dudek, D. Bellotti, A. Miller, A. Mikołajczyk, A. Matera-Witkiewicz, "Antimicrobial Peptide – Metal Interactions – Relationship between Coordination Chemistry, Structure, Thermodynamics and Mode of Action", ICBIC 2019 - 19th International Conference on Biological Inorganic Chemistry, August 11th–16th 2019, Interlaken (Switzerland), p. 241.

15. M. Tegoni, S. Gentili, E. Quartieri, D. Bellotti, M. Remelli, C. Bacchella, S. Dell'Acqua, L. Casella, D. Valensin, "Copper(I) and Copper(II) Binding to R1 and R3 Fragments of Tau Protein", ICBIC 2019 - 19th International Conference on Biological Inorganic Chemistry, August 11th–16th 2019, Interlaken (Switzerland), p. 87.

16. S. Gentili, M. Tegoni, D. Bellotti, C. Bacchella, A. Mazza, E. Quartieri, M. Remelli, S. Dell'Acqua, L. Casella, D. Valensin, "Copper binding to R1 and R3 fragments of Tau protein", Acta of the International Symposia on Metal Complexes, ISMEC GROUP SERIES, Vol. 9, (2019), ISSN: 2239-2459, Symposium Edition: XXX, ISMEC 2019, June 11th–14th 2019, Debrecen (Hungary), pp. 55-56.

17. M. Remelli, M. Perinelli, R. Guerrini, N. Marchetti, D. Bellotti, M. Tegoni, "Macrochelates from rigid polypeptides: a step forward towards synthetic enzymes?", in "XIV International Symposium on Inorganic Biochemistry", Ed. E. Gumienna-Kontecka, K. Krzywoszyńska, S. Potocki, ISBN: 978-83-60043-35-6, 2018, Wrocław (Poland), pp. 33-34.

18. M. Rowińska-Żyrek, D. Bellotti, M. Remelli, "COT1 mediated zinc transport in Candida albicans – searching for the metal binding site", Acta of the International Symposia on Metal Complexes, ISMEC GROUP SERIES, Vol. 7, (2017), ISSN: 2239-2459, Symposium Edition: XXVIII, ISMEC 2017, June 11th–16th 2017, Dijon (France), p. 269.

Abbreviations and symbols

a	activity of the solute
a_i	effective diameter of the hydrated ion i
A	Debye-Hückel constant
A	absorbance
A	EPR hyperfine splitting parameter
ABC	the ATP-binding cassette
AMP	antimicrobial peptide /or protein
AMR	antimicrobial resistance
ATCUN	amino terminal copper- and nickel- binding
β	overall equilibrium constant
β_{sl}	slope factor of experimental Nernst equation
B	second Debye-Hückel constant
B_0	magnetic field
c	speed of light in vacuum
C	concentration
°C	degrees Celsius
CD	circular dichroism
CDF	cation diffusion facilitator
CFT	crystal-field theory
δ	chemical shift
DA	dopamine
DIPCDI	N,N′-diisopropylcarbodiimide
DMF	dimethylformamide
ΔE	energy gap between frontier orbitals
ε	molar extinction coefficient
e	electron charge
E	potential
E^0	standard potential
$E^{0\prime}$	standard potential corrected for constant activity coefficients
E_j	potential of any liquid junctions
ESI	electrospray ionization
F	Faraday's constant
FT-ICR	Fourier transform ion cyclotron resonance
g	EPR constant parameter (g factor)

h	Planck's constant
HOBt	hydroxybenzotriazole
HPLC	high pressure liquid chromatography
θ	molar ellipticity
γ	activity coefficient
γ	giromagnetic ratio
I	ionic strength
I	intensity of the transmitted radiation
I	nuclear spin quantum number
I_0	intensity of the incident monochromatic radiation
j_a	acid liquid junction coefficient
j_b	basic liquid junction coefficient
J	angular momentum
J	spin-spin coupling constant
K	stepwise equilibrium constant
K_a	acid dissociation constant
K_f	equilibrium constant of complex formation
K_w	water self-ionization constant
λ	wavelength
L	ligand
L	length of a drift tube in TOF analyser
l	optical cell path length
L-CPL	left-circularly polarized light
LFT	ligand-field theory
ln	natural logarithm
log	decimal logarithm
μ_B	Bohr magneton
μ	magnetic moment
m	mass
M / M^{m+}	metal ion
MC	4-methylcatechol
MS	mass spectrometry
ν	frequency
N / n	general number
n	number of electrons involved in the electrochemical reaction
N^-	amide nitrogen
NHE	normal hydrogen electrode

N_{Im}	imidazole nitrogen
n_l	refractive index for left-circularly polarized light
N_P	number of titration points
n_r	refractive index for right-circularly polarized light
ORD	optical rotatory dispersion
p	indicates negative log (as in pH, p*K*)
PEM	photoelastic modulator
pH	$-\log[H^+]$
R	universal gas constant
R-CPL	right-circularly polarized light
S	total spin angular momentum
SALC	symmetry-adapted linear combinations
SDS	sodium dodecyl sulfate
SOD	superoxide dismutase
SPPS	solid-phase peptide synthesis
t	time
T	temperature
t_F	time of flight
TFA	trifluoroacetic acid
TOCSY	total ion correlation spectroscopy
TOF	time-of-flight analyser
U	direct current
UV	ultraviolet
v	velocity
V	electric potential
Vis	visible
ω	frequency
TDM	transmembrane domain
z	ion charge
ZIP	ZRT, IRT-like protein

1. Chapter One: Introduction

1.1 Transition metal ion transport as novel drug target candidate

It is well known that the number of pathogenic microorganisms capable to adapt and resist current therapeutic treatments has significantly increased over the last decades; therefore, the necessity of new antimicrobial agents is unarguable. There is currently only a limited number of effective drugs against bacterial and fungal infections and the threat of antimicrobial resistance (AMR) is still a major concern in clinical practice. As a result of antimicrobial resistance, common treatments become inefficient and infections persist in the host organism, making pathogens extremely dangerous for the patient subsistence and increasing the risk of spreading to other individuals. AMR occurs naturally, as a consequence of genetic mutations and organism evolution, but is facilitated by the inappropriate assumption of medicines, low-quality treatments and inadequate prevention and control of infections. The dramatic dissemination of antibiotic-resistant strains represents both a serious threat and a scientific challenge.[1] To date, the available arsenal of therapeutic and diagnostic tools against infectious diseases is insufficient to address the AMR crisis and novel, innovative pharmacological therapies are urgently required. Reports from the European Antimicrobial Resistance Surveillance Network (EARS-Net) estimate that in 2018, 58.3% of the *Escherichia coli* isolates exhibited resistance to the third generation of cephalosporins, fluoroquinolones and even carbapenems, and high levels of *Staphylococcus aureus* infections were caused by methicillin-resistant species (MRSA). The intrinsically drug-resistant *Pseudomonas aeruginosa* still represents the main cause of healthcare-associated infections in Europe, and the percentage for vancomycin-resistant *Enterococcus faecium* increased from 10.5% to 17.3% over three years.[2]

The search for innovative therapies should be aimed not only at clinically more effective drugs, but also at economically attractive compounds with adequate costs and gains for producers. The use of natural compounds, for example, is an advantageous option for attempting production cost-cutting, but still poses the risk of drug-resistance development. In order to devise more attractive therapeutic and diagnostic strategies, as a first step, it is crucial to understand the functioning of the pathogen virulence factors and to aim at them as new clinical targets. Understanding and clarifying the biological phenomena involved in the interactions between pathogens and the host organism, both *in vivo* and *in vitro*, can provide the basis for the rational design of new promising therapies, with high rate of specificity, selectivity and effectiveness. A significant difference between bacterial, fungal and mammalian cells is related to the mechanisms of transition metal ions transport. [3, 4]

The first row d-block metal ions manganese (Mn), iron (Fe), cobalt (Co), nickel (Ni), copper (Cu) and zinc (Zn) are known to be essential for the physiology of living organisms, functioning as cofactors in metalloproteins or structural components for enzymes. It has been estimated that approximately 30% of all proteins require metals for their biological function. Nonetheless, both a reduced and an excessive concentration of metal inside the cell are potentially toxic and fatal for its survival. From this perspective, one can easily understand that metal ions play a key role in the pathogen subsistence and as virulence factors.[5-7] Pathogenic microorganisms, like bacteria and fungi, can meet their physiological metals demand by detracting micronutrients from the surrounding microenvironment during the colonization of a host organism. To prevent infections, the host restricts the access to essential metal micronutrients, withholding and limiting these resources by means of an innate immune response termed “nutritional immunity”.[3, 8] This phenomenon is a primary defence line put in place by vertebrate organisms to limit the

efficiency of the microbial invaders. In fact, during inflammation the concentrations of non-bound trace minerals, such as iron and zinc, proved to undergo a severe drop, which can eventually result in the occurrence of human diseases.[9-12] The host metal homeostasis perturbation is caused by the pathogen organism, which can rely on sophisticated systems to sequester metal micronutrients and overcome their scarce bioavailability. To obtain the necessary metal nutrients, pathogens exploit various mechanisms, including both active and passive transport through the pathogen cell membranes. In the former case, to make the metal recruitment more efficient, pathogens can synthesise proteins, peptides or other molecules with the specific function of metal scavenger, adapting to the host-mediated metal limitations.[6, 13] These so called "metallophores" are intended as specialised extracellular or periplasmic chelators acting as metal shuttles, capable of catching the metal ion from the host microenvironmental niche and transfer it to an appropriate target protein, most often a transmembrane transporter. The amount of free metal ions must be strictly regulated both in the case of pathogens and humans. The overload or shortage of metals can induce cellular apoptosis due to intrinsic cytotoxic effects (inhibition of enzymes through wrong metal coordination, formation of stable, irreversible protein complexes, disruption of the membrane potential, absence of crucial protein cofactors and consequent loss of enzymatic activity). Hence, attempting metals transport-targeted therapies can be an outstanding opportunity to fight pathogens. Moreover, such therapeutics may limit undesirable side effects for the host organism, since most eukaryotes, including humans, frequently exhibit different metal acquisition pathways and totally lack most of the typical extracytosolic metallophores of bacteria and fungi.

1.2 Human versus pathogen: the rules of the metal tug-of-war

To better understand the properties and the mechanisms of action of metallophores and metal transporters, some preliminary considerations are necessary. First of all, we must distinguish between two environmental niches in which pathogens' metal binding proteins can be found: the periplasm and the extracellular space. Gram-negative bacteria are characterized by an additional outer membrane which defines the periplasmic compartment (the space between the outer and the inner/cytoplasmic membranes). On the contrary, Gram-positive bacterial and eukaryotic cells lack the outer membrane and the periplasm, but possess a cell wall mainly containing peptidoglycans (bacteria) or multilayers of chitin, glucans and mannoproteins (fungi). The presence of the periplasm requires a series of import systems to let the metal pass through the outer membrane and make it caught by specialised proteins that transfer it to further cytoplasmic import systems (**Figure 1.1**). This function is usually delegated to diffusible soluble, highly specific, periplasmic metal-binding proteins or low molecular weight metal chelators. The secretion of metal-binding proteins in the Gram-positive bacteria and eukaryotic cells, instead, implies the release of these metallophores directly into the host environment and it requires a further reassociation step with the cell. Alternatively, the metallophore can be a lipid-anchored protein located at the cell surface of Gram-positive bacteria (reaching in some cases up to 40% of Gram-positive surface lipoproteins [14]) and, with less extent, of Gram-negative bacteria (both at outer or inner membrane).[15] Acquisition of metals directly by means of transmembrane systems – not associated with high-affinity proteins acting as metal shuttles – is also possible. The transfer direction can be from and to the cytosol. These systems are often characterized by several transmembrane domains (TDMs) connected by outer-cellular fragments that contain amino acid residues capable of acting as metal binding sites; examples include the ZIP and the CDF family members, drug/metabolite transporters, proton-coupled metals transporters, etc.

On the other hand, the human organism (here named "host") possesses various systems able to withdraw metal ions and limit their availability. The competition for trace minerals is fierce and the host must constantly evolve efficient mechanisms to circumvent the pathogen virulent activity. Numerous antimicrobial peptides and small proteins (AMPs), such as S100 proteins family members, ferritin, transferrin, hepcidin, defensins, histatins, etc., are able to sequester metal ions and starve microbes. They act as mediators of the innate host defence and, more intriguingly, they can serve as starting material to design novel efficient clinical treatments by simply improving their efficacy.[16-18]

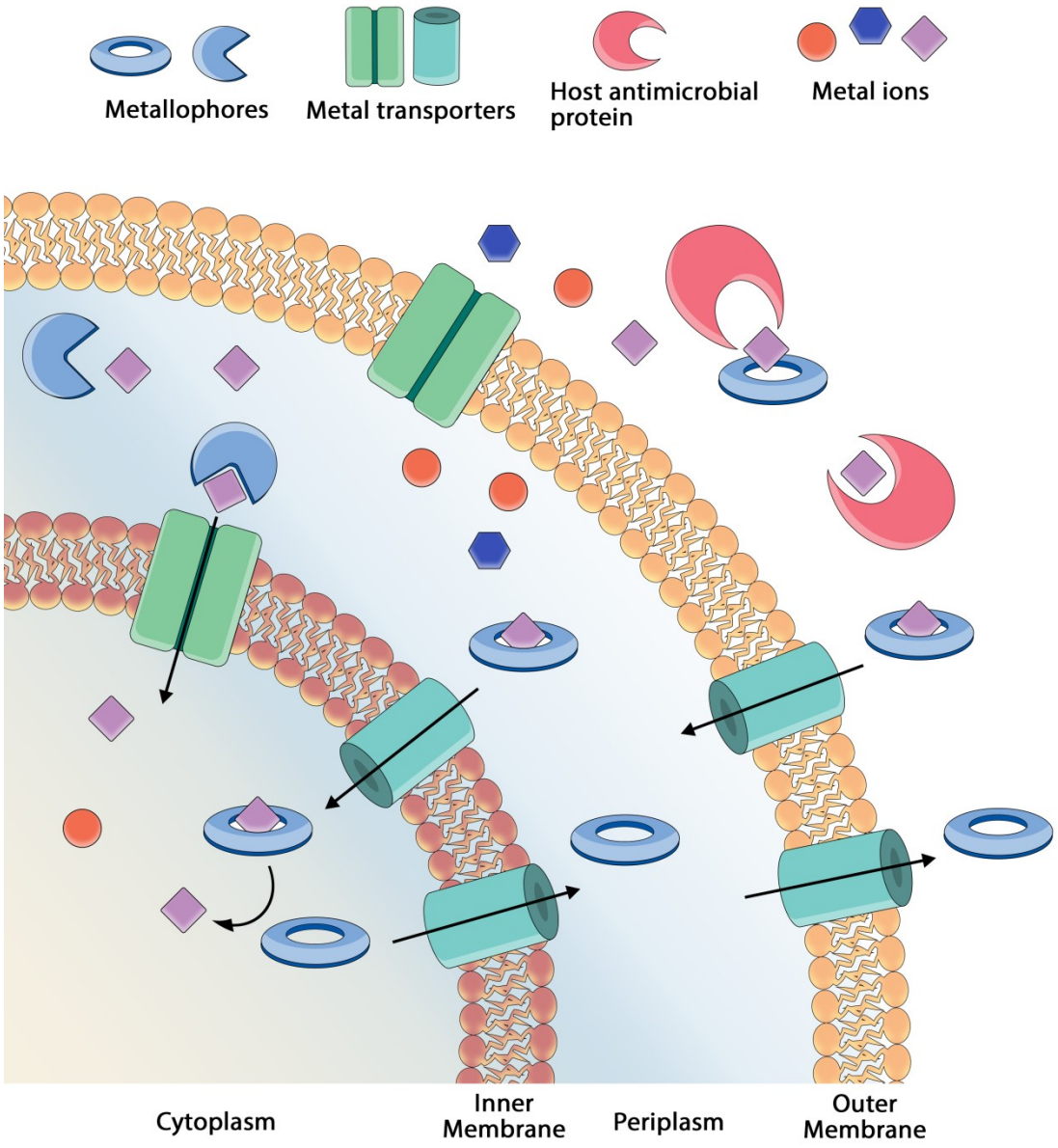

Figure 1.1 - Schematic representation of metal trafficking pathways in Gram-negative bacteria.

Taking into account the whole of the above considerations, this biological context imposes specific metal-coordination features and in particular the necessity of kinetically labile but thermodynamically stable coordination bonds; in other words, the systems involved in the metal trafficking mechanisms must ensure adequate thermodynamic complex stability to

prevent unwanted reactions or the premature release of the loaded ions, at the same time an easy and favourable metal transfer to the proper target must not be hindered. A further complication arises from the presence of different metal ions in the periplasmic and extracellular environments, which can act as competitors for the same binding sites. The Irving-Williams series elucidates the natural order of stability of metal complexes with divalent transition metal atoms: Mg(II), Ca(II) < Mn(II) < Fe(II) < Co(II) < Ni(II) < Cu(II) > Zn(II); in the case of flexible proteins and unstructured portion of polypeptides, the ligand cannot rely on specific steric effects that can favour the interaction with a specific metal ion (such as allostery, protein–protein interaction mediated specificity, steric hindrance, access to the binding site, kinetics, etc.) and therefore the metal selection follows the absolute order of metal affinity, with copper and zinc predominating in the protein bound-form (low bioavailability).[19-21]

Considering the host-pathogen interface, one can distinguish four leading actors: *(i)* metal ions, *(ii)* metallophores, *(iii)* metal transporters and *(iv)* host antimicrobial peptides and proteins (**Figure 1.1**). Each system plays a key role in the phenomenon of metals uptake-associated virulence and the investigation of their mutual interactions opens the way to novel antimicrobial strategies. Further details about each class are given in the next sections, with particular focus on the metal ions and transport systems investigated in this research work. Zinc interaction with zinc-binding proteins is by far the principal mechanism studied in this PhD thesis, therefore, special attention will be devoted to the description of zinc-metallophores ("zincophores") and zinc transporters. Copper binding ability of these proteins has been also investigated by virtue of Cu(II) potential activity as main zinc competitor and of its possible application in antimicrobial strategies. Nickel, instead, played a crucial role when the zinc or copper competition in bacterial nickel-binding proteins (*e.g.* Hpn protein) has been considered.

1.3 Transition metal ions in biological systems

All forms of life require the strict control of transition metal ions homeostasis and the importance of such micronutrients as virulence factors is undoubtedly well recognised and accepted. Metal availability depends on different physiological factors, such as pH, free oxygen concentration, metabolic activity, enzymes expression, imbalance of other free metal ions and the presence of competing chelators from the host organism. Understanding the dynamics behind metal acquisition processes is crucial to direct *in vitro* structural and functional studies and then provide rational guidelines for the design of new antimicrobial agents.[3]

Biological systems, like nature itself, must follow the basic notions of chemistry and, when thinking about metal binding proteins, of metals coordination chemistry. Metal ions and their ligands can be thus classified according to Pearson's theory of hard-soft acids and bases,[22] which predicts the general preference of a metal ion for certain ligands (**Table 1.1**). The two classes are empirically identified on the basis of the thermodynamic stability of the formed complexes (measured by the equilibrium constant for the species formation, K_f). It turns out that hard acids preferentially bind hard bases, and soft acids tend to interact with soft bases. The same also occurs for those acids and bases with an intermediate (borderline) character, which preferentially form complexes together. Furthermore, the metal-ligand interaction can be generally summarized as follow: hard interactions are predominantly electrostatic and soft interactions are predominantly covalent.

In biological systems, and in particular in proteins and peptides, one can identify only a relatively small number of potential metal ligands, corresponding to specific amino acids side-chains, in addition to the amino and carboxylic ends of the sequence. Moreover, the

protein folding must ensure an adequate conformation to locate ligand residues in a position suitable for the metal coordination. Alternatively, the metal binding can occur *via* amino acid residues located in an unstructured, flexible portion of the protein, which can adopt various conformations and properly coordinate the metal ion. The most common metal binding chemical groups are the imidazole of His, the carboxylates of Glu and Asp, the thiolate of Cys and the phenolate of Tyr. Less frequently the metal coordination can occur by means of the thioether moiety of Met, the amino group of Lys, the guanidine of Arg and the amides of Asn and Gln. Metal ions like Cu(II), Ni(II) or Fe(III) can also displace backbone N-amide protons at suitable pH values or bind the carbonyl group of the peptide chain (**Figure 1.2**).

Table 1.1 - Hard-soft classification of Lewis acids and bases.

	Hard	**Borderline**	**Soft**
Acids	H^+, Li^+, Na^+, K^+, Be^{2+}, Mg^{2+}, Ca^{2+}, Cr^{2+}, Fe^{3+}, Cr^{3+}, Al^{3+}, SO_3, BF_3	Fe^{2+}, Co^{2+}, Ni^{2+}, Cu^{2+}, Zn^{2+}, Pb^{2+}, SO_2, BBr_3	Cu^+, Au^+, Ag^+, Tl^+, Hg_2^{2+}, Pd^{2+}, Cd^{2+}, Pt^{2+}, Hg^{2+}, BH_3
Bases	F^-, OH^-, H_2O, NH_3, ROH, CO_3^{2-}, NO_3^-, O^{2-}, SO_4^{2-}, PO_4^{3-}, ClO_4^-	NO_2^-, SO_3^{2-}, Br^-, N_3^-, N_2, C_6H_5N, $SC\underline{N}^-$	H^-, R^-, $\underline{C}N^-$, CO, I^-, $\underline{S}CN^-$, R_3P, C_6H_5, R_2S

Computational approaches applied to experimental evidence (*e.g.* the hard-soft rule) identify a quite ordinary binding preference for each metal ion; for example, Ca(II) favourite amino acids were predicted to be Asp, Glu, Asn and Gly, Cu(II) exhibits a marked preference for His while Zn(II) for His, Asp, Glu and Cys, Mg(II) usually binds Asp and Glu, and Fe(III) His, Asp, Glu, Cys and Tyr.[23, 24] Although metal ion-binding sites in proteins exhibit a wide range of diversity, the regions responsible for the interaction with ligands, substrates or other proteins tend to be conserved both in sequence and structure, and the involved residues are usually in close spatial proximity. Therefore, despite the mere presence of a certain residue in a protein sequence, it is often more useful looking for a particular recurring motif (consensus sequence) by consulting specific database or performing sequences alignment of homologue proteins. Typical examples of metal binding motifs in proteins are the well-known amino terminal copper- and nickel-binding (ATCUN) motif NH_2-X-Y-H-, which commonly results in a Cu(II) and Ni(II) square planar complex where the metal is bound to the terminal amino group, the imidazole nitrogen of His and the two backbone amides (NH_2, N_{Im}, $2N^-$);[25] or the Cys_2His_2 zinc finger motif -X-C-$X_{2,4,5}$-CX_{12}-H-$X_{2,3,4}$H-, consisting of an α-helix and an antiparallel β-sheet, with Zn(II) usually forming a tetrahedral complex.[26] Polyhistidine sequences (consecutive -$(HH)_n$- or alternated -$(HX)_n$-) are also quite common in metallophores or antimicrobial peptides, and several metal transporters contain high percentage of His residues in their flexible, extra-membrane fragments (His-rich loops).[27]

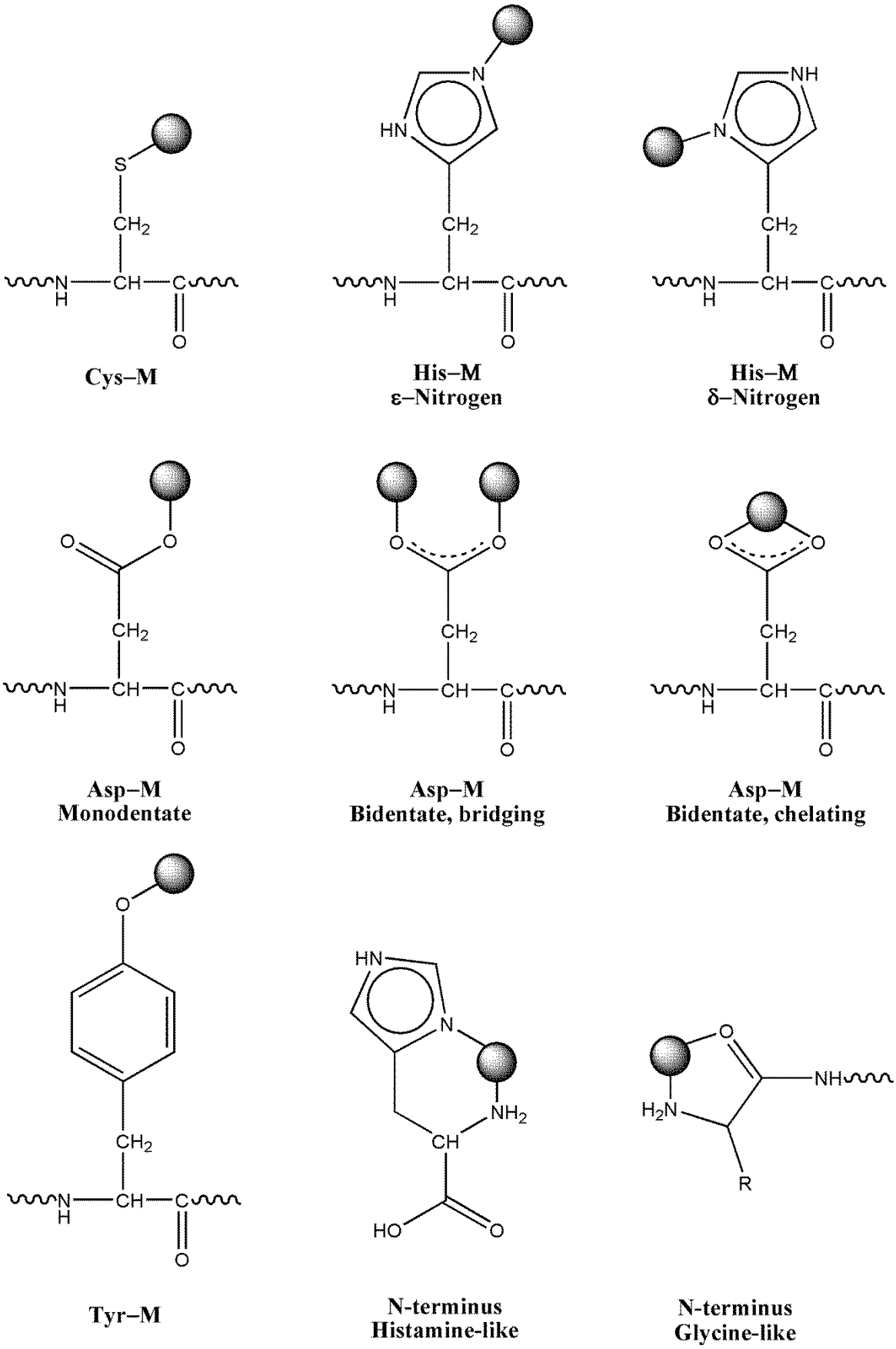

Figure 1.2 - Most common metal binding groups in a protein or peptide system and their metal coordination modes.

This research work is mostly focused on the bioinorganic chemistry of Zn(II), which is crucial for the survival of human and pathogen cells, being indispensable for the function of several metalloproteins and enzymes. Its assimilation by pathogens is extremely challenging: free zinc concentration within cells is normally subnanomolar,[28] and many other divalent endogenous metal ions, first of all Cu(II), but also Fe(II)/Fe(III) and Mg(II) or Ni(II) in certain organisms, can compete for the same protein binding sites, thus requiring an extensive study of the different metals binding abilities of the involved systems. For example, Cu(II) is present in bacterial periplasm, it might enter the cytoplasm *via* the zinc-uptake system ZupT and, depending on its concentration, might represent a strong Zn(II) competitor, unless properly regulated.[29]

1.3.1 Histidine interaction with metal ions

According to Pearson's classification, the imidazole side chain of histidine is a good binding site for the so-called "borderline" metal ions (**Table 1.1**). In fact, although they can form coordination bonds with other donor atoms, such as oxygen and sulphur, divalent cations like Cu(II), Zn(II) and Ni(II) exhibit a marked preference for nitrogen. The imidazole group of His is partially deprotonated at physiological pH ($pK_a \approx 6.5$), exerting a buffer action and being available for metal coordination. Therefore, when a His residue is located in a solvent exposed site or in an accessible unstructured portion of the protein (which can fit itself around the metal centre or extend into the surrounding environment with higher degrees of freedom), Cu(II), Zn(II) or even Ni(II) can easily find an optimal anchor point and coordinate the imidazole.[30] Moreover, in the case of Cu(II) or Ni(II), the His coordination can promote the deprotonation and binding of the peptide backbone amides to occupy the available equatorial coordination positions. The driving force of the amide complexation is usually the formation of stable six- or five-membered chelate rings (see **Figure 1.3a**). An outstanding example is given by the ATCUN motif: the His residue located at position 3 of a peptide chain enables the simultaneous formation of three fused chelate rings and the saturation of the coordination plane when Cu(II) or Ni(II) coordinate the adjacent amides and the terminal amino group (**Figure 1.3b**). The efficiency of His as anchoring site is also underlined by the formation of more stable complexes when several His residues are located in proximal positions. This is certainly true for Zn(II) that usually coordinates several imidazole side chains in order to saturate its coordination sphere or form ($3N_{Im}$, H_2O) complexes, which are quite frequent in biological systems (**Figure 1.4**). Even in the case of Cu(II), Co(II) and Fe(II), poly-His sequences promote the formation of very stable complexes.

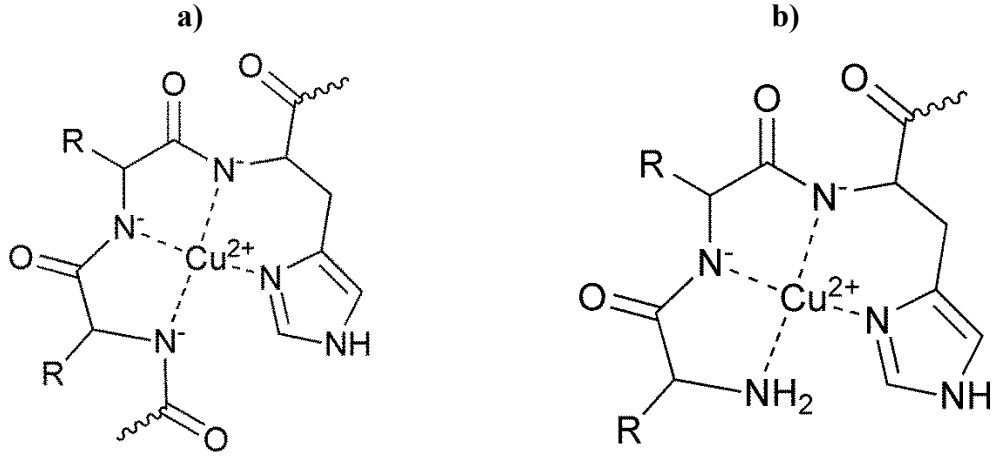

Figure 1.3 - Example of Cu(II) complex with (a) coordination mode (N_{Im}, $3N^-$); (b) ATCUN type coordination mode (N_{Im}, NH_2, $2N^-$).

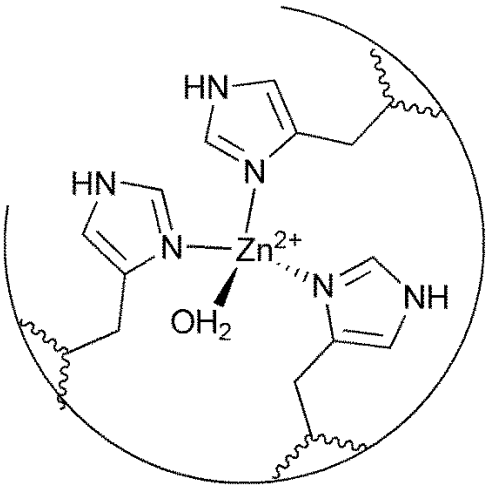

Figure 1.4 - Example of Zn(II) complex with coordination mode ($3N_{Im}$, H_2O).

1.3.2 Zinc

Zinc is the second most abundant transition metal ion in living organisms, after iron. A zinc ion can organize the biological structure and stabilize the folding of a protein, as in zinc fingers proteins. Regulation of the transcription and translation of the genetic message is also dependent on Zn(II), which is required by RNA and DNA polymerases and participates in ribosome activity. The large family of Zn(II)-enzymes includes carbonic anhydrase, carboxypeptidases, alkaline phosphatase, beta-lactamase and alcohol dehydrogenases. Zn(II)-enzymes are also involved in many infectious events (*e.g.* superoxide dismutases, ADAM metalloproteinases or deuterolysin) and play a key role in human innate and adaptive immune responses.[4, 31] The biological significance of Zn(II) is therefore well-documented and a deep look into the (bio-)chemistry of pathogens' primary zinc-thieves is fundamental in order to rationally deal with the discovery and design of new antimicrobial drugs. The divalent Zn(II) ion has a high rate of ligand exchange, a reasonably high electron affinity, a flexibility of coordination geometry (mostly tetrahedral) and no redox activity, which in turns avoids the participation in free-radical cellular damage. The Zn element has the $[Ar]3d^{10}4s^2$ electron configuration and its most common oxidation state is +2. The corresponding Zn(II) ion is therefore characterized by a d^{10} configuration which limits the spectroscopic investigation of zinc complexes: visible light is not absorbed since no *d–d* transitions can take place. Its polarizing power makes the pK_a of coordinated water molecules quite low, displaying Lewis acid properties and allowing a catalytic function when, for instance, it coordinates three rather than four protein ligands. More in general, the zinc-bound water can be either ionized to zinc-bound hydroxide, polarised by a generic base to generate a nucleophile for catalysis, or displaced by an appropriate ligand or substrate.

1.3.3 Copper

Copper is present in many enzymes, with crucial roles in electron transfer and activation of small molecules (e.g. O_2, NO_x, CO). Together with zinc, Cu(II) is an important cofactor for superoxide dismutases (SODs), enzymes that catalyse the dismutation of the superoxide ion, O^{2-}, into oxygen and hydrogen peroxide. Copper is also well-known for its direct pathogenic role in neurotoxic processes, like peptide aggregation and deposition in the brain. In some invertebrates, copper also functions as oxygen carrier. The most common

oxidation states for Cu element ([Ar]$3d^{10}4s^1$) are +1 and +2. The Cu(II) ion has a $3d^9$ electron configuration and its complexes present a coordination number of 4, 5 or 6; they are often characterized by the Jahn-Teller effect, which induces tetragonal, not symmetrical geometry distortions, resulting in a configuration stretched or compressed along a quaternary axis, thus stabilizing (*i.e.* minimizing the energy of) the system. When the tetragonal elongation is enough intense, Cu(II) complexes with coordination 4 can assume a square planar geometry. In a protein/peptide bound form, Cu(II) can also displace backbone N-amide protons at suitable pH values and include the amide-nitrogens in its donor atoms set. In bacterial periplasm Cu(II) can be adventitiously reduced to the more toxic Cu(I), and therefore copper detrimental action must be prevented by oxidation, efflux or sequestration mechanisms. According to the Irving–Williams series of divalent cations, Cu(II) is able to produce the most stable metal complexes and therefore is highly competitive in a biological environment.

1.3.4 Nickel

Nickel plays an essential role as catalytic cofactor in many enzymes from bacteria, fungi and plants. Nickel-containing enzymes, except for urease, are mostly found in microorganisms and they include glyoxalase I, acireductone dioxygenase, urease, superoxide dismutase, [NiFe]-hydrogenase, carbon monoxide dehydrogenase, acetyl-coenzyme A synthase/decarbonylase, methyl-coenzyme M reductase, and lactate racemase.[32] The uptake, trafficking, and storage mechanisms of Ni(II) ion is extremely efficient; nickel deficiency hardly occurs in any organism that requires this metal. The most important nickel import systems are NikABCDE and the nickel/cobalt permeases (NiCoT).[33] Ni element has a [Ar]$3d^8s^2$ electron configuration and its most common oxidation state is +2, although in certain conditions it can present a +1 or +3 oxidation state. The resulting Ni^+ and Ni^{3+}, however, are unstable species and do not contribute to noticeable redox activity in living organisms. Ni(II) is thus the most stable and common ion, with a $3d^8$ electronic configuration. Hexacoordinate nickel forms paramagnetic octahedral complexes (high spin configuration and a triplet ground-state) with three spin-allowed transitions (according to Tanabe-Sugano diagram for d^8 ions): $^3A_{2g} \rightarrow {}^3T_{2g}$ (F), $^3A_{2g} \rightarrow {}^3T_{1g}$ (F), $^3A_{2g} \rightarrow {}^3T_{1g}$ (P). With coordination number 4, Ni(II) tends to preferentially form complexes with a square-planar arrangement (point group D_{4h}) in order to increase the electronic stabilization energy of its d-orbitals. The resulting molecular d-orbital energy levels may favour a low-spin configuration (d_{xz}^2, d_{xz}^2, d_{z2}^2, d_{xy}^2) with an empty $d_{x2\text{-}y2}$ orbital at higher energy. In this case there are three spin-allowed transitions: $^1A_{1g} \rightarrow {}^1B_{2g}$, $^1A_{1g} \rightarrow {}^1E_g$, $^1A_{1g} \rightarrow {}^1B_{1g}$. Therefore, the spin state of Ni(II) complexes depends on the coordination number and geometry. In square-planar complexes, Ni(II) shows diamagnetic behaviour with S = 0 (singlet ground-state), but if the geometry changes to tetrahedral or the coordination number increases to five or six, the spin state changes to S = 1 (triplet ground-state), resulting in a paramagnetic complex. This effect is termed coordination-induced spin-state switching (CISSS).[34] The formation of Ni(II) complexes with peptides proceeds in a way similar to Cu(II), displaying a preference for nitrogen and oxygen donor atoms and being able to promote the deprotonation of the backbone N-amides. In contrast with Cu(II), increasing the pH value, the coordination of the peptide chain (namely the deprotonation of N-amides) occurs cooperatively and promotes the transition from an initial octahedral distorted arrangement (most frequent with amine ligands) to a square-planar geometry. An important limitation of Ni(II) ion is the relatively slow kinetic of ligand exchange and complexation reactions, the first-order water exchange rate constant for Ni(II) is 100 times slower than for Co(II) and 1000 times slower than for Zn(II).[35]

1.4 Zincophores

Many bacteria possess high-affinity uptake systems to transport a specific nutrient or ligand, in general a target substrate, across their membranes. Zincophores are such systems in charge of zinc recruitment from the extracytosolic space (host environment or periplasm). Therefore, it is possible to distinguish different classes of zincophores: *(i)* the bacterial ABC transporter related zincophores, *i.e.* the zinc-specific substrate binding proteins (SBPs) constituting the extramembrane component of the ABC import systems, *(ii)* their associated zinc-chaperones (when existing), which are a miscellaneous group of proteins able to bind and transfer zinc to the SBP-zincophore, *(iii)* the bacterial nicotianamine-like zincophores (also known as opine metallophores) and, analogously to bacterial microorganisms, *(iv)* fungal macromolecules able to bind zinc and deliver it to a target membrane transporter.

1.4.1 ABC transporter-related zincophores and their zinc-chaperones

The most important bacterial transport systems are the ATP-binding cassette (ABC) transporters, consisting of three main components: a substrate binding-protein (SBP), a membrane permease and an ATPase. The ABC transporters are extremely important and often involved in the processes of metal homeostasis, being able to translocate the bound targets across the cell membranes in both the directions (they can be classified as importers or exporters). There are seven different classes ("clusters") of SBPs, including metal-binding proteins. Phylogenetical and structural analyses on a wide variety of known SBPs highlight that Zn(II)-substrate binding proteins share certain evolutionarily conserved structural characteristics, although they display different sizes, poor or no sequence homology and have multiple biological roles. Therefore, only one class (cluster A) is representative of Zn(II)-related chelators and currently all of them are known as extra-membrane components of the ATP-binding cassette (ABC) transporters, with the function of withdrawing and delivering the cognate substrate to the transmembrane domains of the ABC transport system.[36] Cluster A consists, in general, of SBP-dependent ABC transporter proteins able to directly bind free Zn(II), Mn(II), Fe(II)/Fe(III) ions (cluster A-I) or to interact with metals in their protein-bound form, like siderophore, catecholate, heme (cluster A-II). The main common feature of the cluster A metallophores is the presence of a single rigid α-helical hinge region that links the two globular, pseudo symmetrical α/β domains typical of all the SBPs. This α-helix linker makes the structure relatively rigid and seems to be responsible for the different substrate delivery mechanism proposed for cluster A-I SBPs, which significantly differs from the common "Venus flytrap" identified in SBPs with non-metal cognate substrate.[36-38] A further sub-classification differentiates cluster A-I zincophores on the basis of (*i*) the donor atoms of the metal coordination sphere, (*ii*) the organism type, (*iii*) the presence of a flexible loop near the metal-binding site, (*iv*) the length of the loop, and (*v*) the presence of histidine residues in the loop.[15] In the case of cluster A-I Zn(II) binding proteins, it is possible to summarize the following common characteristics: (1) they generally display a tetrahedral ($3N_{Im}$, COO^- or H_2O) metal coordination mode, that means that Zn(II) is bound to 3 histidine residues and 1 carboxylate group from glutamic acid or aspartic acid or 1 exchangeable water molecule; (2) the flexible loop is always present, with only one exception represented by TroA protein, and it generally indicates specificity for Zn(II); (3) in Gram-negative bacteria there is always a long His-rich loop while (4) in Gram-positive bacteria the loop is usually shorter and may or may not contain His residues. The proper coordination mode and the presence of a flexible loop close to the binding site are therefore two indispensable features that ABC-transporter related zincophores must display to perform their biological role and facilitate the interconversion between their metal -free and -loaded forms. To date, only a relatively limited number of cluster A-I zincophores

have been identified (**Table 1.2**). Unfortunately, neither their three-dimensional structures nor the mechanistic implications of their metal uptake function are always clear.

Table 1.2 - Representative bacterial Zn(II) specific substrate-binding proteins of cluster A-I. A three-dimensional structure of the protein in the zinc bound form is available for the underlined species. Hypothetical zinc coordination mode for SBP lacking a 3D structure is written in italics.

Protein	**Coordination mode**	**SBP classification**	**Species**	**Ref.**
AdcAII	3His, 1Glu	Ia (lipid-anchored)	<u>*S. pneumoniae*</u> (G+)	[39]
	3His, 1Glu or H_2O		*S. agalactiae* (G+)	
Lbp (or Lsp)	3His, 1Glu	Ia (lipid-anchored)	<u>*S. pyogenes*</u> (G+)	[40]
Lmb	3His, 1Glu	Ia (lipid-anchored)	<u>*S. agalactiae*</u> (G+)	[41]
AdcA	*3His, 1Glu* or *H_2O* (N-terminal domain); *3His* (C-terminal domain)	Ib (lipid-anchored)	*S. pneumoniae* (G+) *S. agalactiae* (G+) *S. pyogenes* (G+)	[42]
ZnuA	3His, 1Glu	II (soluble)	<u>*E. coli*</u> (G-) <u>*S. enterica*</u> (G-)	[43-45]
	3His, 1H_2O		*P. aeruginosa* (G-) *T. pallidum* (G-) *H. ducreyi* (G-) *H. influenzae* (G-) *Y. pestis* (G-)	
TroA	3His, 1Asp	III (lipid-anchored)	<u>*T. pallidum*</u> (G-) <u>*S. suis*</u> (G+)	[46, 47]

Understanding how exactly the metal ions are recruited and how these zincophores discriminate within the variegated pool of available metal micronutrients remains a challenge. Many studies underline the crucial contribute of the metal binding sites specificity and of the consequent resulting coordination mode, that can facilitate or block the conformational changes required to perform a specific function. An elegant example is provided by the pneumococcal surface adhesin A (PsaA) protein, which belongs to cluster A-I SBPs. Its structural studies revealed that "imperfect", far-from-ideal metal coordination modes are preferable to favour the metal transport processes. This is also the reason why Zn(II) ion (coordinated to His67, His139, Asp280 and Glu205) poisons PsaA, blocking the protein in its closed conformation and preventing the metal release after binding.[37] Therefore, it is desirable that Zn(II)-specific SBPs avoid strong interactions

with the metal substrate and this can be achieved by means of different sets of donor atoms, possibly located at mobile, flexible regions of the protein, or close to them, that make the ideal coordination sphere enough distorted, or occupying some coordination positions with exchangeable solvent molecules, *i.e.* water. Interestingly small changes in helices and in the loop spatial conformation near the metal-binding site are observed between apo- and holo- forms in many Zn(II) specific SBPs, suggesting that metal uptake and release is likely mediated by the structural rearrangements of secondary elements, as also recently proposed for the SBP protein ZnuA of *Escherichia coli* (*Eco*ZnuA).[48] However, the role of the flexible region rich in acidic and histidine residues near the metal binding site has not been established yet. It is supposed to facilitate zinc acquisition, to serve as a sensor under zinc-exceeding conditions or to be recognised by the membrane permease component. Some studies revealed that the His-rich loops of ZnuA homologues in *E. coli* and *Salmonella enterica* can bind Zn(II) through their His and Asp/Glu residues, providing secondary metal binding sites.[43] Moreover, the loop can be involved in specific protein-protein interaction and potential Zn(II) acquisition from additional metallochaperones (**Table 1.3**): the most interesting example concerns the formation of the protein binary complex between *Sen*ZnuA and the periplasmic zinc binding protein *Sen*ZinT, where the N-terminal histidine-rich loop of ZnuA proved to play a critical role, embedding into a structural cavity of the partner protein.[49]

Table 1.3 - Summary of Zn(II) specific substrate binding proteins (SBPs) and their associated accessory zinc-chaperone.

SBP-dependent ABC transporter	Associated zinc-chaperone component	Ref.
ZnuA	ZinT (periplasmic protein)	[49]
AdcA (N-terminal domain)	AdcA (C-terminal domain)	[50]
AdcAII	PhtD (surface protein)	[51]
AztC	AztD (periplasmic protein)	[52]

1.4.2 Nicotianamine-like zincophores

Staphylococcus aureus, *Pseudomonas aeruginosa* and *Yersinia pestis* are human pathogenic bacteria which, in a metal-deficient environment, can express specific opine-type metallophores called staphylopine (StP), pseudopaline and yersinopine, respectively. These chelators are similar to nicotianamine and their biosynthesis proceeds in the following steps: 1) CntK, a histidine racemase (if present, as in *S. aureus*) converts L-His into D-His; 2) CntL, a nicotianamine synthase enzyme, attaches the aminobutyrate chain of S-adenosyl-L-methionine (SAM) to the histidine amino group, to form an intermediate called xNA (if contains D-His) or yNA (if contains L-His); 3) the opine dehydrogenase (ODH) enzyme, CntM, condenses the intermediate with an α-keto acid and, after reduction with NAD(P)H, the obtained opine-type metallophore has stereochemistry (L, L) or (D,

L).[53] An additional nicotianamine-like metallophore belongs to *Paenibacillus mucilaginosus* and has been named bacillopaline. The role of this metallophores in zinc uptake has been confirmed in the context of nutritional immunity, for example staphylopine was shown to compete with human calprotectin for zinc binding and import by *S. aureus*. The mechanism of metal recruitment by means of such metallophores consists of the internalization of the Zn(II)-opine complex through an appropriate transporter.

1.4.3 Fungal zincophores: Pra1 and Aspf2

Fungal zincophores are small proteins, able to sequester zinc from the host tissue by interacting either with the free soluble metal ion or with the metal coordinated to different ligands. The concept of fungal protein zincophores and the discovery of how they work is relatively new to the world of science. In 2012, Citiulo *et al*. explained the details of this mechanism in *C. albicans:* the zincophore is expressed under zinc limited conditions and neutral to basic pH, it is then released from the hyphal surface into the surrounding environment of the host, where it binds the Zn(II) ion and delivers it to the fungal pathogen *via* physical interactions with an appropriate zinc transporter. In the case of *C. albicans*, the 299 amino acid zincophore is named Pra1 (pH-regulated antigen 1); it captures zinc and returns to the cell via a syntenically expressed receptor, Zrt1 (*A. fumigatus* orthologues: Aspf2 and ZrfA, respectively).[54] Although our knowledge on the inorganic biochemistry of zincophores keeps expanding and is starting to be considered as a stepping stone towards finding new, specific antifungal therapeutics based on zincophore fragments connected with antifungal drugs, there are numerous issues that keep surprising us, such as the recent data which shows that the Pra1 zincophore may collaborate with Sap6, a secreted aspartyl protease involved in zinc scavenging. It was suggested that Sap6 may act upstream in the zincophore pathway, delivering the substrate to the Pra1/Zrt1 system.[55] In this context, Sap6 may function as a zinc-chaperone and may take the role of the above mentioned bacterial SBP associated zincophores (*e.g.* ZinT), highlighting more similarities with bacteria than might be expected. It is also worth to mention that, from the functional point of view, the Pra1/Zrt1 zinc uptake system is analogous to bacterial zinc ABC transporters, involving a secreted zinc scavenger (*e.g.* ZnuA) and a transmembrane protein (*e.g.* ZnuB). Hence, the nutrient sequestration strategy from *C. albicans* appears to be well conserved in other pathogens

1.5 Zinc transporters

Several bacterial proteins involved in the transmembrane transport of zinc, along with those devoted to the transport of other metal ions, have been characterised in the past decade. Zinc transporters can be classified as channels and pores, electrochemical potential-driven transporters and primary active transporters. According to the known systems, zinc transport tends to mostly occur by means of active mechanisms, although also passive transport is possible. The major bacterial zinc importers are the members of the ABC transporters family, which has been described in detail in the previous section and makes use of substrate-binding proteins in order to sequester the metal ion from the surrounding environment. Adequate zinc acquisition is also critical for the survival and virulence of fungal pathogens, and – as in the case of bacteria – the tug-of-war between the fungus and its host can be regarded as a potential target for new antifungal therapies. In order to develop a highly specific antifungal medication, it is important to precisely understand and aim at the differences in human and fungal Zn(II) transport.[56, 57] One of the biggest obstacles in finding effective and drug-specific antifungal agents with negligible side effects for patients comes from the fact that fungi share many basic

metabolic pathways with their human hosts (both are eukaryotes), much more than with prokaryotic bacteria. Unlike bacterial pathogens, fungi do not rely on ABC transporters for zinc transport, but they encode two independent classes of zinc transporters: *(i)* ZIPs (Zrt/Irt-like proteins), which transport zinc from outside the cell into the cytoplasm, and *(ii)* ZnTs (zinc transporters) which transport zinc from the cytoplasm out of the cell and from the cytoplasm into vesicles. ZIP proteins consist of several (6 to 9) transmembrane domains connected by outer-cellular fragments that may contain amino acid residues capable of acting as metal binding sites. In most cases, such potential metal-binding sites are histidine rich motifs.

1.6 Host antimicrobial proteins and peptides

Antimicrobial peptides and antimicrobial proteins (AMPs) are phylogenetically ancient biomolecules with a broad spectrum of activity and scarce attitude to induce antimicrobial resistance. They are known to be effective against a wide variety of pathogens, like Gram-positive and Gram-negative bacteria, fungi, viruses and even cancer cells and are present in all living organisms (invertebrates, vertebrates, plants, prokaryotes).[18] Interestingly, AMPs also exhibit different desirable and attractive medicinal properties, hopefully translatable into an appropriate bioactive system that will serve as an efficient clinical treatment. Nevertheless, these extraordinary candidate molecules present some drawbacks. The AMPs activity level is subject to modulation or degradation by both human and pathogenic proteolytic enzymes; in fact, many endo- and exo-peptidases act to transform high molecular weight peptides into shorter oligopeptides, making them inactive. Another challenge to overcome is the decrease of biological activity *in vivo* (compared to *in vitro* experiments): differences in the pH and salt concentrations and the presence of a variety of interacting molecules can inhibit the AMPs efficacy.[58, 59]

As already mentioned, AMPs act as mediators of innate host defence, and their antimicrobial activity can be expressed in different ways, including the interaction with cell membranes and the sequestration of metal nutrients such as Zn(II), Cu(II), Mn(II) or Ca(II). The main AMP mechanisms of action on a membrane concern the possibility to promote cell wall permeabilization and to inhibit its biosynthesis, resulting in a loss of pathogenic cell membrane integrity. On the other hand, several AMPs have also been suggested to be involved in the disruption of metal homeostasis of pathogens.[60] The presence of some divalent metal ions can modulate the efficacy of some AMPs (psoriasin, kappacin, microplusin, calcitermin, histatin, etc.); and some interesting studies demonstrate that Zn(II) and Cu(II) can play a role as structural cofactors,[61, 62] inducing desirable and significant conformational changes in peptide structures with possibly a better microbicide activity; this is the case of kappacin and dermicidin, which can adopt an amphiphilic α-helical structure in bacterial membrane-like environments.[63, 64] The importance of these metal ions in the process of nutritional immunity is crucial as well: antimicrobial peptides like psoriasin, histatins and microplusin, in particular, act by chelating zinc and copper ions.[65-67]

1.7 Overview of the presented research

In this work we mostly focus on Zn(II), Cu(II) and Ni(II) acquisition by bacterial and fungal human pathogens. Our aim is to understand the bioinorganic chemistry of the main systems involved in metals uptake from the periplasmic and/or extracellular space, with particular emphasis on the very first step of metal sequestration at the interface with the

host organism, that is the “place” where most of these processes occur and where the actual “metal tug-of-war” befalls. Once the bioinorganic chemistry of the involved systems is known, the further step can be devoted to the design of novel metal-related therapeutic strategies. The whole of the obtained information can allow to correlate the metal coordination behaviour with the corresponding biological function. Furthermore, metal complexes are not only a promising tool in antimicrobial treatments, but they can also find application against pathologies which, in general, involve metal ions: a well-known example is that of neurodegenerative diseases. In fact, the onset and progression of disorders like Alzheimer's, Parkinson's and Huntington's diseases as well as amyotrophic lateral sclerosis are closely related to the imbalance of transition metal ions in the brain, clearly suggesting the crucial importance of metal homeostasis. The first essential step to develop novel metal-based therapeutics is the elucidation of coordination chemistry of the metal chelators involved in pathogenic events.

Genome analyses have identified numerous homologues of each metallophore and import system, and various genes encoding further putative metal transporters in human pathogenic species. The vastness of the topic forces us to focus on a restricted pool of biological systems. Different pathogenic species and their most promising metal acquisition pathways (as potential drug-targets) have been selected and investigated in terms of coordination properties of the involved metal binding proteins. A detailed description of the systems investigated in this work is given in the next chapters and is schematically reported in **Figure 1.5**.

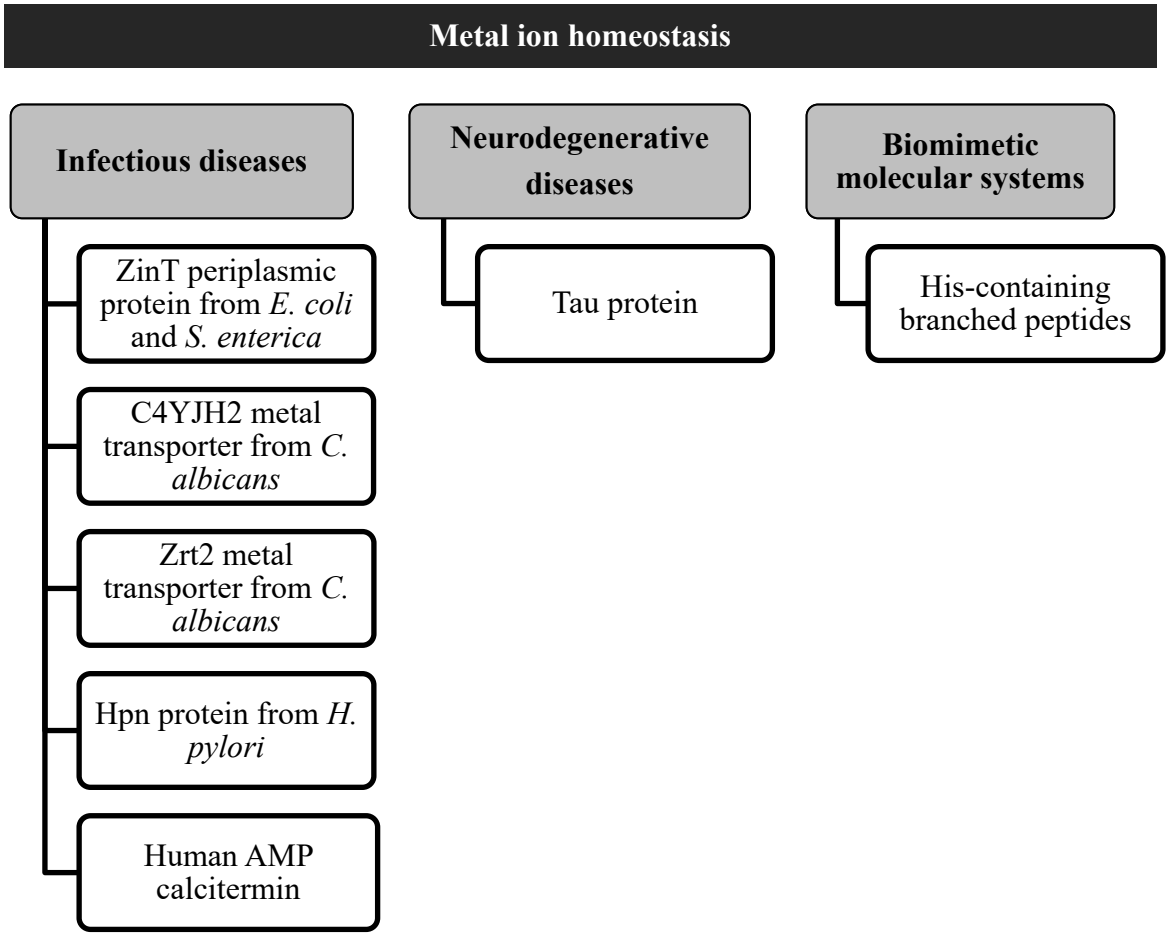

Figure 1.5 - Schematic overview of the research work.

The studied systems include: *(i)* the ZinT periplasmic protein from *E. coli* and *S. enterica*, the metal transporter proteins *(ii)* C4YJH2 and *(iii)* Zrt2 from *C. albicans*, *(iv)* the Hpn protein from *Helicobacter pylori* and *(v)* the human antimicrobial peptide calcitermin. Moreover, there are several hypotheses and existing evidence of infectious agents, like *H. pylori* and other pathogens, contributing to neurodegenerative diseases etiology in human and animal models.[68] *H. pylori* associated worsening of neurological disorders can be related to the disruption of the blood-brain barrier and to the formation of amyloid-like fibrils, which is promoted by the Hpn protein in the brain.[69, 70] The metal-binding ability of Hpn is also well documented.[71, 72] Therefore, considering the possible link among metal ions, neurodegenerative disorders and infectious pathologies, it is worth it to investigate the metal ion interaction with metal-binding proteins associated to neurodegeneration. From this perspective, the Cu(II)/Cu(I) binding and oxidation activity has been studied in relation to the *(vi)* human tau protein. In this context of characterization of biological systems, a different – but closely related – field of research is instead focused on the design and study of artificial systems that can mimic the functions of natural biomolecules or can display multivalent interactions with various biomolecular targets, including the ability of showing specific, selected metal binding properties: *(vii) ad hoc* designed His-containing branched peptides have been studied for their ability to bind metal ions. Although the design of promising therapeutic agents does not represent the goal of this PhD research work, the overall of the obtained results is certainly a solid steppingstone to rationally develop novel strategy against several human pathologies.

1.8 References

[1] R. E. W. Hancock, H.-G. Sahl, *Nat. Biotechnol.* **2006**, *24(12)*, 1551-1557.
[2] European Centre for Disease Prevention and Control, Surveillance of antimicrobial resistance in Europe 2018, **2019**, https://www.ecdc.europa.eu/sites/default/files/documents/surveillance-antimicrobial-resistance-Europe-2018.pdf *(Access on 04 December 2019)*.
[3] M. I. Hood, E. P. Skaar, *Nat. Rev. Microbiol.* **2012**, *10*, 525-537.
[4] W. Maret, *Int. J. Mol. Sci.* **2016**, *17(1)*, 66.
[5] G. Porcheron, A. Garénaux, J. Proulx, M. Sabri, C. M. Dozois, *Front. Cell. Infect. Microbiol.* **2013**, *3*, 90.
[6] Z. Ma, F. E. Jacobsen, D. P. Giedroc, *Chem. Rev.* **2009**, *109(10)*, 4644-4681.
[7] T. Fukada, S. Yamasaki, K. Nishida, M. Murakami, T. Hirano, *J. Biol. Inorg. Chem.* **2011**, *16(7)*, 1123-1134.
[8] E. D. Weinberg, *JAMA* **1975**, *231(1)*, 39-41.
[9] K. Y. Djoko, C.-l. Y. Ong, M. J. Walker, A. G. McEwan, *J. Biol. Chem.* **2015**, *290(31)*, 18954-18961.
[10] M. Umair, M. Alfadhel, *Cells* **2019**, *8(12)*, 1598.
[11] K. Grüngreiff, D. Reinhold, H. Wedemeyer, *Ann. Hepatol.* **2016**, *15(1)*, 7-16.
[12] P. D. Zalewski, A. Q. Truong-Tran, D. Grosser, L. Jayaram, C. Murgia, R. E. Ruffin, *Pharmacol. Ther.* **2005**, *105(2)*, 127-149.
[13] D. A. Capdevila, K. A. Edmonds, D. P. Giedroc, *Essays Biochem.* **2017**, *61(2)*, 177-200.
[14] M. I. Hutchings, T. Palmer, D. J. Harrington, I. C. Sutcliffe, *Trends Microbiol.* **2009**, *17(1)*, 13-21.
[15] R. P. A. Berntsson, S. H. J. Smits, L. Schmitt, D.-J. Slotboom, B. Poolman, *FEBS Lett.* **2010**, *584(12)*, 2606-2617.
[16] A. J. Battersby, J. Khara, V. J. Wright, O. Levy, B. Kampmann, *Front. Immunol.* **2016**, *7*, 309.
[17] D. Łoboda, H. Kozłowski, M. Rowińska-Żyrek, *New J. Chem.* **2018**, *42(10)*, 7560-7568.
[18] G. Wang, X. Li, Z. Wang, *Nucleic Acids Res.* **2016**, *44*, D1087-D1093.
[19] K. J. Waldron, N. J. Robinson, *Nat. Rev. Microbiol.* **2009**, *7(1)*, 25-35.
[20] J. J. Braymer, D. P. Giedroc, *Curr. Opin. Chem. Biol.* **2014**, *19*, 59-66.
[21] L. A. Finney, T. V. Halloran, *Science* **2003**, *300(5621)*, 931-936.
[22] R. G. Pearson, *J. Am. Chem. Soc.* **1963**, *85(22)*, 3533-3539.
[23] J. A. Tainer, V. A. Roberts, E. D. Getzoff, *Curr. Opin. Biotechnol.* **1992**, *3(4)*, 378-387.
[24] L. Regan, *Annu. Rev. Biophys. Biomol. Struct.* **1993**, *22(1)*, 257-281.
[25] C. Harford, B. Sarkar, *Acc. Chem. Res.* **1997**, *30(3)*, 123-130.
[26] M. Isalan, in *Encyclopedia of Biological Chemistry*, Second ed. (Eds.: W. J. Lennarz, M. D. Lane), Academic Press, Waltham, **2013**, pp. 575-579.

[27] M. Rowinska-Zyrek, D. Witkowska, S. Potocki, M. Remelli, H. Kozlowski, *New J. Chem.* **2013**, *37(1)*, 58-70.
[28] M. Maares, H. Haase, *Nutrients* **2020**, *12(3)*, 762.
[29] D. H. Nies, M. Herzberg, *Mol. Microbiol.* **2013**, *87(3)*, 447-454.
[30] E. Farkas, E. Csapó, P. Buglyó, C. A. Damante, G. D. Natale, *Inorg. Chim. Acta* **2009**, *362(3)*, 753-762.
[31] N. Giebeler, P. Zigrino, *Toxins (Basel)* **2016**, *8(4)*, 122.
[32] J. L. Boer, S. B. Mulrooney, R. P. Hausinger, *Arch. Biochem. Biophys.* **2014**, *544*, 142-152.
[33] Y. Li, D. B. Zamble, *Chem. Rev.* **2009**, *109(10)*, 4617-4643.
[34] M. Dommaschk, F. Gutzeit, S. Boretius, R. Haag, R. Herges, *Chem. Commun.* **2014**, *50(83)*, 12476-12478.
[35] R. B. Martin, in *Metal Ions in Biological Systems: Nickel and Its Role in Biology, Vol. 23* (Eds.: A. Sigel, H. Sigel), Marcel Dekker, New York, **1988**, pp. 123-164.
[36] G. H. Scheepers, J. A. Lycklama a Nijeholt, B. Poolman, *FEBS Lett.* **2016**, *590(23)*, 4393-4401.
[37] R. M. Couñago, M. P. Ween, S. L. Begg, M. Bajaj, J. Zuegg, M. L. O'Mara, M. A. Cooper, A. G. McEwan, J. C. Paton, B. Kobe, C. A. McDevitt, *Nat. Chem. Biol.* **2014**, *10(1)*, 35-41.
[38] Y.-H. Lee, M. R. Dorwart, K. R. O. Hazlett, R. K. Deka, M. V. Norgard, J. D. Radolf, C. A. Hasemann, *J. Bacteriol.* **2002**, *184(8)*, 2300-2304.
[39] E. Loisel, L. Jacquamet, L. Serre, C. Bauvois, J. L. Ferrer, T. Vernet, A. M. Di Guilmi, C. Durmort, *J. Mol. Biol.* **2008**, *381(3)*, 594-606.
[40] C. Linke, T. T. Caradoc-Davies, P. G. Young, T. Proft, E. N. Baker, *J. Bacteriol.* **2009**, *191(18)*, 5814-5823.
[41] P. Ragunathan, D. Sridaran, A. Weigel, S. Shabayek, B. Spellerberg, K. Ponnuraj, *PLoS One* **2013**, *8(6)*, e67517.
[42] K. Cao, N. Li, H. Wang, X. Cao, J. He, B. Zhang, Q.-Y. He, G. Zhang, X. Sun, *J. Biol. Chem.* **2018**, *293(16)*, 6075-6089.
[43] L. A. Yatsunyk, J. A. Easton, L. R. Kim, S. A. Sugarbaker, B. Bennett, R. M. Breece, I. I. Vorontsov, D. L. Tierney, M. W. Crowder, A. C. Rosenzweig, *J. Biol. Inorg. Chem.* **2008**, *13(2)*, 271-288.
[44] A. Ilari, F. Alaleona, P. Petrarca, A. Battistoni, E. Chiancone, *J. Mol. Biol.* **2011**, *409(4)*, 630-641.
[45] V. G. Pederick, B. A. Eijkelkamp, S. L. Begg, M. P. Ween, L. J. McAllister, J. C. Paton, C. A. McDevitt, *Sci. Rep.* **2015**, *5(1)*, 13139.
[46] Y.-H. Lee, R. K. Deka, M. V. Norgard, J. D. Radolf, C. A. Hasemann, *Nat. Struct. Biol.* **1999**, *6(7)*, 628-633.
[47] B. Zheng, Q. Zhang, J. Gao, H. Han, M. Li, J. Zhang, J. Qi, J. Yan, G. F. Gao, *PLoS One* **2011**, *6(5)*, e19510.
[48] M. Falconi, F. Oteri, F. Di Palma, S. Pandey, A. Battistoni, A. Desideri, *J. Comput. Aided Mol. Des.* **2011**, *25(2)*, 181-194.
[49] A. Ilari, F. Alaleona, G. Tria, P. Petrarca, A. Battistoni, C. Zamparelli, D. Verzili, M. Falconi, E. Chiancone, *Biochim. Biophys. Acta* **2014**, *1840(1)*, 535-544.
[50] C. D. Plumptre, B. A. Eijkelkamp, J. R. Morey, F. Behr, R. M. Couñago, A. D. Ogunniyi, B. Kobe, M. L. O'Mara, J. C. Paton, C. A. McDevitt, *Mol. Microbiol.* **2014**, *91(4)*, 834-851.
[51] B. Bersch, C. Bougault, L. Roux, A. Favier, T. Vernet, C. Durmort, *PLoS One* **2013**, *8(11)*, e81168-e81168.
[52] D. P. Neupane, D. Avalos, S. Fullam, H. Roychowdhury, E. T. Yukl, *J. Biol. Chem.* **2017**, *292(42)*, 17496-17505.
[53] J. S. McFarlane, C. L. Davis, A. L. Lamb, *J. Biol. Chem.* **2018**, *293(21)*, 8009-8019.
[54] F. Citiulo, I. D. Jacobsen, P. Miramón, L. Schild, S. Brunke, P. Zipfel, M. Brock, B. Hube, D. Wilson, *PLoS Path.* **2012**, *8(6)*, e1002777.
[55] R. Kumar, C. Breindel, D. Saraswat, P. J. Cullen, M. Edgerton, *Sci. Rep.* **2017**, *7(1)*, 2908.
[56] P. K. Walencik, J. Wątły, M. Rowinska-Zyrek, *Curr. Med. Chem.* **2016**, *23(32)*, 3717-3729.
[57] J. Wątły, S. Potocki, M. Rowińska-Żyrek, *Chemistry – A European Journal* **2016**, *22(45)*, 15992-16010.
[58] K. A. Brogden, *Nat. Rev. Microbiol.* **2005**, *3*, 238-250.
[59] C. M. Agbale, J. K. Sarfo, I. K. Galyuon, S. A. Juliano, G. G. O. Silva, D. F. Buccini, M. H. Cardoso, M. D. T. Torres, A. M. Angeles-Boza, C. de la Fuente-Nunez, O. L. Franco, *Biochemistry* **2019**, *58(36)*, 3802-3812.
[60] J. L. Alexander, Z. Thompson, J. A. Cowan, *ACS Chem. Biol.* **2018**, *13(4)*, 844-853.
[61] W. M. Tay, A. I. Hanafy, A. Angerhofer, L.-J. Ming, *Bioorg. Med. Chem. Lett.* **2009**, *19(23)*, 6709-6712.
[62] D. Brewer, G. Lajoie, *Rapid Commun. Mass Spectrom.* **2000**, *14(19)*, 1736-1745.
[63] M. Malkoski, S. G. Dashper, N. M. O'Brien-Simpson, G. H. Talbo, M. Macris, K. J. Cross, E. C. Reynolds, *Antimicrob. Agents Chemother.* **2001**, *45(8)*, 2309-2315.

[64] M. Paulmann, T. Arnold, D. Linke, S. Özdirekcan, A. Kopp, T. Gutsmann, H. Kalbacher, I. Wanke, V. J. Schuenemann, M. Habeck, J. Bürck, A. S. Ulrich, B. Schittek, *The Journal of biological chemistry* **2012**, *287(11)*, 8434-8443.
[65] R. Gläser, J. Harder, H. Lange, J. Bartels, E. Christophers, J.-M. Schröder, *Nat. Immunol.* **2005**, *6(1)*, 57-64.
[66] F. D. Silva, C. A. Rezende, D. C. P. Rossi, E. Esteves, F. H. Dyszy, S. Schreier, F. Gueiros-Filho, C. B. Campos, J. R. Pires, S. Daffre, *J. Biol. Chem.* **2009**, *284(50)*, 34735-34746.
[67] J. Grogan, C. J. McKnight, R. F. Troxler, F. G. Oppenheim, *FEBS Lett.* **2001**, *491(1-2)*, 76-80.
[68] F. Mawanda, R. Wallace, *Epidemiol. Rev.* **2013**, *35(1)*, 161-180.
[69] M. Doulberis, G. Kotronis, R. Thomann, S. A. Polyzos, M. Boziki, D. Gialamprinou, G. Deretzi, P. Katsinelos, J. Kountouras, *Helicobacter* **2018**, *23(1)*, e12454.
[70] R. Ge, X. Sun, D. Wang, Q. Zhou, H. Sun, *Biochim. Biophys. Acta* **2011**, *1813(8)*, 1422-1427.
[71] Z. Saylor, R. Maier, *Microbiology* **2018**, *164(8)*, 1059-1068.
[72] D. Witkowska, R. Politano, M. Rowinska-Zyrek, R. Guerrini, M. Remelli, H. Kozlowski, *Chem. – Eur. J.* **2012**, *18(35)*, 11088-11099.

2. Chapter Two: Instrumental techniques

2.1 Complex-formation equilibria in solution

A metal complex can be defined as a species resulting from the interaction of one or more metal ions (M) with another species (ligand, L) able to independently exist in solution. Their interaction is based on Lewis theory of electron pairs donors and acceptors. According to the type and number of metal ions (acceptors) and ligands (donors), a complex can be: positively or negatively charged, neutral, mononuclear (one metal ion), polynuclear (multiple metal ions), bis-, tris-, etc. complex (multiple ligand molecules), etc. The required parameters for the characterization of simultaneous complex-formation equilibria in solution are contained in the so-called "speciation model", which provides the stoichiometry of the different formed species and their formation constants at a given temperature (T) and ionic strength (I). The speciation model allows to calculate the composition of a system in different conditions of pH, absolute concentrations of the components and metal to ligand ratios. For a generic system constituted by the metal ion M, the ligand L and a proton H, the stoichiometry and the stability constant are described by the following equations:

$$\mathrm{pM + qL + rH \rightleftharpoons M_pL_qH_r} \tag{2.1}$$

$$\beta_{pqr} = \frac{[\mathrm{M}_p\mathrm{L}_q\mathrm{H}_r]}{[\mathrm{M}]^p[\mathrm{L}]^q[\mathrm{H}]^r} \tag{2.2}$$

where the terms in square brackets in equation (2.2) represent the molar concentrations of the different species present at equilibrium (2.1). The charges and the solvent molecules are omitted for the sake of simplicity. β_{pqr} is the global (or cumulative) formation constant and provides quantitative information about the interaction between the metal ion M and ligand L. The stoichiometric coefficient r for the proton may also be negative if the number of protons dissociated from the ligand is greater than the maximum number of dissociated protons in the absence of metal ion. A detailed description of the different equilibria in solution can be obtained by stepwise constants, K_n (or X_n, when they refer to the ligand protonation). The overall formation constant is equal to the product of the individual stepwise constants (equations 2.4 and 2.5).

When working in aqueous solutions, besides the complex-formation equilibria, the metal ion and the ligand participate in other equilibria which are influenced by the pH value, *i.e.* they are involved in acid/based reactions: the metal ion can form complexes with the hydroxide ion ($[M^{m+}(OH^-)_n]^{m-n}$) and/or become insoluble and precipitate in solution, while the ligand can undergo protonation equilibria. The first step to determine the speciation model of a system is to experimentally determine such equilibria and measure the corresponding equilibrium constants. The metal hydrolysis constants are often available from literature and calculated at specific value of T and I. Ligand protonation (stepwise or cumulative) constants must instead be determined and refer to the following equilibria:

$$\mathrm{L + H \rightleftharpoons HL} \qquad X_1 = \frac{[\mathrm{HL}]}{[\mathrm{H}][\mathrm{L}]}$$

$$\mathrm{HL + H \rightleftharpoons H_2L} \qquad X_2 = \frac{[\mathrm{H_2L}]}{[\mathrm{H}][\mathrm{HL}]}$$

$$H_{n-1}L + H \rightleftharpoons H_nL \qquad X_n = \frac{[H_nL]}{[H][H_{n-1}L]} \tag{2.3}$$

$$L + H \rightleftharpoons HL \qquad \beta_{011} = \frac{[HL]}{[H][L]} = X_1$$

$$L + 2H \rightleftharpoons H_2L \qquad \beta_{012} = \frac{[H_2L]}{[H]^2[L]} = X_1X_2$$

$$L + nH \rightleftharpoons H_nL \qquad \beta_{01n} = \frac{[H_nL]}{[H]^n[L]} = X_1X_2 \dots X_n \tag{2.4}$$

Once the protonation equilibria are described, it is possible to move forward to the determination of complex-formation constants.

$$M + L \rightleftharpoons ML \qquad \beta_{110} = \frac{[ML]}{[L][M]} = K_1$$

$$M + 2L \rightleftharpoons ML_2 \qquad \beta_{120} = \frac{[ML_2]}{[L]^2[M]} = K_1K_2$$

$$M + nL \rightleftharpoons ML_n \qquad \beta_{1n0} = \frac{[ML_n]}{[L]^n[M]} = K_1K_2 \dots K_n \tag{2.5}$$

The stepwise constants are usually sought in order to understand the relationships between structure and reactivity; while to calculate the concentration of the final product (the complex ML_n) the overall formation constant, β_n, is frequently used.

Any system with *n* components (metal/s, ligand/s and proton) can be described by the following equations:

a) *n* mass balances of the *n* components;
b) charge balance;
c) *N* formation constants β_i for the present species.

For a binary system, there are three mass balances:

$$C_M = [M] + [ML] + [ML_2] \dots + [ML_n] = [M] + \sum \beta_n [M][L]^n \tag{2.6}$$

$$C_L = [L] + [HL] \dots + [ML] \dots + N[ML_n] = [L] + \sum X_r [L][H]^r + \sum N\beta_n [M][L]^n \tag{2.7}$$

$$C_H = [H] - [OH] + [HL] \dots + r[H_rL] = [H] - K_w[H]^{-1} + \sum rX_r [L][H]^r \tag{2.8}$$

where C_M, C_L and C_H are the stoichiometric concentration of the metal, the ligand and the proton respectively, and [M], [L], [H] are the corresponding free concentration. C_M, C_L and C_H are usually known, as they are suitably set by the experimenter, while [M], [L] and [H] can be directly or indirectly experimentally obtained (for example with potentiometric measurements). To properly solve the problem, it is necessary to build up mass balances models, that represent the system and consider all the possible species in which the main components are partitioned (see equations 2.6, 2.7 and 2.8). The binary system consisting of these three equations contains 3+N unknowns, that are the free concentrations of the components and the overall formation constants. Therefore, it is not univocally solvable. If [M], [L] or [H] and the protonation stepwise constants X_i are known, this set of

simultaneous equations can be solved respect to the N overall formation constants β_i. The ligand protonation constants X_i must be determined accordingly, as previously mentioned. For this purpose, a strong base is added to an acidic solution of the ligand in its protonated form H_rL and pH is measured for each addition (potentiometric titration).

Experimental methods for the study of these systems are, thus, based on the determination of the free concentration of at least one component and re-test to different conditions in which the formation constants remain unchanged (temperature and ionic strength are kept constant). In the case of labile complexes, *i.e.* for those complexes in which the ligands are not irreversibly bound to the metal but may be replaced by other ligands with fast kinetics and there is competition between the metal ion and the proton for the donor sites of the ligand, an experiment can be performed through an acid-base potentiometric titration. For each titration point the concentration of free proton can be estimated. For each of the N_p points of the titration, a system of three mass balances can be written. The result is a total system of $3N_p$ equations and $(3–1)N_p + N$ unknowns, because for every point we have 3–1 unknown free concentrations and the same N formation constants for all the points. The system can be solved if the number of unknowns equals the number of equations, namely the number of experimental points ($N = N_p$). Normally, the exact solution of these systems can be achieved only in very simple cases. For systems with an equation order higher than one, it is possible to get a good approximate result with statistical methods of nonlinear least squares fitting. In this case, the number of needed points is at least double that of the parameters to be determined and, furthermore, a greater number of points will increase the accuracy of the results. Nowadays there are several available software programs which are able to process hundreds of experimental points related to systems with several metals and ligands, where there are many simultaneous equilibria. The program usually gives a statistical analysis of the goodness of fit, that provides an assessment of the model reliability and results. Although potentiometry is the most widely used technique for this purpose, thanks to its simplicity and accuracy, this method of calculation may be coupled to any analytical technique capable of measuring the free concentration of at least one component of the system in variable experimental conditions.

2.1.1 Potentiometry

In potentiometry, the determination of the free concentration of a component present in solution is performed using a glass electrode. A glass electrode is a type of ion-selective electrode made of a doped glass membrane, that is sensitive to changes in the content of a certain type of ions in a solution. Glass electrodes are commonly used for pH measurements. The potentiometric method is used for the determination of both the protonation constants and the complexes formation constants. It is important that the ligand is involved in both acid/base type equilibria and complex-formation equilibria (*i.e.* there must be competition between metal ion and proton for the ligand binding sites). A glass electrode measures the potential E of the system, which correlates with the activity of the hydrogen ions through the Nernst equation:

$$E = E^0 + \frac{RT}{nF}\, ln\, a_{H+} + E_j \tag{2.9}$$

where E^0 is the standard potential, E_j represents any liquid junction potential of the system, R is the universal gas constant (8.314 J K^{-1} mol^{-1}), T is the absolute temperature (in Kelvin, K), F is the Faraday constant (96840 C mol^{-1}), n is the number of transferred electrons and for the glass electrode is 1 and a_{H+} is the activity of the H^+ ion. E_j can be minimized to negligible and reproducible values by providing a salt bridge (conventional saturated KCl solution) and a constant ionic medium. Corrections for the effect of the liquid junction can be included in the calibration procedure in the region of low pH;[1] E_j is

then revealed as a deviation from linearity of the observed potential as a function of pH, since the liquid junction potential in a solution of constant ionic strength can be defined as:

$$E_j = j_a[\mathrm{H}^+] + j_b K_w[\mathrm{H}^+]^{-1} \tag{2.10}$$

where j_a and j_b are the so-called parameters of the ionic medium: the acid liquid junction coefficient and the basic liquid junction coefficient, respectively, and K_w is the water self-ionization constant. Converting now the Neperian logarithm into the decimal one, at room temperature T = 25 °C, and approximating the effect of E_j to a negligible value, equation 2.9 can be rewritten as:

$$E = E^0 + 0.05916\ log\ a_{H+} \tag{2.11}$$

The rigorous thermodynamic equilibrium constant is expressed in terms of activities, which are quite impractical. For the sake of convenience and reproducibility, concentrations are preferred. The proton activity can then be expressed as:

$$a_{H+} = [\mathrm{H}^+]\,\gamma_{H+} \tag{2.12}$$

and thus, considering both equations 2.9 and 2.12:

$$E = E^0 + \frac{RT}{nF} ln[\mathrm{H}^+] + \frac{RT}{nF} ln\,\gamma_{H+} \tag{2.13}$$

where $[H^+]$ is the proton molar concentration and γ_{H+} is the activity coefficient, which is related to the interactions occurring between the solute molecules. γ describes the deviation from the solution ideal behaviour and its value tends to unity in very dilute conditions (*i.e.* when particles encounters approach zero). Experimentally, the Debye-Hückel limiting law is valid only for very dilute solutions ($C \leq 10^{-3}$ M). According to the Debye-Hückel limiting law, the $\log\gamma_i$ should also decrease with the square root of increasing ionic strength, *I*:

$$log\,\gamma_i = -\frac{Az_i^2\sqrt{I}}{1 + Ba_i\sqrt{I}} \tag{2.14}$$

A and B are constants depending on the ion charge, the temperature, the density and the dielectric constant of the solvent, for aqueous solutions at T = 25 °C A = 0.509 and B = 0.3284, z_i is the ion charge number, and a_i is the effective diameter of the hydrated ion. The most significant aspect of equation 2.14 is the prediction that the activity coefficient is a function of ionic strength rather than the electrolyte concentration. Hence, for high and constant concentrations of ionic strength, the activity coefficients remain constant with respect to the variation of the other species in solution, when their concentration is 10% lower than the ionic medium concentration. Therefore, in order to avoid complications due to variation of activity coefficients, it is customary to perform stability constant determinations in solutions of relatively high and constant ionic strength (~ 0.1 M).

In condition of constant temperature and ionic strength, the activity coefficient is constant and it could be incorporated into the standard potential E^0:

$$E = E^{0\prime} + \frac{RT}{nF}\ ln[\mathrm{H}^+] \tag{2.15}$$

with

$$E^{0\prime} = E^0 + \frac{RT}{nF} ln\,\gamma_{H+} \tag{2.16}$$

The Nernst equation applies to an ideal situation, and a real system can actually undergo some slight deviations from the theoretical Nernstian behaviour due to experimental

fluctuations. Thus, it is convenient to introduce the slope factor β_{sl}, an experimental parameter that takes into account the deviation from the theoretical slope of Nernst equation (~ 59.16 mV, see equation 2.11). The resulting equation is:

$$E = E^{0\prime} + \beta_{sl}\frac{RT}{nF}ln[H^+] \tag{2.17}$$

The values of β_{sl} and $E^{0\prime}$ are obtained through a specific daily calibration consisting in a strong acid titration using a strong base as titrant. In this way, the measured values of potential E can be directly related to the concentration of the proton [H^+] and the obtained equilibrium constants can be expressed in terms of concentration.

2.1.2 Data analysis and processing

The analysis of potentiometric data are performed using the following computer programs: Tiamo 2.4, Microsoft EXCEL, GLEE,[2] HYPERQUAD[3] and HYSS.[4]

Tiamo 2.4 is the software package interfaced with the potentiometric instrument Metrohm 905 Titrando, it allows to acquire titration curves and to modify the experimental measuring parameters. GLEE is exploited mainly to process the calibration curves of the electrode. Indeed, if the hydrogen ion concentration, indicated by [H^+] in equation 2.17, is known for a series of measurements of electrode potential it is possible to determine both the standard potential and the slope factor. Calculations proceed using Gran's method (**Figure 2.1**).[5] The perfect linearity is a good estimate of the proper electrode function and the absence of convergence between the acidic and basic lines (ideally the end point of the titration) allows to calculate the amount of impurity of the solutions, often corresponding to the carbonate contamination of the alkaline titrant. The acceptable error on the alkaline concentration is about 2–3%.

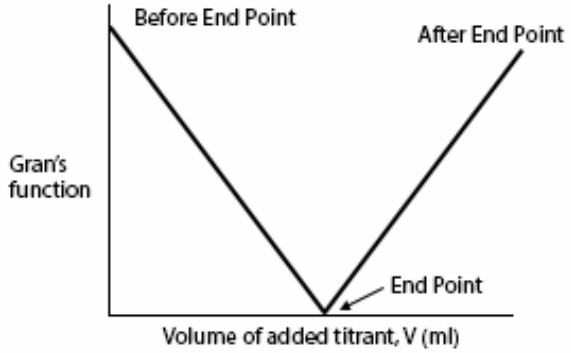

Figure 2.1 - Gran's linearization

Microsoft EXCEL software is used to derive the exact concentration of the ligand in the prepared solutions, once again taking advantage of the Gran's method: applying the Gran plot theory, it is possible to precisely detect the end-points of the potentiometric titration curve. The first end-point corresponds to the volume at which the number of equivalents of strong base (NaOH or KOH) corresponds to that of added strong acid (HCl or $HClO_4$):

$$n°_{eq}acid = n°_{eq}base \tag{2.18}$$

The second end-point indicates the volume at which the sum of equivalents of acid and ligand is equal to the equivalents of the base (equation 2.19).

$$n°_{eq}ligand + n°_{eq}acid = n°_{eq}base \quad (2.19)$$

Therefore, the difference between the above two points is the volume of strong base necessary to titrate the ligand. Then, multiplying this volume for the base concentration and dividing it by the number of protonable sites, it is possible to obtain the concentration of the ligand in the solution.

The above calculated parameters and the titration curve points can be also processed with the HYPERQUAD program, to compute the protonation constants for the ligand and the stability constants for the complexes. HYPERQUAD input files contain a list of parameters that describe the sample analysis: millimoles of ligand, acid and metal, titrant base concentration, electrode standard potential $E^{0\prime}$ and slope factor β_{sl}, initial volume of the analysed sample and temperature. The data refinement is a least-squares based procedure, in which the sum of squared residuals is minimized. The results of a least-squares calculation include the standard deviations and correlation coefficients of the refined parameters, giving information on the goodness of fit. In the input speciation model for HYPERQUAD calculations, hydrolysis constants for metal ions are also included.

2.2 UV-Vis spectrophotometry

Ultraviolet-visible spectrophotometry is a technique widely used to analyse complex formation in solution. The interpretation of the absorption spectra, and hence the analysis of the position and intensity of the experimental bands, provides information about number and nature of the donor sites involved in the metal coordination. UV-Vis spectrophotometry allows to determine the concentration of a species in solution, since it is linearly related to the absorbance of the solution (equation 2.20). The quantitative analysis in spectrophotometric methods is based on the Beer-Lambert law. According to Beer, for a dilute solution the absorption intensity is proportional to the number of the attenuating species, and therefore, to their concentration; while Lambert's law states that the fraction of absorbed radiation is independent of the radiation intensity. Combining these two laws, we can derive the Beer-Lambert law:

$$A = log\frac{I_0}{I} = \varepsilon\, l\, C \quad (2.20)$$

where A is the observable absorbance of the solution, I_0 is the intensity of the incident monochromatic radiation, I is the intensity of the transmitted radiation, ε represent the molar extinction coefficient, an intrinsic property of the absorbing species and thus independent of the other parameters, l is the path length of the absorbing solution expressed in cm and C the concentration of the absorbing species expressed in molarity. The value of $log(I_0/I)$ is commonly known as the absorbance A of the solution and it can be directly read from the experimentally recorded spectrum; A is often expressed as "absorbance units". The absorbance is an additive property of the system, therefore when more than one absorbing species coexist in solution, the measured total absorbance is a sum of each single component contribution.

$$A = l\,(\varepsilon_1\, C_1 + \varepsilon_2\, C_2 \ldots + \varepsilon_n\, C_n) \quad (2.21)$$

In the field of inorganic chemistry, UV-Vis spectral range is usually associated with metal-centered d–d electronic transitions. Indeed, transition metals appear coloured because they are able to absorb visible light (wavelength range: 400–800 nm). Higher energy transitions

may also occur in the ultraviolet range (200–400 nm). When a complex absorbs enough energy in form of quantized ultraviolet or visible light, the valence electrons can be excited to higher energy orbitals depending on the energetic separation between them (ΔE). Different compound will have unique energy spacing between electronic levels, and therefore changes in the absorption spectra of a metal complex solution can provide information about the type of ligand and the metal coordination sphere under different experimental conditions (*e.g.* pH, metal-ligand ratio). The value of ΔE can be directly correlated to the frequency of the absorbed light (ν) and thus to its wavelength (λ). The higher the energy gap ΔE the smaller the value of λ:

$$\Delta E = h\nu = h\frac{c}{\lambda} \tag{2.22}$$

h is Planck's constant ($6.626 \cdot 10^{-34}$ J s) and c is the speed of light in vacuum ($3.00 \cdot 10^{8}$ m s^{-1}). However, the rigorous discussion of electronic transitions must take into account that light-induced electronic excitation also causes many rotational and vibrational transitions of the molecule, and the result is a gaussian band-shape absorption instead of a single line corresponding to the expected ΔE energy (Franck-Condon principle). The maximum of the absorption band is centred on a λ_{max} value which gives information on the ΔE and therefore on the energy distribution and electron occupancy of the complex orbitals. Besides λ_{max}, another important parameter provided by absorption spectra is the molar absorptivity ε at a given wavelength. It is an estimate of the probability that a specific transition between two states separated by $\Delta E \propto \lambda^{-1}$ occurs. Indeed, certain transitions are allowed and certain transitions are forbidden depending on the nature of the involved orbitals and electrons. Without going into the details of the theory, it is possible to distinguish between allowed and forbidden transitions simply investigating the interaction of the complex with the electromagnetic moment induced by the incident photon. The resulting spectroscopic selection rules impose *(i)* a symmetry requirement of the involved orbitals on the basis of the representation of the point group to which the molecule belongs, this also includes the Laporte rule for centrosymmetric complexes, which states that allowed electronic transitions cause a change of the parity (*Germ.* g, *gerade* and u, *ungerade*); *(ii)* a spin state requirement by which electronic transitions which cause a change of the electron spin state are forbidden ($\varepsilon_{max} < 1$ $M^{-1}cm^{-1}$). Nevertheless, selection rules may undergo some exceptions. The spin selection rule may be broken by the coupling of spin and orbital angular momenta, which is greater for heavy atoms. The symmetry/Laporte selection rule can be circumvented by molecular vibrations, which can perturb the symmetry and destroy the centre of inversion, or by intrinsic asymmetry of the complex structure due to distorted arrangements of the ligand around the metal ion. The breakdown of Laporte rule allows to detect roughly intense d-d bands in the absorption spectra of transition metal complexes, which are instead expected to be forbidden ($t_{2g} \rightarrow e_g$). To briefly summarise, the types of electronic transition which are possible to detect by means of UV-Vis absorption (**Figure 2.2**) are:

- transitions between orbitals mostly localized on the metal ion (MC, *i.e.* d-d transitions; $\varepsilon_{max} \sim 100–200$ $M^{-1}cm^{-1}$), typically observable in the visible spectral range;
- transitions between orbitals mostly localized on the ligands (LC), whose UV-Vis bands are almost independent of the presence of the metal;
- transitions between orbitals that are predominantly ligand in character and orbitals that are predominantly metal in character (metal-to-ligand charge transfer MLCT, ligand-to-metal charge transfer LMCT), which are characterized by extremely intense bands ($\varepsilon_{max} \sim 1000–50000$ $M^{-1}cm^{-1}$) in the ultraviolet spectral range, although may have a tail into the visible.

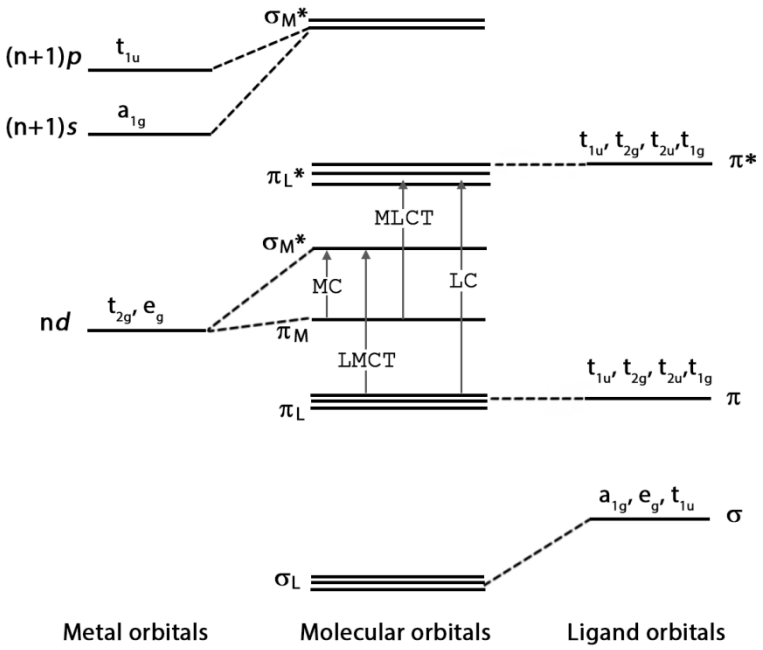

Figure 2.2 - Molecular orbital diagram for a generic ML_6 complex with O_h symmetry representing various types of electronic transitions.

2.2.1 Crystal Field (CF) and Ligand Field (LF) Theories

The above considerations arise from a specific theoretical background that allows to rationalise the absorption spectra of a metal complex by means of both the crystal-field theory (CFT) and the ligand-field theory (LFT). A transition-metal ion in a compound or complex is supposed to be subjected to an electrostatic field produced by molecules and ions in its environment. Reasonably, only the nearest neighbours of the metal ion need to be considered. According to the crystal-field theory, the ligands are either negative ions or molecules with unshared electron pairs directed towards the metal. When forming a complex, the electrons from the ligands will be closer to some of the metal d-orbitals and farther away from others, causing a loss of degeneracy in the orbital energetic levels. The electrons in the d-orbitals and those in the ligands repel each other due to repulsion between charges of the same sign. Thus, the d-electrons closer to the ligands will have a higher energy than those further away, which results in the d-orbitals splitting in energy. The magnitude of the energy separation between the d-orbitals, and hence the colour of the complex (that is due to the d–d transition), depends on: *(i)* the nuclear charge and the identity of the central metal ion, *(ii)* the ligand charge density, *(iii)* the geometry of the complex ion (the electric field created by the lone-pair of the ligand depends on the geometry of the complex ion), *(iv)* the number of d-electrons, and *(v)* the oxidation number of the central ion. CFT focuses on the d-orbitals energy separation, being crucial to understand and rationalize experimental spectra, thermodynamics stability and magnetic properties of the metal complexes. In an octahedral model six ligands (*i.e.* six point charges) are located around the metal ion and cause a lowering of the d_{xy}, d_{xz} and d_{yz} orbital energy and the increase of the d_{z2} and d_{x2-y2} one, as shown in **Figure 2.3**. The difference in energy between the two sets of d-orbitals is called the ligand-field splitting parameter Δ_o where the subscript "o" stands for octahedral.

Tetrahedral complexes are the second most common type of complexes for the first-row transition metals (*i.e.* Zn(II)) after the octahedral ones; they are characterized by four ligands that form a tetrahedron around the metal ion. In a tetrahedral distribution of charges, metal d-orbitals split again into two groups, with an energetic gap of Δ_t. The lower energy orbitals are d_{z2} and d_{x2-y2}, while the higher energy orbitals are d_{xy}, d_{xz} and d_{yz}, opposite to the octahedral situation. Furthermore, since the ligand electrons in the tetrahedral symmetry are not oriented directly towards the d-orbitals, the energy splitting is lower than in octahedral field ($\Delta_t = 0.4\overline{4}\,\Delta_o$). Crystal-field theory is also successful in describing square planar and other geometries, including the tetragonal distortion due to Jahn-Teller effect (see **Figure 2.3**), and allows to introduce the concept of high-spin and low-spin configurations for d^4, d^5, d^6 and d^7 metal ions. Depending on the ligand-field splitting parameter, Δ, and on the pairing energy (electron–electron Coulombic repulsion), the d-electrons may occupy all the available (not degenerate) five d-orbitals with parallel spin (high-spin) or proceed first filling the lower degenerate d-orbitals, allocating two paired electrons per orbital (low-spin), fully in accordance with Pauli exclusion principle.

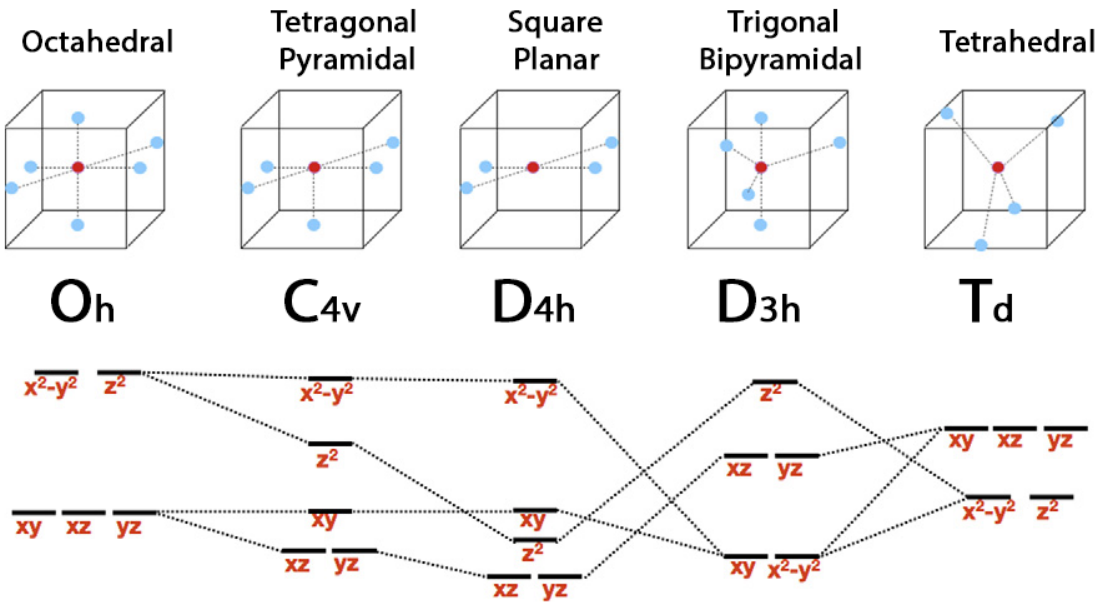

Figure 2.3 - Distribution of the five d-orbitals in different ligand fields. The elongation on one axis causes the decrease in energy of the orbitals lying along the axis direction.

The splitting of d-orbitals in the crystal field model not only depends on the geometry of the complex, but also on the nature of the metal ion, its charge and the surrounding ligands. For instance, the higher the oxidation state of the metal or the stronger the ligand, the larger the splitting. A list of ligands ranked in order of their ability to cause large orbital separations is known as spectrochemical series. In case of octahedral field:

— increasing Δ_o →

$$I^- < Br^- < Cl^- < \underline{S}CN^- < F^- < OH^- < \underline{O}NO^- < H_2O < SC\underline{N}^- < NH_3 < \underline{N}O_2^- < CN^- < CO$$

weak-field ligands *strong-field ligands*

When the geometry and the ligands are held constant, the metals spectrochemical series is approximately the following one:

— increasing Δ_o →

$Mn^{2+} < Ni^{2+} < Co^{2+} < Fe^{2+} < V^{2+} < Fe^{3+} < Ru^{3+} < Pd^{4+} < Pt^{4+}$

In an octahedral field, the value of Δ_o increases as the oxidation state increases and moving down the group. This trend agrees with the decrease of the atomic radius in higher oxidation state ions, that means smaller distances between metal and ligands and larger interaction energies.

An advanced theory to explain the spectroscopic properties of metal complexes is based on the ligand-field model, which takes into account the overlap between the orbitals of the metal ion and of the ligands. LFT arises from the application of the molecular orbital theory and allows to build-up a molecular orbital energy level diagram from metal atom orbitals and symmetry-adapted linear combinations (SALC) of ligand orbitals. In an octahedral complex, the result is an electronic rearrangement which is qualitatively the same as in crystal-field theory with five molecular orbitals which are mainly metal-orbital in character (three triply degenerate nonbonding orbitals with t_{2g} symmetry and two doubly degenerate antibonding e_g orbitals). Moreover, when ligands have orbitals with local π symmetry with respect to the M–L axis, it is possible to form SALCs of t_{2g} symmetry and to combine them with the three metal t_{2g} orbitals. With respect to the atomic nonbonding orbitals, the resulting t_{2g} molecular orbitals of the complex can have higher or lower energy (depending on the relative energies of the ligand and metal orbitals) and Δ_o is decreased or increased, respectively (**Figure 2.5**). The ligands can be then classified as π-donor or π-acceptor depending on the presence (π-donor) or absence (π-acceptor) of electrons in their available π orbitals; this also affects the energy of such orbitals and therefore the Δ_o gap. The spectrochemical series introduced by CFT can be then explained on the basis of the π bonding effect, when feasible, and most of the above considerations on the frontier orbitals are also reflected in LFT model, but with the advantage of a detailed description (and prediction) of the complex molecular orbital energy diagram which rigorously clarify most of the observable absorption phenomena.

— increasing Δ_o →

LFT	π donor < weak π donor < no π effects < π acceptor
CFT	*weak-field ligands* *strong-field ligands*

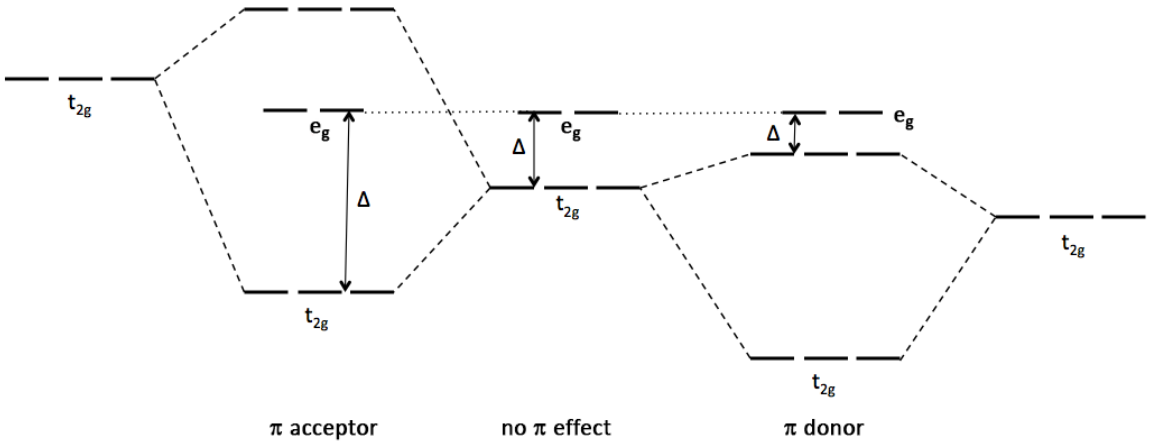

Figure 2.4 - Effect of π-donor and π-acceptor ligands on the energy gap between HOMO and LUMO orbitals of a generic metal complex with O_h symmetry.

2.2.2 Data analysis and processing

The UV-Vis spectra were acquired in the spectral range 200–900 nm at a temperature of 25°C, in a quartz cuvette with an optical path of 1 cm. Spectrophotometric titrations allowed to follow the changes in absorbance throughout the pH range 2–12. The pH was varied approximately half unit for each measurement by manual addition of a little amount of HCl and NaOH 0.1 M. Obtained UV-Vis spectra at different pH values were analysed using the Origin software. For each spectrum, the absorbance was converted in ε ($M^{-1}cm^{-1}$) dividing it by the overall metal concentration and the optical pathway ($\varepsilon = A/Cl$). Molar extinction coefficient values are reported on y-axis, while wavelengths are maintained on x-axis. The position and the intensity of the main bands were derived and the corresponding values of wavelength of maximum absorption (λ_{max}, nm), absorbance (A_{max}, au) or absorptivity with respect to the total metal ion concentration (ε_{max}, $M^{-1}cm^{-1}$) were obtained. In literature it is possible to find the value of λ_{max} expected for a d-d transition of Cu(II) and Ni(II) complexes. In **Tables 2.1** and **2.2** are listed some values that will be useful for the interpretation of the spectrophotometric results in the visible spectral range. In particular, the method here employed to analyse the spectroscopic data is based on the "rule of average environment" (Billo's method).[6-8]

Table 2.1 - Expected λ_{max} for Cu(II) complexes with different coordination modes.

Donor atoms	**λ_{max} (nm)**
N_{Im}, COO^-	731
2 N_{Im}	687
3 N_{Im}	627
2 N_{Im}, N^-	604
4 N_{Im}	576
3 N_{Im}, N^-	557
2 N_{Im}, 2 N^-	539
N_{Im}, 3 N^-	522
4 N^-	506

Table 2.2 - Expected λ_{max} for Ni(II) complexes with different coordination geometries.

Coordination geometry	**λ_{max} (nm)**
Square planar	420 – 600
Octahedral	≈ 650; ≈ 380

For Cu(II) complexes the wavelength related to the maximum absorption λ_{max} can also be estimated using the following empirical equation:

$$\lambda_{max} = \frac{10^3}{[0.294\, n_{CO/H_2O} + 0.346\, n_{COO^-} + 0.434\, n_{N_{Im}} + 0.460\, n_{NH_2} + 0.494\, n_{N^-}]} \quad (2.23)$$

where n_{COO^-} refers to the number of carboxyl groups, $n_{N_{Im}}$is the number of imidazole moieties, n_{NH_2} represents the number of amines and n_{N^-} the number of amides coordinated to the metal ion.[8] As already mentioned above, unfortunately, Zn(II) complexes are not spectrophotometrically active.

2.3 Circular Dichroism (CD)

Asymmetric chromophores or symmetric chromophores in an asymmetric environment can interact differently with right- and left-circularly polarized light. When a circularly polarized light beam passes through an optically active medium, it experiences different velocities depending on the different refraction indices for right- and left-circularly polarized light ($n_r \neq n_l$); this phenomenon is called optical rotation and it results in the rotation of the polarization axis. The variation of optical rotation as a function of wavelength is known as optical rotatory dispersion (ORD). Similarly, right- and left-circularly polarized light at certain wavelengths can be differently absorbed due to differences in the extinction coefficients ($\varepsilon_r \neq \varepsilon_l$) for the two polarized rays, giving rise to the phenomenon called circular dichroism (CD). Therefore, two types of circularly polarized light interact in different ways with optically active chiral molecules. In a CD experiment, right- and left-handed circularly polarized light at different wavelength pass through the sample and the difference in the two light components absorption is measured. The interaction with the sample usually causes an elliptically polarised vector of the transmitted radiation, due to the different interaction with the left- and right- circularly polarised components. If one component is completely absorbed, the resultant wave will be circularly polarized. A circular dichroism signal can be positive or negative, depending on whether L-CPL (left-circularly polarized light) is absorbed to a greater extent than R-CPL (right-circularly polarized light) or to a lesser extent, giving rise to a positive or negative CD signal, respectively. A schematic representation of the instrumental apparatus for a generic CD experiment is shown in **Figure 2.5**.

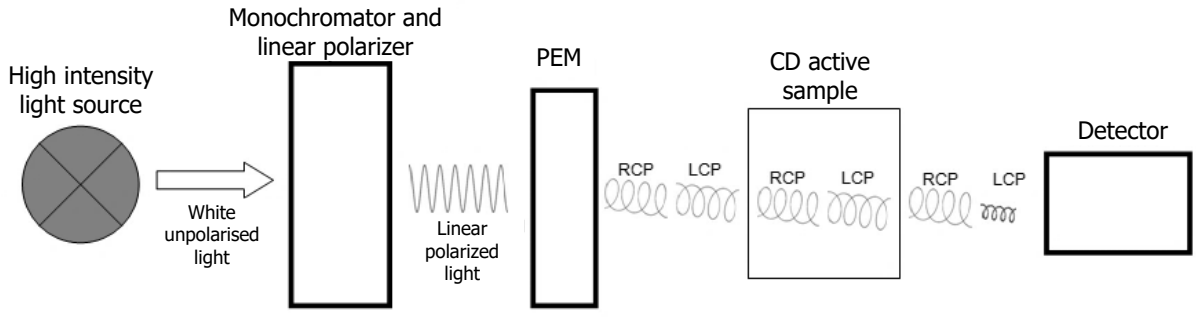

Figure 2.5 - Schematic representation of a CD instrument. The incident radiation passes through a modulating device, usually a photoelastic modulator (PEM), which transforms the linear light to circular polarized light. The PEM is able to let pass either the left (L-CPL) and the right (R-CPL) light component depending on the applied alternating electric field. The direction of polarization and the absorption changes are measured by a detector, and circular dichroism is calculated.

2.3.1 Data analysis and processing

The CD spectra were acquired in the spectral range 200–900 nm. Analogously to UV-Vis measurements, spectrophotometric titrations have been performed to follow the changes in the CD signals throughout the pH range 2–12. The pH was varied approximately half unit for each measurement, by manual addition of a little amount of HCl and NaOH 0.1 M. Obtained CD spectra at different pH values were analysed using the software Origin. In general, any electronic transition that gives rise to a UV-Vis absorption also gives rise to a CD band, with the maximum (or minimum) located at approximately the same wavelength of the maximum absorption on UV-Vis spectra (**Figure 2.6**).

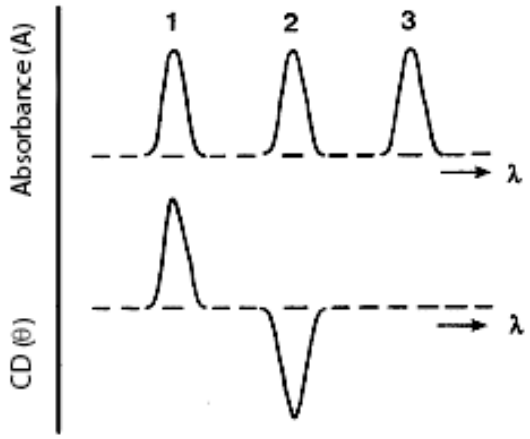

Figure 2.6 - The relationship between UV-Vis absorption and CD spectra. Band 1 has a positive CD spectrum with L-CPL absorbed more than R-CPL; band 2 has a negative CD spectrum with R-CPL absorbed more than L-CPL; band 3 is due to an achiral chromophore.

Historically, circular dichroism is represented in terms of ellipticity (θ), which is defined as the tangent of the ratio of minor to major elliptical axis. Modern CD instruments are capable of millidegree precision. Molar ellipticity can also be defined as $\theta = 3298\,\Delta\varepsilon$. The unit ellipticity persists even though CD is now measured as the difference in absorbance between right- and left-circularly polarized light as a function of wavelength ($\Delta A = A_l - A_r$). The Beer-Lambert law ($\Delta\varepsilon = \Delta A/lC$) states that the difference in extinction coefficients ($\Delta\varepsilon = \varepsilon_l - \varepsilon_r$, where ε_l and ε_r are the molar extinction coefficients expressed as $M^{-1}cm^{-1}$ for left- and right-circularly polarized light, respectively), at a given wavelength, is equal to the difference in absorbance divided by the product of the path-length and the concentration. Therefore, circular dichroism spectra usually present $\Delta\varepsilon$ along y-axis and λ along x-axis. Besides d-d transitions in the visible region, circular dichroism allows to detect intense bands in the ultraviolet region mostly due to charge transfer transitions between metal and ligand. **Table 2.3** reports the maximum wavelengths of absorption for CD bands of Cu(II) and Ni(II) complexes, which can help predicting the coordination modes of the studied complexes.

Table 2.3 - Expected λ_{max} for the most characteristic CD bands of Cu(II) and Ni(II) complexes with different donor atoms.[9]

Metal ion	Donor	λ_{max} (nm)
Cu(II)	N_{Im}	220 245 – 260 280 – 345
	N^-	295 – 315
	OH	285
	O_{tyr}^-	300 – 310
	NH_2	233 – 245
	COO^-	255 – 265
Ni(II)	S	220 – 27 320 – 350
	N^-	250 – 270
	N_{Im}	260 – 270

It is also worth to mention that the chirality of the molecule can arise from both its conformation and its structure. This means, for instance, that the CD spectra of a protein molecule with a specific secondary structure can undergo some variations if its conformation changes (for example from random coil to β-sheet). Such analyses are commonly performed in the far-ultraviolet spectroscopic range (180–350 nm) and require a low concentrated solution of the interested biomolecule (or peptide with an adequate large sequence of amino acids) and a quartz cuvette with 0.1 mm path length. It is useful to measure far-UV CD spectra for both the apo-peptide and the metal-ligand complexes in order to verify possible conformational changes in the peptide folding, which may occur upon the metal coordination. CD signals for specific secondary structures are shown in **Figure 2.7**.

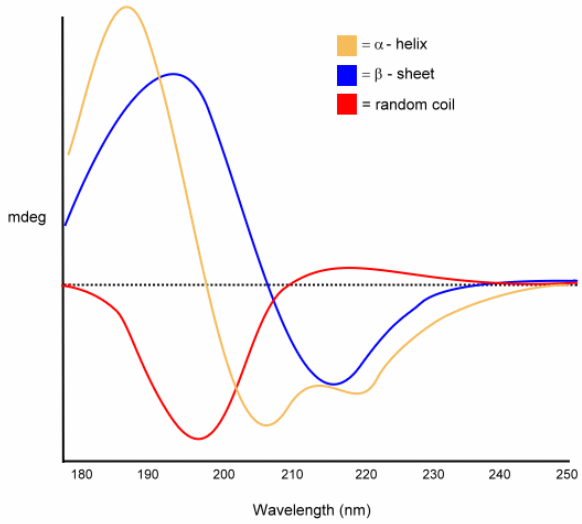

Figure 2.7 - Typical CD bands for α-helix (yellow), β-sheet (blue) and random coil (red) conformations.[10]

2.4 Electrospray Ionization Mass Spectrometry (ESI-MS)

Mass spectrometry is an analytical technique that can provide both qualitative and quantitative information (such as structure, molecular mass, concentration and isotopic ratios of atoms) on organic and inorganic analytes in complex mixtures after their conversion to positively or negatively charged ions. A mass spectrum is a graphical representation of the relative abundance of the obtained ions as a function of their mass/charge (*m/z*) ratio. The most intense peak has 100% of abundance and it is called base peak. Since a mass spectrometer separates and detects ions of slightly different masses (modern instrumentations can resolve ions differing by only a single atomic mass unit), it distinguishes different isotopes of a given element.

Mass spectrometers can be divided into three fundamental parts, namely the ionization source, the analyser and the detector system. Since ions are easier to manipulate than natural molecules, the sample must be first introduced into the ionization source where the ionization process takes place. The obtained ions are sent to the analyser region of the mass spectrometer, where they are separated according to their *m/z* values. The separated ions are thus detected to generate the signal and plot the spectrum. The analyser and detector components, and often the ionisation source too, are maintained under high vacuum to prevent any hindrance from air molecules and let the ions travel throughout the instrument. The main function of the mass analyser is to separate the formed ions according to their mass-to-charge ratios. There are a large number of currently available mass analysers, which include quadrupoles, time-of-flight analysers (TOF), magnetic sectors, Fourier transform ion cyclotron resonance (FT-ICR) and quadrupole ion traps. These mass analysers have different features, including the *m/z* range that can be covered, the mass accuracy and the achievable resolution. The analysers listed above can be used in conjunction with electrospray ionization source (ESI). ESI is suitable for polymers, proteins, peptides and small polar molecules, allowing very high sensitivity and an easy coupling to high-performance liquid chromatography HPLC, μ-HPLC or capillary electrophoresis. The transfer of ionic species from solution into the gas phase by ESI involves three steps: (1) dispersion of a fine spray of charged droplets, followed by (2) solvent evaporation and (3) ion ejection from the highly charged droplets (**Figure 2.8**).

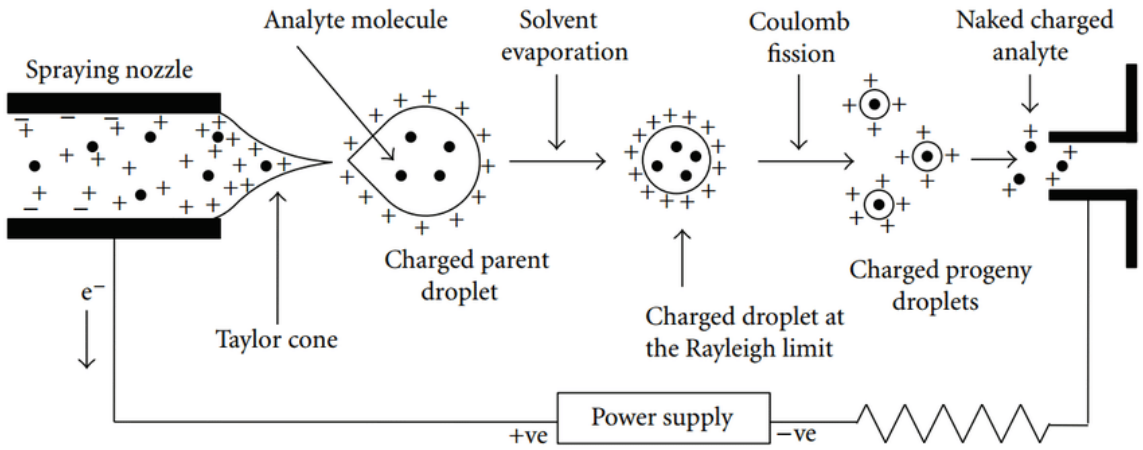

Figure 2.8 - Schematic representation of the electrospray ionization process.

Spray is produced by applying a strong electric field (3–6 kV), under atmospheric pressure, to a liquid passing through a capillary tube with a weak flux. The applied electric field induces a charge accumulation at the liquid surface, which then results in the formation of

highly charged droplets, which are carried by a nebulising gas (*e.g.* nitrogen) and pass down pressure potential gradients toward the analyser region. With the aid of temperature and/or stream of drying gas, the charged droplets are continuously reduced in size by evaporation of the solvent, with consequent increase of surface charge density until the reach of their Rayleigh limit. At this point the surface tension cannot compensate for the electrostatic repulsion and the droplets undergo a "Coulomb explosion" creating many smaller and more stable droplets. Finally, the electric field strength within the charged droplet reaches a critical point and the formation of ions in gaseous phase becomes kinetically and energetically favourable. The ions are then accelerated into the analyser for subsequent analysis.

A brief description of one of the analysers used for the ESI-MS measurements of this work is also given. The Quadrupole-time-of-flight analyser is a high mass accuracy and high-resolution instrument, ideal for peptide sequencing, where a time-of-flight analyser is coupled with a linear series of two quadrupoles. The first quadrupole can be used as a precursor mass selector, *i.e.* an ion mass filter, while the second quadrupole is employed as a collision cell using Ar, He, or N_2 gas, in order to produce further fragmentations. A mass spectrum is obtained by monitoring the ions passing through the quadrupole filter as the voltages on the four paired rods, which composed it, are varied. The two opposite rods have an applied potential of $\pm(U + V\cos(\omega t))$, where U is a direct current voltage and $V\cos(\omega t)$ is an alternating current voltage. There are two operating procedures: varying ω and holding U and V constant, or varying U and V with the ratio U/V fixed for a constant angular frequency, ω. Then the product ions are analysed in the TOF analyser. Resolution for such instrument can be higher than 18000. In a time-of-flight analyser ions "drift" down an evacuated tube of a suitable length (usually 1 m) with different velocities depending on their mass-to-charge ratios (heavier ions of the same charge reach lower speeds, while ions with higher charge have an increased velocity). For a tube of known length, velocity is inversely proportional to the time of flight, t_F, of the ions:

$$t_F = \frac{L}{v} = L\sqrt{\frac{m}{2zeV}} \tag{2.24}$$

where L is the distance between the source and the detector, v is the ion rate after acceleration, m is the mass, e is the electron charge ($e = 1.60 \cdot 10^{-19}$ C) and V is the accelerating electric field potential. Times of flight are typically on the order of microseconds (1–50 μs) for a drift tube (L) of 1 meter long. TOF instrument offers a wide number of advantages respect to other types of mass spectrometers, as it is simple to use and sturdy enough. Furthermore, TOF is the fastest MS analyser, it is well suited for pulsed ionization methods (*i.e.* MALDI ion source), it has high ion transmission and the highest practical mass range (theoretically unlimited). However, it requires fast digitizers which can have limited dynamic range and it has limited resolution and sensitivity.

2.4.1 Data analysis and processing

The interpretation of mass spectra was achieved using the program Bruker Compass Data Analysis 4.0; with this software, it was possible to compare the experimental spectrum with the isotopic pattern of a simulated spectrum, in order to obtain a validation of the ion attribution. The physical property of ions that is measured is the mass-to-charge ratio rather than the simple mass. Therefore, it should be mentioned that for multiply charged ions the apparent *m/z* values are fractional parts of their actual masses. ESI-MS is a soft ionization technique which allows a gentle handling of the sample ions, this is a great advantage since it prevents the molecule fragmentation. As a consequence, ESI mass spectra of peptides and proteins usually appear as a collection of various multiply charged ions of the intact

analyte molecule forming adducts with other metal ions (such as K^+ or Na^+) or protons deriving from the chosen experimental conditions (*e.g.* pH).

2.5 Nuclear Magnetic Resonance Spectroscopy (NMR)

Nuclear magnetic resonance (NMR) is a spectroscopic technique widely used for the determination of molecular structures in solution and pure liquids. This spectroscopic method applies to atomic nuclei which are sensitive to an external magnetic field, B_0, and it measures the absorption of radiofrequency electromagnetic radiation. Atomic nuclei are characterised by the nuclear spin quantum number, *I*. When an atomic nucleus possesses a non-zero net nuclear spin ($I \neq 0$), it can be investigated by NMR. Examples of nuclei relevant for biomolecular NMR include ^{1}H (spin = ½), deuterium ^{2}H or D (spin = 1), ^{13}C (spin = ½), ^{14}N (spin = 1), ^{15}N (spin = ½), ^{31}P (spin = ½). A rotating particle possesses an angular momentum, **J**, and a magnetic moment, **μ**; these vectorial quantities are related by the giromagnetic ratio, γ, which is constant and typical for each nucleus.

$$\boldsymbol{\mu} = \gamma \boldsymbol{J} \tag{2.25}$$

When a nucleus interacts with an external magnetic field, the motion of the electrons around the atom generates an opposite magnetic field and the nucleus precesses about the direction of the field. The angular momentum vector **J** precesses about the external field axis with an angular frequency known as the Larmor frequency, ω, which is proportional to γ and B_0 (Larmor equation, 2.26). Therefore, in the presence of an external magnetic field, nuclei with different gyromagnetic ratios can be discriminated by means of their precession frequency.

$$\omega = \gamma B_0 \tag{2.26}$$

In the presence of an external magnetic field, two spin states exist for a nucleus. The magnetic moment of the lower energy +1/2 state is aligned with the external field, while the higher –1/2 spin state is opposite. The nuclear magnetic moment, oscillating at the Larmor frequency, can be in resonance with the magnetic component of an incident electromagnetic radiation of frequency equal to ω. Under these conditions, the radiation is absorbed (its energy exactly corresponds to the spin state separation of a specific set of nuclei) and the nuclear spin rotates changing orientation from the +1/2 state to the higher –1/2 spin state. The frequency of a NMR transition depends on the local magnetic field experienced by the nucleus and is expressed in terms of the chemical shift, δ, that is the difference between the resonance frequency of nuclei in the sample and that of a reference compound, usually tetramethylsilane $Si(CH_3)_4$. Chemical shifts are different for the same element in inequivalent positions within a molecule, therefore NMR can be used to study the structure of a molecule and the interaction with a metal ion. Moreover, the use of two-dimensional nuclear magnetic resonance spectroscopy allows the dispersion of the signals in various dimensions and the observation of correlations between different signals. Interactions between nuclear spins is also possible and can be observed by NMR. The so-called spin-spin coupling gives rise to multiplets due to small changes in the resonance energy associated to a nucleus affected by the orientation of the spin of a nearby nucleus. The strength of spin-spin coupling, which is reported as the spin-spin coupling constant, J (in hertz, Hz), decreases rapidly with distance through chemical bonds. Chemically equivalent nuclei, however, do not display the effects of their mutual spin-spin coupling.

2.5.1 Data analysis and processing

The TOCSY (Total Correlation Spectroscopy) experiment has been the most employed method to record NMR spectra in this work; it shows the correlations (cross peaks) for nuclei which are directly coupled and nuclei which are connected by a chain of subsequent couplings. A comparison between the observed chemical shifts of a peptide sample in absence and presence of metal ion allows to identify which proton signals are more affected by the addition of the metal and therefore which residues are most likely involved in the interaction with it. In the case of paramagnetic metals, like Cu(II), NMR proton signals of the residues close to the metal ion undergo an intense line broadening, therefore the selective signal disappearance can give information on the involved donor groups. Spectral processing and analysis was performed using Bruker TOPSPIN 2.1 and Sparky.[11]

2.6 Electron Paramagnetic Resonance (EPR)

Electron paramagnetic resonance spectroscopy (EPR) corresponds to the observation of a resonant absorption by unpaired electrons in a magnetic field. It is suitable for paramagnetic species. By analogy with NMR, the application of an external magnetic field B_0 produces a difference in energy between the possible spin states of the unpaired electrons (Zeeman effect) and the absorption of the microwave radiation can cause the excitation of the particle from its low energy state to a higher energy state:

$$\Delta E = g\mu_B B_0 \tag{2.27}$$

where μ_B is the Bohr magneton ($9.2740 \cdot 10^{-24}$ J T^{-1}) and g is a numerical factor known as the "g value". Usually the resonance conditions are obtained at a fixed incident radiation ($\Delta E = h\nu$, with constant ν), by varying the intensity of the magnetic field. The most used frequencies are in the microwave range (9.5 GHz). The proportionality constant g is the primary empirical parameter which is determined in an EPR experiment: this value is specific for the molecule under investigation and contains information on the chemical environment, *e.g.* the coordination sphere of a paramagnetic metal ion. For a free electron in vacuum $g_e = 2.00232$, but in compounds this value is affected by spin-orbit coupling, which alters the local magnetic field experienced by the electron. The unpaired electron of a paramagnetic molecule does not only experience the external magnetic field, but it is also affected by the molecular electronic structure. Then, the g values can be highly anisotropic so that the resonance condition depends on the rotation of the molecule in the applied field (or, alternatively, rotation of the field around the magnet). A metal ion at the centre of a perfect octahedron with six identical ligands with identical metal-to-ligand bond lengths will give a single (derivative) line EPR spectrum, called an isotropic pattern, with $g_z = g_y = g_x$. An axial pattern with $g_z \neq g_y \approx g_x$ can occur when a perfect octahedron is elongated or compressed along one of the axes. More generally, if one, or two of the ligands along this axis are different from the others the structure and the spectrum are (near) axial and it is possible to define two g values, $g_{//}$ (for the component parallel to the applied magnetic field) and $g_\perp$ (for the other two components, which are perpendicular to the field).

The coupling of the electron spin to any magnetic nucleus with $I \neq 0$ gives rise to hyperfine interaction, which results in the multiplet (2I+1) structure of each EPR line. The hyperfine interaction parameter, A, expressed in gauss, represents the magnitude of the splitting and is also generally anisotropic. Taking a metal complex as an example, besides the hyperfine structure, which describes the coupling of the unpaired electron to the atom on which it is primarily located, the superhyperfine structure refers to the coupling to ligands nuclei and

gives further information about the formed complexes (*e.g.* the extent of electron delocalization and covalence in metal complexes).

2.6.1 Data analysis and processing

The EPR parameters, g and A, for Cu(II) complexes were obtained by means of computer simulation of the experimental spectra using the WIN-EPR SIMFONIA software (Bruker). Since these parameters are determined by the chemical composition and the position of the atoms nearest to the metal ion, they provide information on the coordination sphere and the donor atoms set. The metal-ligand interaction can be predicted by a comparison with literature values for the EPR parameters (**Table 2.4**).[12] EPR analyses can also give information on the possible formation of bi-nuclear copper complexes, since the magnetic interaction between the two metal centers – unless very distant in the molecule – produces an antiferromagnetic coupling that renders Cu(II) ions silent.

Table 2.4 - Expected values of $g_{//}$ and $A_{//}$ in Cu(II) complexes with different equatorial donor atoms.

Donor atoms	**$g_{//}$**	**$A_{//}$ (G)**
1N, 3O	2.34 – 2.32	140 – 160
2N, 2O	2.30 – 2.27	160 – 180
3N, 1O	2.25 – 2.19	170 – 200
4N	2.21 – 2.16	190 – 215

2.7 Solid-phase peptide synthesis

Solid-Phase Peptide Synthesis (SPPS) is a common technique for peptide synthesis. The method is based on the use of a solid resin as support material, the use of an excess of reagents in order to promote a faster synthetic process with high purity, and the construction of the peptide from the carbonyl group side (C-terminus) to amino group side (N-terminus) of the amino acid chain. The employed synthetic strategy is Sheppard's α-Fmoc strategy, where the α-amino group is protected with the Fmoc (9-fluorenylmethoxycarbonyl) labile base protecting group. The Fmoc strategy is overall accessible, simple and inexpensive and it allows a wide choice of both resins and amino acid side chains protecting groups, ensuring high yields. The general synthetic scheme is shown in **Figure 2.9**: the first amino acid, which is protected at its α-amino group and at the reactive lateral groups (Fmoc-Xaa), is anchored to the resin through its C-terminus; the Fmoc group is then removed and the unprotected amino group can react with a second Fmoc-amino acid (Fmoc-Xbb) to form a peptide bond. The use of coupling reagents (*e.g.* carbodiimides) is also crucial to activate the reactive groups and enhance the efficiency of amide bond formation. The above steps are repeated for each amino acid added to the peptide chain. Under strong acidic conditions the peptide chain is then cleaved from the resin and the side chains protecting groups are removed.

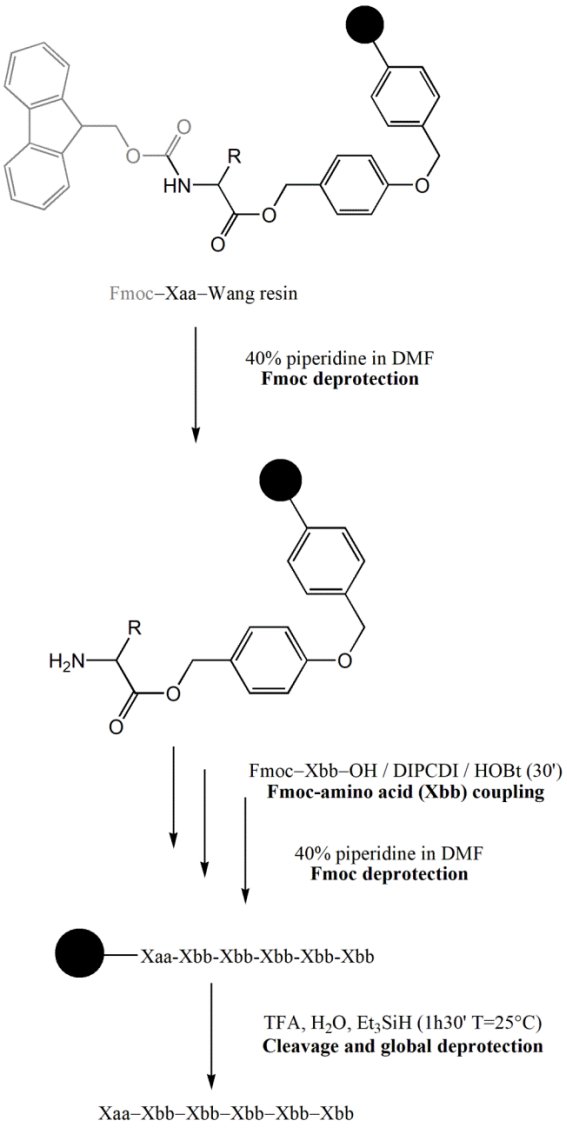

Figure 2.9 - Synthetic scheme of SPPS.

2.8 References

[1] A. Braibanti, G. Ostacoli, P. Paoletti, L. D. Pettit, S. Sammartano, *Pure Appl. Chem.* **1987**, *59(12)*, 1721-1728.
[2] P. Gans, B. O'Sullivan, *Talanta* **2000**, *51(1)*, 33-37.
[3] P. Gans, A. Sabatini, A. Vacca, *Talanta* **1996**, *43(10)*, 1739-1753.
[4] L. Alderighi, P. Gans, A. Ienco, D. Peters, A. Sabatini, A. Vacca, *Coord. Chem. Rev.* **1999**, *184*, 311-318.
[5] G. Gran, *Acta Chem. Scand.* **1950**, *4*, 559-577.
[6] E. J. Billo, *Inorganic and Nuclear Chemistry Letters* **1974**, *10(8)*, 613-617.
[7] E. Prenesti, P. G. Daniele, M. Prencipe, G. Ostacoli, *Polyhedron* **1999**, *18(25)*, 3233-3241.
[8] H. Sigel, R. B. Martin, *Chemical Reviews* **1982**, *82(4)*, 385-426.
[9] P. G. Daniele, E. Prenesti, G. Ostacoli, *Dalton Trans.* **1996***(15)*, 3269-3275.
[10] N. J. Greenfield, *Nat. Protoc.* **2006**, *1(6)*, 2876-2890.
[11] W. Lee, M. Tonelli, J. L. Markley, *Bioinformatics* **2015**, *31(8)*, 1325-1327.
[12] J. Peisach, W. E. Blumberg, *Arch. Biochem. Biophys.* **1974**, *165(2)*, 691-708.

3. Chapter Three: ZinT periplasmic protein

3.1 Outline of the work

ZinT (formerly known as YodA) is a periplasmic protein primarily found in Gram-negative bacteria. ZinT is defined as a lipocalin/calycin-like protein because of its major β-barrel domain, which is structurally related to this protein family; additionally, it also contains a small helical domain. Lipocalins are extracellular proteins associated to several functions, including ligand binding, receptor binding and interaction with other macromolecules to form complexes. Therefore, it is not surprising that ZinT may function as a zinc-chaperone for the ZnuABC system. Although different crystal structures of ZinT identify several possible zinc metal binding residues (His167, His176, His178, Glu212, His216, His24, His26, His27 and His29) there is a general consensus that the three highly conserved His residues (His167, His176 and His178) facing the centre of the calycin like-domain should be a favourable zinc binding site.[1, 2] Interestingly, the sequence portion between residues 24 and 29 (-HXHHXH-) is rich in histidines and is highly conserved in ZinT homologues from different bacterial species; moreover it is highly flexible and it is reminiscent of the His-rich loop typical of zinc-specific SBPs. As already mentioned, the Zn(II)-ZinT complex from *S. enterica* can interact with ZnuA forming a binary complex where both proteins expose their binding pocket to the Zn(II) ion and where the His-rich loop of ZnuA enters the space delimited by the calycin and helical domains of ZinT.[3]

The above results prompted us to deeply investigate the coordination chemistry of ZinT complexes with Zn(II) and Cu(II), two endogenous and competing metal ions. For this purpose, we studied the following amino- and carboxyl-terminal protected peptides: L1 = Ac-HGHHSH-Am and L2 = Ac-HGHHAH-Am, which serve as models for the N-terminal histidine-rich loop (the 24–29 amino acid sequence) of *Eco*ZinT and *Sen*ZinT, respectively, and L3 = Ac-DHIIAPRKSSHFH-Am from *Eco*ZinT and L4 = Ac-DHIIAPRKSAHFH-Am from *Sen*ZinT, which correspond to the 166–178 amino acid sequence encompassing three highly conserved His residues. It is important to stress out that the investigated model peptides are very similar in the two bacteria, but in the case of *S. enterica*, two serine residues (position 28 and 175 of ZinT protein sequence) are substituted by alanines. There are no explanations for such substitution in terms of ZinT biological role or virulence efficacy. Nevertheless, it is quite interesting to notice that this variation occurs in both the metal binding domains of ZinT. Since small changes in the peptide primary structure can affect the metal binding behaviour, a deep investigation of the complex-formation equilibria is required to fully understand the coordination properties of *Eco*ZinT and *Sen*ZinT and to highlight the possible differences between the behaviours of the two bacterial species.

3.2 Experimental procedure

Analyses performed on the above mentioned peptides follow the scheme:

- Potentiometric determination of ligand protonation and Zn(II) and Cu(II) complex-formation constants.
- Mass spectrometric analysis to evaluate ligand purity and the stoichiometry of the formed Zn(II) and Cu(II) complexes.
- Spectrophotometric (UV-Vis and CD) analyses of Cu(II) complexes.
- EPR measurements of Cu(II) complexes.

- Far-UV CD spectroscopy to investigate the structural conformations of apo-peptides, Cu(II) and Zn(II) complexes.

From the obtained equilibrium constants it is possible to plot the species distribution diagram for each system. It shows the formation percentage of each complex as a function of pH. Both the equilibrium constants and the spectroscopic data from UV-Vis and CD measurements help defining the most probable coordination modes for the Cu(II) ion by comparing the observed wavelengths of absorption of a certain complex (corresponding to the pH value at which the species reaches its maximum of formation in solution) with the expected theoretical λ_{max} value obtained from literature. EPR $g_{//}$ and $A_{//}$ parameters also give information on the metal coordination sphere.

The employed experimental conditions, instruments and materials are reported in details below, in Bellotti *et al.*, 2020.[4]

3.3 Results and discussion

The overall stability constants (logβ) and acid dissociation constants (pK_a) for the formed metal complexes are reported in **Table 3.1** together with the proposed coordination mode for each species. In the case of Cu(II) systems, increasing the pH value, a general shift of the visible absorption bands towards shorter wavelengths is observed (**Figure 3.1**); this behaviour typically indicates the increase of the number of coordinated nitrogen atoms around the Cu(II) ion. Therefore, moving to alkaline conditions and with all the studied peptides, Cu(II) is able to gradually form complexes where 2, 3 and 4 nitrogen atoms are coordinated to the metal center (**Figure 3.2**). Under physiological and alkaline conditions, the binding of a larger number of N-amides to the Cu(II) ion, gradually substituting imidazole nitrogens in the equatorial coordination plane, is confirmed by the increased intensity of the CD signals. The metal interaction with the peptide backbone, in fact, usually produces a stronger CD absorption, due to the proximity of the N-amide donor groups to the peptide chiral centres. An increased square-planar character of the complex geometry is conceivable (**Figure 3.3a**), as indicated by the typical shape of CD bands in the visible region.[5]

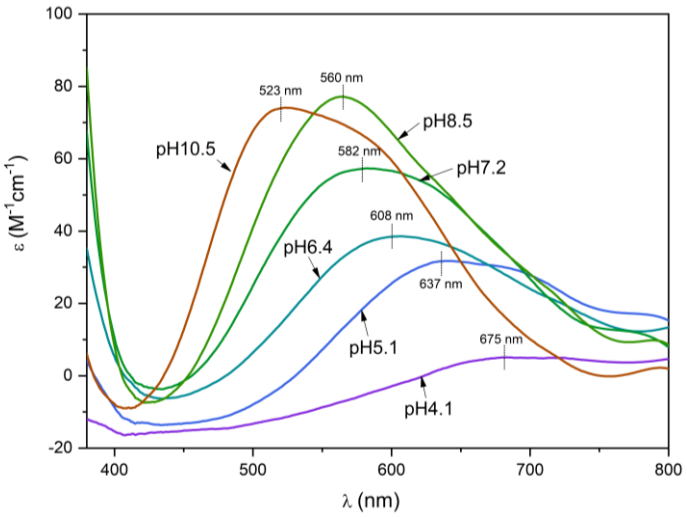

Figure 3.1 - Vis absorption spectra of Cu(II)/L1 complexes; M:L ratio 0.9:1; C_M = $0.45 \cdot 10^{-3}$ M, optical path 1 cm.

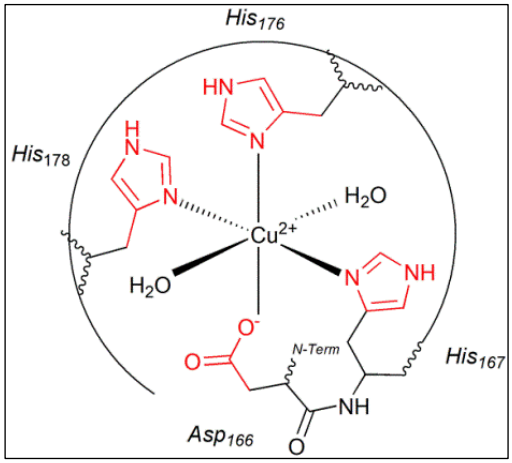

Figure 3.2 - Proposed coordination mode ($3N_{Im}$, COO^-) for Cu(II) complexes with L3 and L4 under acidic conditions.

Table 3.1 - Equilibrium constants and proposed coordination modes for Cu(II) and Zn(II) complexes at T=298 K and I=0.1 M ($NaClO_4$). Values in parentheses are standard deviations on the last significant figure.

Species	**log*β***	**p*K*$_a$**	**Coord.**	**log*β***	**p*K*$_a$**	**Coord.**
	L1			**L2**		
$[CuH_2L]^{4+}$	19.72(8)	4.45	$2N_{Im}$	19.4(1)	4.46	$2N_{Im}$
$[CuHL]^{3+}$	15.27(3)	6.26	$3N_{Im}$	14.93(4)	6.37	$3N_{Im}$
$[CuL]^{2+}$	9.00(7)	7.15	$2N_{Im}$, N^-	8.56(8)	7.24	$2N_{Im}$, N^-
$[CuH_{-1}L]^{+}$	1.85(8)	7.31	$2N_{Im}$, $2N^-$	1.32(9)	7.38	$2N_{Im}$, N^-
$[CuH_{-2}L]$	-5.46(7)	9.31	$2N_{Im}$, $2N^-$	-6.06(8)	9.52	$2N_{Im}$, $2N^-$
$[CuH_{-3}L]^{-}$	-14.78(8)	-	N_{Im}, $3N^-$	-15.59(9)	-	N_{Im}, $3N^-$, $N_{Im(ax.)}$
	L3			**L4**		
$[CuH_2L]^{4+}$	22.26(3)	5.32	$2N_{Im}$, COO^-	22.53(4)	5.40	$2N_{Im}$, COO^-
$[CuHL]^{3+}$	16.94(4)	5.74	$3N_{Im}$, COO^-	17.13(5)	5.68	$3N_{Im}$, COO^-
$[CuL]^{2+}$	11.19(4)	6.19	$3N_{Im}$, N^-	11.45(5)	6.35	$3N_{Im}$, N^-
$[CuH_{-1}L]^{+}$	5.00(4)	9.03	$2N_{Im}$, $2N^-$	5.10(4)	9.65	$2N_{Im}$, $2N^-$
$[CuH_{-2}L]$	-4.03(7)	10.18	$2N_{Im}$, $2N^-$, $\varepsilon NH_{2(ax.)}$	-4.54(6)	10.35	$2N_{Im}$, $2N^-$
$[CuH_{-3}L]^{-}$	-14.20(7)	-	$2N_{Im}$, $2N^-$, $\varepsilon NH_{2(ax.)}$	-14.90(5)	-	$2N_{Im}$, $2N^-$
	L1			**L2**		
$[ZnH_2L]^{4+}$	-	-	-	17.3(1)	5.78	$2N_{Im}$
$[ZnHL]^{3+}$	11.85(7)	6.4	$3N_{Im}$	11.5(1)	6.0	$3N_{Im}$
$[ZnL]^{2+}$	5.5(1)	6.3	$3N_{Im}$	5.5(1)	6.1	$3N_{Im}$
$[ZnH_{-1}L]^{+}$	-0.82(7)	-	$3\text{-}4N_{Im}$	-0.57(3)	-	$3\text{-}4N_{Im}$
	L3			**L4**		
$[ZnH_2L]^{4+}$	20.04(7)	6.28	$2N_{Im}$, COO^-	20.17(5)	6.47	$2N_{Im}$, COO^-
$[ZnHL]^{3+}$	13.76(5)	6.51	$3N_{Im}$	13.70(5)	6.61	$3N_{Im}$
$[ZnL]^{2+}$	7.25(3)	-	$3N_{Im}$	7.09(2)	-	$3N_{Im}$

When the coordination geometry undergoes a tetragonal distorted environment due to a more or less intense apical interaction (*e.g.* in the case of $[CuH_{-3}L]^{-}$ for L2 and $[CuH_{-2}L]$ for L3), spectroscopic methods provide indication of such perturbation. An example is given by the amino group of lysine residue (ε-NH_2) in L3, which can apically interact with Cu(II) under alkaline conditions causing a slight "red-shift" towards 544 nm of the wavelength of maximum absorption of $[CuH_{-2}L]$ (pH ≈ 10). The slight changes of EPR parameters also suggest an apical perturbation in the complex, due to the possible interaction of Cu(II) with the lysine ε-NH_2 moiety (**Figure 3.3b**). On the contrary, in the case of L4 (which is the analogue of L3) no spectroscopic changes are observed and Lys merely deprotonates without any particular effect on Cu(II) complexation. Furthermore, in both the systems (Cu(II)/L3 and Cu(II)/L4) under the most basic pH, the deprotonation of the pyrrole-type nitrogen of a coordinated histidine may occur. For all the investigated copper complexes the octahedral distorted geometry is likely predominant at acidic and physiological pH, while moving to alkaline conditions the square planar character increases with the simultaneous coordination of backbone amides.

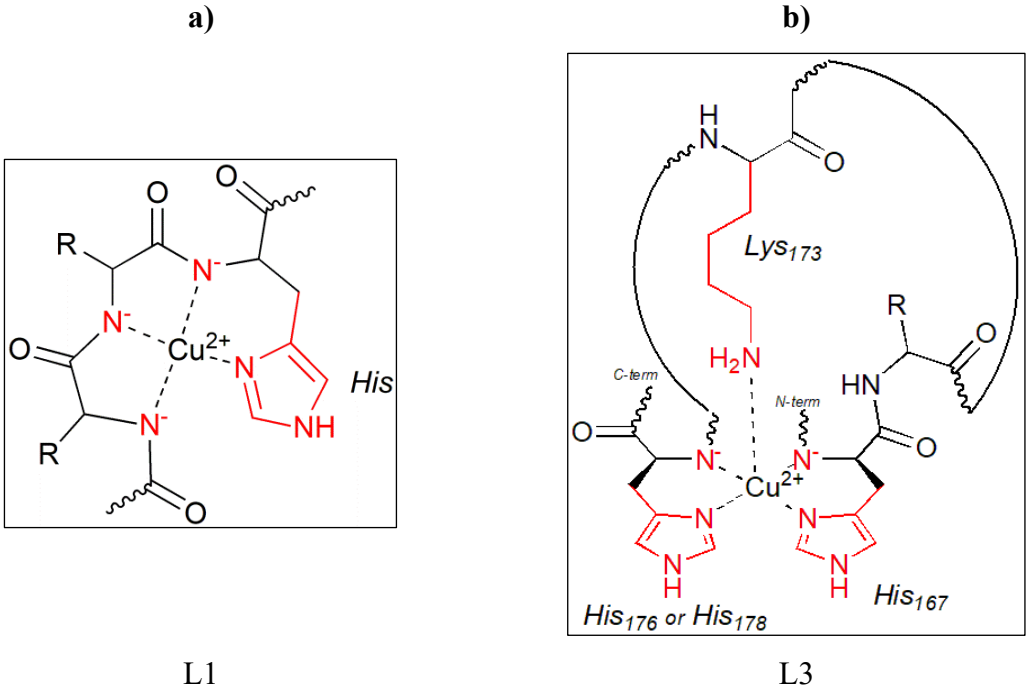

Figure 3.3 - Proposed coordination mode for Cu(II) complexes with (a) L1 (N_{Im}, $3N^{-}$) and (b) L3 ($2N_{Im}$, $2N^{-}$, $\varepsilon NH_{2(ax.)}$) under alkaline conditions.

In the case of Zn(II) complexes, potentiometric measurements have been performed until pH 8, due to the formation of a precipitate at more alkaline conditions. The tetrahedral geometry is by far the most probable (**Figure 3.4**), even though a pentacoordinate system ($4N_{Im}$, O^{-}) with a distorted pyramidal arrangement has been suggested for a Zn(II)-L1 complex ($[ZnH_{-1}L]^{+}$); this is not surprising considering the conformational flexibility of Zn(II) ion.[6, 7] A mix of tetrahedral and pyramidal species can also be hypothesized.

High resolution mass spectra confirmed the formation of mononuclear Zn(II) and Cu(II) complexes under the employed experimental conditions. Signals corresponding to various sodium and potassium adducts, together with the differently protonated free ligand and metal complexes have been detected. No poly-nuclear complexes or bis-complexes have been identified. An exemplificative mass spectra is given in **Figure 3.5**.

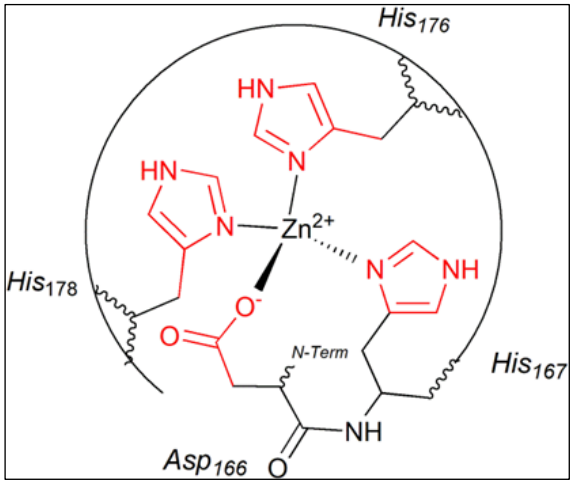

Figure 3.4 - Proposed coordination mode ($3N_{Im}$, COO^-) for Zn(II) complexes with L3 and L4 under acidic conditions.

a)

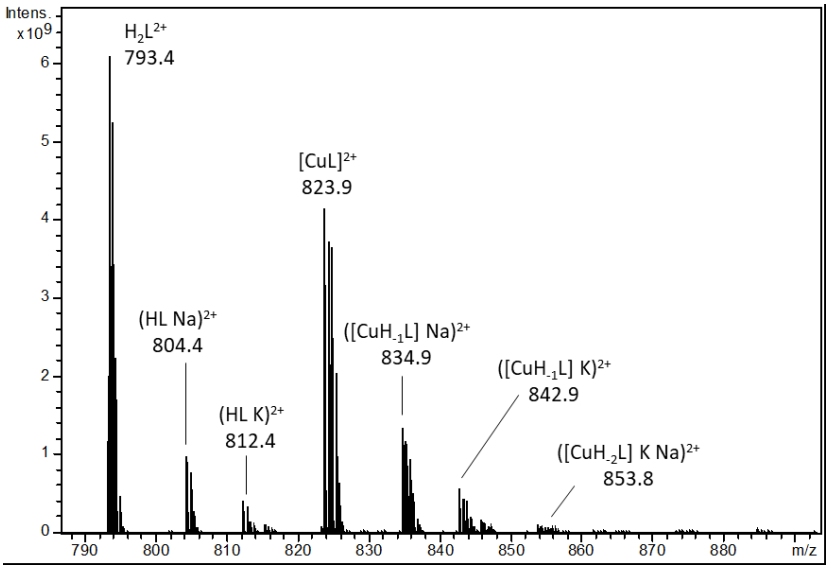

b)

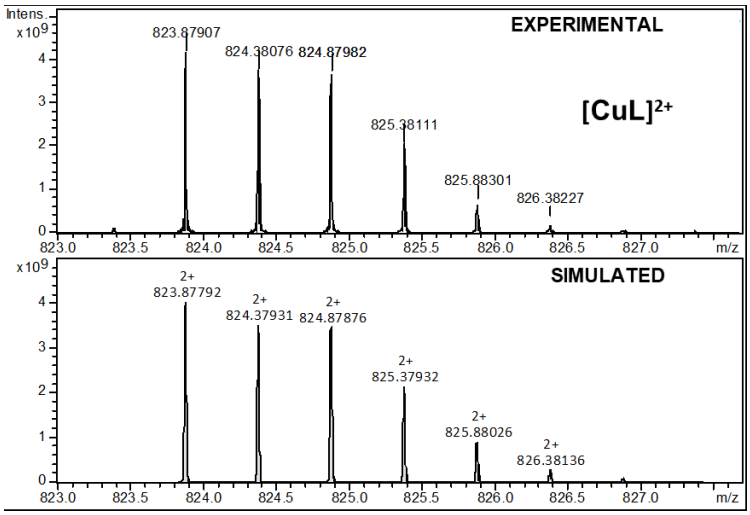

Figure 3.5 - (a) ESI-MS spectrum for Cu(II)/L3 system at L:M molar ratio 1:0.9 in MeOH:H_2O (1:1) mixture solution at pH=7. (b) Comparison of experimental and simulated isotopic pattern of the chosen metal complex $[CuL]^{2+}$. For the sake of simplicity only one mass spectrum, corresponding to L3/Cu(II) complex is reported.

It is worth to mention that the thermodynamic and spectroscopic results obtained in the present work are consistent with previous biological studies conducted on ZinT. The metal binding site corresponding to the 166–178 amino acid sequence (*E. coli* L3 = Ac-DHIIAPRKSSHFH-NH_2 and *S. enterica* L4 = Ac-DHIIAPRKSAHFH-NH_2) is confirmed to be fundamental for metal coordination, particularly involving the three histidines (His167, His176, His178) and the aspartic acid (Asp166). Furthermore, the spectroscopic far-UV CD structural characterization of L3 and L4 apo-peptides and of their Cu(II) and Zn(II) complexes does not highlight the formation of any particular α-helical or β-sheet structure and the typical band obtained at around 200 nm confirms a flexible random coil conformation (**Figure 3.6**).

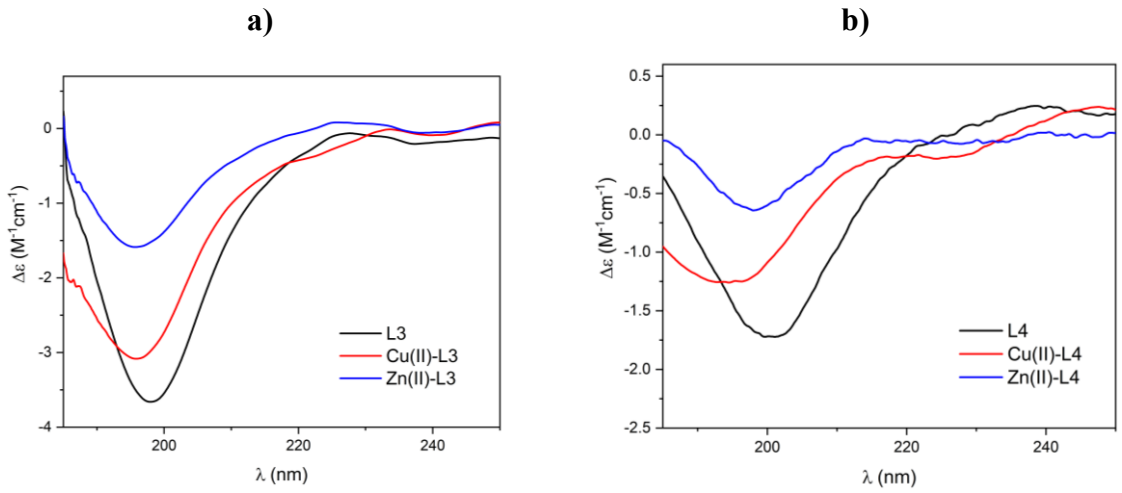

Figure 3.6 - Far-UV CD spectra of (a) L3, (b) L4 apo-peptides and their Cu(II) and Zn(II) complexes. M:L molar ratio 0.9:1; $C_L = 0.1 \cdot 10^{-3}$ M; optical path 0.01 cm; pH = 7.

Nevertheless, the obtained thermodynamic equilibrium constants designate also the N-terminal histidine-rich fragment (^{24}HGHHXH^{29}) as a very effective metal binding domain. We calculated two competition plots to qualitatively evaluate the ligand affinity for Cu(II) and Zn(II) (**Figure 3.7**). They represent a simulation of solutions containing equimolar concentrations of the metal and the chosen ligands, admitting that all the peptides compete for the metal recruitment and that they form only the binary complexes described in the speciation models (**Table 3.1**). The histidine-rich fragments L1 and L2 are better ligands for zinc ion than L3 and L4, confirming the general assumption that a higher number of histidine residues favours the metal complexation.[8-11] Indeed, according to the proposed speciation models, ZinT short fragments form stable 4N complexes with Zn(II) already at pH around 6. On the contrary, L3 and L4 contain only 3 imidazole groups and they can only coordinate the metal ion by means of a ($3N_{Im}$, O^-) binding mode. Therefore, the proposed coordination hypotheses are in good agreement with the competition plot trend, which also confirms a comparable stability among the studied systems below pH 6, *i.e.* where all the peptides display a 3N coordination. In the case of copper ion, once again the crowded cluster of histidines in L1 and L2 provides a higher number of anchoring sites to favour the first steps of complexation. On the contrary, in L3 and L4 the available binding sites are located at the peptide sequence opposite sides (Ac-DHXXXXXXXXHFH-Am), likely preventing an effective complexation. However, increasing the pH value, the calculated competition plots designate the longer fragments as the most effective ligands. In order to explain this result, it can be useful to observe that, under alkaline conditions,

backbone amides gradually substitute His residues as donor groups. As a consequence, the number of histidines in the peptide sequence contributes to a lesser extent to the complex stabilization, while the length of the peptide (clearly greater for L3 and L4) could favour the wrap and protection of the metal binding site, thus increasing the complex stability. No remarkable differences between *E. coli* and *S. enterica* model systems have been observed. The coordination behaviour is similar for L1 and L2 as well as for L3 and L4, respectively, although some minor differences occur under the most alkaline conditions. However, it is worth to underline that peptides from *Ec*ZinT show a higher tendency to stabilize Cu(II) complexes at neutral and alkaline pH, *i.e.* when backbone amides participate in Cu(II) coordination. Although serine residues are not coordinated to the metal ion, this trend has been observed in many other systems and it has been ascribed to a possible electronic effect of serine residues, capable of favouring the amidic proton displacement by the Cu(II) ion.[8, 12] It is worth to note that the higher Cu(II) affinity for L3 is consistent with the hypothesis of the metal interaction with an apical lysine (see above), which contributes to stabilize the complex by "wrapping" the metal centre.

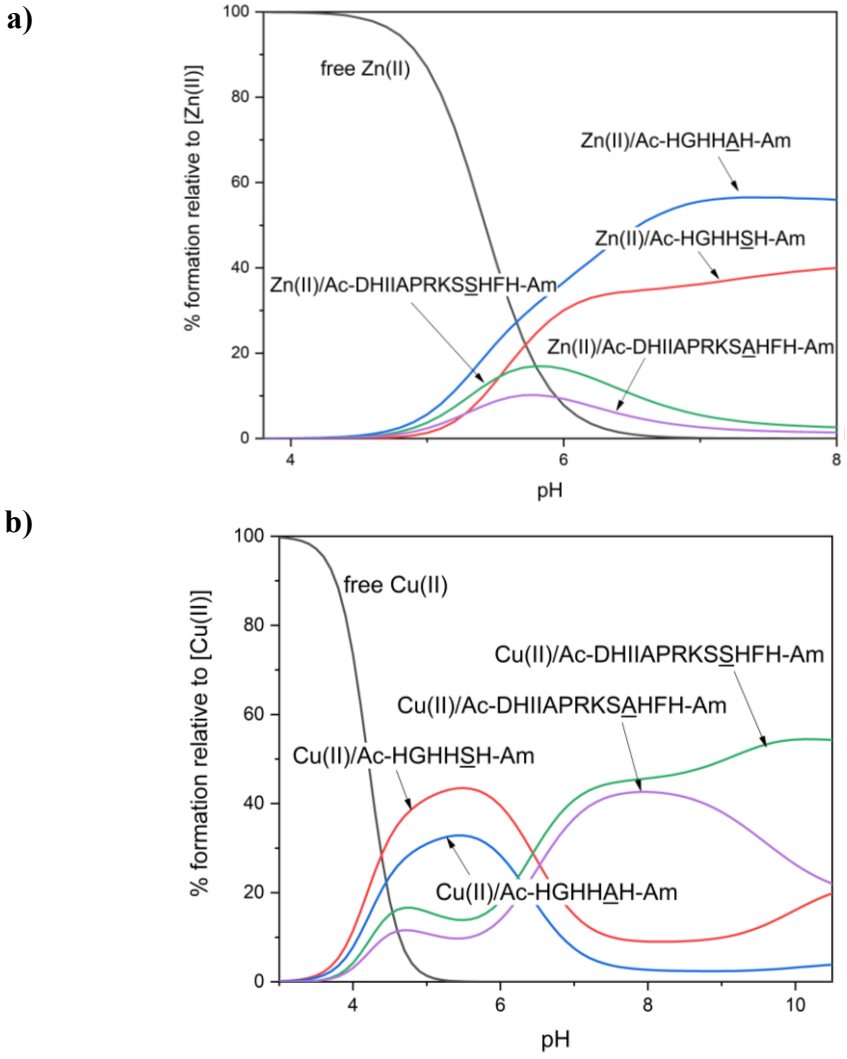

Figure 3.7 - Competition plots for a solution containing equimolar concentration ($1 \cdot 10^{-3}$ M) of metal ion, L1: Ac-HGHHSH-Am, L2: Ac-HGHHAH-Am, L3: Ac-DHIIAPRKSSH FH-Am and L4: Ac-DHIIAPRKSAHFH-Am. (a) Zn(II); (b) Cu(II).

According to recent studies performed on *Se*ZinT, the metal recruitment mechanism of this protein should involve the formation of a binary complex with ZnuA, the soluble periplasmic component of the ZnuABC transporter. This interaction has not been fully elucidated, but the Zn(II) binding seems to be crucial. Moreover, the N-terminal His-rich loop of ZnuA proved to play a critical role, and some evidence also suggests that ZnuA may interact with other metal ions, including Cu(II). In order to compare the Zn(II) and Cu(II) metal binding ability of the ZinT fragments with that of the two identified metal binding sites of ZnuA protein from *E. coli* (Ac-^{115}MKSIHGDDDDHDHAEKSDEDHHHGDFNMHLW^{145}-Am, corresponding to the N-terminal His-rich loop, and Ac-^{223}GHFTVNPEIQPGAQRLHE^{240}-Am, a secondary and less effective binding site),[13] the two competition plots shown in **Figure 3.8** have been computed. The comparison shows that ZnuA His-rich loop located in the domain 115–145 is by far the most effective ligand for Zn(II) ion. This is not surprising and confirms that a higher number (seven in this case) of histidines in the sequence favours the Zn(II) complexation and stabilizes the system.[11] On the other hand, Cu(II) complexes of ZnuA His-rich loop do not exhibit an improved metal affinity with respect to ZinT, unless at the most acidic pH values. Interestingly, from the chemical point of view, although both ZnuA and ZinT systems L1 and L2, under acidic conditions, form macrochelated complexes with the same $3N_{Im}$ coordination, the smaller number of His residues in ZinT leads to the binding of N-amides at lower pH and therefore "earlier" with respect to ZnuA. The N-amides coordination induces an increased square-planar character and the possible formation of stable 5/6-membered-rings involving the imidazole and vicinal peptide amides. Above physiological conditions, as previous described, L3 and L4 peptides are able to form 4N complexes and exhibit the highest binding ability. Lastly, the two His-containing ZnuA fragment Ac-^{223}GHFTVNPEIQPGAQRLHE^{240}-Am has been proved to be the less effective ligand.

The different results obtained for Zn(II) and Cu(II) complexes may explain the ZinT biological activity towards these metals. Although ZinT is able to bind both the ions and participate to Zn(II) recruitment, no evidence of its role in Cu(II) homeostasis has been found and indeed some studies exclude this function.[2] Moreover, the extremely high binding affinity of ZnuA His-rich loop towards Zn(II) is fully consistent with the putative mechanism of zinc transfer from ZinT to ZnuA *via* the formation of the protein binary system. Based on our results, such process can not occur in the case of Cu(II), since the ZnuA fragments proved to be inadequate to catch the metal ion.

a)

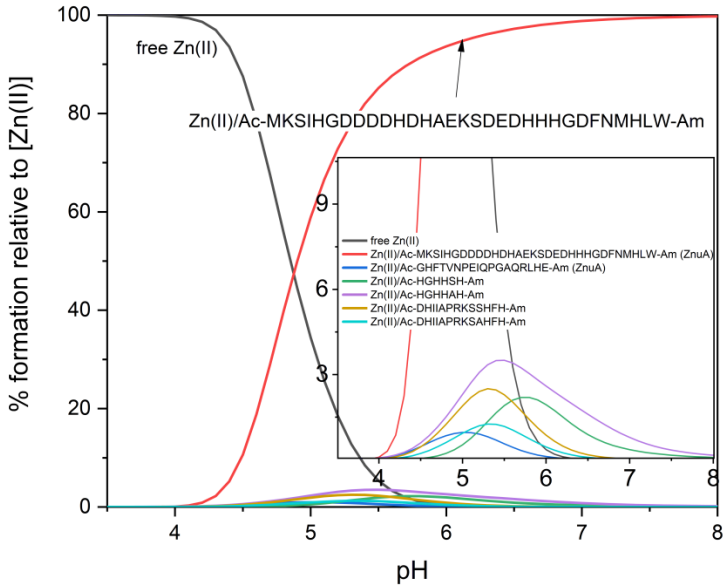

b)

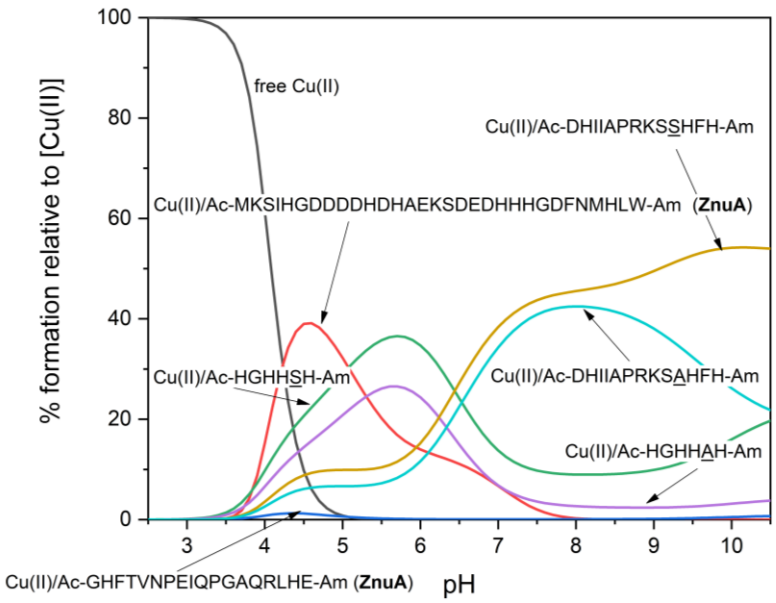

Figure 3.8 - Competition plots for a solution containing equimolar concentration ($1 \cdot 10^{-3}$ M) of metal ion, L1: Ac-HGHHSH-Am, L2: Ac-HGHHAH-Am, L3: Ac-DHIIAPRKSSH FH-Am, L4: Ac-DHIIAPRKSAHFH-Am, *E. coli* ZnuA peptide Ac-MKSIHGDDDDHDH AEKSDEDHHHGDFNMHLW-Am and *E. coli* ZnuA peptide Ac-GHFTVNPEIQPGAQR LHE-Am. (a) Zn(II); (b) Cu(II).

3.4 Conclusions

The metal binding behaviour of ZinT fragments is fully consistent with the hypotheses about the protein biological role.[3] The high efficacy of HGHHXH in metal chelation is in line with the necessity to recover and stabilize as much micronutrients as possible from the medium, acting as a primary metal scavenger. Subsequently, its function may involve the delivery of the metal ion to ZinT canonical binding site (L3 and L4 fragments) for storage and/or transfer to other proteins (*e.g.* ZnuA). The His-rich loop may therefore represent the first, but temporary, stop station for the metal ion on its route to cellular import. Indeed, a relatively high metal binding affinity is crucial to ensure the acquisition process in an environment rich of competitive systems. It is therefore not surprising that the histidine-rich loop of *E. coli* ZnuA (Ac-MKSIHGDDDDHDHAEKSDEDHHHGDFNMHLW-Am) exhibits the strongest Zn(II) affinity in comparison with the ligands studied in this work. ZinT is supposed to directly interact with ZnuA, forming a binary complex in the presence of zinc ions and likely transferring the metal to the partner protein through the His-rich loop of ZnuA. This process can be successfully achieved only if the ZnuA metal binding site has a higher affinity for Zn(II) than ZinT, and this is the case highlighted by our results. Surprisingly, Cu(II) complexes behave in a different way. In this case, the ZnuA His-rich loop shows a less effective metal binding ability, resulting in a higher stability of Cu(II) complexes with ZinT. Although further investigations are necessarily required, our thermodynamic results reflect previous observations according to which ZinT should not participate in Cu(II) homeostasis.

The research on ZinT complexes has been published in the paper “D. Bellotti, M. Rowińska-Żyrek, M. Remelli, *Dalton Trans*., 2020, 49(27), 9393–9403”.

3.5 References

[1] J. Chen, L. Wang, F. Shang, Y. Dong, N.-C. Ha, K. H. Nam, C. Quan, Y. Xu, *Biochem. Biophys. Res. Commun.* **2018**, *500(2)*, 139-144.

[2] H. G. Colaço, P. E. Santo, P. M. Matias, T. M. Bandeiras, J. B. Vicente, *Metallomics* **2016**, *8(3)*, 327-336.

[3] A. Ilari, F. Alaleona, G. Tria, P. Petrarca, A. Battistoni, C. Zamparelli, D. Verzili, M. Falconi, E. Chiancone, *Biochim. Biophys. Acta* **2014**, *1840(1)*, 535-544.

[4] D. Bellotti, M. Rowińska-Żyrek, M. Remelli, *Dalton Trans.* **2020**, *49(27)*, 9393-9403.

[5] H. F. Stanyon, X. Cong, Y. Chen, N. Shahidullah, G. Rossetti, J. Dreyer, G. Papamokos, P. Carloni, J. H. Viles, *The FEBS Journal* **2014**, *281(17)*, 3945-3954.

[6] L. Casella, M. E. Silver, J. A. Ibers, *Inorg. Chem.* **1984**, *23(10)*, 1409-1418.

[7] M. Sola, A. Lledos, M. Duran, J. Bertran, *Inorg. Chem.* **1991**, *30(11)*, 2523-2527.

[8] D. Bellotti, C. Tocchio, R. Guerrini, M. Rowińska-Żyrek, M. Remelli, *Metallomics* **2019**, *11(12)*, 1988-1998.

[9] D. Brasili, J. Watly, E. Simonovsky, R. Guerrini, N. A. Barbosa, R. Wieczorek, M. Remelli, H. Kozlowski, Y. Miller, *Dalton Trans.* **2016**, *45(13)*, 5629-5639.

[10] H. Kozlowski, M. Łuczkowski, M. Remelli, *Dalton Trans.* **2010**, *39(28)*, 6371-6385.

[11] E. Farkas, I. Sóvágó, in *Amino Acids, Peptides and Proteins: Volume 37, Vol. 37*, The Royal Society of Chemistry, **2012**, pp. 66-118.

[12] D. Bellotti, D. Łoboda, M. Rowińska-Żyrek, M. Remelli, *New J. Chem.* **2018**, *42(10)*, 8123-8130.

[13] A. Hecel, A. Kola, D. Valensin, H. Kozlowski, M. Rowinska-Zyrek, *Inorg. Chem.* **2020**, *59(3)*, 1947-1958.

4. Chapter Four: C4YJH2, a putative fungal metal transporter

4.1 Outline of the work

C4YJH2 (UniProt Knowledgebase [1]) is a 199 amino acid sequence corresponding to the gene CAWG_03987 found in the strain WO-1 of *C. albicans*. The encoded protein is classified as a putative cation transmembrane transporter and its sequence analysis highlighted a significantly high number of histidine and serine residues, especially in its C-terminal domain. C4YJH2 shares 60% identity with the Zrc1 zinc transporter. Its structure remains unsolved, but can be modelled with Phyre2, a remote homology recognition technique, able to regularly generate reliable protein models to simulate and predict their likely structure.[2] It occurs that C4YJH2 possesses four transmembrane domains, and its most probable Zn(II) binding sites are located in the C-terminal region, *i.e.* in the extracellular portion of the protein characterized by two poly-His tags: FHEHGHSHSHGSGGGGGGSDHSGDSKSHSHSHSHS (131–165 residues). Our previous work, carried out within my Master's thesis, confirmed that the main histidine-rich sequences between 131–148 (FHEHGHSHSHGSGGGGGG) and 157–165 (SHSHSHSHS) amino acid residues are involved in metal coordination.[3] In the native protein, these two His-rich domains are linked by the 9-residue sequence GSDHSGDSK (148–156), also containing a histidine and thus possibly contributing to the metal binding. Therefore, we decided to study Zn(II) and Cu(II) complexes with the protected peptide Ac-GSDHSGDSK-Am (WT, wild type) and its analogues Ac-GSDHSGASK-Am (D7A), Ac-GADHAGDAK-Am (S2A/S5A/S8A), Ac-GSDH-Am (GSDH) and Ac-HSGD-Am (HSGD). The Asp-to-Ala substitution in D7A allows to investigate the role of Asp-7 in the wild-type peptide protonation (possible hydrogen bond with Lys-9) and metal coordination. The nonapeptide S2A/S5A/S8A has been studied to evaluate the role of serines in stabilizing the formed complexes. Although the Ser hydroxymethyl group is generally not expected to interact with Cu(II) or Zn(II) ions, an electronic effect on the adjacent residues binding ability has been hypothesized. The two short peptides provide information on Cu(II) attitude to coordinate amidic nitrogen atoms in the amino- or carboxyl-terminus direction.

4.2 Experimental procedure

Analyses performed on the above mentioned peptides follow the scheme:

- Peptide synthesis by means of solid-phase technique.
- Potentiometric determination of ligand protonation and Zn(II) and Cu(II) complex-formation constants.
- Mass spectrometric analysis to evaluate ligand purity and the stoichiometry of the formed Zn(II) and Cu(II) complexes.
- Spectrophotometric (UV-Vis and CD) analyses of Cu(II) complexes.
- EPR measurements of Cu(II) complexes.
- Far-UV CD spectroscopy to investigate the structural conformations of apo-peptides, Cu(II) and Zn(II) complexes.
- NMR measurements of apo-peptides and Zn(II) complexes.

The employed experimental conditions, instruments and materials are reported in details below, in Bellotti *et al.*, 2019.[4]

4.3 Results and discussion

The investigated peptides proved to be able to form stable 1:1 complexes with Zn(II) and Cu(II); no poly-nuclear or bis-complexes have been detected either by potentiometry, mass spectrometry or EPR in the case of copper ion. In all the systems the Cu(II) coordination begins at about pH 3.5. After a first anchoring step to the histidine residue, up to three deprotonated amidic groups of the peptide backbone bind the Cu(II) ion, occupying the equatorial position of its coordination sphere. At physiological pH, the species (N_{Im}, $2N^-$) (**Figure 4.1**) is always the most abundant in solution, with the only exception for HSGD, which rather displays a ($2N^-$, COO^-) coordination mode. These complexes are rather stable and reach about 90% of formation in solution. The overall stability constants (logβ) and acid dissociation constants (pK_a) for the formed metal complexes are reported in **Table 4.1** together with the proposed coordination mode for each species.

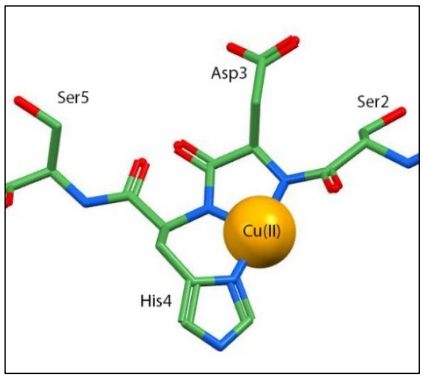

Figure 4.1 - Proposed coordination sphere of Cu(II) complexes with WT ligand at physiological pH. Explicit hydrogen atoms and water molecules are omitted for clarity.

The comparison between measured and expected λ_{max} values, together with EPR results allowed to determine the differences in the copper coordination modes above neutral pH. In the case of WT and D7A the values of λ_{max} (≈ 560 nm) suggest the substitution of the imidazole nitrogen by the N-amide in the Cu(II) equatorial plane, to obtain a ($3N^-$) coordination mode (expected λ_{max} value: 563 nm) with a water molecule in the fourth equatorial position, rather than a (N_{Im}, $3N^-$) coordination sphere, which is the case of S2A/S5A/S8A. The study of the two tetra-peptides, Ac-GSDH-Am and Ac-HSGD-Am allowed to qualitatively describe the Cu(II) N-amide-coordination attitude, since they correspond to the left-hand and the right-hand side fragments around histidine, respectively. It can be assumed that the nona-peptide WT is able to form a mixture of isomeric species in which the amide coordination towards the N-terminal direction is favoured by the formation of a stable 6-membered ring. The lower pK_a value of the step associated to the first N-amide binding in GSDH and, consequently, the higher value of the overall stability constant of [$CuH_{-1}L$] (about one order of magnitude with respect to that of HSGD) support the above hypothesis. The substitution of serine with alanine residues significantly lowers the peptide affinity for the Cu(II) ion (**Figure 4.2**), suggesting a possible role of Ser residues (quite abundant in C4YHJ2 protein sequence) in the biological task of metal uptake and regulation. On the contrary, this trend does not occur

for Zn(II) complexes where amides are not involved in the coordination. This is in agreement with the above hypothesis that serines are responsible for an electronic effect that makes amide protons much more acidic.

In Zn(II) complexes, the metal coordination at physiological pH occurs mainly by means of (at least) one aspartic acid and the histidine residue. The Asp in position 7 is likely a crucial residue for the formation and stabilization of Zn(II) complexes, as indicated by the decrease of Zn(II) affinity for ligand D7A (**Figure 4.3**), where the proposed metal coordination does not involve the aspartic acid.

Table 4.1 - Equilibrium constants and proposed coordination modes for Cu(II) and Zn(II) complexes at T=298 K and I=0.1 M (KCl). Values in parentheses are standard deviations on the last significant figure.

Species	**logβ**	**pK_a**	**Coord.**	**logβ**	**pK_a**	**Coord.**
	WT			**S2A/S5A/S8A**		
$[CuHL]^{+}$	15.66(4)	-	N_{Im}, COO^-	14.63(3)	6.58	N_{Im}, COO^-
[CuL]	-	-	-	8.05(3)	6.63	N_{Im}, N^- (COO^-)
$[CuH_{-1}L]^{-}$	3.54(3)	8.15	N_{Im}, $2N^-$	1.42(3)	9.59	N_{Im}, $2N^-$
$[CuH_{-2}L]^{2-}$	-4.61(5)	10.46	$3N^-$	-8.27(4)	10.65	N_{Im}, $3N^-$
$[CuH_{-3}L]^{3-}$	-15.07(7)	-	$3N^-$	-18.81(5)	-	N_{Im}, $3N^-$
	D7A					
$[CuHL]^{2+}$	14.04(6)	5.57	N_{Im}			
$[CuL]^{+}$	8.48(3)	5.84	N_{Im}, N^-			
$[CuH_{-1}L]$	2.64(2)	8.29	N_{Im}, $2N^-$			
$[CuH_{-2}L]^{-}$	-5.65(4)	10.38	$3N^-$			
$[CuH_{-3}L]^{2-}$	-16.03(5)	-	$3N^-$			
	HSGD			**GSDH**		
$[CuL]^{+}$	4.21(2)	6.79	N_{Im}, COO^-	4.24(5)	5.87	N_{Im}
$[CuH_{-1}L]$	-2.58(2)	6.91	N_{Im}, N^-, COO^-	-1.63(3)	5.92	N_{Im}, N^-
$[CuH_{-2}L]^{-}$	-9.50(2)	8.78	$2N^-$, COO^-	-7.56(2)	8.53	N_{Im}, $2N^-$
$[CuH_{-3}L]^{2-}$	-18.27(2)	-	$3N^-$, COO^-, $N_{Im(ax.)}$	-16.09(4)	-	$3N^-$, $N_{Im(ax.)}$
	WT			**S2A/S5A/S8A**		
$[ZnHL]^{+}$	14.11(6)	-	N_{Im}, 1-2 COO^-	13.37(9)	-	N_{Im}, 1-2 COO^-
$[ZnH_{-1}L]^{-}$	-1.86(4)	10.39	N_{Im}, COO^-	-2.15(4)	10.35	N_{Im}, COO^-
$[ZnH_{-2}L]^{2-}$	-12.25(5)	-	N_{Im}, COO^-	-12.50(6)	-	N_{Im}, COO^-
	D7A					
$[ZnH_{-1}L]$	-2.57(3)	10.36	N_{Im}			
$[ZnH_{-2}L]^{-}$	-12.93(6)	-	N_{Im}			
	HSGD			**GSDH**		
$[ZnL]^{+}$	2.9(1)	-	N_{Im}, COO^-	2.85(9)	-	N_{Im}, COO^-
$[ZnH_{-2}L]^{-}$	-12.43(4)	-	N_{Im}, COO^-	-12.41(3)	-	N_{Im}, COO^-

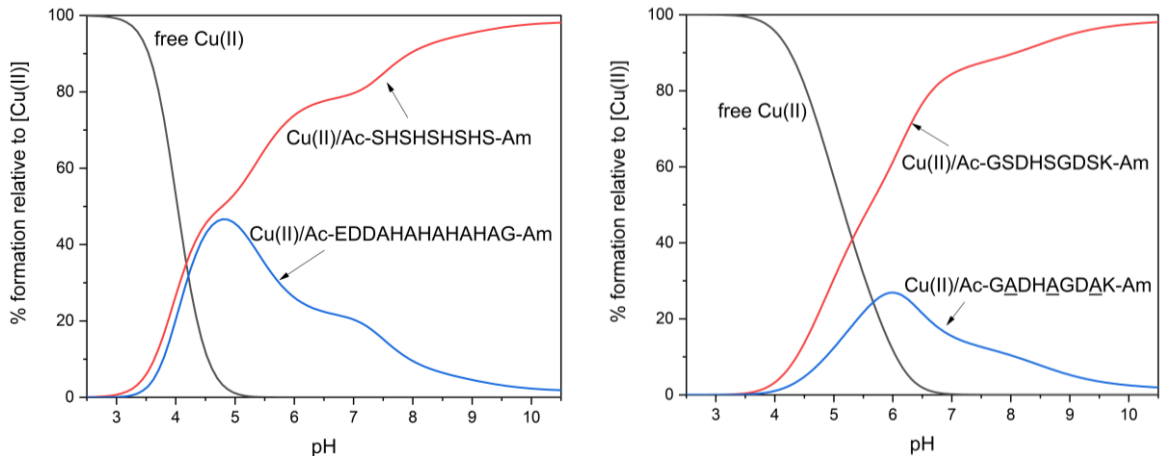

Figure 4.2 - Competition plots for solutions containing equimolar concentrations of each component ($1 \cdot 10^{-3}$ M). The difference in the % of complex formation suggests an effect of Ser residues on the stabilization of Cu(II) complexes.

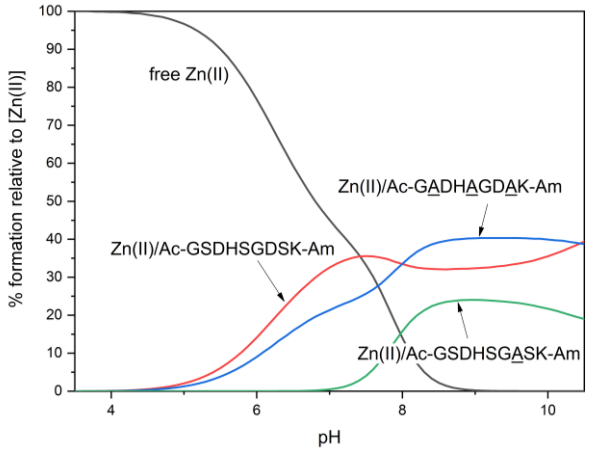

Figure 4.3 - Competition plot for a solution containing equimolar concentrations ($1 \cdot 10^{-3}$ M) of Zn(II), WT, D7A and S2A/S5A/S8A.

^{1}H-^{1}H TOCSY spectra recorded at physiological pH (**Figure 4.4**) confirm the suggested coordination hypotheses, since the major Zn(II)-induced shifts are those of histidine protons ($H_{\varepsilon 1}$–$H_{\delta 2}$), (H_{α}–$H_{\beta 1}$), (H_{α}–$H_{\beta 2}$) and aspartic acids protons (H_{α}–$H_{\beta 1}$), (H_{α}–$H_{\beta 2}$). Furthermore, in the case of WT ligand, the pronounced deshielding effect exhibited by His $H_{\varepsilon 1}$ protons (Δ_{δ}=0.125 ppm) compared to the shift of His $H_{\delta 2}$ (Δ_{δ}=0.050 ppm), in the presence of Zn(II) ions, suggests a coordination through the imidazole-N_{δ}.[5-7] This difference is less pronounced in S2A/S5A/S8A, thus suggesting that the presence of the Ser residues may influence the binding behaviour of histidine. It is also worth of note that in Zn(II)-S2A/S5A/S8A system, the protons of lysine display a moderate downfield shift (**Figure 4.5**): since Lys does not directly participate in coordination, these perturbations suggest the Zn(II) coordination *via* the aspartic acid in position 7, the nearest the Lys residue. In the case of WT ligand, only Lys-H_{α} exhibits a small perturbation after Zn(II) addition, possibly because the presence of serine residues reduces the deshielding effect on Lys. In the case of the WT ligand, only Lys-H_{α} exhibits a small perturbation after Zn(II) addition, possibly because the presence of serine residues reduces the deshielding effect on Lys. As for peptide D7A, Zn(II) complexes begin to form only at pH 6.5, *i.e.* when

imidazole nitrogen is deprotonated and available for complexation. Evidently, the presence, at lower pH, of only one Asp carboxylate is not sufficient to stabilize the metal ion binding. Thus, the first detected species is $[ZnH_{-1}L]$, most likely deriving from the binding of D7A to the hydrolytic species $[ZnOH]^+$ already present in solution in small amount, as revealed by the species distribution diagram. Rather unexpectedly, the ^{1}H-^{1}H TOCSY spectra recorded at pH 7.2 suggest that the aspartic acid in position 3 should not participate in complex formation. Indeed, the metal addition causes only a selective shift of histidine ($H_{\varepsilon 1}$–$H_{\delta 2}$) imidazole protons (more pronounced for His-$H_{\varepsilon 1}$ protons, as already observed above for WT and possibly due to the presence of Ser residues) leaving the signals of H_α–$H_{\beta 1}$/$H_{\beta 2}$ unchanged, therefore suggesting that no other residues are involved in the complexation. Signals corresponding to the aspartic acid (H_α–$H_{\beta 1}$), (H_α–$H_{\beta 2}$) protons undergo only a slight shift, supposedly due to the proximity to the histidine anchoring site.

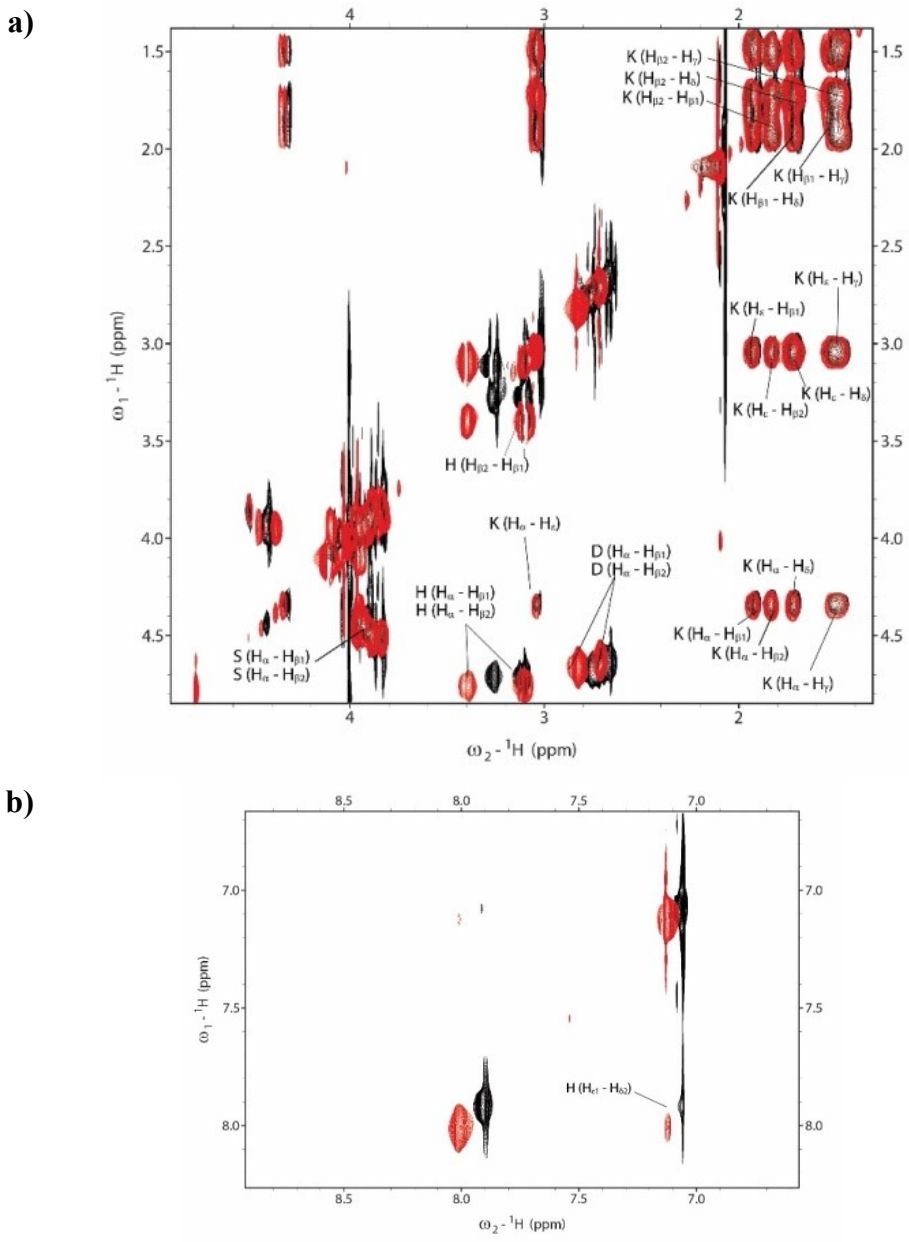

Figure 4.4 - (a) Aliphatic and (b) aromatic regions of ^{1}H-^{1}H TOCSY NMR spectra for ligand WT, $C_L = 3 \cdot 10^{-3}$ M, pH 7.3, *T*=298 K, in the absence (black) and in the presence (red) of 1 equivalent of Zn(II).

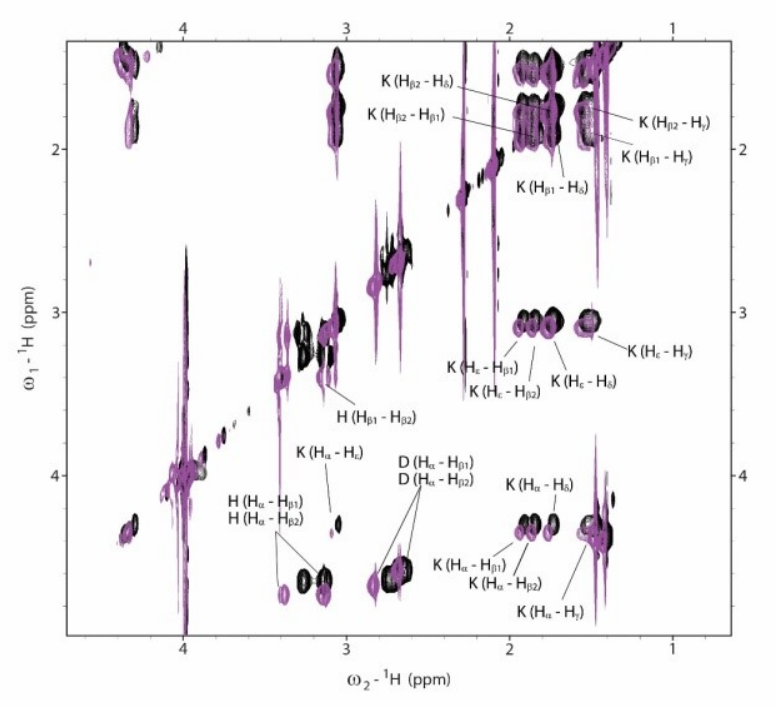

Figure 4.5 - Aliphatic region of ^{1}H-^{1}H TOCSY NMR spectra for ligand S2A/S5A/S8A, C_L = $3 \cdot 10^{-3}$ M, pH 7.4, T = 298 K, in the absence (black) and in the presence (purple) of 1 equivalent of Zn(II).

4.4 Conclusions

An overall comparison of the studied domains of C4YJH2 is shown in **Figure 4.6**. The calculated competition plots take into account the Cu(II) and Zn(II) binding ability of the "linker" Ac-GSDHSGDSK-Am (148–156) and of the two poly-His sequences Ac-FHEHGHSHSHGSGGGGGG-Am (131–148) and Ac-SHSHSHSHS-Am (157–165).[3] The obtained results emphasize that the ligand efficiency mainly arises from the high number of histidine residues, nevertheless there is a minor but not negligible contribution of the linker sequence in the complexes formation at acidic pH. Indeed, both the metal ions show a preference for the binding site corresponding to the 131–148 sequence. A deeper look into the C4YJH2 metal biding sites highlights that the two His-rich fragments bind the metal ion by means of three histidine residues ($3N_{Im}$) and an oxygen (carboxylic O^- or a water molecule); this is a very common zinc coordination mode which is extremely frequent in zinc-binding protein involved in the processes of metal transport. In condition of metal excess, it is reasonable to suppose that the zinc ions can coordinate the two major clusters of histidines and that the two coordination sites should be independent due to the presence of a rather long linker between them. A detailed study of the system with an excess of metal would be required to clarify this aspect. Nonetheless, many biological systems, like ZinT, ZnuA or Pht proteins, contain different metal binding sequences (often rich in histidines) with different metal binding affinities and which play different biological roles: they can function as primary scavengers capable of delivering the metal to other fragments, which are instead involved in the substrate transfer; or they can simply increase the local concentration of metal around the most effective transport site. The same cannot be excluded for the extra-membrane loop of C4YJH2.

This research work includes the publications "D. Bellotti, C. Tocchio, M. Rowinska-Zyrek, M. Remelli, *Metallomics* 2019, 11(12), 1988–1998" and "D. Bellotti, D. Łoboda, M. Rowińska-Żyrek, M. Remelli, *New J. Chem*. 2018, 42(10), 8123-8130".

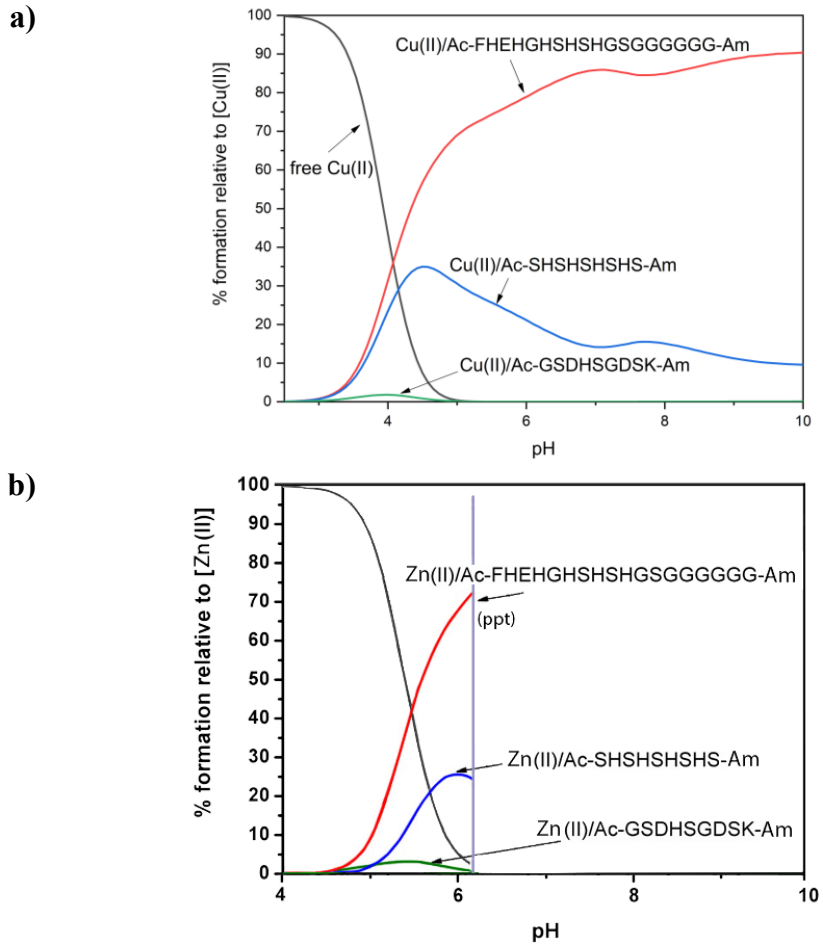

Figure 4.6 - Competition plots for solutions containing equimolar concentrations ($1 \cdot 10^{-3}$ M) of metal ion, Ac-FHEHGHSHSHGSGGGGGG-Am (131–148), Ac-GSDHSGDSK-Am (148–156) and Ac-SHSHSHSHS-Am (157–165). (a) Cu(II); (b) Zn(II).

4.5 References

[1] The UniProt Consortium, *Nucleic Acids Res.* **2018**, *46(5)*, 2699-2699.

[2] L. A. Kelley, S. Mezulis, C. M. Yates, M. N. Wass, M. J. E. Sternberg, *Nat. Protoc.* **2015**, *10(6)*, 845-858.

[3] D. Bellotti, D. Łoboda, M. Rowińska-Żyrek, M. Remelli, *New J. Chem.* **2018**, *42(10)*, 8123-8130.

[4] D. Bellotti, C. Tocchio, R. Guerrini, M. Rowińska-Żyrek, M. Remelli, *Metallomics* **2019**, *11(12)*, 1988-1998.

[5] M. Remelli, M. Peana, S. Medici, L. G. Delogu, M. A. Zoroddu, *Dalton Trans.* **2013**, *42(17)*, 5964-5974.

[6] S. Medici, M. Peana, L. G. Delogu, M. A. Zoroddu, *Dalton Trans.* **2012**, *41(15)*, 4378-4388.

[7] A. Urbani, R. Bazzo, M. C. Nardi, D. O. Cicero, R. De Francesco, C. Steinkuhler, G. Barbato, *J. Biol. Chem.* **1998**, *273(30)*, 18760-18769.

5. Chapter Five: Zrt2 fungal metal transporter

5.1 Outline of the work

Zrt2 is a zinc transporter of the Zip family. It is predicted to be found in the plasma membrane and is essential for *C. albicans* zinc uptake and growth at acidic pH. Zrt2 from *C. albicans* is composed of 370 amino acids and its three-dimensional structure has been predicted using Phyre2 software:[1] eight putative transmembrane domains have been identified together with an extra-membrane, disordered loop corresponding to the amino acids sequence 126–215. This protein portion contains at least three possible metal binding motifs: -HxHxHxxD- (144–153), -HxxHxxEHxDx- (181–193) and the Glu- and Asp- rich sequence DDEEEDxE (161–168) (**Scheme 5.1**). The corresponding model peptides protected at their termini (Ac-GPHTHSHFGD-Am, Ac-DDEEEDLE-Am and Ac-PSHFAHAQEHQDP-Am) have been investigated in order to elucidate the thermodynamic and coordination properties of their Zn(II) and Cu(II) complexes, with the further aim to identify the most effective metal binding site among the three fragments. Furthermore, according to our previous results concerning the possible role of serine residues in stabilizing copper complexes,[2, 3] the Ser-to-Ala substitution has been considered and, therefore, we extended the investigation to the following two peptides: Ac-GPHTHAHFGD-Am and Ac-PAHFAHAQEHQDP-Am.

```
         10         20         30         40         50
MNSDSISQVF EYLNKRDECP TDNDYNGNIG TRISSIFVIM VTSAIGTLLP
         60         70         80         90        100
LLSSKYSFIR LPPMVYFICK YFGSGVIVAT AFIHLLEPAA DSLGNKCLTG
        110        120        130        140        150
PITEYPWAFG ICLMTLFLLF FFELLAYQGI DRKIAKESQL DNQGPHTHSH
        160        170        180        190        200
FGDASMYVKK DDEEEDLENQ NEKQADANPY PSHFAHAQEH QDPDVMGTTV
        210        220        230        240        250
NDQSKEQYYG QLLGVFVLEF GVMFHSVFIG LALAVSGDEF KSLYIVLVFH
        260        270        280        290        300
QMFEGLGLGT RIATTNWARH RYTPWILAIC YTLCTPIAIA VGLGVRKSYP
        310        320        330        340        350
PGSRRALITN GVFDSISAGI LLYTGIVELM AHEFLYSGEF KGPGGFKNML
        360        370
LAYFVMCWGA GLMALLGKWA
```

Scheme 5.1 - Amino acid sequence of Zrt2 from *C. albicans*.

5.2 Experimental Procedures

Analyses performed on the above mentioned peptides follow the scheme:

- Potentiometric determination of ligand protonation and Zn(II) and Cu(II) complex-formation constants.
- Spectrophotometric (UV-Vis and CD) analyses of Cu(II) complexes.
- Far-UV CD spectroscopy to investigate the structural conformations of apo-peptides, Cu(II) and Zn(II) complexes.

The employed experimental conditions, instruments and materials are reported in details below, in Bellotti *et al.*, 2019.[4] Peptides have been purchased and used without further purification.

5.3 Results and discussion

Analogously to previous discussed systems (see Chapters 3 and 4), by means of titrimetric and spectrophotometric techniques the speciation models for the studied peptides have been obtained (L1: Ac-GPHTHSHFGD-Am, L2: Ac-GPHTHAHFGD-Am, L3: Ac-PSHFAHAQEHQDP-Am, L4: Ac-PAHFAHAQEHQDP-Am and L5: Ac-DDEEEDLE-Am): the protonation constants are reported in **Table 5.1**, while the complex-formation constants are reported in **Table 5.2** together with the most probable coordination environment for the formed species.

Table 5.1 - Protonation constants for all the investigated ligands at T=298 K and I=0.1 M (KCl). Values in parentheses are standard deviations on the last significant figure.

	log*β*	**log*K***	**log*β***	**log*K***	**log*β***	**log*K***	**log*β***	**log*K***	**log*β***	**log*K***
	L1		**L2**		**L3**		**L4**		**L5**	
HL	6.96(4)	6.96	6.96(4)	6.96	7.39(4)	7.39	7.34(5)	7.34	5.92(4)	5.92
H_2L	13.32(3)	6.36	13.32(3)	6.36	13.90(3)	6.50	13.87(3)	6.53	11.15(3)	5.23
H_3L	18.71(4)	5.39	18.87(4)	5.55	19.79(4)	5.89	19.66(4)	5.79	15.95(6)	4.80
H_4L	21.71(4)	3.00	22.79(4)	3.92	24.08(4)	4.28	23.87(5)	4.21	20.55(3)	4.60
H_5L	-	-	-	-	27.23(4)	3.15	26.73(5)	2.86	24.45(5)	3.90
H_6L	-	-	-	-	-	-	-	-	28.28(3)	3.83
H_7L	-	-	-	-	-	-	-	-	31.01(3)	-

As already widely discussed in the previous chapters, both the equilibrium constants and the spectroscopic data from UV-Vis and CD measurements can help defining the most probable coordination mode for the Cu(II) ion. The observed wavelength of maximum absorption at a given pH value (corresponding to the conditions at which a selected species reaches its maximum of formation in solution) can be compared with the expected theoretical λ_{max} value obtained from literature.[5-7] From UV-Vis spectra of the native peptides Ac-GPHTHSHFGD-Am and Ac-PSHFAHAQEHQDP-Am (**Figures 5.1a** and **5.2a** respectively) it is possible to clearly distinguish the gradual shift of the λ_{max} value towards higher energies (blue-shift) with the increase of the pH. This trend is obtained with all the studied peptides and agrees with the hypothesis that, moving to alkaline conditions, a general increase of the number of coordinated nitrogen atoms is observed. The acidic residues (Asp and Glu) present in the peptide sequences may also participate in the coordination at acidic pH, however the employed experimental techniques leave this point questionable. The Cu(II) coordination to the backbone amides likely begins at around pH 6–6.5 in the case of Ac-GPHTHSHFGD-Am, and around pH 7–7.5 in the case of Ac-PSHFAHAQEHQDP-Am.

Table 5.2 - Equilibrium constants and proposed coordination modes for Cu(II) and Zn(II) complexes at T=298 K and I=0.1 M (KCl). Values in parentheses are standard deviations on the last significant figure.

Species	logβ	pK_a	Coord.	logβ	pK_a	Coord.
	Ac-GPHTHSHFGD-Am			**Ac-GPHTHAHFGD-Am**		
$[CuH_2L]^{3+}$	-	-	-	17.68(3)	4.27	N_{Im}, COO^-
$[CuHL]^{2+}$	13.21(2)	5.13	$2N_{Im}$	13.42(1)	5.32	$2N_{Im}$, COO^-
$[CuL]^{+}$	8.08(2)	6.85	$3N_{Im}$	8.10(2)	7.05	$3N_{Im}$
$[CuH_{-1}L]$	1.22(4)	6.99	$3N_{Im}$, N^-	1.05(3)	7.27	$3N_{Im}$, N^-
$[CuH_{-2}L]^{-}$	-5.77(3)	9.53	$2N_{Im}$, $2N^-$	-6.22(2)	9.80	$2N_{Im}$, $2N^-$
$[CuH_{-3}L]^{2-}$	-15.30(4)	-	N_{Im}, $3N^-$	-16.02(3)	-	N_{Im}, $3N^-$
	Ac-PSHFAHAQEHQDP-Am			**Ac-PAHFAHAQEHQDP-Am**		
$[CuH_2L]^{2+}$	18.45(3)	4.71	N_{Im} (COO^-)	18.36(3)	4.64	N_{Im} (COO^-)
$[CuHL]^{+}$	13.74(2)	5.46	$2N_{Im}$	13.72(2)	5.33	$2N_{Im}$
[CuL]	8.27(2)		$3N_{Im}$	8.39(2)		$3N_{Im}$
$[CuH_{-2}L]^{2-}$	-6.96(2)	8.61	$2N_{Im}$, $2N^-$	-6.91(2)	8.34	$2N_{Im}$, $2N^-$
$[CuH_{-3}L]^{3-}$	-15.57(3)		N_{Im}, $3N^-$	-15.25(3)		N_{Im}, $3N^-$
	Ac-DDEEEDLE-Am					
$[CuH_4L]^{-}$	23.78(6)	-				
$[CuH_2L]^{3-}$	14.94(5)	5.10				
$[CuHL]^{4-}$	9.84(5)	6.04				
$[CuL]^{5-}$	3.81(6)	-				
$[CuH_{-2}L]^{7-}$	-13.6(1)	-				
	Ac-GPHTHSHFGD-Am			**Ac-GPHTHAHFGD-Am**		
$[ZnHL]^{2+}$	10.48(9)	5.48	$2N_{Im}$ (COO^-)	10.71(4)	5.54	$2N_{Im}$ (COO^-)
$[ZnL]^{+}$	5.00(2)	7.51	$3N_{Im}$	5.17(1)	7.44	$3N_{Im}$
$[ZnH_{-1}L]$	-2.51(4)	9.78	$3N_{Im}$	-2.27(2)	9.43	$3N_{Im}$
$[ZnH_{-2}L]^{-}$	-12.29(5)		$3N_{Im}$	-11.69(3)		$3N_{Im}$
	Ac-PSHFAHAQEHQDP-Am			**Ac-PAHFAHAQEHQDP-Am**		
$[ZnH_2L]^{2+}$	-	-	-	17.1(1)	5.75	N_{Im} (COO^-)
$[ZnHL]^{+}$	11.22(5)	6.03	$2N_{Im}$ (COO^-)	11.36(6)	5.90	$2N_{Im}$ (COO^-)
[ZnL]	5.19(2)	8.04	$3N_{Im}$	5.46(4)	8.02	$3N_{Im}$
$[ZnH_{-1}L]^{-}$	-2.85(3)	9.69	$3N_{Im}$	-2.56(5)	9.82	$3N_{Im}$
$[ZnH_{-2}L]^{2-}$	-12.54(5)		$3N_{Im}$	-12.38(7)		$3N_{Im}$
	Ac-DDEEEDLE-Am					
$[ZnH_2L]^{3-}$	14.4(1)	-				
$[ZnL]^{5-}$	3.6(1)	7.45				
$[ZnH_{-1}L]^{6-}$	-3.9(1)	8.24				
$[ZnH_{-2}L]^{7-}$	-12.2(1)	-				

This is confirmed by the obtained circular dichroism spectra (**Figures 5.1b** and **5.2b**), where the increase of CD signals intensity can be ascribed to the formation of Cu(II)–amide bonds. According to the proposed speciation model and to the species distribution diagrams, $[CuH_{-1}L]$, $[CuH_{-2}L]$ and $[CuH_{-3}L]$ (charges omitted) are the most abundant species found above physiological pH and display a coordination sphere with up to three deprotonated amides located in the equatorial plane of the complex.

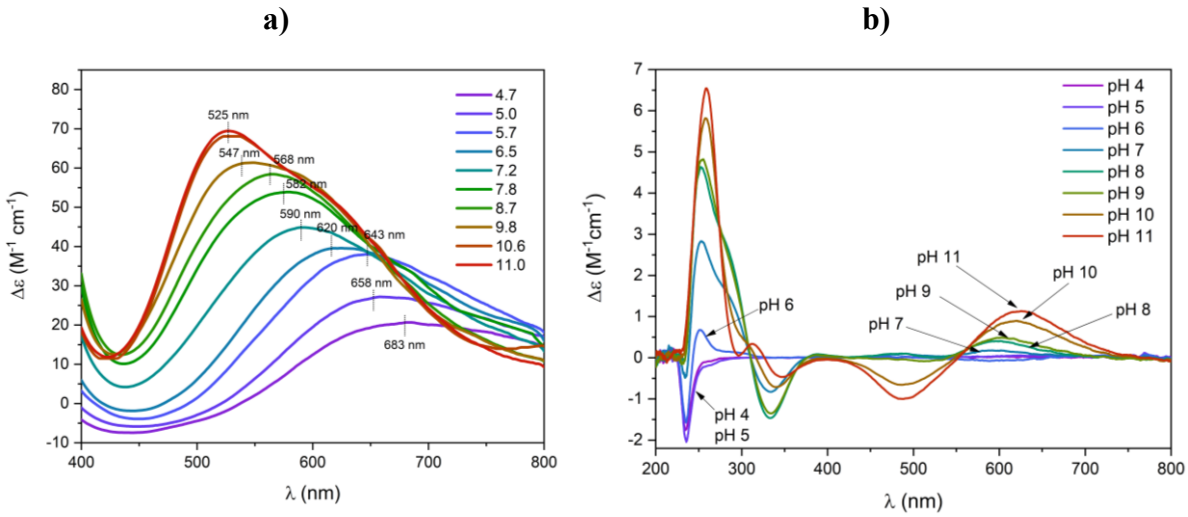

Figure 5.1 - (a)Vis absorption spectra, (b) CD spectra of Cu(II)/Ac-GPHTHSHFGD-Am system; M:L ratio 0.9:1. $C_M = 0.63 \cdot 10^{-3}$ M, optical path 1 cm.

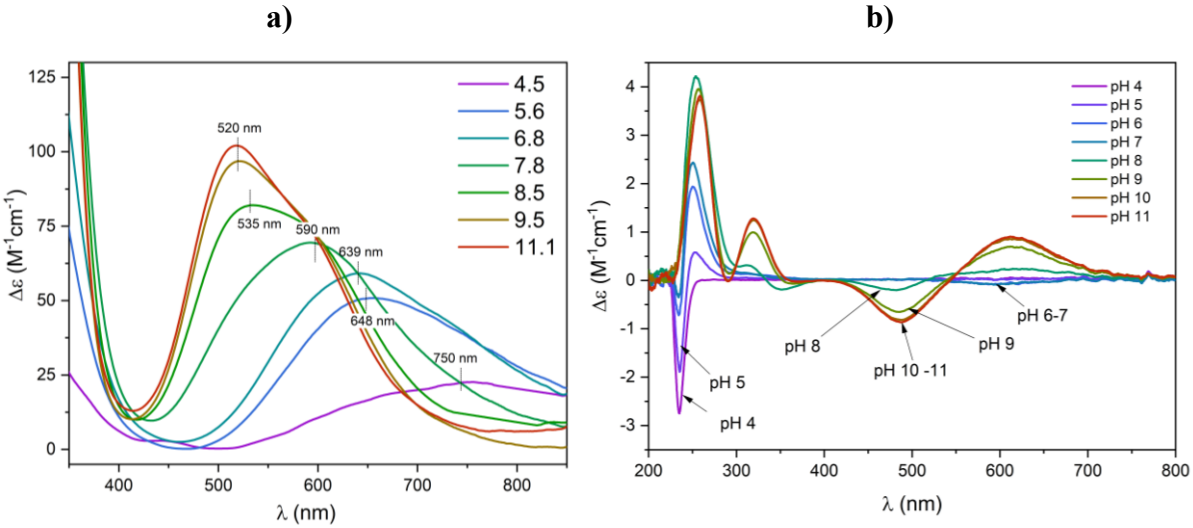

Figure 5.2 - (a)Vis absorption spectra, (b) CD spectra of Cu(II)/Ac-PSHFAHAQEHQDP-Am system; M:L ratio 0.9:1. $C_M = 0.63 \cdot 10^{-3}$ M, optical path 1 cm.

Interestingly, in the case of ligand Ac-DDEEEDLE-Am, the obtained spectroscopic data suggest that, after the anchor to the carboxylic moieties of the peptide, the Cu(II) ion interacts with the backbone amides at pH > 10 (**Figure 5.3**). Moreover, in this system copper hydroxo species are present in solution in large extent, dominating in the alkaline pH range.

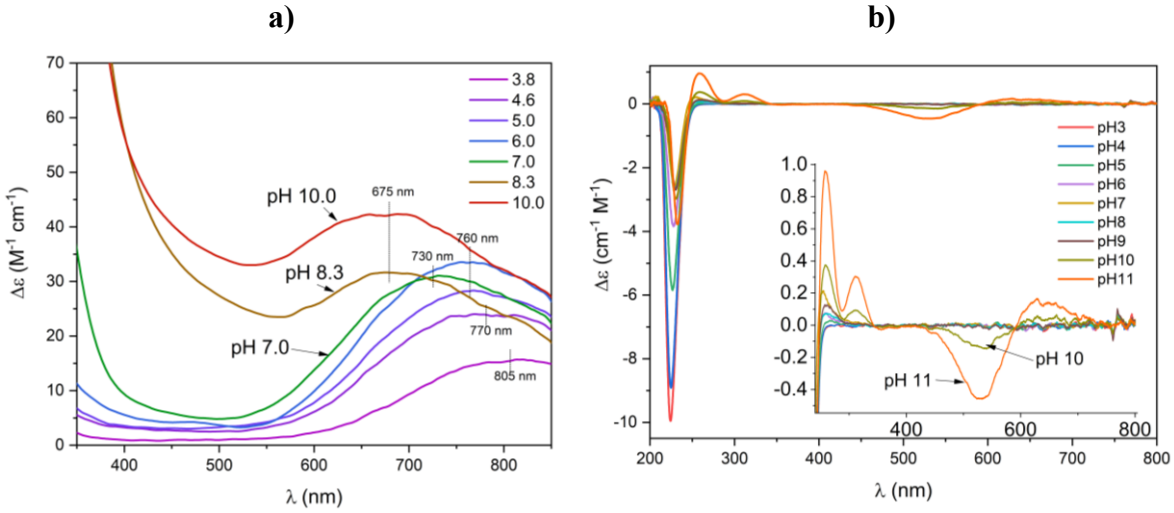

Figure 5.3 - (a)Vis absorption spectra, (b) CD spectra of Cu(II)/Ac-DDEEEDLE-Am system; M:L ratio 0.9:1. $C_M = 0.56 \cdot 10^{-3}$ M, optical path 1 cm.

In the case of zinc complexes, a tetrahedral coordination geometry is expected where up to three imidazole nitrogens belonging to the His residues participate in the complexation, forming ($3N_{Im}$, O) species where the oxygen atom may be a carboxylic O^- or may belong to a coordinated water molecule. Alternatively, in the case of ligand Ac-DDEEEDLE-Am the coordination sphere exclusively involves the carboxylic side chains of Asp and Glu. Hydrolysis steps are then observed at alkaline pH values.

The Ser-to-Ala substitution does not incisively affect the coordination properties of the peptide analogues Ac-GPHTHAHFGD-Am and Ac-PAHFAHAQEHQDP-Am and the above considerations remain valid also for those systems. Nonetheless, the role played by the serine residue in metal complexation can be qualitatively evaluated by means of a competition diagram where each couple of analogues is considered. In the case of Ac-GPHTHSHFGD-Am and Ac-GPHTHAHFGD-Am, the presence of the serine stabilizes copper complexes above pH 6.5, *i.e.* when the metal ion begins to interact with backbone amides. Although this behaviour is not fully elucidated, it quite frequently occurs in Cu(II) complexes with peptides, and it is also verified by the other systems studied in this thesis. Apparently, the only exception (in this PhD work) is represented by the two analogues Ac-PSHFAHAQEHQDP-Am and Ac-PAHFAHAQEHQDP-Am, where this serine-associated trend is not respected. One can hypothesise that, in this case, the coordinated amides are mainly located to the C-terminal portion of the peptide, rather far away from the serine in position 2, and therefore they are not affected by the electrostatic effect of the serine.

5.4 Conclusions

The zinc transporter Zrt2 possesses three possible metal binding sites located at the extramembrane loop between amino acid residues 140 and 200. The corresponding three studied peptides have proved excellent ligands for Zn(II) and Cu(II) ions, although from these preliminary results they are not expected to equally contribute to the metal binding. In fact, according to the obtained competition diagrams (**Figure 5.4**), which have been calculated on the basis of the thermodynamic constants of each binary system, in the native Zrt2 protein the peptide Ac-GPHTHSHFGD-Am should exhibit the highest metal binding affinity. It contains three alternated histidines separated by only one residue (-HxHxH-).

On the other hand, Ac-PSHFAHAQEHQDP-Am contains three histidines separated by two and three residues (-HxxHxxxH-), respectively. The alternated sequence of Ac-GPHTHSHFGD-Am is confirmed to be more effective. It is also worth noting that the peptide Ac-DDEEEDLE-Am is the most efficient ligand at pH lower than 5–5.5 and therefore it may play a crucial role in metal acquisition under the most acidic conditions. Taking into account that Zrt2 is essential for *C. albicans* growth at acidic pH, the different metal binding affinities displayed by the studied peptide sequences may somehow modulate the protein activity in a wider pH range, being indispensable for ensuring the metal transfer inside the pathogenic cell.

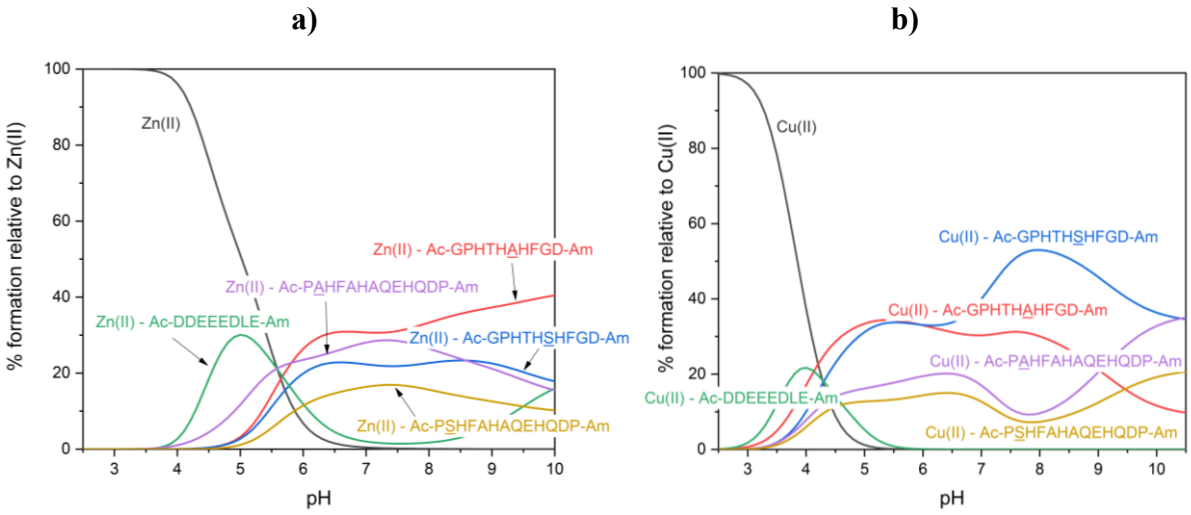

Figure 5.4 - Competition plots for a solution containing equimolar concentrations ($1 \cdot 10^{-3}$ M) of Ac-GPHTHSHFGD-Am, Ac-GPHTHAHFGD-Am, Ac-PSHFAHAQEHQDP-Am, Ac-PAHFAHAQEHQDP-Am and Ac-DDEEEDLE-Am. (a) Zn(II); (b) Cu(II).

5.5 References

[1] L. A. Kelley, S. Mezulis, C. M. Yates, M. N. Wass, M. J. E. Sternberg, *Nat. Protoc.* **2015**, *10(6)*, 845-858.

[2] D. Bellotti, D. Łoboda, M. Rowińska-Żyrek, M. Remelli, *New J. Chem.* **2018**, *42(10)*, 8123-8130.

[3] D. Bellotti, M. Rowińska-Żyrek, M. Remelli, *Dalton Trans.* **2020**, *49(27)*, 9393-9403.

[4] D. Bellotti, C. Tocchio, R. Guerrini, M. Rowińska-Żyrek, M. Remelli, *Metallomics* **2019**, *11(12)*, 1988-1998.

[5] E. Prenesti, P. G. Daniele, M. Prencipe, G. Ostacoli, *Polyhedron* **1999**, *18(25)*, 3233-3241.

[6] P. G. Daniele, E. Prenesti, G. Ostacoli, *Dalton Trans.* **1996***(15)*, 3269-3275.

[7] H. Sigel, R. B. Martin, *Chem. Rev.* **1982**, *82(4)*, 385-426.

6. Chapter Six: Calcitermin antimicrobial peptide

6.1 Outline of the work

Among several uncharacterized molecules that contribute to the overall antimicrobial activity of human nasal fluid, a 15-residue antimicrobial peptide named calcitermin has been recently identified. Its sequence (VAIALKAAHYHTHKE) exactly corresponds to the C-terminal domain of calgranulin C, a pro-inflammatory protein of the S100 family.[1] Several studies have reported that cleavage fragments of parent proteins have potent antimicrobial activity (*e.g.* buforin I,[2] lactoferricin,[3] KDAMP,[4] vasostatin-1 [5]). While calcitermin did not express any antimicrobial activity in phosphate buffer at pH 7.4, under more acidic conditions (pH 5.4) – which are quite common in biological fluids during inflammation – it proved active against *E. coli*, *P. aeruginosa* and *C. albicans*. Furthermore, it was demonstrated that the presence of micromolar concentrations of Zn(II) enhances its antimicrobial activity against *E. coli* and *L. monocytogenes*.

Calcitermin contains a putative metal-binding domain with three alternated histidine residues in position 9, 11 and 13, and the free terminal amino and carboxylic groups. In addition, it has the potential to adopt a helical conformation in membranes. The above results prompted us to deeply investigate the complex-formation equilibria of calcitermin with Zn(II) and Cu(II) ions. The unprotected wild-type peptide VAIALKAAHYHTHKE (WT) has been considered, along with its three mutants, in which each His residue is replaced with one alanine (Ala-scan strategy): VAIALKAAAYHTHKE (H9A), VAIALKAAHYATHKE (H11A), VAIALKAAHYHTAKE (H13A). The comparison among the behaviours of the different analogues helps to shed light on the role played by each His residue in metal coordination and complex stability and on the impact of the formed complexes on antimicrobial activity.

6.2 Experimental procedure

Analyses performed on the above mentioned peptides follow the scheme:

- Peptide synthesis by means of solid-phase technique.
- Potentiometric determination of ligand protonation and Zn(II) and Cu(II) complex-formation constants.
- Mass spectrometric analysis to evaluate ligand purity and the stoichiometry of the formed Zn(II) and Cu(II) complexes.
- Spectrophotometric (UV-Vis and CD) analyses of Cu(II) complexes.
- Far-UV CD spectroscopy to investigate the structural conformations of apo-peptides, Cu(II) and Zn(II) complexes.
- NMR measurements of apo-peptides, Zn(II) complexes and Cu(II) complexes.
- Antimicrobial activity tests of apo-peptides, Zn(II) complexes and Cu(II) complexes, carried out in collaboration with Wrocław Medical University.

The employed experimental conditions, instruments and materials are reported in details below, in Bellotti *et al.*, 2019.[6]

6.3 Results and discussion

The present study shows that calcitermin is a very good chelator for both Cu(II) and Zn(II) ions. Wild type calcitermin (WT = VAIALKAAHYHTHKE) contains nine groups involved in acid-base reactions: two lysines (K), one tyrosine (Y), the amino-terminus, three histidines (H), one glutamic acid side chain (E) and the carboxylic-terminus. The three peptide mutants H9A, H11A, H13A lack one His residue, which has been substituted by one alanine in position 9, 11 and 13, respectively. As a general trend, Cu(II) coordination occurs with the progressive binding of the available histidine residues (except for H11A where only His13 binds the ion), followed by the interaction with the terminal free amino group and the further deprotonation and coordination of three backbone N-amides, which gradually substitute the donor groups in the equatorial plane of Cu(II) complexes (**Table 6.1**). A comparison between the obtained thermodynamic constants for copper complexes and for ligands protonation, together with the absence of changes in the Vis absorption and CD spectra at alkaline pH values, suggested that tyrosil-O^- and the two lysil ε-NH_2 groups do not participate in the metal complexation with all the investigated peptides. Spectroscopic data are in good agreement with the proposed speciation models; in fact, with the increase of pH, a blue-shift of Vis spectra is observed (**Figure 6.1a**), suggesting the increase of the number of coordinated nitrogen atoms. Considering the wild-type system WT as an example, the wavelength of maximum absorption shifts from 800 nm at pH 3.0, corresponding to the $[Cu(H_2O)_6]^{2+}$ species, to 612 nm at pH 6.3, where the $[CuH_4L]^{3+}$ complex reaches almost 60% of formation, supporting the hypothesis of a ($3N_{Im}$) coordination (expected λ_{max} = 625 nm[7]) with a distorted octahedral geometry. Moving to alkaline conditions, the wavelengths shift continues due to the formation of 4N complexes with all the studied peptides. Under physiological and alkaline conditions, the binding of a larger number of N-amides is also confirmed by the increased intensity of the CD signals (**Figure 6.1b**).[8]

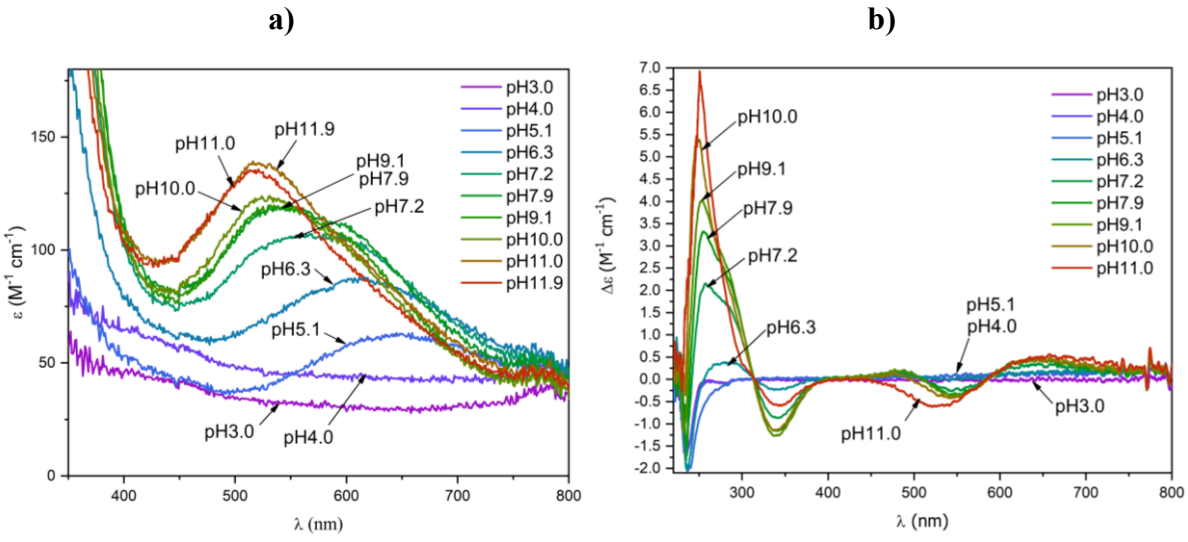

Figure 6.1 - (a) Vis absorption spectra, (b) CD spectra of Cu(II)/WT system; M:L ratio = 0.9:1; $C_M = 0.4 \cdot 10^{-3}$ M, optical path 1 cm.

Table 6.1 - Equilibrium constants and proposed coordination modes for Cu(II) and Zn(II) complexes at T=298 K and I=0.1 M ($NaClO_4$). Values in parentheses are standard deviations on the last significant figure.

Species	logβ	pK_a	Coord.	logβ	pK_a	Coord.
	WT			**H9A**		
$[CuH_7L]^{6+}$	62.6(1)	3.9	N_{Im}	-	-	-
$[CuH_6L]^{5+}$	58.69(3)	4.90	$2N_{Im}$	56.72(6)	4.51	N_{Im}
$[CuH_5L]^{4+}$	53.79(3)	5.94	$3N_{Im}$	52.21(3)	5.66	$2N_{Im}$
$[CuH_4L]^{3+}$	47.85(3)	6.95	$3N_{Im}$	46.55(4)	7.25	$2N_{Im}$
$[CuH_3L]^{2+}$	40.90(4)	7.40	$3N_{Im}$, NH_2	39.30(5)	7.62	$2N_{Im}$, NH_2
$[CuH_2L]^{+}$	33.50(4)	8.88	$2N_{Im}$, NH_2, N^-	31.68(5)	8.87	$2N_{Im}$, NH_2, N^-
[CuHL]	24.62(5)	9.74	$2N_{Im}$, $2N^-$	22.81(6)	9.64	$2N_{Im}$, NH_2, N^-
$[CuL]^{-}$	14.88(5)	10.16	$2N_{Im}$, $2N^-$	13.18(6)	9.84	N_{Im}, NH_2, $2N^-$
$[CuH_{-1}L]^{2-}$	4.72(5)	-	N_{Im}, $3N^-$	3.33(5)	-	NH_2, $3N^-$
$[CuH_{-3}L]^{4-}$	-16.71(8)	-	N_{Im}, $3N^-$	-18.01(6)	-	NH_2, $3N^-$
	H11A			**H13A**		
$[CuH_6L]^{5+}$	55.71(6)	5.35	N_{Im}	-	-	-
$[CuH_5L]^{4+}$	50.37(5)	6.55	N_{Im}	51.82(1)	5.74	$2N_{Im}$ or N_{Im}, NH_2
$[CuH_4L]^{3+}$	43.82(6)	7.53	N_{Im}, N^-	46.08(2)	6.70	$2N_{Im}$ or N_{Im}, NH_2
$[CuH_3L]^{2+}$	36.28(7)	8.71	N_{Im}, N^-	39.38(2)	7.97	$2N_{Im}$, NH_2
$[CuH_2L]^{+}$	27.57(7)	9.17	N_{Im}, NH_2, N^-	31.41(3)	9.75	$2N_{Im}$, NH_2, N^-
[CuHL]	18.40(7)	10.18	N_{Im}, NH_2, N^-	21.66(4)	10.21	$2N_{Im}$, NH_2, N^-
$[CuL]^{-}$	8.22(9)	10.23	N_{Im}, NH_2, $2N^-$	11.45(4)	10.93	$2N_{Im}$, $2N^-$
$[CuH_{-1}L]^{2-}$	-2.01(7)	-	NH_2, $3N^-$	0.52(7)	-	N_{Im}, $3N^-$
$[CuH_{-3}L]^{4-}$	-24.19(8)	-	NH_2, $3N^-$	-21.8(1)	-	N_{Im}, $3N^-$
	WT			**H9A**		
$[ZnH_5L]^{4+}$	51.02(5)	6.47	$2N_{Im}$, COO^-	-	-	-
$[ZnH_4L]^{3+}$	44.55(7)	7.00	$3N_{Im}$, COO^-	42.80(6)	7.82	$2N_{Im}$
$[ZnH_3L]^{2+}$	37.55(8)	7.52	$3N_{Im}$ (COO^-)	34.88(8)	8.78	$2N_{Im}$
$[ZnH_2L]^{+}$	30.03(7)	8.31	$3N_{Im}$	26.20(1)	8.81	$2N_{Im}$
[ZnHL]	21.72(7)	-	$3N_{Im}$	17.39(8)	-	$2N_{Im}$
$[ZnH_{-1}L]^{2-}$	3.5(1)	-	$3N_{Im}$	-2.6(1)	-	$2N_{Im}$
	H11A			**H13A**		
$[ZnH_5L]^{4+}$	48.4(1)	6.24	N_{Im}, COO^-	49.44(4)	6.22	N_{Im}
$[ZnH_4L]^{3+}$	42.14(4)	7.56	$2N_{Im}$, COO^-	43.23(3)	-	$2N_{Im}$
$[ZnH_3L]^{2+}$	34.58(5)	8.25	$2N_{Im}$ (COO^-)	-	-	$2N_{Im}$
$[ZnH_2L]^{+}$	26.32(6)	8.70	$2N_{Im}$	27.24(5)	-	$2N_{Im}$
[ZnHL]	17.62(6)	9.70	$2N_{Im}$	-	-	-
$[ZnL]^{-}$	7.9(1)	9.94	$2N_{Im}$	-	-	-
$[ZnH_{-1}L]^{2-}$	-2.02(9)	-	$2N_{Im}$	-	-	-

As for zinc complexes, the metal coordination is very similar with all the four ligands: Zn(II) binding occurs by means of all the available histidine residues, giving rise to tetrahedral complexes. The N-terminus, the tyrosine and the two lysine residues are not involved in complexes formation. Furthermore, approaching the physiological/alkaline pH, the deprotonation of a coordinated water molecule leads to the formation of monohydroxo species with all the investigated peptides (**Table 6.1**).

The metal coordination modes at physiological pH are unambiguously confirmed by NMR spectra, where distinct changes can be observed after the addition of Cu(II) or Zn(II): *(i)* broadening of the signals assigned to specific His residues H_δ-H_ε correlations, confirming their participation in coordination, *(ii)* the shift of valine H_α-H_γ and H_β-H_γ correlations, which is likely related to the involvement of terminal amine in the metal coordination sphere (**Figure 6.2**), and *(iii)* the variation of the signals assigned to carboxylic moieties, corresponding to the Glu or C-terminus binding to the metal ion (the involvement of the C-terminal carboxyl group, instead of the Glu side chain carboxylate, although less likely, cannot be excluded, since it would also affect the H_α correlations of the C-terminal Glu). By means of NMR spectra and Ala-scan strategy it has been possible to elucidate the role of each histidine in metal coordination: at physiological pH all the available His residues are bound to the metal ion, except for Cu(II)-H11A system, where only His in position 13 participates in the complexation, probably due to less hindered surroundings.

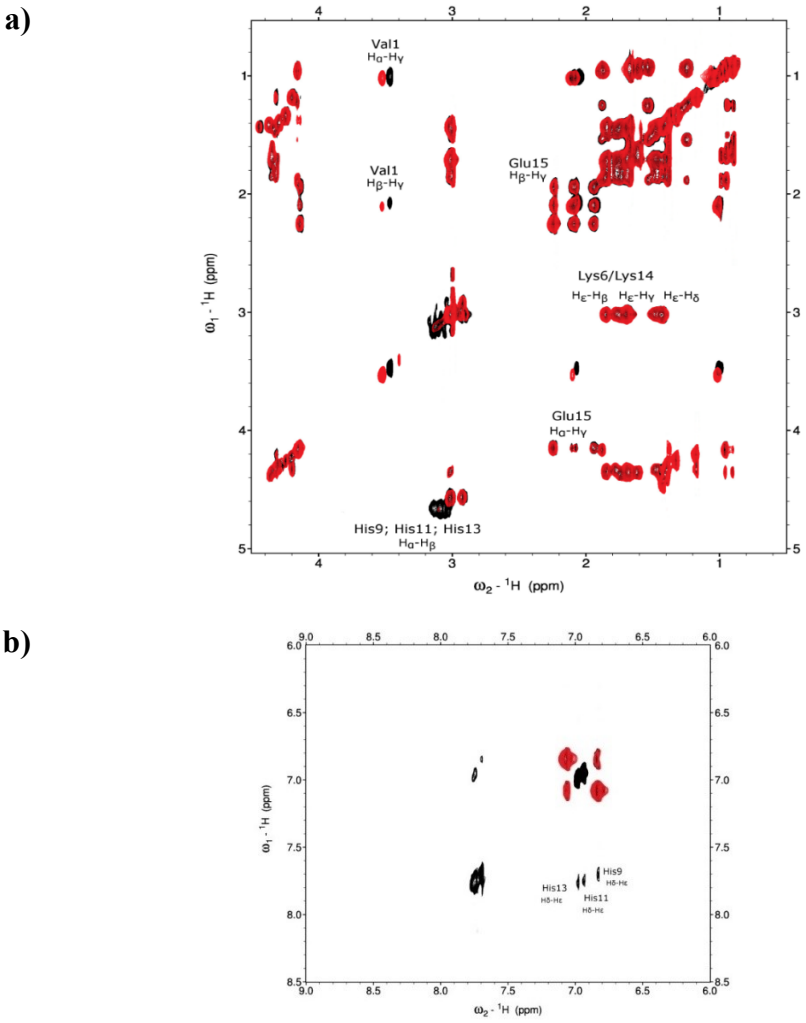

Figure 6.2 - (a) Aliphatic and (b) aromatic region of ^{1}H-^{1}H TOCSY NMR spectra for wild-type calcitermin, $C_L = 3 \cdot 10^{-3}$ M, pH 7.4, $T = 298$ K, in the absence (black) and in the presence (red) of 1 equivalent of Cu(II).

His-to-Ala substitutions have a significant effect on both the thermodynamic stability and the structure of the metal complexes. As expected, the increased number of histidines makes the coordination of both the metals more effective. In fact, the most remarkable differences in binding affinity between calcitermin and its mutants occur from pH 5.5 in the case of Zn(II), and pH 4.5 in the case of Cu(II), *i.e.* when the third histidine residue of WT calcitermin comes into play (**Figure 6.3**). There is no preferred Cu(II) binding site in calcitermin: the stabilities of the complexes with H9A and H13A are almost identical. H11A mutant – where two histidines are separated by three amino acids – displays the lower affinity for Cu(II) and in its complexes only one His residue is involved in binding (**Table 6.1**): clearly the coordination His-Xxx-His is preferred to His-$(Xxx)_3$-His. As for Zn(II) complexes, the higher stability of the species formed by H13A, with respect to those formed by H9A and H11A, suggests a pivotal role of His9 and His11 in zinc complexation. It is also noteworthy that the coordination of Zn(II) to the glutamic acid side chain of H11A mutant is not reflected by an increased stability of the complex.

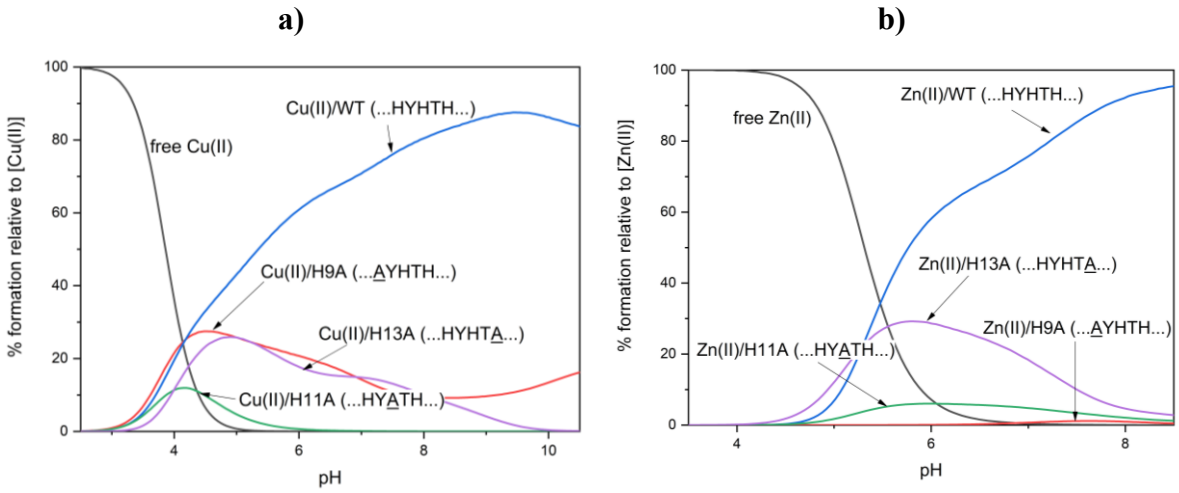

Figure 6.3 - Competition plots for a solution containing equimolar concentrations ($1 \cdot 10^{-3}$ M) of metal ion, WT calcitermin, H9A, H11A and H13A. (a) Cu(II); (b) Zn(II).

All compounds were tested for their antimicrobial activity against a representative panel of pathogenic organisms: *Pseudomonas aeruginosa 15442*, *Klebsiella pneumoniae 13883*, *Escherichia coli 25922*, *Staphylococcus aureus 29213*, *Enterococcus faecalis 29212* and *Candida albicans 10231*. The minimal inhibitory concentration (MIC) has been determined for free ligand and metal complexes at pH 5.4 (**Table 6.2**). Only WT and the three Zn(II) complex systems with H9A, H11A and H13A are effective against Gram-negative species (MIC=128 μg/ml), although their activity is lower than against Gram-positive bacteria. The most promising MIC values have been obtained for H13A, H13A/Cu(II) and H11A/Zn(II) (MIC = 4 μg/ml) and for H13A/Zn(II) (MIC = 0.5 μg/ml) against *E. faecalis*. Relevant MIC values were also detected against *S. aureus* for all the H13A systems (0.25 μg/ml). Activity against *C. albicans* has been also detected, in particular for WT and H9A metal complexes (MIC = 0.25–2 μg/ml). At pH 7.4, none of the analysed systems showed any antimicrobial activity.

In order to better understand the mechanism of action of calcitermin and of its His-to-Ala mutants **Table 6.3** has been produced: it highlights differences between each system at acidic and physiological pH in terms of their binding ability. The calculated dissociation constant (K_d) refers to the hypothetical general equilibrium: M + L = ML, where the

protonation of both the ligand and the complex are not explicitly considered. The pM value is the negative logarithm of the concentration of the free metal ion (pCu or pZn in the present case) under given experimental conditions, here $[L]_{total} = 10^{-5}$ M and $[M]_{total} = 10^{-6}$ M, at pH 7.4 or 5.4.

Table 6.2 - *In vitro* antimicrobial activity of WT, H9A, H11A, H13A expressed as a minimal inhibitory concentration (μg/ml), at pH = 5.4.

Strain	*C. albicans*	*E. faecalis*	*S. aureus*	*E. coli*	*K. pneumoniae*	*P. aeruginosa*
WT	n/d	n/d	**128**	n/d	**128**	n/d
WT-Cu(II)	**1**	n/d	**128**	n/d	n/d	n/d
WT-Zn(II)	**1**	n/d	n/d	n/d	n/d	n/d
H9A	**1**	n/d	n/d	n/d	n/d	n/d
H9A- Cu(II)	**2**	**128**	n/d	n/d	n/d	n/d
H9A- Zn(II)	**0.25**	n/d	**64**	n/d	n/d	**128**
H11A	n/d	**64**	n/d	n/d	n/d	n/d
H11A Cu(II)	n/d	**32**	**64**	n/d	n/d	n/d
H11A-Zn(II)	n/d	**4**	n/d	n/d	**128**	n/d
H13A	n/d	**4**	**0.25**	n/d	n/d	n/d
H13A Cu(II)	n/d	**4**	**0.25**	n/d	n/d	n/d
H13A-Zn(II)	**128**	**0.5**	**0.25**	n/d	n/d	**128**

*n/d- not determined

Table 6.3 - Calculated dissociation constants (K_d/M), pM values and coordination hypotheses for Cu(II) and Zn(II) complexes at pH 5.4 and 7.4.

	pH 5.4			**pH 7.4**		
	Coord. (% of M complexation)	K_d	**pM**	**Coord.**	K_d	**pM**
WT-Cu(II)	$3N_{Im}$ (100%)	$1.16 \cdot 10^{-6}$	6.95	$3N_{Im}$, NH_2	$1.31 \cdot 10^{-10}$	10.83
H9A-Cu(II)	$2N_{Im}$ (97%)	$3.95 \cdot 10^{-6}$	6.53	$2N_{Im}$, NH_2	$3.07 \cdot 10^{-9}$	9.47
H11A-Cu(II)	N_{Im} (84%)	$5.40 \cdot 10^{-5}$	6.07	N_{Im}, NH_2, N^-	$8.15 \cdot 10^{-7}$	7.08
H13A-Cu(II)	$2N_{Im}$ or N_{Im}, NH_2 (94%)	$4.03 \cdot 10^{-6}$	6.52	$2N_{Im}$, NH_2	$2.50 \cdot 10^{-9}$	9.56
WT-Zn(II)	$2N_{Im}$, COO^- (36%)	$1.02 \cdot 10^{-3}$	6.00	$3N_{Im}$, COO^-	$3.07 \cdot 10^{-7}$	7.48
H9A-Zn(II)	$2N_{Im}$ (4%)	$6.08 \cdot 10^{-2}$	6.00	$2N_{Im}$	$4.32 \cdot 10^{-5}$	6.09
H11A-Zn(II)	N_{Im}, COO^- (10%)	$8.60 \cdot 10^{-3}$	6.00	$2N_{Im}$, COO^-	$4.35 \cdot 10^{-5}$	6.10
H13A-Zn(II)	N_{Im} (35%)	$1.24 \cdot 10^{-3}$	6.00	$2N_{Im}$	$1.16 \cdot 10^{-6}$	6.26

It is not straightforward to link the antimicrobial activity of the studied systems with their charge, structure or metal binding mode, although an hypothesis may concern the presence of the non-bound amino terminal group. Far-UV CD measurements in water also revealed a disordered structure for all the systems (ligands and their complexes), while they adopt a helical-like structure in the presence of membrane-mimicking SDS. A further question may arise from the relative competitivness of the two metal ions: can Cu(II) oust Zn(II) in binding to calcitermin? According to the Irving-Williams series the answer looks quite obvious and Cu(II) complexes should be the most favoured, at least under equimolar concentrations. By means of the calculated stability constants, a comparison between zinc and copper systems under physiological concentrations in human lungs (a tenfold excess of Zn(II) over Cu(II)[9]) suggests the predominance of copper/calcitermin complex.[6]

The metal complexation ability of ZinT (see Chapter 3) has been compared with that of calcitermin, since it represents a possible natural competitor and antagonist of ZinT in the host human organism for zinc and copper acquisition. The obtained competition plots (**Figure 6.4)** show that, under acidic conditions, calcitermin binds both Zn(II) and Cu(II) ions with the highest affinity. At such pH values its coordination sphere is very similar to that of ZinT complexes, with a ($3N_{Im}$, O^-) binding mode; however, the alternated His-tag (HxHxH) is confirmed to be an extremely effective binding motif, even with respect to the four histidine sequence HxHHxH of ZinT. Moreover, in the case of zinc, calcitermin almost steadily maintains its efficacy as ligand throughout the explored pH range.

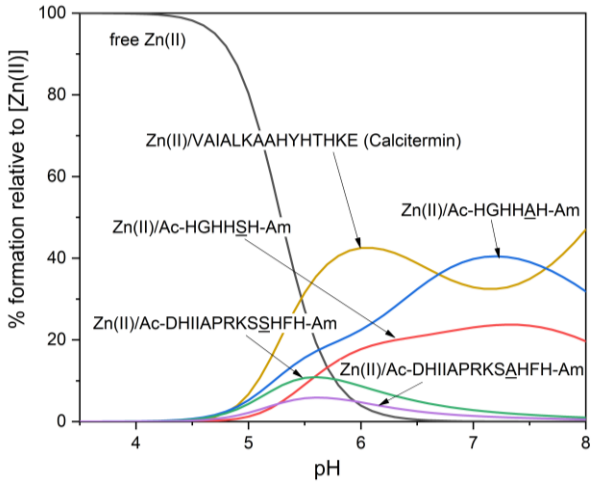

Figure 6.4 - Competition plot for a solution containing equimolar concentrations ($1 \cdot 10^{-3}$ M) of Zn(II), calcitermin and peptides L1, L2, L3 and L4 of ZinT.

6.4 Conclusions

The present work is a comprehensive description of the thermodynamics, structure, coordination chemistry and antimicrobial acitivity of the studied metal-calcitermin complexes. Novel antimicrobial peptides with very promising efficacies are presented: both His-to-Ala substitutions and the presence of metal ions have a significant influence on the antimicrobial activity of the studied systems, in particular, *(i)* Cu(II) and Zn(II) complexes of both wild type calcitermin and H9A mutant are active against fungi (*C. albicans*); *(ii)* mutating His11 and His13 to H11A and H13A, respectively, extinguishes the antifungal activity; *(iii)* relevant antimicrobial effects against Gram-positive bacteria are detected, in particular by the H13A systems against *S. aureus* and *E. faecalis*; *(iv)* no intrinsic activity has been determined against Gram-negative strains for all the analysed

compounds. These outstanding results clearly place calcitermin in a privileged position for further attempts to understand the relationships between antimicrobial peptide-metal coordination, structure, stability, efficacy and mode of action, with the final aim of designing novel effective therapeutics.

This research work includes the publication "D. Bellotti, M. Toniolo, D. Dudek, A. Mikolajczyk, R. Guerrini, A. Matera-Witkiewicz, M. Remelli, M. Rowinska-Zyrek, *Dalton Trans*. 2019, 48(36), 13740-13752".

6.5 References

[1] A. M. Cole, Y.-H. Kim, S. Tahk, T. Hong, P. Weis, A. J. Waring, T. Ganz, *FEBS Lett.* **2001**, *504*, 5-10.

[2] I. Minn, H. S. Kim, S. C. Kim, *Biochimica et Biophysica Acta (BBA) - Molecular Basis of Disease* **1998**, *1407(1)*, 31-39.

[3] K. Yamauchi, M. Tomita, T. J. Giehl, R. T. Ellison, 3rd, *Infect. Immun.* **1993**, *61(2)*, 719-728.

[4] C. Tam, J. J. Mun, D. J. Evans, S. M. J. Fleiszig, *The Journal of clinical investigation* **2012**, *122(10)*, 3665-3677.

[5] K. Lugardon, R. Raffner, Y. Goumon, A. Corti, A. Delmas, P. Bulet, D. Aunis, M. H. Metz-Boutigue, *J. Biol. Chem.* **2000**, *275(15)*, 10745-10753.

[6] D. Bellotti, M. Toniolo, D. Dudek, A. Mikołajczyk, R. Guerrini, A. Matera-Witkiewicz, M. Remelli, M. Rowińska-Żyrek, *Dalton Trans.* **2019**, *48(36)*, 13740-13752.

[7] H. Sigel, R. B. Martin, *Chem. Rev.* **1982**, *82(4)*, 385-426.

[8] H. F. Stanyon, X. Cong, Y. Chen, N. Shahidullah, G. Rossetti, J. Dreyer, G. Papamokos, P. Carloni, J. H. Viles, *The FEBS Journal* **2014**, *281(17)*, 3945-3954.

[9] K. Jensen, in *Peptide and Protein Design for Biopharmaceutical Applications* (Ed.: K. Jensen), John Wiley and Sons Ltd, Chirchester, UK, **2009**, pp. 207-248.

7. Chapter Seven: Hpn protein

7.1 Outline of the work

Nickel is crucial for the virulence of *H. pylori*, whose machinery for the homeostasis of this metal ion is rather complicated. This system includes a small cytoplasmic His-rich protein called Hpn (*Helicobacter pylori* protein with affinity for nickel), which accounts for about 2% of the total synthesized proteins.[1] This protein was initially considered to store Ni(II) in the cell and to alleviate the metal toxicity by sequestering the intracellular excess of metal.[2] Interestingly, it has been observed that, under acidic conditions, Hpn releases the bound nickel and it has been suggested that this allows the protein to supply nickel to the cell when urease activity needs to be stimulated for pH regulation.[3, 4] Recently, it has also been proposed that Hpn interacts with many other proteins to perform various cellular functions connected with the maturation of nickel-containing enzymes, with the recovery of peptides and the acquisition of nitrogen.[5]

Hpn contains 60 amino acids, 28 of which (47%) are histidines[1]), thus it has several domains capable of coordinating metal cations: the poly-histidine sequences in positions 11–17 and 28–33,[6] the two motifs 38–42 and 51–55 encompassing a double cysteine residue (EEGCC),[7] and the amino-terminal sequence (Met-Ala-His-) corresponding to a typical ATCUN motif. Although the first ATCUN sequence play a major role in the Hpn binding ability towards Ni(II), the histidines in positions 4 and 8 can contribute to the stability of the metal complexes by participating in the complexation and forming macrochelated species, or by favouring the formation of bi-nuclear complexes. We therefore compared the affinity for Cu(II), Ni(II) and Zn(II) ions of the wild-type peptide WT (corresponding to the N-terminal domain of Hpn, MAHHEEQHG-Am) with that of its His-to-Ala mutants: MAAHEEQHG-Am (H3A), MAHAEEQHG-Am (H4A), MAHHEEQAG-Am (H8A) and MAHAEEQAG-Am (H4A/H8A). The complex-formation equilibria in condition of Cu(II) excess have also been studied in order to detect the formation of binuclear complexes.

7.2 Experimental procedure

Analyses performed on the above mentioned peptides follow the scheme:

- Peptide synthesis by means of solid-phase technique.
- Potentiometric determination of ligand protonation and Ni(II), Zn(II) and Cu(II) complex-formation constants.
- Mass spectrometry analysis to evaluate ligand purity and the stoichiometry of the formed Ni(II), Zn(II) and Cu(II) complexes.
- Spectrophotometric (UV-Vis and CD) analyses of Ni(II) and Cu(II) complexes.
- EPR measurements of Cu(II) complexes.

The employed experimental conditions, instruments and materials are reported in details below, in Bellotti *et al.*, 2021.[8]

7.3 Results and discussion

With the exception of H3A, all the investigated sequences contain a very efficient Cu(II) and Ni(II) ATCUN-binding site (N_{Im}, NH_2, $2N^-$) which is confirmed to confer great stability to copper and nickel complexes. The presence of additional histidines in position 4 and 8 allows the formation of stable homo- and hetero- binuclear complexes (**Table 7.1**). When Cu(II) and WT are present in solution at a nearly equimolar ratio, six variously protonated mononuclear 1:1 complexes are formed. However, at acidic pH, when "free" Cu(II) ions are still available in solution, a not negligible amount of the binuclear species $[Cu_2H_{-1}L]^+$ is formed (about 12%) (**Figure 7.1a**). On the other hand, in conditions of metal excess, practically only binuclear complexes are formed above pH 5 (**Figure 7.1b**). Spectroscopic data are in good agreement with the proposed speciation model. When M/L molar ratio is about 1:1, a single intense absorption located at 525 nm dominates the UV-Vis spectra. This d-d band is almost entirely attributable to [CuL] and is compatible with the coordination hypothesis (N_{Im}, NH_2, $2N^-$) suggested above (expected λ_{max} = 531 nm). EPR data at pH 5.5 ($g_{//}$ = 2.19, $A_{//}$ = 197.0) agree with a 4N coordination around Cu(II) in the equatorial plane of the complex.[9, 10] This is also confirmed by CD spectra, where the typical double band characteristic of the ATCUN-type coordination was observed.

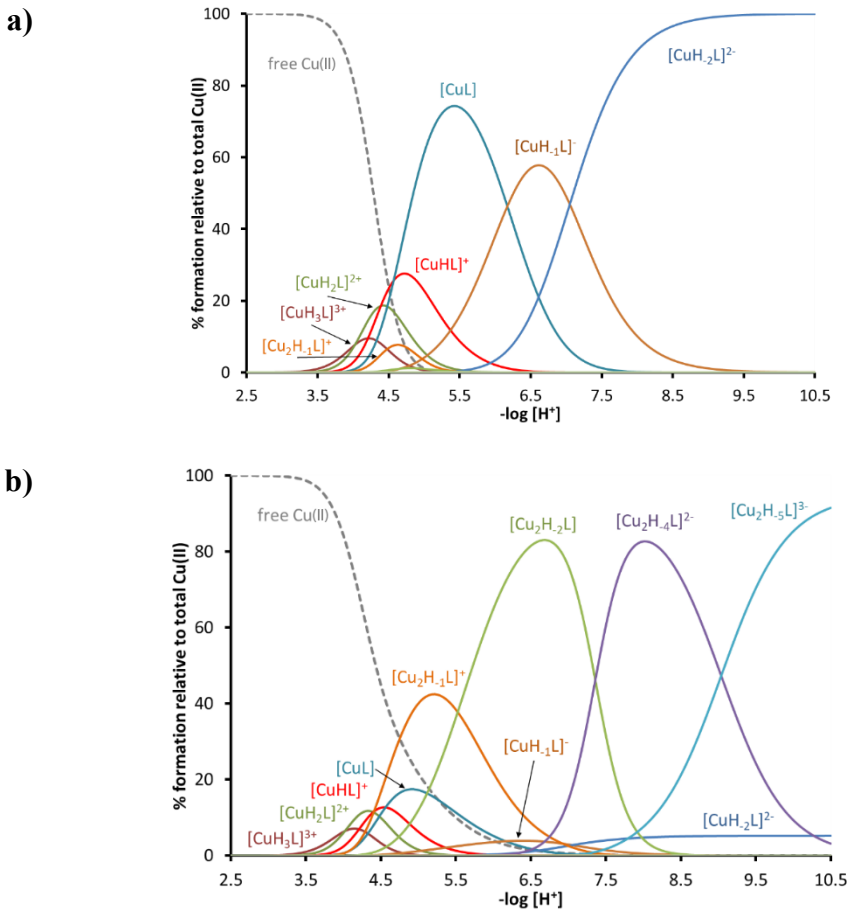

Figure 7.1 - Representative species distribution diagrams for complex-formation of WT with Cu(II), at *T*=298 K and *I*=0.1 M (KCl). C_L=1·10^{-3} M and (a) M/L molar ratio 0.8:1; (b) M/L molar ratio 1.9:1.

Table 7.1 - Equilibrium constants and proposed coordination modes for Cu(II) complexes at T=298 K and I=0.1 M (KCl). Values in parentheses are standard deviations on the last significant figure.

Species	**logβ**	**pK_a**	**Coord.**	**logβ**	**pK_a**	**Coord.**
	WT			**H3A**		
$[CuH_3L]^{3+}$	25.52(8)	4.03	N_{Im} (COO^-)	-	-	-
$[CuH_2L]^{2+}$	21.49(6)	4.39	N_{Im}, NH_2	19.59(3)	4.93	N_{Im}, COO^-
$[CuHL]^{+}$	17.10(5)	4.57	N_{Im}, NH_2, N^-	14.66(2)	5.62	$2N_{Im}$, COO^-
[CuL]	12.53(2)	6.17	N_{Im}, NH_2, $2N^-$	9.04(3)	6.82	N_{Im}, NH_2, COO^-
$[CuH_{-1}L]^{-}$	6.36(3)	7.05	N_{Im}, NH_2, $2N^-$	2.22(4)	7.30	N_{Im}, NH_2, N^-
$[CuH_{-2}L]^{2-}$	-0.69(4)	-	N_{Im}, NH_2, $2N^-$	-5.08(5)	10.14	N_{Im}, NH_2, $2N^-$
$[CuH_{-3}L]^{3-}$	-	-	-	-15.22(7)	-	N_{Im}, $3N^-$
$[Cu_2H_{-1}L]^{+}$	10.98(2)	5.52	(N_{Im}, NH_2, $2N^-$) (N_{Im}, COO^-)	6.76(4)	-	(N_{Im}, NH_2, COO^-) (N_{Im}, N^-)
$[Cu_2H_{-2}L]$	5.46(3)	-	(N_{Im}, NH_2, $2N^-$) ($2N_{Im}$, COO^-)	-	-	-
$[Cu_2H_{-3}L]^{-}$	-	-	-	-6.53(4)	7.68	
$[Cu_2H_{-4}L]^{2-}$	-9.27(3)	9.04	(N_{Im}, NH_2, $2N^-$) ($2N_{Im}$, $2N^-$)	-14.21(6)	9.03	
$[Cu_2H_{-5}L]^{3-}$	-18.31(5)	-	(N_{Im}, NH_2, $2N^-$) ($2N_{Im}$, $3N^-$)	-23.24(7)	11.0	
$[Cu_2H_{-6}L]^{4-}$	-	-	-	-34.2(1)	-	
	H4A			**H8A**		
$[CuH_2L]^{2+}$	-	-	-	19.33(2)	-	N_{Im} (COO^-)
$[CuHL]^{+}$	15.15(3)	4.60	N_{Im}, NH_2	-	-	-
[CuL]	10.55(3)	4.71	N_{Im}, NH_2, N^-	10.55(1)	4.87	N_{Im}, NH_2, N^-
$[CuH_{-1}L]^{-}$	5.84(2)	6.83	N_{Im}, NH_2, $2N^-$	5.68(2)	6.76	N_{Im}, NH_2, $2N^-$
$[CuH_{-2}L]^{2-}$	-0.99(4)	-	N_{Im}, NH_2, $2N^-$	-1.08(4)	-	N_{Im}, NH_2, $2N^-$
$[Cu_2H_{-1}L]^{+}$	8.74(5)	5.76	N_{Im}, NH_2, N^- N_{Im}, COO^-	8.82(5)	5.82	N_{Im}, NH_2, N^- N_{Im}, COO^-
$[Cu_2H_{-2}L]$	2.98(7)	6.56	(N_{Im}, NH_2, $2N^-$) (N_{Im}, COO^-)	3.00(7)	-	(N_{Im}, NH_2, $2N^-$) (N_{Im}, COO^-)
$[Cu_2H_{-3}L]^{-}$	-3.58(7)	6.34	(N_{Im}, NH_2, $2N^-$) (N_{Im}, N^-)	-	-	(N_{Im}, NH_2, $2N^-$) (N_{Im}, N^-)
$[Cu_2H_{-4}L]^{2-}$	-9.92(3)	8.88	(N_{Im}, NH_2, $2N^-$) (N_{Im}, $2N^-$)	-13.12(3)	9.32	(N_{Im}, NH_2, $2N^-$) (N_{Im}, $2N^-$)
$[Cu_2H_{-5}L]^{3-}$	-18.80(4)	-	(N_{Im}, NH_2, $2N^-$) (N_{Im}, $3N^-$)	-22.44(4)	-	(N_{Im}, NH_2, $2N^-$) (N_{Im}, $3N^-$)
	H4A/H8A					
$[CuHL]^{+}$	12.95(1)	-	N_{Im} (COO^-)			
$[CuH_{-1}L]^{-}$	4.27(1)	5.28	N_{Im}, NH_2, N^-			
$[CuH_{-2}L]^{2-}$	-0.99(1)	-	N_{Im}, NH_2, $2N^-$			

In condition of metal excess, as previously mentioned, binuclear species are formed by means of the two additional histidines in position 4 and 8. After the second Cu(II) ion anchors the His residues ($2N_{Im}$), the binding of up to three N-amides occurs leading to the formation of $[Cu_2H_{-5}L]^{3-}$, (N_{Im}, NH_2, $2N^-$)(N_{Im}, $3N^-$). In principle, both His4 and His8 can originate this binding mode. The significant difference is that, if His4 is bound to copper in the equatorial plane of the complex, the amide coordination should proceed in the C-terminal direction (due to the presence of the other complexed metal ion) while, in the case of His8, it can proceed towards the N-terminus. It is well known in the literature that both these modes are possible, but the latter produces more stable complexes due to the different dimension of the formed chelation rings. Spectroscopic data confirm the above hypotheses. The two Vis absorption spectra recorded at pH 4.5 and 5.0, where the complex $[Cu_2H_{-1}L]^+$ is the prevailing species in solution, show two maxima: the first, more intense, at λ_{max} = 528 nm corresponds to the ATCUN coordination mode of the first Cu(II) ion; the second band, around λ_{max} = 740–730 nm, can be attributed to the coordination of an imidazole nitrogen to the second copper atom with the possible participation of the side carboxylate group of one Glu residue (expected absorption maximum: 731 nm). Increasing the pH, the second band shifts to shorter wavelengths, as a consequence of the coordination of further nitrogens to the second Cu(II) in the C-terminal portion of WT. At pH = 11, only one intense absorption band is observed at 520 nm, typical of a (N_{Im}, $3N^-$) Cu(II) complex (expected λ_{max} = 522 nm). This band is superimposed to that of the ATCUN-type copper. EPR spectra recorded in the presence of excess of Cu(II) are very weak, confirming the formation of binuclear complexes. In ligand H3A, the absence of histidine in position 3 definitively influences the ability to coordinate Cu(II), resulting in complexes which are significantly weaker than those formed by WT. Both the histidine residues can function as metal anchor site, thus favouring the formation of binuclear complexes in the case of metal excess in solution. The metal coordination sphere also involves the amino terminal group and, starting from pH 6, the backbone amides (**Table 7.1**). Such behaviour occurs for both the bound Cu(II) ions, in accordance with the general trend already discussed for His-containing peptides without an ATCUN site (see previous chapters). The speciation model of H4A and H8A does not differ very much from that determined for the WT peptide, except for the absence of the most protonated species; this is obviously due to the lack of one histidine residue. It is worth of note that two consecutive histidines really do give rise to binuclear complexes, as in the case of H8A. Lastly, in H4A/H8A only the histidine in third position is present and, therefore, only mononuclear ATCUN-type complexes are formed in the explored pH range. In addition, Vis absorption data show that, in the presence of Cu(II) excess, the solution precipitates at pH > 7, most likely due to Cu(II) hydroxide.

The complex-formation equilibria with the Ni(II) ion have been investigated only in the presence of a slight ligand excess and thus only mono-nuclear complexes have been detected. Adequate long waiting times between each titrant addition have been employed due to nickel slow kinetics. The formation of yellow, diamagnetic, square-planar complexes has been observed at alkaline pH in every system. The presence of the ATCUN type sequence in all peptides, with the exception of H3A, favours the Ni(II) coordination to the amino-terminal domain, as already described for copper. The main species at neutral pH is the (N_{Im}, NH_2, $2N^-$) complex, characterized by an intense absorption around 422 nm;[11, 12] the corresponding CD spectrum contains, in the Vis range, two bands of opposite sign, at 415 (positive) and 480 (negative) nm, respectively,[13-15] and a positive and intense charge-transfer band in the UV region around 260 nm.[16, 17] The obtained stability constants and coordination modes for the formed Ni(II) species are reported in **Table 7.2**. Since ligand H3A lacks the ATCUN-type domain, its interaction with nickel differs from the other investigated peptides. Ni(II) first coordinates one His residue, then proceeds with the formation of macrochelated species, with the involvement of the second histidine

and/or of the terminal amino group. The species formed at acidic pH are probably octahedral; with the increase of pH they evolve to the classical square planar, low spin complex *via* the interaction with deprotonated backbone amides.

Table 7.2 - Equilibrium constants and proposed coordination modes for Ni(II) complexes at T=298 K and I=0.1 M (KCl). Values in parentheses are standard deviations on the last significant figure.

	Species	logβ	pK_a	Coord.
WT	$[NiHL]^{+}$	12.90(8)	5.77	N_{Im}, NH_2, N^-
	[NiL]	7.13(6)	6.26	N_{Im}, NH_2, $2N^-$
	$[NiH_{-1}L]^-$	0.87(5)	6.95	N_{Im}, NH_2, $2N^-$
	$[NiH_{-2}L]^{2-}$	-6.08(5)	-	N_{Im}, NH_2, $2N^-$
H3A	$[NiH_2L]^{2+}$	18.0(2)	6.0	N_{Im}
	$[NiHL]^{+}$	11.98(8)	6.25	$2N_{Im}$ or N_{Im}, NH_2
	[NiL]	5.73(6)	7.78	$2N_{Im}$ or $2N_{Im}$, NH_2
	$[NiH_{-1}L]^-$	-2.05(8)	-	$2N_{Im}$, N^- or $2N_{Im}$, NH_2, N^-
	$[NiH_{-3}L]^{3-}$	-18.64(7)	9.1	N_{Im}, $3N^-$
	$[NiH_{-4}L]^{4-}$	-27.7(1)	-	$4N^-$
H4A	[NiL]	6.25(8)	5.49	N_{Im}, NH_2, N^-
	$[NiH_{-1}L]^-$	0.76(2)	6.89	N_{Im}, NH_2, $2N^-$
	$[NiH_{-2}L]^{2-}$	-6.13(5)	-	N_{Im}, NH_2, $2N^-$
H8A	[NiL]	6.01(6)	5.75	N_{Im}, NH_2, N^-
	$[NiH_{-1}L]^-$	0.26(3)	6.72	N_{Im}, NH_2, $2N^-$
	$[NiH_{-2}L]^{2-}$	-6.46(4)	-	N_{Im}, NH_2, $2N^-$
H4A/H8A	$[NiH_{-1}L]^-$	-0.48(5)	5.55	N_{Im}, NH_2, N^-
	$[NiH_{-2}L]^{2-}$	-6.03(1)	-	N_{Im}, NH_2, $2N^-$

In the case of Zn(II) ion, the ligand effectiveness is not strictly affected by the presence of the ATCUN sequence, but mostly depends on the number of available histidines, which act as multiple metal anchoring sites and allow the formation of macrochelated systems. The stoichiometry of the first detected species with all the investigated peptides requires that two nitrogen atoms are deprotonated and bound to the metal ($2N_{Im}$ or in the case of H4A/H8A N_{Im}, NH_2). In the case of WT, which contains three histidines, a mixture of complexes, with identical stoichiometry and coordination mode but involving different

donor atoms, can be formed. This may explain why zinc complexation with WT starts at lower pH (= 4.5) than with the other peptides. It is also worth noting that, when the histidine in position 8 is replaced by one alanine (peptides H8A and H4A/H8A) the first complexes are formed only at pH around 5.5, suggesting an important role of His-8 as the first metal anchor. As the pH increases, Zn(II) binds all the available histidines and terminal amino group, forming 3N complexes or, in the case of WT, a 4N complex theoretically corresponding to [ZnL]; this could be the reason for its greater stability (almost two orders of magnitude) compared to the other complexes of the same stoichiometry formed by the other peptides (see **Table 7.3**). All these complexes should have a tetrahedral geometry, with water molecules occupying the "vacant" coordination positions. Further deprotonation steps can be then attributed to water molecules deprotonation.

Table 7.3 - Equilibrium constants and proposed coordination modes for Zn(II) complexes at T=298 K and I=0.1 M (KCl). Values in parentheses are standard deviations on the last significant figure.

	Species	logβ	pK_a	Coord.
WT	$[ZnH_2L]^{2+}$	18.79(6)	6.23	$2N_{Im}$
	$[ZnHL]^{+}$	12.56(6)	6.46	$3N_{Im}$ or $2N_{Im}$, NH_2
	[ZnL]	6.10(4)	-	$3N_{Im}$, NH_2
H3A	$[ZnHL]^{+}$	11.71(4)	6.93	$2N_{Im}$
	[ZnL]	4.78(4)	8.02	$2N_{Im}$, NH_2
	$[ZnH_{-1}L]^{-}$	-3.24(5)	-	$2N_{Im}$, NH_2
H4A	$[ZnHL]^{+}$	11.69(3)	7.22	$2N_{Im}$
	[ZnL]	4.47(6)	8.37	$2N_{Im}$, NH_2
	$[ZnH_{-1}L]^{-}$	-3.9(1)	-	$2N_{Im}$, NH_2
H8A	$[ZnHL]^{+}$	10.71(6)	6.58	$2N_{Im}$
	[ZnL]	4.13(3)	8.23	$2N_{Im}$, NH_2
	$[ZnH_{-1}L]^{-}$	-4.10(4)	-	$2N_{Im}$, NH_2
H4A/H8A	[ZnL]	3.88(6)	7.84	N_{Im}, NH_2
	$[ZnH_{-1}L]^{-}$	-3.96(6)	8.46	$2N_{Im}$, NH_2
	$[ZnH_{-2}L]^{2-}$	-12.42(6)	-	$2N_{Im}$, NH_2

The formation of hetero Cu(II) and Ni(II) binucelar complexes with WT have been also investigated. Potentiometric data processing revealed the formation of three hetero-metallic binuclear species: $[CuNiH_{-1}L]^{+}$ (logβ=9.97), $[CuNiH_{-2}L]$ (logβ=3.40) and $[CuNiH_{-5}L]^{3-}$ (logβ=-23.74). It can be assumed that, at acidic condition, Cu(II) coordinates the N-terminal ATCUN site, while increasing the pH, a nickel ion binds the two histidine residues not involved in copper coordination. Starting from pH about 9, the Ni(II) ion forms the classic planar and diamagnetic 4N complex. In the pH range 4.5–8.5, the Vis

absorption spectra remain virtually unchanged, showing the d-d transition of the Cu(II) ATCUN-type complex; under more alkaline pH values, the typical band of the diamagnetic Ni(II) complex becomes instead evident (**Figure 7.2**).

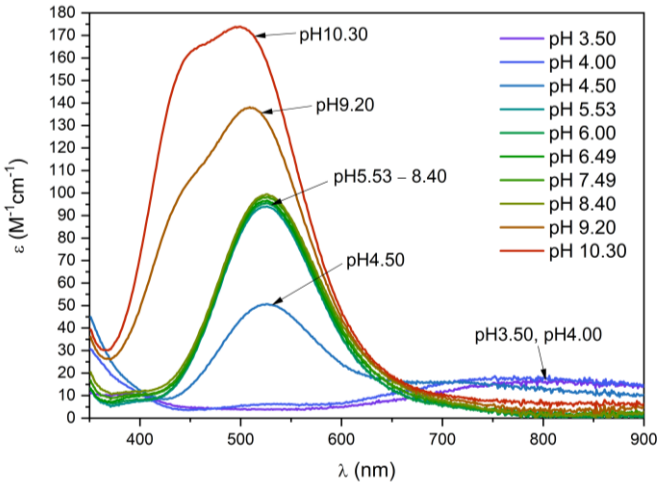

Figure 7.2 - Vis absorption spectra for Cu(II)/Ni(II) complexes with WT; $C_L = 1.0 \cdot 10^{-3}$ M, Cu(II):L = 0.8:1, Ni(II):L = 0.9:1.

7.4 Conclusions

The studied fragments of Hpn protein proved to be good chelators for divalent copper, nickel and zinc ions. The formation of binuclear Cu(II) complexes have been extensively studied; from the obtained results one can generally assume that the first Cu(II) ion interacts with the peptide at the very effective N-terminal ATCUN site (if present), while a second Cu(II) ion can further coordinate the histidine residues in position 4 and 8. However, His-8 seems to be the favourite site, due to the possibility to further coordinate the amide nitrogen towards the N-terminal direction, forming a stable 5/6-membered chelate rings. Moreover, the WT model peptide proved to form hetero-binuclear complexes, where the ATCUN sequence interacts exclusively with Cu(II), while nickel preferentially binds the histidine residue in position 8 (second binding site) to form its typical square planar complex (N_{Im}, $3N^-$). In the interaction of Cu(II) with a binary Ni(II)/WT complex, the nickel ion can be either released or even moved from the ATCUN site to the second binding site. In both cases, the activity of Hpn protein is disturbed. In fact, in the presence of only a 20% of Cu(II) with respect to Ni(II), not only mixed Cu(II)/Ni(II) species are formed in the entire pH range, but, at neutral pH, some Ni(II) is still not complexed (**Figure 7.3**). When thinking about possible antimicrobial strategies, a suitable Cu(II) complex, sufficiently stable to reach the bacterium but weaker than that formed with Hpn, could be employed as a pharmacophore, with the aim of producing a "ligand exchange" reaction, where Cu(II) ions substitute Ni(II) ions at the Hpn ATCUN domain; in a possible additional second step, the released Ni(II) ions could even be sequestered by the metal-free pharmacophore and eliminated. This action would partially inhibit the Hpn efficiency in Ni(II) recruitment and storage, thus helping the nutritional immunity mechanism to starve the pathogen. A similar action could also be obtained with Zn(II) ion, but it would require very high Zn(II) concentration, since its affinity for Hpn, at least as far as the N-terminus is concerned, is much lower. **Figure 7.4** shows that, in the presence of a 10-fold excess of Zn(II) with respect to Ni(II), the most acidic pH values are dominated by Zn(II) complexes, and, at neutral pH, about 30% of the peptide is engaged

with zinc. Therefore, distressing the bacterial nickel homeostasis by means of competing metals (or ligands) seems to be a promising strategy to find new therapeutic ways to eradicate *H. pylori*.

This research work includes the publication "D. Bellotti, A. Sinigaglia, R. Guerrini, E. Marzola, M. Rowińska-Żyrek, M. Remelli, *J. Inorg. Biochem.*, 2021, 214, 111304".

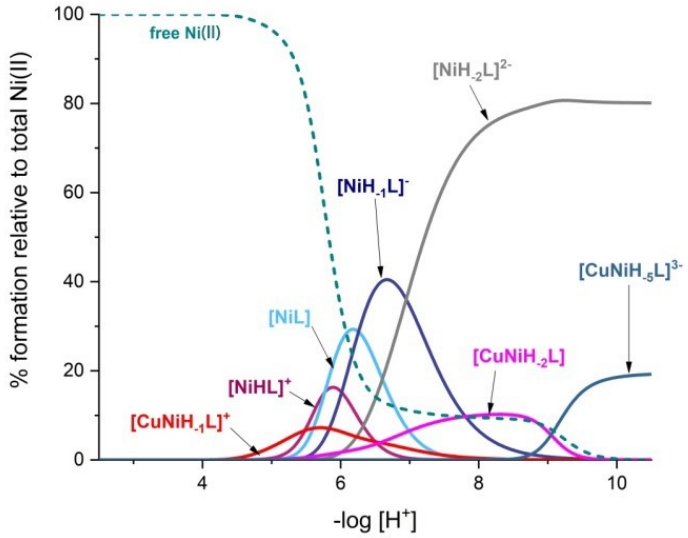

Figure 7.3 - Simulation of species distribution in the ternary Cu(II)/Ni(II)/WT system. C_L=1·10^{-3} M; L:Ni(II):Cu(II) ratio = 1:1:0.2.

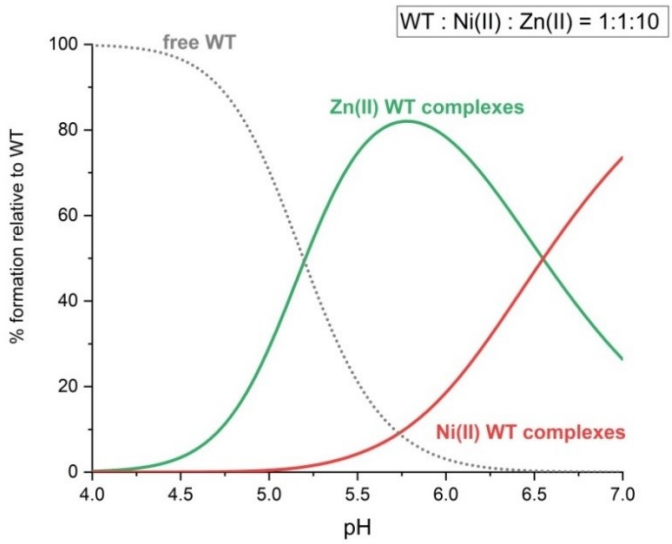

Figure 7.4 - Competition plots for a solution containing L=WT, Ni(II) and Zn(II). C_L=1·10^{-3} M; L:Ni(II):Zn(II) ratio = 1:1:10.

7.5 References

[1] J. V. Gilbert, J. Ramakrishna, F. W. Sunderman, A. Wright, A. G. Plaut, Infect. Immun. 1995, 63(7), 2682.

[2] R. J. Maier, S. L. Benoit, S. Seshadri, BioMetals 2007, 20(3-4), 655-664.
[3] G. Wang, P. Alamuri, R. J. Maier, Mol. Microbiol. 2006, 61(4), 847-860.
[4] H. Zeng, G. Guo, X. H. Mao, W. De Tong, Q. M. Zou, Curr. Microbiol. 2008, 57(4), 281-286.
[5] Z. Saylor, R. Maier, Microbiology 2018, 164(8), 1059-1068.
[6] D. Witkowska, R. Politano, M. Rowinska-Zyrek, R. Guerrini, M. Remelli, H. Kozlowski, Chem. – Eur. J. 2012, 18(35), 11088-11099.
[7] M. Rowinska-Zyrek, D. Witkowska, S. Bielinska, W. Kamysz, H. Kozlowski, Dalton Trans. 2011, 40(20), 5604-5610.
[8] D. Bellotti, A. Sinigaglia, R. Guerrini, E. Marzola, M. Rowińska-Żyrek, M. Remelli, J. Inorg. Biochem. 2021, 214, 111304.
[9] E. Farkas, É. A. Enyedy, G. Micera, E. Garribba, Polyhedron 2000, 19(14), 1727-1736.
[10] G. Tabbì, A. Giuffrida, R. P. Bonomo, J. Inorg. Biochem. 2013, 128, 137-145.
[11] C. Harford, B. Sarkar, Acc. Chem. Res. 1997, 30(3), 123-130.
[12] M. Rowińska-Żyrek, H. Kozłowski, in The Biological Chemistry of Nickel, The Royal Society of Chemistry, 2017, pp. 43-59.
[13] W. Bal, M. Jeżowska-Bojczuk, K. S. Kasprzak, Chem. Res. Toxicol. 1997, 10(8), 906-914.
[14] M. Sokolowska, A. Krezel, M. Dyba, Z. Szewczuk, W. Bal, Eur. J. Biochem. 2002, 269(4), 1323-1331.
[15] M. Peana, K. Zdyb, S. Medici, A. Pelucelli, G. Simula, E. Gumienna-Kontecka, M. A. Zoroddu, J. Trace Elem. Med Biol. 2017, 44, 151-160.
[16] J. D. Van Horn, G. Bulaj, D. P. Goldenberg, C. J. Burrows, J. Biol. Inorg. Chem. 2003, 8(6), 601-610.
[17] W. Bal, J. Lukszo, K. S. Kasprzak, Chem. Res. Toxicol. 1996, 9(2), 535-540.

8. Chapter Eight: R1 and R3 regions of tau protein

8.1 Outline of the work

Compared to the interaction of copper with other neuronal peptides involved in the pathogenesis of neurodegenerative diseases, which has been deeply elucidated, the interaction of copper with tau protein is poorly characterized, even if the relevance and the impact of tau homoeostasis in neurodegenerative diseases progression is taking a central stage in the last years. Tau proteins are present in the axon terminals of neurons and are mostly associated with microtubules, the major constituent of the cytoskeleton, composed of a dynamic tubulin polymer. The human brain contains six main tau isoforms that can be categorized depending on whether they contain three or four pseudorepeats (R1-R4) in the C-terminal region that constitutes the microtubule-binding domain. Tau proteins are highly soluble and show little tendency to aggregation. However, tau aggregation is characteristic of several neurodegenerative diseases known as tauopathies (including Alzheimer's disease).[1-3] The structure of the tau fibrils from a diseased brain obtained with cryo-EM shows the formation of cross-β/β-helix structure between residues 306–378, which is the portion of tau comprising R3 and R4 regions.[4] The region encompassing the R1–R4 repeats represents a potential binding site for metal ions, since each repeat contains at least one histidine (His268, His299 and His362 in R1, R2 and R4, respectively); R3 contains two vicinal histidine residues (His329 and His330).

In the present study, we investigate the properties and the reactivity of the copper complexes formed with R1 (Ac-^{256}VKSKIGSTENLKHQPGGG^{273}-Am) and R3 (Ac-^{323}GSLGNIHHKPGGG^{335}-Am) fragments. These two fragments were chosen because they have different behaviour in the intraneuronal tau neurofibrillary tangles formation. In particular, R3 portion is found inside the cross-β/β-helix structure of tau filament, whereas R1 is outside.[4] Moreover, these two peptides allow to clarify how the presence of one histidine or two vicinal histidines affects the affinity for copper and the reactivity of the complexes. We also justify the choice to use a truncated R3 fragment excluding the cysteine residue (Cys322) according to the evidence that Cu(II) is able to oxidize *in vitro* the cysteine residue inducing the formation of a disulfide intermolecular bond.[5] However, the two cysteine residues in tau protein (Cys291 and Cys322) are likely involved in disulfide bond in the native protein, even if formation of intramolecular or intermolecular bonds may play an important role in tau aggregation.[6, 7] The speciation of the Cu(I) and Cu(II) complexes with both R1 and R3 peptides were studied, together with the oxidation of the dopamine (DA) neurotransmitter, as physiological model of induced copper redox cycling, and the related, but with a simpler oxidation pattern, 4-methylcatechol (MC).

8.2 Experimental Procedures

Analyses performed on the above mentioned peptides follow the scheme:

- Peptide synthesis by means of solid-phase technique.
- Potentiometric determination of ligand protonation and Cu(II) complex-formation constants.
- Spectrophotometric (UV-Vis and CD) analyses of Cu(II) complexes.
- EPR measurements of Cu(II) complexes.
- Study of Cu(I) complex formation equilibria by means of UV-visible competition experiments with ferrozine (Fz^{2-}) as competing metallochromic indicator.

- NMR measurements of apo-peptides, Cu(II) and Cu(I) complexes.
- Kinetics study of oxidation of catecholic substrates.
- Evaluation of SOD-like activity of free Cu(II) and of its complexes.

The employed experimental conditions, instruments and materials are reported in details below, in Bacchella *et al.*, 2020.[8]

8.3 Results and discussion

All the formed Cu(II) complexes correspond to 1:1 metal/peptide stoichiometry. For the R1 system, the predominant species in the pH range 6–8.5 is $[CuHL]^{2+}$ which reaches 95% total copper at pH 7.2. Above pH 8.5 $[CuL]^{+}$ becomes the most abundant species, reaching its maximum at pH 9 (ca. 60 % total copper). The last three deprotonation steps only involve the deprotonation of the lysine residues. In the case of R3, under acidic conditions both the histidine residues bind the cupric ion in the equatorial plane, while at neutral pH (pH 7–7.5) the $[CuL]^{2+}$ and $[CuH_{-1}L]^{+}$ species predominate. In $[CuL]^{2+}$ the metal ion likely adopts an equatorial (3N, O) coordination mode that involves one deprotonated peptide nitrogen, two imidazole donors, and a water molecule. The expected λ_{max} for this coordination environment is 604 nm. Moving to pH 7.8 where $[CuH_{-1}L]^{+}$ dominates, the complex shows a (N_{Im}, $2N^{-}$, O) donor-atom set. The proposed equatorial coordination of N-amides extends toward the N-terminal and a stable 6-membered (N_{Im}, N^{-}) chelation ring is formed; the deprotonation of amides in the C-terminal direction for R1 and R3 peptides is prevented by the presence of a proline residue. The copper coordination environments proposed in **Table 8.1** are based on visible absorption and CD spectra and on EPR magnetic parameters at different pH.

The calculated conditional affinities for Cu(II) for both the peptides (K_d) revealed that the R3 peptide has higher affinity for Cu(II) than R1, as a consequence of the presence of two His donors. However, the affinity of R3 is only 2-fold higher than that of R1 at pH 7.4, and 5-fold at pH 6.5; this indicates that R3 region is not selective in binding copper but that, in tau protein, the metal may rather be distributed over multiple sites, or likely be bound to one preferential site as the consequence of additional structural features not modelled using R1 and R3 peptides. On the other hand, UV-visible competition experiments performed on Cu(I) complexes highlight that the R1 peptide does not significantly bind Cu(I), while the R3 peptide has a high affinity for this metal ion (**Figure 8.1**). The proposed coordination mode is a ($2N_{Im}$) with a possible weak interaction of the carbonyl oxygen of His329. The characterization of R3 complexes with both Cu(I) and Cu(II) by NMR spectroscopy is in full agreement with the proposed binding modes.

To gain information on the potential catalytic role of R1 and R3 complexes in oxidative reactions, a comparative study of their oxidative activity against catecholic substrates with respect to that of free Cu(II) has been performed. Both in the case of dopamine (DA) and 4-methylcatechol (MC), the substrate catalyzed by Cu(II) is strongly promoted by the addition of R3 but it is only slightly enhanced by the presence of R1. The oxidation proceeds with a biphasic behaviour where a fast initial step is followed by a second linear phase; however, in the case of DA such behaviour is less clear due to the presence of several absorbing species in solution (**Figures 8.2** and **8.3**). It was previously demonstrated that the presence of tandem His-His sites promotes the reduction of Cu(II) to Cu(I), mainly through the formation of stable Cu(I)/peptide adducts.[9-12]

Table 8.1 - Equilibrium constants and proposed coordination modes for Cu(II) complexes at T=298 K and I=0.1 M (KCl). Values in parentheses are standard deviations on the last significant figure.

Species	Logβ	pK_a	Coord.	
	R1			
$[CuH_3L]^{4+}$	34.84(8)	6.74	N_{Im} (COO^-)	K_d **(R1)**
$[CuH_2L]^{3+}$	28.1(3)	5.40	N_{Im}, N^-	
$[CuHL]^{2+}$	22.70(5)	8.62	N_{Im}, $2N^-$	pH 6.5
$[CuL]^{+}$	14.08(8)	9.62	N_{Im}, $3N^-$	$13.1(1) \cdot 10^{-6}$ M
$[CuH_{-1}L]$	4.46(7)	10.31	N_{Im}, $3N^-$	pH 7.4
$[CuH_{-2}L]^{-}$	-5.85(9)	10.50	N_{Im}, $3N^-$	$150(10) \cdot 10^{-9}$ M
$[CuH_{-3}L]^{2-}$	-16.35(7)	-	N_{Im}, $3N^-$	
	R3			
$[CuH_2L]^{4+}$	20.48(7)	4.67	N_{Im}	K_d **(R3)**
$[CuHL]^{3+}$	15.81(2)	6.42	$2N_{Im}$	
$[CuL]^{2+}$	9.39(3)	6.91	$2N_{Im}$, N^-	pH 6.5
$[CuH_{-1}L]^{+}$	2.48(2)	8.70	N_{Im}, $2N^-$	$2.8(5) \cdot 10^{-6}$ M
$[CuH_{-2}L]$	-6.22(3)	10.09	N_{Im}, $3N^-$	pH 7.4
$[CuH_{-3}L]^{-}$	-16.31(4)	-	N_{Im}, $3N^-$	$71(5) \cdot 10^{-9}$ M

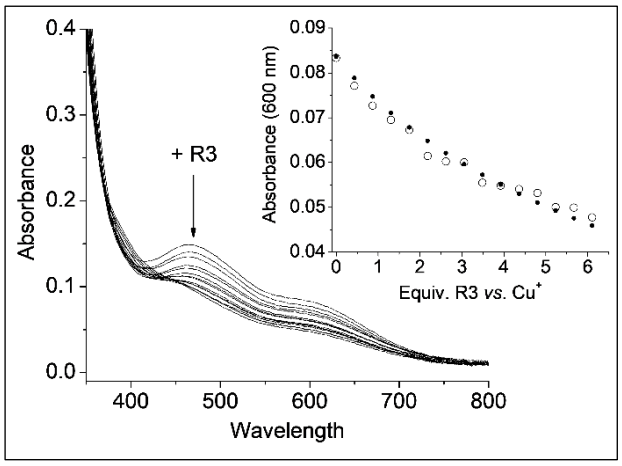

Figure 8.1 - Spectral dataset for the titration of a solution of $[Cu(CH_3CN)_4]BF_4$ and Fz^{2-} with R3 (Cu:Fz = 1:2.15, C_{Cu} = 41 μM, $C_{ascorbate}$ = 10 mM, 100 mM aqueous HEPES buffer solution, pH 7.4). Insect: absorbance values at 600 nm. Open circles: observed; filled circles: calculated.

It is however worth noting that here, for both R1 and R3 fragments, the estimated potential is lower than that observed for copper adducts with tau (340 mV vs NHE).[13] Assuming a similar affinity for Cu(I) for both R3 region and tau protein, the difference of one order of magnitude in the affinities for Cu(II) accounts only for 60 mV of the difference in their

redox potentials. Overall, these data suggest that there are structural or second-shell interactions in copper/tau adducts that determine the redox potential in the protein and that are not completely modelled by R1 and R3 peptides.

The reaction mechanism proposed for the oxidation of catechols by copper-tau peptide complexes may involve the following reaction steps, where P is tau-peptide:

1. Cu(II) + P ⇄ [Cu(II)P]

2. [Cu(II)P] + catechol → [Cu(I)P] + semiquinone$^{\bullet+}$

3. [Cu(I)P] + catechol ⇄ [Cu(I)P-catechol]

4. [Cu(I)P-catechol] + O_2 → [CuP-catechol-O_2]

5. [CuP-catechol-O_2] →→ [Cu(II)P] + quinone

After rapid complexation (1), the reaction proceeds with a fast step of Cu(II) reduction by the catechol (2). The rate-determining step is the reaction of [Cu(I)P-catechol] complex with O_2, to generate the ternary complex indicated as [CuP-catechol-O_2]. Previous studies on copper-peptide complexes indicate that the reaction rate depends also on catechol concentration, suggesting that substrate binding occurs as a pre-equilibrium step (3) before the rate-determining binding of molecular oxygen (4).[14-16] The complexation between Cu(I) and R3 facilitates the reaction with molecular oxygen, increasing the reaction rate, while with R1 the metal ion is mostly unbound and the reactivity reflects that of "free" copper (**Figures 8.2** and **8.3**).

The reduction of Cu(II) during the catechol oxidation generate Cu/O_2 species capable to oxidize other cellular components through Fenton chemistry. LC-MS analysis allows to evaluate the oxidative modifications on R1 and R3 peptide upon oxidation of DA and MC. R3 undergoes extensive modifications through oxygen insertion and/or quinone-derivatized histidines, in fact the amount of unmodified peptide is only 8% after 90 min of time incubation (**Figure 8.4**).

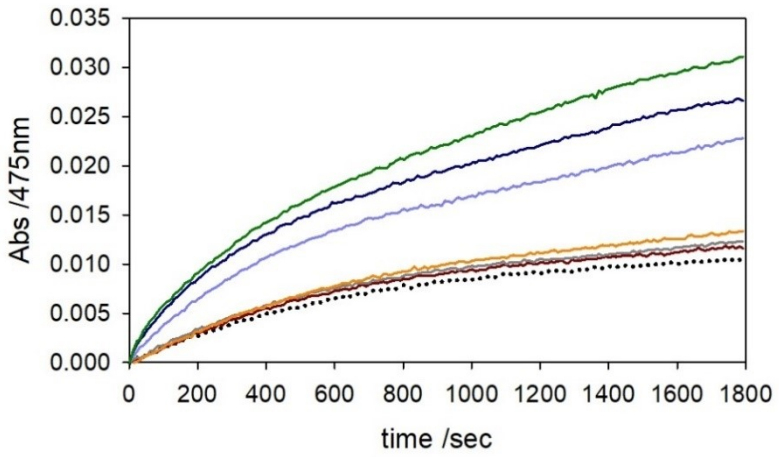

Figure 8.2 - Kinetic profile of DA (3 mM) oxidation with time in 50 mM HEPES buffer solution at pH 7.4 and 20 °C in the presence of only Cu(II) (25 μM) (brown trace) and with 2 equiv. (grey), 4 equiv. (orange) of R1 peptide or 1 equiv. (light blue), 2 equiv. (blue) and 4 equiv. (green) of R3. Autoxidation of substrate is also shown (black dotted trace).

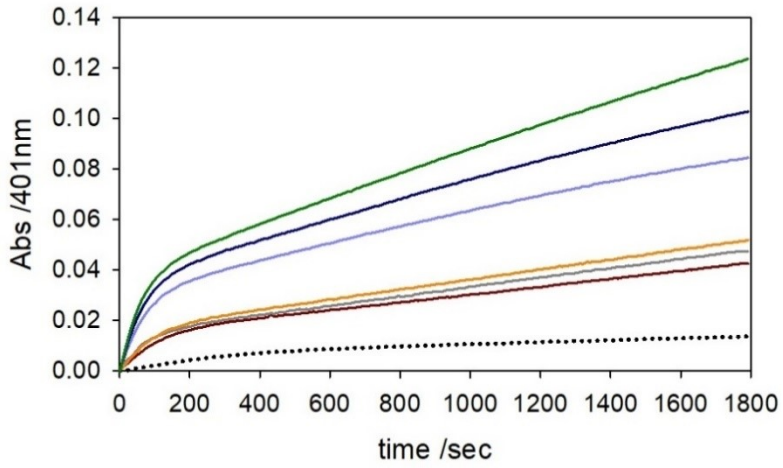

Figure 8.3 - Kinetic profile of MC (3 mM) oxidation with time in 50 mM HEPES buffer solution at pH 7.4 and 20 °C in the presence of only copper(II) (25 μM) (brown trace) and with 2 equiv. (grey), 4 equiv. (orange) of R1 peptide or 1 equiv. (light blue), 2 equiv. (blue) and 4 equiv. (green) of R3. Autoxidation of substrate is also shown (black dotted trace).

The LC-MS data are in agreement with the catalytic data on catechol oxidation. R1 fragment is weakly bound to Cu(I), leading to a slow reaction with molecular oxygen and thus to weak catalytic activity in catechol oxidation and limited "self-modification". By considering the percentage of unmodified peptide after 90 min in the presence of copper and MC under the same experimental conditions, it is possible to list the neuronal peptides in this order of reactivity: R3 > prion fragment 76–114 (PrP_{76-114})[16] > Aβ16 ≈ Aβ28[15] >> R1 > α-synuclein fragment 1–15.[14] Moreover, neither Cu(II)-R1, nor Cu(II)-R3 significantly increase the SOD-like activity of free Cu(II).

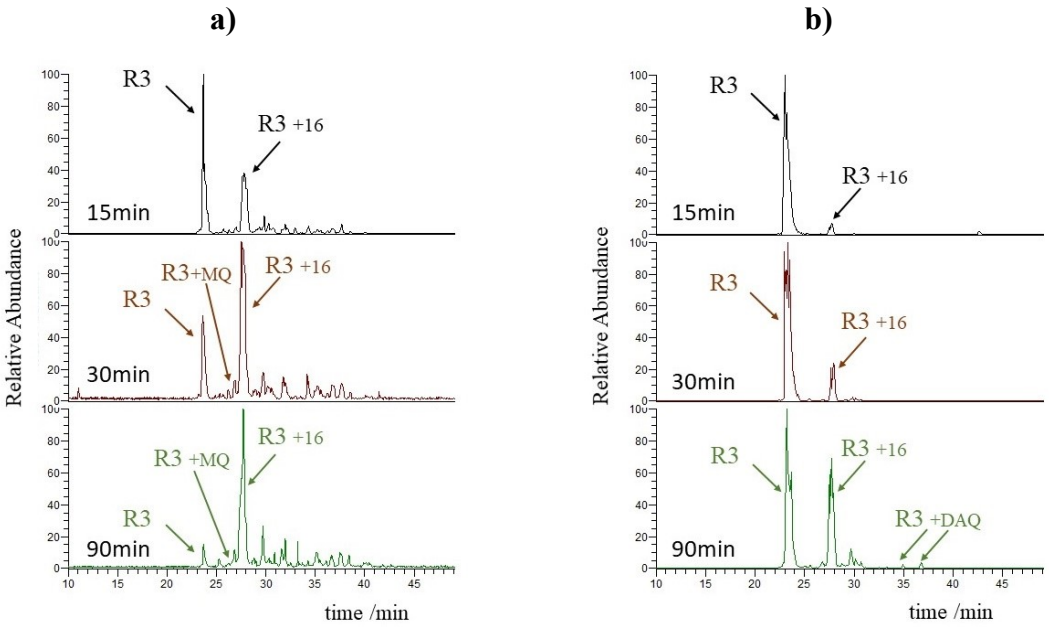

Figure 8.4 - HPLC-MS elution profiles of R3 peptide (50 μM) in HEPES buffer (50 mM) pH 7.4 in the presence of Cu(II) (25 μM) and MC (panel A) or DA (panel B) (3 mM) after 15, 30 and 90 min reaction time.

8.4 Conclusions

Potentiometric measurements suggest that the vicinal His-His residues in R3 guarantee a strong binding site for copper in both the oxidation states, whereas the single histidine in R1 is not able to stably interact with Cu(I). The study of the oxidative reactivity of these copper-tau peptide complexes confirms that R3 coordination sphere guarantees an efficient Cu(I)/(II) redox cycling. In particular, copper-R3 complex is able to strongly enhance the metal ion ability to oxidize cathecolic substrates, like dopamine and 4-methylcatechol, whereas copper-R1 complex reactivity is similar to that of free copper. Moreover, by comparing the tendency to undergo copper-mediated oxidative modification of tau R3 and R1 peptides with other neuronal peptides analysed in previous studies, it turns out that R3 is the most reactive, followed by prion protein fragment ($PrP_{76–114}$) and N-terminal portion of A□ peptide.

The His-His tandem site ability to bind copper in both oxidation states provides an active catalyst for reactions that activate oxygen and are potentially dangerous for the cellular compartment. The different binding of Cu(I) for R3 and R1 fragments is particularly important for this interaction because tau protein is located intracellularly where the reductive redox potential implies that copper is mostly in the reduced state.

This research work includes the publication "C. Bacchella, S. Gentili, D. Bellotti, E. Quartieri, S. Draghi, M. C. Baratto, M. Remelli, D. Valensin, E. Monzani, S. Nicolis, L. Casella, M. Tegoni, S. Dell'Acqua, *Inorg. Chem*. 2020, 59(1), 274-286".

8.5 References

[1] Y. Wang, E. Mandelkow, *Nature Reviews Neuroscience* **2015**, *17*, 22.
[2] M. G. Spillantini, M. Goedert, *Lancet Neurol.* **2013**, *12(6)*, 609-622.
[3] A. Fuster-Matanzo, F. Hernández, J. Ávila, *Int. J. Mol. Sci.* **2018**, *19(3)*.
[4] A. W. P. Fitzpatrick, B. Falcon, S. He, A. G. Murzin, G. Murshudov, H. J. Garringer, R. A. Crowther, B. Ghetti, M. Goedert, S. H. W. Scheres, *Nature* **2017**, *547*, 185.
[5] X.-Y. Su, W.-H. Wu, Z.-P. Huang, J. Hu, P. Lei, C.-H. Yu, Y.-F. Zhao, Y.-M. Li, *Biochem. Biophys. Res. Commun.* **2007**, *358(2)*, 661-665.
[6] S. Walker, O. Ullman, C. M. Stultz, *J. Biol. Chem.* **2012**, *287(12)*, 9591-9600.
[7] Y. Furukawa, K. Kaneko, N. Nukina, *J. Biol. Chem.* **2011**, *286(31)*, 27236-27246.
[8] C. Bacchella, S. Gentili, D. Bellotti, E. Quartieri, S. Draghi, M. C. Baratto, M. Remelli, D. Valensin, E. Monzani, S. Nicolis, L. Casella, M. Tegoni, S. Dell'Acqua, *Inorg. Chem.* **2020**, *59(1)*, 274-286.
[9] B. Alies, B. Badei, P. Faller, C. Hureau, *Chemistry (Easton)* **2012**, *18(4)*, 1161-1167.
[10] K. L. Haas, A. B. Putterman, D. R. White, D. J. Thiele, K. J. Franz, *J. Am. Chem. Soc.* **2011**, *133(12)*, 4427-4437.
[11] R. A. Himes, G. Y. Park, G. S. Siluvai, N. J. Blackburn, K. D. Karlin, *Angew. Chem. Int. Ed. Engl.* **2008**, *47(47)*, 9084-9087.
[12] S. E. Conklin, E. C. Bridgman, Q. Su, P. Riggs-Gelasco, K. L. Haas, K. J. Franz, *Biochemistry* **2017**, *56(32)*, 4244-4255.
[13] S. Martic, M. K. Rains, H.-B. Kraatz, *Anal. Biochem.* **2013**, *442(2)*, 130-137.
[14] S. Dell'Acqua, V. Pirota, C. Anzani, M. M. Rocco, S. Nicolis, D. Valensin, E. Monzani, L. Casella, *Metallomics* **2015**, *7(7)*, 1091-1102.
[15] V. Pirota, S. Dell'Acqua, E. Monzani, S. Nicolis, L. Casella, *Chemistry – A European Journal* **2016**, *22(47)*, 16964-16973.
[16] S. Dell'Acqua, C. Bacchella, E. Monzani, S. Nicolis, G. Di Natale, E. Rizzarelli, L. Casella, *Inorg. Chem.* **2017**, *56(18)*, 11317-11325.

9. Chapter Nine: Linear and branched Cu(II) binding peptides

9.1 Outline of the work

The metal-binding properties of branched peptides and more in general of oligopeptides covalently mounted on a molecular scaffold have been widely explored in the last decade;[1] several examples are known in the literature, from short dipeptides,[2-4] to long oligopeptides that spontaneously fold into supersecondary structures.[5-7] The metal binding affinities and the coordination modes depend on the peptide chain sequence and preorganization or fold of the overall branched structure; in fact, as a general assumption, one can consider the chains of a branched construct as independent metal binding moieties in absence of folded architectures, while they can act as single metal binding sites in a structured molecule.[8]

The two branched homomeric tetrapeptides, $(AAHAWG)_4$-PWT2 and $(HAWG)_4$-PWT2 where synthesized by mounting the linear peptides on a PWT2 cyclam-based scaffold provided with four maleimide chains.[9] The peptides used (AAHAWGC-Am and HAWGC-Am) reacted with PWT2 through a thio-Michael reaction which resulted in the formation of thioether bonds. The used ligands ensure a high degree of flexibility of the construct and the possibility to bind four or less metal ions, one per arm or two to four peptides coordinated to one metal center. The aim of this work is to demonstrate that the ligand $(AAHAWG)_4$-PWT2, which bears four ATCUN-type AAH N-terminal sequences, is capable to bind four Cu(II) ions and form stable (N_{Im}, NH_2, $2N^-$) complexes in a wide pH range. On the other hand, the use of $(HAWG)_4$-PWT2, whose branches present His as the N-terminal amino acid, could stabilize Cu(II) histamine- or glycine-like coordination modes under pH conditions at which they are less common; in fact, with the single-chain HAWG-Am they are expected to mostly occur at acidic pH.[10-12] Both the branched peptides, $(AAHAWG)_4$-PWT2 and $(HAWG)_4$-PWT2, and single-chain peptides, AAHAWG-Am and HAWG-Am, have been studied in the absence/presence of Cu(II) ions. The addition of a C-terminal methylated cysteine residue in the single-chain peptides to obtain AAHAWGC(SMe)-Am and HAWGC(SMe)-Am has been also considered to simulate the thioether moiety of the branched systems. Finally, a preliminary investigation of Zn(II) complexes with the single-chain peptides has been performed. As a general perspective, the stabilization of specific metal coordination environments in conditions (*e.g.* pH) where they are not expected to be stable may lead, for instance, to the design and isolation of new bioinspired catalytic systems or efficient metal-based sensors and receptors.

9.2 Experimental Procedures

Analyses performed on the above mentioned peptides follow the scheme:

- Synthesis of linear and branched peptides by means of solid-phase technique and peptide welding technology.
- Potentiometric determination of ligand protonation and Zn(II) and Cu(II) complex-formation constants.
- Mass spectrometric analysis to evaluate ligand purity and the stoichiometry of the formed Cu(II) complexes.

- Spectrophotometric (UV-Vis and CD) analyses of Cu(II) complexes.

The employed experimental conditions, instruments and materials are reported in details below, in Perinelli *et al.*, 2020.[13]

9.3 Results and discussion

All the investigated linear peptides bear one histidine residue, and therefore an imidazole donor group, and a Trp residue as a spectroscopic tag. Single-chain peptides can be grouped into two couples possessing an Xxx-Xxx-His- N-terminus or a His- N-terminus, respectively. For each couple of peptides, the difference stands in the presence at the C-terminus of a Cys(S-Me) residue. The obtained results confirmed that this moiety does not particularly affect the peptides metal binding ability (**Table 9.1**). Our results demonstrate that Cu(II) is bound to both the single-chain and the branched peptides preferentially at the N-termini, as previewed by our design. The ATCUN terminus in AAHAWG-Am gives rise to mononuclear complexes of high stability with a (N_{Im}, NH_2, $2N^-$) coordination. A further deprotonation step at alkaline pH to form the $[CuLH_{-3}]^-$ species has been assigned to the deprotonation of the second imidazolic proton to form a coordinated imidazolate ion.[14-16] The deprotonation of axially-bound water molecule has been excluded since the corresponding *m/z* signal is completely absent in the ESI-MS spectra. On the other hand, HAWG-Am is able to form 1:2 copper:peptide adducts at pH 7 with mixed histamine-like and glycine-like coordination, where the second amino group likely binds Cu(II) in axial position (**Figure 9.1**) and is responsible of the small red-shift of the Vis absorption band, from the expected 607–617 nm to the observed 634 nm. Conversely, in the alkaline pH range the peptide forms 1:1 adducts: the deprotonation of three amides of the peptide backbone occurs and the ligand wraps around the metal, with the participation of the terminal amine, in a (4N) coordination mode.

Bimetallic species, with different protonation degrees, were also detected in this system by potentiometric data analysis. These are however minor species if compared to monometallic ones, and their characterization was not carried out in further detail. Therefore, the major difference between the two peptides is that the ATCUN coordination mode for AAHAWG-Am is stable in a wide pH range (4–10), while for HAWG-Am there is a profound change of Cu(II) coordination from pH 7 to pH 9.

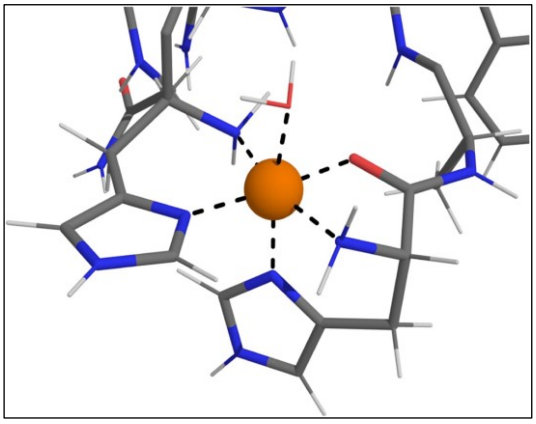

Figure 9.1 - Structural hypothesis for the complex $[Cu(II)(HAWG\text{-}Am)_2]^{2+}$. Color code: orange=copper, blue=nitrogen, red=oxygen, light grey=hydrogen, grey = carbon.

Table 9.1 - Equilibrium constants and proposed coordination modes for Cu(II) and Zn(II) complexes at T=298 K and I=0.1 M ($NaClO_4$). Values in parentheses are standard deviations on the last significant figure.

Species	logβ	pK_a	Coord.	logβ	pK_a	Coord.
	HAWG-Am			**HAWGC(SMe)-Am**		
$[CuL]^{2+}$	8.24(1)	7.5	N_{Im}, NH_2	8.21(1)	7.4	N_{Im}, NH_2
$[CuLH_{-1}]^{+}$	0.7(3)	8.0	N_{Im}/NH_2, N^-	0.8(4)	7.6	N_{Im}/NH_2, N^-
$[CuLH_{-2}]$	-7.3(1)	7.7	N_{Im}/NH_2, $2N^-$	-6.8(1)	7.8	N_{Im}/NH_2, $2N^-$
$[CuLH_{-3}]^{-}$	-15.04(3)	-	N_{Im}/NH_2, $3N^-$	-14.57(4)	-	N_{Im}/NH_2, $3N^-$
$[CuL_2]^{2+}$	14.26(3)	-	2 (N_{Im}, NH_2)	14.63(4)	-	2 (N_{Im}, NH_2)
$[Cu_2L_2H_{-2}]^{2+}$	5.5(1)	7.8		5.9(1)	7.4	
$[Cu_2L_2H_{-3}]^{+}$	-2.3(1)	-		-1.5(1)	-	
	AAHAWG-Am			**AAHAWGC(SMe)-Am**		
$[CuH_{-2}L]$	-0.47(1)	11.59	N_{Im}, NH_2, $2N^-$	-0.86(1)	11.7	N_{Im}, NH_2, $2N^-$
$[CuH_{-3}L]^{-}$	-12.06(3)	-	N_{Im}, NH_2, $2N^-$	-12.6(2)	-	N_{Im}, NH_2, $2N^-$
	HAWG-Am			**HAWGC(SMe)-Am**		
$[ZnL]^{2+}$	4.7(1)	7.58	N_{Im}, NH_2	4.35(5)	-	N_{Im}, NH_2
$[ZnH_{-1}L]^{+}$	-2.87(4)	8.73	N_{Im}, NH_2	-	-	-
$[ZnH_{-2}L]$	-11.61(4)	-	N_{Im}, NH_2	-12.40(3)	-	N_{Im}, NH_2
$[ZnH_2L_2]^{4+}$	21.50(7)	-	2 (N_{Im})	-	-	-
$[ZnL_2]^{2+}$	9.96(7)	-	2 (N_{Im}, NH_2)	8.86(5)	-	2 (N_{Im}, NH_2)
	AAHAWG-Am			**AAHAWGC(SMe)-Am**		
$[ZnL]^{2+}$	3.18 (6)	7.90	N_{Im}, NH_2	3.28(7)	7.77	N_{Im}, NH_2
$[ZnH_{-1}L]^{+}$	-4.72 (4)	8.21	N_{Im}, NH_2	-4.49(4)	8.68	N_{Im}, NH_2
$[ZnH_{-2}L]$	-12.92 (3)	-	N_{Im}, NH_2	-13.17(5)		N_{Im}, NH_2

In the case of Zn(II) ion, the formation of complexes with AAHAWG-Am and HAWG-Am exclusively occurs by means of the histidine residue and the terminal amino group, giving rise to (N_{Im}, NH_2) complexes. A tetrahedral geometry is conceivable, where coordinated water molecules complete the zinc coordination sphere. Interestingly, these preliminary data reveal that in Zn(II)/HAWG-Am system, bis-complexes dominate in the pH range 4.5–8.5; while they have not been detected in the case of AAHAWG-Am.

The interaction of Cu(II) with the two tetramers built on the cyclam scaffold has been studied through spectroscopic and spectrometric techniques at fixed pH. In the case of $(AAHAWG)_4$-PWT2, mass spectrometry identified the species $[Cu_4LH_{-8}]K_4^{4+}$ (m/z = 1029.4) and $[Cu_4LH_{-8}]K_3^{3+}$ (m/z = 1359.7), suggesting that each branch of the tetramer behaves exactly like the monomer and independently binds one Cu(II) ion. This hypothesis is confirmed by spectrophotometric and spectrofluorimetric titrations performed at pH 7.4 and pH 9. At both pH values the absorbance increases and the fluorescence intensity decreases during the addition of Cu(II), reaching a plateau when the metal ion is equimolar to the peptide branches, *i.e.* when the concentration of copper is four times that of $(AAHAWG)_4$-PWT2. In the case of $(HAWG)_4$-PWT2, mass spectra show the signals of mono- to tetra-nuclear complexes. Based on fluorescence measurements at pH 7, we

suggest the formation of a species where the metal ion is bound to two peptide arms, according to the species $[CuL_2]^{2+}$ observed for the single peptide. This hypothesis is confirmed by the Vis absorption spectra, since we observed a d-d band at 630 nm, which is very close to the λ_{max} of $[CuL_2]^{2+}$ complex of HAWG-Am. Moreover, CD spectra are perfectly superimposable to those recorded for the system Cu(II)/HAWG-Am, at neutral pH and in excess of ligand. The fluorescence binding isotherm at pH 9.0 shows that the emission intensity of the tryptophan residue is very rapidly quenched with Cu(II) addition, with an equivalence point corresponding to 2 copper ions per ligand. In these conditions the hypothesis of the formation of a 2:1 Cu:L complex (each Cu(II) coordinated by two peptide arms) is in full agreement with visible absorption data. Moreover, since in our experiments the $(HAWG)_4$-PWT2 concentration is 0.20 mM (corresponding to a formal concentration of the peptide branches of 0.80 mM), our data suggest that through $(HAWG)_4$-PWT2 we could achieve an increase of the peptide "local concentration" of 2–3 orders of magnitude compared to the same conditions using the single-chain analogue. Finally, *in silico* analyses showed that the four branches (peptide plus spacer) have an adequate length and a sufficient degree of flexibility to place the N-termini of the peptides close to each other, allowing the formation of histamine-like $[Cu(peptide)_2]$ adducts (**Figure 9.2**).

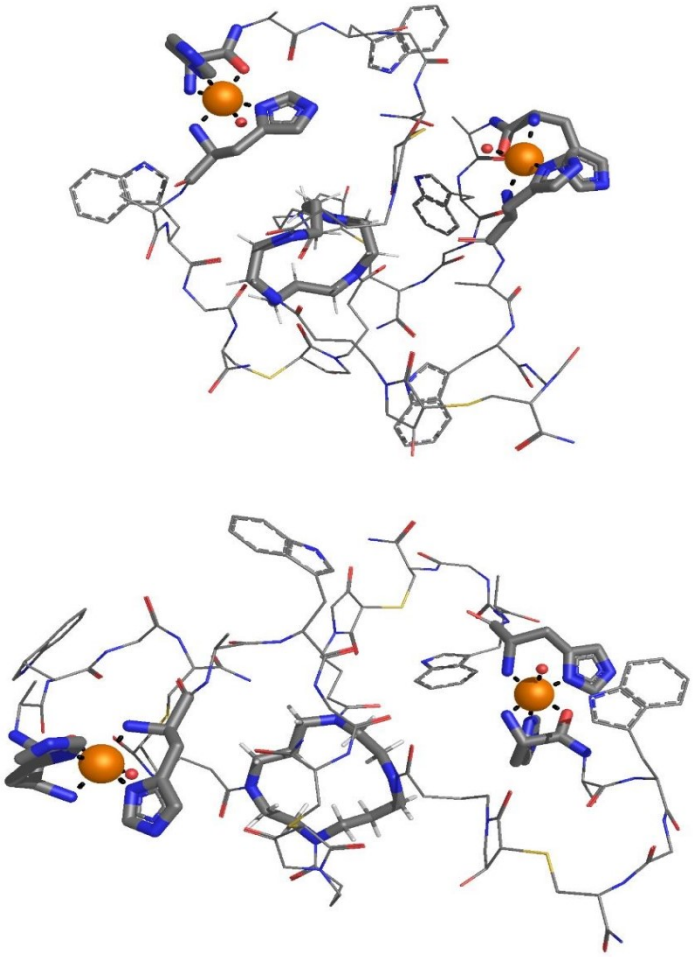

Figure 9.2 - Representation of two model structures of different atropoisomers of the adducts $[Cu_2(HAWG)_4$-PWT2]. The cyclam scaffold and the two histamine-like copper binding sites are represented as thick sticks, Cu(II) ion is the orange sphere. In the figure, the imidazole of the terminal His (N_{NH2}, O)-coordinated and a water molecule (red sphere) are in axial position.

9.4 Conclusions

Each AAHAWG peptide mounted on the cyclam scaffold retains the property to form ATCUN-type adducts with copper. However, in the AAHAWG-PWT2 the affinity of the four chelating groups is not exactly the same and the metal binding ability decreases as the amount of Cu(II) bound to the ligand increases. With the ligand HAWG-Am we were able to qualitatively obtain what we expected from our design. On one hand, the nature of the scaffold and the length of the spacer allowed a large degree of freedom of the peptides which, at pH 7, can form 1:2 adducts with copper, adopting the mixed *histamine-like* and *glycine-like* coordination, as the single-chain peptide does. Most importantly, the latter coordination mode is predominant also at pH 9, unlike what occurs with free HAWG-Am. This behaviour (*i.e.* avoiding peptide nitrogen deprotonation) is unachievable at pH 9 for the single chain-peptides unless its concentration is in the molar range. This is not only an extraordinarily high concentration for model peptides, but it is also out of the solubility range for the vast majority of proteins. Therefore, with our branched peptides we were able to shift up the effective molar concentration of the chelating groups (N-termini) of 2 to 3 orders of magnitude by mounting 4 equivalent peptides on a cyclam scaffold. We expect that avoiding peptide nitrogen deprotonation and coordination will have, for instance, a noticeable effect on the Cu(I)/Cu(II) redox potential, since amide nitrogen coordination stabilizes Cu(II). Along with this consideration we preview that the development of these branched peptides will get into the development of copper bioinspired catalysts based on stable coordination environments at pH conditions unachievable with the use of single-chain peptides.

This research work includes the publication "M. Perinelli, R. Guerrini, V. Albanese, N. Marchetti, D. Bellotti, S. Gentili, M. Tegoni, M. Remelli, *J. Inorg. Biochem.* 2020, *205*, 110980-110993".

9.5 References

[1] T. Yi-Hsuan, H. Adela Ya-Ting, C. Po-Yu, C. Hui-Ting, K. Chai-Lin, *Curr. Pharm. Des.* **2011**, *17(22)*, 2308-2330.

[2] Ł. Szyrwiel, J. S. Pap, Ł. Szczukowski, Z. Kerner, J. Brasuń, B. Setner, Z. Szewczuk, W. Malinka, *RSC Advances* **2015**, *5(70)*, 56922-56931.

[3] J. S. Pap, Ł. Szyrwiel, D. Srankó, Z. Kerner, B. Setner, Z. Szewczuk, W. Malinka, *Chem. Commun.* **2015**, *51(29)*, 6322-6324.

[4] E. Farkas, D. Srankó, Z. Kerner, B. Setner, Z. Szewczuk, W. Malinka, R. Horvath, Ł. Szyrwiel, J. S. Pap, *Chemical Science* **2016**, *7(8)*, 5249-5259.

[5] K. Jensen, in *Peptide and Protein Design for Biopharmaceutical Applications* (Ed.: K. Jensen), John Wiley and Sons Ltd, Chirchester, UK, **2009**, pp. 207-248.

[6] A. G. Tebo, V. L. Pecoraro, *Curr. Opin. Chem. Biol.* **2015**, *25*, 65-70.

[7] M. Tegoni, *Eur. J. Inorg. Chem.* **2014**, *2014(13)*, 2177-2193.

[8] M. Mutter, G. Tuchscherer, *Cell. Mol. Life Sci.* **1997**, *53(11)*, 851-863.

[9] G. Calo, A. Rizzi, C. Ruzza, F. Ferrari, S. Pacifico, E. C. Gavioli, S. Salvadori, R. Guerrini, *Peptides* **2018**, *99*, 195-204.

[10] R.-P. Martin, L. Mosoni, B. Sarkar, *J. Biol. Chem.* **1971**, *246(19)*, 5944-5951.

[11] T. Szabó-Plánka, A. Rockenbauer, L. Korecz, D. Nagy, *Polyhedron* **2000**, *19(9)*, 1123-1131.

[12] Y. Altun, F. Köseoĝlu, *J. Solution Chem.* **2005**, *34(2)*, 213-231.

[13] M. Perinelli, R. Guerrini, V. Albanese, N. Marchetti, D. Bellotti, S. Gentili, M. Tegoni, M. Remelli, *J. Inorg. Biochem.* **2020**, *205*, 110980-110993.

[14] P. Mlynarz, D. Valensin, K. Kociolek, J. Zabrocki, J. Olejnik, H. Kozlowski, *New J. Chem.* **2002**, *26(2)*, 264-268.

[15] K. Ősz, K. Várnagy, H. Süli-Vargha, A. Csámpay, D. Sanna, G. Micera, I. Sóvágó, *J. Inorg. Biochem.* **2004**, *98(1)*, 24-32.

[16] R. B. Martin, J. T. Edsall, *J. Am. Chem. Soc.* **1960**, *82(5)*, 1107-1111.

10. Chapter Ten: Future perspectives

The importance of transition metals as virulence factors is undoubtedly well recognised and accepted. Metal binding proteins, and in particular zinc binding proteins, represent the main targets in an antimicrobial scenario aimed at knocking out the pathogen through cellular starvation and inhibition of the metal import systems. The amount of free metal ions, in fact, must be strictly regulated both in the case of pathogens and humans. If one thinks about zinc, overload and shortage of the metal can certainly induce cellular apoptosis due to intrinsic cytotoxic effects (inhibition of enzymes through wrong metal coordination, formation of stable, irreversible protein complexes, disruption of the membrane potential, absence of crucial protein cofactors and consequent loss of enzymatic activity). Moreover, zinc binding proteins-targeted therapies may limit undesirable side effects for the host organism, since most eukaryotes, including humans, frequently exhibit different zinc acquisition pathways and totally lack most of the extracytosolic zinc-binding proteins here described for bacteria and fungi.

Since the host and the pathogen organisms compete for the acquisition of transition metal ions, any antimicrobial agent whose activity depends on the metal coordination must exhibit proper thermodynamic features in order to avoid the loss of its metallic substrate or its sequestration by a more efficient pathogenic protein. It is therefore necessary to clearly elucidate the thermodynamic and coordination chemistry behind metal binding proteins at the host/pathogen interface, and this PhD thesis gets a glimpse of the variety of existing systems. Moreover, the study of the antimicrobial peptide calcitermin represented an effective object of comparison to qualitatively speculate on the possible competition between the investigated pathogenic systems and the calcitermin-mediated host defence. An example is given in **Figure 10.1**, where the metal binding affinity of calcitermin is compared with that of Zrt2 metal binding sites. Calcitermin activity against *C. albicans* is enhanced by the presence of Zn(II) and Cu(II) and according to our thermodynamic results calcitermin is also a better ligand for such metal ions in the pH range where it is biologically active. The same is verified in the case of the bacterial protein ZinT (Chapter 3). Thus, the present results suggest that one possible calcitermin antimicrobial way of action may be related to the metal binding affinities of the competing systems.

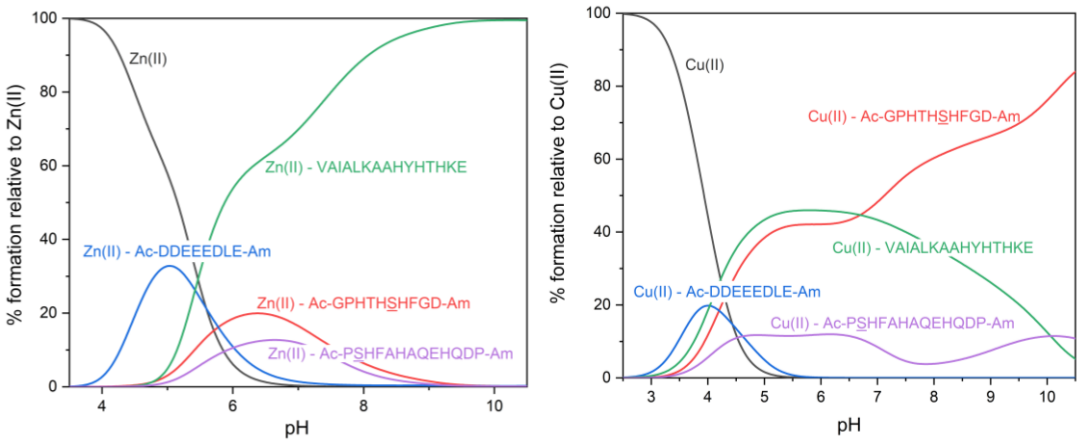

Figure 10.1 - Competition plot for a solution containing equimolar concentrations ($1 \cdot 10^{-3}$ M) of metal ion, calcitermin VAIALKAAHYHTHKE (see Chapter 6) and Zrt2 binding sites (Ac-GPHTHSHFGD-Am, Ac-DDEEEDLE-Am and Ac-PSHFAHAQEHQDP-Am) (see Chapter 5).

Hence, impairing the cell metals homeostasis can represent a promising antimicrobial strategy with a high rate of selectivity and specificity. The administration of compounds able to mimic, undermine or inactivate metal-binding proteins activity can result in a less morbidity and in the attenuation of the pathogen virulence, until a most desirable microbicide property. For this purpose, one can rely on *de novo* designed molecules with inedited characteristics and way of actions or on derivatives of already existing natural antimicrobial agents that commonly reside in the host organism and participate in the nutritional immunity process (*e.g.* calcitermin). These systems, and their *ad hoc* synthetized derivatives, may exhibit the antimicrobial activity by simply displaying higher metal binding affinity and thermodynamic stability, which in turn allows the metal ions sequestration and the reduction of their bioavailability.

The results obtained in this work are the basis of a further research project focused on calcitermin peptide derivatives, with the aim of obtaining novel, potent and stable antimicrobial agents. This project has been already financed by the Polish National Science Centre (Preludium Grant no. UMO-2020/37/N/ST4/03165). The peptidomimetic strategy, *i.e.* the modification of the native peptide structure in order to improve its potential, will be applied to calcitermin. The synthetic approach includes the insertion/substitution of D-amino acids, non-proteinogenic amino acids or β-amino acids, and the synthesis of peptoids. All these mutations should increase the proteolytic stability of native calcitermin, giving rise to novel classes of potential metal-based-AMPs.

Annexes

The full version of the published journal articles are reported as annexes.

Dalton Transactions

ROYAL SOCIETY OF CHEMISTRY

PAPER

View Article Online
View Journal | View Issue

Cite this: *Dalton Trans.*, 2020, **49**, 9393

Novel insights into the metal binding ability of ZinT periplasmic protein from *Escherichia coli* and *Salmonella enterica*†

Denise Bellotti, [a,b] Magdalena Rowińska-Żyrek [b] and Maurizio Remelli *[a]

Received 4th May 2020,
Accepted 18th June 2020

DOI: 10.1039/d0dt01626h

rsc.li/dalton

The ZinT mediated Zn(II) uptake is one of the major differences in the metabolism of human and bacterial cells that can be challenged when looking for possible highly selective metal-based therapeutics. ZinT is a 216-amino acid periplasmic protein expressed by Gram-negative bacteria, which shuttles Zn(II) ions to the ZnuABC transporter under zinc-limiting conditions. The suggested metal-binding sites of ZinT correspond to a domain containing three highly conserved histidine residues (His 167, 176 and 178) and to the N-terminal histidine-rich loop HGHHXH (residues 24–29). The coordination chemistry of the ZinT complexes with Zn(II) and Cu(II) has been investigated. The present work is focused on the protected peptides Ac-^{24}HGHHSH^{29}-NH_2 and Ac-^{166}DHIIAPRKSSHFH^{178}-NH_2 as models for the putative metal binding sites of ZinT from *Escherichia coli* (*Ec*ZinT), and Ac-^{24}HGHHAH^{29}-NH_2 and Ac-^{166}DHIIAPRKSAHFH^{178}-NH_2 from the ZinT protein expressed by *Salmonella enterica* sv. Typhimurium (*Se*ZinT). The investigated peptides are able to form stable mono-nuclear complexes where the histidine residues represent the principal metal anchoring sites. The ZnuA (a periplasmic component of the ZnuABC transporter) metal binding site exhibits higher affinity for Zn(II) than ZinT, suggesting that the interaction of the two proteins through the formation of a binary complex may involve the metal transfer from ZinT to ZnuA. In contrast, this would not occur in Cu(II), since the ZinT complexes are more stable. Furthermore, at acidic pH, where the antimicrobial peptide calcitermin is biologically active, it also binds the metal ions with higher affinity than ZinT, representing a possible efficient competitor and antagonist of ZinT in the host human organism.

Introduction

The dramatic dissemination of antibiotic-resistant microorganisms represents both a serious threat and a scientific challenge of the modern age. The acquisition of metals from the host environment is a fundamental aspect of infections and deeper insights into the mechanism of metal trafficking in pathogens can provide crucial information to design new effective antimicrobial treatments.[1–3] Several pathogenic microorganisms are capable of expressing metallophore systems for the purpose to sequester metals from the host environment. In the process of nutritional immunity, in fact, the host and the pathogen compete for the acquisition of metallic nutrients and, therefore, the relative metal binding affinity and the specific coordination properties can seriously affect the activity and the effectiveness of the involved systems.[4–7]

The Zn(II) assimilation pathway provided by the ZinT/ZnuABC transport system is a promising strategy to develop novel treatments against infectious diseases, since this metal transporter does not have homologues in eukaryotic cells and it can therefore assure high specificity and selectivity, minimizing collateral side effects in patients.[8] The high-affinity Zn(II) uptake system ZnuABC belongs to the family of ATP-binding cassette transporters and it is composed of three proteins: ZnuA (periplasmic metallochaperone), ZnuB (membrane permease) and ZnuC (the ATPase component).[9,10] Recent studies have also identified an additional auxiliary periplasmic component of the bacterial ZnuABC system, which collaborates with ZnuA in the mechanism of Zn(II) recruitment from the periplasmic environment under severe zinc-limiting conditions. This protein is known as ZinT (formerly named YodA) and it is expressed by many Gram-negative bacteria, including *Escherichia coli* and *Salmonella enterica*.[11–14] Interestingly, recent studies have also demonstrated that ZinT and ZnuA can specifically interact together to form a binary system, but only if they are in a Zn(II)-bound form.[8,14,15]

[a]*Department of Chemical and Pharmaceutical Sciences, University of Ferrara, Luigi Borsari 46, 44121 Ferrara, Italy. E-mail: maurizio.remelli@unife.it*
[b]*Faculty of Chemistry, University of Wrocław, F. Joliot-Curie 14, 50-383 Wrocław, Poland*

†Electronic supplementary information (ESI) available. See DOI: 10.1039/D0DT01626H

An efficient metal ion import is doubtlessly critical for *Escherichia coli* and *Salmonella enterica* pathogenicity, together with a proficient resistance system that can prevent microbial cells from heavy metal poisoning. Interestingly, the physiological role of ZinT is related not only to Zn(II) homeostasis but also to cellular metal detoxification. In fact, beside zinc shortage, its expression can be upregulated upon cadmium stress, inducing protein accumulation in the periplasmic region.[16] Furthermore, ZinT exhibits extremely versatile metal binding properties and affinity for several other divalent metal ions.[15,17]

Various crystal structures of ZinT from *Escherichia coli* (*Ec*ZinT) and *Salmonella enterica* sv. Typhimurium (*Se*ZinT) have been reported, including Zn(II), Ni(II) and Cd(II) complexes (Protein Data Bank (PDB) entries: 1OEJ, 1OEK, 1OEE, 5AQ6, 5YXC, 1S7D, 1TXL, 5XM5, 4AW8, 4AYH, and 4ARH). According to the evolutionarily highly conserved amino acid sequence of ZinT and its three-dimensional structures, the most probable identified metal-binding sites are two regions, corresponding to (i) the sequence containing three histidine residues at positions 167, 176 and 178,[18,19] and (ii) the highly conserved histidine-rich loop (HGHHXH) located at the N-terminal position of the protein.[8,15,20] No thermodynamic data are available for ZinT metal binding sites and the accepted evidence encouraged us to proceed with the investigation of Zn(II) and Cu(II) complexes with ZinT in both *E. coli* (*Ec*ZinT) and *S. enterica* (*Se*ZinT) species. Although the physiological role of ZinT in Cu(II) metabolism has not been confirmed yet, Cu(II) is essential for many enzymatic processes and it can be extremely toxic to microbes, since it generates reactive oxygen species (ROS), increasing the cellular oxidative stress.[21,22] In contrast, Zn(II) is redox inactive and is crucial for pathogen subsistence, participating in many cellular reactions as a coenzyme or cofactor.[23–25] Moreover, the importance of these ions in the process of nutritional immunity is decisive as well; human organisms can rely on a variety of proteins and antimicrobial peptides in order to sequester Zn(II) and Cu(II) and induce pathogen starvation, interfering with their virulence and survival in the host organism.[26,27]

The present paper describes a detailed study on Zn(II) and Cu(II) complexes with the following amino- and carboxyl-terminal protected peptides: Ac-HGHHSH-NH_2 (**L1**) and Ac-HGHHAH-NH_2 (**L2**), which serve as models for the N-terminal histidine-rich loop (the 24–29 amino acid sequence) of *Ec*ZinT and *Se*ZinT, respectively, and Ac-DHIIAPRKSSHFH-NH_2 from *Ec*ZinT (**L3**) and Ac-DHIIAPRKSAHFH-NH_2 from *Se*ZinT (**L4**), which correspond to the 166–178 amino acid sequence encompassing three highly conserved His residues (see Fig. 1). It is worth emphasizing the punctual Ser-to-Ala substitution occurring in each couple of the peptide homologues **L1**/**L2** and **L3**/**L4**. Since small changes in the peptide primary structure can affect the metal binding behaviour, a deep investigation of the complex-formation equilibria is required to fully understand the coordination properties of *Ec*ZinT and *Se*ZinT and to highlight the possible differences between the behaviors of the two bacterial species. The thermodynamic and spectroscopic analyses of metal-ZinT complexes have been performed by means of several experimental techniques. The complex formation equilibria have been investigated over a wide pH range through high-resolution mass spectrometry and potentiometric titrations. A complementary description of the metal coordination sphere and molecular geometry has been provided by UV-Vis spectrophotometry, circular dichroism (CD) spectroscopy and electronic paramagnetic resonance (EPR).

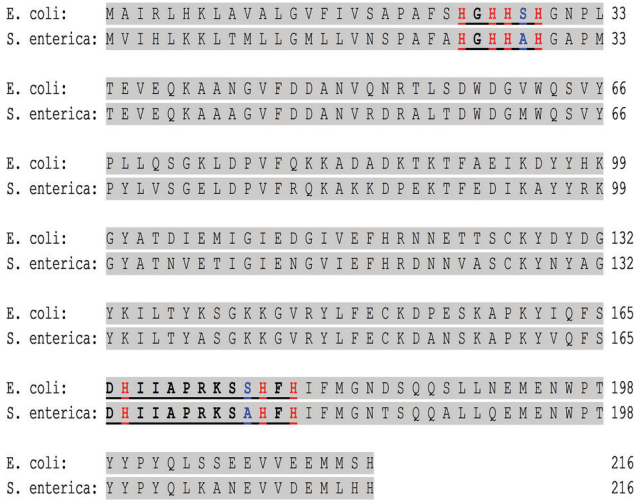

Fig. 1 Protein sequence alignment between *Ec*ZinT and *Se*ZinT.[15,20] The studied regions are marked in color.

Experimental

Materials

All peptides (Ac-HGHHSH-NH_2, Ac-HGHHAH-NH_2, Ac-DHIIAPRKSSHFH-NH_2 and Ac-DHIIAPRKSAHFH-NH_2) were purchased from KareBay Biochem (USA) with a certified purity of 98%. They were used as received. $Zn(ClO_4)_2{\cdot}6H_2O$ and $Cu(ClO_4)_2{\cdot}6H_2O$ were extra pure products (Sigma-Aldrich); the concentrations of their stock solutions were standardised by EDTA titration and periodically analysed *via* ICP-MS. The carbonate-free stock solution of 0.1 mol dm^{-3} NaOH was purchased from Sigma-Aldrich and standardized with the primary standard potassium hydrogen phthalate (99.9% purity) by potentiometry. The $HClO_4$ stock solution was prepared by diluting concentrated $HClO_4$ (Sigma-Aldrich) and then standardizing it with NaOH. The ionic strength was adjusted to 0.1 mol dm^{-3} by adding $NaClO_4$ (Sigma-Aldrich). Grade A glassware was employed throughout. All sample solutions were prepared with fresh doubly distilled water.

Potentiometric measurements

The stability constants for proton and metal complexes were calculated from the pH-metric titration curves registered at T = 298 K and an ionic strength of 0.1 mol dm^{-3} ($NaClO_4$) with a total volume of 3 cm^{-3}. The potentiometric apparatus consisted of a Metrohm 905 Titrando pH-meter system provided

with a Metrohm LL Unitrode glass electrode and a dosing system 800 Dosino, equipped with a 2 ml micro burette. High purity grade argon was gently blown over the sample solution to ensure an inert atmosphere. The solutions were titrated under constant-speed magnetic stirring with 0.1 mol dm^{-3} carbonate-free NaOH. The electrode was daily calibrated for hydrogen ion concentration by titrating $HClO_4$ with standard NaOH under the same experimental conditions as above. The standard potential and the slope of the electrode couple were computed by means of the Glee[28] program. The purity and the exact concentrations of the ligand solutions were potentiometrically determined using the Gran method.[29] The HYPERQUAD[30] program was employed to calculate the overall formation constant (β), referring to the following equilibrium:

$$pM + qL + rH \leftrightarrows M_pL_qH_r$$

(the charges are omitted; p is 0 in the case of ligand protonation; r can be negative). The step formation constants (K) and/or acid dissociation constants (K_a) were also reported. The computed standard deviations (referring to random errors only) were given by the program itself and are shown in parentheses as uncertainties in the last significant figure. The hydrolysis constants for the Cu(II) and Zn(II) ions were taken from the literature: $[CuH_{-1}]^{+}$ $\log\beta = -7.7$, $[Cu_2H_{-2}]^{2+}$ $\log\beta = -10.75$, $[Cu_3H_{-4}]^{2+}$ $\log\beta = -21.36$, and $[CuH_{-4}]^{2-}$ $\log\beta = -39.08$;[31] $[ZnH_{-1}]^{+}$ $\log\beta = -8.96$, $[ZnH_{-2}]$ $\log\beta = -16.9$, $[ZnH_{-3}]^{-}$ $\log\beta = -28.4$, and $[ZnH_{-4}]^{2-}$ $\log\beta = -41.2$.[32] The distribution diagrams were computed using the HYSS program.[33] A comparison of the overall metal binding ability of different ligands was performed by computing the competitive diagrams. They represent the simulation of a solution containing the metal and two (or more) ligands (or *vice versa*) and are based on previously obtained binary speciation models, admitting that all the components compete to form the respective binary complexes without mixed species formation. This is a reasonable approximation in the case of peptides, which most often form only 1 : 1 complexes where the peptide completely wraps the metal ion.

Mass spectrometric measurements

High-resolution mass spectra were obtained on a BrukerQ-FTMS spectrometer (Bruker Daltonik, Bremen, Germany), equipped with an Apollo II electrospray ionization source with an ion funnel. The mass spectrometer was operated in the positive ion mode. The instrumental parameters were as follows: scan range m/z 100–2500, dry gas nitrogen, temperature 453 K and ion energy 5 eV. The capillary voltage was optimized to the highest signal-to-noise ratio, corresponding to 4500 V. The small changes in the voltage (±500 V) did not significantly affect the optimized spectra. The samples (Zn(II) : ligand and Cu(II) : ligand in a 0.9 : 1 stoichiometry, $[ligand]_{tot} = 0.5 \times 10^{-3}$ mol dm^{-3}) were prepared with a 1 : 1 methanol–water mixture at different pH values and were infused at a flow rate of 3 μL min^{-1}. The instrument was externally calibrated with a Tunemix™ mixture (Bruker Daltonik, Germany) in the quadratic regression mode. The data were processed using the Bruker Compass DataAnalysis 3.4 program. The mass accuracy for the calibration was greater than 5 ppm, showing together with the true isotopic pattern (using SigmaFit) an unambiguous confirmation of the elemental composition of the obtained complex.

Spectroscopic measurements

The absorption spectra were recorded on a Varian Cary300 Bio spectrophotometer, in the range of 200–800 nm, using a quartz cuvette with an optical path of 1 cm. Circular dichroism (CD) experiments were performed using a Jasco J-1500 CD spectrometer at 298 K in 0.01 cm and 1 cm quartz cells in the spectral ranges of 180–270 and 200–800 nm, respectively. The ligands were dissolved in a water solution containing 4×10^{-3} mol dm^{-3} $HClO_4$ and 0.1 mol dm^{-3} $NaClO_4$. The ligand concentration was 0.5×10^{-3} mol dm^{-3} (200–800 nm range) and 0.1×10^{-3} mol dm^{-3} (180–270 nm range). The Cu(II) to ligand molar ratio was 0.9 : 1. The UV-Vis and CD spectroscopic parameters were extracted from the spectra obtained at the pH values corresponding to the maximum concentration of each particular species, based on the distribution diagrams. Electron paramagnetic resonance (EPR) spectra were recorded in liquid nitrogen on a Bruker ELEXSYS E500 CW-EPR spectrometer at an X-band frequency (9.5 GHz), equipped with an ER 036TM NMR teslameter and an E41 FC frequency counter. Ethylene glycol (30%) was used as a cryoprotectant. The ligand concentration was 1.0×10^{-3} mol dm^{-3} and the Cu(II) to ligand ratio = 0.9 : 1. The EPR parameters were analysed by simulating the experimental spectra using the WIN-EPR SIMFONIA software, version 1.2 (Bruker).

Results and discussion

Ligand protonation

The investigated peptides are protected at their amino- and carboxyl-termini by means of acetylation and amidation, respectively. The ligand acid–base behaviour, therefore, only depends on the amino acid side chain properties; the corresponding experimental overall and step protonation constants are reported in Table 1. The amide groups of the peptide backbone are very weak acids ($pK_a \approx 15$)[34] and the spontaneous release of their protons cannot occur in the explored pH range (2.5–10.5). For each peptide, the obtained *macro*-constants reported in Table 1 were compared with the literature data in order to assign the protonation step to the corresponding functional group. The term L here indicates the ligand in its unprotonated form where all the dissociable protons have been released; the net charge of L is zero for all the investigated ligands. However, in the case of **L1** and **L2**, L corresponds to a peptide without any charged groups, while in **L3** and **L4** L is a zwitterionic species, due to the presence of the negatively charged carboxylate group of the Asp residue and the positively charged arginyl guanidinium group, which is always protonated in the pH range here employed.

In ligands **L1** and **L2** there are four histidine residues which are involved in the acid–base equilibria. The obtained

Table 1 Overall ($\log\beta$) and step ($\log K$) protonation constants for all the investigated ligands (Ac-HGHHSH-NH_2 (**L1**), Ac-HGHHAH-NH_2 (**L2**), Ac-DHIIAPRKSSHFH-NH_2 (**L3**) and Ac-DHIIAPRKSAHFH-NH_2 (**L4**)) at T = 298 K and I = 0.1 mol dm^{-3} ($NaClO_4$). Values in parentheses are standard deviations in the last significant figure

	L1		**L2**		**L3**		**L4**	
Species	$\log\beta$	$\log K$	$\log\beta$	$\log K$	$\log\beta$	$\log K$	$\log\beta$	$\log K$
HL^{+}	7.38(9)	7.38	7.16(9)	7.16	9.53(3)	9.53	9.65(2)	9.65
H_2L^{2+}	13.87(6)	6.50	13.75(5)	6.59	16.27(3)	6.74	16.56(4)	6.90
H_3L^{3+}	19.87(9)	6.00	19.68(8)	5.93	22.59(2)	6.32	22.91(3)	6.35
H_4L^{4+}	25.60(7)	5.73	25.46(6)	5.78	28.17(3)	5.58	28.64(3)	5.74
H_5L^{5+}					32.22(3)	4.06	32.56(4)	3.92

pK_a values range from 5.73 to 7.38, in good agreement with the literature protonation constants for histidine residues.[35] Ligands **L3** and **L4** contain five functional groups with dissociable protons: the carboxylic side chain of aspartic acid, the imidazole groups of the three histidine residues and the lysyl amino group. In the case of both the ligands, we attribute the lowest pK_a value to the carboxylic acid of the Asp residue (4.06 and 3.92), while the next three protonation steps can be assigned to the histidine residues with the pK_a values ranging from 5.61 to a maximum of 6.91. The highest formation constants, 9.50 (**L3**) and 9.65 (**L4**), most likely correspond to the lysine ε-amino groups. The rather low pK_a values can be related to the Lys proximity to the protonated arginyl guanidinium group. Indeed, the low pK_a values (even lower than 9) for lysine deprotonation are comparable with those found in the literature, where the increased acidity is explained by the presence of vicinal positively charged side chains (Lys, Orn and Arg).[36–38] Notably, the Ser-to-Ala substitution does not significantly affect the acid–base properties of the investigated peptides, since the obtained protonation constants of each homologue couple Ac-HGHHSH-NH_2/Ac-HGHHAH-NH_2 and Ac-DHIIAPRKSSHFH-NH_2/Ac-DHIIAPRKSAHFH-NH_2 are comparable.

Cu(II) complexes

The high resolution mass spectra revealed the formation of mononuclear Cu(II) complexes under the employed experimental conditions. Signals corresponding to various sodium and potassium adducts, together with differently protonated free ligand and metal complexes, have been detected. No polynuclear complexes or bis-complexes have been identified. The mass spectra are reported in Fig. S1–S4, ESI.† The speciation models obtained by potentiometry confirm the occurrence in the solution of 1 : 1 metal complexes, in accordance with the MS results. The complex-formation constants for Cu(II) are reported in Table 2, and the corresponding species distribution diagrams are shown in Fig. 2 and S5–S7, ESI.† The spectroscopy data are summarised in Tables S1–S4, ESI† and the UV-Vis, CD and EPR spectra are depicted in Fig. 3, 4 and S8–S16, ESI.†

Potentiometric measurements revealed that Cu(II) is able to interact with **L1** and **L2** starting from pH 3. The first identified species is $[CuH_2L]^{4+}$; the speciation diagrams plotted in Fig. 2 and S5, ESI† show that its percentage of formation in solution remains rather low (25%) since this complex is quickly substituted with the $[CuHL]^{3+}$ species, that is by far the most abundant complex in solution is observed from pH 4.5 up to pH 6. In $[CuH_2L]^{4+}$ the ligand has already lost two acidic protons from its fully protonated histidine residues which can thus bind the metal ion and form a ($2N_{Im}$) species. The following deprotonation step, associated with the formation of the $[CuHL]^{3+}$ complex, has a pK_a value of 4.45 (**L1**) and 4.46 (**L2**), both attributable to the deprotonation and binding of the third imidazole group. This step is also accompanied by a shift of the visible absorption spectra towards shorter wavelengths, thus indicating an increase of the number of coordinated nitrogen atoms around Cu(II) (Fig. 3 and S9, ESI†). The measured λ_{max} values for the complex solutions at pH ≈ 5.5 – where $[CuHL]^{3+}$ is the most abundant species – are 637 nm for Cu(II)–**L1** and 626 nm for Cu(II)–**L2**, and suggest a ($3N_{Im}$) coordination for both the systems. The next deprotonation step occurs with pK_a = 6.26 (**L1**) and 6.37 (**L2**), leading to the

Table 2 Overall stability constants ($\log\beta$) and acid dissociation constants (pK_a) of Cu(II) complexes with all the investigated ligands (Ac-HGHHSH-NH_2 (**L1**), Ac-HGHHAH-NH_2 (**L2**), Ac-DHIIAPRKSSHFH-NH_2 (**L3**) and Ac-DHIIAPRKSAHFH-NH_2 (**L4**)) at T = 298 K and I = 0.1 mol dm^{-3} ($NaClO_4$). Values in parentheses are standard deviations in the last significant figure

	L1		**L2**		**L3**		**L4**	
Species	$\log\beta$	pK_a	$\log\beta$	pK_a	$\log\beta$	pK_a	$\log\beta$	pK_a
$[CuH_2L]^{4+}$	19.72(8)	4.45	19.4(1)	4.46	22.26(3)	5.32	22.53(4)	5.40
$[CuHL]^{3+}$	15.27(3)	6.26	14.93(4)	6.37	16.94(4)	5.74	17.13(5)	5.68
$[CuL]^{2+}$	9.00(7)	7.15	8.56(8)	7.24	11.19(4)	6.19	11.45(5)	6.35
$[CuH_{-1}L]^{+}$	1.85(8)	7.31	1.32(9)	7.38	5.00(4)	9.03	5.10(4)	9.65
$[CuH_{-2}L]$	−5.46(7)	9.31	−6.06(8)	9.52	−4.03(7)	10.18	−4.54(6)	10.35
$[CuH_{-3}L]^{-}$	−14.78(8)		−15.59(9)		−14.20(7)		−14.90(5)	

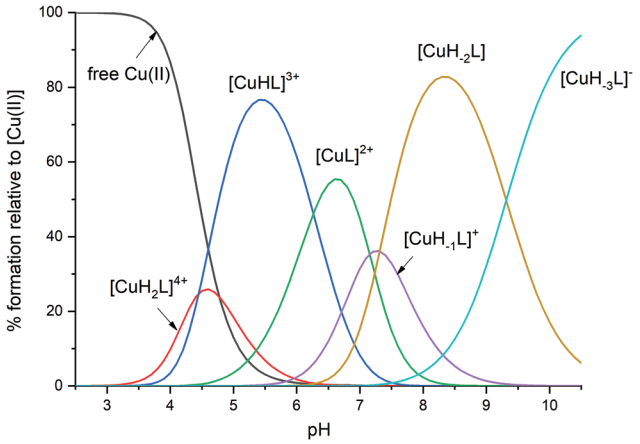

Fig. 2 Species distribution diagram relative to Cu(II)/**L1** complexes; M : L molar ratio = 0.9 : 1; $C_{Cu(II)}$ = 0.45 × 10^{-3} mol dm^{-3}.

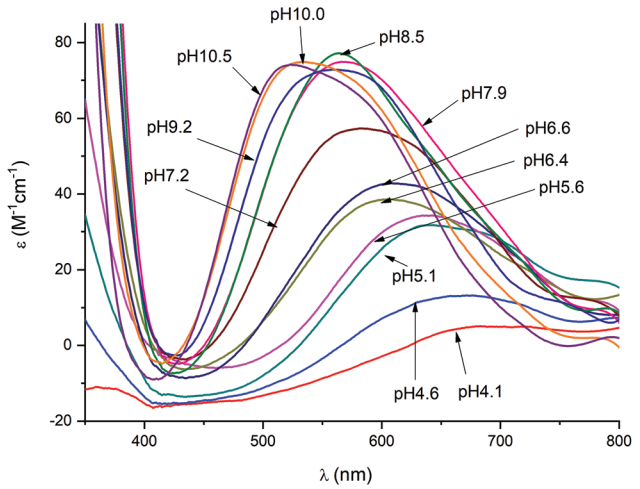

Fig. 3 Vis absorption spectra for Cu(II) complexes with **L1**; M : L ratio = 0.9 : 1. $C_{Cu(II)}$ = 0.45 × 10^{-3} mol dm^{-3}; optical path 1 cm.

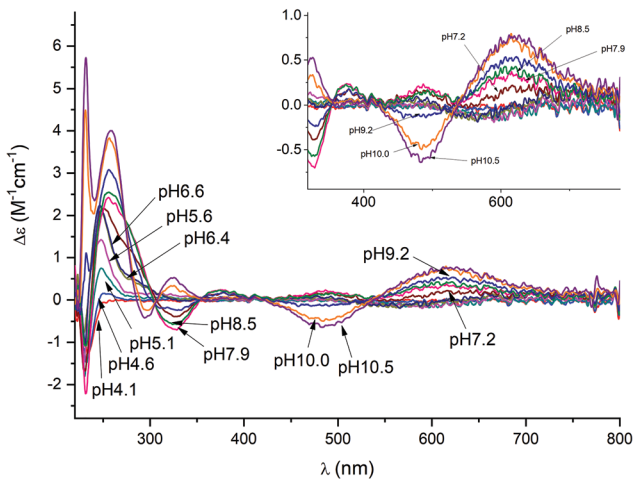

Fig. 4 CD spectra for Cu(II) complexes with **L1**; M : L ratio = 0.9 : 1. $C_{Cu(II)}$ = 0.45 × 10^{-3} mol dm^{-3}; optical path 1 cm.

formation of the species $[CuL]^{2+}$. In this case the most reasonable hypothesis is the release of the proton from an amide group of the peptide backbone, which can be ionized, thanks to the interaction with the Cu(II) ion. In fact, the corresponding d–d band in the UV-Vis spectra at pH around 6.5–7, where $[CuL]^{2+}$ reaches its maximum of formation (Fig. 2 and S5, ESI†), is characterized by the λ_{max} value (**L1**: 608 nm and **L2**: 600 nm) very close to the expected absorption wavelength for the ($2N_{Im}$, N^-) complex (604 nm (ref. 34)); the fourth equatorial position should be occupied by a water molecule. Therefore, in the formation of the $[CuL]^{2+}$ species, a N-amide group should substitute one histidine residue in the equatorial plane of the metal coordination sphere. Moreover, starting from pH 6, a slight variation in the CD spectra likely confirms the Cu(II) interaction with the backbone N-amide (Fig. 4 and S10, ESI†). The EPR parameters at pH 6.5 also indicate the prevalence of a 3N coordination (**L1**: $g_{\|}$ = 2.25, $A_{\|}$ = 180.4; **L2**: $g_{\|}$ = 2.22, $A_{\|}$ = 175.3).[39] Upon increasing the pH value, the species $[CuH_{-1}L]^+$ and $[CuH_{-2}L]$ are formed with the following corresponding acid dissociation constants: pK_a = 7.15 and 7.31 (**L1**) and pK_a = 7.24 and 7.38 (**L2**). From pH 6.5 to pH 9, the absorption spectra of both the systems undergo a further blue-shift towards the wavelengths of maximum absorption around 560 nm, suggesting the binding of one additional nitrogen atom, most likely with the substitution of the water molecule. An unequivocal description of the coordination mode of each formed complex in this pH range is not possible. However, one deprotonation step can be attributed to the mere release of the proton from the last protonated histidine residue, without directly participating in the metal complexation – the corresponding step constants (7.31 for **L1** and 7.24 for **L2**) are in fact very close to those measured in the absence of metal ions. The other step can be ascribed to the release of the acidic proton from a second backbone amide, which binds Cu (II) in the equatorial position, finally obtaining a ($2N_{Im}$, $2N^-$) coordination. The 4N binding mode for $[CuH_{-2}L]$ is also confirmed by EPR results.[39] Moreover, the increased signal intensity of the CD spectra in the above considered pH range is consistent with the increase of N-amide donors. Finally, at pH > 9, the last complex $[CuH_{-3}L]^-$ can be detected, characterized by pK_a = 9.31 (**L1**) or pK_a = 9.52 (**L2**). The visible spectra in the most alkaline pH range suggest the coordination of a third N-amide in the equatorial plane of the complex, with the substitution of an imidazole. The formation of the $[CuH_{-3}L]^-$ species causes a clear blue-shift of the Vis-absorption band to λ_{max} = 523 nm, in the case of the Cu(II)–**L1** system, and 540 nm in Cu(II)–**L2**. While the former wavelength perfectly agrees with the expected literature value (522 nm) for the (N_{Im}, $3N^-$) coordination mode, the latter value suggests the presence of an axial donor group, most likely a further histidine residue, which is known to induce a red-shift. An exhaustive explanation of this different behaviour is not simple; it can be suggested that, in **L2**, the additional coordination of an axial imidazole is (possibly electrostatically) hindered by the serine residue of **L1**.

In the case of **L3** and **L4**, Cu(II) complexes begin to form at pH 3.5. Under such acidic conditions, the metal coordination

can involve the carboxylate side chain of Asp and the histidine residues. The stoichiometry of the first detected complex $[CuH_2L]^{4+}$ suggests that two histidine residues and the carboxylic acid are already deprotonated. At such acidic pH the binding of the two imidazole groups likely occurs, while the coordination of COO^- is questionable. However, by subtracting the $\log\beta_{012}$ value from the $\log\beta_{112}$ value for each ligand, *i.e.* the contribution of the still protonated groups, one obtains 5.85 (**L1**), 5.65 (**L2**), 5.99 (**L3**) and 5.97 (**L4**). The latter two values are slightly higher than the former ones, supporting the hypothesis of the additional carboxylate coordination, in agreement with the spectroscopy results. The UV-Vis spectra recorded at pH 5 (Fig. S12 and S15, ESI†), where $[CuH_2L]^{4+}$ reaches its maximum of formation in solution, show a d–d band centred at λ = 654 nm (Cu(II)–**L3**) and 650 nm (Cu(II)–**L4**), which is in reasonably good agreement with the literature data for the ($2N_{Im}$, COO^-) Cu(II) complex (λ = 663 nm).[34] The binding groups most likely occupy three equatorial positions of the metal coordination sphere in a distorted octahedral geometry. The obtained $g_{\parallel}$ and $A_{\parallel}$ values of the EPR spectra recorded at pH 5.3 (Fig. S14, S17, Tables S3 and S4, ESI†) also confirm the (2N, O) coordination. The $[CuH_2L]^{4+}$ species loses a further proton with pK_a = 5.32 (**L3**) or 5.40 (**L4**), as a result of the deprotonation of the third histidine residue which can coordinate the metal ion in the fourth equatorial position. This hypothesis is supported by the fact that the expected wavelength of maximum absorption for the ($3N_{Im}$, COO^-) complex is 607 nm and the experimentally obtained λ_{max} values for $[CuHL]^{3+}$ are 603 nm and 610 nm for **L3** and **L4**, respectively. Upon increasing the pH value, two further deprotonation steps give rise to $[CuL]^{2+}$ and $[CuH_{-1}L]^{+}$, respectively. The corresponding pK_a values (see Table 2) agree with the hypothesis of the Cu(II)-induced ionization of two backbone amides. The metal interaction with the peptide backbone usually produces a stronger CD absorption, due to the proximity of the N-amide donor group to the peptide chiral centres, and the CD spectra in Fig. S13 and S16, ESI† do not show a remarkable CD activity up to pH = 6, *i.e.* when the $[CuL]^{2+}$ and $[CuH_{-1}L]^{+}$ complexes become the predominant species in solution. According to the UV-Vis absorption spectra and EPR data, the formed complexes likely involve 4 N equatorial donor groups, with a ($3N_{Im}$, N^-) and ($2N_{Im}$, $2N^-$) coordination mode for $[CuL]^{2+}$ and $[CuH_{-1}L]^{+}$, respectively. The next deprotonation step leads to the formation of the $[CuH_{-2}L]$ complex. The proton release occurs with pK_a = 9.03 for **L3** and pK_a = 9.65 for **L4** and it is reasonably attributable to the lysine ε-amino group. In the case of **L3** the recorded UV-Vis spectra for $[CuH_{-2}L]$ (pH ≈ 10) show a red-shift towards λ_{max} = 544 nm, suggesting a variation in the Cu(II) coordination environment. The slight changes of the EPR parameters (Fig. S14, ESI†) also suggest an apical perturbation in the Cu(II) coordination sphere, due to the possible interaction with the lysine ε-NH_2 moiety. In contrast, in the case of **L4** no spectroscopic changes were observed. The dissociation constant of 9.65 is also in perfect agreement with the hypothesis of the lysine deprotonation without being involved in the metal complexation (pK_a = 9.65 in the free ligand). Lastly, under the most alkaline conditions, the release of a further proton occurs with pK_a = 10.18 (**L3**) and 10.35 (**L4**), most likely corresponding to the deprotonation of the pyrrole-type nitrogen of a coordinated histidine group.[40,41] This hypothesis is supported by the absence of spectroscopic changes during the formation of the $[CuH_{-3}L]^{-}$ complex, thus excluding the coordination of a third amidic nitrogen group.

Zinc complexes

The investigated systems are able to form Zn(II) complexes in a stoichiometric ratio of 1 : 1 under the employed experimental conditions. The electrospray ionization mass spectra confirm the presence of only mononuclear species at different protonation degrees with all the studied systems. The most intense signals correspond to the free ligands and to their adducts with sodium and potassium ions; nevertheless, it was also possible to detect various Zn(II) complexes, confirming the speciation model obtained from the potentiometric data. The corresponding *m*/*z* values and the superimposition of the experimental and simulated isotopic patterns for the most intense Zn(II) complexes are shown in Fig. S18–S21, ESI.† Potentiometric calculations have been performed up to pH 8, due to the formation of a precipitate at alkaline pH. The complex-formation constants are shown in Table 3 and the species distribution diagrams are plotted in Fig. 5 and S22–S24, ESI.†

In the case of Ac-HGHHSH-NH_2 (**L1**) and Ac-HGHHAH-NH_2 (**L2**), at the most acidic pH values, the free metal ion is prevailing and Zn(II) complexes begin to form only above pH 4.5–5 (Fig. 5 and S22, ESI†). The di-protonated complex $[ZnH_2L]^{4+}$ is the first detected species in the **L2**-Zn(II) system. Notably, its formation is not detectable in the case of **L1**, where the first identified species is instead $[ZnHL]^{3+}$. Most likely, the **L1** di-

Table 3 Overall stability constants ($\log\beta$) and acid dissociation constants (pK_a) of Zn(II) complexes with all the investigated ligands (Ac-HGHHSH-NH_2 (**L1**), Ac-HGHHAH-NH_2 (**L2**), Ac-DHIIAPRKSSHFH-NH_2 (**L3**) and Ac-DHIIAPRKSAHFH-NH_2 (**L4**)) at T = 298 K and I = 0.1 mol dm^{-3} ($NaClO_4$). Values in parentheses are standard deviations in the last significant figure

	L1		**L2**		**L3**		**L4**	
Species	$\log\beta$	pK_a	$\log\beta$	pK_a	$\log\beta$	pK_a	$\log\beta$	pK_a
$[ZnH_2L]^{4+}$	—	—	17.3(1)	5.78	20.04(7)	6.28	20.17(5)	6.47
$[ZnHL]^{3+}$	11.85(7)	6.4	11.5(1)	6.0	13.76(5)	6.51	13.70(5)	6.61
$[ZnL]^{2+}$	5.5(1)	6.3	5.5(1)	6.1	7.25(3)	—	7.09(2)	—
$[ZnH_{-1}L]^{+}$	−0.82(7)	—	−0.57(3)	—	—	—	—	—

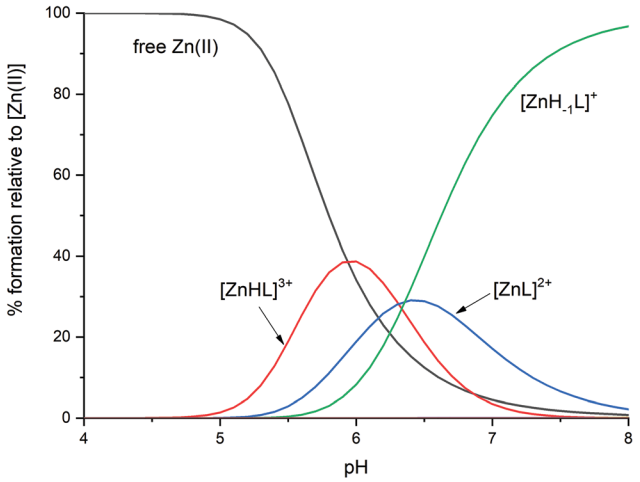

Fig. 5 Species distribution diagram relative to Zn(II)/**L1** complexes; M : L molar ratio = 0.9 : 1; $C_{Zn(II)}$ = 0.45 × 10^{-3} mol dm^{-3}.

protonated complex is only a transient species, which cannot be detected by potentiometry due its low percentage of formation in solution. In the $[ZnH_2L]^{4+}$ complex two histidine residues should have already deprotonated and bound to the metal ion; the complex geometry is likely tetrahedral, where two water molecules complete the Zn(II) coordination sphere. The stoichiometry of the $[ZnHL]^{3+}$ complex for both systems suggests that the Zn(II) coordination occurs by means of three imidazole groups ($3N_{Im}$). In the case of **L2** – where it was possible to calculate the corresponding step dissociation constant – the pK_a value of 5.78 agrees with the hypothesis of the deprotonation and coordination of a third His residue to form $[ZnHL]^{3+}$. The tetrahedral complex geometry most likely exists also in this species, where the fourth donor group is a water molecule. Upon increasing the pH value, two further complexes are formed, $[ZnL]^{2+}$ and $[ZnH_{-1}L]^{+}$. The former species most likely is derived from the $[ZnHL]^{3+}$ complex through the simple release of a proton from the coordinated water molecule; in the latter, the binding of a fourth histidine group possibly takes place. Once again, the preferred Zn(II) tetrahedral geometry should be retained in $[ZnL]^{2+}$ with the formation of the mono-hydroxo complex ($3N_{Im}$, O^-). The coordination of the fourth histidine group in $[ZnH_{-1}L]^{+}$ would instead lead to the formation of a pentacoordinate system ($4N_{Im}$, O^-) with a distorted pyramidal geometry, which is not surprising considering the conformational flexibility of the Zn(II) ion.[42,43] A mixture of tetrahedral and pyramidal species can also be hypothesized.

With the ligands Ac-DHIIAPRKSSHFH-NH_2 (**L3**) and Ac-DHIIAPRKSAHFH-NH_2 (**L4**), the Zn(II) complexation begins at pH 4.5 with the formation of $[ZnH_2L]^{4+}$ and $[ZnHL]^{3+}$, although the solution remains dominated by the presence of free Zn(II) up to about pH 6.5 (Fig. S23 and S24, ESI†). In the first identified species $[ZnH_2L]^{4+}$, the proposed hypothesized coordination is ($2N_{Im}$, COO^-), where two histidine residues and the Asp carboxylic side chain are bound to Zn(II) and occupy three coordination positions with a tetrahedral conformation. The fourth donor group should be a water molecule. The $[ZnHL]^{3+}$ complex begins to form at around pH 5–5.5. The related acid dissociation constants (**L3**: pK_a = 6.28; **L4**: pK_a = 6.47) suggest the coordination of the third His residue, which likely substitutes the carboxylate donor group in the metal coordination sphere to obtain a ($3N_{Im}$) binding mode. The thirdly formed complex $[ZnL]^{2+}$ becomes the most abundant species above neutral pH in both the systems. According to its stoichiometry and the corresponding pK_a values, the ionization of the coordinated water molecule probably takes place and a ($3N_{Im}$, O^-) tetrahedral complex is obtained. Indeed, the relatively low pK_a values are not compatible with the hypothesis of lysine deprotonation in the explored pH range, since its ε-amino group dissociates at higher pH values (pK_a = 9.50 (**L3**) and 9.65 (**L4**) in the free ligands).

ZinT complex stability: pointing out the most effective metal binding site

In order to better evaluate and compare the coordination ability of the investigated systems, some competition plots have been drawn. They represent the simulation of the solutions containing equimolar concentrations of the metal and the chosen ligands, admitting that all the peptides compete for the metal recruitment and that they form only the binary complexes described in the speciation models reported above.

It is important to point out that the investigated model peptides belong to the ZinT proteins of different pathogenic organisms, *i.e. E. coli* and *S. enterica*. The sequences are very similar in the two bacteria, but in the case of *S. enterica*, two serine residues (positions 28 and 175 of the ZinT protein sequence) are substituted by alanines. There are no explanations for such substitution in terms of the ZinT biological role or virulence efficacy. Nevertheless, it is quite interesting to note that this variation occurs in both the metal binding domains of ZinT. The competition diagrams plotted in Fig. S25 and S26, ESI† show the effects of the Ser-to-Ala substitution on the Cu(II) and Zn(II) complex stability. Although serine residues are not coordinated to the metal ion, their presence seems to contribute to the overall stability of the Cu(II) systems when the deprotonation of backbone amides occurs, as already previously observed for similar systems.[44] This effect is particularly evident in the case of **L1** and **L2**, where the lack of serine in the sequence causes a decrease of the metal affinity around pH 6 (Fig. S25a, ESI†). The Cu(II) complexes with **L3** (*E. coli* fragment) are also more stable than the Cu(II)–**L4** systems; however, here the difference is smaller (Fig. S25b, ESI†), possibly due to the presence of an additional serine residue in the sequence which reduces the effect of the Ser-to-Ala substitution. It is worth noting that the higher Cu(II) affinity for **L3** is consistent with the hypothesis of the metal interaction with an apical lysine (see above), which contributes to the stability of the complex by wrapping the metal centre. In the case of the Zn(II) complexes (Fig. S26, ESI†), where amides are not involved in the coordination, the contribution of the serine residue to the complexation does not have a clear and definite trend; the behaviour of the two binding sites is

different although the binding modes are quite similar. A deeper investigation would be required to completely analyse these features.

An overall comparison among the four systems gives some clues about the biological role of the two identified metal binding sites in the ZinT protein, corresponding to the N-terminal His-rich sequence (**L1** and **L2**) and to the 166–178 fragments (**L3** and **L4**). We obtained two competition plots to qualitatively evaluate the ligand affinity for Cu(II) and Zn(II) (Fig. 6). The histidine-rich fragments **L1** and **L2** are better ligands for the Zn(II) ion, confirming the general assumption that a higher number of histidine residues favour the metal complexation.[45–47] Indeed, according to the proposed speciation models, the ZinT short fragments form stable 4N complexes with Zn(II) already at pH around 6. In contrast, **L3** and **L4** contain only 3 imidazole groups and they can only coordinate the metal ion by means of a ($3N_{Im}$, O^-) binding mode. Therefore, the proposed coordination hypotheses are in good agreement with the competition plot trend, which also confirms the comparable stability of the studied systems below pH 6, *i.e.* where all the peptides display a 3N coordination.

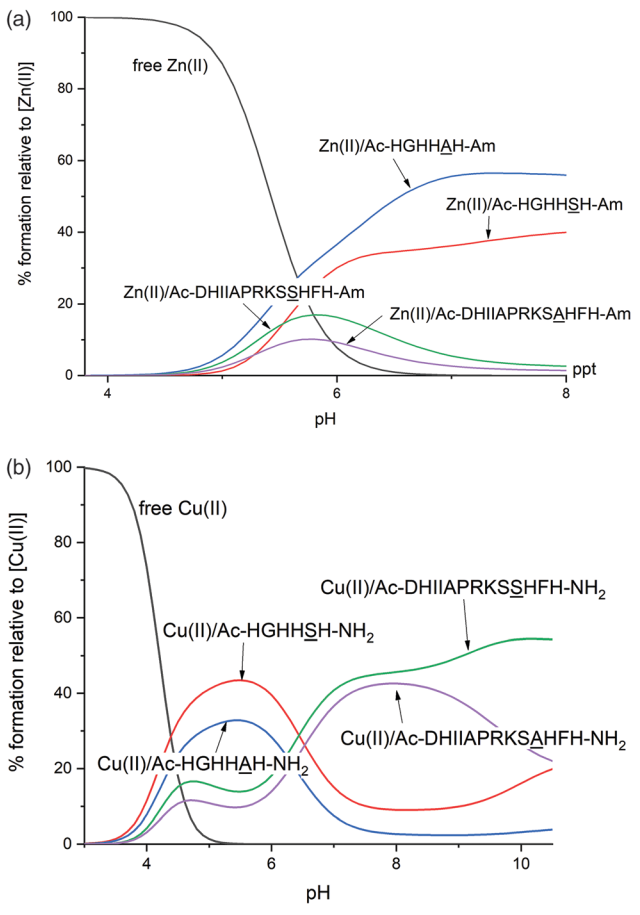

Fig. 6 Competition plots for a solution containing an equimolar concentration (1×10^{-3} mol dm^{-3}) of the metal ion, **L1** = Ac-HGHHSH-NH_2, **L2** = Ac-HGHHAH-NH_2, **L3** = Ac-DHIIAPRKSSHFH-NH_2 and **L4** = Ac-DHIIAPRKSAHFH-NH_2. (A) Zn(II); (B) Cu(II).

In the case of copper ions (Fig. 6b), once again the crowded cluster of histidines in **L1** and **L2** provides a higher number of anchoring sites to favour the first step of complexation. In contrast, in **L3** and **L4** the available binding sites are located on the opposite sides of the peptide sequence (Ac-DHXXXXXXXXXHFH-NH_2), likely preventing an effective complexation. However, upon increasing the pH value the calculated competition plots designate the longer fragments as the most effective ligands. In order to explain this result, it can be useful to observe that, under alkaline conditions, the backbone amides gradually substitute the His residues as donor groups. As a consequence, the number of histidines in the peptide sequence contributes to a lesser extent to the complex stabilization, while the length of the peptide (clearly greater for **L3** and **L4**) could favour the wrapping and protection of the metal binding site, thus increasing the complex stability.

ZinT complex stability: a comparison with other biologically relevant metal binding systems

The above results of the complex-formation behaviour of ZinT allow for a comparison with some biologically relevant metal binding systems in order to shed light on its mechanism of action in the metal acquisition processes at the host/pathogen interface.

The metal complexation ability of ZinT can be compared with that of the antimicrobial peptide calcitermin (VAIALKAAHYHTHKE), which is present in human airways and is able to bind quite effectively Zn(II) and Cu(II) ions (Fig. S27, ESI†).[48] Calcitermin contains three alternated histidines (HXHXH), two lysines, one glutamic acid and free amino- and carboxyl-termini. Furthermore, its antimicrobial activity is enhanced in the presence of Zn(II) and Cu(II) under acidic conditions,[48] representing a possible natural competitor and antagonist of ZinT in the host human organism. The competition plots of Fig. S27, ESI† show that, under acidic conditions, calcitermin binds both Zn(II) and Cu(II) ions with the highest affinity. At such pH values its coordination sphere is very similar to those of ZinT complexes, with a ($3N_{Im}$, O^-) binding mode; however, the alternated His-tag (HXHXH) is confirmed to be an extremely effective binding motif, even with respect to the four histidine sequences, HXHHXH, of **L1** and **L2**. On the other hand, in the case of Cu(II) ions, starting from physiological pH, the **L3** and **L4** fragments become more efficient ligands than calcitermin. Interestingly, previous studies show that the antimicrobial activity of calcitermin is lost at physiological pH.[48] Thus, the present results can suggest that its antimicrobial way of action is related to the metal binding affinities of the competing systems. A slight different behaviour is observed, instead, in the case of Zn(II) ions, where calcitermin almost steadily maintains its efficacy as a ligand throughout the explored pH range.

According to recent studies performed on *Se*ZinT,[14] the metal recruitment mechanism of this protein should involve the formation of a binary complex with ZnuA, the soluble periplasmic component of the ZnuABC transporter. This interaction has not been fully elucidated, but the presence of both

the proteins in the Zn(II)-bound form seems to be crucial. Moreover, the N-terminal histidine-rich loop of ZnuA has been proved to play a critical role,[14] and some evidence also suggests that ZnuA may interact with other metal ions, including Cu(II).[49] In order to compare the Zn(II) and Cu(II) metal binding ability of the ZinT fragments with that of the two identified metal binding sites of ZnuA from *E. coli*[50] (Ac-^{115}MKSIHGDDDDHDHAEKSDEDHHHGDFNMHLW^{145}-NH_2, corresponding to the N-terminal His-rich loop, and Ac-^{223}GHFTVNPEIQPGAQRLHE^{240}-NH_2, the secondary and less effective binding site), the two competition plots shown in Fig. S28, ESI† have been computed. The comparison shows that the ZnuA His-rich loop located in the domain 115–145 is by far the most effective ligand for the Zn(II) ion. This is not surprising and confirms that a higher number (seven in this case) of histidines in the sequence favour the Zn(II) complexation and stabilize the system. On the other hand, the Cu(II) complexes of the ZnuA His-rich loop do not exhibit an improved metal affinity with respect to ZinT, unless at the most acidic pH values. Interestingly, from the chemical point of view, although both ZnuA and ZinT (**L1** and **L2**) systems, under acidic conditions, form macrochelated complexes with the same $3N_{Im}$ coordination, the smaller number of His residues in ZinT leads to the binding of N-amides at lower pH and therefore earlier with respect to ZnuA. The N-amide coordination induces an increased square-planar character and the possible formation of stable 5/6-membered-rings involving the imidazole and vicinal peptide amides. Under physiological conditions, as previous described, the **L3** and **L4** peptides are able to form 4N complexes and exhibit the highest binding ability. Lastly, the two His-containing ZnuA fragment Ac-^{223}GHFTVNPEIQPGAQRLHE^{240}-NH_2 has been proved to be the less effective ligand.

The different results obtained for the Zn(II) and Cu(II) complexes may explain the ZinT biological activity towards these metals. Although ZinT is able to bind both the ions and participate in Zn(II) recruitment, no evidence of its role in Cu(II) homeostasis has been found and indeed some studies exclude this function.[15] Moreover, the extremely high binding affinity of the ZnuA His-rich loop towards Zn(II) is fully consistent with the putative mechanism of zinc transfer from ZinT to ZnuA *via* the formation of the protein binary system. Based on our results, such a process cannot occur in the case of Cu(II), since the ZnuA fragments proved to be inadequate to catch the metal ion.

Conclusions

The thermodynamic and spectroscopy results obtained in the present work are consistent with previous biological studies conducted on ZinT. The metal binding site corresponding to the 166–178 amino acid sequence (*E. coli* **L3** = Ac-DHIIAPRKSSHFH-NH_2 and *S. enterica* **L4** = Ac-DHIIAPRKSAHFH-NH_2) is confirmed to be fundamental for metal coordination, particularly involving the three histidine residues (H167, H176, H178) and the aspartic acid (D166) residue. Furthermore, the spectroscopic near-UV CD structural characterization of the **L3** and **L4** apo-peptides and of their Cu(II) and Zn(II) complexes does not highlight the formation of any particular α-helical or β-sheet structures and the typical band at around 200 nm confirms the flexible random coil conformation (Fig. S29 and S30, ESI†).

However, the obtained thermodynamic equilibrium constants designate also the N-terminal histidine-rich fragment (^{24}HGHHXH^{29}) as a very effective metal binding domain. In fact, the results presented in this work reveal that **L1** = Ac-HGHHAH-NH_2 (*Ec*ZinT) and especially **L2** = Ac-HGHHAH-NH_2 (*Se*ZinT) exhibit the highest affinity for the Zn(II) ion all over the explored pH range. These fragments are also able to better stabilize the Cu(II) complexes, but only under acidic conditions, which is, nonetheless, quite common during infections.

No remarkable differences between the *E. coli* and *S. enterica* model systems have been observed. The coordination behaviour is similar for **L1** and **L2** as well as for **L3** and **L4**, respectively, although some minor differences are observed under the most alkaline conditions. However, it is worth underlining that the peptides from *Ec*ZinT show a higher tendency to stabilize the Cu(II) complexes at neutral and alkaline pH, *i.e.* when the backbone amides participate in Cu(II) coordination. This trend has been observed in many other systems and ascribed to the possible electronic effect of serine residues, capable of favouring the amidic proton displacement by the Cu(II) ion.[44,45,51]

The metal binding behaviour of the ZinT fragments is fully consistent with the previously formulated hypotheses about the protein biological role. The high efficacy of HGHHXH in metal chelation is in line with the necessity to recover and stabilize as much micronutrients as possible from the medium, acting as a primary metal scavenger. Subsequently, its function may involve the delivery of the metal ion to the ZinT canonical binding site (**L3** and **L4** fragments) for storage and/or transfer to other proteins (*e.g.* ZnuA). The His-rich loop may therefore represent the first, but temporary, stop station for the metal ion on its route to cellular import. Indeed, a relatively high metal binding affinity is crucial to ensure the acquisition process in an environment rich of competitive systems. It is therefore not surprising that the histidine-rich loop of *E. coli* ZnuA (Ac-MKSIHGDDDDHDHAEKSDEDHHHGDFNMHLW-NH_2) exhibits the strongest Zn(II) affinity in comparison with the ligands studied in this work. ZinT is supposed to directly interact with ZnuA, forming a binary complex in the presence of zinc ions and likely transferring the metal to the partner protein through the His-rich loop of ZnuA. This process can be successfully achieved only if the ZnuA metal binding site has a higher affinity for Zn(II) than ZinT, and this is the case highlighted by our results. Surprisingly, the Cu(II) complexes behave in a different way. In this case, the ZnuA His-rich loop shows a less effective metal binding ability, resulting in a higher stability of the Cu(II) complexes with ZinT. Although further investigations are necessarily required, our thermo-

dynamic results reflect previous observations according to which ZinT should not participate in Cu(II) homeostasis.

The results of the present study shed new light on the way of action of the ZinT/ZnuABC transport system. The elucidation of the metal–protein interaction based on thermodynamics and coordination chemistry is an indispensable starting point to develop metal-based drugs. Taking advantage of the Zn(II) chelating properties, a possible antimicrobial strategy can be related to the design of a Zn(II) chelating system that can ultimately interact with both ZinT and ZnuA forming an irreversible (ternary) complex ZinT–(Zn(II)-pharmacophore)–ZnuA. This may starve the pathogen by preventing the transfer of the metal ion to the ZnuB component and eliminating both the proteins in charge of metal recruitment.

Conflicts of interest

There are no conflicts to declare.

Acknowledgements

Financial support from the National Science Centre (UMO-2017/26/A/ST5/00363 and UMO-2017/26/A/ST5/00364), the University of Ferrara (FAR 2019) and the Erasmus + Programme is gratefully acknowledged. This paper is based on the work from COST Action CA18202, NECTAR – Network for Equilibria and Chemical Thermodynamics Advanced Research, supported by COST (European Cooperation in Science and Technology).

Notes and references

1 J. P. Zackular, R. J. Knippel, C. A. Lopez, W. N. Beavers, C. N. Maxwell, W. J. Chazin and E. P. Skaar, *mSphere*, 2020, **5**, e00061–e00020.
2 P. Chandrangsu, C. Rensing and J. D. Helmann, *Nat. Rev. Microbiol.*, 2017, **15**, 338–350.
3 R. E. W. Hancock and H.-G. Sahl, *Nat. Biotechnol.*, 2006, **24**, 1551.
4 P. Kumar, V. Dalal, N. Sharma, S. Kokane, D. K. Ghosh, P. Kumar and A. K. Sharma, *Metallomics*, 2020, **12**, 280–289.
5 Z. Ma, F. E. Jacobsen and D. P. Giedroc, *Chem. Rev.*, 2009, **109**, 4644–4681.
6 K. P. Grim, J. N. Radin, P. K. Párraga Solórzano, J. R. Morey, K. A. Frye, K. Ganio, S. L. Neville, C. A. McDevitt and T. E. Kehl-Fie, *J. Bacteriol.*, 2020, **202**(9), e00014-00020.
7 S. Gillet, E. Lawarée and J.-Y. Matroule, in *Microbial Diversity in the Genomic Era*, ed. S. Das and H. R. Dash, Academic Press, 2019, vol. ch. 23, pp. 409–426.
8 P. Petrarca, S. Ammendola, P. Pasquali and A. Battistoni, *J. Bacteriol.*, 2010, **192**, 1553–1564.
9 S. I. Patzer and K. Hantke, *Mol. Microbiol.*, 1998, **28**, 1199–1210.
10 Z. R. Lonergan and E. P. Skaar, *Trends Biochem. Sci.*, 2019, **44**, 1041–1056.
11 S. Campoy, M. Jara, N. Busquets, A. M. Pérez De Rozas, I. Badiola and J. Barbé, *Infect. Immun.*, 2002, **70**, 4721–4725.
12 R. Gabbianelli, R. Scotti, S. Ammendola, P. Petrarca, L. Nicolini and A. Battistoni, *BMC Microbiol.*, 2011, **11**, 36–36.
13 S. Ammendola, P. Pasquali, C. Pistoia, P. Petrucci, P. Petrarca, G. Rotilio and A. Battistoni, *Infect. Immun.*, 2007, **75**, 5867–5876.
14 A. Ilari, F. Alaleona, G. Tria, P. Petrarca, A. Battistoni, C. Zamparelli, D. Verzili, M. Falconi and E. Chiancone, *Biochim. Biophys. Acta*, 2014, **1840**, 535–544.
15 H. G. Colaço, P. E. Santo, P. M. Matias, T. M. Bandeiras and J. B. Vicente, *Metallomics*, 2016, **8**, 327–336.
16 T. Stojnev, J. Harichová, P. Ferianc and T. Nyström, *Curr. Microbiol.*, 2007, **55**, 99–104.
17 C. J. Kershaw, N. L. Brown and J. L. Hobman, *Biochem. Biophys. Res. Commun.*, 2007, **364**, 66–71.
18 G. David, K. Blondeau, M. Schiltz, S. Penel and A. Lewit-Bentley, *J. Biol. Chem.*, 2003, **278**, 43728–43735.
19 J. Chen, L. Wang, F. Shang, Y. Dong, N.-C. Ha, K. H. Nam, C. Quan and Y. Xu, *Biochem. Biophys. Res. Commun.*, 2018, **500**, 139–144.
20 The UniProt Consortium, *Nucleic Acids Res.*, 2018, **47**, D506–D515.
21 J. A. Lemire, J. J. Harrison and R. J. Turner, *Nat. Rev. Microbiol.*, 2013, **11**, 371–384.
22 K. S. Chaturvedi and J. P. Henderson, *Front. Cell. Infect. Microbiol.*, 2014, **4**, 1–12.
23 J. B. Cross, J. S. Duca, J. J. Kaminski and V. S. Madison, *J. Am. Chem. Soc.*, 2002, **124**, 11004–11007.
24 N. Fushimi, C. n. E. Ee, T. Nakajima and E. Ichishima, *J. Biol. Chem.*, 1999, **274**, 24195–24201.
25 N. Giebeler and P. Zigrino, *Toxins*, 2016, **8**, 122–122.
26 S. Damo and T. E. Kehl-Fie, in *Antimicrobial Peptides: Role in Human Health and Disease*, ed. J. Harder and J.-M. Schröder, Springer International Publishing, Cham, 2016, pp. 89–100.
27 S. R. Hennigar and J. P. McClung, *Am. J. Lifestyle Med.*, 2016, **10**, 170–173.
28 P. Gans and B. O'Sullivan, *Talanta*, 2000, **51**, 33–37.
29 G. Gran, *Acta Chem. Scand.*, 1950, **4**, 559–577.
30 P. Gans, A. Sabatini and A. Vacca, *Talanta*, 1996, **43**, 1739–1753.
31 G. Arena, R. Cali, E. Rizzarelli and S. Sammartano, *Thermochim. Acta*, 1976, **16**, 315–321.
32 C. F. Baes and R. E. Mesmer, *The hydrolysis of cations*, John Wiley & Sons, Ltd., New York, 1976.
33 L. Alderighi, P. Gans, A. Ienco, D. Peters, A. Sabatini and A. Vacca, *Coord. Chem. Rev.*, 1999, **184**, 311–318.
34 H. Sigel and R. B. Martin, *Chem. Rev.*, 1982, **82**, 385–426.
35 L. D. Pettit and H. K. J. Powell, *The IUPAC Stability Constants Database*, Royal Society of Chemistry, London, 1992–2000.

36 J. Makowska, K. Bagińska, A. Liwo, L. Chmurzyński and H. A. Scheraga, *Biopolymers*, 2008, **90**, 724–732.
37 J. Makowska, A. Liwo, L. Chmurzyński and H. A. Scheraga, *J. Solution Chem.*, 2012, **41**, 1738–1746.
38 B. Noszál and E. Osztás, *Int. J. Pept. Protein Res.*, 1989, **33**, 162–166.
39 J. Peisach and W. E. Blumberg, *Arch. Biochem. Biophys.*, 1974, **165**, 691–708.
40 K. Ősz, K. Várnagy, H. Süli-Vargha, A. Csámpay, D. Sanna, G. Micera and I. Sóvágó, *J. Inorg. Biochem.*, 2004, **98**, 24–32.
41 P. Deschamps, P. P. Kulkarni, M. Gautam-Basak and B. Sarkar, *Coord. Chem. Rev.*, 2005, **249**, 895–909.
42 L. Casella, M. E. Silver and J. A. Ibers, *Inorg. Chem.*, 1984, **23**, 1409–1418.
43 M. Sola, A. Lledos, M. Duran and J. Bertran, *Inorg. Chem.*, 1991, **30**, 2523–2527.
44 D. Bellotti, C. Tocchio, R. Guerrini, M. Rowińska-Żyrek and M. Remelli, *Metallomics*, 2019, **11**, 1988–1998.
45 D. Bellotti, D. Łoboda, M. Rowińska-Żyrek and M. Remelli, *New J. Chem.*, 2018, **42**, 8123–8130.
46 M. Remelli, M. Peana, S. Medici, L. G. Delogu and M. A. Zoroddu, *Dalton Trans.*, 2013, **42**, 5964–5974.
47 H. Kozlowski, M. Łuczkowski and M. Remelli, *Dalton Trans.*, 2010, **39**, 6371–6385.
48 D. Bellotti, M. Toniolo, D. Dudek, A. Mikołajczyk, R. Guerrini, A. Matera-Witkiewicz, M. Remelli and M. Rowińska-Żyrek, *Dalton Trans.*, 2019, **48**, 13740–13752.
49 L. A. Yatsunyk, J. A. Easton, L. R. Kim, S. A. Sugarbaker, B. Bennett, R. M. Breece, I. I. Vorontsov, D. L. Tierney, M. W. Crowder and A. C. Rosenzweig, *J. Biol. Inorg. Chem.*, 2008, **13**, 271–288.
50 A. Hecel, A. Kola, D. Valensin, H. Kozlowski and M. Rowinska-Zyrek, *Inorg. Chem.*, 2020, **59**, 1947–1958.
51 P. Mlynarz, D. Valensin, K. Kociolek, J. Zabrocki, J. Olejnik and H. Kozlowski, *New J. Chem.*, 2002, **26**, 264–268.

NJC

PAPER

Cite this: *New J. Chem.*, 2018, **42**, 8123

Investigation on the metal binding sites of a putative Zn(II) transporter in opportunistic yeast species *Candida albicans*†

Denise Bellotti,[a] Dorota Łoboda,[b] Magdalena Rowińska-Żyrek *[b] and Maurizio Remelli *[a]

Received 30th January 2018,
Accepted 26th February 2018

DOI: 10.1039/c8nj00533h

rsc.li/njc

In the present work, we focus on C4YJH2, a protein sequence of 199 amino acid residues, found in the genome of *Candida albicans*, and suggested to be involved in metal transport. *Candida albicans* is a member of the normal human microbiome; under certain circumstances that allow it to grow out of control, it can transform into a very dangerous fungal pathogen. The most probable Zn(II) binding domain of this sequence was identified at its C-terminus, a histidine-rich region, well conserved in numerous fungal Zn(II) transporters. The Zn(II) binding behaviour towards the three peptides Ac-FHEHGHSHSHGSGGGGGG-NH_2 (residues 131–148), Ac-SHSHSHSHS-NH_2 (residues 157–165), and Ac-FHEHGHSHSHGSGGGGGGSDHSGDSKSHSHSHSHS-NH_2 (residues 131–165) was explored by means of different thermodynamic and spectroscopic techniques. Cu(II) was also investigated since this endogenous metal can compete with Zn(II) for the same binding sites. The results indicate that the peptides under investigation have the ability to tightly coordinate Zn(II), at physiological pH, thus suggesting that the whole protein sequence can play a role in Zn(II) acquisition and regulation. Cu(II) is able to form even stronger complexes than Zn(II) but it is normally present in very low concentrations in the biological environment. The competition between Zn(II) and Cu(II) could be exploited to impair the Zn(II) acquisition routes of *Candida albicans*. Among the two binding sites, the affinity of both Zn(II) and Cu(II) is higher for that located at the residues 131–148, although the coordination geometry is rather different for the two metal ions.

Introduction

Candida albicans is a commensal part of the physiological flora in the oral cavity, skin, gastrointestinal and urogenital tracts. In the case of its pathological overgrowth, it is also the most common fungal pathogen found in humans, the cause of candidiasis, a condition that encompasses infections that range from superficial (such as oral thrush or vaginitis), chronic (reoccurring ulcers or painful sores that require long-term treatment) to systemic and potentially life-threatening candidemia (invasive candidiasis). The condition is usually confined to severely immunocompromised patients (undergoing organ transplantation, major surgery and those with AIDS or neoplastic disease).[1] However, untreated invasive candidiasis is also a serious problem in non-immunosuppressed patients,[2–4] and may ultimately become a greater problem than drug resistant bacterial "superbugs".[5]

Despite the progress of antifungal therapies and the ongoing search for new therapeutic strategies, there is currently only a limited number of truly effective treatments: the ability of pathogenic microorganisms to adapt and therefore resist drug action still causes thousands of deaths every year. One of the biggest obstacles in finding fungus-specific therapeutics is the fact that humans and fungi share essential metabolic pathways (they are both eukaryotes, unlike disease-causing bacteria). Lack of specificity is an important concern in the development of novel, specific agents towards which fungi will not be resistant. In order to design new antifungal drugs, it is crucial to find and aim at differences in the human and fungal metabolism. One of these differences is the metal transport mechanism and, in particular, the transport of Zn(II) into the fungal cell. Understanding the bioinorganic chemistry of this process is therefore of particular interest; in fact, a deep knowledge of the coordination modes and thermodynamics of metal–metal transporter interactions is the first step towards the design of a highly specific therapeutic.[6–9]

Zn(II) is crucial for the virulence and survival of fungal pathogens in humans, being indispensable, together with

[a] *Department of Chemical and Pharmaceutical Sciences, University of Ferrara, via Luigi Borsari 46, I-44121 Ferrara, Italy. E-mail: rmm@unife.it*
[b] *Faculty of Chemistry, University of Wroclaw, F. Joliot-Curie 14, 50-383 Wroclaw, Poland. E-mail: magdalena.rowinska-zyrek@chem.uni.wroc.pl*

† Electronic supplementary information (ESI) available. See DOI: 10.1039/c8nj00533h

Cu(II), in the expression of many metal–proteins and enzymes.[10,11] Zn(II) uptake is a challenge for microbes, since the concentration of this metal in free, non-protein bound form is as low as sub-nanomolar.[12] Cu(II) is not only an endogenous metal that can generally compete with Zn(II) for the same binding sites, but it can take part in the host–microbe "tug of war".[13–15]

C4YJH2 (UniProt Knowledgebase[16]) is a 199 amino acid sequence corresponding to the gene CAWG_03987 found in the strain WO-1 of *Candida albicans*.[17] "CAWG_03987 has domains with predicted cation transmembrane transporter activity, a role in transmembrane transport, cation transport and is integral to membrane localization".[18] In contrast to most metal-sequestering proteins, C4YJH2 has a significantly higher number of histidine and serine residues, especially in its C-terminal domain, where two sequences containing His alternated with other amino acids are located and can both act as metal binding sites.

In this work, we focus on the interactions of Zn(II) and Cu(II) with three C-terminal C4YJH2 sequences: Ac-FHEHGHSHSHGSGGGGGG-NH_2 (residues 131–148, L1), Ac-SHSHSHSHS-NH_2 (residues 157–165, L2), and Ac-FHEHGHSHSHGSGGGGGGSDHSGDSKSH SHSHSHS-NH_2 (residues 131–165, encompassing the two shorter fragments, L3). The studied sequences are very similar to those present in several putative Zn(II) transporters and proteins involved in metal homeostasis (Scheme S1, ESI†).

Mass spectrometric measurements and potentiometric titrations provided information about stoichiometry, coordination modes and stability of the formed complexes. In combination with spectroscopic techniques, these methods allowed us to identify and discuss the metal binding sites of the investigated ligands.

Results and discussion

Ligand protonation

All the peptides L1, L2 and L3 (see Experimental) were protected at their N-terminus by acetylation and at their C-terminus by amidation. The amidic protons of the peptide backbone cannot be spontaneously released in the pH range explored by potentiometry, since they are very weak acids ($pK_a \approx 15$),[19] but they can be displaced by Cu(II) at a suitable pH value, to form complexes. The distribution diagrams for protonation equilibria of L1, L2 and L3 are shown in Fig. S1–S3 (ESI†) and the corresponding constants are reported in Tables S1–S3 (ESI†). Ligand L1 (Ac-FHEHGHSHSHGSGGGGGG-NH_2) has six groups involved in acid–base reactions: one glutamic acid and five histidines. Glutamic acid has the lowest pK_a value (4.18), as predicted by its acid moiety, while His residues are characterized by log *K* values ranging from 5.74 to 7.50. Ligand L2 (Ac-SHSHSHSHS-NH_2) contains four basic sites, corresponding to its four histidines. The obtained protonation constants (5.48, 6.08, 6.47, and 7.12) are in excellent agreement with theoretical expectations based on His protonation equilibria.[20] Ligand L3 has fourteen groups involved in acid–base reactions: one glutamic acid, two aspartic acids, ten histidines and one lysine. In the considered pH range of 3–9, deprotonation of both an aspartic acid and the lysine could not be detected. The first two acidic constants of L3, characterized by pK_a values of 3.52 and 3.90, likely correspond to the second aspartic acid and to the glutamic acid side groups, while the other ten pK_a values, ranging from 5.14 to 7.78, arise from the deprotonation of the ten histidines. The pK_a of Lys (necessary for computations but irrelevant to the results in the pH range 3–9) is assumed to be equal to the averaged literature value for Lys-containing peptides, under the same experimental conditions (10.54 [21]). Potentiometric data do not allow us to understand which specific His residue is involved in each deprotonation step, as all the histidines are almost equivalent from the chemical point of view. For this purpose, NMR studies would be useful and they will be the subject of further investigation.

Zn(II) complexes

All the present results show that L1 and L2 peptides are able to form 1 : 1 complexes with the Zn(II) ion; no poly-nuclear or bis-complexes have been detected either by potentiometry or by mass spectrometry. The formation constant values are shown in Table 1 and the corresponding distribution diagrams are plotted in Fig. 1–3; ESI-MS spectra are also reported in Fig. S4–S14 (ESI†). Stability constants for the system Zn(II)/L1 have been calculated only up to pH 6, because, at higher pH, precipitation occurred. However, no precipitation has been observed over the explored pH range in the case of L2 and L3.

Zn(II) binds L1 starting from pH 4.3 with the formation of the species $[ZnH_3L]^{4+}$, where the most likely coordination mode is *via* two histidine residues and the carboxyl group of the glutamic acid ($2N_{Im}$; COO^-). The next step involves the release of a third proton with a pK_a value of 4.9, giving rise to the species $[ZnH_2L]^{3+}$. This complex begins to form at a pH close to that of the previous one. The most likely coordination mode for this species is three histidine residues and one oxygen atom with a tetrahedral geometry, rather common in zinc-transporting proteins.[22–25] Analogously, in the case of L2, the first detected

Table 1 Overall stability constants (log β) and acid dissociation constants (pK_a) of zinc(II) complexes with L1, L2 and L3 at T = 298 K, I = 0.1 mol dm^{-3} ($NaClO_4$). Values in parentheses are standard deviations on the last significant figure

Ligand	Species	log β	pK_a
L1	$[ZnH_3L]^{4+}$	24.1 (1)	4.9
	$[ZnH_2L]^{3+}$	19.21 (2)	—
	$[ZnL]^{+}$	7.51 (2)	—
L2	$[ZnHL]^{3+}$	11.55 (3)	5.97
	$[ZnL]^{2+}$	5.58 (2)	7.22
	$[ZnH_{-1}L]^{+}$	−1.65 (4)	8.20
	$[ZnH_{-2}L]$	−9.85 (6)	—
L3	$[ZnH_8L]^{7+}$	62.32 (5)	—
	$[ZnH_6L]^{5+}$	51.65 (6)	—
	$[ZnH_4L]^{3+}$	39.89 (3)	—
	$[ZnH_2L]^{+}$	26.40 (3)	7.84
	$[ZnHL]$	18.57 (7)	8.57
	$[ZnL]^{-}$	10.0 (1)	8.6
	$[ZnH_{-1}L]^{2-}$	1.35 (1)	—
	$[Zn_2H_3L]^{4+}$	38.8 (2)	—

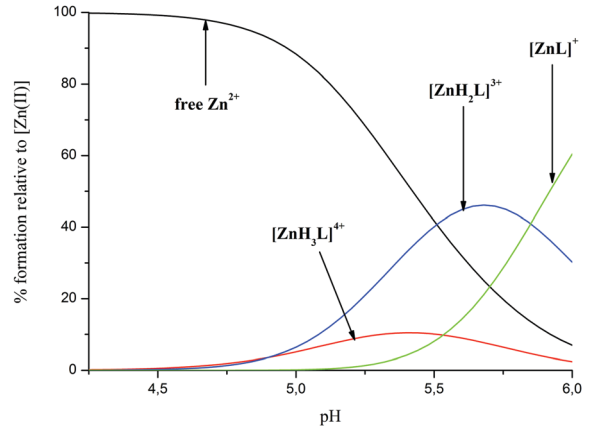

Fig. 1 Exemplificative species distribution diagram relative to Zn(II)/L1 complexes; metal/ligand molar ratio = 1 : 1.25.

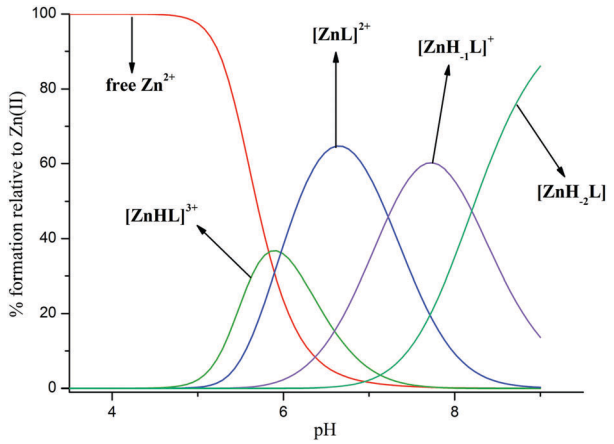

Fig. 2 Exemplificative species distribution diagram relative to Zn(II)/L2 complexes; metal/ligand molar ratio = 1 : 1.25.

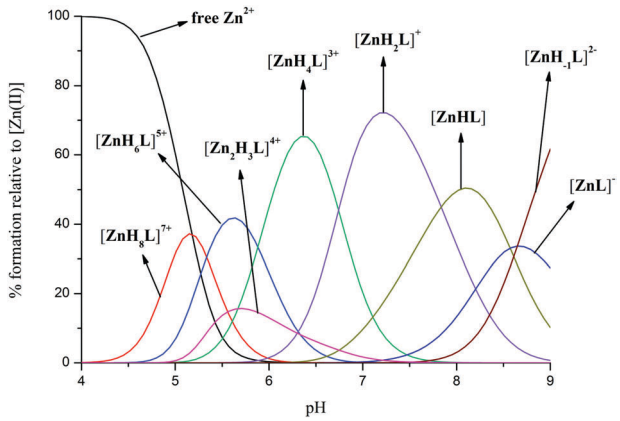

Fig. 3 Exemplificative species distribution diagram relative to Zn(II)/L3 complexes; metal/ligand molar ratio = 1 : 1.25.

complex $[ZnHL]^{3+}$ is also characterized by the ($3N_{Im}$; O) configuration; in this case, the oxygen atom should belong to a water molecule. Further deprotonation gives rise to the species $[ZnL]^{+}$ (L1) and $[ZnL]^{2+}$ (L2). In the case of L1, two protons are most likely released almost simultaneously by the remaining two histidines, which are not involved in the coordination. As for L2, the acidic proton of the coordinated water molecule is instead released, giving rise to a ($3N_{Im}$; OH^{-}) complex. Moreover, at higher pH values, the species $[ZnH_{-1}L]^{+}$ is formed: the corresponding $\log K$ value 7.22 is practically identical to that of the fourth His residue (7.12, Table S2, ESI†), which most likely deprotonates without interacting with the metal ion. Further hydrolysis is observed at the most alkaline pH values.

In the system Zn(II)/L3, the availability of a larger number of histidine residues gives rise to a complicated, pH-dependent, mixture of metal complexes (Fig. 3), where different histidines are coordinated to Zn(II) in a high number of combinations. The MS spectra (Fig. S10–S14, ESI†), recorded at pH 5.30, reveal the presence of both mononuclear ($[ZnH_5L]^{4+}$ at m/z = 900.6, $([ZnH_4L]\cdot K)^{4+}$ at m/z = 910.1 and $([ZnH_3L]\cdot K_2)^{4+}$ at m/z = 919.8) and binuclear ($[Zn_2H_3L]^{4+}$ at m/z = 916.5) species. The latter complex has been successfully introduced in the speciation model for the fitting of potentiometric data (Table 1). It is reasonable to suppose that, in the complex $[Zn_2H_3L]^{4+}$, the two Zn(II) ions are bound to the two major clusters of histidines, located near the C- and N-terminus, respectively. Thus, the L3 peptide possesses two (most likely) independent coordination sites separated by a rather long linker. It is reasonable to suggest that, in the simultaneous presence of different, competing, metal ions – as can happen *in vivo* – the two binding sites can be occupied by different metals. This hypothesis could be checked through further thermodynamic studies on the ternary system Cu(II)/Zn(II)/L3, on the basis of the binary speciation models reported here. Circular dichroism measurements performed in the far-ultraviolet spectroscopic range (Fig. S15, ESI†) reveal that there is no significant pH-dependant variation in the secondary structure of the Zn(II)/L3 complexes. The band at 200 nm points out the absence of a specific conformation and the prevalence of random coils.

Cu(II) complexes

The three investigated peptides proved to be able to form stable 1 : 1 complexes with the Cu(II) ion; no poly-nuclear or bis-complexes have been detected either by potentiometry or by mass spectrometry under the experimental conditions here employed. Complex-formation constants are reported in Table 2 and the corresponding distribution diagrams are plotted in Fig. 4–6; ESI-MS results are also shown in Fig. S16–S25 (ESI†), UV-Vis spectra are reported in Fig. S26–S28 (ESI†) and CD spectra are reported in Fig. S29–S32 (ESI†).

Cu(II) starts to interact with L1 at pH lower than 3 and the first detected complex is $[CuH_4L]^{5+}$. The stoichiometry of this species indicates that two acid/base sites are deprotonated and it can be suggested that Cu(II) binds a histidine and the carboxylate group of the glutamic acid (N_{Im}; COO^{-}), in fact, these two residues (pK_a values: 5.7 and 4.2, respectively) can be deprotonated at such an acidic pH value only if they are bound to the metal ion.

As for L2 peptide, the stoichiometry of the first detected species is $[CuH_2L]^{4+}$: in this case, potentiometric data do not

Table 2 Overall stability constants (log β) and acid dissociation constants (pK_a) of copper(II) complexes with L1, L2 and L3 at T = 298 K, I = 0.1 mol dm^{-3} ($NaClO_4$). Values in parentheses are standard deviations on the last significant figure

Ligand	Species	log β	pK_a
L1	$[CuH_4L]^{5+}$	31.63 (5)	4.30
	$[CuH_3L]^{4+}$	27.33 (5)	4.63
	$[CuH_2L]^{3+}$	22.70 (4)	4.92
	$[CuHL]^{2+}$	17.78 (2)	5.77
	$[CuL]^{+}$	12.00 (2)	—
	$[CuH_{-2}L]^{-}$	−3.04 (2)	8.43
	$[CuH_{-3}L]^{2-}$	−11.47 (3)	—
L2	$[CuH_2L]^{4+}$	20.00 (2)	—
	$[CuL]^{2+}$	10.04 (2)	—
	$[CuH_{-2}L]$	−4.50 (2)	8.94
	$[CuH_{-3}L]^{-}$	−13.44 (4)	—
L3	$[CuH_{10}L]^{9+}$	73.4 (1)	4.0
	$[CuH_9L]^{8+}$	69.4 (1)	4.1
	$[CuH_8L]^{7+}$	65.30 (8)	4.72
	$[CuH_7L]^{6+}$	60.58 (6)	5.20
	$[CuH_6L]^{5+}$	55.38 (6)	5.72
	$[CuH_5L]^{4+}$	49.65 (7)	6.09
	$[CuH_4L]^{3+}$	43.56 (7)	6.39
	$[CuH_3L]^{2+}$	37.16 (5)	6.83
	$[CuH_2L]^{+}$	30.34 (4)	7.19
	$[CuHL]$	23.14 (2)	—
	$[CuH_{-1}L]^{2-}$	7.01 (2)	—
	$[CuH_{-3}L]^{4-}$	−10.85 (3)	—

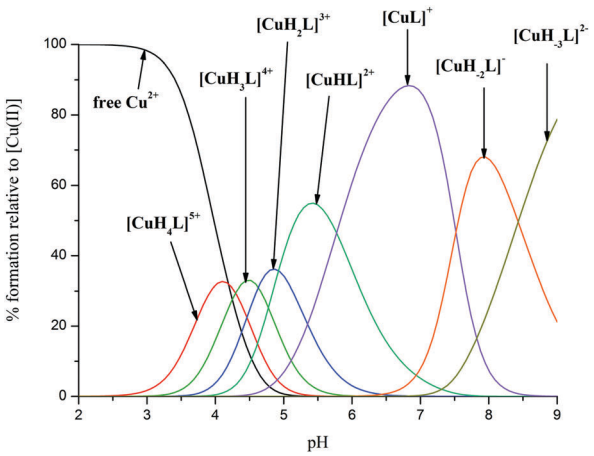

Fig. 4 Exemplificative species distribution diagram relative to Cu(II)/L1 complexes; metal/ligand molar ratio = 1 : 1.25.

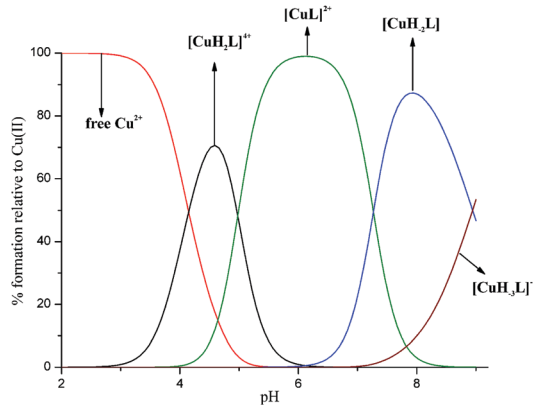

Fig. 5 Exemplificative species distribution diagram relative to Cu(II)/L2 complexes; metal/ligand molar ratio = 1 : 1.25.

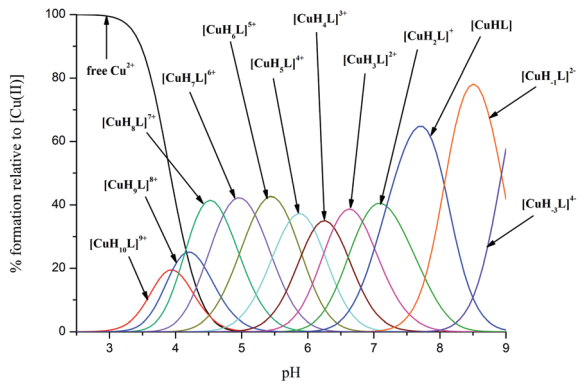

Fig. 6 Exemplificative species distribution diagram relative to Cu(II)/L3 complexes; metal/ligand molar ratio = 1 : 1.25.

reveal the formation of the $1N_{Im}$ complex. Most likely, the absence of a carboxylate side chain makes the hypothetical species $[CuH_3L]^{5+}$ less stable than the corresponding complex formed by L1. It can be suggested, for the complex $[CuH_2L]^{4+}$, that two imidazole nitrogens are coordinated to Cu(II). The position of the d–d band of the UV-Vis spectra at pH 5 (660 nm, see Fig. S27 and Table S4, ESI†) is in good agreement with this hypothesis.

Two different hypotheses are instead possible for the coordination mode of the first identified complex of L3 peptide, $[CuH_{10}L]^{9+}$, where, besides the Asp residues, two additional acid/base side groups of the ligand are deprotonated. It can be suggested that Cu(II) binds a histidine and the carboxylate group of the Glu residue ($1N_{Im}$; COO^-), as in the case of L1, or that the binding occurs *via* two histidine residues ($2N_{Im}$) while the glutamic acid is still protonated. This latter hypothesis is well supported by the Vis absorption data at pH 3 (see Fig. S28 and Table S5, ESI†), which show a λ_{max} = 660 nm, as expected for a complex where Cu(II) is bound to two imidazole nitrogens.[19] Subsequently, the species $[CuH_9L]^{8+}$, characterized by a protonation constant of 4.0 (Table 2), is compatible with the hypothesis of the mere deprotonation of the Glu residue without any relevant change in the complex geometry; in fact, the wavelength of maximum absorption of the d–d band measured at pH 4 is 658 nm, suggesting again a ($2N_{Im}$) coordination.

Increasing the pH value, Cu(II) binds a larger number of nitrogen atoms, as the blue-shift of Vis spectra for the three ligands indicates (Tables S4–S6, ESI†). In the case of L1, the ($2N_{Im}$; COO^-) and ($3N_{Im}$; COO^-) configurations are the most probable for $[CuH_3L]^{4+}$ and $[CuH_2L]^{3+}$, respectively. Starting from pH 4, the complex loses a further proton to form the species $[CuHL]^{2+}$ where Cu(II) should bind a fourth *N*-imidazole with a pK_a = 4.92. It is reasonable that this His residue substitutes the carboxylate group in the equatorial plane,

moving it to the axial position. The presence of an axial binding group produces a red-shift in the Vis spectra[19] that can explain the fact that the wavelength of maximum absorption at pH 6.3 (593 nm, see Fig. S26 and Table S6, ESI†) is slightly higher than the predicted value for a ($4N_{Im}$) complex (576 nm).[19] At neutral pH, the species $[CuL]^+$ is formed from the deprotonation of a histidine residue not involved in the coordination (d–d band at 590 nm).

A ($4N_{Im}$) configuration is also hypothesized for the $[CuL]^{2+}$ complex formed by the L2 ligand at pH 6. Since the corresponding ($3N_{Im}$) complex was not detected by potentiometry, a cooperative binding effect can be suggested leading to the coordination of the third and the fourth histidine, in quick sequence. The formation of a 4N species is also confirmed by EPR spectra (Tables S4 and S6, ESI†).[26]

In the case of L3, when increasing the pH value, several species with the same stoichiometry but different donor atom set can form in solution at the same time, giving rise to a complicated mixture, as happens in the presence of Zn(II). The formation of macrochelates is also possible. At pH 5, where the species $[CuH_7L]^{6+}$ is the most abundant complex in solution, the first amide proton is displaced by the Cu(II) ion. In fact, CD spectra show a negative band at 309 nm (see Fig. S31 and Table S5, ESI†), attributable to the *N*-amide charge transfer to the metal ion.[19] The d–d band of the Vis spectra is located at 602 nm (pH 5.06) and it is compatible with the hypothesis of a ($2N_{Im}$; N^-) complex.[19] At physiological pH, a mixture of ($2N_{Im}$; N^-) and ($3N_{Im}$; N^-) species can be suggested.

Under alkaline conditions, the remarkable change in the visible CD spectra of Cu(II) complexes with all three ligands (see Fig. S29–S31, ESI†) suggests an important variation in coordination modes: up to three deprotonated amides of the peptide backbone can gradually substitute imidazole nitrogens in the metal coordination sphere with a square-planar molecular geometry to form ($2N_{Im}$; $2N^-$) and (N_{Im}; $3N^-$) complexes. The formation of some of these mononuclear Cu(II) complexes has been also confirmed by mass spectrometry (Fig. S16–S25, ESI†).

As a final point, it is worth noting that the experimental far UV-CD spectra for the system Cu(II)/L3 (Fig. S32, ESI†) show the absence of any pH-dependant variation in the secondary structure and the prevalence of a random coil conformation (band at 200 nm).

A comparison of metal binding abilities

In order to better understand the binding ability of the investigated ligands towards Zn(II) and Cu(II) ions, some competition plots (see Experimental) were built up at equimolar concentrations of ligands and metal ions. As shown in Fig. 7 and 8, the L3 species formed with both the Zn(II) and Cu(II) ions are the most stable, while complexes with L2 reach the lowest formation percentages. Complexes with the L1 ligand, containing one more histidine than L2, are in an intermediate situation. These results confirm the previous observation that with the increase in the number of histidines, the coordination becomes more effective.[27–30] It is important to emphasize that L3 contains both the other two peptides. No direct evidence for the preferred metal

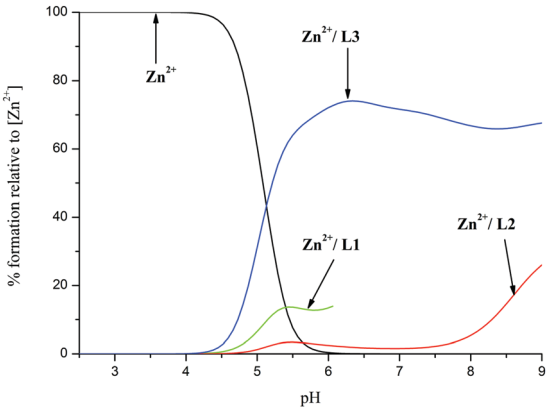

Fig. 7 Competition plot for a quaternary solution containing equimolar concentrations (1 mM) of Zn(II), L1, L2 and L3.

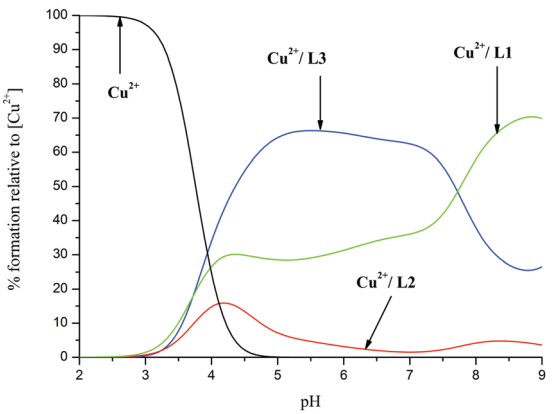

Fig. 8 Competition plot for a quaternary solution containing equimolar concentrations (1 mM) of Cu(II), L1, L2 and L3.

binding site of L3 is available, although the higher affinity of L1 with respect to L2 suggests that the distribution of mono-nuclear species where the metal ion is bound to L3 is unbalanced in favour of the N-terminal binding site.

In the attempt to get more information on the role played by the number and position of His residues on the coordination ability of the ligand, other competition plots have been built up, where the complex-formation behaviour of L1, L2 and L3 is compared to that of other similar peptides. Four other histidine-rich sequences have been taken into account: (i) the fragment of the prion protein of zebrafish, Ac-PVHTGHMGHIGHTGHTG HTGSSGHG-NH_2 (zp-PrP63-87), which contains seven separated His residues;[31,32] (ii) the peptides Ac-EDDAHAHAHAHAG-NH_2 and (iii) Ac-EDDHAHAHAHAHG-NH_2,[27] shorter analogues of the peptide pHpG-1 ($EDDH_9GVG_{10}$-NH_2) found in the venom of the snake *Atheris squamigera*,[28,33] which contain four and five alternate His residues, respectively; (iv) the peptide Ac-THHHHYHGG-NH_2, corresponding to the 18–26 domain of the Hpn protein from *H. pylori* and containing five His residues, four of which are consecutive.[34]

The competition plots that compare the zp-PrP63-87 peptide with L3 (Fig. S33 and S34, ESI†) show a similar trend for both

the Zn(II) and Cu(II) complexes and confirm that the larger the number of histidines in the sequence, the better the ability to bind both Zn(II) and Cu(II) ions.

A comparison between L2 and Ac-EDDAHAHAHAHAG-NH_2 – both containing four histidines but separated by serine or alanine residues, respectively – in the case of the Cu(II) ion, shows a similar trend for both the ligands up to pH about 5 (Fig. S35, ESI†). On the other hand, Cu(II)/L2 complexes are instead significantly more stable at higher pH values, where the Cu(II)–amide binding comes into play. Evidently, the presence of (non-coordinating) serines has an impact on amide deprotonation, possibly through their electronic effect on amidic nitrogens, making amide protons more acidic. In addition, if the EDD-sequence is involved in Cu(II) coordination, this could somehow hinder the binding with amides. On the contrary, Fig. S36 (ESI†) shows that the peptide sequence Ac-EDDAHAHAHAHAG-NH_2 is a better ligand for Zn(II) than the serine-substituted sequence L2, even though the difference between the two curves is not excessive (25% at physiological pH). In this case, Zn(II) is not able to deprotonate *N*-amides, which do not come into play. The coordination mode is almost the same for both the peptides: Zn(II) binds L2 *via* ($3N_{Im}$; H_2O), while Zn(II)/Ac-EDDAHAHAHAHAG-NH_2 complexes involve a carboxylic oxygen of the acidic terminus EDD-, and this may be the difference that makes the Zn(II) complexes of the latter more stable. At alkaline pH, the two systems become equivalent, since coordination modes for L2 and Ac-EDDAHA HAHAHAG-NH_2 ($3N_{Im}$; HO^-) are the same.

In Fig. S37 and S38 (ESI†), the competition diagrams involving L1 and Ac-EDDHAHAHAHAHG-NH_2 complexes are plotted: both of them have five His residues alternated with other amino acids. As in the previous case, the alanine-substituted peptide is a less effective Cu(II) ligand than L1, where histidines are alternated with a glutamic acid, a glycine and two serines. The explanation for this behaviour may be the same as above, although here, both the ligands contain carboxylate side chains which, in principle, can be involved in coordination. For Zn(II) complexes, up to pH 6 (where precipitation occurs in the Zn(II)/L1 system), the difference in stability between the two systems is very small.

A comparison between alternate and consecutive His sequences is shown in Fig. S39 (ESI†), where the competition plot between L1 and the peptide Ac-THHHHYHGG-NH_2 to form Cu(II) complexes is reported. Both the ligands contain 5 histidines, but the alternate sequence seems to be more effective in binding the Cu(II) ion at physiological pH, in agreement with the literature, where it is reported that the alternate His-tag -AHAHAHAH- confers more stability to the Cu(II) complexes than the consecutive His-tag with four histidines.[27]

Experimental

Materials

All peptides (Ac-FHEHGHSHSHGSGGGGGG-NH_2, Ac-SHSHSHSHS-NH_2, Ac-FHEHGHSHSHGSGGGGGGSDHSGDSKSHSHSHSHS-NH_2) were purchased from KareBay Biochem (USA) (certified purity: 98%) and were used as received. $Zn(ClO_4)_2{\cdot}6H_2O$ and $Cu(NO_3)_2{\cdot}3H_2O$ were extra pure products (Sigma-Aldrich); the concentrations of their stock solutions were standardised by EDTA titration and periodically checked *via* ICP-MS. The carbonate-free stock solutions of 0.1 mol dm^{-3} KOH and NaOH were purchased from Sigma-Aldrich and then potentiometrically standardized with the primary standard potassium hydrogen phthalate (99.9% purity). All sample solutions were prepared with freshly doubly distilled water. The $HClO_4$ stock solution was prepared by diluting concentrated $HClO_4$ (Sigma-Aldrich) and then standardized with KOH or NaOH. The ionic strength was adjusted to 0.1 mol dm^{-3} by adding $NaClO_4$ (Sigma-Aldrich). Grade A glassware was employed throughout.

Potentiometric measurements

Stability constants for proton and metal complexes were calculated from pH-metric titration curves registered at T = 298 K and ionic strength 0.1 mol dm^{-3} ($NaClO_4$); experimental details are reported as supplementary information (Tables S7 and S8, ESI†). The potentiometric apparatus consisted of a Metrohm 905 Titrando pH-meter system provided with a Mettler-Toledo InLab® Micro, glass-body, micro combination pH electrode and a dosing system 800 Dosino, equipped with a 2 mL micro burette. High purity grade argon was gently blown over the test solution in order to maintain an inert atmosphere. Constant-speed magnetic stirring was applied throughout. Solutions were titrated with 0.1 mol dm^{-3} carbonate-free KOH or NaOH. The electrode was daily calibrated for hydrogen ion concentration by titrating $HClO_4$ with alkaline solution under the same experimental conditions as above. The standard potential and the slope of the electrode couple were computed by means of the Glee[35] program. The purities and the exact concentrations of the ligand solutions were determined by the Gran method.[36] The HYPERQUAD[37] program was employed for the overall (β) and step (K) stability constant calculations, referring to the following equilibrium:

$$pM + qL + rH \leftrightarrows M_pL_pH_r$$

(charges omitted; p is 0 in the case of ligand protonation; r can be negative). Reported K_a values are instead the acid dissociation constants of the corresponding species. The computed standard deviations (referring to random errors only) were given by the program itself and are shown in parentheses as uncertainties on the last significant figure. Hydrolysis constants for the Zn(II) and Cu(II) ions were taken from the literature.[21,38] The distribution diagrams were computed using the HYSS program.[39] The overall metal binding ability can be evaluated in a wide pH range by computing and plotting the competition diagrams, starting from the binary speciation models. A solution containing the metal and the two (or more) ligands (or *vice versa*) is simulated, admitting that all the components compete with each other to form the respective binary complexes, without mixed species formation. This is a reasonable approximation in the case of peptides, which most often form only 1 : 1 complexes in which the peptide completely wraps the metal ion.

Mass spectrometric measurements

High-resolution mass spectra were obtained on a Bruker MicrOTOF-Q spectrometer (Bruker Daltonik, Bremen, Germany),

equipped with an Apollo II electrospray ionization source with an ion funnel. The mass spectrometer was operated in the positive ion mode. The instrumental parameters were as follows: scan range *m*/*z* 300–4000, dry gas nitrogen, temperature 453 K, and ion energy 5 eV. The capillary voltage was optimized to the highest S/N ratio and it was 4800 V. The small changes in voltage (±500 V) did not significantly affect the optimized spectra. The samples were prepared in a 1 : 1 acetonitrile–water mixture at different pH values (experimental details are reported in Table S9, ESI†). The samples were infused at a flow rate of 3 μL min^{-1}. The instrument was calibrated externally with a Tunemix™ mixture (Bruker Daltonik, Germany) in quadratic regression mode. Data were processed using the Bruker Compass DataAnalysis 4.0 program. The mass accuracy for the calibration was better than 5 ppm, enabling together with the true isotopic pattern (using SigmaFit) an unambiguous confirmation of the elemental composition of the obtained complex.

Spectroscopic measurements

The absorption spectra were recorded on Varian Cary50 Bio and Varian Cary300 Bio spectrophotometers, in the range 200–800 nm, using a quartz cuvette with an optical path of 1 cm. Circular dichroism (CD) spectra were recorded on a Jasco J-1500 CD spectrometer in the 200–800 nm range, using a quartz cuvette with an optical path of 1 cm in the visible and near-UV range or with a cuvette with an optical path of 0.01 cm in the wavelength range 180–300. The UV-Vis and CD spectroscopic parameters were calculated from the spectra obtained at the pH values corresponding to the maximum concentration of each particular species, based on distribution diagrams. Electron paramagnetic resonance (EPR) spectra were recorded in liquid nitrogen on a Bruker ELEXSYS E500 CW-EPR spectrometer at X-band frequency (9.5 GHz) and equipped with an ER 036TM NMR teslameter and an E41 FC frequency counter. Ethylene glycol (30%) was used as a cryoprotectant for EPR measurements. The EPR parameters were analyzed by computer simulation of the experimental spectra using WIN-EPR SIMFONIA software, version 1.2 (Bruker). The concentrations of sample solutions used for spectroscopic studies were similar to those employed in the potentiometric experiment (experimental details are reported in Tables S10–S12, ESI†).

Conclusions

In the present work, three peptide fragments corresponding to two possible metal binding sites, located in the C-terminal region of the putative fungal protein C4YJH2, have been investigated for their ability to interact with Zn(II) and Cu(II) ions. All the peptides demonstrated a very good affinity for these metals, in a wide pH range; the competition plots reported in Fig. S40–S42 (ESI†) show that complexes formed with Cu(II) are always more stable than those formed with Zn(II) throughout the explored pH range. As a consequence, the two metal ions should compete *in vivo* for these binding sites, copper being favoured by its higher affinity and zinc instead by its larger concentration.

Both the metal ions showed a preference for the binding site corresponding to peptide L1, although the coordination modes are different. As for Zn(II) complexes, all the investigated peptides bind the metal ion by means of three histidine residues ($3N_{Im}$) and an oxygen (carboxylic O^- or a water molecule), with a tetrahedral coordination geometry. The hypothesized molecular structure for Zn(II)/L2 complexes with the ($3N_{Im}$; O) configuration at physiological pH is illustrated in Fig. S43 (ESI†), by way of example. Concerning copper, it is supposed that, at acidic pH, the metal coordination sphere mainly involves the imidazole ring of histidine residues, while, at neutral or alkaline pH, the coordination of amide nitrogens of the peptidic backbone prevails. In addition, a role for Ser residues has been also hypothesized, *i.e.* that of reinforcing the Cu(II)–amide bonds.

The evolutionarily conserved sequence in C4YJH2 is probably fully involved in the task of Zn(II) acquisition and regulation, which is crucial for the growth and subsistence of pathogenic species like *Candida albicans.* A better understanding of the thermodynamics behind biological metal transport processes has been obtained, highlighting both the coordination modes used by Zn(II) to bind the proposed amino-acid sequence of C4YJH2 and the competition with Cu(II). This knowledge can contribute to the design and tuning of new antibiotic strategies against all the fungal pathogens using zinc transporters or zincophores containing these or similar peptide sequences in their metal binding sites.

Conflicts of interest

There are no conflicts to declare.

Acknowledgements

The present research was financially supported by: National Science Centre (nr UMO-2014/13/D/ST5/02868), University of Ferrara (FAR 2016), CIRCMSB (Consorzio Interuniversitario di Ricerca in Chimica dei Metalli nei Sistemi Biologici, Bari, Italy), MIUR (Ministero dell'Istruzione, dell'Università e della Ricerca) projects PRIN2015-2015MP34H3 and PRIN2015-2015T778JW) and Erasmus+ programme of the European Union.

Notes and references

1 T. Kourkoumpetis, D. Manolakaki, G. C. Velmahos, Y. C. Chang, H. B. Alam, M. M. De Moya, E. A. Sailhamer and E. Mylonakis, *Virulence*, 2010, **1**, 359–366.
2 S. Campoy and J. L. Adrio, *Biochem. Pharmacol.*, 2017, **133**, 86–96.
3 A. L. Mavor, S. Thewes and B. Hube, *Curr. Drug Targets*, 2005, **6**, 863–874.
4 M. W. McCarthy and T. J. Walsh, *Expert Rev. Anti-Infect. Ther.*, 2017, **15**, 577–584.
5 M. A. Pfaller, D. J. Diekema and P. Int Fungal Surveillance, *Clin. Microbiol. Infect.*, 2004, **10**, 11–23.
6 M. Blatzer and J.-P. Latgé, *Curr. Opin. Microbiol.*, 2017, **40**, 152–159.

7 M. I. Hood and E. P. Skaar, *Nat. Rev. Microbiol.*, 2012, **10**, 525.
8 E. R. Ballou and D. Wilson, *Curr. Opin. Microbiol.*, 2016, **32**, 128–134.
9 P. K. Walencik, J. Watly and M. Rowinska-Zyrek, *Curr. Med. Chem.*, 2016, **23**, 3717–3729.
10 C. S. Hwang, G. E. Rhie, J. H. Oh, W. K. Huh, H. S. Yim and S. O. Kang, *Microbiology*, 2002, **148**, 3705–3713.
11 I. Yike, *Mycopathologia*, 2011, **171**, 299–323.
12 I. Bremner and P. M. May, in *Zinc in Human Biology*, ed. C. F. Mills, Springer, London, 1989, pp. 95–108.
13 A. N. Besold, E. M. Culbertson and V. C. Culotta, *J. Biol. Inorg. Chem.*, 2016, **21**, 137–144.
14 S. García-Santamarina and D. J. Thiele, *J. Biol. Chem.*, 2015, **290**, 18945–18953.
15 A. N. Besold, B. A. Gilston, J. N. Radin, C. Ramsoomair, E. M. Culbertson, C. X. Li, B. P. Cormack, W. J. Chazin, T. E. Kehl-Fie and V. C. Culotta, *Infect. Immun.*, 2018, **86**, e00779-17.
16 The_UniProt_Consortium, *Nucleic Acids Res.*, 2017, **45**, D158–D169.
17 G. Butler, M. D. Rasmussen, M. F. Lin, M. A. S. Santos, S. Sakthikumar, C. A. Munro, E. Rheinbay, M. Grabherr, A. Forche, J. L. Reedy, I. Agrafioti, M. B. Arnaud, S. Bates, A. J. P. Brown, S. Brunke, M. C. Costanzo, D. A. Fitzpatrick, P. W. J. de Groot, D. Harris, L. L. Hoyer, B. Hube, F. M. Klis, C. Kodira, N. Lennard, M. E. Logue, R. Martin, A. M. Neiman, E. Nikolaou, M. A. Quail, J. Quinn, M. C. Santos, F. F. Schmitzberger, G. Sherlock, P. Shah, K. A. T. Silverstein, M. S. Skrzypek, D. Soll, R. Staggs, I. Stansfield, M. P. H. Stumpf, P. E. Sudbery, T. Srikantha, Q. Zeng, J. Berman, M. Berriman, J. Heitman, N. A. R. Gow, M. C. Lorenz, B. W. Birren, M. Kellis and C. A. Cuomo, *Nature*, 2009, **459**, 657.
18 M. S. Skrzypek, J. Binkley, G. Binkley, S. R. Miyasato, M. Simison and G. Sherlock, *Nucleic Acids Res.*, 2017, **45**, D592–D596.
19 H. Sigel and R. B. Martin, *Chem. Rev.*, 1982, **82**, 385–426.
20 G. Borghesani, F. Pulidori, M. Remelli, R. Purrello and E. Rizzarelli, *J. Chem. Soc., Dalton Trans.*, 1990, 2095–2100.
21 L. D. Pettit and H. K. J. Powell, *The IUPAC Stability Constants Database*, Royal Society of Chemistry, London, 1992–2000.
22 W. Maret, *J. Inorg. Biochem.*, 2012, **111**, 110–116.
23 D. S. Auld, *Biometals*, 2001, **14**, 271–313.
24 S. F. Sousa, A. B. Lopes, P. A. Fernandes and M. J. Ramos, *Dalton Trans.*, 2009, 7946–7956, DOI: 10.1039/b904404c.
25 I. L. Alberts, K. Nadassy and S. J. Wodak, *Protein Sci.*, 1998, **7**, 1700–1716.
26 J. Peisach and W. E. Blumberg, *Arch. Biochem. Biophys.*, 1974, **165**, 691–708.
27 D. Brasili, J. Watly, E. Simonovsky, R. Guerrini, N. A. Barbosa, R. Wieczorek, M. Remelli, H. Kozlowski and Y. Miller, *Dalton Trans.*, 2016, **45**, 5629–5639.
28 F. Pontecchiani, E. Simonovsky, R. Wieczorek, N. Barbosa, M. Rowinska-Zyrek, S. Potocki, M. Remelli, Y. Miller and H. Kozlowski, *Dalton Trans.*, 2014, **43**, 16680–16689.
29 J. Watly, E. Simonovsky, N. Barbosa, M. Spodzieja, R. Wieczorek, S. Rodziewicz-Motowidlo, Y. Miller and H. Kozlowski, *Inorg. Chem.*, 2015, **54**, 7692–7702.
30 J. Watly, E. Simonovsky, R. Wieczorek, N. Barbosa, Y. Miller and H. Kozlowski, *Inorg. Chem.*, 2014, **53**, 6675–6683.
31 L. Szyrwiel, E. Jankowska, A. Janicka-Klos, Z. Szewczuk, D. Valensin and H. Kozlowski, *Dalton Trans.*, 2008, 6117–6120.
32 D. Valensin, L. Szyrwiel, F. Camponeschi, M. Rowinska-Zyrek, E. Molteni, E. Jankowska, A. Szymanska, E. Gaggelli, G. Valensin and H. Kozlowski, *Inorg. Chem.*, 2009, **48**, 9042.
33 M. Remelli, D. Brasili, R. Guerrini, F. Pontecchiani, S. Potocki, M. Rowinska-Zyrek, J. Watly and H. Kozlowski, *Inorg. Chim. Acta*, 2018, **472**, 149–156.
34 D. Witkowska, R. Politano, M. Rowinska-Zyrek, R. Guerrini, M. Remelli and H. Kozlowski, *Chem. – Eur. J.*, 2012, **18**, 11088–11099.
35 P. Gans and B. O'Sullivan, *Talanta*, 2000, **51**, 33–37.
36 G. Gran, *Acta Chem. Scand.*, 1950, **4**, 559–577.
37 P. Gans, A. Sabatini and A. Vacca, *Talanta*, 1996, **43**, 1739–1753.
38 G. Arena, R. Cali, E. Rizzarelli and S. Sammartano, *Thermochim. Acta*, 1976, **16**, 315–321.
39 L. Alderighi, P. Gans, A. Ienco, D. Peters, A. Sabatini and A. Vacca, *Coord. Chem. Rev.*, 1999, **184**, 311–318.

Volume 11 | Number 12 | December 2019 | Pages 1967–2112

Metallomics

rsc.li/metallomics

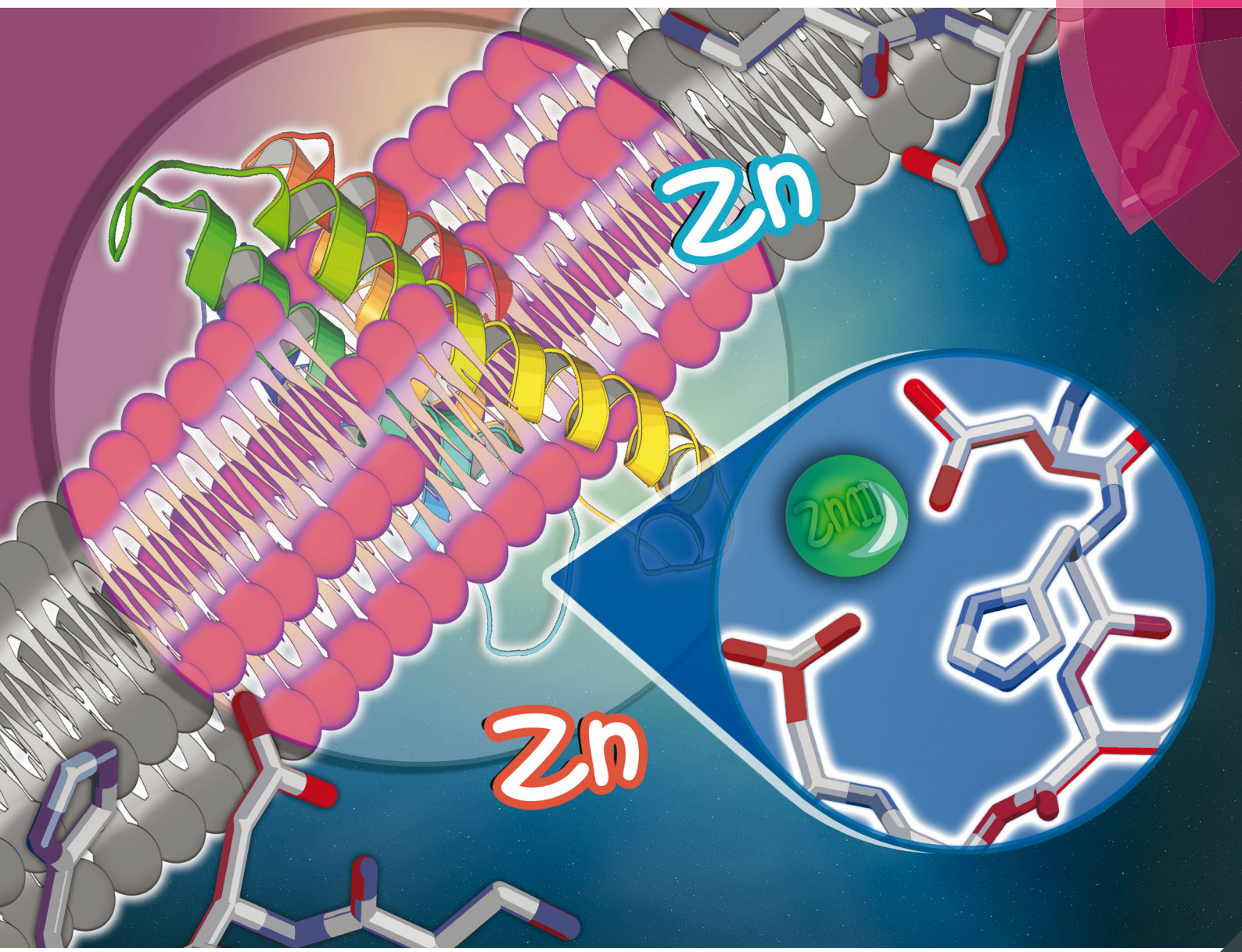

ISSN 1756-591X

ROYAL SOCIETY OF CHEMISTRY | Celebrating IYPT 2019

PAPER
Maurizio Remelli *et al.*
Thermodynamic and spectroscopic study of Cu(II) and Zn(II) complexes with the (148–156) peptide fragment of C4YJH2, a putative metal transporter of *Candida albicans*

Indexed in Medline!

Metallomics

PAPER

View Article Online
View Journal | View Issue

Cite this: *Metallomics*, 2019, **11**, 1988

Thermodynamic and spectroscopic study of Cu(II) and Zn(II) complexes with the (148–156) peptide fragment of C4YJH2, a putative metal transporter of *Candida albicans*†

Denise Bellotti,[ab] Cinzia Tocchio,[a] Remo Guerrini,[a] Magdalena Rowińska-Żyrek[b] and Maurizio Remelli*[a]

Received 9th October 2019,
Accepted 8th November 2019

DOI: 10.1039/c9mt00251k

rsc.li/metallomics

Candida albicans is a widespread human pathogen which can infect humans at different levels. Like the majority of microorganisms, it needs transition metals as micronutrients for its subsistence. In order to acquire these nutrients from the host, *C. albicans* employs various strategies, also involving chelating proteins specifically expressed to sequester metals from the environment. A histidine-rich protein sequence identified in the *C. albicans* genome, named C4YJH2, has been recently studied for its putative role in Zn(II) transport. Two outer membrane major histidine-rich clusters of C4YJH2, namely the domains 131–148 (FHEHGHSHSHGSGGGGGG) and 157–165 (SHSHSHSHS), have been confirmed as strong binding sites for the Cu(II) and Zn(II) ions. Nevertheless, the 9-residue "linker" sequence 148–156 (GSDHSGDSK) between the two His-rich fragments of C4YJH2, containing an additional His residue, can also contribute to metal binding. In the present work, the protected peptide Ac-GSDHSGDSK-NH_2 and some analogues (Ac-GSDHSGASK-NH_2, Ac-GADHAGDAK-NH_2, Ac-GSDH-NH_2, and Ac-HSGD-NH_2) have been synthesized and their metal binding properties have been studied in detail. The thermodynamics of complex-formation equilibria of the above reported ligands with Cu(II) and Zn(II) ions have been studied by potentiometry in a wide pH range and the stoichiometry of the formed species has been confirmed by mass spectrometry; the most likely solution structures of the metal complexes are also discussed on the basis of NMR, UV-vis, circular dichroism (CD) and EPR data. The results show the importance of Asp7 in the stabilization of Zn(II) complexes and suggest a significant role of the (quite abundant) Ser residues in the task of metal uptake and regulation.

Significance to metallomics

The mechanism of metal acquisition at the host/pathogen interface can be a fertile ground for the design of new antibiotics. The present paper deals with the characterization of Cu(II) and Zn(II) binding to the putative metal transporter C4JYH2, found in the genome of *Candida albicans*. The thermodynamic investigation of the formed metal complexes and their spectroscopic characterization in solution opens the way to the discovery of possible new pharmacological targets based on metal ions.

Introduction

The constant increase of the drug-resistance phenomenon against antibiotics and antifungal agents, with a high incidence especially in hospitals, represents a heavy burden for the healthcare systems: a deep reconsideration of commonly used therapies and the availability of innovative drugs are definitely required. *Candida albicans* is one of the most diffused opportunistic pathogenic yeasts that can affect the human organism. The pathological conditions associated to *C. albicans* frequently involve skin, oral cavity, oesophageal, vaginal and gastrointestinal tract infections ranging from superficial disorders to invasive systemic diseases that can eventually involve the vascular system and various organs anywhere in the body. Infections caused by *C. albicans* represent a serious threat for the subsistence of immunocompromised or debilitated

[a] *Department of Chemical and Pharmaceutical Sciences, University of Ferrara, Via L. Borsari 46, 44121, Ferrara, Italy. E-mail: rmm@unife.it*
[b] *Faculty of Chemistry, University of Wrocław, F. Joliot-Curie 14, 50-383, Wrocław, Poland*

† Electronic supplementary information (ESI) available. See DOI: 10.1039/c9mt00251k

individuals and it is by far the major cause of severe mucosal infections (invasive candidiasis) with an elevated mortality rate.[1–5] Furthermore, the phenomenon of drug resistant mycoses has become a serious clinical and financial burden on the world healthcare systems: in the long run it may become a critical and dangerous threat comparable to the increase of ''superbug'' infections.[6,7] As a consequence, the need of innovative antifungal treatments with high selectivity, specificity and effectiveness is undeniable.

Since the eukaryotic cells of human and fungal pathogens share several biological processes, in order to identify new pharmacological targets, one possible strategy is to focus on the differences in the metabolic pathways of these species. One difference concerns the mechanism of metal uptake and transport into the fungal cell. In fact, several lines of evidence confirm that one critical aspect of fungal infection and survival is the ability of the pathogenic microorganism to assimilate metal nutrients from the host environment.[8] Since metals are essential for many vital cellular functions, to avoid infection, the host restricts the access to the essential nutrients by means of a process known as ''nutritional immunity''.[9] The first step towards the design of a highly specific metal transport targeting therapeutic is therefore to obtain relevant information about thermodynamics and coordination chemistry of the interacting systems (metal–metal transporter).[9–12]

Zn(II), as well as several other transition metals, including Cu(II), is crucial for life and it is frequently involved in many cellular processes, where it can play the role of coenzyme or cofactor. Since Zn(II) concentration in a free, nonprotein-bound form is estimated to be sub-nanomolar,[13] its uptake becomes extremely challenging for the fungal pathogen. *C. albicans* has evolved several mechanisms to overcome host nutritional immunity by expressing zinc transporters (*e.g.* Zrt1/Zrt2/Pra1 for Zn(II))[14,15] or redundant enzymes that withhold the host stocks. Also Cu(II) is an endogenous metal and a necessary nutrient for *C. albicans*; it can compete with Zn(II) for the same binding sites and actively participate in the host–pathogen strife.[16,17]

In this context, we recently started a study on Zn(II) and Cu(II) binding behaviour towards C4YJH2 (UniProt Knowledgebase),[18] a protein sequence of 199 amino acid residues, found in the genome of *Candida albicans* (strain WO-1), which is supposed to be involved in metal transport processes. In fact, it shares a high percentage of identity with putative Zn(II) transporters and proteins involved in metal homeostasis.[19] Its amino acid sequence contains a remarkably high number of alternating histidine and serine residues, mostly located in the domains 131–148 (FHEHGHSHSHGSGGGGGG) and 157–165 (SHSHSHSHS) and confirmed to be involved in Zn(II) and Cu(II) coordination.[20] In the native protein, these two His-rich domains are linked by the 9-residue sequence GSDHSGDSK (148–156), also containing a histidine and thus possibly contributing to the metal binding. Therefore, we decided to extend our investigation focusing on this ''linker''. The protected peptide **WT** = Ac-GSDHSGDSK-NH_2 has been considered, along with its analogues **D7A** = Ac-GSDHSGASK-NH_2, **S2A/S5A/S8A** = Ac-GADHAGDAK-NH_2, **GSDH** = Ac-GSDH-NH_2, and **HSGD** = Ac-HSGD-NH_2. The peptide sequence of **D7A** lacks the aspartic acid in position 7, which is substituted by an alanine in order to investigate the role of Asp-7 in the wild-type peptide (**WT**) protonation (possible hydrogen bond with Lys-9) and metal coordination. The nonapeptide **S2A/S5A/S8A** is an analogue of **WT** where serine residues have been replaced by alanines. Serine residues are rather abundant in C4YJH2 protein sequence. Although the serine side hydroxymethyl group has no acidic properties in the explored pH range and it is generally not expected to significantly interact with Cu(II) or Zn(II) ions, an electronic effect on the histidine residues and/or on the amides of the peptide backbone has previously been suggested.[20] Finally, the study of the two short peptides, Ac-GSDH-NH_2 and Ac-HSGD-NH_2, corresponding to the left-hand and the right-hand side fragments around histidine, provides information on the Cu(II) attitude to coordinate amidic nitrogen atoms in the amino- or carboxyl-terminus direction.

Results and discussion

Ligand protonation

All the investigated peptides, **WT**, **D7A**, **S2A/S5A/S8A**, **GSDH** and **HSGD**, were protected at their N-terminus by acetylation and at their C-terminus by amidation; therefore, their acid–base behaviour depends on the amino acid side-chain properties, *i.e.* on the imidazole ring of His, the carboxylic group of Asp and the amino group of Lys. The amidic protons of the peptide backbone cannot be spontaneously released in the pH range explored by potentiometry, since they are very weak acids ($pK_a \approx 15$),[21] but they can be displaced by Cu(II) at a mildly acidic pH value, to form a coordination bond. The protonation constants of **WT**, **D7A**, **S2A/S5A/S8A**, **GSDH** and **HSGD** are reported in Table 1 while the corresponding distribution diagrams are shown in Fig. S1–S5 (ESI†).

The obtained protonation constants are consistent with the literature values for similar systems[22] and show reasonable

Table 1 Overall ($\log\beta$) and step ($\log K$) protonation constants for **WT**, **D7A**, **S2A/S5A/S8A**, **HSGD** and **GSDH** at T = 298 K and I = 0.1 mol dm^{-3} (KCl). Values in parentheses are standard deviations on the last significant figure

	WT		**S2A/S5A/S8A**			**D7A**		**HSGD**		**GSDH**	
Species	$\log\beta$	$\log K_{step}$	$\log\beta$	$\log K_{step}$	Species	$\log\beta$	$\log K_{step}$	$\log\beta$	$\log K_{step}$	$\log\beta$	$\log K_{step}$
HL^-	10.84 (2)	10.84	10.39 (1)	10.39	HL	10.21 (2)	10.21	6.58 (2)	6.58	6.83 (2)	6.83
H_2L	17.72 (3)	6.88	17.19 (2)	6.80	H_2L^+	16.70 (3)	6.49	10.44 (2)	3.86	10.60 (2)	3.77
H_3L^+	21.82 (3)	4.10	21.29 (2)	4.10	H_3L^{2+}	20.46 (3)	3.76	—	—	—	—
H_4L^{2+}	25.01 (3)	3.19	24.63 (2)	3.34	—	—	—	—	—	—	—

similarities among the considered peptides; the variability can be mainly ascribed to the charge of the different species. The histidine protonation constant ranges from 6.49 to 6.88; this interval is rather small, suggesting the absence of specific behaviours depending on the ligand sequence. Furthermore, the presence or absence of the serine residues nearby the histidine does not seem to significantly affect its protonation constant. The lysine $\log K$ value is rather high (10.84) for the "wild-type" peptide (Ac-GSDHSGDSK-NH_2), although still measurable under the employed experimental conditions. Finally, the Asp residues have the lowest $\log K$ values, due to their acidic moiety, which vary between 3.19 and 4.10, depending on the primary structure of the peptide and its charge.

The comparison between **WT** and its mutants does not point out any significant change in the protonation behaviour attributable to Ala substitutions. The difference in the $\log K$ values of Lys residues between **WT** and **D7A** does not suggest the formation of a hydrogen bond between the protonated amino group of Lys-9 and the carboxylate group of Asp-7, but it can be simply due to the higher charge of the former ligand, which contains an additional carboxylate group. Analogously, the Ala-Ser substitutions do not significantly affect the protonation constants of peptide side chains.

Cu(II) complexes

All the investigated peptides proved to be able to form stable 1 : 1 complexes with the Cu(II) ion; no poly-nuclear or bis-complexes have been detected either by potentiometry, mass spectrometry or EPR. No precipitation has been observed over the explored pH range. Overall complex-formation constants ($\log \beta$) and corresponding acidity constants (pK_a) are reported in Table 2 and the corresponding distribution diagrams are plotted in Fig. 1 and Fig. S6–S9 (ESI†); ESI-MS results are shown in Table S1 (ESI†). UV-vis, CD and EPR results are reported in Tables S2–S6 (ESI†) and Fig. 2, 3 and Fig. S10–S17 (ESI†).

Cu(II) starts to interact with **WT** and its mutants around pH 3.5 and the first detected complex is the mono-protonated species ($[CuHL]^+$ for **WT** and **S2A/S5A/S8A**; $[CuHL]^{2+}$ in the case of **D7A**). The stoichiometry of these species indicates that the ligand is mono-protonated, most likely at its Lys residue. Doubtless, Cu(II) is anchored to the imidazole nitrogen of histidine, while the possible participation in coordination by the carboxylic group(s) of the Asp residue(s) is arguable. The wavelength of maximum absorption expected for a coordination (N_{Im}, COO^-) is 731 nm,[21] in good agreement with the VIS

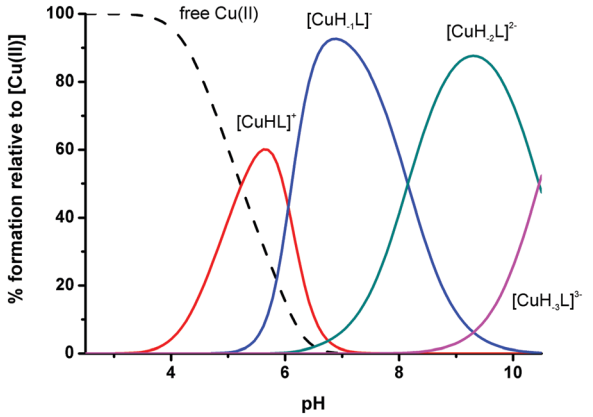

Fig. 1 Representative species distribution diagram relative to Cu(II) complexes with **WT**; Cu(II) : L molar ratio = 0.8 : 1.

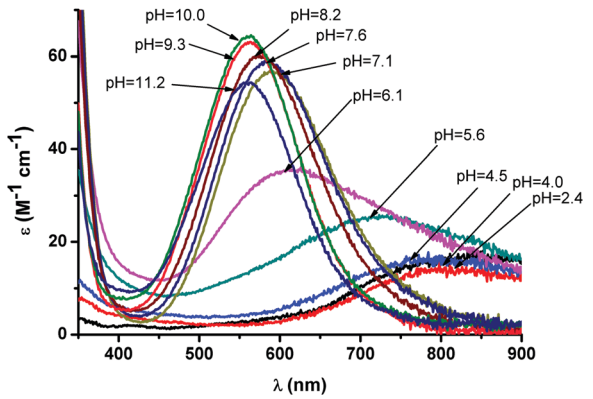

Fig. 2 Vis absorption spectra [350–900 nm; optical path 1 cm] for Cu(II) complexes with **WT**; Cu(II) : L molar ratio = 0.8 : 1.

absorption data in the pH range 5–6 for **WT** and **S2A/S5A/S8A** (λ_{max} = 726 nm and 735 nm, respectively) (see Tables S2 and S3, ESI†). Otherwise, in the case of **D7A**, we found λ_{max} = 750 nm, a value closer to that expected for a Cu(II) complex with a ($1N_{Im}$) configuration (760 nm). Increasing the pH value, the species [CuL] (for **S2A/S5A/S8A**) and $[CuL]^+$ (for **D7A**) are formed with pK_a values of 6.58 and 5.57, respectively. This complex was not observed in the case of **WT**. It is well known[23] that, in this pH range, the cupric ion already bound to the ligand can displace one peptide hydrogen of the backbone to bind the amide nitrogen. In that case, the coordination geometry should be ($1N_{Im}$, $1N^-$) or ($1N_{Im}$, $1N^-$, COO^-). The presence of two

Table 2 Overall stability constants ($\log \beta$) and acid dissociation constants (pK_a) of Cu(II) complexes with **WT**, **S2A/S5A/S8A**, **D7A**, **HSGD** and **GSDH** at T = 298 K and I = 0.1 mol dm^{-3} (KCl). Values in parentheses are standard deviations on the last significant figure

	WT		**S2A/S5A/S8A**			**D7A**		**HSGD**		**GSDH**	
Species	$\log \beta$	pK_a	$\log \beta$	pK_a	Species	$\log \beta$	pK_a	$\log \beta$	pK_a	$\log \beta$	pK_a
$[CuHL]^+$	15.66 (4)	—	14.63 (3)	6.58	$[CuHL]^{2+}$	14.04 (6)	5.57	—	—	—	—
$[CuL]$	—	—	8.05 (3)	6.63	$[CuL]^+$	8.48 (3)	5.84	4.21 (2)	6.79	4.24 (5)	5.87
$[CuH_{-1}L]^-$	3.54 (3)	8.15	1.42 (3)	9.59	$[CuH_{-1}L]$	2.64 (2)	8.29	−2.58 (2)	6.91	−1.63 (3)	5.92
$[CuH_{-2}L]^{2-}$	−4.61 (5)	10.46	−8.27 (4)	10.65	$[CuH_{-2}L]^-$	−5.65 (4)	10.38	−9.50 (2)	8.78	−7.56 (2)	8.53
$[CuH_{-3}L]^{3-}$	−15.07 (7)	—	−18.81 (5)	—	$[CuH_{-3}L]^{2-}$	−16.03 (5)	—	−18.27 (2)	—	−16.09 (4)	—

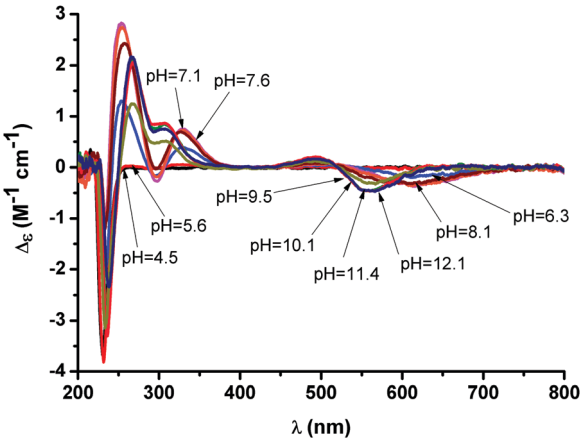

Fig. 3 Circular dichroism spectra [200–800 nm; optical path 1 cm] for Cu(II) complexes with **WT**; Cu(II) : L molar ratio = 0.8 : 1.

nitrogens in the first coordination sphere of Cu(II) is confirmed by EPR spectra (see Tables S3 and S4, ESI†). At higher pH, the ionization/binding of a second amide occurs with values of pK_a = 6.63 (for **S2A/S5A/S8A**) and 5.84 (for **D7A**) and leads to the formation of the species $[CuH_{-1}L]^-$ and $[CuH_{-1}L]$, respectively. The complex $[CuH_{-1}L]^-$ was also detected in the system containing **WT**, where, however, a cooperative binding effect leads to the simultaneous coordination of the first and second amide nitrogens. These complexes reach about 90% of formation at physiological pH. The most plausible coordination hypothesis for these species is ($1N_{Im}$, $2N^-$) (see Fig. 4). In fact, the wavelengths of maximum absorption recorded at neutral pH are consistent with the expected value for a Cu(II) complex with this donor-atom set (λ_{max} = 583 nm) and the EPR results at physiological pH confirm a 3N coordination.

In the alkaline pH range, the deprotonation of the third amide likely occurs (pK_a values = 8.15, 9.59 and 8.29 for **WT**, **S2A/S5A/S8A** and **D7A**, respectively). The visible absorption

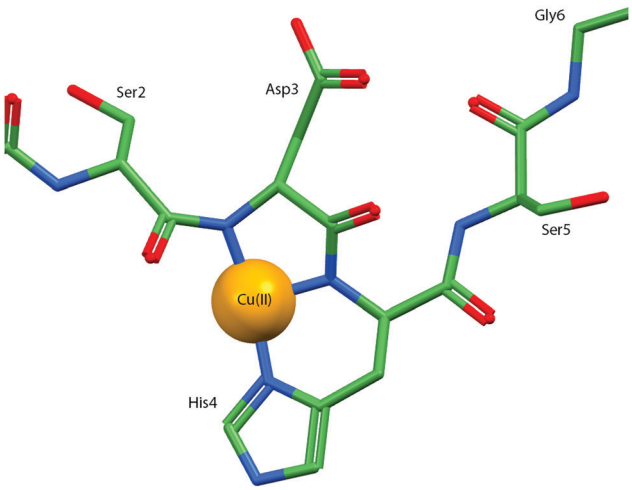

Fig. 4 Proposed coordination sphere of Cu(II) complexes with **WT** ligand at physiological pH. Explicit hydrogen atoms and water molecules are omitted for clarity.

bands always shift to shorter wavelengths, suggesting the increase of the number of coordinated nitrogen atoms. Based on spectroscopic results it is possible to suggest two possible configurations. In the case of ligands **WT** and **D7A**, the values of λ_{max} (≈560 nm) suggest the substitution of the imidazole nitrogen by the N-amide in the Cu(II) equatorial plane, to obtain a ($3N^-$) coordination mode (expected λ_{max} value: 563 nm) with a water molecule in the fourth equatorial position. On the other hand, in the case of ligand **S2A/S5A/S8A**, the obtained wavelength of maximum absorption at pH 10.3 (529 nm) strongly suggests a ($1N_{Im}$, $3N^-$) configuration (expected λ_{max} value: 522 nm). The experimental values of $A_{\parallel}$ and $g_{\parallel}$ (Tables S2–S4, ESI†) for all three systems agree with the hypothesis of both a 3N coordination and a 4N coordination. It is worth noting that the acidity constants of the three amide groups of **S2A/S5A/S8A** involved in complexation are approximately one order of magnitude lower (pK_a one unit higher) than the corresponding constants of **WT** and **D7A**. Since no steric effect comes into play, an electronic effect due to the hydroxyl side chain of Ser can be the source of this difference and of the consequent lower stability of Cu(II) complexes with **S2A/S5A/S8A** with respect to the analogous complexes with the other mutants. A similar hypothesis was already put forward in the previous study on the main metal binding domains of C4YJH2.[20] In addition, among the three Ser residues of **S2A/S5A/S8A**, a significant role should be played by Ser-2, as suggested by the constant values obtained for the systems Cu(II)/**GSDH** and Cu(II)/**HSGD** (see below).

Finally, under the most alkaline conditions, a further deprotonation step is observed and $[CuH_{-3}L]^{2-}$ (for **WT** and **S2A/S5A/S8A**) and $[CuH_{-3}L]^{2-}$ (for **D7A**) species are formed, without any significant variation in the spectroscopic parameters. This suggests that the last deprotonation step does not affect the Cu(II) coordination and likely corresponds to the deprotonation of a not-coordinated lysine. This hypothesis is also in good agreement with the thermodynamics results, since the corresponding pK_a values (10.46, 10.65 and 10.38) are practically identical to those obtained from ligand protonation measurements.

Cu(II) interaction with **HSGD** and **GSDH** begins at pH lower than 4. The speciation model is the same for the two ligands, with four mononuclear 1 : 1 complexes, variously protonated. However, the distribution diagrams (Fig. S8 and S9, ESI†) show that the behaviour is not exactly the same, as explained below.

The first detected complex is $[CuL]^+$; the stoichiometry of this species suggests that both the histidine and the aspartic acid are not protonated. The imidazole nitrogen of the histidine can be deprotonated at such an acidic pH value only if it is bound to the metal ion; instead, the side carboxylate of the Asp residue can be involved or not in the metal coordination. In the case of **HSGD**, the obtained wavelength of maximum absorption at pH 6 – where the $[CuL]^+$ complex is the most abundant species in solution – is 715 nm, suggesting the formation of a macrocycle with a ($1N_{Im}$, COO^-) coordination mode (expected λ_{max} value: 731 nm). On the other hand, in the case of **GSDH**, the wavelength of maximum absorption at pH 5.5 is significantly higher (763 nm), suggesting a ($1N_{Im}$) coordination (expected λ_{max} value: 760 nm). Most likely, in the latter case,

the carboxylate group of the Asp residue (close to histidine), being at the opposite side of the backbone with respect to the imidazole ring, cannot bind the same Cu(II) ion due to steric hindrance. On increasing the pH value, three successive deprotonation steps are observed, giving rise to the species $[CuH_{-1}L]$, $[CuH_{-2}L]^-$ and $[CuH_{-3}L]$.[2] The corresponding pK_a values (6.79, 6.91 and 8.78 for **HSGD** and 5.87, 5.92 and 8.53 for **GSDH**, respectively) suggest the progressive coordination of amide nitrogens of the peptide backbone. Considering the complex $[CuH_{-1}L]$ formed by **HSGD**, a ($1N_{Im}$, $1N^-$, and COO^-) coordination mode can be suggested. In fact, the wavelength of maximum absorption at pH 7 – where this species reaches its higher percentage – (λ_{max} = 636 nm) is very close to the expected λ_{max} value (638 nm).[21] It is not possible, from the present experimental data, to state which one of the backbone amides is bound to copper; as a matter of fact, the coordination of the amide nitrogen most close to His will lead to the formation of a 7-membered chelate ring. On the other hand, in the case of **GSDH**, the amide nitrogen which binds the metal ion should be that of His, the first one in the N-terminal direction, forming a stable 6-membered ring. The lower pK_a value of this step for **GSDH** and, consequently, the higher value of the overall stability constant of $[CuH_{-1}L]$ (about one order of magnitude with respect to that of **HSGD**) support the above hypothesis.

At higher pH, the deprotonation/coordination of a second amide occurs in a quick sequence in both the systems, giving rise to the $[CuH_{-2}L]^-$ complex, the predominant species at physiological pH. In the case of **HSGD**, the positions of the d–d band in the UV-vis spectra both at pH 7.60 and 8.12 (615 nm and 612 nm, respectively, see Fig. S12 and Table S5 ESI†) suggest a coordination mode where the two amides and the carboxyl group occupy the equatorial positions of the metal coordination sphere ($2N^-$, COO^-; expected λ_{max} = 614 nm). EPR data at pH 8.7 agree with a [2N,O] coordination mode; in the CD spectra, the typical[24] charge transfer band at 301 nm, due to the formation of the amide-copper bond, has been observed (Table S5, ESI†). As for **GSDH**, the wavelength of maximum absorption at neutral pH (λ_{max} = 585 nm) is very close to the one expected for a coordination ($1N_{Im}$, $2N^-$) (583 nm), where Cu(II) coordinates one imidazole and two amide nitrogens in the equatorial plane of the complex. The EPR data at pH 8.6 ($A_{\parallel}$ = 191.6, and $g_{\parallel}$ = 2.215, Table S6, ESI†) clearly indicate a 3N coordination mode. The last deprotonation step is associated with the binding of a third amide in the main coordination plane; the corresponding species is $[CuH_{-3}L]^{2-}$. In the case of **HSGD**, a further blue-shift is observed in the vis absorption spectra with a wavelength of maximum absorption at pH 11 of 575 nm, only slightly higher than the predicted value for a ($3N^-$, COO^-) complex (547 nm). This difference can be ascribed to the presence of an axial binding group, most likely the His imidazole.[21] EPR spectra at pH 10–11 are in agreement with both 3N and 4N coordination modes.[25] Also in the case of the ligand **GSDH**, at very alkaline pH, the deprotonation of a further amide occurs, with a pK_a 8.53. The visible absorption band shifts to a lower wavelength (560 nm), suggesting that the third backbone amide substitutes the imidazole nitrogen in the Cu(II) main coordination plane; in fact, the expected value of λ_{max} for a ($3N^-$) coordination mode is 563 nm, very close to the experimental one. As for the ($1N_{Im}$, $3N^-$) coordination mode, the expected λ_{max} value would be 522 nm, rather far from the experimental one. A similar behaviour was already previously observed for the protected tetrapeptide Boc-Ala-Gly-Gly-His.[26] Actually, EPR spectra at pH 10–11 indicate a 4N coordination mode, thus suggesting that the imidazole ring can be still bound in an axial position.

Zn(II) complexes

The characterization of the Zn(II) complexes has been achieved by means of mass spectrometry, potentiometry and nuclear magnetic resonance. Mass spectrometric measurements provided information on the stoichiometry of the formed species, potentiometry allowed the partial and overall stability constants of the detected metal complexes to be determined and NMR spectra recorded both in the presence and in the absence of Zn(II) ion pointed out the precise metal binding sites. All the peptides studied here are able to form 1 : 1 complexes with the Zn(II) ion; no polynuclear or bis-complexes have been detected either by potentiometry or by mass spectrometry. No precipitation has been observed in the explored pH range. The formation constant values are shown in Table 3 and the corresponding distribution diagrams are plotted in Fig. 5 and Fig. S18–S21 (ESI†); ESI-MS results are reported in Table S1, ESI.†

WT and **S2A/S5A/S8A** peptides behave in a very similar manner in coordination to the Zn(II) ion. In both systems, the metal/ligand interaction starts at pH 4 and the first detected species is $[ZnHL]^+$, which is also the prevailing complex at physiological pH. The stoichiometry of this complex suggests that only the side chain of Lys is protonated. The metal ion should be anchored at the His residue and one or both of the carboxylate moieties of the Asp residues can be involved in complexation; the corresponding coordination mode can either be ($1N_{Im}$, COO^-) or ($1N_{Im}$, $2COO^-$). The suggested geometry

Table 3 Overall stability constants (log β) and acid dissociation constants (pK_a) of Zn(II) complexes with **WT**, **S2A/S5A/S8A**, **D7A**, **HSGD** and **GSDH** at T = 298 K and I = 0.1 mol dm^{-3} (KCl). Values in parentheses are standard deviations on the last significant figure

	WT		**S2A/S5A/S8A**			**D7A**		**HSGD**		**GSDH**	
Species	log β	pK_a	log β	pK_a	Species	log β	pK_a	log β	pK_a	log β	pK_a
$[ZnHL]^+$	14.11 (6)	—	13.37 (9)	—		—	—	—	—	—	—
$[ZnL]$	—	—	—	—	$[ZnL]^+$	—	—	2.9 (1)	—	2.85 (9)	—
$[ZnH_{-1}L]^-$	−1.86 (4)	10.39	−2.15 (4)	10.35	$[ZnH_{-1}L]$	−2.57 (3)	10.36	—	—	—	—
$[ZnH_{-2}L]^{2-}$	−12.25 (5)	—	−12.50 (6)	—	$[ZnH_{-2}L]^-$	−12.93 (6)	—	−12.43 (4)	—	−12.41 (3)	—

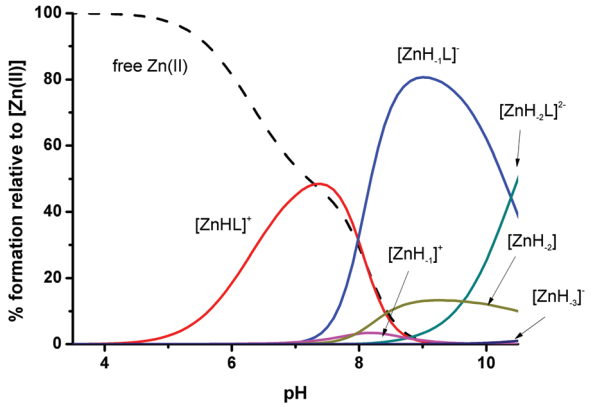

Fig. 5 Representative species distribution diagram relative to Zn(II) complexes with **WT**; Zn(II) : L molar ratio = 0.8 : 1.

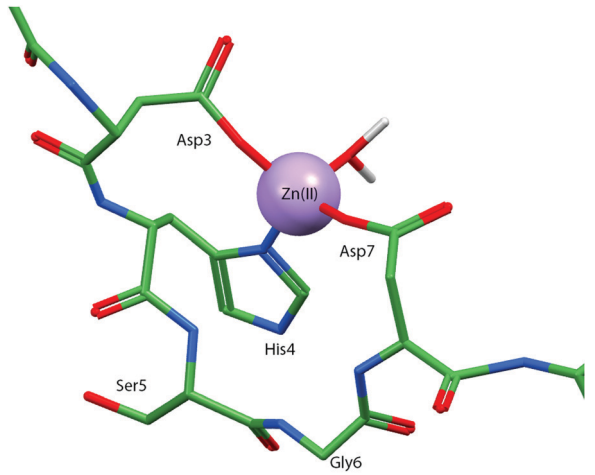

Fig. 6 Proposed molecular structure of Zn(II) complexes with **WT** ligand at physiological pH. Explicit hydrogen atoms are omitted for clarity.

can be either tetrahedral or trigonal bipyramid, as most frequently found in proteins,[27] where the additional coordination positions are occupied by water molecules (Fig. 6). On increasing the pH value, two simultaneous deprotonation steps occur, giving rise to the $[ZnH_{-1}L]^-$ complex, the most abundant species in the pH range 8–10. It is reasonable to suggest the hydrolysis of two coordinated water molecules. The [ZnL] complex has not been detected by potentiometry, thus suggesting it is only a transient species. ^{1}H–^{1}H TOCSY spectra recorded at physiological pH (Fig. S22 and S23, ESI†) confirm the suggested coordination hypotheses, since the major Zn(II)-induced shifts are those of histidine protons ($H_{\varepsilon1}$–$H_{\delta2}$), (H_α–$H_{\beta1}$), and (H_α–$H_{\beta2}$) and aspartic acid protons (H_α–$H_{\beta1}$), and (H_α–$H_{\beta2}$). Furthermore, in the case of **WT** ligand, the pronounced deshielding effect exhibited by His $H_{\varepsilon1}$ protons (Δ_δ = 0.125 ppm) compared to the shift of His $H_{\delta2}$ (Δ_δ = 0.050 ppm) (Fig. S22, ESI†), in the presence of Zn(II) ions, suggests a coordination through the imidazole-N_δ.[28–31] This difference is less pronounced in **S2A/S5A/S8A**, thus suggesting that the presence of the Ser residues may influence the binding behaviour of histidine. It is also worth noting that in the Zn(II)/**S2A/S5A/S8A** system, the protons of lysine display a moderate downfield shift (Fig. S23, ESI†): since Lys does not directly participate in coordination, these perturbations can suggest an interaction of Zn(II) with the aspartic acid in position 7, the nearest the Lys residue. In the case of the **WT** ligand, only Lys-H_α exhibits a small perturbation after Zn(II) addition, possibly because the presence of serine residues reduces the deshielding effect on Lys. Finally, starting from pH 8.5, the complex $[ZnH_{-1}L]^-$ releases a further proton, giving rise to the species $[ZnH_{-2}L]^{2-}$. The corresponding pK_a values for the two systems (10.39 and 10.35 for **WT** and **S2A/S5A/S8A**, respectively) are very similar to those obtained in the absence of Zn(II), suggesting the simple deprotonation of the Lys residue without any involvement in complexation.

As for peptide **D7A**, Zn(II) complexes begin to form only at pH 6.5, *i.e.* when imidazole nitrogen is deprotonated and available for complexation. Evidently, the presence, at lower pH, of only one Asp carboxylate is not sufficient to stably bind the metal ion. Thus, the first detected species is $[ZnH_{-1}L]$, most likely derived from the binding of **D7A** to the hydrolytic species $[ZnOH]^+$ already present in solution in small amount (see distribution diagram of Fig. S19, ESI†). In the complex $[ZnH_{-1}L]$, the dominant species throughout all the explored pH range, the Zn(II) ion is certainly bound to the histidine residue. Rather unexpectedly, the ^{1}H–^{1}H TOCSY spectra recorded at pH 7.2 (Fig. S24, ESI†) suggest that the aspartic acid in position 3 should not participate in complex formation. Indeed, the metal addition causes only a selective shift of histidine ($H_{\varepsilon1}$–$H_{\delta2}$) imidazole protons (more pronounced for His $H_{\varepsilon1}$ protons, as already observed above for **WT** and possibly due to the presence of Ser residues) leaving the signals of H_α–$H_{\beta1}$/$H_{\beta2}$ unchanged, therefore suggesting that no other residues are involved in the complexation. Signals corresponding to the aspartic acid (H_α–$H_{\beta1}$), and (H_α–$H_{\beta2}$) protons undergo only a slight shift, supposedly due to the proximity to the histidine anchor site. Starting form pH 8.5, the complex $[ZnH_{-2}L]^-$ begins to form with pK_a = 10.36, likely corresponding to the deprotonation of a not-coordinated lysine.

For the sake of completeness, Zn(II) complexes with ligands **HSGD** and **GSDH** have been also investigated. These peptides only possess two possible donor groups: one histidine and one aspartic acid. No precipitation has been observed in the explored pH range. In both the systems Zn(II) complexes begin to form at pH 4 and only two major species were detected by potentiometry: $[ZnL]^+$, where both the Asp and His residues should be bound to the metal ion, and $[ZnH_{-2}L]^-$, where the Zn(II) coordination sphere possibly involves also two ionized water molecules, as already hypothesised for the systems **WT**, **D7A** and **S2A/S5A/S8A**. The participation of His and Asp residues in the Zn(II) complex formation is also confirmed by the general changes of their proton correlations in ^{1}H–^{1}H TOCSY spectra (Fig. S25 and S26, ESI†). It is also reasonable to assume that both the low availability of donor groups and the relatively small dimensions of these peptides can encourage the formation of bis-/(poly)-complexes, although they should represent only a minor species under the experimental

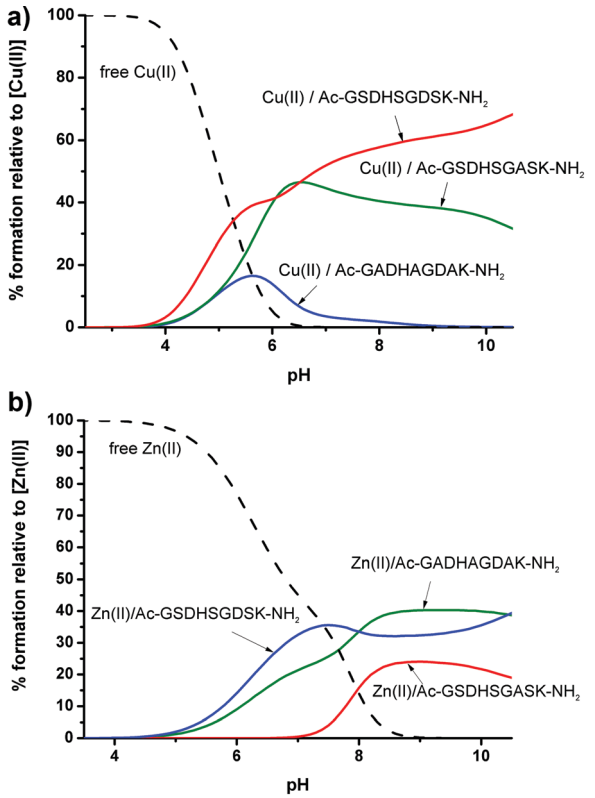

Fig. 7 Competition plots for solutions containing equimolar concentrations of M(II), **WT**, **D7A** and **S2A/S5A/S8A**. M(II) = (a) Cu(II) and (b) Zn(II).

conditions employed here (ligand and metal ion in almost equimolar concentration) and therefore not detectable. The MS spectra recorded at pH 6 confirm the presence of mononuclear complexes as major species (see Table S1, ESI†).

Comparison of complex stability

In an attempt to better understand the binding ability of the investigated ligands towards Zn(II) and Cu(II) ions, competition plots have been built up at equimolar concentrations of ligands and metal ions. The diagrams plotted in Fig. 7 compare the thermodynamic stability of **WT**, **D7A** and **S2A/S5A/S8A** peptide complexes with Cu(II) and Zn(II). The replacement of the Asp residue in position 7 seems to affect the affinity with both the metal ions. In the case of Cu(II), the absence of Asp7 makes the metal complexation only slightly less efficient under acidic pH values (Fig. 7a). It is noteworthy that at pH 6.5 the competition curves of Cu(II)-**WT** and Cu(II)-**D7A** coincide; this is in agreement with the proposed speciation models, since at that pH value, the species $[CuH_{-1}L]$ dominate in solution and have the same coordination geometry in both systems. The importance of the Asp residue in position 7 is much more evident in the case of Zn(II) (Fig. 7b), since **WT** and **S2A/S5A/S8A** show a much better binding ability throughout all the explored pH range, thus suggesting that the carboxyl group of Asp7 is of fundamental importance for the complex stability. As for the possible role of serine residues, in the case of Cu(II) (Fig. 7a), the presence of non-coordinating serines seems to have an impact on amide deprotonation, making complexes with **WT** and **D7A** more stable than the species formed by **S2A/S5A/S8A**, starting from pH 5 on, when amides come into play. On the contrary, this trend does not occur for Zn(II) complexes where amides are not involved in the coordination. This is in agreement with the above hypothesis that serines are responsible for an electronic effect that makes amide protons much more acidic.

The calculated competition diagram for the Cu(II)/**WT**/**HSGD**/**GSDH** system is shown in Fig. S27 (ESI†). The **HSGD** and **GSDH** tetra-peptides coincide with the 151–154 and 148–151 amino acid sequence of the C4YJH2 protein and are coincidentally composed by the same amino acid residues with a different order. They also correspond to the minimal coordination site for a Cu(II) ion when anchored to the His residue of the linker sequence **WT** ($C4YJH2_{148–156}$). After the histidine binding, the N-amide coordination can only proceed towards the N-terminus in the **GSDH** ligand – forming a 6-membered ring between the imidazole nitrogen and the first amide – and towards the C-terminus in the case of **HSGD** – with instead the formation of an initial 7-membered ring. These two different coordination modes are certainly in competition also in the **WT** peptide (Ac-GSDHSGDSK-NH_2). The comparison among these systems reveals that under acidic conditions the two short peptides have similar behaviour, while starting from pH 5.5 (when the amide coordination comes into play), **GSDH** complexes are by far more stable than **HSGD** species, suggesting that in **WT** the amide coordination is unbalanced in favour of the N-terminal direction. In the case of the Zn(II) ion, which is not able to deprotonate and bind amide nitrogens, the two tetra-peptides **HSGD** and **GSDH** have exactly the same behaviour all over the explored pH range (Fig. S28, ESI†). On the other hand, **WT** ligand shows a slightly higher affinity for Zn(II) under acidic and physiological pH, probably due to the presence of two Asp residues, which can both contribute to the metal coordination. At alkaline pH, the stability of **WT** complexes becomes a little lower than that of the species formed by the two short fragments, possibly only because the lower negative charge of the latter species stabilizes the hydroxo-complexes.

Conclusions

The present work represents an in-depth analysis of the thermodynamic and spectroscopic properties of Ac-GSDHSGDSK-NH_2 (**WT**) solution complex-formation equilibria. Four analogues were also taken into account, for the sake of comparison. **WT**, corresponding to the 148–156 amino acid sequence of C4YJH2, acts as a linker between the two main poly-histidine domains of the mentioned protein and proved able to coordinate both the Cu(II) and Zn(II) ions.

For all the investigated peptides (Ac-GSDHSGDSK-NH_2, Ac-GSDHSGASK-NH_2, Ac-GADHAGDAK-NH_2, Ac-GSDH-NH_2 and Ac-HSGD-NH_2) the Cu(II) coordination begins at about pH 3.5. After a first anchoring step to the histidine residue, up to three deprotonated amidic groups of the peptide backbone can bind the Cu(II) ion, occupying the equatorial position of

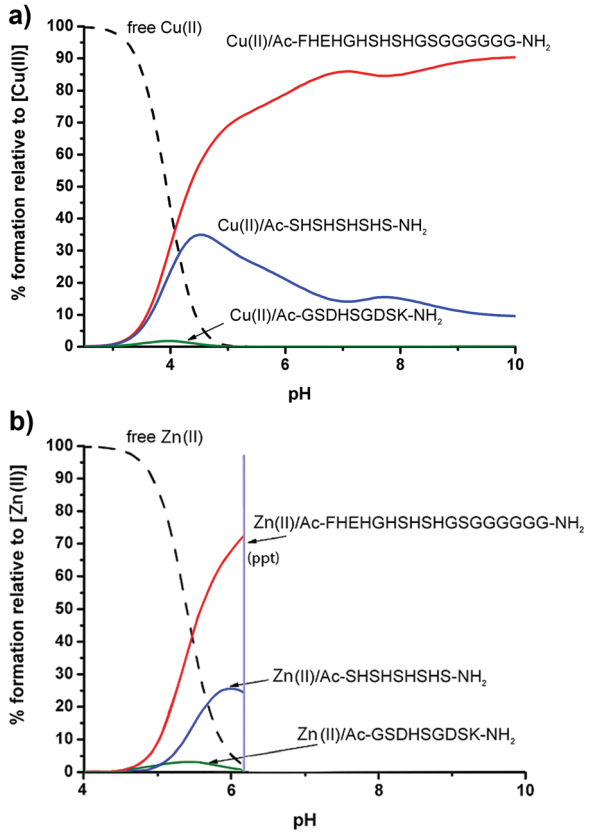

Fig. 8 Competition plots for solutions containing equimolar concentrations of M(II), Ac-FHEHGHSHSHGSGGGGGG-NH_2 (131–148), Ac-GSDHSGDSK-NH_2 (148–156) and Ac-SHSHSHSHS-NH_2 (157–165). M(II) = (a) Cu(II) and (b) Zn(II).

its coordination sphere. At physiological pH, the species ($1N_{Im}$, $2N^-$) is always the most abundant in solution. This complex is rather stable and reaches about 90% of formation with all the investigated peptides. The study of the two tetra-peptides, Ac-GSDH-NH_2 and Ac-HSGD-NH_2 allowed us to qualitatively describe the Cu(II) N-amide-coordination attitude: it can be assumed that the nona-peptide **WT** is able to form a mixture of isomeric species in which the amide coordination towards the N-terminal direction is favoured. Furthermore, the substitution of serine with alanine residues significantly lowers the peptide affinity for the Cu(II) ion, suggesting a possible role of Ser residues (quite abundant in C4YHJ2 protein sequence) in the biological task of metal uptake and regulation.

In Zn(II) complexes, the metal coordination at physiological pH occurs mainly by means of (at least) one aspartic acid moiety and the histidine residue. The Asp in position 7 is likely a crucial residue for the formation and stabilization of Zn(II) complexes, as indicated by the decrease of Zn(II) affinity for ligand Ac-GSDHSGASK-NH_2 (Fig. 7b), where the proposed metal coordination does not involve the aspartic acid.

An overall comparison of the stabilities of the studied domains of C4YJH2 is shown in Fig. 8. The calculated competition plots take into account the Cu(II) and Zn(II) binding abilities of the studied "linker" Ac-GSDHSGDSK-NH_2 (148–156) and of the two poly-His sequences Ac-FHEHGHSHSHGSGGGGGG-NH_2 (131–148) and Ac-SHSHSHSHS-NH_2 (157–165).[20] The obtained results emphasize that the ligand metal binding efficiency comes mainly from the high number of histidine residues, however highlighting a minor, but non-negligible contribution of the linker sequence in the complex formation, which, in the acidic pH range, is most likely due to the impact of the further histidine and the additional serine residues.

As for the histidine rich fragments of C4YJH2, it is possible to summarize that Zn(II) coordination mostly occurs by means of three histidine residues ($3N_{Im}$) and an oxygen atom belonging to the aspartic acid side chain (in the case of Ac-FHEHGHSHSHGSGGGGGG-NH_2) or to a water molecule (in the case of Ac-SHSHSHSHS-NH_2). Similarly, in the case of Cu(II) complexation, histidine residues promote the metal binding at acidic pH, while, moving to alkaline conditions, the amide nitrogens of the peptide backbone gradually bind copper, eventually substituting the imidazole nitrogens in the equatorial positions. No direct evidence for the preferred metal binding site of the C4YJH2 sequence is available, although the higher affinity of Ac-FHEHGHSHSHGSGGGGGG-NH_2 suggests that the distribution of mono-nuclear species is in favour of this fragment, most likely due to the availability of both a higher number of His imidazoles and the Asp carboxylic side-chain.

As a matter of fact, the presence of specific, highly conserved, histidine-rich motifs (*e.g.* HXHXH or HXXHXH) determines the metal-binding ability of the protein and then its capability to affect the host/pathogen Zn(II) homeostasis.[32–34] However, it is also clear that different coordination modes, like those found at different pH values, can definitely affect the efficacy of the protein activity in the task of metal recruitment, as previously shown in the case of calcitermin, a human antimicrobial peptide.[32] The rational understanding of such correlation is still ongoing, especially in the case of C4YJH2, the biological activity of which is still completely unknown, and the door is open to further investigations.

Experimental

Materials

$ZnCl_2$ and $CuCl_2$ were extra pure products (Sigma-Aldrich); the concentrations of their stock solutions were standardised by EDTA titration and periodically checked *via* ICP-MS. The carbonate-free stock solutions of 0.1 mol dm^{-3} KOH were prepared by diluting concentrated KOH (Sigma-Aldrich) and then potentiometrically standardized with the primary standard potassium hydrogen phthalate (99.9% purity). All sample solutions were prepared with freshly prepared Milli-Q® water. The HCl and HNO_3 stock solutions were prepared by diluting concentrated HCl and HNO_3 (Sigma-Aldrich) and then standardized with KOH. The ionic strength was adjusted to 0.1 mol dm^{-3} by adding KCl (Sigma-Aldrich). Grade A glassware was employed throughout.

Peptide synthesis and purification

Peptides: Ac-GSDHSGDSK-NH_2; Ac-GSDHSGASK-NH_2; Ac-GAD HAGDAK-NH_2; Ac-GSDH-NH_2; and Ac-HSGD-NH_2 were synthesized

according to published methods[35] using Fmoc/*t*-butyl chemistry with a Syro XP multiple peptide synthesizer (MultiSynTech GmbH, Witten, Germany). Rink amide MBHA resin was used as a solid support for the synthesis of all derivatives. Fmoc-amino acids (4-fold excess) were sequentially coupled to the growing peptide chain using DIPCDI/HOBt (*N*,*N*′-diisopropylcarbodiimide/1-hydroxybenzotriazole) (4-fold excess) as an activating mixture for 1 h at room temperature. Cycles of deprotection of Fmoc (40% piperidine/*N*,*N*-dimethylformamide) and coupling with the subsequent amino acids were repeated until the desired peptide-bound resin was completed. N-Terminal acetylation was performed with acetic anhydride (0.5 M) in the presence of *N*-methylmorpholine (0.25 M) (3 : 1 v/v; 2 mL/0.2 g of resin) as the last synthetic step. The protected peptide-resin was treated with reagent B[36] (trifluoroacetic acid (TFA)/H_2O/phenol/triisopropylsilane 88 : 5 : 5 : 2; v/v; 10 mL/0.2 g of resin) for 1.5 h at room temperature. After filtration of the resin, the solvent was concentrated *in vacuo* and the residue triturated with ethyl ether. Crude peptides were purified by preparative reversed-phase HPLC using a Water Delta Prep 3000 system with a Jupiter column C18 (250 × 30 mm, 300 A, and 15 μm spherical particle size). The column was perfused at a flow rate of 20 mL min^{-1} with a mobile phase containing solvent A (5%, v/v, acetonitrile in 0.1% TFA), and a linear gradient from 0 to 30% of solvent B (60%, v/v, acetonitrile in 0.1% TFA) over 25 min for the elution of peptides. Analytical HPLC analyses were performed on a Beckman 116 liquid chromatograph equipped with a Beckman 166 diode array detector. Analytical purity of the peptides has been assessed using a Zorbax C18 column (4.6 × 150 mm, 3 μm particle size) with the above solvent system (solvents A and B) programmed at a flow rate of 0.5 mL min^{-1} using a linear gradient from 0% to 50% B over 25 min. All analogues showed ≥95% purity when monitored at 220 nm. The molecular weight of the final compounds was determined by an ESI Micromass ZMD-2000 mass spectrometer.

Potentiometric measurements

Stability constants for proton and metal complexes were calculated from pH-metric titration curves registered at T = 298 K and ionic strength 0.1 mol dm^{-3} (KCl). The potentiometric apparatus consisted of an Orion EA 940 pH-meter system provided with a Metrohm 6.0234.100, glass-body, micro combination pH electrode and a Hamilton MICROLAB 500 dosing system, equipped with a 0.5 mL micro burette. The thermostated glass-cell was equipped with a magnetic stirring system, a microburet delivery tube and an inlet–outlet tube for nitrogen. High purity grade nitrogen gas was gently blown over the test solution in order to maintain an inert atmosphere. Constant-speed magnetic stirring was applied throughout. Solutions were titrated with 0.1 mol dm^{-3} carbonate-free KOH. The electrode was daily calibrated for hydrogen ion concentration by titrating HNO_3 with alkaline solution under the same experimental conditions as above. The standard potential and the slope of the electrode couple were computed by means of the SUPERQUAD[37] and Glee[38] programs. The purities and the exact concentrations of the ligand solutions were determined by the Gran method.[39] The HYPERQUAD[40] program was employed for the overall formation constant (β) calculations, referring to the following equilibrium:

$$pM + qL + rH \leftrightarrows M_pL_qH_r$$

(charges omitted; p is 0 in the case of ligand protonation; r can be negative). Step formation constants (K_{step}) and/or acid dissociation constants (K_a) are also reported. The computed standard deviations (referring to random errors only) were given by the program itself and are shown in parentheses as uncertainties on the last significant figure. Hydrolysis constants for Zn(II) and Cu(II) ions were taken from the literature (Table S7, ESI†).[22,41] The distribution and the competition diagrams were computed using the HYSS program.[42] In fact, the overall metal binding ability of the different ligands can be compared in a wide pH range by computing the competition diagrams, starting from the binary speciation models. A solution containing the metal and the two (or more) ligands (or *vice versa*) is simulated, admitting that all the components compete with each other to form the respective binary complexes, without mixed species formation. This is a reasonable approximation in the case of peptides, which most often form only 1 : 1 complexes in which the peptide completely wraps the metal ion.

Mass spectrometric measurements

High-resolution mass spectra were obtained on a BrukerQ-FTMS spectrometer (Bruker Daltonik, Bremen, Germany), equipped with an Apollo II electrospray ionization source with an ion funnel. The mass spectrometer was operated in the positive and negative ion modes. The instrumental parameters were as follows: scan range m/z 300–4000, dry gas-nitrogen, temperature 453 K and ion energy 5 eV. The capillary voltage was optimized to the highest S/N ratio and it was 4500 V. The small changes in voltage (±500 V) did not significantly affect the optimized spectra. The samples were prepared in a 1 : 1 methanol–water mixture at different pH values. The samples (Zn(II) : ligand and Cu(II) : ligand in a 0.8 : 1 stoichiometry, $[ligand]_{tot} = 5 \times 10^{-4}$ mol dm^{-3}) were infused at a flow rate of 3 μL min^{-1}. The instrument was calibrated externally with a Tunemix™ mixture (Bruker Daltonik, Germany) in a quadratic regression mode. Data were processed using the Bruker Compass DataAnalysis 4.2 program. The mass accuracy for the calibration was better than 5 ppm, enabling, together with the true isotopic pattern (using SigmaFit), an unambiguous confirmation of the elemental composition of the obtained complex.

Spectroscopic measurements

The absorption spectra were recorded on a Varian Cary50 Probe spectrophotometer, in the range 350–900 nm, using a quartz cuvette with an optical path of 1 cm. Circular dichroism (CD) spectra were recorded on a Jasco J-1500 CD spectrometer in the 200–800 nm range, using a quartz cuvette with an optical path of 1 cm in the visible and near-UV range. Electron paramagnetic resonance (EPR) spectra were recorded in liquid nitrogen on a Bruker ELEXSYS E500 CW-EPR spectrometer at X-band frequency (9.5 GHz) and equipped with an ER 036TM NMR teslameter and

an E41 FC frequency counter. Ethylene glycol (30%) was used as a cryoprotectant for EPR measurements. The EPR parameters were analysed by computer simulation of the experimental spectra using the WIN-EPR SIMFONIA software, version 1.2 (Bruker). The concentrations of sample solutions used for spectroscopic studies were similar to those employed in the potentiometric experiment. The UV-vis, CD and EPR spectroscopic parameters were calculated from the spectra obtained at the pH values corresponding to the maximum concentration of each particular species, based on distribution diagrams.

NMR measurements

NMR spectra were recorded at 14.1 T on a Bruker Avance III 600 MHz system equipped with a Silicon Graphics workstation. The temperatures were controlled with an accuracy of ±0.1 K. Suppression of the residual water signal was achieved by excitation sculpting, using a selective square pulse 2 ms long on water. All the samples were prepared in D_2O (99.9% from Merck) solution. Proton resonance assignment was accomplished by 2D ^1H–^1H total correlation spectroscopy (TOCSY) experiments carried out with standard pulse sequences. Samples of analysed complexes (Zn(II) : ligand in a 1 : 1 stoichiometry, $[ligand]_{tot}$ = 0.003 mol dm^{-3}) were prepared by adding metal ions to the acidic solution of a ligand (pH 3), and the pH was then increased to a higher value (pH 7.4). Spectral processing and analysis was performed using Bruker TOPSPIN 2.1 and Sparky.[43]

Complex structure drawings

The pictures of the complex structural hypotheses have been drawn with ACD/ChemSketch and the 3D structure visualisation was obtained with Mercury (The Cambridge Crystallographic Data Centre, CCDC).

Author contributions

D. Bellotti carried out potentiometric, CD, EPR, ESI-MS and NMR measurements on Zn(II) and Cu(II) systems. C. Tocchio carried out potentiometric and UV-Vis measurements on Cu(II) systems. R. Guerrini performed peptide synthesis and purification. M. Remelli and M. Rowińska-Żyrek designed and coordinated the experiments. D. B., M. R. and M. R.-Z. contributed to the data interpretation. All the authors contributed equally to the writing of the paper.

Conflicts of interest

There are no conflicts to declare.

Acknowledgements

The present research was financially supported by the National Science Centre (UMO-2017/26/A/ST5/00364, SONATA BIS grant to MR-Z), University of Ferrara (FAR 2018), CIRCMSB (Consorzio Interuniversitario di Ricerca in Chimica dei Metalli nei Sistemi Biologici, Bari, Italy), MIUR (Ministero dell'Istruzione, dell'Università e della Ricerca) projects (PRIN2015-2015MP34H3 and PRIN2015-2015T778JW) and Erasmus+ programme of the European Union. The CD measurements were carried out with the equipment purchased thanks to the financial support of the Polish National Science Centre (Grant UMO 2015/19/B/ST5/00413).

Notes and references

1 T. Kourkoumpetis, D. Manolakaki, G. C. Velmahos, Y. C. Chang, H. B. Alam, M. M. De Moya, E. A. Sailhamer and E. Mylonakis, *Virulence*, 2010, **1**, 359.
2 S. Campoy and J. L. Adrio, *Biochem. Pharmacol.*, 2017, **133**, 86.
3 A. L. Mavor, S. Thewes and B. Hube, *Curr. Drug Targets*, 2005, **6**, 863.
4 T. J. Walsh, *Expert Rev. Anti-Infect. Ther.*, 2017, **15**, 577.
5 A. Pitarch, C. Nombela and C. Gil, *Curr. Top. Med. Chem.*, 2018, **18**, 1375.
6 V. Srivastava, R. K. Singla and A. K. Dubey, *Curr. Top. Med. Chem.*, 2018, **18**, 759.
7 M. A. Pfaller and D. J. Diekema, *Clin. Microbiol. Rev.*, 2007, **20**, 133.
8 P. Chandrangsu, C. Rensing and J. D. Helmann, *Nat. Rev. Microbiol.*, 2017, **15**, 338.
9 M. I. Hood and E. P. Skaar, *Nat. Rev. Microbiol.*, 2012, **10**, 525.
10 M. Blatzer and J.-P. Latgé, *Curr. Opin. Microbiol.*, 2017, **40**, 152.
11 E. R. Ballou and D. Wilson, *Curr. Opin. Microbiol.*, 2016, **32**, 128.
12 K. W. Paulina, W. Joanna and R.-Z. Magdalena, *Curr. Med. Chem.*, 2016, **23**, 3717.
13 I. Bremner and P. M. May, in *Zinc in Human Biology*, ed. C. F. Mills, Springer London, London, 1989, p. 95.
14 T. Yi-Hsuan, H. Adela Ya-Ting, C. Po-Yu, C. Hui-Ting and K. Chai-Lin, *Curr. Pharm. Des.*, 2011, **17**, 2308.
15 F. Citiulo, I. D. Jacobsen, P. Miramón, L. Schild, S. Brunke, P. Zipfel, M. Brock, B. Hube and D. Wilson, *PLoS Pathog.*, 2012, **8**, e1002777.
16 G. Butler, M. D. Rasmussen, M. F. Lin, M. A. S. Santos, S. Sakthikumar, C. A. Munro, E. Rheinbay, M. Grabherr, A. Forche, J. L. Reedy, I. Agrafioti, M. B. Arnaud, S. Bates, A. J. P. Brown, S. Brunke, M. C. Costanzo, D. A. Fitzpatrick, P. W. J. de Groot, D. Harris, L. L. Hoyer, B. Hube, F. M. Klis, C. Kodira, N. Lennard, M. E. Logue, R. Martin, A. M. Neiman, E. Nikolaou, M. A. Quail, J. Quinn, M. C. Santos, F. F. Schmitzberger, G. Sherlock, P. Shah, K. A. T. Silverstein, M. S. Skrzypek, D. Soll, R. Staggs, I. Stansfield, M. P. H. Stumpf, P. E. Sudbery, T. Srikantha, Q. Zeng, J. Berman, M. Berriman, J. Heitman, N. A. R. Gow, M. C. Lorenz, B. W. Birren, M. Kellis and C. A. Cuomo, *Nature*, 2009, **459**, 657.
17 A. N. Besold, B. A. Gilston, J. N. Radin, C. Ramsoomair, E. M. Culbertson, C. X. Li, B. P. Cormack, W. J. Chazin, T. E. Kehl-Fie and V. C. Culotta, *Infect. Immun.*, 2018, **86**, e00779.

18 T. UniProt Consortium, *Nucleic Acids Res.*, 2018, **46**, 2699.
19 G. Binkley, J. Binkley, M. S. Skrzypek, M. Simison, S. R. Miyasato and G. Sherlock, *Nucleic Acids Res.*, 2016, **45**, D592.
20 D. Bellotti, D. Łoboda, M. Rowińska-Żyrek and M. Remelli, *New J. Chem.*, 2018, **42**, 8123.
21 H. Sigel and R. B. Martin, *Chem. Rev.*, 1982, **82**, 385.
22 L. D. Pettit and H. K. J. Powell, *The IUPAC Stability Constants Database*, Royal Society of Chemistry, London, 1992–2000.
23 R. J. Sundberg and R. B. Martin, *Chem. Rev.*, 1974, **74**, 471.
24 R. Hennig, A. Veser, S. Kirchhof and A. Goepferich, *Mol. Pharmaceutics*, 2015, **12**, 3292.
25 J. Peisach and W. E. Blumberg, *Arch. Biochem. Biophys.*, 1974, **165**, 691.
26 L. D. Pettit, S. Pyburn, W. Bal, H. Kozlowski and M. Bataille, *J. Chem. Soc., Dalton Trans.*, 1990, 3565.
27 A. R. Borges and C. L. Schengrund, *Curr. Drug Targets: Infect. Disord.*, 2005, **5**, 247.
28 M. Remelli, M. Peana, S. Medici, L. G. Delogu and M. A. Zoroddu, *Dalton Trans.*, 2013, **42**, 5964.
29 S. Medici, M. Peana, L. G. Delogu and M. A. Zoroddu, *Dalton Trans.*, 2012, **41**, 4378.
30 M. A. Zoroddu, S. Medici, M. Peana and R. Anedda, *Dalton Trans.*, 2010, **39**, 1282.
31 A. Urbani, R. Bazzo, M. C. Nardi, D. O. Cicero, R. De Francesco, C. Steinkuhler and G. Barbato, *J. Biol. Chem.*, 1998, **273**, 18760.
32 D. Bellotti, M. Toniolo, D. Dudek, A. Mikołajczyk, R. Guerrini, A. Matera-Witkiewicz, M. Remelli and M. Rowińska-Żyrek, *Dalton Trans.*, 2019, **48**, 13740.
33 D. Łoboda and M. Rowińska-Żyrek, *Dalton Trans.*, 2017, **46**, 13695.
34 A. Miller, D. Dudek, S. Potocki, H. Czapor-Irzabek, H. Kozłowski and M. Rowińska-Żyrek, *Metallomics*, 2018, **10**, 1631.
35 N. L. Benoiton, *Chemistry of Peptide Synthesis*, Taylor & Francis, 2005.
36 N. A. Sole and G. Barany, *J. Org. Chem.*, 1992, **57**, 5399.
37 P. Gans, A. Sabatini and A. Vacca, *J. Chem. Soc., Dalton Trans.*, 1985, 1195.
38 P. Gans and B. O'Sullivan, *Talanta*, 2000, **51**, 33.
39 G. Gran, *Acta Chem. Scand.*, 1950, **4**, 559.
40 P. Gans, A. Sabatini and A. Vacca, *Talanta*, 1996, **43**, 1739.
41 G. Arena, R. Cali, E. Rizzarelli and S. Sammartano, *Thermochim. Acta*, 1976, **16**, 315.
42 L. Alderighi, P. Gans, A. Ienco, D. Peters, A. Sabatini and A. Vacca, *Coord. Chem. Rev.*, 1999, **184**, 311.
43 W. Lee, M. Tonelli and J. L. Markley, *Bioinformatics*, 2015, **31**, 1325.

Dalton Transactions

PAPER

View Article Online
View Journal | View Issue

Check for updates

Cite this: *Dalton Trans.*, 2019, **48**, 13740

Bioinorganic chemistry of calcitermin – the picklock of its antimicrobial activity†

Denise Bellotti,[a,b] Mattia Toniolo,[a] Dorota Dudek,[b] Aleksandra Mikołajczyk,[c] Remo Guerrini,[a] Agnieszka Matera-Witkiewicz,[c] Maurizio Remelli *[a] and Magdalena Rowińska-Żyrek *[b]

Received 10th July 2019,
Accepted 26th August 2019

DOI: 10.1039/c9dt02869b

rsc.li/dalton

Calcitermin, an antimicrobial peptide from the fluid of the human airways, is a well-conserved, 15 amino acid C-terminal cleavage fragment of calgranulin C (VAIALKAAHYHTHKE), which is active under acidic pH conditions (pH 5.4). In an attempt to understand the impact of the coordination of Zn(II) and Cu(II) on the biological activity of calcitermin, we mutated each of the histidines with an alanine and studied the thermodynamics, binding mode and antimicrobial activity of wild type calcitermin and its H9A, H11A and H13A mutants and their Zn(II) and Cu(II) complexes. Both metals strongly enhance the antimicrobial activity of calcitermin-like peptides, although the link between the minimal inhibitory concentration (MIC) values and the stability, charge or structure of the complexes is not so obvious. As expected, the increase in the number of histidines makes the coordination of both metals more effective. There is no preferred Cu(II) binding site in calcitermin: the stabilities of the Cu(II)–H9A and Cu(II)–H13A complexes are almost identical, while the Cu(II)–H11A complex (in which two histidines are separated by three amino acids and only one His residue is involved in binding) is less stable. On the other hand, the higher stability of the Zn(II)–H13A complex with respect to those formed by H9A and H11A suggests a pivotal role of His9 and His11 in Zn(II) complexation. Impressive MIC breakpoints were obtained, similar and lower than those for commonly used antimicrobial agents that treat *Candida albicans* (Zn(II) and Cu(II) complexes of WT calcitermin and H9A, as well as H9A alone), Enterococcus faecalis (H11A, H13A and their metal complexes) and *Staphylococcus aureus* (H13A and its complexes).

Introduction

Antimicrobial peptides (AMPs, also known as host defence peptides), are small, polycationic peptides that form part of the innate immune response shared by all classes of life. Different AMPs are active against fungi, bacteria, viruses, protozoa, and even cancer cells.[1] There are numerous ways in which AMPs might interact with pathogens, such as membrane disruption, production of reactive oxygen species, inhibition of cell wall, nucleic acid and protein synthesis, or by the involvement of essential metal ions.[1,2] Presumably, bacteria have been exposed to AMPs for millions of years and, with the exception of a few species,[3] widespread resistance has not been reported, making them a potential 'treasure trove' of starting points for rational, focused antimicrobial drug design.[4,5]

Calcitermin is one of the antimicrobial peptides found in the fluid of the human airways. It is a 15 amino acid C-terminal cleavage fragment of calgranulin C, a member of the S100 family of antibacterial proteins, produced by neutrophils, monocytes and keratinocytes.[6] Calcitermin is only active under acidic pH conditions (pH 5.4), which are often present during inflammation; no antimicrobial activity was detected at pH 7.4.[7] What is of particular interest for this work, calcitermin antimicrobial activity is enhanced in the presence of Zn(II) ions.[7] How does Zn(II) coordination contribute to the biological activity? Could the same enhancement be achieved in the presence of Cu(II)? In general, metal ions have a dual effect on the activity of antimicrobial peptides: (i) AMPs bind them, so that microbes cannot get enough metals essential for their life and virulence and/or (ii) AMPs need the given metal ion as a booster of their antimicrobial activity, affecting the charge and/or structure of the peptide.[8] Therefore, it is reasonable to hypothesize that calcitermin mode of action may be connected

[a]*Department of Chemical and Pharmaceutical Sciences, University of Ferrara, Luigi Borsari 46, 44121 Ferrara, Italy. E-mail: rmm@unife.it*
[b]*Faculty of Chemistry, University of Wrocław, F. Joliot-Curie 14, 50-383 Wrocław, Poland*
[c]*Screening Laboratory of Biological Activity Test and Collection of Biological Material, Faculty of Pharmacy with Division of Laboratory Diagnostics, Wrocław Medical University, Borowska 211A, 50-556 Wrocław, Poland*
†Electronic supplementary information (ESI) available. See DOI: 10.1039/c9dt02869b

with (i) the increase of the positive charge (coming from the protonation of its residues and from the metal ion itself) that may facilitate interaction with the negatively charged groups on the bacterial and fungal surfaces and/or (ii) with metal-induced structural stabilization.[7] In an attempt to understand the impact of Zn(II) and Cu(II) on calcitermin antimicrobial activity, we described the bioinorganic chemistry and the antimicrobial potential of Cu(II) and Zn(II) complexes with calcitermin and its three His-to-Ala mutants, in which each histidine residue is replaced with one alanine (wild type calcitermin, WT = VAIALKAAHYHTHKE; H9A = VAIALKAAAYHTHKE; H11A = VAIALKAAHYATHKE; H13A = VAIALKAAHYHTAKE). Complexes were characterized by mass spectrometry, potentiometry, UV-Vis spectrophotometry, circular dichroism (CD) and nuclear magnetic resonance (NMR). Antimicrobial activity assays of ligand/complex system were also performed.

Results and discussion

Ligand protonation

All investigated peptides are unprotected fragments and thus their acid–base behaviour not only depends on the amino acids side chains properties, but also on their amino and carboxyl termini. The amide groups of the peptide backbone cannot spontaneously release their protons in the pH range explored by potentiometry, since they are very weak acids ($pK_a \approx 15$);[9] however, these protons can be displaced by Cu(II) at a suitable pH value, to form complexes. The distribution diagrams for protonation equilibria of wild type calcitermin and its mutants are shown in Fig. S1–S4 (ESI†) and the corresponding constants are reported in Table 1. Wild type calcitermin (WT = VAIALKAAHYHTHKE) contains nine groups involved in acid–base reactions: two lysines (K), one tyrosine (Y), the amino-terminus, three histidines (H), one glutamic acid side chain (E) and the carboxylic-terminus. The three peptide mutants H9A (VAIALKAAAYHTHKE), H11A (VAIALKAAHYATHKE), H13A (VAIALKAAHYHTAKE) lack one His residue, which has been substituted by an alanine in position 9, 11 and 13, respectively. All of them, once completely deprotonated, bear a triple negative charge (L^{3-}). The obtained protonation constants are in good agreement with literature values for similar systems[10] and show reasonable similarities among the considered peptides. Lysines are the most basic residues; although their $\log K$ values are rather high, they could be measured under the considered experimental conditions (pH range 2.5–10.5). $\log K$ value of tyrosine falls in the range 9.37–9.65, among the studied peptides; this interval is rather small, suggesting the lack of a specific behaviour depending on the ligand sequence. Neither the presence or absence of one histidine residue nearby the tyrosine significantly affects its protonation constant. Analogously, the obtained protonation constants for the amino-terminus are quite close to each other (8.70, 8.57, 8.38, 8.61). Histidine residues are characterized by $\log K$ values ranging from 6.11 to 7.30: the acidity of imidazole groups increases with the positive charge of the peptide, as expected. Finally, the lowest $\log K$ values can be attributed to the carboxylic groups of the Glu residue (rather high for a carboxylate, but already reported in the literature,[11] and comparable in all mutants: 5.33, 5.59, 5.49, 5.36) and of the C-terminus (3.89, 4.11, 3.93, 3.80).

Cu(II) complexes

Calcitermin (WT) and its mutants H9A, H11A and H13A are able to form 1 : 1 complexes with the Cu(II) ion; no polynuclear or bis-complexes have been detected by potentiometry or mass spectrometry under the experimental conditions here employed. No precipitation has been observed over the explored pH range. Overall complex-formation constants ($\log \beta$) and corresponding acidity constants (pK_a) are reported in Tables 2, S1–S3 (ESI†), along with the spectroscopic results. The corresponding distribution diagrams are plotted in Fig. 1 and S5–S7 (ESI†). ESI-MS results are shown in Table S4 (ESI†): the prevailing signals correspond to equimolar Cu(II) complexes. UV-Vis and CD spectra are reported in Fig. 2, 3 and S8–S13 (ESI†).

The Cu(II) coordination to WT calcitermin starts at about pH 3. The first detected complex is $[CuH_7L]^{6+}$; the stoichiometry of this species indicates that two acid–base sites are already deprotonated. Besides the terminal carboxyl group, it is reasonable to claim that the first metal anchor site is one His residue. In addition, NMR spectra (Fig. S14 ESI†) suggest

Table 1 Overall ($\log \beta$) and step ($\log K$) protonation constants for calcitermin, H9A, H11A and H13A at T = 298 K and I = 0.1 mol dm^{-3} ($NaClO_4$). Values in parentheses are standard deviations on the last significant figure

	WT			H9A			H11A			H13A		
Species	$\log \beta$	$\log K$		$\log \beta$	$\log K$		$\log \beta$	$\log K$		$\log \beta$	$\log K$	
HL^{2-}	10.3 (1)	10.3	Lys	10.22 (7)	10.22	Lys	10.14 (9)	10.14	Lys	10.27 (5)	10.27	Lys
H_2L^{-}	20.13 (6)	9.83	Lys	20.26 (3)	10.04	Lys	20.03 (4)	9.89	Lys	20.15 (2)	9.88	Lys
H_3L	29.78 (6)	9.65	Tyr	29.77 (4)	9.51	Tyr	29.41 (5)	9.38	Tyr	29.52 (3)	9.37	Tyr
H_4L^{+}	38.50 (5)	8.70	NH_2	38.34 (4)	8.57	NH_2	37.79 (4)	8.38	NH_2	38.13 (2)	8.61	NH_2
H_5L^{2+}	45.80 (7)	7.30	His	45.44 (5)	7.10	His	44.88 (6)	7.09	His	45.25 (3)	7.13	His
H_6L^{3+}	52.43 (6)	6.62	His	52.00 (5)	6.56	His	51.42 (5)	6.54	His	51.69 (3)	6.43	His
H_7L^{4+}	58.54 (6)	6.11	His	57.59 (5)	5.59	Glu	56.91 (6)	5.49	Glu	57.05 (3)	5.36	Glu
H_8L^{5+}	63.89 (6)	5.33	Glu	61.71 (5)	4.11	COO^{-}	60.83 (6)	3.93	COO^{-}	60.85 (3)	3.80	COO^{-}
H_9L^{6+}	67.78 (7)	3.89	COO^{-}	—	—		—	—		—	—	

Table 2 Potentiometric and spectroscopic data for Cu(II) complexes with ligand calcitermin (VAIALKAAHYHTHKE), T = 298 K, I = 0.1 mol dm^{-3} ($NaClO_4$) and M : L molar ratio = 0.9 : 1. Values in parentheses are standard deviations on the last significant figure

			UV-Vis		CD		
Species	log β	pK_a	λ_{max} (nm)	$\Delta\varepsilon$ (M^{-1} cm^{-1})	λ (nm)	$\Delta\varepsilon$ (M^{-1} cm^{-1})	pH
$[CuH_7L]^{6+}$	62.6 (1)	3.9	800		233	−1.6	3.0
$[CuH_6L]^{5+}$	58.69 (3)	4.90	800		233	−1.6	4.0
$[CuH_5L]^{4+}$	53.79 (3)	5.94	650	63	235	−2.0	5.1
$[CuH_4L]^{3+}$	47.85 (3)	6.95	612	87	340	−0.22	6.3
					283	0.39	
					235	−2.03	
$[CuH_3L]^{2+}$	40.90 (4)	7.40	570	108	640	0.34	7.2
					550	−0.25	
					340	−0.88	
					257	2.10	
					235	−1.77	
$[CuH_2L]^{+}$	33.50 (4)	8.88	540	120	640	0.46	7.9
					550	−0.35	
					340	−1.19	
					255	3.31	
					235	−1.48	
[CuHL]	24.62 (5)	9.74	540	120	640	0.46	9.1
					550	−0.35	
					340	−1.24	
					253	4.02	
					235	−1.11	
$[CuL]^{-}$	14.88 (5)	10.16	525	125	640	0.46	10.0
					541	−0.40	
					340	−1.15	
					249	5.38	
$[CuH_{-1}L]^{2-}$	4.72 (5)		520	140	640	0.46	11.0
					525	−0.58	
					340	−0.56	
					250	6.90	
$[CuH_{-3}L]^{4-}$	−16.71 (8)		520	140	340	−0.22	11.0
					283	0.39	
					235	−2.03	

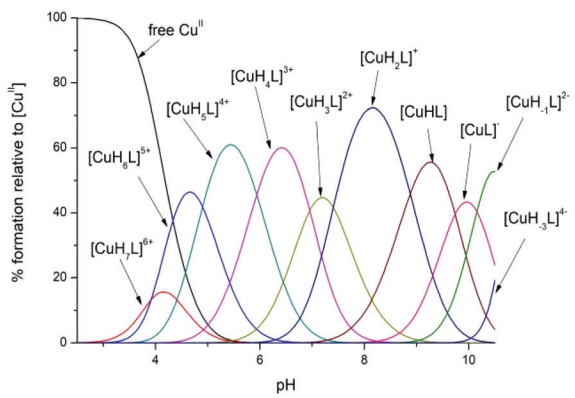

Fig. 1 Exemplificative species distribution diagram relative to Cu(II)/WT complexes; M : L molar ratio = 0.9 : 1.

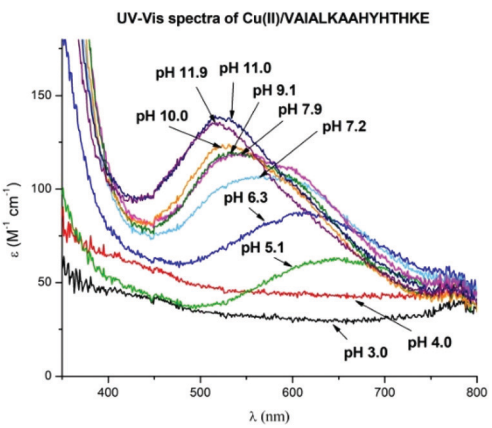

Fig. 2 Vis absorption spectra [350–800 nm; optical path 1 cm] for Cu(II) complexes with WT; M : L ratio = 0.9 : 1.

that the carboxylic groups are not involved in Cu(II) complexation. With the increase of pH value two subsequent deprotonation steps occur with pK_a values of 3.9 and 4.90, respectively, most likely corresponding to the deprotonation and coordination of the other two histidine residues to form the ($2N_{Im}$) complex $[CuH_6L]^{5+}$ and the ($3N_{Im}$) species $[CuH_5L]^{4+}$. In fact, in the acidic pH range (4.5–5.5), the second and third His residues of WT calcitermin can be deprotonated only if they are bound to the metal ion. It is not possible to exactly determine the wavelength of maximum absorption of $[CuH_7L]^{6+}$ and $[CuH_6L]^{5+}$, because of interference of the solvated Cu(II) ion, always present in solution until pH 5.5. Starting from pH 6, the $[CuH_4L]^{3+}$ species is the most abundant in solution. It

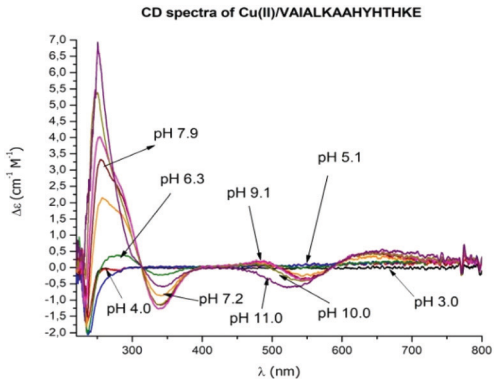

Fig. 3 CD spectra [220–800 nm; optical path 1 cm] for Cu(II) complexes with WT; M : L ratio = 0.9 : 1.

derives from the $[CuH_5L]^{4+}$ complex which releases a proton with a pK_a value of 5.94, compatible with the hypothesis of the deprotonation of the Glu residue, without any relevant change in the complex geometry. Spectroscopic data (Table 2) are in good agreement with the thermodynamic results. With the increase of pH, a blue-shift of Vis spectra is observed (Fig. 2), suggesting the increase of the number of coordinated nitrogen atoms: the wavelength of maximum absorption shifts to 612 nm at pH 6.3, where the $[CuH_4L]^{3+}$ complex reaches almost 60% of formation, supporting the hypothesis of a ($3N_{Im}$) coordination.[9] The ($3N_{im}$) coordination mode is also confirmed by NMR spectra where we can observe broadening of all His H_δ–H_ε correlations (Fig. S14 ESI†). Starting from pH 5.5, the complex releases a further proton with a pK_a = 6.95 to form the $[CuH_3L]^{2+}$ species. This pK_a value is attributable to the deprotonation and binding of the terminal amino group to form a ($3N_{Im}$, NH_2) complex (see Fig. 4A). This pK_a, in fact, is significantly lower than the deprotonation constant of the N-terminus in the free WT ligand (pK_a = 8.70) (Table 1). The coordination of the N-terminal amino group is suggested by a significant shift of the H_α–H_β correlations of Val1 in NMR spectra (Fig. S14 ESI†). The Vis spectrum recorded at pH 7 (Fig. 2) shows a quite broadened absorption band, likely due to the presence of different species in solution ($[CuH_4L]^{3+}$, $[CuH_3L]^{2+}$ and $[CuH_2L]^{+}$).

The measured λ_{max} is in the range 570–560 nm, which is consistent with the hypothesis of a ($3N_{Im}$, NH_2) coordination mode (568 nm)[9] for $[CuH_3L]^{2+}$. At physiological pH, the amount of this species present in solution is comparable with the amount of the $[CuH_2L]^{+}$ complex. It can be suggested that, to form $[CuH_2L]^{+}$, one amide proton is displaced by the Cu(II) ion (pK_a = 7.40) and that the corresponding amide nitrogen substitutes a donor group already bound in the equatorial plane. Indeed, a significant change in the visible CD spectra could be detected at pH > 7.2 (Fig. 3), thus suggesting a remarkable variation in the coordination mode, attributable to the involvement of a backbone amide.[12] Furthermore, at pH 7.9, where the $[CuH_2L]^{+}$ species is the most abundant complex in solution, the d–d band of the Vis spectra is located at

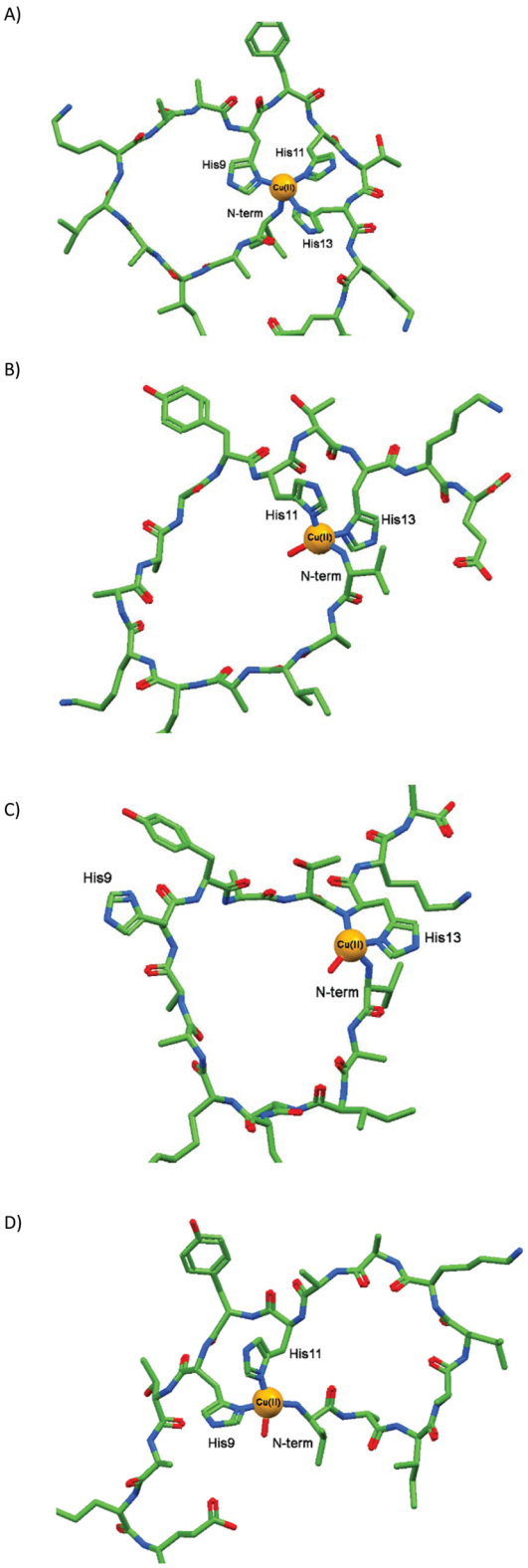

Fig. 4 Proposed coordination sphere of Cu(II) complexes with (A) wild-type calcitermin, (B) H9A mutant of calcitermin, (C) H11A mutant of calcitermin, (D) H13A mutant of calcitermin, at physiological pH.

540 nm and this is compatible with the hypothesis of a ($2N_{Im}$, $1NH_2$, $1N^-$) complex (549 nm).[9] The formation of the next species [CuHL], detected at higher pH (pK_a = 8.88), is consistent with the coordination of a further amide nitrogen, suggesting a ($2N_{Im}$, $2N^-$) coordination mode; the wavelength of maximum absorption predicted for this type of coordination is 539 nm.[9] The Vis absorption spectrum at pH 9.1 overlaps with the one recorded at pH 7.9 (Fig. 2), both characterized by a λ_{max} = 540 nm, in agreement with the two proposed Cu(II) configurations for the $[CuH_2L]^+$ and [CuHL] species. The seventh detected complex ($[CuL]^-$) derives from the release of the tyrosine proton (pK_a = 9.74) without any interaction with the metal ion. At pH higher than 9, the $[CuH_{-1}L]^{2-}$ species is formed: the corresponding deprotonation step (pK_a = 10.16) can be attributed to the binding of a third amide nitrogen in the main coordination plane, resulting in a ($1N_{Im}$, $3N^-$) coordination mode (predicted λ_{max} = 522 nm).[9] A square-planar complex geometry is conceivable, as indicated by the CD bands in the visible region (Fig. 3). Finally, at pH higher than 10, two further deprotonation steps occur, giving rise to the $[CuH_{-3}L]^{4-}$ species, no changes in the Vis absorption and CD spectra are observed suggesting that the two Lys residues spontaneously deprotonate without being involved in complexation.

The coordination behaviour of the Cu(II)/H9A mutant system is very similar to that of the wild-type calcitermin. The formation of the first detected species, $[CuH_6L]^{5+}$, is associated with the coordination of the first histidine, while the C-terminal carboxyl group is already deprotonated. The first deprotonation step (pK_a = 4.51) likely corresponds to the displacement of the acidic proton from the second histidine to obtain a 2N coordination mode (expected λ_{max} = 687 nm, measured λ_{max} = 670 nm at pH = 5.0). At higher pH, the glutamic acid deprotonates without being involved in Cu(II) coordination (pK_a = 5.66). At physiological pH, the $[CuH_3L]^{2+}$ species reaches its maximum of formation (40%) and the corresponding protonation constant of 7.25 suggests that the Cu(II) ion binds the N-terminal amine to obtain an equatorial configuration ($2N_{Im}$, NH_2) (Fig. 4B); the corresponding value of λ_{max} is 613 nm, measured at pH 7.0 (expected λ_{max} = 617 nm). The coordination mode at physiological pH is also confirmed by NMR spectra, where distinct changes are observed after the addition of Cu(II): (i) broadening of both the signals assigned to His H_δ–H_ε correlations, confirming their participation in coordination (Fig. S15A ESI†), and (ii) the shift of valine H_α–H_γ and H_β–H_γ correlations (Fig. S15B ESI†), which is most probably related to N-terminal amine involvement in complexation. No changes in correlation signals assigned to glutamic acid are observed. The release of a further proton with a pK_a = 7.62 gives rise to the $[CuH_2L]^+$ species, where the most probable deprotonated site is one N-amide, as suggested by the remarkable change in the visible portion of CD spectra at pH > 8. Under the most alkaline conditions, up to three deprotonated amides of peptide backbone can gradually substitute imidazole nitrogens in the metal coordination sphere. At the most alkaline pH values the recorded d–d bands show a λ_{max} of about 515 nm, slightly lower than the one obtained for the Cu(II)/WT system and exactly the expected value for a (NH_2, $3N^-$) coordination mode.[9]

As for Cu(II) complexes with H11A mutant, in the first detected species ($[CuH_6L]^{5+}$), the Cu(II) ion is most likely anchored to a His residue. The following complex, $[CuH_5L]^{4+}$, is obtained with a pK_a = 5.35 which suggests the deprotonation of the glutamic acid, without any change in Cu(II) coordination. In NMR spectra, the addition of Cu(II) to the peptide solution does not trigger any significant change of glutamic acid signals (Fig. S16B ESI†), further confirming that this residue is not involved in binding. The formation of the third detected species, $[CuH_4L]^{3+}$, is characterized by a pK_a value of 6.55; this is the most abundant species in the pH range 6.5–7.5. In the visible portion of the CD spectra in the pH range 6–8, the onset of an intense negative band at 650 nm can be observed, only in this Cu(II)/H11A system (Fig. S12 ESI†). This is a clue that an amide nitrogen is already involved in coordination, as confirmed by the CD band at 316 nm. Since the amides are closer to the chiral centers of the peptide than the imidazole side chains, it is expected that their involvement in Cu(II) coordination gives rise to more intense CD signals. Therefore, the binding of a backbone-amide nitrogen leads to the formation of a (N_{Im}, N^-) complex (expected λ_{max} = 660 nm). It is worth of note that H11A is the only peptide of the series where the two histidines of the sequence are separated by 3 residues; evidently, this His disposition favours the amide ionization rather than the coordination of the second imidazole ring, as confirmed by NMR spectra. Apart from the N-terminal Val1 signals, only the His13 H_δ–H_ε correlations broaden after the metal ion addition (Fig. S16A ESI†), while the His9 aromatic signals do not undergo any significant change, which points out the involvement of only the His13 in Cu(II) binding (Fig. 4C). At pH higher than 9, significant changes in UV-Vis and CD spectra support the hypothesis of further important variations in the coordination mode, suggesting that up to three deprotonated amides of the peptide backbone can gradually be involved in the metal coordination sphere. As in the case of H9A, the obtained wavelength of maximum absorption at pH > 10 (λ_{max} = 513 nm) suggest a (NH_2, $3N^-$) configuration for Cu(II) complexes at the most alkaline conditions.

A substantial difference in coordination modes at the most acidic pH values can be hypothesized for Cu(II) complexes with the H13A mutant, where the His residue in position 13 is substituted by an alanine. Cu(II) starts to interact with the ligand at pH around 3.5 and the first detected complex is $[CuH_5L]^{4+}$, in which three acidic sites are already deprotonated. The wavelength of maximum absorption in the visible region at pH 5.2 (λ_{max} = 653 nm) suggests a (2N) coordination for the metal ion. Both the ($2N_{Im}$) and (N_{Im}, NH_2) equatorial configurations are possible: the expected λ_{max} values for these structures are 687 nm and 675 nm, respectively, not far from the experimental value. Evidently, the absence of His13 in H13A destabilizes the (N_{Im}) complex, favouring the early formation of a (2N) species. This behaviour suggests a role for His13 in the first

Cu(II) anchorage in WT calcitermin and its H9A and H11A mutants. At pH 4, the $[CuH_4L]^{3+}$ species begins to form. The calculated pK_a value of 5.74 can be attributed to the deprotonation of the Glu residue without any involvement in Cu(II) coordination. With the increase of pH, the $[CuH_3L]^{2+}$ complex is detected; the corresponding pK_a value (6.70) can be attributed to the coordination of either the N-terminal amine or the second His residue. In any case, the suggested configuration for $[CuH_3L]^{2+}$, which is the major species at physiological pH, is characterized by three N-donor groups ($2N_{Im}$, NH_2) (see Fig. 4D). This coordination mode is supported by NMR spectroscopy, where the broadening of both histidine H_δ–H_ε signals and the shift of the valine signals can be observed (Fig. S17A and B ESI†). Once again, increasing the pH value Cu(II) coordinates amide nitrogens to form a ($1N_{Im}$, $3N^-$) complex under the most alkaline conditions (experimental λ_{max} = 520 nm at pH 11.0).

As in the case of WT, the obtained experimental results for all the three mutants suggest that tyrosine does not directly interact with the metal ion. Furthermore, increasing the pH, the $[CuH_{-3}L]^{4-}$ complex is formed in all the systems at the most alkaline pH values. No spectroscopic changes are observed, thus indicating that lysine residues release their additional proton without participating to Cu(II) coordination.

Zn(II) complexes

All the investigated peptides are able to form 1 : 1 complexes with the Zn(II) ion; no poly-nuclear or bis-complexes have been detected neither by potentiometry, nor by mass spectrometry. The complex formation constant values for wild-type calcitermin are shown in Table 3 and for the three mutants (H9A, H11A and H13A) are reported in Tables S1–S3 (ESI†); the corresponding distribution diagrams are plotted in Fig. 5 and S18–S20 (ESI†). ESI-MS results are reported in Table S4 (ESI†) and NMR spectra are shown in Fig. S21–S24 (ESI†).

In the case of wild type calcitermin, the first observed Zn(II) complex is $[ZnH_5L]^{4+}$ which begins to form around pH 4.5 and reaches its maximum concentration at pH 6. A reasonable structural hypothesis for this species is that 2 histidine imidazoles and the side chain of glutamic acid are involved in Zn(II) coordination (the involvement of the C-terminal carboxyl group, instead of the Glu side chain carboxylate, although less likely, cannot be excluded, since it would also affect the Hα

Table 3 Overall stability constants (log β) and acid dissociation constants (pK_a) for Zn(II) complexes with calcitermin, T = 298 K, I = 0.1 mol dm^{-3} ($NaClO_4$) and M : L molar ratio = 0.9 : 1. Values in parentheses are standard deviations on the last significant figure

Species	log β	pK_a
$[ZnH_5L]^{4+}$	51.02 (5)	6.47
$[ZnH_4L]^{3+}$	44.55 (7)	7.00
$[ZnH_3L]^{2+}$	37.55 (8)	7.52
$[ZnH_2L]^{+}$	30.03 (7)	8.31
[ZnHL]	21.72 (7)	—
$[ZnH_{-1}L]^{2-}$	3.5 (1)	—

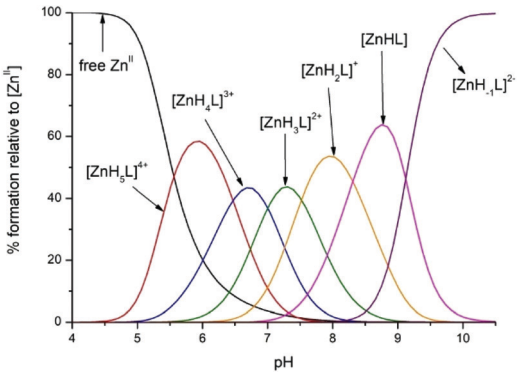

Fig. 5 Exemplificative species distribution diagram relative to Zn(II)/WT complexes; M : L molar ratio = 0.9 : 1.

correlations of the C-terminal Glu (Fig. S21B†)). The next deprotonation step gives rise to the $[ZnH_4L]^{3+}$ species; the corresponding pK_a = 6.47 can be ascribed to the deprotonation of a further histidine. This pK_a value is lower than that measured for the third His residue (7.30) in the free ligand and this suggests the participation of a third imidazole in Zn(II) binding (Fig. 6A). This hypothesis is also supported by NMR spectra, where H_δ–H_ε protons signals of His9, His11 and His13 are broadened to baseline (Fig. S21 ESI†) in the presence of the metal ion. The deprotonation of a coordinated water molecule leads to the formation of the $[ZnH_3L]^{2+}$ species, which dominates around pH 7. The remaining three complexes $[ZnH_2L]^+$, [ZnHL] and $[ZnH_{-1}L]^{2-}$ are related to the deprotonations of the terminal amine, tyrosine and two lysine residues, which are not involved in the coordination.

The first detected complex for the H9A mutant is $[ZnH_4L]^{3+}$, which reaches its maximum of formation in solution around pH 7. The stoichiometry of this species suggests that four acid–base sites are already deprotonated. It is reasonable that 2 histidine residues are involved in Zn(II) coordination (Fig. 6B); the glutamic acid does not interact with the metal ion, as indicated by the lack of any changes in its NMR correlations (Fig. S22 ESI†). The next four species $[ZnH_3L]^{2+}$, $[ZnH_2L]^+$, [ZnHL] and $[ZnH_{-1}L]^{2-}$, are most likely obtained from the deprotonation of the non-coordinating N-terminus, tyrosine and two lysine residues, respectively, without being involved in complexation.

In case of the H11A mutant, the first Zn(II) complex, $[ZnH_5L]^{4+}$, begins to form around pH 4.5 with a maximum of formation at pH 6. Only three groups are deprotonated at this point, *i.e.* the two carboxylic groups and one histidine. The proposed coordination mode for this species is (N_{Im}, COO^-), where one histidine and the glutamic acid side chain are involved in binding. The next species, $[ZnH_4L]^{3+}$, dominates in solution at neutral pH; its metal coordination sphere includes a second histidine residue (pK_a = 6.24) (Fig. 6C). This coordination mode is also supported by NMR spectra where we can observe the broadening of histidine signals (Fig. S23A ESI†) and a slight shift of the glutamic acid signals (Fig. S23B ESI;† however, as in the case of wild type calcitermin Zn(II) complex,

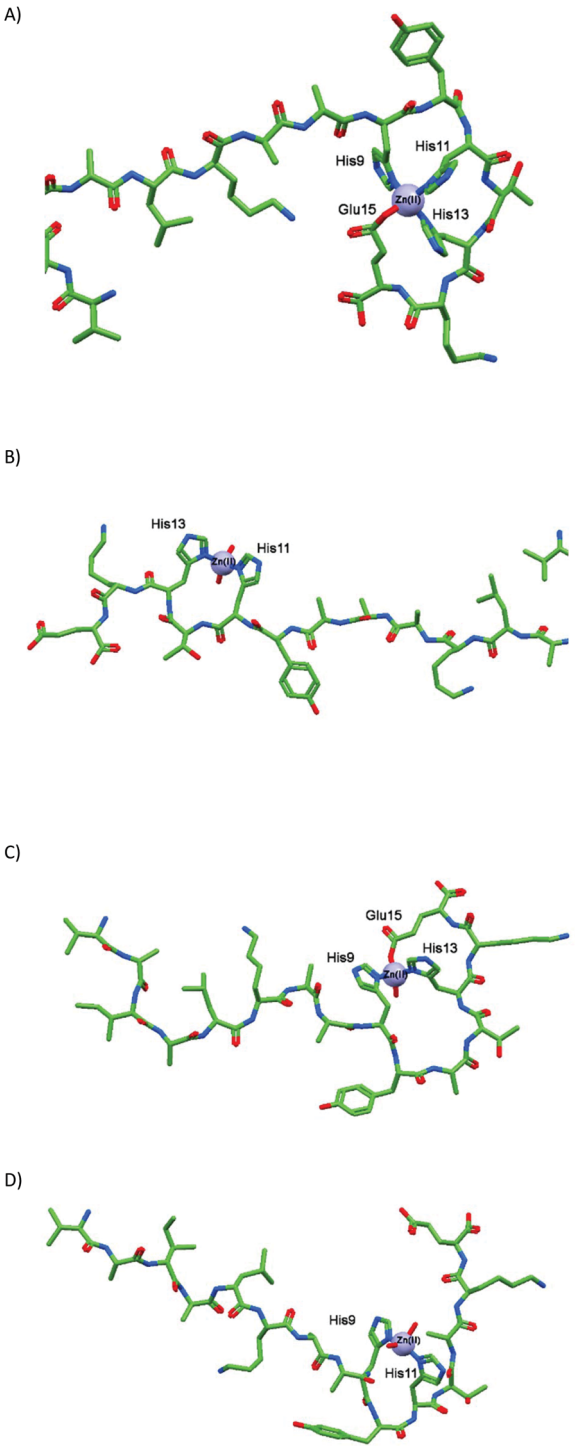

Fig. 6 Proposed coordination sphere of Zn(II) complexes with (A) wild-type calcitermin, (B) H9A mutant of calcitermin, (C) H11A mutant of calcitermin, (D) H13A mutant of calcitermin, at physiological pH.

the involvement of the C-terminal carboxyl group, instead of the Glu side chain carboxylate, is less likely, but cannot be excluded, since it would also affect the Hα correlations of the C-terminal Glu). A further deprotonation step gives rise to the $[ZnH_3L]^{2+}$ complex with a pK_a = 7.56, which can be ascribed to the ionization of the coordinated water molecule. The following four deprotonations lead to the formation of $[ZnH_2L]^+$, $[ZnHL]$, $[ZnL]^-$ and $[ZnH_{-1}L]^{2-}$ complexes, which derive from the deprotonation of the N-terminus, tyrosine and two lysine residues, respectively. None of them are involved in Zn(II) binding.

The first observed zinc complex of the H13A mutant is $[ZnH_5L]^{4+}$ reaching its maximum amount around pH 6. As in the case of H11A mutant, in this complex only one histidine imidazole is involved in Zn(II) coordination. At neutral pH, the species $[ZnH_4L]^{3+}$ dominates in solution; the corresponding protonation constant of 6.22 is consistent with the hypothesis of the coordination of a second His residue. As in the case of H9A mutant, Glu residue does not interact with the metal ion (Fig. 6D). This hypothesis is supported by NMR spectra (Fig. S24B ESI†): after the addition of one equivalent of Zn(II) ions, the signals corresponding to glutamic acid side chain correlations remain unchanged. The release of two further protons leads to the formation of the $[ZnH_2L]^+$ complex; the corresponding deprotonation steps can be assigned to the ionization of a coordinated water molecule and to the deprotonation of the N-terminal amino group. Analysis of the complex solution at pH above 8 was not possible, due to precipitation.

Comparison of complex stability

The stability constants of metal complexes characterized by different stoichiometries and/or protonation degrees cannot be directly compared. The parameters most commonly used to evaluate the overall binding affinity of different ligands towards a metal ion, the dissociation constant (K_d)[13] and the pM value[14] (Table S7†) are reasonably comparable to those of similar systems found in the literature. K_d values of Cu(II) complexes at pH 5.4 are in the micromolar range, while those calculated for pH 7.4 are close to the nanomolar range, with the exception of A11H (8.15×10^{-7}), which involves (N_{Im}, NH_2, N–) in binding, and the wild type calcitermin (1.31×10^{-10}), which employs a ($3N_{im}$, NH_2) binding mode. Considering that for histidine a K_d value of 3 nM has been reported,[15] calcitermin can compete with amino acids and low molecular weight ligands to bind the accessible pool of Cu(II) *in vivo*. K_d values of Zn(II) complexes are in the millimolar range at pH 5.4, while at pH 7.4, they are around micromolar, with the exception of the wild type calcitermin (3.07×10^{-7} M), which involves an additional imidazole in Zn(II) binding in comparison to other mutants.

In addition, in the attempt to get more information on the role played by the number and position of His residues on the coordination ability of calcitermin, two competition plots (plots based on the calculated constants, showing a hypothetical situation, in which equimolar amounts of Cu(II)/Zn(II), WT calcitermin, H9A, H11A and H13A mutants, are present see Experimental) were built up at equimolar concentrations of ligands and metal ions (Fig. 7). The wild-type calcitermin is the most effective ligand for both the investigated metal ions. The most remarkable differences in binding affinity between calcitermin and its mutants occur from pH = 5.5 in the case of

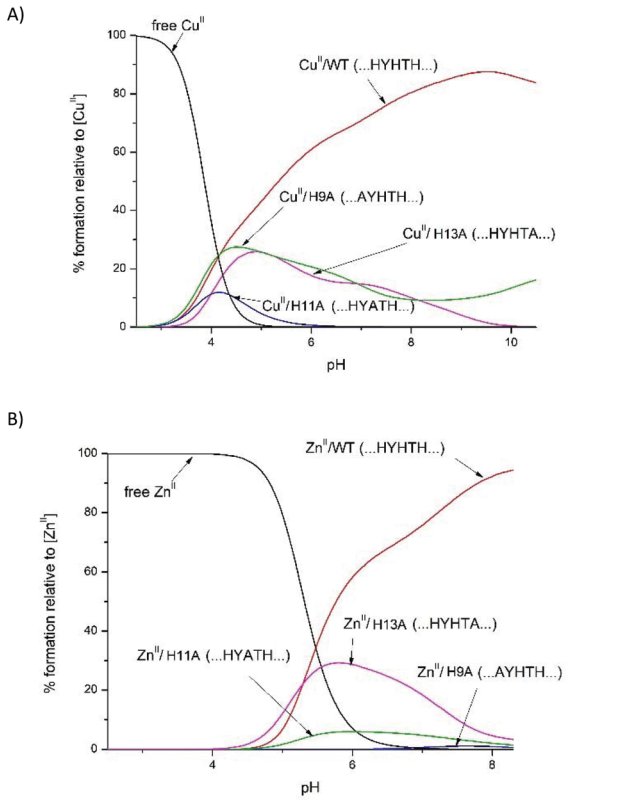

Fig. 7 Competition plots for solutions containing equimolar concentrations of M(II), WT wild-type calcitermin, H9A, H11A and H13A. M(II) = (A) Cu(II) and (B) Zn(II).

Zn(II) and pH = 4.5 in the case of Cu(II), *i.e.* when the third histidine residue of WT calcitermin comes into play. This confirms once again that an increase in the number of histidines makes the coordination more effective.[16–18] At the most acidic pH values the affinity of WT, H9A and H13A for Cu(II) ion is comparable, in agreement with the above hypothesis that the coordination behaviour towards the metal ion is very similar for these three peptides. No direct evidence for the preferred metal binding site of calcitermin comes out, since the two curves referring to H9A and H13A complexes are practically superimposable throughout the entire pH range. On the other hand, the lowest affinity of H11A is in good agreement with the hypothesis of the initial involvement of only one His residue and it also suggests that two histidines separated by only one amino acid (ligands H9A and H13A) are more effective in chelating copper than two histidines more far apart (as in H11A).

In the case of Zn(II) ion, the calculated competition plot shows different trends. The stability of the mutant complexes is much more affected by the position of His residues in the amino-acid sequence. The higher stability of Zn(II) complexes formed by H13A with respect to those formed by H9A and H11A suggests a pivotal role of His9 and His11 in zinc complexation. It is also noteworthy that, the coordination of Zn(II) to the glutamic acid side chain of H11A mutant is not reflected by an increased stability of the complex.

In order to better understand the binding ability of the calcitermin sequence, other competition plots have been built up, where the complex-formation behaviour of WT is compared to that of other similar peptides. Four other histidine rich sequences have been taken into account: (i) the neuropeptide gamma DAGHGQISHKRHKTDSFVGLM-NH_2 (NPG),[19] which contains three histidines separated by four and two residues (HxxxxHxxH) and a free N-terminus, (ii) the protected fragment Ac-SHSHSHSHS-NH_2 of C4YJH2, a putative metal transporter of *Candida albicans*,[16] with four alternated His residues (HxHxHxH), (iii) the N-terminally free multihistidine peptide HAVAHHH-NH_2,[20] which bears four histidines with a HxxxHHH motif, and (iv) the polyhistidine triad motif from *Streptococcus pneumoniae* Ac-HGDHYH-NH_2,[21] which contains three histidines separated by two and one residues (HxxHxH). In the case of Zn(II) complexes, the comparison between calcitermin, Ac-SHSHSHSHS-NH_2, HAVAHHH-NH_2 and Ac-HGDHYH-NH_2 (Fig. S25 ESI†) reveals that, under the most acidic conditions (pH 4.5–6), the participation of Glu residue in the complexation likely contributes to the stabilization of Zn(II)/WT system, making this ligand more efficient than Ac-SHSHSHSHS-NH_2, in which only 3 histidines participate in the coordination.[16] In Fig. S26 (ESI†), the competition diagram of Cu(II) complexes with WT, NPG and Ac-SHSHSHSHS-NH_2 is plotted: under the most acidic condition Cu(II) coordination mostly involves the His residues in all the systems. Starting from pH 5, the higher affinity of Ac-SHSHSHSHS-NH_2 is consistent with the binding of the fourth imidazole nitrogen, that is absent in WT and NPG. These latter systems, instead, contain three His and the free N-terminus and show a similar trend up to pH 5.5. The increase of stability of Cu(II)/WT complexes is due to the presence of a 4N coordination mode ($3N_{Im}$, NH_2), rather than a 3N configuration ($2N_{Im}$, NH_2) suggested for NPG, where the third histidine should not bind the metal ion.

Can Cu(II) outcompete Zn(II) in binding to calcitermin? The Irving–Williams series suggests it definitely would, at least under equimolar concentrations. The same situation would be observed under physiological concentrations of the studied metals in the lung (a tenfold excess of Zn(II) over Cu(II))[22]– Zn(II) would be outcompeted by Cu(II) in all the studied pH range (Fig. S27†).

Antimicrobial activity

All compounds were tested for their antimicrobial activity against a representative panel of microbials: *Pseudomonas aeruginosa* 15442, *Klebsiella pneumoniae* 13883, *Escherichia coli* 25922, *Staphylococcus aureus* 29213, *Enterococcus faecalis* 29212 and *Candida albicans* 10231. The *in vitro* antimicrobial activity was screened using microdilution method and modified Richard's method. The results showed no MBC/MFC activity. However, the minimal inhibitory concentration (MIC) has been determined for all active compounds and their metal complexes (Table 4).

Obtained results suggest that the structure modification in all analysed systems (WT, H9A, H11A, H13A) determine

Table 4 *In vitro* antimicrobial activity of WT, H9A, H11A, H13A expressed as a minimal inhibitory concentration (MIC), at pH = 5.4

Strain	*Candida albicans* 10231 MIC (μg mL^{-1})	*Enterococcus faecalis* 29212 MIC (μg mL^{-1})	*Staphylococcus aureus* 29213 MIC (μg mL^{-1})	*Escherichia coli* 25922 MIC (μg mL^{-1})	*Klebsiella pneumoniae* 13883 MIC (μg mL^{-1})	*Pseudomonas aeruginosa* 15442 MIC (μg mL^{-1})
WT	n/d	n/d	**128**	n/d	**128**	n/d
WT–Cu(II)	**1**	n/d	**128**	n/d	n/d	n/d
WT–Zn(II)	**1**	n/d	n/d	n/d	n/d	n/d
H9A	**1**	n/d	n/d	n/d	n/d	n/d
H9A–Cu(II)	**2**	**128**	n/d	n/d	n/d	n/d
H9A–Zn(II)	**0.25**	n/d	**64**	n/d	n/d	**128**
H11A	n/d	**64**	n/d	n/d	n/d	n/d
H11A Cu(II)	n/d	**32**	**64**	n/d	n/d	n/d
H11A–Zn(II)	n/d	**4**	n/d	n/d	**128**	n/d
H13A	n/d	**4**	**0.25**	n/d	n/d	n/d
H13A Cu(II)	n/d	**4**	**0.25**	n/d	n/d	n/d
H13A–Zn(II)	**128**	**0.5**	**0.25**	n/d	n/d	**128**

n/d, not detected.

Table 5 Examples of MIC breakpoints values from EUCAST/2019/01/01 for bacteria and 2018/02 for fungi

Enterococcus ssp. (for *E. faecalis*)	MIC breakpoints (μg mL^{-1}) S(sensitive)≤	R(resistant)>	*Staphylococcus* ssp. (for *S. aureus*)	MIC breakpoints (μg mL^{-1}) S≤	R>	*C. albicans*	MIC breakpoints (μg mL^{-1}) S≤	R>
Ampicillin	4	8	Azithromycin	1	2	Amhotericin B	1	1
Ampicillin-Sulbactam	4	8	Ceftobiprole	2	2	Fluconazole	2	4
Amoxicillin	4	8	Ciprofloxacin	1	1			
Amoxicillin-clavulanic acid	4	8	Chloramphenicol	8	8			
Imipenem	4	8	Maxifloxacin	0.25	0.25			
Ciprofloxacin	4	4	Amikacin	8	8			
Levofloxacin	4	4	Gentamicin	1	1			
Vancomycin	4	4	Tobramycin	1	1			
Linezolid	4	4	Teicoplanin	2	2			
Nitrofurantoin (only *E. faecalis*)	64	64	Clindamycin	0.25	0.5			

specific and strictly directed activity. A different sensitivity of all investigated strains is presented. Among all, Gram-negative species (*Escherichia coli* 25922, *Klebsiella pneumoniae* 13883, *Pseudomonas aeruginosa* 15442) are resistant for almost all investigated compounds. Only WT and the three Zn(II) complex systems with H9A, H11A and H13A present activity against Gram-negative species (MIC = 128 μg mL^{-1}), although their activity was lower than those exhibited towards Gram-positive bacteria. In fact, activity against *Enterococcus faecalis* 29212 and *Staphylococcus aureus* 29213 was detected for both H11A and H13A mutants, although the most relevant MIC values are shown for H13A, H13A/Cu(II) and H11A/Zn(II) against *Enterococcus faecalis* 29212 (MIC = 4 μg mL^{-1}) and for H13A/Zn(II) (MIC = 0.5 μg mL^{-1}) (Table 4).

According to the newest EUCAST (European Committee on Antimicrobial Susceptibility Testing) validated "*Clinical Breakpoints and dosing* v.9.0", which have been obtained for the same *Enterococcus faecalis* 29212 strain (Table 5) the MIC breakpoints are similar and lower than those for commonly used antimicrobial agents. Promising MIC values were also detected against *Staphylococcus aureus* 29213 for all the H13A systems: their MIC values (0.25 μg mL^{-1}) are significantly lower than those obtained for common used antibiotics and chemotherapeutics (Table 5, an EUCAST validation was obtained for the same strain). Finally, comparison of the results obtained against *Candida albicans* 10231 clearly shows that WT complexes with Cu(II) and Zn(II) and also H9A mutant and metal ion complexes present competitive values for currently used antimicrobial agents used in therapies (Tables 4 and 5). Antimicrobial activity of ligands/complexes, which were active at pH 5.4 (discussed so far), was also tested at pH 7.4. At this pH, none of the analysed systems presented any antimicrobial activity. A Neutral Red (NR) cytotoxicity *in vitro* assay (Table S6 ESI†) performed on a regular fibroblast show that the used metal concentration range is not toxic to regular cells.

Conclusions

The present study shows that calcitermin is a very good chelator for both Cu(II) and the Zn(II) ions. His-to-Ala substitutions have a significant effect on both the thermodynamic stability

and the structure of the metal complexes. As expected, the increase in the number of histidines makes the coordination of both the metals more effective. There is no preferred Cu(II) binding site in calcitermin: the stabilities of the Cu(II) complexes with H9A and H13A are almost identical. In the least stable Cu(II) complexes formed by H11A, in which two histidines are separated by three amino acids, only one His residue is involved in binding: clearly the coordination HisxHis is preferred to HisxxxHis. As for the Zn(II) complexes, the higher stability of the species formed by H13A, with respect to those formed by H9A and H11A, suggest a pivotal role of His9 and His11 in zinc complexation.

Both His-to-Ala substitutions and the presence of metal ions have a significant influence on the antimicrobial activity of the studied systems: (i) Cu(II) and Zn(II) complexes of both wild type calcitermin and the three systems containing the H9A mutant are active against fungi (*C. albicans*); (ii) mutating His11 and His13 to H11A and H13A, respectively, puts out the antifungal activity; (iii) relevant antimicrobial effects against Gram-positive bacteria are detected, in particular by the H13A systems against *S. aureus* and *E. faecalis*; (iv) no intrinsic activity has been determined against Gram-negative strains for all analysed compounds.

Several AMPs require metal ions for their antimicrobial activity. Often, metal coordination triggers the preorganization of the AMP and/or various charge–charge or metal–ligand interactions that may lead to the destabilization or permeabilization of the cell wall.[8,23] In the present case, it is not straightforward to link the antimicrobial activity of the studied systems with their charge, structure or metal binding mode (Table S7†). The peptides and their metal complexes seem to be random coils in water (data not shown) while they adopt a helical-like structure in the presence of membrane-mimicking SDS; no clear influence of the His-to-Ala substitutions or metal coordination is observed (Fig. S28–S31 ESI†).

In conclusion, the present work is a comprehensive description of the thermodynamics, structure and coordination chemistry of the studied metal-calcitermin complexes, with the aim to find a link between these properties and the antimicrobial mode of action. No such link became obvious so far, however, what is of particular interest, novel antimicrobial peptides with very promising antimicrobial efficacies are presented and the antimicrobial-activity enhancing effect of the metal binding is observed in numerous cases. This clearly opens the door for further attempts to understand the relationships between antimicrobial peptide-metal coordination, structure, stability, efficacy and mode of action.

Experimental

Materials

$Zn(ClO_4)_2{\cdot}6H_2O$ and $Cu(ClO_4)_2{\cdot}6H_2O$ were extra pure products (Sigma-Aldrich); the concentrations of their stock solutions were standardised by EDTA titration and periodically checked *via* ICP-MS. The carbonate-free stock solution of 0.1 mol dm^{-3} NaOH was purchased from Sigma-Aldrich and then potentiometrically standardized with the primary standard potassium hydrogen phthalate (99.9% purity). All sample solutions were prepared with freshly doubly distilled water. The $HClO_4$ stock solution was prepared by diluting concentrated $HClO_4$ (Sigma-Aldrich) and then standardizing with NaOH. The ionic strength was adjusted to 0.1 mol dm^{-3} by adding $NaClO_4$ (Sigma-Aldrich). Grade A glassware was employed throughout.

Peptide synthesis and purification

Peptides WT, H9A, H11A and H13A were synthesized according to published methods[24] using Fmoc/*t*-butyl chemistry with a Syro XP multiple peptide synthesizer (MultiSynTech GmbH, Witten Germany). Wang resin preloaded with Fmoc-Glu(O*t*Bu) was used as a solid support for the synthesis of all derivatives. Fmoc-amino acids (4-fold excess) were sequentially coupled to the growing peptide chain using DIPCDI/HOBt (*N*,*N*′-diisopropylcarbodiimide/1-hydroxybenzotriazole) (4-fold excess) as activating mixture for 1 h at room temperature. Cycles of deprotection of Fmoc (40% piperidine/*N*,*N*-dimethylformamide) and coupling with the subsequent amino acids were repeated until the desired peptide-bound resin was completed. The protected peptide-resin was treated with reagent B[25] (trifluoroacetic acid (TFA)/H20/phenol/triisopropylsilane 88 : 5 : 5 : 2; v/v; 10 mL per 0.2 g of resin) for 1.5 h at room temperature. After filtration of the resin, the solvent was concentrated *in vacuo* and the residue triturated with ethyl ether. Crude peptides were purified by preparative reversed-phase HPLC using a Water Delta Prep 3000 system with a Jupiter column C18 (250 × 30 mm, 300 A, 15 μm spherical particle size). The column was perfused at a flow rate of 20 mL min^{-1} with a mobile phase containing solvent A (5%, v/v, acetonitrile in 0.1% TFA), and a linear gradient from 0 to 65% of solvent B (60%, v/v, acetonitrile in 0.1% TFA) over 25 min for the elution of peptides. Analytical HPLC analyses were performed on a Beckman 116 liquid chromatograph equipped with a Beckman 166 diode array detector. Analytical purity of the peptides was assessed using a Zorbax C18 column (4.6 × 150 mm, 3 μm particle size) with the above solvent system (solvents A and B) programmed at a flow rate of 0.7 mL min^{-1} using a linear gradient from 0% to 100% B over 25 min. All analogues showed ≥ 95% purity when monitored at 220 nm. Molecular weight of final compounds was determined by a mass spectrometer ESI Micromass ZMD-2000.

Potentiometric measurements

Stability constants for proton and metal complexes were calculated from pH-metric titration curves registered at T = 298 K and ionic strength 0.1 mol dm^{-3} ($NaClO_4$). The potentiometric apparatus consisted of a Metrohm 905 Titrando pH-meter system provided with a Mettler-Toledo InLab® Micro, glass-body, micro combination pH electrode and a dosing system 800 Dosino, equipped with a 2 ml micro burette. High purity grade argon was gently blown over the test solution in order to maintain an inert atmosphere. A constant-speed magnetic stirring was applied throughout. Solutions were titrated with

0.1 mol dm^{-3} carbonate-free NaOH. The electrode was daily calibrated for hydrogen ion concentration by titrating $HClO_4$ with alkaline solution under the same experimental conditions as above. The reaction kinetics was always fast and an average waiting time of 50 s seconds was employed between two burette additions; acceptable signal drift was 2 mV min^{-1}. The standard potential and the slope of the electrode couple were computed by means of the Glee[26] program. The purities and the exact concentrations of the ligand solutions were potentiometrically determined using the Gran method.[27] The HYPERQUAD[28] program was employed for the overall formation constant (β) calculations, referred to the following equilibrium:

$$pM + qL + rH \leftrightarrows M_pL_qH_r$$

(charges omitted; p is 0 in the case of ligand protonation; r can be negative). Step formation constants (K) and/or acid dissociation constants (K_a) are also reported. The computed standard deviations (referring to random errors only) were given by the program itself and are shown in parentheses as uncertainties on the last significant figure. Hydrolysis constants for Zn(II) and Cu(II) ions were taken from the literature[10,29] and are reported in Table S5 (ESI†). The distribution diagrams were computed using the HYSS program.[30] The overall metal binding ability of the different ligands can be compared in a wide pH range by computing the competition diagrams, starting from the binary speciation models. A solution containing the metal and the two (or more) ligands (or *vice versa*) is simulated, admitting that all the components compete with each other to form the respective binary complexes, without mixed species formation. This is a reasonable approximation in the case of peptides, which most often form only 1 : 1 complexes in which the peptide completely wraps the metal ion.

The dissociation constant (K_d) refers to the hypothetical general equilibrium: M + L = ML, where the protonation of both the ligand and the complex are not explicitly considered.[13] The pM value is the negative logarithm of the concentration of the free metal ion (pCu or pZn in the present case), under given experimental conditions,[14] here $[L]_{total}$ = 10^{-5} M and $[M]_{total} = 10^{-6}$ M, at pH 7.4 or 5.4.[13]

Mass spectrometric measurements

High-resolution mass spectra were obtained on a BrukerQ-FTMS spectrometer (Bruker Daltonik, Bremen, Germany), equipped with an Apollo^{II} electrospray ionization source with an ion funnel. The mass spectrometer was operated in the positive ion mode. The instrumental parameters were as follows: scan range m/z 100–2500, dry gas nitrogen, temperature 453 K and ion energy 5 eV. The capillary voltage was optimized to the highest S/N ratio and it was 4500 V. The small changes in voltage (±500 V) did not significantly affect the optimized spectra. The samples were prepared in a 1 : 1 methanol–water mixture at different pH values. The samples (Zn(II) : ligand and Cu(II) : ligand in a 0.9 : 1 stoichiometry, $[ligand]_{tot} = 0.5 \times 10^{-3}$ mol dm^{-3}) were infused at a flow rate of 3 μL min^{-1}. The instrument was externally calibrated with a Tunemix™ mixture (Bruker Daltonik, Germany) in quadratic regression mode. Data were processed using the Bruker Compass DataAnalysis 4.2 program. The mass accuracy for the calibration was better than 5 ppm, enabling together with the true isotopic pattern (using SigmaFit) an unambiguous confirmation of the elemental composition of the obtained complex.

Spectroscopic measurements

The absorption spectra were recorded on a Varian Cary300 Bio spectrophotometer, in the range 200–800 nm, using a quartz cuvette an optical path of 1 cm. The solutions were prepared in water solution of 4 mM $HClO_4$ at 0.1 M $NaClO_4$ ionic strength. Ligand concentration was 1 mM. Circular dichroism (CD) spectroscopy experiments were recorded on a Jasco J-1500 CD spectrometer at 298 K in a 0.01 cm and 1 cm quartz cells. The spectral range was 180–300 and 200–800 nm respectively. The solutions were prepared in water solution of 4 mM $HClO_4$ at 0.1 M $NaClO_4$ ionic strength and in the water solution of 4 mM $HClO_4$ at 10 mM SDS ionic strength (180–300 nm range). Ligand concentration was 1 mM (200–800 nm range) or 0.1 mM (180–300 nm range). Cu(II) to ligand molar ratio was 0.9 : 1. The UV-Vis and CD spectroscopic parameters were calculated from the spectra obtained at the pH values corresponding to the maximum concentration of each particular species, based on distribution diagrams.

NMR measurements

NMR spectra were recorded at 14.1 T on a Bruker Avance III 600 MHz equipped with a Silicon Graphics workstation. The temperatures were controlled with an accuracy of ±0.1 K. Suppression of the residual water signal was achieved by excitation sculpting, using a selective square pulse on water 2 ms long. All the samples were prepared either in D_2O or in a 90% H_2O and 10% D_2O (99.95% from Merck) mixture. Proton resonance assignment was accomplished by 2D ^1H–^1H total correlation spectroscopy (TOCSY) and nuclear Overhauser effect spectroscopy (NOESY) experiments, carried out with standard pulse sequences. Samples of analysed complexes (metal : ligand in a 1 : 1 stoichiometry, $[ligand]_{tot}$ = 0.003 mol dm^{-3}) were prepared by adding metal ions to the acidic solution of a ligand (pH 3), and the pH was then increased to a higher value. Spectral processing and analysis was performed using Bruker TOPSPIN 2.1 and Sparky.[31]

Antimicrobial activity assay of ligand/complex system

Three reference strains from ATCC collection (*Pseudomonas aeruginosa* 15442, *Klebsiella pneumoniae* 13883, *Escherichia coli* 25922, *Staphylococcus aureus* 29213, *Enterococcus faecalis* 29212 and *Candida albicans* 10231) were used for antimicrobial activity assay. The pH of experiment condition was 5.4 in Tryptone Soy Broth (TSB) medium (as suggested by A.M. Cole *et al.*, that when the acidity of the medium was increased (until pH 5.4) calcitermin was active against selected pathological strains and did not present any activity against any tested microorganisms at pH 7.4.[7] Before the general experi-

ment, the validation of method concerning lower pH conditions has been proceeded. Preliminary experiments, where all examined strains have been incubated 24 h/37 °C in pH 5.4 TSB did not present any influence on growth conditions. The antimicrobial effect of analysed ligands/complexes was performed according to the standard protocol using microdillution method with spectrophotometric measurement (λ = 580 nm in starting point and after 24 h) and modified Richard's method.[32–34] After 24 h/37 °C in TSB medium incubation, a density of bacterial suspension was measured using a densitometer and a proper dilution were prepared (0.005 MF). Afterwards, a 96-well microplate was prepared with the range from 128 μg mL^{-1} to 0.0625 μg mL^{-1} of ligand/complex solution. A positive (TSB + strain) and negative control (TSB) was also included in the test. Microplates were incubated 37 ± 1 °C for 24 hours on the shaker. After this, the spectrophotometric measurement has been done, then aliquots of 5 μL of 1% (m/v) 2,3,5-triphenyltetrazolium chloride (TTC) solution were added in each well. TTC is converted into red formazan crystals in microbial live cells. MBC/MFC can be observed as the lowest concentration that did not show microbial growth by visual analysis after 24 h incubation with TTC (did not change the colour to pink). Thanks to both methods, MIC, MBC or MFC can be determined.

Abbreviations

MIC	Minimum inhibitory concentration/minimum concentration, where microbial growth is inhibited
MBC	Minimum bactericidal concentration/minimum concentration, where 99.9% bacteria died
MFC	Minimum fungicidal concentration/minimum concentration, where 99.9% fungi died
TTC	Triphenyl tetrazolium chloride
TSB	Tryptone soy broth
ATCC	American type culture collection
S	Sensitive
R	Resistant

Conflicts of interest

There are no conflicts to declare.

Acknowledgements

The present research was financially supported by the National Science Centre (UMO-2017/26/A/ST5/00364, SONATA BIS grant to MRZ), University of Ferrara (FAR 2017), CIRCMSB (Consorzio Interuniversitario di Ricerca in Chimica dei Metalli nei Sistemi Biologici, Bari, Italy), MIUR (Ministero dell'Istruzione, dell'Università e della Ricerca) projects (PRIN2015-2015MP34H3 and PRIN2015-2015T778JW) and Erasmus + programme of the European Union.

Notes and references

1 C.-F. Le, C.-M. Fang and S. D. Sekaran, *Antimicrob. Agents Chemother.*, 2017, **61**, e02340.
2 S. Damo and T. E. Kehl-Fie, in *Antimicrobial Peptides: Role in Human Health and Disease*, ed. J. Harder and J.-M. Schröder, Springer International Publishing, Cham, 2016, pp. 89–100, DOI: 10.1007/978-3-319-24199-9_6.
3 S. A. Loutet and M. A. Valvano, *Front. Microbiol.*, 2011, **2**, 159–159.
4 J. L. Alexander, Z. Thompson and J. A. Cowan, *ACS Chem. Biol.*, 2018, **13**, 844–853.
5 C. D. Fjell, J. A. Hiss, R. E. W. Hancock and G. Schneider, *Nat. Rev. Drug Discovery*, 2011, **11**, 37.
6 J. D. Gottsch, S. W. Eisinger, S. H. Liu and A. L. Scott, *Infect. Immun.*, 1999, **67**, 6631.
7 A. M. Cole, Y.-H. Kim, S. Tahk, T. Hong, P. Weis, A. J. Waring and T. Ganz, *FEBS Lett.*, 2001, **504**, 5–10.
8 D. Łoboda, H. Kozłowski and M. Rowińska-Żyrek, *New J. Chem.*, 2018, **42**, 7560–7568.
9 H. Sigel and R. B. Martin, *Chem. Rev.*, 1982, **82**, 385–426.
10 L. D. Pettit and H. K. J. Powell, *The IUPAC Stability Constants Database*, Royal Society of Chemistry, London, 1992–2000.
11 G. R. Grimsley, J. M. Scholtz and C. N. Pace, *Protein Sci.*, 2009, **18**, 247–251.
12 L. D. Pettit, S. Pyburn, W. Bal, H. Kozlowski and M. Bataille, *J. Chem. Soc., Dalton Trans.*, 1990, 3565–3570, DOI: 10.1039/dt9900003565.
13 H. Kozlowski, M. Łuczkowski and M. Remelli, *Dalton Trans.*, 2010, **39**, 6371–6385.
14 G. Crisponi and M. Remelli, *Coord. Chem. Rev.*, 2008, **252**, 1225–1240.
15 R. M. C. Dawson, D. C. Elliot, W. H. Elliot and K. M. Jones, *Data for Biochemical Research*, Clarendon Press, Oxford, 1986.
16 D. Bellotti, D. Łoboda, M. Rowińska-Żyrek and M. Remelli, *New J. Chem.*, 2018, **42**, 8123–8130.
17 F. Pontecchiani, E. Simonovsky, R. Wieczorek, N. Barbosa, M. Rowinska-Zyrek, S. Potocki, M. Remelli, Y. Miller and H. Kozlowski, *Dalton Trans.*, 2014, **43**, 16680–16689.
18 J. Watly, E. Simonovsky, N. Barbosa, M. Spodzieja, R. Wieczorek, S. Rodziewicz-Motowidlo, Y. Miller and H. Kozlowski, *Inorg. Chem.*, 2015, **54**, 7692–7702.
19 M. Pietruszka, E. Jankowska, T. Kowalik-Jankowska, Z. Szewczuk and M. Smuzynska, *Inorg. Chem.*, 2011, **50**, 7489–7499.
20 B. D. Balogh, Z. Bihari, P. Buglyo, G. Csire, Z. Kerekes, M. Lukacs, I. Sovago and K. Varnagy, *New J. Chem.*, 2019, **43**, 907–916.
21 A. Miller, D. Dudek, S. Potocki, H. Czapor-Irzabek, H. Kozlowski and M. Rowinska-Zyrek, *Metallomics*, 2018, **10**, 1631–1637.
22 J. Morton, E. Tan and S. K. Suvarna, *J. Trace Elem. Med. Biol.*, 2017, **43**, 63–71.
23 N. M. Revie, K. R. Iyer, N. Robbins and L. E. Cowen, *Curr. Opin. Microbiol.*, 2018, **45**, 70–76.

24 N. L. Benoiton, *Chemistry of Peptide Synthesis*, Taylor & Francis, 2005.
25 N. A. Sole and G. Barany, *J. Org. Chem.*, 1992, **57**, 5399–5403.
26 P. Gans and B. O'Sullivan, *Talanta*, 2000, **51**, 33–37.
27 G. Gran, *Acta Chem. Scand.*, 1950, **4**, 559–577.
28 P. Gans, A. Sabatini and A. Vacca, *Talanta*, 1996, **43**, 1739–1753.
29 G. Arena, R. Cali, E. Rizzarelli and S. Sammartano, *Thermochim. Acta*, 1976, **16**, 315–321.
30 L. Alderighi, P. Gans, A. Ienco, D. Peters, A. Sabatini and A. Vacca, *Coord. Chem. Rev.*, 1999, **184**, 311–318.
31 W. Lee, M. Tonelli and J. L. Markley, *Bioinformatics*, 2015, **31**, 1325–1327.
32 J. Gabrielson, M. Hart, A. Jarelöv, I. Kühn, D. McKenzie and R. Möllby, *J. Microbiol. Methods*, 2002, **50**, 63–73.
33 P. Sabaeifard, A. Abdi-Ali, M. R. Soudi and R. Dinarvand, *J. Microbiol. Methods*, 2014, **105**, 134–140.
34 F. L. Francisco, A. M. Saviano, T. d. J. A. Pinto and F. R. Lourenço, *J. Microbiol. Methods*, 2014, **103**, 104–111.

Journal of Inorganic Biochemistry 214 (2021) 111304

Contents lists available at ScienceDirect

Journal of Inorganic Biochemistry

journal homepage: www.elsevier.com/locate/jinorgbio

The N-terminal domain of *Helicobacter pylori*'s Hpn protein: The role of multiple histidine residues

Denise Bellotti [a,b], Angelica Sinigaglia [a], Remo Guerrini [a], Erika Marzola [a], Magdalena Rowińska-Żyrek [b], Maurizio Remelli [a,*]

[a] Department of Chemical and Pharmaceutical Sciences, University of Ferrara, Via L. Borsari 46, 44121 Ferrara, Italy
[b] Faculty of Chemistry, University of Wrocław, F. Joliot-Curie 14, 50-383 Wrocław, Poland

ARTICLE INFO

Keywords:
Copper
Nickel
Zinc
Metal complexes
Hpn protein
ATCUN motif

ABSTRACT

Helicobacter pylori is a gram-negative bacterium with gastric localization that can cause many gastrointestinal disorders. Its survival in the host environment strictly requires an efficient regulation of its metal homeostasis, in particular of Ni(II) ions, crucial for the synthesis of some essential enzymes. Hpn is a protein of 60 amino acids, 47% of which are histidines, expressed by *H. pylori* and avid for nickel, characterized by the presence of an ATCUN (Amino Terminal Cu(II)- and Ni(II)-binding) motif and by two further histidine residues which can act as additional metal anchoring sites. We decided to deepen the following aspects: (i) understanding the role of each histidine in the coordination of metal ions; (ii) comparing the binding affinities for Cu(II), Ni(II) and Zn(II) ions, which are potentially competing metals in vivo; (iii) understanding the Hpn ability of forming ternary and polynuclear complexes. For these purposes, we synthesized the Hpn N-terminal "wild-type" sequence (MAHHEEQHG-Am) and the following peptide analogues: MAAHEEQHG-Am, MAHAEEQHG-Am, MAHHEEQAG-Am and MAHAEEQAG-Am. Our results highlight that the histidines in position 4 and 8 lead to the formation of Cu(II) binuclear complexes. The ATCUN motif is by far the most efficient binding site for Cu(II) and Ni(II), while macrochelate Zn(II) complexes are formed thanks to the presence of several suitable anchoring sites (His and Glu). The metal binding affinities follow the order Zn(II) < Ni(II) < < Cu(II). In solutions containing equimolar amount of wild-type ligand, Cu(II) and Ni(II), the major species above pH 5.5 are hetero-binuclear complexes.

1. Introduction

Helicobacter pylori is a spiral-shaped gram-negative bacterium that can survive and proliferate in the human stomach; it is present in about half of the Earth population. *H. pylori* infection can cause serious disorders such as gastro-duodenal ulcer, MALT (mucosa-associated lymphoid tissue) lymphoma and gastric cancer, which is responsible for almost one million deaths worldwide every year [1]. The World Health Organization has classified *H. pylori* as a "Group 1" human carcinogen [2]. The survival capacity of the bacterium is especially based on the activity of urease, a nickel-containing enzyme that catalyzes the hydrolysis of urea to ammonia and bicarbonate which act as buffers and allow *H. pylori* to keep neutral the pH of its cytoplasm [3]. Urease represents about 10% of the total soluble proteins of *H. pylori* and requires up to 24 nickel ions [4]. Another enzyme that contains nickel, and also important for *H. pylori*, is the [NiFe] hydrogenase, which allows the bacterium to exploit molecular hydrogen as an alternative energy source [5].

Nickel is therefore crucial for the virulence of *H. pylori*, which contains a rather complicated management system for the homeostasis of this metal ion. This system includes a small cytoplasmic protein, called Hpn (*Helicobacter pylori* protein with affinity for nickel) [6], rich in histidine, which accounts for about 2% of the total synthesized proteins.

The role played by Hpn in *H. pylori* is not fully understood; this protein was initially considered to store nickel in the cell and to alleviate the metal toxicity by sequestering the intracellular excess of nickel [7]. In fact, it was reported that *H. pylori* mutants with Hpn deficiencies are more sensitive to excess of Ni(II) than the wild-type bacterium [8]. Interestingly, it has also been observed that, under acidic conditions, Hpn releases the bound nickel and it has been suggested that this allows the protein to supply nickel to the cell when urease activity needs to be stimulated for pH regulation [9,10]. Recently, it has also been proposed that Hpn interacts with many other proteins to perform various cellular functions connected with the maturation of enzymes that contain nickel,

* Corresponding author.
E-mail address: rmm@unife.it (M. Remelli).

https://doi.org/10.1016/j.jinorgbio.2020.111304
Received 30 July 2020; Received in revised form 27 October 2020; Accepted 27 October 2020
Available online 4 November 2020
0162-0134/

MAHHEEQHGG[10] HHHHHHHTHH[20] HHYHGGEHHH[30] HHHSSHHEEG[40] CCSTSDSHHQ[50]
EEGCCHGHHE[60]

Scheme 1. Amino acid sequence of Hpn protein. The studied N-terminal fragment is underlined.

with the recovery of peptides and the acquisition of nitrogen [2].

Using equilibrium dialysis and subsequent analysis by ICP-MS and UV/visible spectrophotometry, Ge et al. have shown that Hpn binds five Ni(II) ions per monomer at pH 7.4 [11]; however, the measured dissociation constant was quite modest ($K_d = 7.1 \cdot 10^{-6}$ mol dm^{-3}). A more recent study has confirmed that Hpn can bind up to six Ni(II) ions per monomer [12]. On the other hand, an investigation carried out by converting Hpn into a FRET (fluorescence resonance energy transfer)-based fluorescent sensor [13] reported a K_d value in vitro as low as $7.89 \cdot 10^{-8}$ mol dm^{-3}, while it was not possible to measure any affinity of the Hpn-FRET probe for Ni(II) within *E. coli*, most likely due to the severe control of the levels of this potentially toxic metal inside the cell.

Hpn contains 60 amino acids, 28 of which (47%) are histidines [6] (see Scheme 1). Hpn has several domains capable of coordinating metal cations [14–16], such as the poly-histidine sequences in the positions 11–17, 18–26 and 28–33 [14], the two motifs encompassing a double cysteine residue (EEGCC), in the positions 38–42 and 51–55 [17] and the amino-terminal sequence (Met-Ala-His-), containing a His residue in the third position, which makes it particularly suitable to bind divalent metal ions such as Cu(II) and Ni(II) [18,19]. The coordination ability of this latter sequence, called "ATCUN" (Amino Terminal Cu(II)- and Ni(II)-binding motif) is highly recognized [20] and it has already been studied in the past by our research team, but only in conditions of ligand excess [18].

Although the first three Hpn residues play a major role in the Hpn binding ability towards Ni(II), the additional histidines in positions 4 and 8 can have a non-negligible effect on the stability of the metal complexes, for two main reasons: (i) they can take part in the formation of complexes, forming macrochelated species; (ii) they can anchor a second metal ion. We therefore decided to take a deeper look to these aspects by following two main lines of investigation. First, comparing the affinity towards the Cu(II), Ni(II) and Zn(II) ions of the model peptide corresponding to the N-terminal domain of Hpn, MAHHEEQHG-Am (wild-type, **WT**), with that of its mutants obtained by substitution of one or two His residues with alanine (Ala-scan): MAAHEEQHG-Am (**H3A**), MAHAEEQHG-Am (**H4A**), MAHHEEQAG-Am (**H8A**) and MAHAEEQAG-Am (**H4A/H8A**) (Scheme S1, SI†). All the peptides are protected by amidation at their C-terminus to better simulate the behaviour of the entire protein. Second, in the case of the cupric ion, the complex-formation equilibria under condition of metal excess have been studied, in order to detect the formation of binuclear complexes. Stoichiometry and thermodynamic stability of the formed species have been studied by mass spectrometry and potentiometry under a wide range of pH; the structural hypotheses of the main complexes detected in solution have been suggested on the basis of the results of several spectroscopic techniques.

2. Experimental

2.1. Materials

$CuCl_2$, $ZnCl_2$ and $NiCl_2$ were extra pure products (Sigma-Aldrich); the concentrations of their stock solutions were standardized by EDTA titration and periodically checked via ICP-OES. The carbonate-free stock solutions of 0.1 mol dm^{-3} KOH were prepared by diluting concentrated KOH (Sigma-Aldrich) and then potentiometrically standardized with the primary standard potassium hydrogen phthalate (99.9% purity). All sample solutions were prepared with freshly prepared Milli-Q® water. The HCl and HNO_3 stock solutions were prepared by diluting concentrated ultra-pure HCl and HNO_3 (Sigma-Aldrich) and then standardized with KOH. The ionic strength was adjusted to 0.1 mol dm^{-3} by adding KCl (Sigma-Aldrich). Grade A glassware was employed throughout.

2.2. Peptide synthesis and purification

All the peptides were synthesized according to published methods [21] using Fmoc (fluorenylmethoxycarbonyl protecting group)/t-butyl chemistry with a Syro XP multiple peptide synthesizer (MultiSynTech GmbH, Witten Germany). Rink amide MBHA resin was used as a solid support for the synthesis of all derivatives. Fmoc-amino acids (4-fold excess) were sequentially coupled to the growing peptide chain using DIPCDI/HOBt (N,N′-diisopropylcarbodiimide/1-hydroxybenzotriazole) (4-fold excess) as activating mixture for 1 h at room temperature. Cycles of deprotection of Fmoc (40% piperidine/*N*,*N*-dimethylformamide) and coupling with the subsequent amino acids were repeated until the desired peptide-bound resin was completed. N-terminal acetylation has been performed with acetic anhydride (0.5 mol dm^{-3}) with the presence of *N*-methylmorpholine (0.25 mol dm^{-3}) (3:1 *v*/v; 2 ml/0.2 g of resin) as the last synthetic step. The protected peptide-resin was treated with reagent B [22] (trifluoroacetic acid (TFA)/H20/phenol/triisopropylsilane 88: 5: 5: 2; v/v; 10 mL/0.2 g of resin) for 1.5 h at room temperature. After filtration of the resin, the solvent was concentrated in vacuo and the residue triturated with ethyl ether. Crude peptides were purified by preparative reversed-phase HPLC using a Water Delta Prep 3000 system with a Jupiter column C18 (250 × 30 mm, 300 A, 15 μm spherical particle size). The column was perfused at a flow rate of 20 mL/min with a mobile phase containing solvent A (5%, *v*/v, acetonitrile in 0.1% TFA), and a linear gradient from 0 to 30% of solvent B (60%, v/v, acetonitrile in 0.1% TFA) over 25 min for the elution of peptides. Analytical HPLC analyses were performed on a Beckman 116 liquid chromatograph equipped with a Beckman 166 diode array detector. Analytical purity of the peptides has been assessed using a Zorbax C18 column (4.6 × 150 mm, 3 μm particle size) with the above solvent system (solvents A and B) programmed at a flow rate of 0.5 ml/min using a linear gradient from 0% to 50% B over 25 min. All analogues showed ≥95% purity when monitored at 220 nm. Molecular weight of final compounds was determined by a mass spectrometer ESI Micromass ZMD-2000.

2.3. Potentiometry

Stability constants for proton and metal complexes were calculated from pH-metric titration curves registered at $T = 298$ K and ionic strength 0.1 mol dm^{-3} (KCl). The potentiometric apparatus consisted of an Orion EA 940 pH-meter system provided with a Metrohm 6.0234.100, glass-body, micro combination pH electrode and a dosing system Hamilton MICROLAB 500, equipped with a 0.5 ml micro burette. The thermostated glass-cell was equipped with a magnetic stirring system, a microburet delivery tube and an inlet-outlet tube for the inert gas. High purity grade nitrogen was gently blown over the test solution in order to maintain an inert atmosphere. A constant-speed magnetic stirring was applied throughout. Solutions were titrated with 0.1 mol dm^{-3} carbonate-free KOH. The electrode was daily calibrated for hydrogen ion concentration by titrating HNO_3 with alkaline solution under the same experimental conditions as above. The standard potential and the slope of the electrode couple were computed by means of SUPERQUAD [23] and Glee [24] programs. The purities and the exact concentrations of the ligand solutions were determined by the Gran method [25]. The HYPERQUAD [26] program was employed for the overall formation constant (β) calculations, referred to the following equilibrium:

Table 1
Overall (log β) and step (log K) protonation constants for the studied peptides at $T = 298$ K and $I = 0.1$ mol dm^{-3} (KCl).

Species	WT				H3A		H4A		H8A		H4A/H8A	
	logβ	log$K$	logβ[a]	log$K$[a]	logβ	log$K$	logβ	log$K$	logβ	log$K$	logβ	log$K$
HL^-	7.79(2)	7.79	7.76	7.76	7.81(2)	7.81	7.70(3)	7.70	7.59(1)	7.59	7.59(1)	7.59
H_2L	14.75(1)	6.96	14.69	6.93	14.58(2)	6.77	14.58(3)	6.88	14.41(1)	6.82	14.16(1)	6.57
H_3L^+	21.34(2)	6.59	21.22	6.53	20.87(3)	6.29	20.80(4)	6.22	20.39(2)	5.98	18.76(2)	4.60
H_4L^{2+}	27.06(1)	5.72	27.02	5.80	25.37(2)	4.50	25.24(5)	4.44	24.70(2)	4.31	22.43(2)	3.67
H_5L^{3+}	31.20(2)	4.14	31.17	4.15	28.89(4)	3.52	28.64(3)	3.40	28.29(2)	3.59	–	–
H_6L^{4+}	34.59(2)	3.39	34.56	3.39	–	–	–	–	–	–	–	–

WT - MAHHEEQHG-Am; H3A - MAAHEEQHG-Am; H4A - MAHAEEQHG-Am; H8A - MAHHEEQAG-Am; H4A/H8A - MAHAEEQAG-Am. Values in parentheses are standard deviations on the last significant figure.
[a] Witkowska et al. [18].

$$pM + qL + rH \leftrightarrows M_pL_qH_r$$

(charges omitted; p is 0 in the case of ligand protonation; r can be negative). Step formation constants (K_{step}) and/or acid dissociation constants (K_a) are also reported. The computed standard deviations (referring to random errors only) were given by the program itself and are shown in parentheses as uncertainties on the last significant figure. Hydrolysis constants for metal ions were taken from the literature and suitably extrapolated for the experimental conditions here employed [27,28]. The distribution and the competition diagrams were computed using the HYSS program [29]. In particular, the latter are calculated from the binary speciation models, hypothesizing a solution containing the metal and the various ligands, and admitting that all the components compete with each other to form the respective binary complexes, without mixed species formation.

2.4. Mass spectrometry

High-resolution mass spectra were obtained on a BrukerQ-FTMS spectrometer (Bruker Daltonik, Bremen, Germany), equipped with an Apollo II electrospray ionization source with an ion funnel and on a linear ion trap LTQ XL Mass Spectrometer (Thermo Scientific, Waltham, MA, USA). The mass spectrometer was operated in the positive ion mode. The instrumental parameters for BrukerQ-FTMS spectrometer were as follows: scan range m/z 100–2500, dry gas nitrogen, temperature 453 K and ion energy 5 eV. The capillary voltage was optimized to the highest signal-to-noise ratio, corresponding to 4500 V. Experimental conditions for LTQ XL Mass Spectrometer were as follows: spray voltage 4.8 kV; sheath gas 40 a.u.; capillary temperature 523 K; capillary voltage 8–25 V and tube lens 60–120 V. The samples were prepared in a 1:1 methanol-water mixture at different pH values. The samples ($[ligand]_{tot} = 5 \cdot 10^{-4}$ mol dm^{-3}) were directly infused at a flow rate of 3 μl min^{-1}. Data were processed using the Bruker Compass DataAnalysis 3.4 program. The mass accuracy for the calibration was better than 5 ppm, enabling together with the true isotopic pattern (using SigmaFit) an unambiguous confirmation of the elemental composition of the obtained complex.

2.5. Spectroscopic measurements

The absorption spectra were recorded on a Varian Cary50 Probe spectrophotometer, in the range 350–900 nm, using a quartz cuvette with an optical path of 1 cm. Circular dichroism (CD) spectra were recorded on a Jasco J-1500 CD spectrometer in the 200–800 nm range, using a quartz cuvette with an optical path of 1 cm in the visible and near-UV range. Electron paramagnetic resonance (EPR) spectra were recorded in liquid nitrogen on a Bruker ELEXSYS E500 CW-EPR spectrometer at X-band frequency (9.5 GHz) and equipped with an ER 036TM NMR teslameter and an E41 FC frequency counter. Ethylene glycol (30%) was used as a cryoprotectant for EPR measurements. The EPR parameters were analysed by computer simulation of the experimental spectra using WIN-EPR SIMFONIA software, version 1.2 (Bruker). The concentrations of sample solutions used for spectroscopic studies were similar to those employed in the potentiometric experiment. The UV–Vis, CD and EPR spectroscopic parameters were calculated from the spectra obtained at the pH values corresponding to the maximum concentration of each particular species, based on distribution diagrams.

3. Results and discussion

3.1. Ligand protonation

The five investigated peptides possess two neighbouring Glu residues containing a carboxylic side chain which can release a proton; therefore, they can be represented as H_2L. In addition to these acidic residues, the peptides contain up to three histidines and the unprotected N-terminal amine, which is the most basic group in these ligands. The protonation constants are reported in Table 1, together with the available literature values; representative distribution diagrams are shown as Supplementary Information (Supplementary Figs. S1–S5).

The protonation constants measured in the present work for the wild-type peptide are almost identical to the values previously reported [18]; in the case of mutants, no literature value is available but the present results are in excellent agreement with literature data of other peptides containing the same residues with acid/base properties [30]. The substitution of one or two His residue with Ala does not affect the basicity of the terminal amine, whose log$K$ value ranges in a very narrow interval (7.59–7.81). As for the Glu residues, the most acidic of them is characterized by a log$K$ value of 3.39–3.67 while the second one by a log$K$ value of 4.14–4.60; their acidity increases (and the protonation constant decreases) with the charge of the ligand which in turn depends on the number of (protonated) His residues. Finally, the log$K$ value of the side imidazole groups of histidines spans in the range 5.72–6.96; the available data do not allow to exactly attribute a protonation value to the single His residues, in terms of *micro*-constants. The Ala-scan is unable to identify significant differences in the acidity/basicity of the three single histidines and the only observable trend is the same already reported above for Glu residues: the higher the charge of the peptide, the lower the side-imidazole protonation-constant.

3.2. Binary Cu(II) complexes

3.2.1. MAHHEEQHG-Am (wild-type, **WT**)

As observed above, the N-terminal fragment of Hpn investigated here contains an ATCUN-type metal-binding site, corresponding to the first three residues MAH-, the presence of which strongly characterize the Cu(II) and Ni(II) binding behaviour of this peptide. In a previous investigation on this system [18], performed in the presence of an excess of ligand, only the ATCUN-type coordination mode ($N_{Imidazole}$, N_{NH2}, $2N_{amide}$) was detected and the formation of only mononuclear 1:1 complexes was reported. In that case, only His in position 3 was claimed

Table 2
Cumulative complex-formation constants (β) and acid dissociation constants (K_a) of Cu(II) complexes with the peptide MAHHEEQHG-Am (**WT**), at $T = 298.2$ K and $I = 0.1$ mol dm^{-3} (KCl).

Species	log β	pK_a	log β[a]	pK_a[a]
$[CuH_3L]^{3+}$	25.52(8)	4.03	–	–
$[CuH_2L]^{2+}$	21.49(6)	4.39	–	–
$[CuHL]^{+}$	17.10(5)	4.57	17.38	4.72
[CuL]	12.53(2)	6.17	12.66	5.96
$[CuH_{-1}L]^{-}$	6.36(3)	7.05	−6.70	7.09
$[CuH_{-2}L]^{2-}$	−0.69(4)	–	−0.39	–
$[Cu_2H_{-1}L]^{+}$	10.98(2)	5.52	–	–
$[Cu_2H_{-2}L]$	5.46(3)	–	–	–
$[Cu_2H_{-4}L]^{-2}$	−9.27(3)	9.04		–
$[Cu_2H_{-5}L]^{-3}$	−18.31(5)	–	–	–

Standard deviations on the last figure in parentheses.
[a] Witkowska et al. [18].

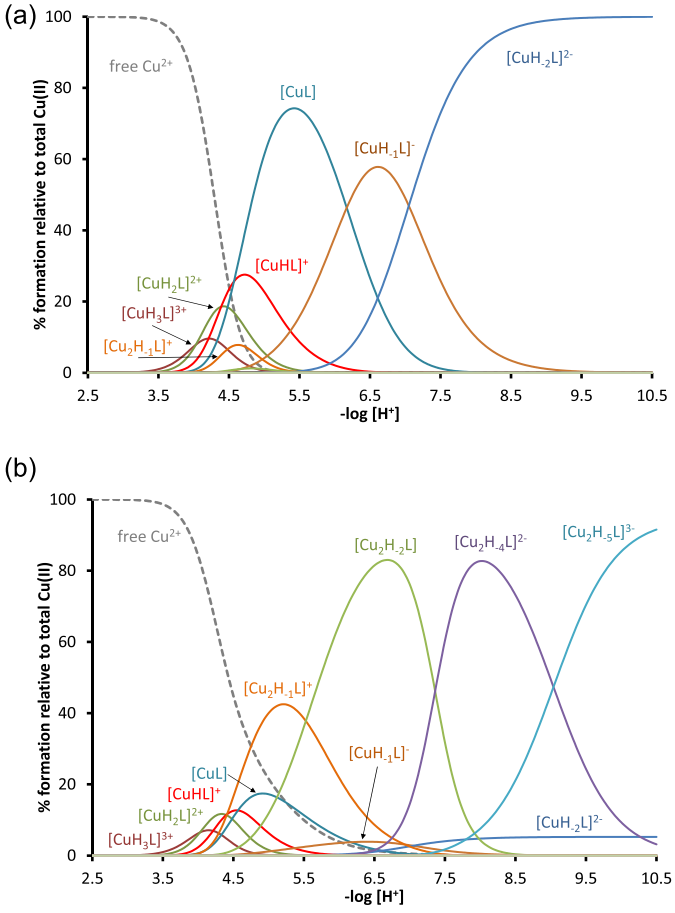

Fig. 1. Representative species distribution diagrams for complex-formation of **WT** with Cu(II), at $T = 25$ °C and $I = 0.1$ mol dm^{-3} (KCl). $C_L = 1.0 \cdot 10^{-3}$ mol dm^{-3} and a) $C_{Cu(II)} = 0.8 \cdot 10^{-3}$ mol dm^{-3}; b) $C_{Cu(II)} = 1.9 \cdot 10^{-3}$ mol dm^{-3}.

to be involved in complexation. However, the presence of two additional His residues can lead to the formation of binuclear complexes also in solutions containing Cu(II) and **WT** in equimolar amount. Therefore, we decided to revisit this system and to extend the investigation to the case of excess of metal ion and to four new mutants where one or two histidines have been replaced by alanine.

As reported in the Experimental section, the thermodynamic investigation of complex-formation equilibria has been performed by means of potentiometric titrations on solutions where the M:L stoichiometric ratio was 0.8:1 or 1.9:1. The speciation model for the system Cu(II)/**WT**, reported in Table 2, was obtained putting all the experimental data together (8 curves, 753 experimental points in the pH range 2.5–11) and a very good fitting was obtained ($\sigma = 1.81$). Of course, given the speciation model, the shape of the corresponding distribution diagram depends on the metal and ligand concentrations: Fig. 1a shows that, when Cu(II) and **WT** are present in solution at a nearly equimolar ratio, six variously protonated mononuclear 1:1 complexes are formed in the explored pH range and they engage all the copper at pH higher than 5.2. The corresponding stoichiometries and formation constants are in very good agreement with literature values. However, at acidic pH, when "free" Cu(II) ions are still available in solution, a not negligible amount of the binuclear species $[Cu_2H_{-1}L]^{+}$ is formed (about 12%). On the other hand, if the metal ion is in excess, practically only binuclear complexes are formed at neutral/alkaline pH (Fig. 1b).

Starting from pH 3.5, the first detected species is $[CuH_3L]^{3+}$, whose stoichiometry indicates that only three residues involved in acid-base reactions are protonated: it is reasonable to assume that the two glutamic acids and a histidine residue are deprotonated. However, at such a pH value, histidine can be deprotonated only if it is coordinated to Cu(II) through the imidazole nitrogen of its side chain (N_{Im}); the participation of one or both carboxylate groups in chelation cannot be excluded. The species $[CuH_3L]^{3+}$ deprotonates with p$K_a = 4.03$ (see Table 2 and mass spectrum in Supplementary Fig. S6, SI†); this value can be explained with the coordination of the terminal amine to form the species $[CuH_2L]^{2+}$, characterized by a "macrocyclic" coordination mode (N_{Im}, NH_2) [31]. By increasing the pH value, the species $[CuHL]^{+}$ and [CuL] begin to form, almost simultaneously, with pK_a values of 4.39 and 4.57, respectively, compatible with the deprotonation and coordination of two amide nitrogens of the peptide chain, which occupy two further equatorial positions in the coordination sphere of the metal ion. This is the "ATCUN coordination mode": (N_{Im}, NH_2, 2 N^-). In excess of ligand (Fig. 1a), the species [CuL] reaches its formation maximum at pH 5.5 and dominates in solution in the range of pH 4.7–6.1, approximately. Since the formation of the first protonated species is extremely overlapped in a narrow pH range, the possibility of formation of binding isomers cannot be excluded. It is worth of note that, also in the presence of a slight excess of peptide with respect to Cu(II) (see the distribution diagram of Fig. 1a), in the acidic pH range, a not negligible amount of the binuclear $[Cu_2H_{-1}L]^{+}$ species is formed. Its possible structure is discussed below where the results of the investigation in excess of metal are reported.

From the qualitative Vis absorption spectra (Supplementary Fig. S7, SI†) recorded at pH lower than 5.0, it is not possible to precisely identify the wavelengths of maximum absorption corresponding to the species $[CuH_3L]^{3+}$, $[CuH_2L]^{2+}$ and $[CuHL]^{+}$, due to the superimposition of these complexes and the interference of the exa-aquo Cu(II) ion, present in solution in a consistent amount up to pH 4.5. In the case of nearly equimolar Cu(II)/**WT** solutions, the UV–Vis spectra recorded at pH 5.0 and 5.5 are instead characterized by a single intense absorption band located at 525 nm (Supplementary Fig. S7a and Supplementary Table S1, SI†), almost entirely attributable to [CuL] and compatible with the coordination hypothesis (N_{Im}, NH_2, 2 N^-) suggested above (expected $\lambda_{max} = 531$ nm [32]). EPR data at pH 5.5 (Supplementary Table S1, SI†) agree with a 4 N coordination around Cu(II) in the equatorial plane of the complex [33]. Above pH 4.5, CD spectra (Supplementary Fig. S8a and Supplementary Table S1, SI†) contain two intense negative bands and one positive signal in the UV region, at 236, 272 and 311 nm, attributable to charge-transfer transitions to Cu(II) by the coordinated amine, imidazole and peptide nitrogens, respectively [34]. As for the Vis range of CD spectra, the typical double band characteristic of the ATCUN-type coordination [20] was observed. No clue was detected of a possible direct involvement of methionine sulphur in peptide coordination.

Finally, again in the presence of ligand excess (Fig. 1a), at neutral/alkaline pH, the species $[CuH_{-1}L]^{-}$ and $[CuH_{-2}L]^{2-}$ are formed, through two deprotonation steps involving the remaining two histidine residues, which do not participate in the complex formation. In fact, the

corresponding pK_a values are respectively 6.17 and 7.05 (Table 2), rather close to those obtained for the free ligand (6.59 and 6.96) (Table 1). This hypothesis is also confirmed by all the spectroscopic data which do not change by increasing the pH value from 5 to 10, as expected if the coordination mode does not change.

The system Cu(II)/**WT** has been explored also at the metal/ligand ratio of (1.9:1)·10^{-3} mol dm^{-3}. As expected, this favours the formation of binuclear species (see ESI-MS spectrum of Supplementary Fig. S9, ESI†) where two Cu(II) ions are coordinated to the same peptide molecule (Fig. 1b). Under these experimental conditions, the complex $[Cu_2H_{-1}L]^+$, which is formed starting from pH 4, reaches a percentage of about 45%, being the predominant species around pH 5.5. It is reasonable to assume that, while one Cu(II) ion is coordinated to the N-terminal domain in the above described ATCUN mode, the second metal atom is bound to one of the two remaining histidines of the chain, with the possible participation of one or both the side carboxylate groups of Glu residues; the stoichiometry of this complex requires that the third histidine is still protonated. Available data do not allow to state if the "anchor" of the second Cu(II) ion is His-4 or His-8; a mixture of these two species is likely. In the pH range 5–8, the third histidine releases its proton, leading to the species $[Cu_2H_{-2}L]$, which dominates at pH 6–7. The corresponding pK_a value (5.52, Table 2) much lower than that measured in the absence of copper (6.96, Table 1), suggests that this His binds the second Cu(II) ion. Moving to alkaline pH, the species $[Cu_2H_{-4}L]^{2-}$ is formed: two protons are released in a quick sequence, probably corresponding to the deprotonation and coordination of two peptide nitrogens. A further deprotonation step is observed at the most alkaline pH values, characterized by a pK_a value of 9.04; it can be attributed to the coordination of a third amide nitrogen, which most likely substitutes one imidazole in the equatorial plane of the complex, leading to the formation of the species $[Cu_2H_{-5}L]^{3-}$, whose binding mode is (N_{Im}, NH_2, 2 N^-)(N_{Im}, 3 N^-). In principle, both His-4 and His-8 can originate this binding mode, where the peptide wraps around the second Cu(II) ion through the coordination of the amide nitrogens of its peptide chain. The significant difference is that, if His-4 is bound to copper in the equatorial plane of the complex, the amide coordination should proceed in the C-terminal direction (due to the presence of the other complexed metal ion) while, in the case of His-8, it can proceed towards the N-terminus. It is well known in the literature that both these modes are possible, but the latter leads to more stable complexes than the former due to the different dimension of the formed chelation rings [35,36].

Spectroscopic data (Supplementary Figs. S7b and S8b; Supplementary Table S2, SI†) confirm the above hypotheses. The two Vis absorption spectra recorded at pH 4.5 and 5.0, where the complex $[Cu_2H_{-1}L]^+$ is the prevailing species in solution, show two maxima: the first, more intense, at $\lambda_{max} = 528$ nm corresponds to the ATCUN coordination mode of the first Cu(II) ion. The second band, around $\lambda_{max} = 740$–730 nm, can be attributed to the coordination of an imidazole nitrogen to the second copper atom with the possible participation of the side carboxylate group of one Glu residue (expected absorption maximum: 731 nm [32]). Increasing the pH, the second band shifts to shorter wavelengths, as a consequence of the coordination of further nitrogens to the second Cu (II) in the C-terminal domain of **WT**. At pH = 11, only one intense absorption band is observed at 520 nm, typical of a Cu(II) species where 3 amidic nitrogens of the peptide chain and one imidazole are bound to the equatorial plane of the complex (expected $\lambda_{max} = 522$ nm [32]). This is exactly the coordination mode suggested above for the second metal ion in the complex $[Cu_2H_{-5}L]^{3-}$. This band is superimposed to that of the ATCUN-type copper. EPR spectra recorded in the presence of excess of Cu(II) are very weak, confirming the formation of binuclear complexes. CD spectra (Supplementary Fig. S8b and Supplementary Table S2, SI†) at pH 5 are practically identical to those already described above for the solutions containing an excess of ligand and referring to the ATCUN-type complex. However, when the Cu(II) ion is instead in excess, increasing the pH value, the shape of CD spectra undergoes a dramatic change, due to the contribution of the second Cu(II) ion. The final spectrum, at pH 10.2, is very similar to that already previously reported for a Cu(II)/peptide binding mode (N_{Im}, 3 N^-) [37], attributable to the species $[Cu_2H_{-5}L]^{3-}$.

Table 3
Cumulative complex-formation constants (β) and acid dissociation constants (K_a) of Cu(II) complexes with the peptide MAAHEEQHG-Am (**H3A**), at T = 298.2 K and I = 0.1 mol dm^{-3} (KCl).

Species	log β	pK_a
$[CuH_2L]^{2+}$	19.59(3)	4.93
$[CuHL]^+$	14.66(2)	5.62
[CuL]	9.04(3)	6.82
$[CuH_{-1}L]^-$	2.22(4)	7.30
$[CuH_{-2}L]^{2-}$	−5.08(5)	10.14
$[CuH_{-3}L]^{3-}$	−15.22(7)	–
$[Cu_2H_{-1}L]^+$	6.76(4)	–
$[Cu_2H_{-3}L]^-$	−6.53(4)	7.68
$[Cu_2H_{-4}L]^{-2}$	−14.21(6)	9.03
$[Cu_2H_{-5}L]^{-3}$	−23.24(7)	11.0
$[Cu_2H_{-6}L]^{-4}$	−34.2(1)	–

Standard deviations on the last figure in parentheses.

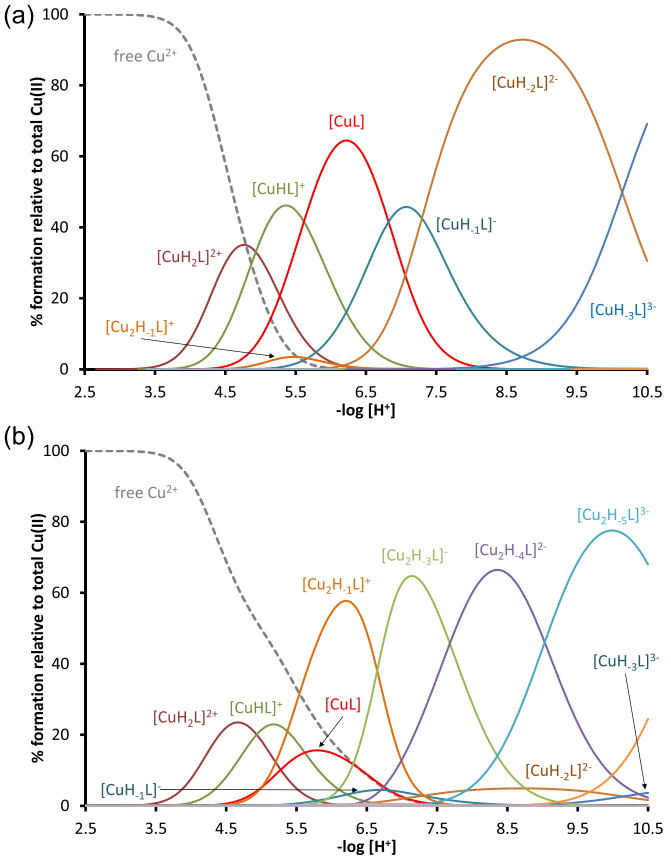

Fig. 2. Representative species distribution diagrams for complex-formation of **H3A** with Cu(II), at T = 25 °C and I = 0.1 mol dm^{-3} (KCl). $C_L = 1.0 \cdot 10^{-3}$ mol dm^{-3} and a) $C_{Cu(II)} = 0.8 \cdot 10^{-3}$ mol dm^{-3}; b) $C_{Cu(II)} = 1.9 \cdot 10^{-3}$ mol dm^{-3}.

3.2.2. *MAAHEEQHG-Am (**H3A**)*

The thermodynamic complex-formation constants for the system Cu (II)/**H3A** are reported in Table 3 and the corresponding distribution diagrams are shown in Fig. 2.

The **H3A** peptide is the only one, in the series here investigated, that does not have a histidine in third position: this definitively influences its ability to coordinate the Cu(II) ion, resulting in complexes which are significantly weaker than those formed by **WT** (over 3.5 orders of

Table 4
Cumulative complex-formation constants (β) and acid dissociation constants (K_a) of Cu(II) complexes with the peptide MAHAEEQHG-Am (**H4A**), at T = 298.2 K and I = 0.1 mol dm^{-3} (KCl).

Species	log β	pK_a
$[CuHL]^{+}$	15.15(3)	4.60
[CuL]	10.55(3)	4.71
$[CuH_{-1}L]^{-}$	5.84(2)	6.83
$[CuH_{-2}L]^{2-}$	−0.99(4)	–
$[Cu_2H_{-1}L]^{+}$	8.74(5)	5.76
$[Cu_2H_{-2}L]$	2.98(7)	6.56
$[Cu_2H_{-3}L]^{-}$	−3.58(7)	6.34
$[Cu_2H_{-4}L]^{-2}$	−9.92(3)	8.88
$[Cu_2H_{-5}L]^{-3}$	−18.80(4)	–

Standard deviations on the last figure in parentheses.

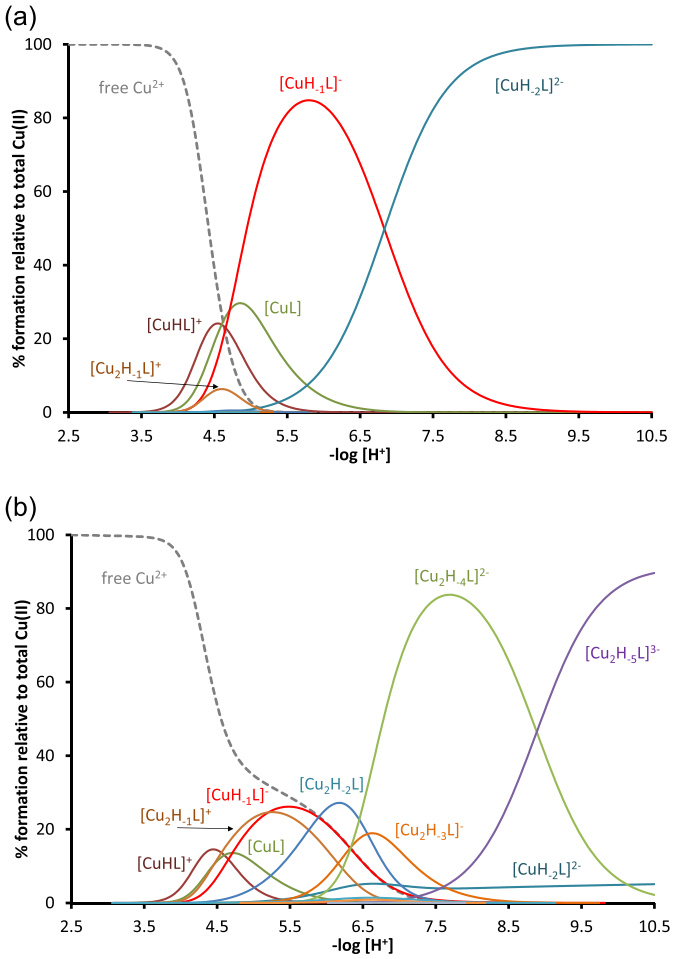

Fig. 3. Representative species distribution diagrams for complex-formation of **H4A** with Cu(II), at T = 25 °C and I = 0.1 mol dm^{-3} (KCl). $C_L = 1.0 \cdot 10^{-3}$ mol dm^{-3} and a) $C_{Cu(II)} = 0.8 \cdot 10^{-3}$ mol dm^{-3}; b) $C_{Cu(II)} = 1.9 \cdot 10^{-3}$ mol dm^{-3}.

magnitude in the case of the species [CuL]). However, the presence of two histidines, separated by three amino acid residues, allows, also in this case, the formation of binuclear complexes, as demonstrated by the mass spectrum of Supplementary Fig. S10b SI†, recorded in excess of metal.

The first species observed at acidic pH is the complex $[CuH_2L]^{2+}$, the main complex up to pH 5. Both its stoichiometry and the spectroscopic parameters (Supplementary Figs. S11 and S12, Supplementary Table S3, SI†) suggest that the metal is bound to the nitrogen of a histidine imidazole side chain, with the possible participation of the carboxylic group of a glutamic acid. Since the sequence contains two His and two Glu residues, it is likely a mixture of complexes in solution with this type of coordination but with different donor atoms involved. The loss of a proton leads to the formation of the $[CuHL]^{+}$ complex, which reaches its maximum at pH 5.5; the experimental value of λ_{max} is very close to that expected for a coordination ($2N_{Im}$, COO^{-}), with the formation of a macrochelate between the two histidines. The corresponding pK_a value (4.98), considerably lower than that measured for the second histidine in the absence of metal (6.77, Table 1), supports this coordination hypothesis.

Starting from pH 4.5, the formation of the complex [CuL] is observed (Fig. 2a). The thermodynamic and spectroscopic parameters suggest the deprotonation and coordination of the terminal amino group, which replaces an imidazole ring in the equatorial plane of the complex (N_{Im}, NH_2, COO^{-}); the fourth vertex of the plane is probably occupied by a water molecule, while the second imidazole ring becomes free or interacts with the metal in axial position. When, on the other hand, the metal ion is in excess, the binuclear complex $[Cu_2H_{-1}L]^{+}$ forms in a considerable amount, in parallel with [CuL]. Here, the additional metal ion is linked to the second histidine and to an amide nitrogen of the peptide chain. Both the complex [CuL] and the species $[Cu_2H_{-1}L]^{+}$, have their formation maximum around pH 6. As pH increases, each metal ion anchored to the peptide is able to gradually displace the amide protons of the chain, thus binding the corresponding amide nitrogens. The wavelength of maximum absorption in the Vis spectra shifts to lower values as the pH increases: the absorption band is narrower and more intense when only mononuclear complexes are present (with a unique and well-defined coordination site) while it is broader for binuclear complexes that contain two similar but not identical metal-binding sites. The CD spectra (Supplementary Fig. S12, SI†) have very similar shapes, especially in their UV portion, confirming that the type of donor atoms is the same in the two cases.

3.2.3. *MAHAEEQHG-Am (**H4A**)*

The thermodynamic complex-formation constants for the system Cu(II)/**H4A** are reported in Table 4 and the corresponding distribution diagrams are shown in Fig. 3.

The replacement of histidine in position 4 with an alanine does not preclude the peptide **H4A** from complexing Cu(II) as described above for **WT**: in fact, His in third position leads to the formation of the stable ATCUN-type complexes, while the presence of a second histidine in position 8 allows the formation of binuclear complexes. The presence of the latter species, detected by potentiometry, was confirmed by the mass spectra recorded in excess of metal (Supplementary Fig. S13, SI†). The speciation model of Table 4 does not differ very much from that determined for the **WT** peptide (Table 2) except for the absence of the most protonated species $[CuH_3L]^{3+}$ and $[CuH_2L]^{2+}$; this is obviously due to the lack of one histidine residue. In excess of ligand, the ATCUN-type complex, with stoichiometry $[CuH_{-1}L]^{-}$, is already the predominant species at pH 5; at alkaline pH, the second histidine releases the proton bound to the pyridine-type nitrogen of its imidazole ring, with a pK_a value (6.83) very similar to that measured in the absence of metal (6.88), thus suggesting the absence of any interaction with the Cu(II) ion already bound to the N-terminal domain. The Vis-absorption (Supplementary Fig. S14a, SI†) and the CD spectra (Supplementary Fig. S15a, SI†) confirm this coordination hypothesis, since they are practically unchanged throughout the explored pH range (Supplementary Table S5, SI†). Interestingly, although the replacement of His in position 4 with Ala does not change the peptide coordination modes, the mono-nuclear complexes of **WT** are more stable than those formed by **H4A** (see competition diagrams discussed below). This result is in agreement with the observation, already widely documented in the literature, that the number of histidine residues of the peptide sequence always has a great influence on the stability of the formed Cu(II) complexes, due to the possibility of forming a number of species with the same stoichiometry but a different set of donor atoms. Lastly, in the presence of metal excess, the spectroscopic data (Supplementary Figs. S14b and S15b,

Table 5
Cumulative complex-formation constants (β) and acid dissociation constants (K_a) of Cu(II) complexes with the peptide MAHHEEQAG-Am (**H8A**), at T = 298.2 K and I = 0.1 mol dm^{-3} (KCl).

Species	log β	pK_a
$[CuH_2L]^{2+}$	19.33(2)	–
$[CuL]$	10.55(1)	4.87
$[CuH_{-1}L]^{-}$	5.68(2)	6.76
$[CuH_{-2}L]^{2-}$	−1.08(4)	–
$[Cu_2H_{-1}L]^{+}$	8.82(5)	5.82
$[Cu_2H_{-2}L]$	3.00(7)	–
$[Cu_2H_{-4}L]^{-2}$	−13.12(3)	9.32
$[Cu_2H_{-5}L]^{-3}$	−22.44(4)	–

Standard deviations on the last figure in parentheses.

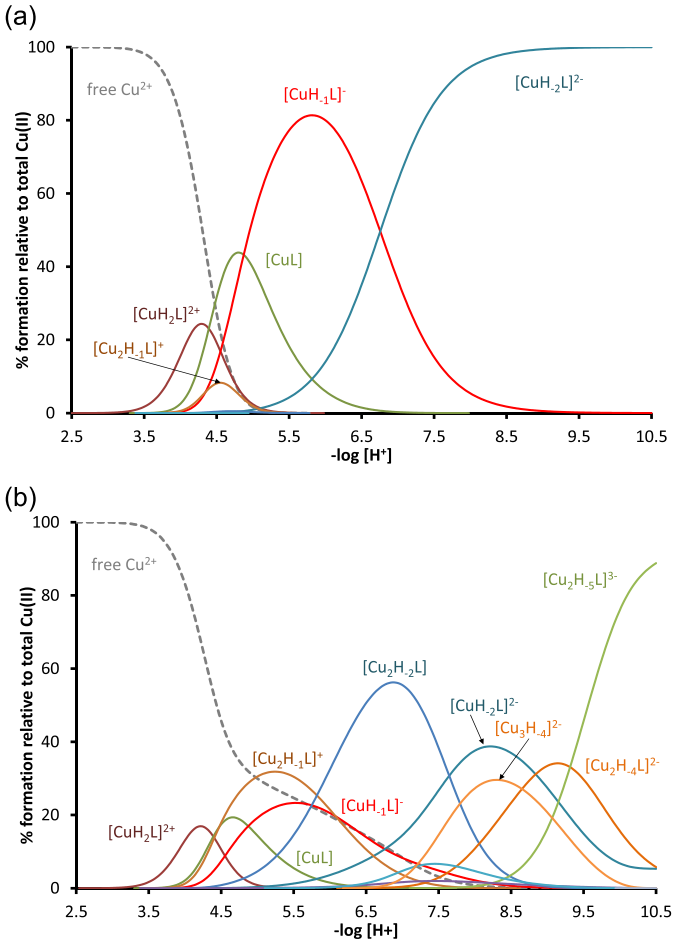

Fig. 4. Representative species distribution diagrams for complex-formation of **H8A** with Cu(II), at T = 25 °C and I = 0.1 mol dm^{-3} (KCl). $C_L = 1.0 \cdot 10^{-3}$ mol dm^{-3} and a) $C_{Cu(II)} = 0.8 \cdot 10^{-3}$ mol dm^{-3}; b) $C_{Cu(II)} = 1.9 \cdot 10^{-3}$ mol dm^{-3}.

Supplementary Table S6, SI†) have a very similar trend to that already discussed above for **WT**, confirming the formation of binuclear species with similar structure and stability of those already described for **WT**.

3.2.4. *MAHHEEQAG-Am (H8A)*

The thermodynamic complex-formation constants for the system Cu(II)/**H8A** are reported in Table 5 and the corresponding distribution diagrams are shown in Fig. 4.

The **H8A** peptide contains two histidine residues which, although close together, can lead to the formation of binuclear species. A first metal ion is bound by the N-terminal ATCUN site, starting from pH 3, and this complex (variously protonated depending on pH) is practically

Table 6
Cumulative complex-formation constants (β) and acid dissociation constants (K_a) of Cu(II) complexes with the peptide MAHAEEQAG-Am (**H4A/H8A**), at T = 298.2 K and I = 0.1 mol dm^{-3} (KCl).

Species	log β	pK_a
$[CuHL]^{+}$	12.95(1)	–
$[CuH_{-1}L]^{-}$	4.27(1)	5.28
$[CuH_{-2}L]^{2-}$	−0.99(1)	–

Standard deviations on the last figure in parentheses.

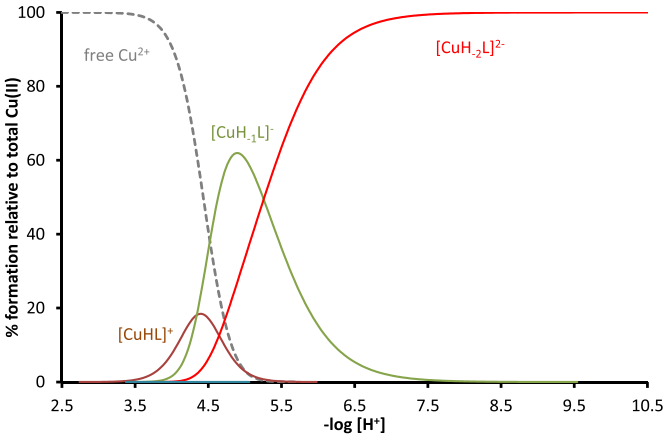

Fig. 5. Representative species distribution diagram for complex-formation of **H4A/H8A** with Cu(II), at T = 25 °C and I = 0.1 mol dm^{-3} (KCl). $C_L = 1.0 \cdot 10^{-3}$ mol dm^{-3} and $C_{Cu(II)} = 0.8 \cdot 10^{-3}$ mol dm^{-3}.

the only species in solution in the presence of ligand excess. If, on the other hand, the metal is in excess, a second Cu(II) ion can first anchor to the histidine in position 4 and then bind, at basic pH, the amides of the peptide backbone in the C-terminal direction. The formation of binuclear complexes, suggested by the potentiometric results of Table 5, is confirmed by the mass spectra, an example of which is shown in Supplementary Fig. S16 SI†. The spectrophotometric results confirm a behaviour similar to that of the other peptides (Supplementary Figs. S17 and S18, Supplementary Tables S7 and S8, SI†). It is worth of note that two consecutive histidines really do give rise to binuclear complexes.

Table 7
Cumulative complex-formation constants (β) and acid dissociation constants (K_a) of Ni(II) complexes with the investigated peptides, at T = 298.2 K and I = 0.1 mol dm^{-3} (KCl).

Ligand	Species	log β	pK_a
MAHHEEQHG-Am (wild-type, **WT**)	$[NiHL]^{+}$	12.90(8)	5.77
	$[NiL]$	7.13(6)	6.26
	$[NiH_{-1}L]^{-}$	0.87(5)	6.95
	$[NiH_{-2}L]^{2-}$	−6.08(5)	–
MAAHEEQHG-Am (**H3A**)	$[NiH_2L]^{2+}$	18.0(2)	6.0
	$[NiHL]^{+}$	11.98(8)	6.25
	$[NiL]$	5.73(6)	7.78
	$[NiH_{-1}L]^{-}$	−2.05(8)	–
	$[NiH_{-3}L]^{3-}$	−18.64(7)	9.1
	$[NiH_{-4}L]^{4-}$	−27.7(1)	–
MAHAEEQHG-Am (**H4A**)	$[NiL]$	6.25(8)	5.49
	$[NiH_{-1}L]^{-}$	0.76(2)	6.89
	$[NiH_{-2}L]^{2-}$	−6.13(5)	–
MAHHEEQAG-Am (**H8A**)	$[NiL]$	6.01(6)	5.75
	$[NiH_{-1}L]^{-}$	0.26(3)	6.72
	$[NiH_{-2}L]^{2-}$	−6.46(4)	–
MAHAEEQAG-Am (**H4A/H8A**)	$[NiH_{-1}L]^{-}$	−0.48(5)	5.55
	$[NiH_{-2}L]^{2-}$	−6.03(1)	–

Standard deviations on the last figure in parentheses.

3.2.5. MAHAEEQAG-Am (H4A/H8A)

The thermodynamic complex-formation constants for the system Cu (II)/MAHAEEQAG-Am (**H4A/H8A**), are reported in Table 6 and the corresponding distribution diagram is shown in Fig. 5. Only the histidine in third position is present in this peptide and, therefore, only mono-nuclear, ATCUN-type complexes are formed in the explored pH range. In addition, Vis absorption data (Supplementary Fig. S19, Supplementary Table S9, SI†) show that, in the presence of Cu(II) excess, the solution becomes cloudy at pH > 7 for the formation of a precipitate, most likely of Cu(II) hydroxide. CD spectra (Supplementary Fig. S20, Supplementary Table S9, SI†) are almost identical at 0.8:1.0 and 1.9:1.0 metal-to-ligand ratios, supporting the absence of polynuclear complexes.

3.3. Binary Ni(II) complexes

The complex-formation equilibria with the Ni(II) ion have been investigated only in the presence of ligand excess and only mono-nuclear complexes have been detected. The speciation models obtained by potentiometry are shown in Table 7, while the corresponding distribution diagrams and all the spectroscopic results are reported as SI† (Supplementary Figs. S22–S41, Supplementary Tables S10–S14). The formation of yellow, diamagnetic, square-planar complexes has been observed at alkaline pH in every system, with a slow kinetics which required rather long waiting times between each titrant addition. No precipitation was observed in the explored pH range.

The presence of the ATCUN type sequence in all peptides, with the exception of **H3A**, favours the Ni(II) coordination to the amino-terminal domain, as already described for copper. The main species at neutral pH is the (N_{Im}, NH_2, 2 N^-) complex, characterized by an intense absorption around 422 nm [20,38]; the corresponding CD spectrum contains, in the Vis range, two bands of opposite sign, at 415 (positive) and 480 (negative) nm, respectively [39–41], and a positive and intense charge-transfer band in the UV region around 260 nm [42,43]. However, it should be noted that the shape of CD spectra referring to the peptides **WT** and **H4A** progressively changes at pH > 9, although no variations are observed either in the absorption spectra or in the distribution diagrams (where the complex $[NiH_{-2}L]^{2-}$ is practically the only species detected in solution at pH > 8). On the contrary, for the **H8A** and **H4A/H8A** peptides, in which the histidine in position 8 has been replaced by an alanine, the CD spectrum simply becomes more intense, as pH increases, without changing shape. Evidently, His-8, when present, is somehow involved in coordination at high pH, for example with a shift of nickel from the N-terminal to the C-terminal domain. However, the available experimental data are not enough to fully clarify this point, which would require further investigation.

A peculiar behaviour is that of **H3A**, due to the lack of the ATCUN-type coordination domain. Likely, at acidic pH, the Ni(II) ion is anchored to one His residue [38,44] and then, as pH increases, macro-chelated species are formed, with the involvement of the second histidine and/or of the terminal amino group. The species formed at acidic pH are probably octahedral; they evolve to the classical square planar, low spin complex at alkaline pH, with the involvement of deprotonated amide nitrogens of the backbone. As a matter of fact, up to four deprotonation steps are revealed by potentiometry at alkaline pH, suggesting the coordination of more than two amide nitrogens to Ni(II). This behaviour is confirmed by spectroscopic data (Supplementary Figs. S28 and S29, SI†): the wavelength of maximum absorption at pH > 10 is 414 nm, lower than that recorded for the other systems (about 422 nm). In addition, the CD spectra in the Vis range show a single broad and intense negative band, located around 440 nm.

3.4. Binary Zn(II) complexes

The Zn(II) ion has a strong affinity for the imidazole nitrogen of histidine, while it is generally accepted that it is not able to displace the protons of the amide nitrogens. In all the studied systems, the formation of 1:1 complexes, variously protonated, was observed (see Table 8, distribution diagrams of Supplementary Figs. S42–S46 SI† and mass spectra of Supplementary Figs. S47–S51 SI†). The first complexes are formed in all systems starting from pH 4.5–5.5: the stoichiometry of these species depends on the number of histidines in the sequence ($[ZnH_2L]^{2+}$ in the case of **WT**; $[ZnHL]^+$ in the case of **H3A**, **H4A** and **H8A**; [ZnL] in the case of **H4A/H8A**). In every case, the stoichiometry requires that two nitrogen atoms are unprotonated and bound to the metal. They should belong to the two available imidazole side chains; or, in the case of **H4A/H8A**, to the histidine and the terminal amino group. It should be noted that, in the case of **WT**, which contains three histidines, a mixture of complexes, with identical stoichiometry and coordination mode but involving different donor atoms, can be formed. This may explain why the $[ZnH_2L]^{2+}$ complex of **WT** begins to form at a pH value (4.5) lower than that observed with the other peptides. It is also worth noting that, when the histidine in position 8 is replaced by an alanine (peptides **H8A** and **H4A/H8A**) the first complexes are formed only at pH around 5.5, suggesting an important role of His-8 as the first metal anchor. All these complexes should be macrochelated, most likely with a tetrahedral geometry, where the two coordination positions not occupied by nitrogens are occupied by water molecules. As the pH increases, the third nitrogen of the peptide, if present, binds the metal by displacing a water molecule. Only in the case of **WT**, zinc can simultaneously coordinate three histidine residues. In addition, also the formation of a species with four nitrogen atoms linked to zinc is theoretically possible for **WT,** corresponding to the complex [ZnL]; this could be the reason for its greater stability (almost two orders of magnitude) compared to the other complexes of the same stoichiometry formed by the other peptides (see Table 8). Unexpectedly, the solutions containing Zn(II) and **WT** are the only ones in which the formation of a precipitate was observed between pH 7 and 10.2. In all other cases, no clouding of the solution was detected, although the potentiometric signal had a slow drift at pH > 8.5. At alkaline pH, further deprotonation steps have been observed, which lead to the formation of the species $[ZnH_{-1}L]^-$ and, only in the case of **H4A/H8A**, also $[ZnH_{-2}L]^{2-}$. The simplest explanation is the deprotonation of the coordinated water molecules.

Table 8
Cumulative complex-formation constants (β) and acid dissociation constants (K_a) of Zn(II) complexes with the investigated peptides, at $T = 298.2$ K and $I = 0.1$ mol dm^{-3} (KCl).

Ligand	Species	log β	pK_a
MAHHEEQHG-Am (wild-type, **WT**)	$[ZnH_2L]^{2+}$	18.79(6)	6.23
	$[ZnHL]^+$	12.56(6)	6.46
	[ZnL]	6.10(4)	–
MAAHEEQHG-Am (**H3A**)	$[ZnHL]^+$	11.71(4)	6.93
	[ZnL]	4.78(4)	8.02
	$[ZnH_{-1}L]^-$	−3.24(5)	–
MAHAEEQHG-Am (**H4A**)	$[ZnHL]^+$	11.69(3)	7.22
	[ZnL]	4.47(6)	8.37
	$[ZnH_{-1}L]^-$	−3.9(1)	–
MAHHEEQAG-Am (**H8A**)	$[ZnHL]^+$	10.71(6)	6.58
	[ZnL]	4.13(3)	8.23
	$[ZnH_{-1}L]^-$	−4.10(4)	–
MAHAEEQAG-Am (**H4A/H8A**)	[ZnL]	3.88(6)	7.84
	$[ZnH_{-1}L]^-$	−3.96(6)	8.46
	$[ZnH_{-2}L]^{2-}$	−12.42(6)	–

Standard deviations on the last figure in parentheses.

3.5. Ternary Cu(II)/Ni(II)/WT complexes

Data reported above show that, in the presence of Cu(II) excess, the **WT** peptide can form binuclear species. Therefore, we decided to test its behaviour in the presence of equimolar quantities of Cu(II) and Ni(II).

Table 9
Cumulative complex-formation constants (β) and acid dissociation constants (K_a) of mixed Cu(II)/Ni(II) complexes with peptide **WT**, at $T = 298.2$ K and $I = 0.1$ mol dm^{-3} (KCl).

Species	log β	pK_a
$[CuNiH_{-1}L]^{+}$	9.97(6)	6.57
$[CuNiH_{-2}L]$	3.40(4)	–
$[CuNiH_{-5}L]^{3-}$	−23.74(4)	–

Standard deviations on the last figure in parentheses.

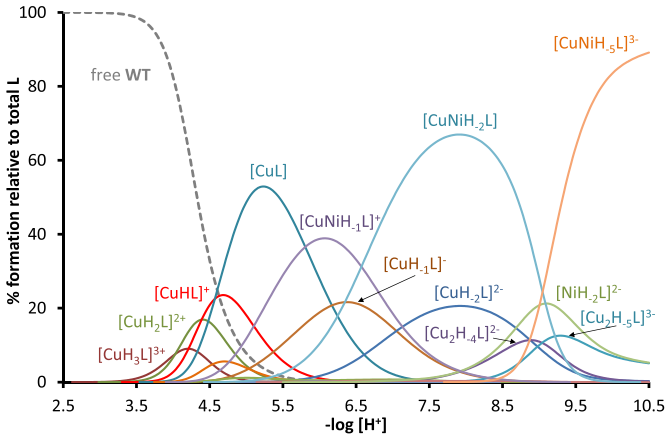

Fig. 6. Representative species distribution diagram for complex-formation in the ternary Cu(II)/Ni(II)/**WT** system, at $T = 25$ °C and $I = 0.1$ mol dm^{-3} (KCl). $C_L = C_{Cu(II)} = C_{Ni(II)} = 1.0 \cdot 10^{-3}$ mol dm^{-3}.

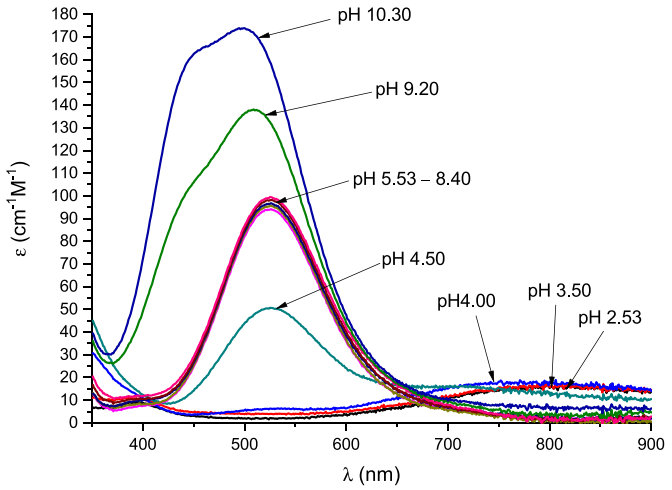

Fig. 7. Vis absorption spectra for Cu(II)/Ni(II) complexes with **WT**; $C_L = 1.0 \cdot 10^{-3}$ mol dm^{-3}, Cu(II):L = 0.8: 1, Ni(II):L = 0.9:1.

First, from a qualitative point of view, it was possible to observe, during the titrations with KOH, that the solution, initially colorless, assumed a pink color at acidic pH close to neutrality and then turned to orange at basic pH.

Potentiometric data processing revealed the formation of three hetero-metallic binuclear species, as reported in Table 9; the corresponding distribution diagram is shown in Fig. 6. This result is in excellent agreement with a recent study carried out under similar conditions on the AAHAAAHG octapeptide [45]. Although that paper does not report the complex-formation constants of the mixed species, the stoichiometry of the ternary complex formed at basic pH, obtained from mass spectra, is exactly $[CuNiH_{-5}L]^{2-}$, which corresponds (except for the different charge due to the different number of carboxylic groups of the sequence) to that obtained in the present investigation. Furthermore, the absorption spectra shown in Fig. 7 are very similar to those reported by Grenacs et al. [45], suggesting the same coordination geometry. Therefore, it can be assumed that, at acidic pH, Cu(II) coordinates at the N-terminus of **WT** (with the ATCUN-type coordination mode); as pH is increased, a nickel ion initially binds the two histidine residues not involved in copper coordination. Starting from pH about 9, the Ni(II) ion displaces up to 3 amide hydrogens of the peptide chain, thus forming the classic planar and diamagnetic 4 N complex. It is reasonable to assume that, in the species $[CuNiH_{-5}L]^{3-}$ (which dominates at pH > 9, see Fig. 6) the Ni(II) ion is bound to His-8 and to the three preceding amides, in the N-terminal direction. In the pH range 4.5–8.5, the absorption spectra are practically identical and dominated by the d-d transition of the Cu(II) ATCUN-type complex; at more alkaline pH values, the typical band of the diamagnetic Ni(II) complex becomes instead evident.

ESI-MS spectra recorded at pH 5.5, 7.8 and 10.2 (Supplementary Fig. S52 SI†) also highlight the formation of binuclear complexes with Cu(II) and Ni(II) at different protonation states and they are in good agreement with the speciation model obtained by potentiometry. Following the distribution diagram plotted in Fig. 6, the observed more intense *m/z* signals correspond to the major species in solution under the given pH.

Table 10
Calculated dissociation constants (K_d/mol dm^{-3}), pM and p$L_{0.5}$ values for Cu(II) complexes with the investigated peptides.

	K_d[a]		pCu[b]		p$L_{0.5}$[c]	
	pH = 7.4	pH = 5.4	pH = 7.4	pH = 5.4	pH = 7.4	pH = 5.4
WT	$2.35 \cdot 10^{-14}$	$9.95 \cdot 10^{-8}$	14.408	7.959	12.27	7.00
H3A	$4.03 \cdot 10^{-10}$	$1.65 \cdot 10^{-5}$	10.173	6.198	9.23	4.59
H4A	$4.48 \cdot 10^{-14}$	$2.26 \cdot 10^{-7}$	14.128	7.610	12.25	6.64
H8A	$4.63 \cdot 10^{-14}$	$1.31 \cdot 10^{-7}$	14.113	7.841	12.24	6.88
H4A/H8A	$4.26 \cdot 10^{-14}$	$2.52 \cdot 10^{-7}$	14.150	7.565	12.25	6.60
DAHK-Am[d]	$1.69 \cdot 10^{-14}$	$7.30 \cdot 10^{-8}$	14.550	8.093	12.28	7.14

[a] Kozlowski et al. [46].
[b] $[L]_{total} = 10^{-5}$ M and $[M]_{total} = 10^{-6}$ M; Crisponi et al. [47].
[c] Crea et al. [48].
[d] Speciation model taken from: Sokolowska et al. [40].

Table 11
Calculated dissociation constants (K_d/mol dm^{-3}), pM and p$L_{0.5}$ values for Ni(II) complexes with the investigated peptides, at pH = 7.4.

	K_d	pNi	p$L_{0.5}$
WT	$6.19 \cdot 10^{-9}$	9.163	8.21
H3A	$5.24 \cdot 10^{-6}$	6.444	5.28
H4A	$5.89 \cdot 10^{-9}$	9.184	8.23
H8A	$1.13 \cdot 10^{-8}$	8.901	7.95
H4A/H8A	$4.72 \cdot 10^{-9}$	9.281	8.33
DAHK-Am[a]	$1.85 \cdot 10^{-9}$	9.689	8.73

[a] Speciation model taken from: Sokolowska et al. [40].

3.6. Comparison of complex stability

When the various histidines of a peptide sequence have very similar chemical environments, spectroscopic techniques are unable to distinguish the behaviour of each specific residue. Hence the need to study series of analogues, e.g. with the Ala-scan method used here. To obtain the required information, the stability of the complexes formed by the different mutants must be compared; however, this cannot be directly

Table 12
Calculated dissociation constants (K_d/mol dm^{-3}), pM and $pL_{0.5}$ values for Zn(II) complexes with the investigated peptides, at pH = 7.4.

	K_d	pZn	$pL_{0.5}$
WT	$3.17 \cdot 10^{-6}$	6.582	5.49
H3A	$4.44 \cdot 10^{-5}$	6.084	4.34
H4A	$6.99 \cdot 10^{-5}$	6.056	4.14
H8A	$1.70 \cdot 10^{-4}$	6.024	3.76
H4A/H8A	$2.65 \cdot 10^{-4}$	6.016	3.56

done through the stability constants, since the complexes have different stoichiometry and/or protonation degree. For this purpose, the parameters reported in Tables 10–12 have been calculated. The general meaning of these parameters is to give an overall estimation of the metal-ligand "affinity", under well-defined experimental conditions of pH and component concentration, which summarizes all the metal-ligand interactions that give rise to the speciation models described above. In particular, K_d (expressed as molarity, mol dm^{-3}) corresponds to the concentration of free metal when the ligand is half in the form of a complex (whatever its stoichiometry) and half not complexed [46]. K_d depends on pH but not on the ligand concentration and the smaller it is, the greater the complexes stability is. This parameter is widely used in biochemistry, assuming that, if the K_d value is equal to or less than the free metal concentration estimated (or measured) in the biological environment, then the ligand can "capture" the metal. A similar meaning can also be attributed to pM (= $-\log[M]_{free}$); in this case a higher value means that the ligand is more effective in metal sequestration [47]. The parameter $pL_{0.5}$, recently introduced by Sammartano and coworkers [48], refers to the quantity of ligand (expressed as -log$[L]_{tot}$) required to bind 50% of the metal present in traces (typically $[M]_{tot} = 1 \cdot 10^{-12}$ mol dm^{-3}). This parameter takes into account the action of all the other possible competing ligands present in solution (the speciation model of which must be known) and it is the greater the smaller the quantity of ligand required, i.e. the stronger the metal-ligand affinity. The values of K_d, pM and $pL_{0.5}$, at different pH and for all the systems studied are shown in Tables 10–12 together with reference values for the tetrapeptide DAHK-Am, corresponding to the ATCUN site of human albumin.

As for the Cu(II) complexes, from Table 10 it is clear that the best ligand in the series is human albumin at both pH 7.4 and 5.4: although the coordination site is always of the ATCUN type and therefore the binding mode is very similar for all peptides (with the exception of **H3A**), the particular albumin sequence is favored probably due to the presence of the aspartic acid residue, whose side carboxyl group can participate in the metal complexation through an axial interaction [49,50]. In the series of Hpn protein analogues, **WT** forms the most stable complexes: the presence of an extra histidine residue and the possibility of forming different complexes with identical stoichiometry but different set of donor atoms is probably the reason of this greater affinity. The differences between the **H4A**, **H8A** and **H4A/H8A** ligands, which have an identical ATCUN site but different combinations of additional histidines, are of minor importance, although it can be observed that the **H4A/H8A** peptide, which only possesses one histidine in position 3 (and which consequently cannot form binuclear complexes), has the lowest affinity. A significantly lower strength as Cu(II) ligand is shown by **H3A**, where the histidine in position 3, responsible for the ATCUN sequence, was replaced by alanine. As expected, the His-3 residue is crucial to confer high Cu(II) binding affinity to the studied peptides like in human albumin. Similar considerations can be deduced from the competition diagram reported as Supplementary Material (Supplementary Fig. S53, SI†), which allow to compare the strength of the ligands in a wide pH range.

Also in the case of Ni(II) complexes, the best ligand proved to be DAHK-Am (Table 11). Surprisingly, the peptide of the series which has the second-best affinity for Ni(II) is **H4A/H8A**, which contains less histidines than all the others. Evidently, the ATCUN binding motif, which leads to the formation of strictly square-planar Ni(II) complexes plays a major role and the presence of additional histidines is negligible, or even disturbing, when moving towards neutral and alkaline pH, as it can be observed from the competition diagram of Supplementary Fig. S54, SI†. On the other hand, His-8 (which is absent in **H8A**) seems to contribute to the stability of the system; moreover, as discussed in the previous section, the obtained CD data for **WT** and **H4A** undergo a shape variation at pH > 9, suggesting that His-8 is somehow involved in coordination at alkaline pH. Once again, the lack of the His residue in position 3 strongly penalizes the **H3A** peptide, as already observed in the case of Cu(II).

The coordination modes of the Zn(II) ion are very different from those of Cu(II) and Ni(II), as described above. In this case, the number of histidine residues of the peptide plays a major role in establishing its affinity towards the metal. The results reported in Table 12 and Supplementary Fig. S55 SI† show that **WT** is by far the strongest ligand of the series, at acidic pH; it is the only one which can form Zn(II) complexes with three imidazole nitrogens as donor atoms. In contrast, **H4A/H8A** is the weakest ligand; in fact, it possesses only one histidine. Moreover, the zinc affinity is significantly lower for the **H3A** and **H8A** peptides than for the **H4A** ligand, although all the three of them possess two histidines. This result suggests a minor role for His-4, with respect to His-3 and His-8, in zinc chelation.

Finally, the data of Tables 10–12 clearly show that, under the same experimental conditions, the N-terminal domain of Hpn (represented by **WT**) has great selectivity towards the metals studied with affinities in the following order: Cu(II) >> Ni(II) > Zn(II). Similar considerations also apply to the other peptides. As already described above, a recent study [13] reported, in the case of Ni(II), a K_d value for the Hpn protein of $7.89 \cdot 10^{-8}$. It can be considered in a reasonably good agreement with the value measured in the present work for the Ni(II)/**WT** system ($6.19 \cdot 10^{-9}$ M, Table 11), also taking into account that the experimental conditions are rather different. Hence, it can be deduced that the amino-terminal ATCUN site of Hpn plays an important role in the nickel coordination. On the contrary, in the case of Zn(II), the K_d value measured here for the peptide **WT** ($3.17 \cdot 10^{-6}$ mol dm^{-3}, Table 12) is much higher than that reported by Wegner et al. for the Hpn protein ($1.03 \cdot 10^{-9}$ mol dm^{-3}). This is attributable to the fact that Hpn has other binding sites rich in histidine and cysteine residues which have a greater affinity for zinc than the amino-terminal domain.

4. Conclusions

The studied peptides proved to be good chelators for divalent copper, nickel and zinc ions. With the exception of **H3A**, all the investigated sequences contain a very efficient Cu(II) and Ni(II) ATCUN-binding site (N_{Im}, NH_2, 2 N^-) which is confirmed to confer great stability to copper and nickel complexes. Furthermore, the presence of additional histidines in position 4 and 8 allows the formation of stable homo- and hetero-binuclear complexes. In the case of Zn(II) ion, the ligand effectiveness is not strictly affected by the presence of the ATCUN sequence, but most likely depends on the number of available histidines, which act as multiple metal anchoring sites and allow the formation of macrochelate systems. The binding strength of the N-terminus of Hpn protein has been compared with that of the other studied binding sites of Hpn, i.e. the two motifs containing a double cysteine residue in the positions 38–42 and 51–55 [17] and the poly-histidine sequence in the positions 18–26 [14]. The corresponding competition diagrams are reported as Supplementary Information (Supplementary Figs. S56, S57 SI†). The -Cys-Cys- motifs are stronger than the N-terminal ATCUN site, both for Ni(II) and Zn(II) coordination. On the other hand, the poly-His sequence corresponding to the 18–26 domain of Hpn can compete with the N-terminus only at acidic pH value. In view of the fact that Hpn can bind up to five Ni(II) ions, we can suggest that all these four studied binding sites are involved in nickel trafficking. It looks reasonable that, at low nickel levels, the

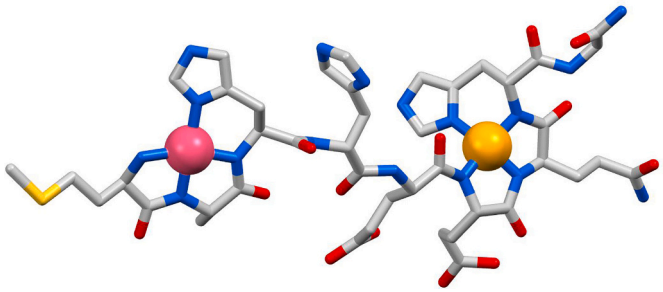

Fig. 8. Proposed molecular structure for the hetero-binuclear complex $[CuNiH_{-5}L]^{3-}$. Cu(II) atom (in purple) is bound to the ATCUN site (N_{Im}, NH_2, 2 N^-), Ni(II) atom (in yellow) displays a (N_{Im}, 3 N^-) coordination mode. (For interpretation of the references to color in this figure legend, the reader is referred to the web version of this article.)

cysteine binding sites are saturated with nickel before than His binding sites.

The formation of binuclear Cu(II) complexes have been extensively studied; from the obtained results one can generally assume that the first Cu(II) ion interacts with the peptide at the very effective N-terminal ATCUN site (if present), while a second Cu(II) ion can further coordinate the histidine residues in position 4 and 8. However, His-8 seems to be the favorite site, due to the possibility to further coordinate the amide nitrogen towards the N-terminal direction, forming a stable 5/6-membered chelate rings.

As expected from the Irving-Williams series [51], the N-terminal domain of Hpn displays metal-binding affinities in the order Zn(II) < Ni (II) << Cu(II). In particular, this means that Cu(II), even if present in low amount, can replace Ni(II) in the Hpn protein coordination. Moreover, the **WT** model peptide was proved to form hetero-binuclear complexes, where the ATCUN sequence interacts exclusively with Cu(II) while nickel preferentially binds the histidine residue in position 8 (second binding site) to form its typical square planar complex (N_{Im}, 3 N^-)(see Fig. 8). In the interaction of Cu(II) with a binary Ni(II)/**WT** complex, the nickel ion can be either released or even moved from the ATCUN site to the second binding site. In both cases the activity of Hpn protein is disturbed. In fact, Supplementary Figs. S58, S59 SI† show that, in the presence of only a 20% of Cu(II) with respect to Ni(II), not only mixed Cu (II)/Ni(II) species are formed in the entire pH range, but, at neutral pH, some Ni(II) is still not complexed (see Supplementary Fig. S23 SI† for the sake of comparison in the absence of copper). When thinking about possible antimicrobial strategies, a suitable Cu(II) complex, sufficiently stable to reach the bacterium but weaker that that formed with Hpn, could be employed as a pharmacophore, with the aim of producing a "ligand exchange" reaction, where Cu(II) ions substitute Ni(II) ions at the Hpn ATCUN domain; in a possible additional second step, the released Ni(II) ions could even be sequestered by the metal-free pharmacophore and eliminated. This action would partially inhibit the Hpn efficiency in Ni(II) recruitment and storage, thus helping the nutritional immunity mechanism to starve the pathogen. A similar action could also be obtained with the more safe Zn(II) ion, but it would require very high Zn(II) concentration, since its affinity for Hpn, at least as far as the N-terminus is concerned, is much lower than that of Ni(II). Anyway, Supplementary Fig. S60 SI† shows that, in the presence of a 10-fold excess of Zn(II) with respect to Ni(II), the most acidic pH values are dominated by Zn(II) complexes, and, at neutral pH, about 30% of the peptide is engaged in zinc binding.

The strategy of distressing bacterial nickel homeostasis by means of competing metals (or ligands) looks promising in order to find new therapeutic ways to eradicate *H. pylori* and a detailed understanding of metal binding modes in bacterial metal chaperones is a valuable "brick in the wall" which aims to stop the pathogens from spreading.

Declaration of Competing Interest

The authors declare that they have no known competing financial interests or personal relationships that could have appeared to influence the work reported in this paper.

Acknowledgements

Financial support by University of Ferrara (FAR 2020), the National Science Centre (UMO-2017/26/A/ST5/00364 and UMO-2017/26/A/ST5/00363) and by the Erasmus+ Programme are gratefully acknowledged. This paper is based upon work from COST Action CA18202, NECTAR – Network for Equilibria and Chemical Thermodynamics Advanced Research, supported by COST (European Cooperation in Science and Technology). The authors would thank dr. Claudia Stevanin for her assistance in the acquisition and interpretation of some ESI-MS spectra.

Appendix A. Supplementary data

Supplementary data to this article can be found online at https://doi.org/10.1016/j.jinorgbio.2020.111304.

References

[1] C. de Martel, J. Ferlay, S. Franceschi, J. Vignat, F. Bray, D. Forman, M. Plummer, Lancet Oncol. 13 (2012) 607–615.
[2] Z. Saylor, R. Maier, Microbiology 164 (2018) 1059–1068.
[3] D.R. Scott, D. Weeks, C. Hong, S. Postius, K. Melchers, G. Sachs, Gastroenterology 114 (1998) 58–70.
[4] N.-C. Ha, S.-T. Oh, J.Y. Sung, K.A. Cha, M.H. Lee, B.-H. Oh, Nat. Struct. Biol. 8 (2001) 505–509.
[5] J.W. Olson, R.J. Maier, Science 298 (2002) 1788.
[6] J.V. Gilbert, J. Ramakrishna, F.W. Sunderman, A. Wright, A.G. Plaut, Infect. Immun. 63 (1995) 2682.
[7] R.J. Maier, S.L. Benoit, S. Seshadri, Biometals 20 (2007) 655–664.
[8] S. Seshadri, S.L. Benoit, R.J. Maier, J. Bacteriol. 189 (2007) 4120–4126.
[9] G. Wang, P. Alamuri, R.J. Maier, Mol. Microbiol. 61 (2006) 847–860.
[10] H. Zeng, G. Guo, X.H. Mao, W. De Tong, Q.M. Zou, Curr. Microbiol. 57 (2008) 281–286.
[11] R. Ge, Rory M. Watt, X. Sun, Julian A. Tanner, Q.-Y. He, J.-D. Huang, H. Sun, Biochem. J. 393 (2005) 285–293.
[12] R.M. Shelake, Y. Ito, J. Masumoto, E.H. Morita, H. Hayashi, PLoS One 12 (2017) e0172182.
[13] S.V. Wegner, E. Ertem, M. Sunbul, C. He, Chem. Sci. 2 (2011) 451–456.
[14] D. Witkowska, R. Politano, M. Rowinska-Zyrek, R. Guerrini, M. Remelli, H. Kozlowski, Chem. Eur. J. 18 (2012) 11088–11099.
[15] M. Rowinska-Zyrek, J. Zakrzewska-Czerwinska, A. Zawilak-Pawlik, H. Kozlowski, Dalton Trans. 43 (2014) 8976–8989.
[16] M. Rowinska-Zyrek, D. Witkowska, S. Potocki, M. Remelli, H. Kozlowski, New J. Chem. 37 (2013) 58–70.
[17] M. Rowinska-Zyrek, D. Witkowska, S. Bielinska, W. Kamysz, H. Kozlowski, Dalton Trans. 40 (2011) 5604–5610.
[18] D. Witkowska, S. Bielinska, W. Kamysz, H. Kozlowski, J. Inorg. Biochem. 105 (2011) 208–214.
[19] N.M. Chiera, M. Rowinska-Zyrek, R. Wieczorek, R. Guerrini, D. Witkowska, M. Remelli, H. Kozlowski, Metallomics 5 (2013) 214–221.
[20] C. Harford, B. Sarkar, Acc. Chem. Res. 30 (1997) 123–130.
[21] N.L. Benoiton, Chemistry of Peptide Synthesis, Taylor & Francis, London, 2005.
[22] N.A. Sole, G. Barany, J. Organomet. Chem. 57 (1992) 5399–5403.
[23] P. Gans, A. Sabatini, A. Vacca, Dalton Trans. (1985) 1195–1200.
[24] P. Gans, B. O'Sullivan, Talanta 51 (2000) 33–37.
[25] G. Gran, Acta Chem. Scand. 4 (1950) 559–577.
[26] P. Gans, A. Sabatini, A. Vacca, Talanta 43 (1996) 1739–1753.
[27] G. Arena, R. Cali, E. Rizzarelli, S. Sammartano, Therm. Acta 16 (1976) 315–321.
[28] C.F. Baes, R.S. Mesmer, The Hydrolysis of Cations, John Wiley & Sons, Ltd, New York, 1976.
[29] L. Alderighi, P. Gans, A. Ienco, D. Peters, A. Sabatini, A. Vacca, Coord. Chem. Rev. 184 (1999) 311–318.
[30] L.D. Pettit, H.K.J. Powell, The IUPAC Stability Constants Database, Royal Society of Chemistry, London, 1992–2000.
[31] I. Sóvágó, K. Várnagy, N. Lihi, Á. Grenács, Coord. Chem. Rev. 327-328 (2016) 43–54.
[32] H. Sigel, R.B. Martin, Chem. Rev. 82 (1982) 385–426.
[33] J. Peisach, W.E. Blumberg, Arch. Biochem. Biophys. 165 (1974) 691–708.
[34] P.G. Daniele, E. Prenesti, G. Ostacoli, Dalton Trans. (1996) 3269–3275.
[35] D. Bellotti, C. Tocchio, R. Guerrini, M. Rowińska-Żyrek, M. Remelli, Metallomics 11 (2019) 1988–1998.

[36] K. Krupa, M. Korabik, T. Kowalik-Jankowska, J. Inorg. Biochem. 201 (2019) 110819.
[37] C. Conato, H. Kozłowski, P. Młynarz, F. Pulidori, M. Remelli, Polyhedron 21 (2002) 1469–1474.
[38] M. Rowińska-Żyrek, H. Kozłowski, Nickel binding sites – coordination modes and thermodynamics, in: The Biological Chemistry of Nickel, The Royal Society of Chemistry, 2017, pp. 43–59.
[39] W. Bal, M. Jeżowska-Bojczuk, K.S. Kasprzak, Chem. Res. Toxicol. 10 (1997) 906–914.
[40] M. Sokolowska, A. Krezel, M. Dyba, Z. Szewczuk, W. Bal, Eur. J. Biochem. 269 (2002) 1323–1331.
[41] M. Peana, K. Zdyb, S. Medici, A. Pelucelli, G. Simula, E. Gumienna-Kontecka, M. A. Zoroddu, J. Trace Elem. Med. Biol. 44 (2017) 151–160.
[42] J.D. Van Horn, G. Bulaj, D.P. Goldenberg, C.J. Burrows, J. Biol. Inorg. Chem. 8 (2003) 601–610.
[43] W. Bal, J. Lukszo, K.S. Kasprzak, Chem. Res. Toxicol. 9 (1996) 535–540.
[44] W. Bal, H. Kozlowski, R. Robbins, L.D. Pettit, Inorg. Chim. Acta 231 (1995) 7–12.
[45] Á. Grenács, A. Kaluha, C. Kállay, V. Jószai, D. Sanna, I. Sóvágó, J. Inorg. Biochem. 128 (2013) 17–25.
[46] H. Kozlowski, M. Łuczkowski, M. Remelli, Dalton Trans. 39 (2010) 6371–6385.
[47] G. Crisponi, M. Remelli, Coord. Chem. Rev. 252 (2008) 1225–1240.
[48] F. Crea, C. De Stefano, C. Foti, D. Milea, S. Sammartano, Curr. Med. Chem. 21 (2014) 3819–3836.
[49] J.P. Laussac, B. Sarkar, J. Biol. Chem. 255 (1980) 7563–7568.
[50] J.P. Laussac, B. Sarker, Biochemistry 23 (1984) 2832–2838.
[51] H. Irving, R.J.P. Williams, J. Chem. Soc. (1953) 3192–3210.

Inorganic Chemistry
Cite This: Inorg. Chem. 2020, 59, 274−286
Article
pubs.acs.org/IC

Binding and Reactivity of Copper to R_1 and R_3 Fragments of tau Protein

Chiara Bacchella,[†] Silvia Gentili,[‡] Denise Bellotti,[§] Eleonora Quartieri,[‡] Sara Draghi,[∥] Maria Camilla Baratto,[∥] Maurizio Remelli,[§] Daniela Valensin,[∥] Enrico Monzani,[†] Stefania Nicolis,[†] Luigi Casella,[†] Matteo Tegoni,*[,‡] and Simone Dell'Acqua*[,†]

[†]Dipartimento di Chimica, Università di Pavia, Via Taramelli 12, 27100 Pavia, Italy

[‡]Dipartimento di Scienze Chimiche, della Vita e della Sostenibilità Ambientale, Università di Parma, Parco Area delle Scienze 11/A, 43124 Parma, Italy

[§]Dipartimento di Scienze Chimiche e Farmaceutiche, Università di Ferrara, Via Luigi Borsari 46, 44121 Ferrara, Italy

[∥]Dipartimento di Biotecnologie, Chimica e Farmacia, Università di Siena, Via A. Moro 2, 53100, Siena, Italy

Supporting Information

ABSTRACT: Tau protein is present in significant amounts in neurons, where it contributes to the stabilization of microtubules. Insoluble neurofibrillary tangles of tau are associated with several neurological disorders known as tauopathies, among which is Alzheimer's disease. In neurons, tau binds tubulin through its microtubule binding domain which comprises four imperfect repeats (R_1−R_4). The histidine residues contained in these fragments are potential binding sites for metal ions and are located close to the regions that drive the formation of amyloid aggregates of tau. In this study, we present a detailed characterization through potentiometric and spectroscopic methods of the binding of copper in both oxidation states to R_1 and R_3 peptides, which contain one and two histidine residues, respectively. We also evaluate how the redox cycling of copper bound to tau peptides can mediate oxidation that can potentially target exogenous substrates such as neuronal catecholamines. The resulting quinone oxidation products undergo oligomerization and can competitively give post-translational peptide modifications yielding catechol adducts at amino acid residues. The presence of His−His tandem in the R_3 peptide strongly influences both the binding of copper and the reactivity of the resulting copper complex. In particular, the presence of the two adjacent histidines makes the copper(I) binding to R_3 much stronger than in R_1. The copper−R_3 complex is also much more active than the copper−R_1 complex in promoting oxidative reactions, indicating that the two neighboring histidines activate copper as a catalyst in molecular oxygen activation reactions.

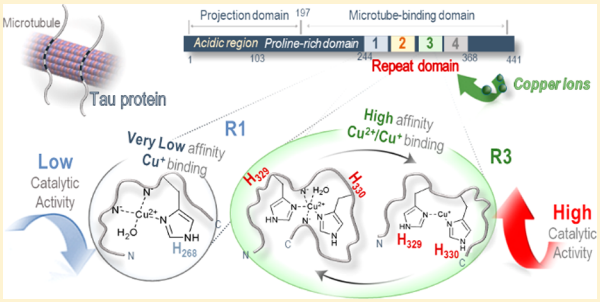

INTRODUCTION

Tau proteins, first discovered and characterized in 1975,[1] are present in the axon terminals of neurons and are mostly associated with microtubules, the major constituent of the cytoskeleton, composed of a dynamic tubulin polymer. In solution, tau proteins are highly unfolded and characterized by high flexibility of the chain.[2] The human brain contains six main tau isoforms that can be categorized depending on whether they contain three or four pseudorepeats (R_1−R_4) in the C-terminal region that constitutes the microtubule-binding domain. Tau proteins are highly soluble and show little tendency to aggregation. However, tau aggregation is characteristic of several neurodegenerative diseases known as tauopathies.[3−5] Among them, Alzheimer's disease (AD) is one of the most relevant and is characterized by the accumulation of extracellular amyloid plaques and intraneuronal tau neurofibrillary tangles (NFT).[6] The mechanism that leads to accumulation of NFT is still poorly understood, but there is evidence that tau undergoes post-translational modifications associated with AD such as abnormal hyperphosphorylation[7,8] and nitration.[9] The failure of therapeutic approaches based on amyloid hypothesis has led to an increasing interest in tau mediated AD etiology.[10] Moreover, the recent application of the cryo-electron microscopy (cryo-EM) technique has allowed a fundamental step for deciphering how the structural conformation might correlate physiological and pathological aspects of tau protein.[11] In particular, the structure of the tau fibrils from a diseased brain obtained with cryo-EM shows the formation of cross-β/β-helix structure between residues 306 and 378, which is the portion of tau comprising the R_3 and R_4 regions.[12]

As for other neurodegenerative diseases, oxidative stress and metal ions are recognized as important factors contributing to AD etiology.[13−17] Copper, zinc, and iron are essential metals for healthy organisms and brain function, but impairment of

Received: July 26, 2019
Published: December 10, 2019

DOI: 10.1021/acs.inorgchem.9b02266
Inorg. Chem. 2020, 59, 274−286

metal homeostasis is a crucial risk factor.[18] Despite the large amount of biophysical and structural studies regarding the interaction of transition metals with other proteins related to neurodegeneration, such as α-synuclein,[19,20] prion proteins,[21] and β-amyloid (Aβ),[22−24] much less is known about the interaction of metals ions with tau. The region encompassing the R_1−R_4 repeats represents a potential binding site for metals, since each repeat contains at least one histidine (His268, His299, and His362 in R_1, R_2, and R_4, respectively); R_3 contains two vicinal histidine residues (His329 and His330; Figure 1).

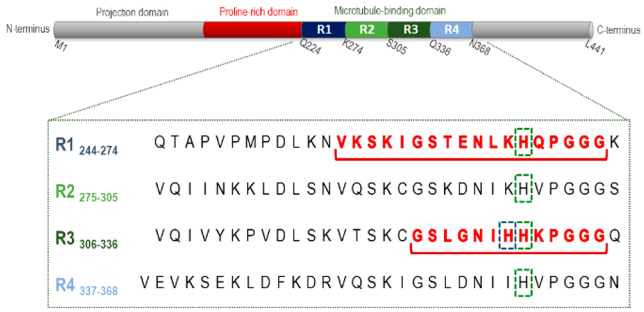

Figure 1. Amino acid sequences of the four pseudorepeats in the longest tau isoform. Each pseudorepeat consists of 31−32 amino acid residues and contains a highly conserved octadecapeptide, which shows >60% homology. The fragments used in this study are underlined and highlighted in red and are defined as R_1 (Ac-^{256}VKSKIGSTENLKHQPGGG^{273}-NH_2) and R_3 (Ac-^{323}GSLGNIHHKPGGG^{335}-NH_2).

Isothermal titration calorimetry shows that zinc(II) binds to tau in a tetrahedral coordination site involving Cys291, Cys322, and two histidines with moderate micromolar affinity.[25] Moreover, zinc(II) promotes tau hyperphosphorylation by inactivation of protein phosphatase 2A.[26] Recently, an important role of zinc in the modulation of the aggregation process of R_3−R_4 has been proposed.[27]

Even if a detailed binding study is still missing, it has been suggested that iron(III) binds to hyperphosphorylated tau and induces its aggregation.[28] Regarding heme-iron, the analysis of the interaction with the R_1 fragment shows that heme binds with moderate affinity to the histidine contained in this region.[29]

The binding of copper to tau has been studied more extensively. In particular, Soragni et al. have suggested that copper(II) binds to a site between R_2 and R_3, even if a definite coordination sphere has not been proposed.[30] The binding of copper(II) to tau fragments R_1,[31] R_2,[32] and R_3[33] has been also reported showing the crucial role of histidine as a coordination site; however, the peptide fragments used in these studies present free amine and carboxylic acid at the *N*-terminus and *C*-terminus, respectively, giving rise to a coordination model which is not suitable for mimicking the binding to full length protein. The same objection can be made with regard to an EPR spectroscopic study on the interaction of copper(II) and different portions of tau including R_1, R_2, R_3, and R_4 regions[34] and a more recent study that analyzes the interaction of copper, in both oxidation states, with the R_2 region.[35]

Another study suggests that also the N-terminal portion of tau protein can bind copper through coordination of His14 and His32.[36] The interaction of copper with the full length tau has been investigated also by laser ablation inductively coupled plasma mass spectrometry[37] and by electrochemical techniques.[38] In particular, the latter study proposes a reduction potential for the Cu(II)/Cu(I) redox couple bound to the tau protein of approximately 340 ± 5 mV versus NHE.

The number of studies that account for the reactivity of the copper−tau complexes and the related oxidative stress is even more limited. Sayre et al. analyzed the metal-catalyzed oxidation of 3,3′-diaminobenzidine in the presence of hydrogen peroxide and propose that copper and iron are involved in the redox reactions occurring in the neurofibrillary tangles as well as in the senile plaques.[39]

It is therefore crucial to better define the nature and strength of the binding of copper to tau by determining the stoichiometry and the structure of the complexes formed in solution and measuring the corresponding stability constants. In addition, the oxidative reactivity associated with these complexes should be explored to assess the potential contribution to oxidative stress arising from the copper−tau interaction.

In the present study, we investigate the properties and the reactivity of the copper complexes formed with *N*-acetylated and *C*-amidated R_1 (Ac-^{256}VKSKIGSTENLKHQPGGG^{273}-NH_2) and R_3 (Ac-^{323}GSLGNIHHKPGGG^{335}-NH_2) fragments. These two fragments were chosen because they have different behavior in the NFT formation. In particular, the R_3 portion is found inside the cross-β/β-helix structure of tau filament whereas R_1 is outside.[12] Moreover, these two peptides allow clarification on how the presence of one histidine or two vicinal histidines affects the affinity for copper and the reactivity of the relative copper complexes. We also justify the choice to use a truncated R_3 fragment excluding the cysteine residue (Cys322) according to the evidence that copper(II) is able to oxidize *in vitro* the cysteine residue inducing the formation of a disulfide intermolecular bond.[40] However, the two cysteine residues in tau protein (Cys291 and Cys322) are likely involved in the disulfide bond in the native protein, even if formation of intramolecular or intermolecular bonds may play an important role in tau aggregation.[41,42]

The speciation of the copper(I) and copper(II) complexes with both R_1 and R_3 peptides was studied by potentiometry, and the coordination environment of copper(II) in its adducts with the peptides was investigated by visible absorption and CD spectroscopy. The copper(I)− and copper(II)−R_3 binding was also studied by NMR and EPR spectroscopy. Finally, we studied the oxidation of the dopamine (DA) neurotransmitter, as a physiological model of induced copper redox cycling, and the related, but with a less complex oxidation pattern, 4-methylcatechol (MC). The present study extends our previous investigations on the redox activity of copper complexes with neuronal peptide fragments of Aβ,[43−45] α-synuclein,[46,47] and prion protein.[48]

RESULTS AND DISCUSSION

Peptide Protonation Equilibria. R_1 in its neutral form is a monoprotic acid (LH, Scheme S1). In its fully protonated form (on the side chains of Glu, His, and the three Lys residues) it is a pentaprotic acid (LH_5^{4+}). The pK_a values determined by potentiometric titrations (Table 1) are fully consistent with the sequential deprotonation of the carboxylic group of Glu, the imidazolium nitrogen of His, and the three protonated amino groups of Lys residues, the latter ones occurring at pH > 8.5. At pH 7.4, the predominant form of R_1 is LH_3^{2+}. The second peptide R_3, in its neutral form, has no

DOI: 10.1021/acs.inorgchem.9b02266
Inorg. Chem. 2020, 59, 274−286

Table 1. Protonation Constants (pK_a) of the Peptides R_1 (LH) and R_3 (L), and Overall Formation Constants of Their Complexes with Copper(II) (Referred to the Global Reaction: pCu + qL + rH = $[Cu_pL_qH_r]$, Charges Omitted)[a]

R_1 = LH		R_3 = L	
pK_{a1}	4.16(3); COOH Glu	pK_{a1}	5.78(4); $N_{im}H^+$ His
pK_{a2}	6.40(2); $N_{im}H^+$ His	pK_{a2}	6.75(3); $N_{im}H^+$ His
pK_{a3}	9.69(1); NH_3^+ Lys	pK_{a3}	10.19(1); NH_3^+ Lys
pK_{a4}	10.32(1); NH_3^+ Lys		
pK_{a5}	10.64(1); NH_3^+ Lys		
species	log β	species	log β
$[Cu(LH_3)]^{4+}$	34.84(8)		
$[Cu(LH_2)]^{3+}$	28.1(3)	$[Cu(LH_2)]^{4+}$	20.48(7)
$[Cu(LH)]^{2+}$	22.70(5)	$[Cu(LH)]^{3+}$	15.81(2)
$[CuL]^+$	14.08(8)	$[CuL]^{2+}$	9.39(3)
$[Cu(LH_{-1})]$	4.46(7)	$[Cu(LH_{-1})]^+$	2.48(2)
$[Cu(LH_{-2})]^-$	−5.85(9)	$[Cu(LH_{-2})]$	−6.22(3)
$[Cu(LH_{-3})]^{2-}$	−16.35(7)	$[Cu(LH_{-3})]^-$	−16.31(4)

[a] T = 298.2 K, I = 0.1 M (KCl). Standard deviations on the last significant figure are given in parentheses. Most relevant species at neutral pH are given in bold.

acidic protons (L, Scheme S1), but it can undergo protonation on the imidazole rings of the two His residues and on the amino group of the Lys chain. In its fully protonated form, it is therefore a triprotic acid (LH_3^{3+}). For this peptide, the observed pK_a values (Table 1) are fully consistent with the deprotonation of the two His residues (in the pH range 4−8.5), and the deprotonation of the Lys side chain at pH > 9. At pH 7.4, the predominant form of R_3 is LH^+.

Copper(II)/R_1 Complex Formation Equilibria. In the presence of copper(II), and in an excess of ligand with respect to the equimolar metal/ligand ratio, the R_1 peptide forms seven complex species. All these complexes correspond to 1:1 copper/peptide stoichiometry and differ for their protonation states. The stoichiometry of these species, along with their log β values, are reported in Table 1. A representative distribution diagram is reported in Figure 2. We will discuss here the speciation at neutral pH, whereas a complete description of the speciation of the systems is reported as Supporting Information. It should be highlighted that we did not examine in depth ligand/Cu ratios lower than 1.5 since reactivity experiments were principally carried out in the excess of peptide. Our conditions are therefore unfavorable for the formation of di- or polynuclear species that, in agreement with this perspective, were not found in our speciation systems.

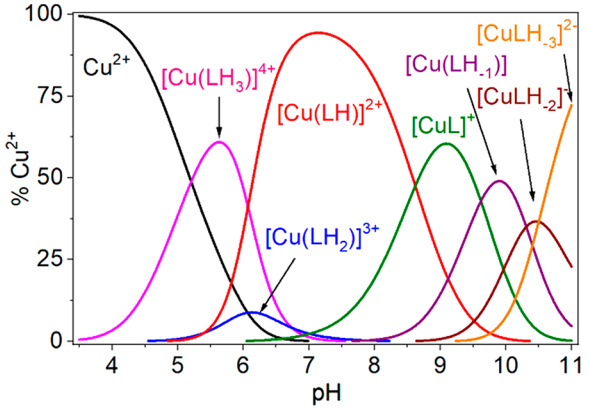

Figure 2. Representative distribution diagram of the copper(II)/R_1 (LH) system in aqueous solution (Cu^{2+}/R_1 = 1:3, C_{Cu} = 0.47 mM, I = 0.1 M (KCl), T = 298.2 K).

The predominant species in the pH range 6−8.5 is $[Cu(LH)]^{2+}$, which reaches 95% total copper at pH 7.2 (Figure 2). Above pH 8.5, $[CuL]^+$ becomes the most abundant species, reaching its maximum at pH 9 (ca. 60% total copper). The last three deprotonation steps lead to $[Cu(LH_{-1})]$, $[Cu(LH_{-2})]^-$, and $[Cu(LH_{-3})]^{2-}$, and they involve solely the deprotonation of the lysine residues. The coordination environment of copper in $[Cu(LH)]^{2+}$ and $[CuL]^+$ (Scheme 1) is proposed on the basis of visible absorption and CD spectra of the copper(II)/R_1 (LH) system at different pH's (Figure 3; UV CD spectra are reported in Figure S1).

The two spectra at pH 6.70 and 7.30, where $[Cu(LH)]^{2+}$ is predominant, exhibit an absorption λ_{max} of ca. 584 nm. By means of the parameters of the average environment (Billo's method)[49−51] this wavelength very well accounted for the presence on the equatorial plane of copper(II) of one imidazole nitrogen, two deprotonated peptide nitrogen atoms, and a water molecule (Scheme 1, left; expected λ_{max} = 583 nm).[49−51] A 6-membered chelate ring is obtained in the hypothesis of coordination of the imidazole N^{δ} and of the deprotonated peptide nitrogen of His268. By increasing the pH from 7.3 to 9.1, the maximum of the ligand field transition shifts from 584 to 523 nm in correspondence with the formation of $[CuL]^+$ (Figures 2 and 3). The latter absorption maximum is very well accounted for by the presence in $[CuL]^+$ of one imidazole and three peptide nitrogen atoms on the equatorial plane of copper(II) (expected λ_{max} = 523 nm).

The coordination mode in $[Cu(LH)]^{2+}$ is confirmed by EPR spectroscopy at pH 7.3 in which the complex between copper(II) and R_1 in slight excess displays a typical axial spectrum with with magnetic parameters: $A_{\parallel}$ = (174 ± 1) × 10^{-4} cm^{-1}, $A_{\perp}$ = 9 ± 1 × 10^{-4} cm^{-1}, $g_{\parallel}$ = 2.22 ± 0.001, and $g_{\perp}$ = 2.055 ± 0.0005. (Figure S2). The simulation allows assignment of 3N atoms in the coordination sphere of Cu(II). Reporting the magnetic parameters in the Peisach and Blumberg diagrams in which $g_{\parallel}$ and $A_{\parallel}$ are plotted for different coordinations of model Cu(II) compounds,[52] it is evident that the parameters of the R_1 EPR spectrum are in agreement with a 3N coordination, confirming the assignment obtained by simulation. A schematic representation of the proposed coordination mode is reported in Scheme 1 (left).

Copper(II)/R_3 Complex Formation Equilibria. In the presence of copper(II) and in an excess of ligand with respect to an equimolar metal/ligand ratio, the R_3 peptide forms six complex species. Similarly to what was observed for R_1, all correspond to 1:1 copper/peptide stoichiometries. The speciation model is reported in Table 1, and a representative distribution diagram is reported in Figure 4. The formation of copper/ligand 1:2 species was examined carefully for this ligand since the presence of two imidazoles may favor these stoichiometries. The fitting analysis suggests negligible formation of 1:2 species under our experimental conditions. A complete discussion of the speciation of the system is reported as Supporting Information.

At neutral pH (pH 7−7.5), the $[CuL]^{2+}$ and $[Cu(LH_{-1})]^+$ species predominate (Figure 4). At pH 6.7, where $[CuL]^{2+}$ is 48% of the total copper, the maximum of absorption of the d−d band is 610 nm. Copper(II) in this species likely adopts an equatorial (3N,O) coordination mode that involves one deprotonated peptide nitrogen, two imidazole donors, and a

DOI: 10.1021/acs.inorgchem.9b02266
Inorg. Chem. 2020, 59, 274−286

Scheme 1. Schematic Representation of the Copper(II) Coordination in $[Cu(LH)]^{2+}$ and $[CuL]^{+}$ Species of R_1 (LH)

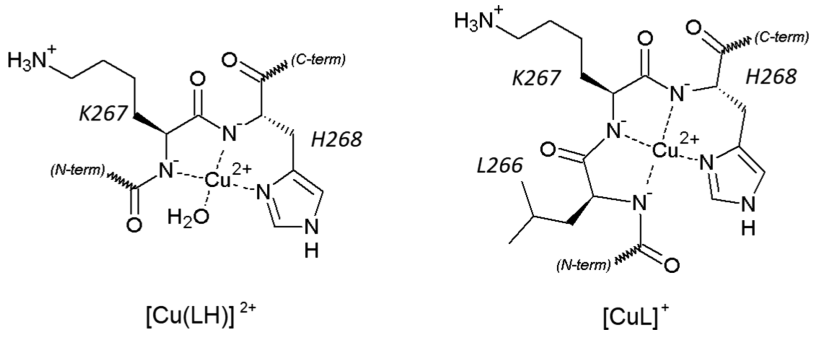

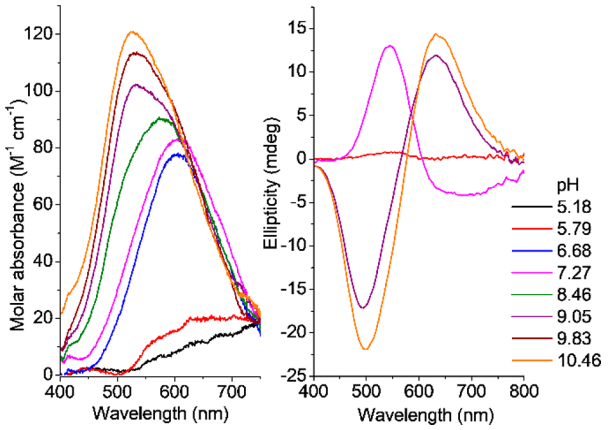

Figure 3. Left: Visible absorption spectra (absorbance/C_{Cu}) of solutions of copper(II) and R_1 (Cu^{2+}/R_1 = 1:1.5, C_{Cu} = 0.39 mM, I = 0.1 M (KCl), T = 298.2 K). Right: Visible CD spectra of solutions of copper(II) and R_1 (Cu^{2+}/R_1 = 1:1.5, C_{Cu} = 0.52 mM, I = 0.1 M (KCl), T = 298.2 K).

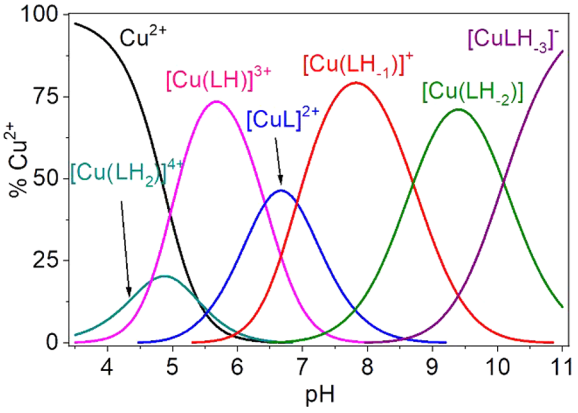

Figure 4. Representative distribution diagram of the copper(II)/R_3 (L) system in aqueous solution (Cu^{2+}/R_3 = 1:3, C_{Cu} = 0.47 mM, I = 0.1 M (KCl), T = 298.2 K).

water molecule (Scheme 2). The expected λ_{max} for this coordination environment is 604 nm. Moving to pH 7.8 where $[Cu(LH_{-1})]^+$ dominates, the spectrum of the solution experiences a blue shift to 585 nm (Figure 5; UV CD spectra are reported in Figure S3). This wavelength is well accounted for a (N_{Im}, $2N^-$, O) donor set. We have also performed EPR experiments at both pH 6.7 and 7.9 in the presence of a slight excess of R_3 compared to copper(II). At pH 6.7, $[CuL]^{2+}$ is the expected predominant species, whereas at pH 7.9, $[Cu(LH_{-1})]^+$ is the most abundant. In both cases, the spectra are characteristic of an axial geometry around the metal center (Figures S4 and S5), but severe broadening of the signal due to aggregation effects prevents reliable simulation and calculation of the magnetic parameters.

For this coordination environment we propose chelation models that are reported in Scheme 2 (modes *a* and *b*). In the first (mode *a*), the imidazole of His329 acts as the anchor and the donor atom set is made by two deprotonated peptide nitrogen donors (Ile328 and His329) and one water molecule on the equatorial plane. In the second (mode *b*), the imidazole of His 330 is the anchor, while the two-deprotonated peptide nitrogen atoms are those of His329 and His330. For each of the two donor atom sets, the expected maximum of absorption calculated using the rule of the average environment (Billo's rule) is 583 nm, in full agreement with experimental 585 nm. ^{1}H NMR data collected on R_3 (see below) show how the proton signals of the Ile328−Pro332 are completely washed out upon the addition of copper(II) to the peptide at neutral pH. These data suggest that possibly both modes *a* and *b* are present in solution. As for the coordination of the second imidazole, our data do not provide information on the occurrence of this interaction.

The proposed equatorial coordination modes in $[Cu(LH_{-1})]^+$ start from one imidazole (either His 329 or 330) and extend toward the N-terminus. In this circumstance, a stable six-membered (N_{Im}, N^-) chelation ring is formed. An alternative coordination mode for the (N_{Im}, $2N^-$, O) donor set has been proposed in the literature, and it involves anchoring to the imidazole and the deprotonation of amides toward the C-terminus.[53,54] For R_1 and R_3 peptides, these coordination modes are prevented by the presence of the proline residue.

Overall, these data suggest that $[CuL]^{2+}$ and $[Cu(LH_{-1})]^+$ markedly differ in their coordination environment since two imidazoles are coordinated in the equatorial plane in the former, while only one is found equatorially coordinated in the latter. This major change in the coordination of copper(II) is consistent with the major changes in the CD spectra that were observed in the pH range 6.7−7.8 (Figure 5). Here, we see that the CD trace at pH 6.7 (green trace) has a similar trend to that of the CD spectrum of copper(II)/R_1 at pH 7.3 (Figure 3), but the sign of the curve is inverted at pH 7.8 (violet trace). We can attribute this CD change to conformational inversion of the six-membered histidine chelate ring occurring upon binding of the axial ligand in $[Cu(LH_{-1})]^+$, as this effect has been observed systematically for a number of copper(II) complexes with histidine-containing multidentate ligands.[55−57] The much stronger CD activity observed in the visible range at high pH for both Cu^{2+}/R_1 and Cu^{2+}/R_3 complexes cannot be attributed to vicinal or conformational effects and is probably

DOI: 10.1021/acs.inorgchem.9b02266
Inorg. Chem. 2020, 59, 274−286

Scheme 2. Schematic Representation of the Copper(II) Coordination in $[CuL]^{2+}$ and $[Cu(LH_{-1})]^{+}$ Species of R_3 (L)

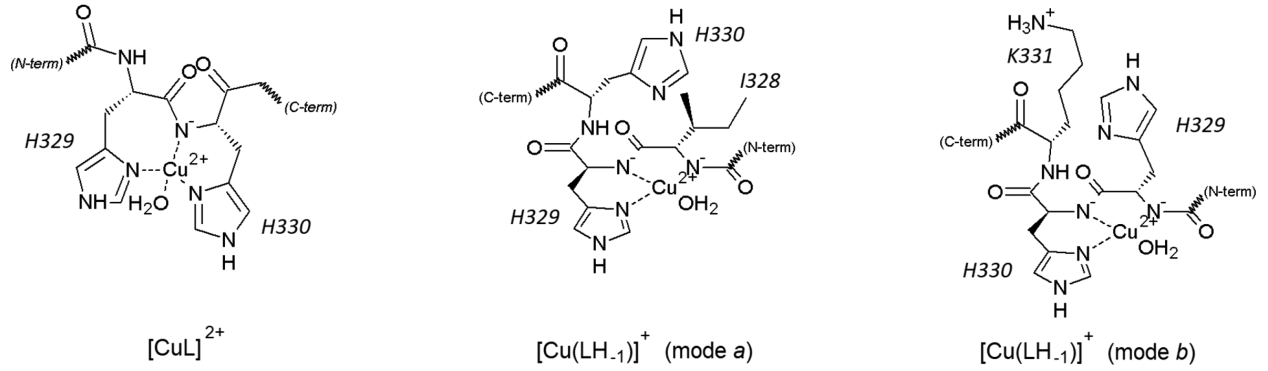

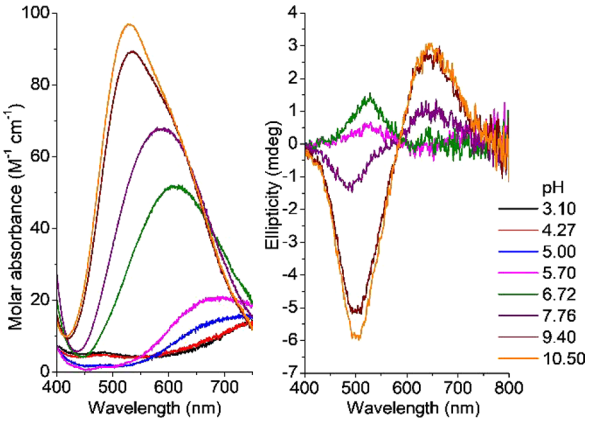

Figure 5. Left: Molar visible absorption spectra (absorbance/C_{Cu}) of solutions of copper(II) and R_3 (Cu^{2+}/R_3 = 1:1.25, C_{Cu} = 0.60 mM, I = 0.1 M (KCl), T = 298.2 K). Right: Visible CD spectra of solutions of copper(II) and R_3 (Cu^{2+}/R_3 = 1:3, C_{Cu} = 0.51 mM, I = 0.1 M (KCl), T = 298.2 K).

due to coupling of transition moments of d−d transitions with the three strong π(amide)−copper(II) charge transfer bands in the near-UV. In the literature, a (3N,O) binding mode at pH 7.4 for copper(II) with several model peptides of R_1 and R_3 was proposed.[34] For some of these peptides the precise coordination environment was not clarified, and the involvement of the peptide groups was proposed to occur through the oxygen atom. Moreover, most of those peptides are not acetylated at their *N*-terminus and, as a consequence, the N-terminal amino group has been proposed as one of the donor groups, especially on the basis of the EPR fingerprints.[34,58] While the coordination modes we propose agree with those in the literature for the presence of (3N,O) binding modes for both peptides at neutral pH, the major difference with the latter models is that the peptide groups are coordinated through the deprotonated nitrogen atoms, and that possibly water is the oxygen donor.[31−34]

With the speciation of the two copper(II)/R_1 and copper(II)/R_3 systems available, we could calculate for both peptides the conditional affinities for copper(II) at pH 6.5 and at pH 7.4 (K_d for the equilibrium [CuL] = Cu + L). These two pH values are those for which the K_d of copper(II)-tau and the copper(II/I)-tau reduction potential are available, respectively. The K_d of the copper(II) adducts with the peptides at pH 7.4 resulted in 150(10) nM for R_1 and 71(5) nM for R_3. Although these two values allow the calculation of the copper(II/I)-tau reduction potentials at this pH (see below), the affinities at pH 6.5 are needed to compare with that of tau.

The conditional K_d at pH 6.5 resulted in 13(1) μM for R_1 and 2.8(5) μM for R_3, respectively. Although these conditional affinities for copper(II) are lower than that determined for tau by ITC (500−700 nM),[30] that of R_3 stays within a factor of 4 to 6 from that of the protein. It is therefore evident that a full-length tau plays a role in modulating on the overall formation constants of the copper(II)−peptide adducts that is not modeled by the fragments used in this study.

As expected, the R_3 peptide has higher affinity for copper(II) than R_1 at both pH values as a consequence of the presence of two His donors. However, the affinity of R_3 is only 2-fold higher than that of R_1 at pH 7.4, and 5-fold higher at pH 6.5, therefore showing that R_3 is not selective in binding copper at both pH values. This is illustrated by the calculated competition diagram reported in Figure S6, which represents a hypothetical system where copper(II), R_1, and R_3 are present in equimolar amounts, as occurs in tau protein. The relative amount of copper(II) bound to R_3 and R_1, respectively, is 65 vs 35% at pH 6.5 and 58 vs 42% at pH 7.4. Therefore, with the presence in tau of one His (R_1, R_2, and R_4 of tau) or a His−His tandem (R_3), the nature of the individual sequences may not be discriminant in defining a unique binding site for copper(II). The metal in tau may rather be distributed over multiple sites, or likely be bound to one preferential site as the consequence of additional structural features not modeled using R_1 and R_3 peptides.

Copper(I)/R_1 and Copper(I)/R_3 Complex Formation Equilibria. The formation constants of copper(I) complexes with R_3 were determined in 100 mM aqueous 4-(2-hydroxyethyl)-1-piperazine ethanesulfonic acid (HEPES) buffer at pH 7.4. As a consequence of the use of the buffer, these are apparent constants. However, there is consensus in the literature for not considering HEPES as a strong competing ligand for copper(I).[59] We expect therefore the values of these apparent formation constants to be not significantly different from conditional ones. UV−visible competition experiments were carried out using ferrozine (Fz^{2-}) as a competing metallochromic indicator for copper(I). By adding R_3 to a $[Cu(Fz)_2]^{3-}$ solution, a decrease in the absorbance values in the range 450−800 nm was observed as a consequence of copper(I) displacement from the indicator (Figure 6).

Conversely, the limited decrease in absorbance observed with R_1 was fully accounted by dilution effects, which suggests that the formation log β value of a possible copper(I)/R_1 adduct is lower than 5 (see Figure S7). Data treatment of the spectral dataset for the titrations with both peptides allowed to

DOI: 10.1021/acs.inorgchem.9b02266
Inorg. Chem. 2020, 59, 274−286

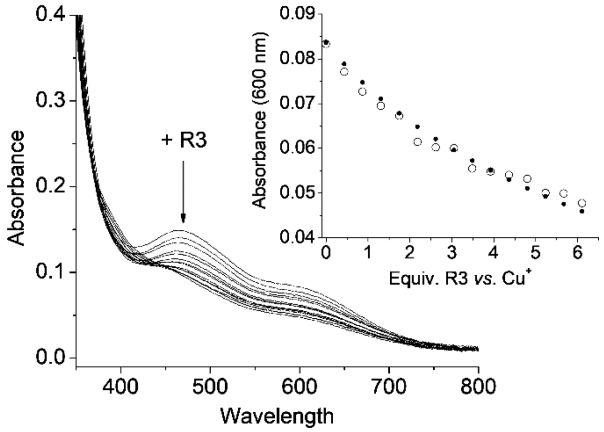

Figure 6. Spectral data set for the titration of a solution of $[Cu(CH_3CN)_4]BF_4$ and Fz^{2-} with R_3 (Cu/Fz = 1:2.15, C_{Cu} = 41 μM, $C_{ascorbate}$ = 10 mM, 100 mM aqueous HEPES buffer solution, pH 7.4). Inset: absorbance values at 600 nm. Open circles, observed; filled circles, calculated.

calculate the conditional log β values for the $Cu^+ + L = [CuL]$ equilibria, which resulted 10.1(2) for R_3 (corresponding to a dissociation constant of 7.9 10^{-11} M) and not significant for R_1. Overall, all these data confirm that the R_1 peptide does not significantly bind copper(I), while the R_3 peptide has a high affinity for copper(I). This result was not unexpected, since previous investigations of histatin peptides and models of Aβ and Ctr1 have proven the affinity of His−His tandem for copper(I).[59−62] For these peptides, we reported affinities in the range of 10^{-10} to 10^{-11} M were reported, although affinities down to 10^{-6} M have been reported in the literature.[59−62] As for the coordination environment, we put forward the hypothesis that the main binding site is at the two imidazole groups of His 329 and His 330: copper(I) is likely (N_{im},N_{im}) two-coordinated with a possible weak interaction of the carbonyl oxygen of His 329. The involvement of the imidazole groups as the donor ligands is in full agreement with NMR data (see below). Finally, in the attempt to exclude a buffer competing effect that could bias the comparison with NMR data, we have performed the same competition experiments in 100 mM phosphate buffer at pH 7.0. Formation constants are not significantly different from those in HEPES (not shown).

Structural Characterization of Copper−R_3 Complexes by NMR Spectroscopy. Copper(II) and copper(I) binding to R_3 at pH 6.8 was also investigated by NMR spectroscopy. Upon the addition of the paramagnetic ion to R_3 solutions, we observed selective line broadening of NMR resonances. As shown in Figure 7, the most affected signals were those belonging to His329, His330 and residues nearby, Ile328, Lys331, and Pro332. As usually found for copper(II)−peptide interactions, the higher is the metal concentration, the larger is the metal induced line broadening of NMR signals, as shown in Figure 7B. The most affected protons are those belonging to His imidazole rings, Hδ and Hε. In particular, the effects are more pronounced on Hε than Hδ, indicating Nδ rather than Nε, as a binding donor atom for both His.[63−65]

Besides copper(II), we also investigated copper(I)−R_3 association. Copper(I) is diamagnetic, and it induces chemical shift variations of protein/peptide nuclei close to the metal coordination sphere. As evident from Figure 8, signals of both His329 and His330 are downfield shifted, supporting their binding to the cuprous ion.[66,67] Moreover, Figure 8 shows changes on Ile328 methyl protons as well; this might be explained by considering their proximity to the metal center. Similar effects were obtained by using Ag(I) as a copper probe. In this case, Ag(I) causes an upfield shift of His protons, in agreement with what we recently reported on copper(I) interaction with Aβ peptides.[66] This similar behavior is consistent with the fact that a His−His tandem is present in Aβ as well as in R_3, and it plays a key role in metal interactions.[68,69]

The interaction between copper(II) and R_1 has been also investigated by NMR spectroscopy. Both ^{1}H 1D and ^{1}H−^{1}H TOCSY NMR spectra (Figure S8) indicate that the presence of copper(II) induces large broadening of the signals of His268 and of the vicinal residues (Leu266, Gln269, and Pro270). These data confirm the relevance of His268 as an anchoring site for the coordination of copper(II).

Oxidation of Dopamine and 4-Methylcatechol by Copper−R_1 and Copper−R_3 Complexes. To gain information on the potential catalytic role of copper−R_1 and

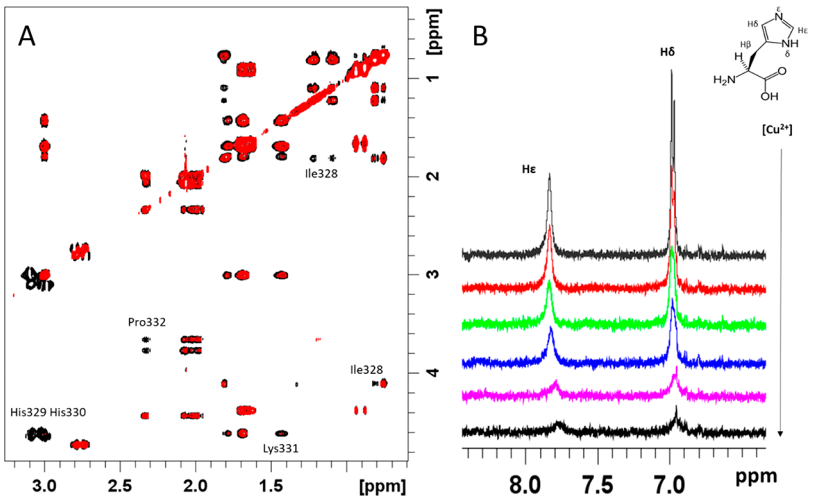

Figure 7. (A) Comparison of the selected region of ^{1}H−^{1}H TOCSY spectra of R_3 in the absence (black contours) and in the presence (red spots) of 0.2 equiv of copper(II). (B) Superimposition of ^{1}H 1D NMR spectra of apo R_3 both free (upper trace) and in the presence of increasing copper(II) concentration.

DOI: 10.1021/acs.inorgchem.9b02266
Inorg. Chem. 2020, 59, 274−286

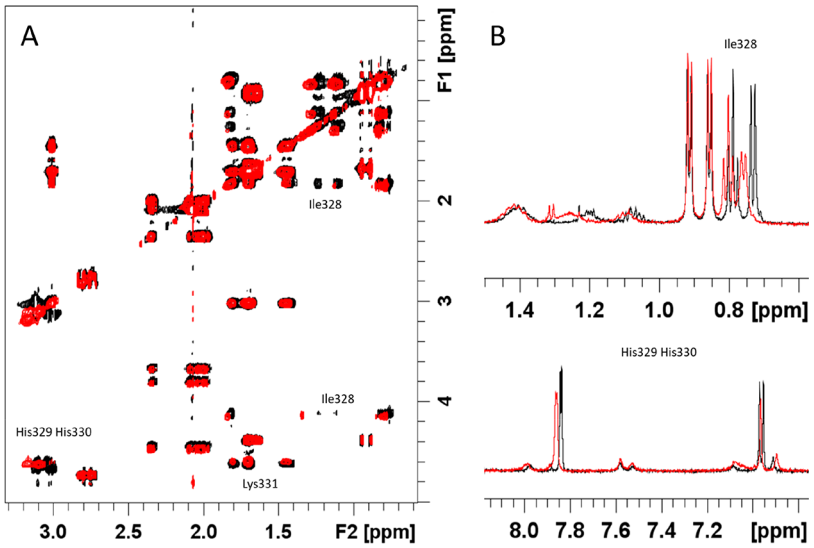

Figure 8. (A) Comparison of selected region of ^{1}H−^{1}H TOCSY spectra of R_3 in absence (black contours) and in presence (red spots) of 0.8 equiv of copper(I). (B) Superimposition of ^{1}H 1D NMR spectra of apo R_3 both free (black trace) and in presence (red trace) of 0.8 equiv of copper(I).

−R_3 complexes in oxidative reactions, we performed a comparative study of their oxidative activity against catecholic substrates with respect to that of free copper(II). The most important substrate that can be involved in this type of reactivity is DA, due to its abundance in *substantia nigra* neurons and because alteration in DA metabolism can be related to several neurodegenerative disorders.[70] Catecholamines are present in many brain areas besides the substantia nigra and, in particular, in those regions which are mostly affected by AD and Parkinson's disease.[71]

The oxidation of DA catalyzed by copper(II) in HEPES buffer at pH 7.4 was studied in the presence of increasing amounts of either R_1 or R_3, in parallel experiments. DA oxidation was monitored by UV−visible spectroscopy through the development of the absorption band of dopaminochrome (DAC) at 475 nm. This product accumulates in the initial stages of the reaction.[72,73] Within about 1 h, formation of insoluble melanic products could be noted; therefore, we focused our attention on the first 30 min of reaction. In these conditions, DA autoxidation is not negligible, as shown by the black dotted trace in Figure 9. DA (3 mM) oxidation catalyzed by copper(II) (25 μM) is strongly promoted by the addition of R_3, but it is only slightly enhanced by the presence of R_1. In both cases, the DA oxidation increases by increasing the tau/copper(II) ratio.

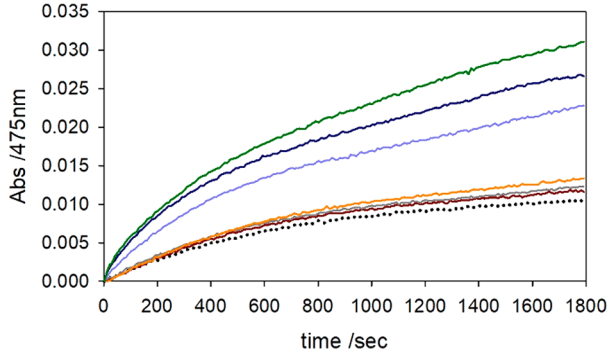

Figure 9. Kinetic profile of DA (3 mM) oxidation with time in 50 mM HEPES buffer solution at pH 7.4 and 20 °C in the presence of only copper(II) (25 μM; brown trace) and with 2 equiv (gray) and 4 equiv (orange) of R_1 peptide or 1 equiv (light blue), 2 equiv (blue), and 4 equiv (green) of R_3. Autoxidation of substrate is also shown (black dotted trace).

Since DA oxidation is rather slow and occurs with the formation of a mixture of products and precipitate, this substrate is not suitable to perform a more detailed kinetic study. Therefore, the oxidation of the more reactive MC (with a lower semiquinone/catechol redox potential)[46] can be conveniently studied as a model substrate of DA. Oxidation of MC (3 mM) promoted by copper(II) (25 μM) and tau peptides at pH 7.4 (50 mM HEPES buffer) proceeds with a biphasic behavior where a fast initial step, concluded after about 100 s, is followed by a second linear phase (Figure 10).

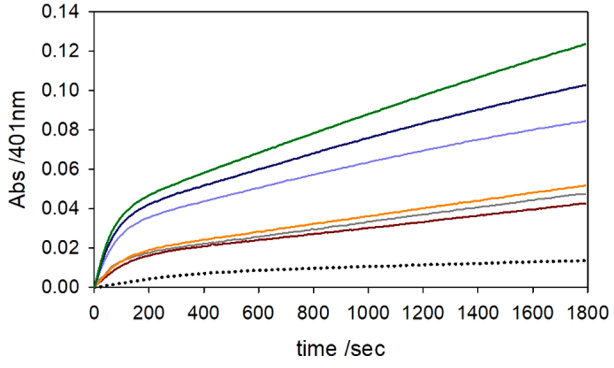

Figure 10. Kinetic profile of MC (3 mM) oxidation with time in 50 mM HEPES buffer solution at pH 7.4 and 20 °C in the presence of only copper(II) (25 μM; brown trace) and with 2 equiv (gray) and 4 equiv (orange) of R_1 peptide or 1 equiv (light blue), 2 equiv (blue), and 4 equiv (green) of R_3. Autoxidation of substrate is also shown (black dotted trace).

The biphasic behavior can be noted also for DA oxidation, but the presence of several absorbing species in solution makes the observation less clear. During the time course of MC oxidation, a shift of the developing absorption bands occurs from the initial value of 401 nm, due to the 4-methylquinone (MQ), to higher wavelengths, which is related to the formation

DOI: 10.1021/acs.inorgchem.9b02266
Inorg. Chem. 2020, 59, 274−286

of the quinone addition product with catechol.[47] By increasing the peptide concentration, the rate of both steps is accelerated with a much stronger effect observed in the presence of R_3 rather than the complex with R_1.

Prior to analysis of the reaction mechanism and comparison of the different behavior in the presence of the two peptides, we could estimate the reduction potential of the copper(II/I) couple by using the formation constants of copper(I) and copper(II) complexes with the two peptides. As for the copper(I)/R_1 adduct, for which a log β value could not be determined, an upper limit of log β = 5 was considered (see above). With these data in our hands, we could estimate a reduction potential of −170(10) and +110(10) mV vs NHE for R_1 and R_3, respectively. The former value (−170 mV for copper/R_1) represents an upper limit under our approximations.

It was previously demonstrated that the presence on peptide sequences of tandem His−His sites promotes the reduction of copper(II) to copper(I), mainly through the formation of stable copper(I)/peptide adducts.[59−62] It is however worth noting that here for both R_1 and R_3 fragments the estimated potential is lower than that observed for copper adducts with tau (340 mV vs NHE).[38] Assuming for R_3 and tau a similar affinity for copper(I), the difference of an order of magnitude in the affinities for copper(II) accounts only for 60 mV of the difference in their redox potentials. Overall, these data suggest that there are structural or second-shell interactions in copper/tau adducts that determine the redox potential in the protein and that are not completely modeled by R_1 and R_3 peptides.

The reaction mechanism previously proposed for the oxidation of catechols by copper-Aβ,[43] copper-α-synuclein,[46] and copper-prion[48] peptide complexes can be extended to the present study on copper-tau peptide complexes. It involves the following reaction steps:

$$Cu^{2+} + \text{peptide} \rightleftarrows [Cu^{2+}\text{-peptide}] \quad (1)$$

$$[Cu^{2+}\text{-peptide}] + \text{catechol} \rightarrow [Cu^{+}\text{-peptide}] + \text{semiquinone}^{\bullet+} \quad (2)$$

$$[Cu^{+}\text{-peptide}] + \text{catechol} \rightleftarrows [Cu^{+}\text{-peptide-catechol}] \quad (3)$$

$$[Cu^{+}\text{-peptide-catechol}] + O_2 \rightarrow [Cu - \text{peptide-catechol-}O_2] \quad (4)$$

$$[\text{Cu-peptide-catechol-}O_2] \rightarrow\rightarrow [Cu^{2+}\text{-peptide}] + \text{quinone} \quad (5)$$

After rapid complexation (reaction 1), the reaction proceeds with the reduction of copper(II) to copper(I) by the catechol, which occurs as a fast phase (reaction 2). The rate-determining step is reaction 4 of the reduced form of the Cu−peptide complex with dioxygen, to generate the ternary complex indicated as [Cu-PrP-catechol-O_2]. Our previous studies on copper−peptide complexes indicate that the reaction rate depends also on catechol concentration, suggesting that substrate binding occurs as a pre-equilibrium step before the rate-determining binding of molecular oxygen.[43,46,48] The R_3 binding to copper(I) facilitates the reaction with molecular oxygen, increasing the reaction rate (Figures 9 and 10). On the other hand, the weak affinity toward R_1 leaves copper(I) mostly unbound to the peptide and, thus, with a reactivity comparable with that observed for "free" copper (Figures 9 and 10). The presence of the catechol, which could bind to the metal ions, could complicate the scenario, perturbing the binding processes. Anyway, the activity data clearly indicate that the turnover reactivity of the copper/peptide complexes is controlled by the copper(I) binding mode, confirming the key role of His−His tandem in the R_3 fragment. An increase of the rate of copper-mediated oxidation of catecholic substrates has been already observed in the presence of Aβ[43,74,75] and prion protein[48] fragments, whereas truncated α-synuclein peptides induce a decrease in the reactivity of copper.[46] This behavior suggests that the multiple histidine residues present in Aβ, prion protein, and R_3 peptides, but not in R_1 and α-synuclein, are crucial for this reactivity.

Conversely, in the presence of other substrates such as ascorbate the rate of oxidation is higher with copper compared to that of copper-Aβ[76,77] or copper-α-synuclein[45] peptide complexes. This behavior can be ascribed to the different coordination properties of different substrates for copper in both oxidation states and to a possible change in the rate limiting step of the overall process.

Competitive Endogenous R_1 and R_3 Peptide Oxidation. Similarly to our previous studies on other copper−peptide complexes,[43,46,48] we investigated the metal-catalyzed oxidation of tau peptides in the reductive environment generated during catechol oxidation, by using LC-MS analysis.

This aspect is important because, unlike copper enzymes that activate oxygen for specific reactions,[78] copper complexes with neuronal peptides generate Cu/O_2 species capable of nonselective oxidations. This reactivity is due to Fenton chemistry yielding harmful reactive oxygen species (ROS) that give rise to oxidative protein damage, through oxidation of amino acid residues, structural alteration, and loss of function.[79−82] These reactions contribute to the oxidative damage observed in AD, especially addressed to Aβ,[83] but they can also reasonably involve tau protein. In this LC-MS analysis, the oxidative modifications on R_1 and R_3 peptides produced upon oxidation of both DA and MC were evaluated. In these experiments, a solution of copper and tau peptides was incubated in the presence of DA or MC under the same conditions as in the catalytic oxidations ([tau peptide] = 50 μM; [Cu^{2+}] = 25 μM; [catechol] = 3 mM; in 50 mM HEPES buffer pH 7.4). Samples were analyzed after 15, 30, and 90 min of reaction time.

The R_1 fragment undergoes a limited pattern of modifications in the presence of MC (Figure 11, panel A), whereas in the presence of DA the peptide remains mostly unmodified (peak with t_R = 26 min, Figure 11, panel B). In the latter case, the peak appearing at a t_R of 24 min, with a relative area of 7%, is not corresponding to an oxidative modification but it is probably due to a fragmentation derivative.

Table 2 reports the variation over time of the percent modification of the native peptide. These data show that in the presence of MC the most abundant modification undergone by R_1 peptide is the nucleophilic addition of MC and MQ to His residue (two adjacent peaks with t_R = 33/34 min). The modification that implies an oxygen atom insertion (R_1 + 16, peak with t_R = 29 min) is limited, and it is only observed in a low amount after prolonged incubation (1% after 30 min and 3% after 90 min).

The oxidative modifications of R_3 peptide are larger both in terms of the number of products and in terms of the extension of the modifications (Figure 12). In the presence of DA (Figure 12, panel B), the most abundant modification

DOI: 10.1021/acs.inorgchem.9b02266
Inorg. Chem. 2020, 59, 274−286

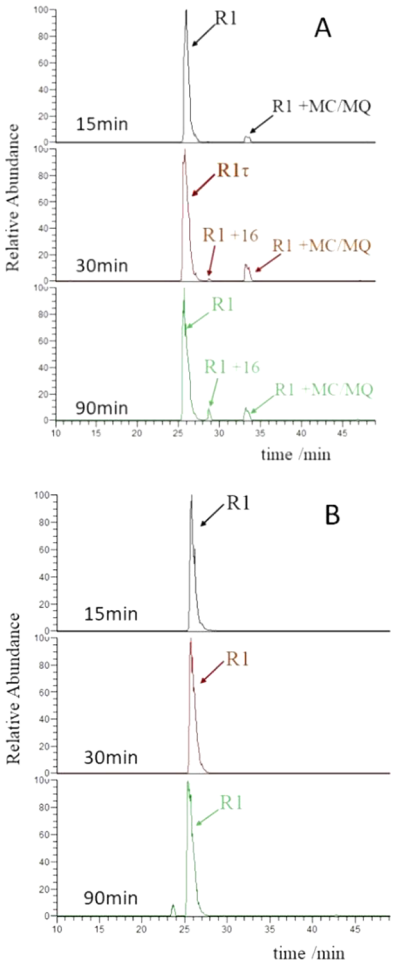

Figure 11. HPLC-MS elution profiles of the R_1 peptide (50 μM) in HEPES buffer (50 mM) at pH 7.4 in the presence of copper(II) (25 μM) and MC (panel A) or DA (panel B; 3 mM) after 15, 30, and 90 min reaction time.

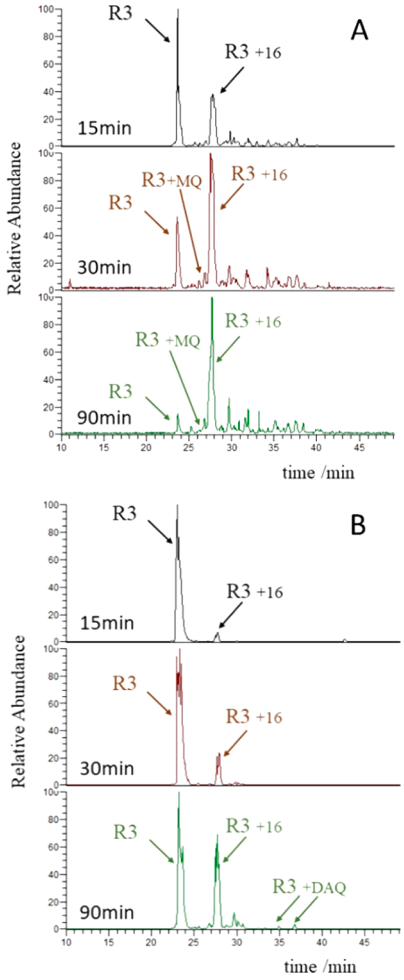

Figure 12. HPLC-MS elution profiles of R_3 peptide (50 μM) in HEPES buffer (50 mM) at pH 7.4 in the presence of copper(II) (25 μM) and MC (panel A) or DA (panel B; 3 mM) after 15, 30, and 90 min of reaction time.

Table 2. Modification of R_1 Peptide (50 μM) Detected by LC-MS Analysis, in the Presence of Copper(II) (25 μM) and MC or DA (3 mM) in HEPES Buffer (50 mM) pH 7.4 at 20 °C

incubation time (min)	R_1	+16	+MQ	+MC	+MQ + 16	+MC + 16
15	95%		3%	2%		
30	88%	1%	6%	5%		
90	85%	3%	5%	5%	1%	1%
incubation time (min)	R_1	+16	+DAQ	+DA	+DAQ + 16	+DA + 16
15	100%					
30	100%					
90	93%					

corresponds to the peak with a mass increment of +16 (t_R = 27 min) that indicates the insertion of an oxygen atom (11% after 30 min and 29% after 90 min, Table 3). It is possible to note also the double insertion of oxygen (+32 total mass increment, −8% after 90 min), whereas a small amount of derivatives obtained from the addition of catechol (2% of R_3-DA+16) or quinone (1% of R_3-DAQ and 2% of R_3-DAQ+16) even after 90 min is observed.

In the presence of MC, the pattern of modification is even more complicated (Figure 12, panel A). The types of modification identified by LC-MS analysis include (i) *O*-atom insertion into His329 or His330 (+16 mass increment); (ii) double *O*-atom insertion into both His residues (+32); (iii) the addition of MQ to one His residue (+120); (iv) the addition of MC to one His residue (+122); (v) a double modification consisting of MQ addition to one His residue (+120) and *O*-atom insertion into His (+16), yielding a total mass increment of 136; (vi) a double modification consisting of MC addition to one His residue (+122) and *O*-atom insertion into His (+16), yielding a total mass increment of 138; and (vii) oxidation of Pro332 to hydroxyproline[84] followed by dehydration (mass loss of 2). Contrary to the data regarding R_1 in which the nucleophilic addition was predominant, in this case, the oxygen insertion is the most abundant modification.

In conclusion, R_3 undergoes extensive modifications, since the amount of unmodified peptide is only 8% after 90 min of time incubation. The LC-MS data are in agreement with the catalytic data on catechol oxidation. The R_1 fragment is weakly bound to copper(I), leading to a slow reaction with molecular oxygen and thus to weak catalytic activity in catechol oxidation and limited "self-modification."

DOI: 10.1021/acs.inorgchem.9b02266
Inorg. Chem. 2020, 59, 274−286

Table 3. Modification of R_3 Peptide (50 μM) Detected by LC-MS Analysis, in the Presence of Copper(II) (25 μM) and MC or DA (3 mM) in HEPES Buffer (50 mM) pH 7.4 at 20 °C

incubation time (min)	R_3	−2	+16	+16 + 16	+MQ	+MC	+MQ + 16	+MC + 16
15 min	40%	5%	27%	13%	1%	1%	6%	7%
30 min	23%	8%	36%	11%	1%	2%	7%	12%
90 min	8%	12%	36%	18%	1%	2%	7%	16%
incubation time (min)	R_3	−2	+16	+16 + 16	+DAQ	+DA	+DAQ + 16	+DA + 16
15 min	97%		3%					
30 min	86%		11%	3%				
90 min	53%	4%	29%	8%	1%		2%	2%

It is also possible to compare the tendency to undergo copper-mediated oxidative modification of tau R_3 and R_1 peptides with other neuronal peptides analyzed under the same experimental conditions in previous studies by our group. By considering the percentage of unmodified peptides after 90 min in the presence of copper and MC, it is possible to list the neuronal peptides in this order of reactivity: R_3 > prion fragment 76−114 (PrP_{76-114})[48] > Aβ16 ≈ Aβ28[43] ≫ R_1 > α-synuclein fragment 1−15.[46]

SOD-Like Reactivity of Copper−R_1 and Copper−R_3 Complexes. We also measured the SOD-like activity of copper(II)−R_1 and copper(II)−R_3 complexes in comparison of the activity of free copper(II) in solution. The activity was evaluated through the direct assay in which O_2^- is supplied as a KO_2-crown ether complex, as we reported previously for copper(II)−-prion,[48] copper(II)−Aβ,[44] and copper(II)−α-synuclein[46] peptide complexes. As shown in Figure S9, neither copper(II)−R_1 nor copper(II)−R_3 significantly increase the SOD activity of free copper(II).

CONCLUSIONS

Compared to the interaction of copper with other neuronal peptides involved in the pathogenesis of neurodegenerative diseases, which has been deeply elucidated, the interaction of copper with tau protein is poorly characterized, even if the relevance and the impact of tau homeostasis in neurodegenerative disease progression has taken center stage in recent years. The present study presents a thorough and detailed analysis of the stability and the structural models of copper (in both oxidation states) complexes with two peptide fragments that are encompassed in the R_1 and R_3 repeats of tau.

Potentiometric measurements suggest that the vicinal His-His residues in R_3 guarantee a strong binding site for copper in both oxidation states (K_d value of 71 nM and 0.08 nM for copper(II) and copper(I), respectively), whereas the single histidine in R_1 can bind copper(II) (K_d = 150 nM) but not copper(I). CD and NMR techniques confirm the involvement of the His−His tandem in the coordination of copper in both oxidation states.

The study of the oxidative reactivity of these copper−tau peptide complexes confirms that the R_3 coordination sphere guarantees an efficient copper(I/II) redox cycling. In particular, the copper−R_3 complex is able to strongly enhance the capability of copper to oxidize cathecolic substrates as DA and MC, whereas copper−R_1 complex reactivity is similar to that of free copper. The reduction of copper during the catechol oxidation generates Cu/O_2 species capable of oxidizing other cellular components through Fenton chemistry. LC-MS analysis of the reaction mixture indicate that R_3 is rapidly and extensively modified, through oxygen insertion and/or quinone-derivatized histidines. By comparing the tendency to undergo copper-mediated oxidative modification of tau R_3 and R_1 peptides with other neuronal peptides analyzed in previous studies by our group, we can conclude that R_3 is the most reactive, followed by the prion protein fragment (PrP_{76-114}) and N-terminal portion of Aβ peptide.

In conclusion, the His−His tandem strongly discriminates the copper binding, rendering the copper(I) coordination more favorable in R_3 compared to R_1. This site accommodates copper in both oxidation states, providing an active catalyst for reactions that activate oxygen and are potentially dangerous for the cellular compartment. The different binding of copper(I) for R_3 and R_1 fragments is particularly important for this interaction because tau protein is located intracellularly where the reductive redox potential implies that copper is mostly in the reduced state.

The next steps of this bottom-up approach for deciphering the copper−tau interaction might include (i) the study of the copper complex with an R_3 peptide that includes the cysteine residue, which has a relevant role in tau aggregation; (ii) the analysis of protein fragments that contain more than one copper binding site in order to understand if the individual binding sites are influenced by each other; (iii) once the individual binding site for copper is characterized, the extension of the study to full length protein; and (iv) the implementation of this *in vitro* approach by introducing other cellular components such as a membrane-like environment.

ASSOCIATED CONTENT

Supporting Information

The Supporting Information is available free of charge at https://pubs.acs.org/doi/10.1021/acs.inorgchem.9b02266.

Materials and methods, detailed description of copper complexes' formation equilibria, EPR spectra, additional CD and UV−visible spectra (PDF)

AUTHOR INFORMATION

Corresponding Authors

*E-mail: matteo.tegoni@unipr.it.
*E-mail: simone.dellacqua@unipv.it.

ORCID

Enrico Monzani: 0000-0002-8791-6446
Stefania Nicolis: 0000-0002-6618-7555
Luigi Casella: 0000-0002-7671-0506
Matteo Tegoni: 0000-0002-9621-0410
Simone Dell'Acqua: 0000-0002-1231-4045

Author Contributions

C.B., preparation and purification of the peptides; acquisition and analysis of kinetic and HPLC-MS experiments. S.G.,

DOI: 10.1021/acs.inorgchem.9b02266
Inorg. Chem. 2020, 59, 274−286

acquisition and analysis of potentiometric, spectrophotometric, and CD data. D.B., acquisition and analysis of potentiometric and spectrophotometric data. E.Q., acquisition and analysis of potentiometric, spectrophotometric, and CD data. S.D., acquisition and analysis of NMR experiments. M.R., analysis and interpretation of copper(II) binding experiments; preparation of the manuscript. M.C.B. analysis and interpretation of EPR experiments. D.V., analysis and interpretation of NMR experiments; preparation of the manuscript. E.M., analysis and interpretation of kinetic experiments. S.N., analysis and interpretation of HPLC-MS experiments. L.C., conception of the project; preparation of the manuscript. M.T., conception of the project; analysis and interpretation of potentiometric, spectrophotometric, and CD data; preparation of the manuscript. S.D.A., conception of the project; analysis and interpretation of kinetic experiments; preparation of the manuscript. All authors critically revised the manuscript and approved its final version.

Funding

Italian Ministry of Education, University, and Research (MIUR) -Research Projects of National Interest (PRIN) 2015 prot. 2015T778JW.

Notes

The authors declare no competing financial interest.

■ ACKNOWLEDGMENTS

The authors acknowledge the Italian Ministry of Education, University, and Research (MIUR) - Research Projects of National Interest (PRIN) 2015 prot. 2015T778JW. CIRCMSB and CIRMMP are also acknowledged.

■ REFERENCES

(1) Weingarten, M. D.; Lockwood, A. H.; Hwo, S. Y.; Kirschner, M. W. A protein factor essential for microtubule assembly. *Proc. Natl. Acad. Sci. U. S. A.* **1975**, *72* (5), 1858.

(2) Jeganathan, S.; von Bergen, M.; Brutlach, H.; Steinhoff, H.-J.; Mandelkow, E. Global Hairpin Folding of Tau in Solution. *Biochemistry* **2006**, *45* (7), 2283−2293.

(3) Wang, Y.; Mandelkow, E. Tau in physiology and pathology. *Nat. Rev. Neurosci.* **2016**, *17*, 22.

(4) Spillantini, M. G.; Goedert, M. Tau pathology and neurodegeneration. *Lancet Neurol.* **2013**, *12* (6), 609−22.

(5) Fuster-Matanzo, A.; Hernández, F.; Ávila, J. Tau spreading mechanisms; Implications for dysfunctional tauopathies. *Int. J. Mol. Sci.* **2018**, *19* (3), 645.

(6) Masters, C. L.; Bateman, R.; Blennow, K.; Rowe, C. C.; Sperling, R. A.; Cummings, J. L. Alzheimer's disease. *Nat. Rev. Dis Primers* **2015**, *1*, 15056.

(7) Gong, C. X.; Iqbal, K. Hyperphosphorylation of microtubule-associated protein tau: a promising therapeutic target for Alzheimer disease. *Curr. Med. Chem.* **2008**, *15* (23), 2321−8.

(8) Brister, M. A.; Pandey, A. K.; Bielska, A. A.; Zondlo, N. J. OGlcNAcylation and Phosphorylation Have Opposing Structural Effects in tau: Phosphothreonine Induces Particular Conformational Order. *J. Am. Chem. Soc.* **2014**, *136* (10), 3803−3816.

(9) Reynolds, M. R.; Reyes, J. F.; Fu, Y.; Bigio, E. H.; Guillozet-Bongaarts, A. L.; Berry, R. W.; Binder, L. I. Tau nitration occurs at tyrosine 29 in the fibrillar lesions of Alzheimer's disease and other tauopathies. *J. Neurosci.* **2006**, *26* (42), 10636−45.

(10) Lindsley, C. W.; Hooker, J. M. Beyond the Amyloid Hypothesis of Alzheimer's Disease: Tau Pathology Takes Center Stage. *ACS Chem. Neurosci.* **2018**, *9* (11), 2519.

(11) Lippens, G.; Gigant, B. Elucidating Tau function and dysfunction in the era of cryo-EM. *J. Biol. Chem.* **2019**, *294*, 9316.

(12) Fitzpatrick, A. W. P.; Falcon, B.; He, S.; Murzin, A. G.; Murshudov, G.; Garringer, H. J.; Crowther, R. A.; Ghetti, B.; Goedert, M.; Scheres, S. H. W. Cryo-EM structures of tau filaments from Alzheimer's disease. *Nature* **2017**, *547*, 185.

(13) Alavi Naini, S. M.; Soussi-Yanicostas, N. Tau Hyperphosphorylation and Oxidative Stress, a Critical Vicious Circle in Neurodegenerative Tauopathies? *Oxid. Med. Cell. Longevity* **2015**, *2015*, 151979.

(14) Ibanez-Salazar, A.; Banuelos-Hernandez, B.; Rodriguez-Leyva, I.; Chi-Ahumada, E.; Monreal-Escalante, E.; Jimenez-Capdeville, M. E.; Rosales-Mendoza, S. Oxidative Stress Modifies the Levels and Phosphorylation State of Tau Protein in Human Fibroblasts. *Front. Neurosci.* **2017**, *11*, 495.

(15) Savelieff, M. G.; Lee, S.; Liu, Y.; Lim, M. H. Untangling Amyloid-β, Tau, and Metals in Alzheimer's Disease. *ACS Chem. Biol.* **2013**, *8* (5), 856−865.

(16) Leal, S. S.; Botelho, H. M.; Gomes, C. M. Metal ions as modulators of protein conformation and misfolding in neurodegeneration. *Coord. Chem. Rev.* **2012**, *256* (19), 2253−2270.

(17) Cheignon, C.; Tomas, M.; Bonnefont-Rousselot, D.; Faller, P.; Hureau, C.; Collin, F. Oxidative stress and the amyloid beta peptide in Alzheimer's disease. *Redox Biol.* **2018**, *14*, 450−464.

(18) Kepp, K. P. Bioinorganic Chemistry of Alzheimer's Disease. *Chem. Rev.* **2012**, *112* (10), 5193−5239.

(19) Valensin, D.; Dell'Acqua, S.; Kozlowski, H.; Casella, L. Coordination and redox properties of copper interaction with α-synuclein. *J. Inorg. Biochem.* **2016**, *163*, 292−300.

(20) Carboni, E.; Lingor, P. Insights on the interaction of alpha-synuclein and metals in the pathophysiology of Parkinson's disease. *Metallomics* **2015**, *7* (3), 395−404.

(21) La Mendola, D.; Rizzarelli, E. Evolutionary Implications of Metal Binding Features in Different Species' Prion Protein: An Inorganic Point of View. *Biomolecules* **2014**, *4* (2), 546.

(22) Kepp, K. P. Alzheimer's disease: How metal ions define β-amyloid function. *Coord. Chem. Rev.* **2017**, *351*, 127−159.

(23) Kozlowski, H.; Luczkowski, M.; Remelli, M.; Valensin, D. Copper, zinc and iron in neurodegenerative diseases (Alzheimer's, Parkinson's and prion diseases). *Coord. Chem. Rev.* **2012**, *256* (19−20), 2129−2141.

(24) Migliorini, C.; Porciatti, E.; Luczkowski, M.; Valensin, D. Structural characterization of Cu2+, Ni2+ and Zn2+ binding sites of model peptides associated with neurodegenerative diseases. *Coord. Chem. Rev.* **2012**, *256* (1−2), 352−368.

(25) Mo, Z. Y.; Zhu, Y. Z.; Zhu, H. L.; Fan, J. B.; Chen, J.; Liang, Y. Low micromolar zinc accelerates the fibrillization of human tau via bridging of Cys-291 and Cys-322. *J. Biol. Chem.* **2009**, *284* (50), 34648−57.

(26) Sun, X. Y.; Wei, Y. P.; Xiong, Y.; Wang, X. C.; Xie, A. J.; Wang, X. L.; Yang, Y.; Wang, Q.; Lu, Y. M.; Liu, R.; Wang, J. Z. Synaptic released zinc promotes tau hyperphosphorylation by inhibition of protein phosphatase 2A (PP2A). *J. Biol. Chem.* **2012**, *287* (14), 11174−82.

(27) Jiji, A. C.; Arshad, A.; Dhanya, S. R.; Shabana, P. S.; Mehjubin, C. K.; Vijayan, V. Zn2+ Interrupts R_4-R_3 Association Leading to Accelerated Aggregation of Tau Protein. *Chem. - Eur. J.* **2017**, *23* (67), 16976−16979.

(28) Yamamoto, A.; Shin, R. W.; Hasegawa, K.; Naiki, H.; Sato, H.; Yoshimasu, F.; Kitamoto, T. Iron (III) induces aggregation of hyperphosphorylated τ and its reduction to iron (II) reverses the aggregation: implications in the formation of neurofibrillary tangles of Alzheimer's disease. *J. Neurochem.* **2002**, *82* (5), 1137−1147.

(29) Pirota, V.; Monzani, E.; Dell'Acqua, S.; Casella, L. Interactions between heme and tau-derived R_1 peptides: binding and oxidative reactivity. *Dalton Transactions* **2016**, *45* (36), 14343−14351.

(30) Soragni, A.; Zambelli, B.; Mukrasch, M. D.; Biernat, J.; Jeganathan, S.; Griesinger, C.; Ciurli, S.; Mandelkow, E.; Zweckstetter, M. Structural Characterization of Binding of Cu(II) to Tau Protein†. *Biochemistry* **2008**, *47* (41), 10841−10851.

DOI: 10.1021/acs.inorgchem.9b02266
Inorg. Chem. 2020, 59, 274−286

(31) Zhou, L. X.; Du, J. T.; Zeng, Z. Y.; Wu, W. H.; Zhao, Y. F.; Kanazawa, K.; Ishizuka, Y.; Nemoto, T.; Nakanishi, H.; Li, Y. M. Copper (II) modulates in vitro aggregation of a tau peptide. *Peptides* **2007**, *28*, 2229−34.
(32) Ma, Q.; Li, Y.; Du, J.; Liu, H.; Kanazawa, K.; Nemoto, T.; Nakanishi, H.; Zhao, Y. Copper binding properties of a tau peptide associated with Alzheimer's disease studied by CD, NMR, and MALDI-TOF MS. *Peptides* **2006**, *27* (4), 841−849.
(33) Ma, Q.-F.; Li, Y.-M.; Du, J.-T.; Kanazawa, K.; Nemoto, T.; Nakanishi, H.; Zhao, Y.-F. Binding of copper (II) ion to an Alzheimer's tau peptide as revealed by MALDI-TOF MS, CD, and NMR. *Biopolymers* **2005**, *79* (2), 74−85.
(34) Shin, B.-k.; Saxena, S. Insight into Potential Cu(II)-Binding Motifs in the Four Pseudorepeats of Tau Protein. *J. Phys. Chem. B* **2011**, *115* (50), 15067−15078.
(35) Du, X.; Zheng, Y.; Wang, Z.; Chen, Y.; Zhou, R.; Song, G.; Ni, J.; Liu, Q. Inhibitory Act of Selenoprotein P on Cu+/Cu2+-Induced Tau Aggregation and Neurotoxicity. *Inorg. Chem.* **2014**, *53* (20), 11221−11230.
(36) Di Natale, G.; Bellia, F.; Sciacca, M. F. M.; Campagna, T.; Pappalardo, G. Tau-peptide fragments and their copper(II) complexes: Effects on Amyloid-β aggregation. *Inorg. Chim. Acta* **2018**, *472*, 82−92.
(37) Susanne Becker, J.; Zoriy, M.; Przybylski, M.; Sabine Becker, J. Study of formation of Cu- and Zn-containing tau protein using isotopically-enriched tracers by LA-ICP-MS and MALDI-FTICR-MS. *J. Anal. At. Spectrom.* **2007**, *22* (1), 63−68.
(38) Martic, S.; Rains, M. K.; Kraatz, H.-B. Probing copper/tau protein interactions electrochemically. *Anal. Biochem.* **2013**, *442* (2), 130−137.
(39) Sayre, L. M.; Perry, G.; Harris, P. L.; Liu, Y.; Schubert, K. A.; Smith, M. A. In situ oxidative catalysis by neurofibrillary tangles and senile plaques in Alzheimer's disease: a central role for bound transition metals. *J. Neurochem.* **2000**, *74* (1), 270−9.
(40) Su, X.-Y.; Wu, W.-H.; Huang, Z.-P.; Hu, J.; Lei, P.; Yu, C.-H.; Zhao, Y.-F.; Li, Y.-M. Hydrogen peroxide can be generated by tau in the presence of Cu(II). *Biochem. Biophys. Res. Commun.* **2007**, *358* (2), 661−665.
(41) Walker, S.; Ullman, O.; Stultz, C. M. Using intramolecular disulfide bonds in tau protein to deduce structural features of aggregation-resistant conformations. *J. Biol. Chem.* **2012**, *287* (12), 9591−600.
(42) Furukawa, Y.; Kaneko, K.; Nukina, N. Tau protein assembles into isoform- and disulfide-dependent polymorphic fibrils with distinct structural properties. *J. Biol. Chem.* **2011**, *286* (31), 27236−46.
(43) Pirota, V.; Dell'Acqua, S.; Monzani, E.; Nicolis, S.; Casella, L. Copper-Aβ Peptides and Oxidation of Catecholic Substrates: Reactivity and Endogenous Peptide Damage. *Chem. - Eur. J.* **2016**, *22* (47), 16964−16973.
(44) Ciregna, D.; Monzani, E.; Thiabaud, G.; Pizzocaro, S.; Casella, L. Copper-β-amyloid peptides exhibit neither monooxygenase nor superoxide dismutase activities. *Chem. Commun. (Cambridge, U. K.)* **2013**, *49* (38), 4027−9.
(45) De Ricco, R.; Valensin, D.; Dell'Acqua, S.; Casella, L.; Hureau, C.; Faller, P. Copper(I/II), alpha/beta-Synuclein and Amyloid-beta: Menage a Trois? *ChemBioChem* **2015**, *16* (16), 2319−28.
(46) Dell'Acqua, S.; Pirota, V.; Anzani, C.; Rocco, M. M.; Nicolis, S.; Valensin, D.; Monzani, E.; Casella, L. Reactivity of copper-[small alpha]-synuclein peptide complexes relevant to Parkinson's disease. *Metallomics* **2015**, *7* (7), 1091−1102.
(47) Dell'Acqua, S.; Pirota, V.; Monzani, E.; Camponeschi, F.; De Ricco, R.; Valensin, D.; Casella, L. Copper(I) Forms a Redox-Stable 1:2 Complex with α-Synuclein N-Terminal Peptide in a Membrane-Like Environment. *Inorg. Chem.* **2016**, *55* (12), 6100−6106.
(48) Dell'Acqua, S.; Bacchella, C.; Monzani, E.; Nicolis, S.; Di Natale, G.; Rizzarelli, E.; Casella, L. Prion Peptides Are Extremely Sensitive to Copper Induced Oxidative Stress. *Inorg. Chem.* **2017**, *56* (18), 11317−11325.
(49) Billo, E. J. Copper(II) chromosomes and the rule of average environment. *Inorg. Nucl. Chem. Lett.* **1974**, *10* (8), 613−617.
(50) Prenesti, E.; Daniele, P. G.; Prencipe, M.; Ostacoli, G. Spectrum-structure correlation for visible absorption spectra of copper(II) complexes in aqueous solution. *Polyhedron* **1999**, *18* (25), 3233−3241.
(51) Sigel, H.; Martin, R. B. Coordinating Properties of the Amide Bond. Stability and Structure of Metal Ion Complexes of Peptides and Related Ligands. *Chem. Rev.* **1982**, *82* (4), 385−426.
(52) Peisach, J.; Blumberg, W. E. Structural implications derived from the analysis of electron paramagnetic resonance spectra of natural and artificial copper proteins. *Arch. Biochem. Biophys.* **1974**, *165* (2), 691−708.
(53) Gralka, E.; Valensin, D.; Porciatti, E.; Gajda, C.; Gaggelli, E.; Valensin, G.; Kamysz, W.; Nadolny, R.; Guerrini, R.; Bacco, D.; Remelli, M.; Kozlowski, H. CuII binding sites located at His-96 and His-111 of the human prion protein: thermodynamic and spectroscopic studies on model peptides. *Dalton Trans* **2008**, No. 38, 5207−19.
(54) Remelli, M.; Valensin, D.; Toso, L.; Gralka, E.; Guerrini, R.; Marzola, E.; Kozlowski, H. Thermodynamic and spectroscopic investigation on the role of Met residues in Cu(II) binding to the non-octarepeat site of the human prion protein. *Metallomics* **2012**, *4* (8), 794−806.
(55) Santagostini, L.; Gullotti, M.; Pagliarin, R.; Bianchi, E.; Casella, L.; Monzani, E. Functional mimics of copper enzymes. Synthesis and stereochemical properties of the copper(II) complexes of a trinucleating ligand derived from L-histidine. *Tetrahedron: Asymmetry* **1999**, *10* (2), 281−295.
(56) Perrone, M. L.; Salvadeo, E.; Lo Presti, E.; Pasotti, L.; Monzani, E.; Santagostini, L.; Casella, L. A dinuclear biomimetic Cu complex derived from l-histidine: synthesis and stereoselective oxidations. *Dalton Trans* **2017**, *46* (12), 4018−4029.
(57) Presti, E. L.; Perrone, M. L.; Santagostini, L.; Casella, L.; Monzani, E. A Stereoselective Tyrosinase Model Compound Derived from an m-Xylyl-l-histidine Ligand. *Inorg. Chem.* **2019**, *58* (11), 7335−7344.
(58) Alies, B.; Renaglia, E.; Rozga, M.; Bal, W.; Faller, P.; Hureau, C. Cu(II) affinity for the Alzheimer's peptide: tyrosine fluorescence studies revisited. *Anal. Chem.* **2013**, *85* (3), 1501−8.
(59) Alies, B.; Badei, B.; Faller, P.; Hureau, C. Reevaluation of copper(I) affinity for amyloid-beta peptides by competition with ferrozine–an unusual copper(I) indicator. *Chem. - Eur. J.* **2012**, *18* (4), 1161−7.
(60) Haas, K. L.; Putterman, A. B.; White, D. R.; Thiele, D. J.; Franz, K. J. Model peptides provide new insights into the role of histidine residues as potential ligands in human cellular copper acquisition via Ctr1. *J. Am. Chem. Soc.* **2011**, *133* (12), 4427−37.
(61) Himes, R. A.; Park, G. Y.; Siluvai, G. S.; Blackburn, N. J.; Karlin, K. D. Structural studies of copper(I) complexes of amyloid-beta peptide fragments: formation of two-coordinate bis(histidine) complexes. *Angew. Chem., Int. Ed.* **2008**, *47* (47), 9084−7.
(62) Conklin, S. E.; Bridgman, E. C.; Su, Q.; Riggs-Gelasco, P.; Haas, K. L.; Franz, K. J. Specific Histidine Residues Confer Histatin Peptides with Copper-Dependent Activity against Candida albicans. *Biochemistry* **2017**, *56* (32), 4244−4255.
(63) Gaggelli, E.; D'Amelio, N.; Valensin, D.; Valensin, G. 1H NMR studies of copper binding by histidine-containing peptides. *Magn. Reson. Chem.* **2003**, *41* (10), 877−883.
(64) Gaggelli, E.; Kozlowski, H.; Valensin, D.; Valensin, G. NMR studies on Cu(II)-peptide complexes: Exchange kinetics and determination of structures in solution. *Mol. BioSyst.* **2005**, *1* (1), 79−84.
(65) Hautier, A.; Carvalho, T.; Valensin, D.; Simaan, A. J.; Faure, B.; Mateus, P.; Delgado, R.; Iranzo, O. The role of methylation in the copper(ii) coordination properties of a His-containing decapeptide. *Dalton Trans* **2019**, *48* (5), 1859−1870.
(66) De Gregorio, G.; Biasotto, F.; Hecel, A.; Luczkowski, M.; Kozlowski, H.; Valensin, D. Structural analysis of copper(I)

DOI: 10.1021/acs.inorgchem.9b02266
Inorg. Chem. 2020, 59, 274−286

interaction with amyloid beta peptide. *J. Inorg. Biochem.* **2019**, *195*, 31−38.
(67) Valensin, D.; Padula, E. M.; Hecel, A.; Luczkowski, M.; Kozlowski, H. Specific binding modes of Cu(I) and Ag(I) with neurotoxic domain of the human prion protein. *J. Inorg. Biochem.* **2016**, *155*, 26−35.
(68) Atrian-Blasco, E.; Gonzalez, P.; Santoro, A.; Alies, B.; Faller, P.; Hureau, C. Cu and Zn coordination to amyloid peptides: From fascinating chemistry to debated pathological relevance. *Coord. Chem. Rev.* **2018**, *371*, 38−55.
(69) Shearer, J.; Szalai, V. A. The amyloid-beta peptide of Alzheimer's disease binds Cu(I) in a linear bis-his coordination environment: insight into a possible neuroprotective mechanism for the amyloid-beta peptide. *J. Am. Chem. Soc.* **2008**, *130* (52), 17826−35.
(70) Monzani, E.; Nicolis, S.; Dell'Acqua, S.; Capucciati, A.; Bacchella, C.; Zucca, F. A.; Mosharov, E. V.; Sulzer, D.; Zecca, L.; Casella, L. Dopamine, Oxidative Stress and Protein-Quinone Modifications in Parkinson's and Other Neurodegenerative Diseases. *Angew. Chem., Int. Ed.* **2019**, *58* (20), 6512−6527.
(71) Zecca, L.; Bellei, C.; Costi, P.; Albertini, A.; Monzani, E.; Casella, L.; Gallorini, M.; Bergamaschi, L.; Moscatelli, A.; Turro, N. J.; Eisner, M.; Crippa, P. R.; Ito, S.; Wakamatsu, K.; Bush, W. D.; Ward, W. C.; Simon, J. D.; Zucca, F. A. New melanic pigments in the human brain that accumulate in aging and block environmental toxic metals. *Proc. Natl. Acad. Sci. U. S. A.* **2008**, *105* (45), 17567−17572.
(72) Pham, A. N.; Waite, T. D. Cu(II)-catalyzed oxidation of dopamine in aqueous solutions: mechanism and kinetics. *J. Inorg. Biochem.* **2014**, *137*, 74−84.
(73) Herlinger, E.; Jameson, R. F.; Linert, W. Spontaneous autoxidation of dopamine. *J. Chem. Soc., Perkin Trans. 2* **1995**, No. 2, 259−263.
(74) da Silva, G. F. Z.; Ming, L.-J. Metallo-ROS in Alzheimer's Disease: Oxidation of Neurotransmitters by CuII-β-Amyloid and Neuropathology of the Disease. *Angew. Chem., Int. Ed.* **2007**, *46* (18), 3337−3341.
(75) Nam, E.; Derrick, J. S.; Lee, S.; Kang, J.; Han, J.; Lee, S. J. C.; Chung, S. W.; Lim, M. H. Regulatory Activities of Dopamine and Its Derivatives toward Metal-Free and Metal-Induced Amyloid-β Aggregation, Oxidative Stress, and Inflammation in Alzheimer's Disease. *ACS Chem. Neurosci.* **2018**, *9* (11), 2655−2666.
(76) Atrián-Blasco, E.; Del Barrio, M.; Faller, P.; Hureau, C. Ascorbate Oxidation by Cu(Amyloid-β) Complexes: Determination of the Intrinsic Rate as a Function of Alterations in the Peptide Sequence Revealing Key Residues for Reactive Oxygen Species Production. *Anal. Chem.* **2018**, *90* (9), 5909−5915.
(77) Yako, N.; Young, T. R.; Cottam Jones, J. M.; Hutton, C. A.; Wedd, A. G.; Xiao, Z. Copper binding and redox chemistry of the Aβ16 peptide and its variants: insights into determinants of copper-dependent reactivity. *Metallomics: integrated biometal science* **2017**, *9* (3), 278−291.
(78) Solomon, E. I.; Heppner, D. E.; Johnston, E. M.; Ginsbach, J. W.; Cirera, J.; Qayyum, M.; Kieber-Emmons, M. T.; Kjaergaard, C. H.; Hadt, R. G.; Tian, L. Copper Active Sites in Biology. *Chem. Rev.* **2014**, *114* (7), 3659−3853.
(79) Smith, D. G.; Cappai, R.; Barnham, K. J. The redox chemistry of the Alzheimer's disease amyloid beta peptide. *Biochim. Biophys. Acta, Biomembr.* **2007**, *1768* (8), 1976−90.
(80) Chassaing, S.; Collin, F.; Dorlet, P.; Gout, J.; Hureau, C.; Faller, P. Copper and heme-mediated Abeta toxicity: redox chemistry, Abeta oxidations and anti-ROS compounds. *Curr. Top. Med. Chem.* **2013**, *12* (22), 2573−95.
(81) Butterfield, D. A.; Reed, T.; Newman, S. F.; Sultana, R. Roles of amyloid beta-peptide-associated oxidative stress and brain protein modifications in the pathogenesis of Alzheimer's disease and mild cognitive impairment. *Free Radical Biol. Med.* **2007**, *43* (5), 658−77.
(82) Hawkins, C. L.; Davies, M. J. Generation and propagation of radical reactions on proteins. *Biochim. Biophys. Acta, Bioenerg.* **2001**, *1504* (2−3), 196−219.
(83) Hureau, C.; Faller, P. Abeta-mediated ROS production by Cu ions: structural insights, mechanisms and relevance to Alzheimer's disease. *Biochimie* **2009**, *91* (10), 1212−7.
(84) Requena, J. R.; Chao, C.-C.; Levine, R. L.; Stadtman, E. R. Glutamic and aminoadipic semialdehydes are the main carbonyl products of metal-catalyzed oxidation of proteins. *Proc. Natl. Acad. Sci. U. S. A.* **2001**, *98* (1), 69.

DOI: 10.1021/acs.inorgchem.9b02266
Inorg. Chem. 2020, 59, 274−286

Journal of Inorganic Biochemistry 205 (2020) 110980

Contents lists available at ScienceDirect

Journal of Inorganic Biochemistry

journal homepage: www.elsevier.com/locate/jinorgbio

Cu(II) coordination to His-containing linear peptides and related branched ones: Equalities and diversities

Monica Perinelli[a,1], Remo Guerrini[b], Valentina Albanese[b], Nicola Marchetti[b], Denise Bellotti[b], Silvia Gentili[a], Matteo Tegoni[a,*,2], Maurizio Remelli[b,*,2]

[a] Dipartimento di Scienze Chimiche, della Vita e della Sostenibilità Ambientale, Università di Parma, Parco Area delle Scienze 11/A, 43124 Parma, Italy
[b] Dipartimento di Scienze Chimiche e Farmaceutiche, Università di Ferrara, via Luigi Borsari 46, 44121 Ferrara, Italy

ARTICLE INFO

Keywords:
Metal complexes
Copper(II)
Branched peptides
Cyclam scaffold
Solution equilibria
Peptide welding technology

ABSTRACT

The two branched peptides $(AAHAWG)_4$-**PWT2** and $(HAWG)_4$-**PWT2** where synthesized by mounting linear peptides on a cyclam-based scaffold (**PWT2**), provided with four maleimide chains, through a thio-Michael reaction. The purpose of this study was primarily to verify if the two branched ligands had a Cu(II) coordination behavior reproducing that of the single-chain peptides, namely AAHAWG-NH_2, which bears an Amino Terminal Cu(II)- and Ni(II)-Binding (ATCUN) Motif, and HAWG-NH_2, which presents a His residue as the N-terminal amino acid, in a wide pH range. The study of Cu(II) binding was performed by potentiometric, spectroscopic (UV–vis absorption, CD, fluorescence) and ESI-MS techniques. ATCUN-type ligands ($(AAHAWG)_4$-**PWT2** and AAHAWG-NH_2) were confirmed to bind one Cu(II) per peptide fragment at both pH 7.4 and pH 9.0, with a [NH_2, $2N^-$, N_{Im}] coordination mode. On the other hand, the ligand HAWG-NH_2 forms a $[CuL_2]^{2+}$ species at neutral pH, while, at pH 9, the formation of 1:2 Cu(II):ligand adducts is prevented by amidic nitrogen deprotonation and coordination, to give rise solely to 1:1 species. Conversely, Cu(II) binding to $(HAWG)_4$-**PWT2** resulted in the formation of 1:2 copper:peptide chain also at pH 9: hence, through the latter branched peptide we obtained, at alkaline pH, the stabilization of a specific Cu(II) coordination mode which results unachievable using the corresponding single-chain peptide. This behavior could be explained in terms of high local peptide concentration on the basis of the speciation of the Cu(II)/single-chain peptide systems.

1. Introduction

Branched peptides have been explored in recent years for the isolation of compounds capable of nucleic acid condensation [1,2] and gene delivery [3–5], characterized by a high resistance to peptidases [6,7] or with application in multivalent interactions with biomolecular targets [8,9]. In the last decade, branched peptides and more in general oligopeptides covalently mounted on a molecular scaffold were explored for their metal-binding properties [10].

Among those presented in the literature, branched peptides studied for metal binding are profoundly diverse in complexity. Examples were given of short dipeptides [11–14] and long oligopeptides that spontaneously fold into supersecondary structures such as coiled coils [15–17]. For this latter class of peptides the term template-assisted synthetic protein (TASP) was coined [18]. All these peptides operate metal binding in a diverse way depending on the amino acid composition and preorganization or fold of the overall branched peptide. As a general observation, the branches in a branch peptide act as independent metal binding moieties for less structured constructs, while single metal binding sites could be obtained for folded architectures [19].

A new, relatively simple and very efficient method for the synthesis of tetrabranched peptides has been recently described [20]. It guarantees very high yields and an excellent purity of the products. The synthetic strategy was named “peptide welding technology” (PWT) and it consists of fixing four identical peptides on a suitable scaffold, by means of a convergent approach. First, the peptide sequence and the scaffold are separately synthesized and purified; then, they are bonded together by exploiting the presence of specific mutually-reactive functional groups. The thiol-Michael reaction, which is highly chemoselective, was used for this PWT strategy. The peptide contains an additional C-terminal cysteine residue and the reaction occurs between the Cys

* Corresponding authors.
E-mail addresses: matteo.tegoni@unipr.it (M. Tegoni), rmm@unife.it (M. Remelli).
[1] Current address: Institute of Inorganic Chemistry, University of Zurich, Winterthurerstrasse 190, 8057 Zurich, Switzerland.
[2] M.T. and M.R. equally contributed to this work.

https://doi.org/10.1016/j.jinorgbio.2019.110980
Received 1 October 2019; Received in revised form 13 December 2019; Accepted 24 December 2019
Available online 03 January 2020
0162-0134/

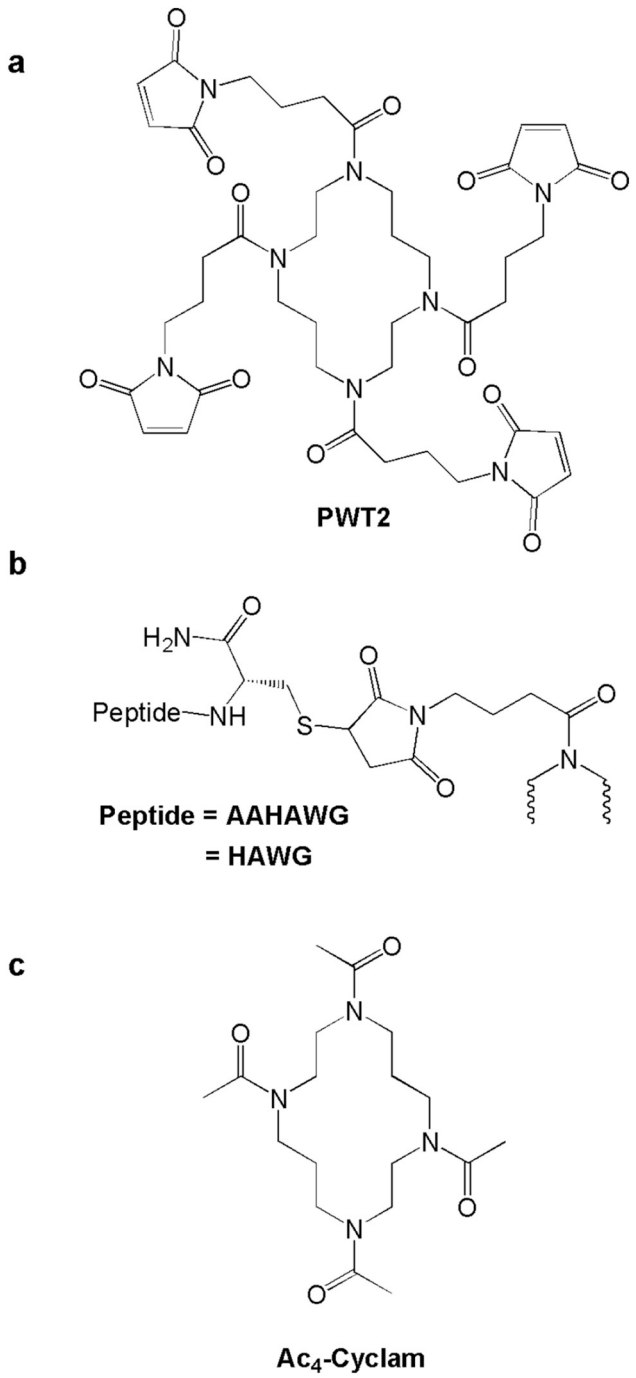

Scheme 1. Representation of a) the **PWT2** scaffold [20]; b) the spacer between the cyclam macrocycle and the peptide moieties; c) the tetra-acetylated cyclam-based scaffold 1,1′,1″,1‴-(1,4,8,11-tetraazacyclotetradecane-1,4,8,11-tetrayl) tetraethanone (Ac_4-cyclam).

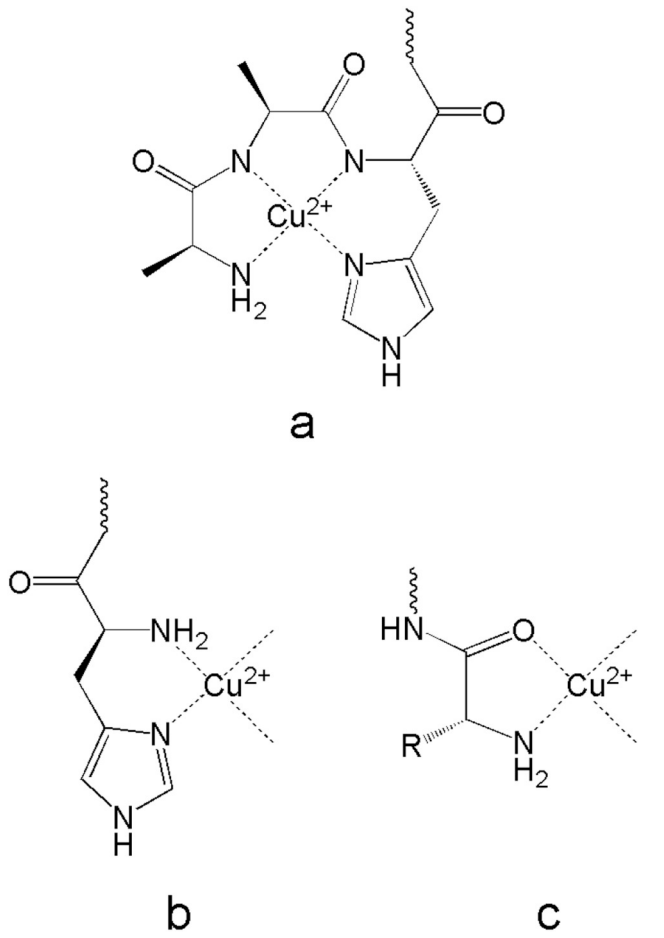

Scheme 2. Representation of a) ATCUN-type coordination; b) *histamine-like* coordination, c) *glycine-like* coordination of the peptide N-terminus to Cu(II) (R = CH_2Im).

thiolic side chain and a α-β-unsaturated carbonyl group present on the platform, thus a thio-ether addition product is obtained. Among several studied cores, we focused our attention on the so called **PWT2**, a scaffold based on the cyclam (1,4,8,11-tetraazacyclotetradecane) moiety, – where four maleimide chains are linked through a spacer to the four nitrogen atoms of the hetero-cycle (Scheme 1).

In this paper we present two branched homomeric tetrapeptides consisting of four linear tetra- or hexa-peptides mounted on a **PWT2** scaffold, capable of binding Cu(II) at their N-termini (Scheme 1). The used linear peptides were AAHAWGC-NH_2 and HAWGC-NH_2. The C-terminal Cys present in each peptide had the thiol function converted into a thioether group as a consequence of the covalent linkage to the cyclam scaffold (Scheme 1). Furthermore, these peptides are characterized by the presence of one histidine residue as the principal metal binding residue, and were designed to achieve the stabilization of two different metal coordination environments, as discussed below. The tetrameric ligand $(AAHAWG)_4$-**PWT2** contains four ATCUN (Amino Terminal Cu(II)- and Ni(II)-Binding Motif) N-termini, corresponding to the Xxx-Xxx-His- sequence, while the ligand $(HAWG)_4$-**PWT2** has a histidine as first amino acid at its four N-termini. These ligands are therefore homomeric branched tetrapeptides with four or six residues plus a spacer between the peptide and the scaffold. Conversely to the examples in literature [21], these ligands ensure a high degree of flexibility of the construct and the possibility to bind either four metal ions (one per arm) or two metal ions (two peptides coordinated to each metal).

The rationale for the use of these ligands is the following: peptides with ATCUN sequence are known to form 1:1 Cu(II)/peptide adducts with a (NH_2, $2N^-$, N_{Im}, Scheme 2a) metal coordination [22–24]. In addition, this binding mode is known to be stable over a quite wide pH range. On the contrary, peptides containing the amino-terminal His residue have been reported to form different complexes with Cu(II) as a function of the pH. In particular, a (2N) mode – known as *histamine-like* mode (Scheme 2b) – or a (N, O) coordination mode – which we can call *glycine-like* mode, for the sake of simplicity, (Scheme 2c) – are expected to be stable at low pH [25–27]. The deprotonation of the peptide nitrogen atoms of the backbone and subsequent coordination to Cu(II)

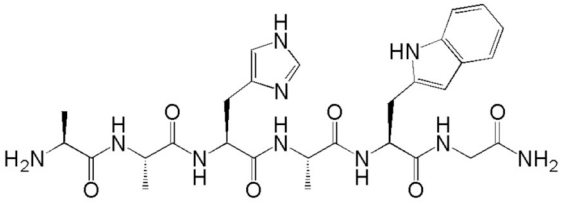

AAHAWG-NH_2

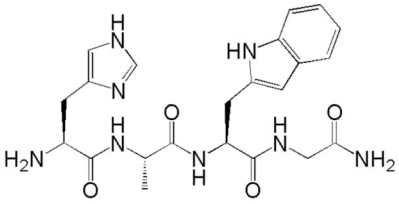

HAWG-NH_2

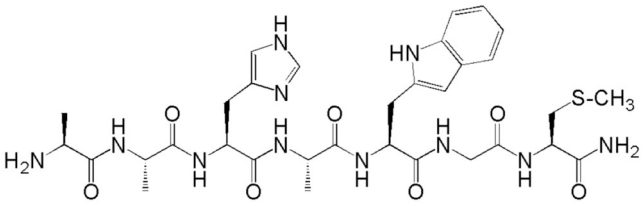

AAHAWGC(SMe)-NH_2

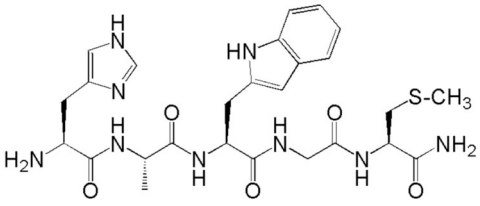

HAWGC(SMe)-NH_2

Scheme 3. Representation of the single-chain peptides studied in this work.

has been observed at higher pH values [28,29]. Here we aimed to take advantage of anchoring of four short peptides to a single scaffold to stabilize specific Cu(II) coordination environments. In particular, we aimed to evaluate if with $(HAWG)_4$-**PWT2** – considering the high local concentration of peptides – a *histamine-like* coordination of the N-terminal His could be stabilized at pH values where, using single-chain peptides, it cannot be formed.

Along with the two branched peptides, in this work we have studied the corresponding single-chain peptides, containing or not a Cys(SMe) residue at their C-terminus to simulate the role played by the spacer in the tetrameric ligands (Scheme 3). The thermodynamic speciation model in solution, in a wide pH range, was obtained through potentiometric titrations and the stoichiometry of the formed species was confirmed by mass spectrometry. A deep spectroscopic investigation with several different techniques allowed to formulate structural hypotheses for the complexes formed in solution, under different experimental conditions.

2. Experimental

2.1. Reagents

2.1.1. Synthesis and purification of the ligands

Tetrabranched peptide derivatives were prepared using a convergent synthetic approach previously optimized and employed by our research group for the synthesis of a series of G-protein coupled receptor ligands [20]. Linear peptides were synthesized by solid phase method with an automatic solid phase peptide synthesizer Syro II (Biotage, Uppsala Sweden) using Fluorenylmethyloxycarbonyl (Fmoc)/tBu chemistry [30]. The resin 4-(2′,4′-dimethoxyphenyl-Fmoc-aminomethyl)-phenoxyacetamido-norleucyl-4-Methylbenzhydrylamine (Rink amide MBHA resin) was used as a solid support.

As an example, for the synthesis of AAHAWGC-NH_2, the following procedure was applied. The resin was treated with 40% piperidine/*N*,*N*-dimethylformamide (DMF) and linked with Fmoc-Cys(Trt)-OH (Trt = Trityl = Triphenylmethyl) by using [O-(7-azabenzotriazol-1-yl)-1,1,3,3-tetramethyluronium hexafluorophosphate] (HATU) as the coupling reagent. The following Fmoc amino acids were sequentially coupled to the growing peptide chain: Fmoc-Gly-OH, Fmoc-Trp(Tert-butyloxycarbonyl = Boc)-OH, Fmoc-Ala-OH, Fmoc-His(Trt)-OH, Fmoc-Ala-OH, Fmoc-Ala-OH. All the Fmoc amino acids (4 equiv.) were coupled to the growing peptide chain by using HATU (4 equiv.) in DMF in the presence of an equimolar concentration of 4-methylmorpholine (NMM), and the coupling reaction time was 1 h. To improve the analytical profile of the crude peptide, capping with acetic anhydride (0.5 M/DMF) in the presence of NMM (0.25 M/DMF) (3:1 *v*/v; 2 mL/0.2 g of resin) was performed at any step. 40% Piperidine/DMF was used to remove the Fmoc protecting group. The protected peptide-resin was treated with reagent B [31] (trifluoroacetic acid (TFA)/H_2O/phenol/triisopropylsilane 88:5:5:2; v/v; 10 mL/0.2 g of resin) for 1.5 h at room temperature. After filtration of the resin, the solvent was concentrated in vacuo and the residue triturated with ether. Crude peptide was purified by preparative reversed-phase HPLC using a Water Delta Prep 3000 system with a Jupiter column C_{18} (250 × 30 mm, 300 A, 15 μm spherical particle size). The column was perfused at a flow rate of 20 mL/min with a mobile phase containing solvent A (5% *v*/v acetonitrile/water, 0.1% TFA), and a linear gradient from 0 to 60% of solvent B (60% v/v acetonitrile/water, 0.1% TFA) over 25 min for the elution of peptides.

In order to obtain the branched peptide $(AAHAWG)_4$-**PWT2**, purified AAHAWGC-NH_2 x TFA (37 mg; 0.044 mmol) was reacted in solution (H_2O/CH_3CN 1/1; 2 mL) with **PWT2** [20] core (8.6 mg; 0.01 mmol) in the presence of 100 μL of 5% $NaHCO_3$ in a classical thio-Michael reaction previously optimized for the synthesis of Nociceptin/orphanin FQ tetra branched derivatives [32]. As expected, the reaction reached completion in a few minutes and the mixture was directly purified by preparative HPLC using experimental condition previously reported for the purification of the linear peptide. The compound $(HAWG)_4$-**PWT2** was synthesized in a similar manner.

Analytical HPLC analyses were performed on a Beckman 116 liquid chromatograph equipped with a Beckman 166 diode array detector. The analytical purity of the final compounds (the branched: $(AAHAWG)_4$-**PWT2**, $(HAWG)_4$-**PWT2** and the linear: AAHAWG-NH_2, HAWG-NH_2, AAHAWGC-NH_2, HAWGC-NH_2, AAHAWGC(SMe)-NH_2, HAWGC(SMe)-NH_2,) was determined using a Luna C_{18} column (4.6 × 100 mm, 3 μm particle size) with the above solvent system (solvents A and B) programmed at a flow rate of 0.5 mL/min using a linear gradient from 0% to 70% B over 25 min. Final products showed ≥95% purity when monitored at 220 nm. Molecular weights of final compounds were determined by a mass spectrometer ESI Micromass ZMD-2000 (Waters®).

The tetra-acetylated cyclam-based scaffold 1,1′,1″,1‴-(1,4,8,11-tetraazacyclotetradecane-1,4,8,11-tetrayl)tetraethanone (Ac_4-cyclam) was obtained by dissolving 1,4,8,11-tetraazacyclotetradecane (1.0 mmol) in

acetic anhydride (2 mL). The reaction was then left to stir overnight. After this time, the solvent was removed under vacuum and the crude product was purified via silica gel column chromatography using EtOAc as eluent. ^{1}H and ^{13}C NMR measurements confirmed the synthesis of Ac_4-cyclam, giving the following values of chemical shift: ^{1}H NMR (400 MHz, DMSO-d_6) = δ 3.58–3.25 (m, 16H), 2.03–1.66 (m, 12H), 1.92–1.62 (m, 4H); 13C NMR = δ 170.03, 169.99, 169.84, 169.68, 48.37, 48.05, 47.19, 46.66, 45.71, 44.90, 44.44, 43.72, 43.10, 28.09, 27.63, 27.12, 21.34, 20.77.

2.2. Solution studies

All the linear and branched peptide solutions were prepared in freshly-boiled bidistilled water, in the presence of HCl 2 mM; the peptide (single chain) concentration was always about 10 mM. The stock solution of Ac_4-cyclam was prepared in D_2O and its concentration (19.1 mM) was determined by H^1-NMR using an external standard (L-Phe).

2.2.1. Potentiometric measurements

The potentiometric titrations of AAHAWG-NH_2, HAWG-NH_2, AAHAWGC(SMe)-NH_2 and HAWGC(SMe)-NH_2 were carried out in aqueous solution at T = 25 ± 0.1 °C and I = 0.1 M (KCl) under N_2 stream, using 2.2 mL samples. The potentiometric apparatus was previously described [33]. The Hamilton combined glass electrode (P/N 238000) was calibrated in terms of [H^+] by titrating HCl solutions with a 0.1 M carbonate-free standardized solution of KOH and the pK_w value resulted to be 13.76(1). Protonation data were obtained by alkalimetric titration of 3 samples (C_L = 1.2–1.3 10^{-3} M). Formation constants for the Cu(II) complexes were determined from 3 titrations carried out on sample solutions where the total concentration of metal ranged from 0.5 to 1.1 mM and the copper/ligand molar ratio ranged from 1:2 to 2:1. All the systems were studied between pH 3 and 11.

The protonation and complex-formation constants of the systems were calculated with the software HyperQuad 2013 [34] and the results were used to draw the species distribution curves with the software Hyss 2009 [35].

2.2.2. UV–visible and circular dichroism data

UV and visible spectra of the Cu(II)/AAHAWG-NH_2, Cu(II)/HAWG-NH_2, Cu(II)/$(AAHAWG)_4$-**PWT2** and Cu(II)/$(HAWG)_4$-**PWT2** systems were collected with a spectrophotometer Evolution 260 Bio (Thermo Scientific, Waltham, MA, USA) provided with a Peltier thermostat, using quartz cuvettes of 1 cm path length. The absorption spectra of the Cu(II)/AAHAWGC(SMe)-NH_2 and Cu(II)/HAWGC(SMe)-NH_2 systems were recorded on a Varian Cary50 Probe spectrophotometer, using quartz cuvettes with an optical path of 1 cm. For the studies performed at fixed pH, aqueous HEPES 25 mM (pH 7.0 for Cu(II)/HAWG-NH_2; pH 7.4 for Cu(II)/AAHAWG-NH_2) or CHES 25 mM (pH 9.0) were employed. The used Cu(II) and peptide concentrations were $C_{peptide}$ = 0.70 mM, Cu:peptide = 0–1.32:1. Studies at variable pH were performed by direct addition of NaOH. Spectra were collected every half pH unit between pH 3 and 11 (Cu:peptide = 1:1.3–1.4, C_{Cu} = 0.50 mM). Spectrophotometric titrations of the Cu(II)/$(AAHAWG)_4$-**PWT2** and Cu(II)/$(HAWG)_4$-**PWT2** systems were performed only at fixed pH, under the conditions used for linear peptides, by the addition of Cu(II) aliquots to the buffered ligand solutions (C_{ligand} = 0.17 mM, Cu:ligand = 0–8.2:1).

CD spectra of the Cu(II)/AAHAWG-NH_2, Cu(II)/HAWG-NH_2, Cu(II)/$(AAHAWG)_4$-**PWT2** and Cu(II)/$(HAWG)_4$-**PWT2** systems were collected with a Jasco J715 spectropolarimeter, using 0.1 and 1 cm path length cuvettes for the UV and the Vis range, respectively. CD data collection at variable pH for Cu(II)/AAHAWG-NH_2 and Cu(II)/HAWG-NH_2 was performed between pH 3.2 and 12 by direct addition of NaOH. For spectra collected in the UV region the concentrations were Cu:peptide = 1:2–2.2, C_{Cu} = 48–52 μM; for spectra collected in the visible region the concentrations were Cu:peptide = 1:2–2.2, C_{Cu} = 0.48–0.52 mM. CD data collection at fixed pH was performed at pH 7.4 for Cu(II)/AAHAWG-NH_2 and pH 7.0 or pH 9.0 for Cu(II)/HAWG-NH_2. The same buffer conditions of absorption measurements were employed. The Cu(II)/$(AAHAWG)_4$-**PWT2** and Cu(II)/$(HAWG)_4$-**PWT2** systems were studied only at fixed pH (7.4 and 9.0 for the former, 7.0 for the latter, same buffer solutions as above). For both UV and visible regions, the following conditions were employed: C_{ligand} = 0.20 mM, Cu:ligand = 0–4:1. For Cu(II)/$(AAHAWG)_4$-**PWT2**, opalescence was observed at pH 9.0 for Cu(II):ligand > 1. For Cu(II)/$(HAWG)_4$-**PWT2**, opalescence was observed at pH 9.0 upon addition of small quantities of Cu(II), which prevented the collection of reliable CD data. CD data at pH 7.0 for $(HAWG)_4$-**PWT2** were limited to Cu:ligand = 0–4:1 due to opalescence for higher amounts of Cu(II).

2.2.3. Spectrofluorometric titrations

Emission spectra were collected on a Horiba Jobin Yvon Fluoromax 3 spectrofluorimeter, using a 1 cm path length quartz cuvette. The protonation equilibria of AAHAWG-NH_2 and HAWG-NH_2 were studied in aqueous solution between pH 3 and 10.5 by addition of small aliquots of concentrated NaOH to an acidic solution of the ligands (C_L = 9.5 and 4.8 μM for the two peptides, respectively, I = 0.1 M (KCl), T = 298.2 K). The Cu(II)/AAHAWG-NH_2 and Cu(II)/HAWG-NH_2 systems were studied at fixed pH (7.4 for the former, 7.0 and 9.0 for the latter) by titration of the peptide solution with Cu(II) (C_L = 48 μM, Cu(II)/peptide = 0–1.46). The Cu(II)/$(AAHAWG)_4$-**PWT2** and Cu(II)/$(HAWG)_4$-**PWT2** systems were studied at fixed pH (7.4 for the former, 7.0 and 9.0 for the latter) by titration of the peptide solution with Cu(II) (C_L = 20 μM, Cu/ligand = 0–5). Buffer conditions were the same as described above for absorption studies. Buffer solutions used to prepare the samples were passed through a 0.45 μm nylon filter immediately prior their use.

2.2.4. ^{1}H-NMR

^{1}H NMR spectra were collected on a Bruker AVANCE 400 MHz spectrometer. The Ac_4-cyclam system was studied with ^{1}H NMR and ^{1}H-COSY (C_L = 19.1 mM in D_2O). The variable temperature spectra were collected from 25 to 75 °C. The ^{1}H NMR spectrum in the presence of an equimolar amount of Cu(II) was also collected. The 2D spectra were collected at 75 °C. Spectra were referenced to the residual HDO peak [36].

2.2.5. Electrospray-Ionization Mass-Spectrometry (ESI-MS)

ESI mass spectra were recorded on a linear ion trap LTQ XL Mass Spectrometer (Thermo Scientific, Waltham, MA, USA). Data were processed by using the spectrometer software. The measurements were performed on binary metal/ligand solutions at appropriate pH values, chosen in order to maximize the formation of a single complex species. The samples were prepared in a similar way as described for potentiometric studies without the addition of background electrolyte, in water/methanol 50:50 *V*/V. The counter-ion was supplied by the base employed to adjust the pH value (KOH). Direct infusion analyses were always performed at 5 μL/min. Experimental conditions were as follows: spray voltage 4.8 kV; sheath gas 40 a.u.; capillary temperature 250 °C; capillary voltage 8–25 V and tube lens 60–120 V.

3. Results

3.1. Study of Cu(II)/Ac_4-cyclam system

The compound Ac_4-cyclam has been synthesized and used as a model to study the possible binding of Cu(II) to the functionalized cyclam scaffold. Ac_4-cyclam has been characterized by ^{1}H NMR and ^{1}H-COSY experiments (Figs. S1 and S2, Supplementary Information). Multiple peaks are present in the 1.5–2.2 ppm (alkyl C-CH_2-C and acyl CH_3CO protons) and 3.3–3.8 ppm ranges (CH_2-N protons). Increasing

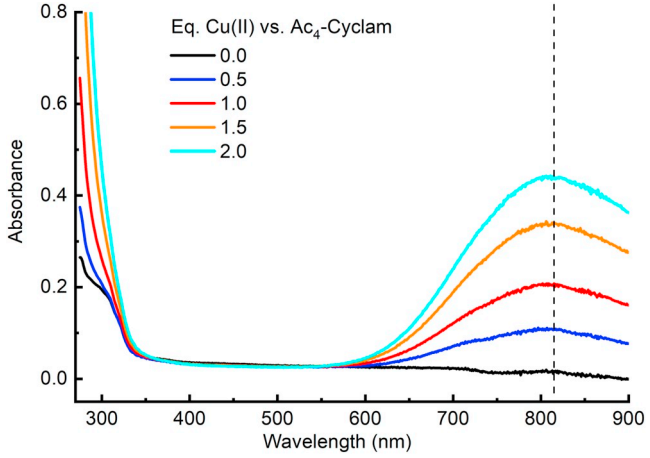

Fig. 1. UV–visible spectra for the titration of a water solution containing Ac_4-cyclam (19.1 mM) and $CuCl_2$ (Cu:Ac_4-cyclam ratio = 0–2).

the temperature up to 75 °C, we observed progressive broadening of the alkyl signals and coalescence of the acyl ones (Fig. S2, Supplementary Information). These data overall demonstrate that the conformation of the scaffold is fluxional in intermediate exchange on the NMR time scale with prevalence of slow exchange at 25 °C.

The acid-base behavior of Ac_4-cyclam has been investigated by potentiometry. The obtained titration curve (Fig. S3, Supplementary Information) is nicely superimposable to that calculated for the titration of HCl alone, without Ac_4-cyclam. This result confirms that Ac_4-cyclam does not have any acid-base activity which could interfere with the potentiometric study of the apo-peptidic chains. Furthermore, in order to exclude Cu(II) binding to Ac_4-cyclam, a series of UV–Vis spectra have been recorded at different metal/ligand ratios. No changes in the wavelength of maximum of absorption have been observed and the obtained λ_{max} = 815 nm is consistent with the presence of solely Cu(II) aqua ion (Fig. 1). Further evidence comes from the NMR spectra of Ac_4-cyclam registered in the absence and in the presence of an equimolar amount of Cu(II) (Fig. S4, Supplementary Information), since signals broadening, expected for the presence of coordinated Cu(II), are completely absent.

3.2. Ligand protonation equilibria

The protonation constants of the single-chain peptides are reported in Table 1; the corresponding distribution diagrams are reported as Supplementary Information (Figs. S5 – S8).

All the linear peptides bear two basic sites, i.e. the terminal amine and the side imidazole of the His residue. Data of Table 1 are *macro*-constants and the corresponding *micro*-constants are not available; however, on the basis of literature [37] the highest log*K* value can be mainly attributed to the former functional group and the lowest to His. The protonation equilibria of AAHAWG-NH_2 and HAWG-NH_2 have also

Table 1
Protonation constants for the single-chain peptides at T = 298.2 K and I = 0.1 M (KCl). Standard deviations on the last figure in parentheses.

Ligand	Species	logβ	log$K$	Residue
AAHAWG-NH_2	LH^+	7.94(1)	7.94	Terminal NH_2
	LH_2^{2+}	14.30(1)	6.36	His
AAHAWGC(SMe)-NH_2	LH^+	7.86(2)	7.86	Terminal NH_2
	LH_2^{2+}	14.09(3)	6.23	His
HAWG-NH_2	LH^+	7.33(5)	7.33	Terminal NH_2
	LH_2^{2+}	12.89(3)	5.56	His
HAWGC(SMe)-NH_2	LH^+	7.27(3)	7.27	Terminal NH_2
	LH_2^{2+}	12.58(4)	5.31	His

Table 2
Cumulative complex-formation constants (β) and acid dissociation constants (K_a) of Cu(II) complexes with AAHAWG-NH_2 and AAHAWGC(SMe)-NH_2, at T = 298.2 K and I = 0.1 M (KCl). Standard deviations on the last figure in parentheses.

Ligand	Species	logβ	pK_a	Coordination mode
AAHAWG-NH_2	$[CuLH_{-2}]$	−0.47(1)	11.59	$[N_{NH2},N_{Im},2N^-]$
	$[CuLH_{-3}]^-$	−12.06(3)	–	$[N_{NH2},N_{Im},2N^-]$
AAHAWGC(SMe)-NH_2	$[CuLH_{-2}]$	−0.86(1)	11.7	$[N_{NH2},N_{Im},2N^-]$
	$[CuLH_{-3}]^-$	−12.6(2)	–	$[N_{NH2},N_{Im},2N^-]$

been investigated by means of spectrofluorimetric titrations and the results are shown in Fig. S9 (Supplementary Information): interestingly, the intensity of the emission band of the indole group of Trp increases as a consequence of imidazole deprotonation. As it was already previously reported [38,39], the close proximity of a protonated histidine to tryptophan promotes a charge-transfer between the two aromatic rings which, in turn, quenches the indole fluorescence. Although this behavior is more evident for AAHAWG-NH_2 (Fig. S9a), for both AAHAWG-NH_2 and HAWG-NH_2 the assignment of the residues involved in ligand deprotonation are in agreement with the spectrofluorimetric data.

3.3. Cu(II) complexes with AAHAWG-NH_2 and AAHAWGC(SMe)-NH_2

The complex-formation constants obtained by potentiometric studies of the single-chain peptides AAHAWG-NH_2 and AAHAWGC(SMe)-NH_2 are reported in Table 2. The corresponding distribution diagrams are shown in Fig. 2 and Fig. S10 (Supplementary Information). For both these ATCUN-type peptides, the potentiometric titrations confirmed their high affinity for Cu(II) ion. The obtained speciation models are in very good agreement with those reported for other similar systems [40–43] (see also Table S1, Supplementary Information). Moreover, the minor behavior difference between the two peptides (Table 2) suggests that the additional Cys(SMe) residue has a negligible impact on their Cu(II) binding ability. For this reason, only the Cu(II)/AAHAWG-NH_2 equilibria are described below.

Starting from pH 4, the interaction between Cu(II) and AAHAWG-NH_2, after a plausible anchoring of the metal ion to either the imidazole or the amine nitrogen, leads to the concerted deprotonation of two amide nitrogens of the peptide backbone to form the complex $[CuLH_{-2}]$ which quickly becomes the most abundant copper species in solution, the only one present in the pH range 5.5–9.0. The coordination geometry is most likely almost planar with the $[N_{NH2}, N_{Im}, 2N^-]$ donor-atom set, as represented in Scheme 2a. Further deprotonation step at alkaline pH gives the $[CuLH_{-3}]^-$ species. Our hypothesis is that

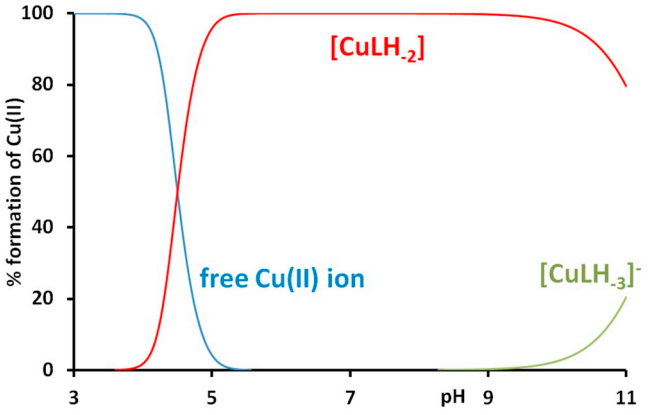

Fig. 2. Representative species distribution diagram for complex-formation of AAHAWG-NH_2 with Cu(II), at T = 25 °C and I = 0.1 M (KCl). C_{Cu} = 1 mM; Cu:L = 1:1.

the deprotonation of the second imidazolic proton occurs to form a coordinated imidazolate ion, rather than of an axially-coordinated water molecule. Although observed as a bridging group between two metal ions, the coordination of His in the imidazolate form to one Cu(II) has been previously observed [42,44,45]. Here we exclude the deprotonation of axially-bound water molecule since the signal of this ion is completely absent in the ESI-MS spectra. Rather, the speciation model of Table 2 is nicely confirmed by ESI-MS spectra recorded at slightly alkaline pH, where both the $[CuLH_{-2}]$ and $[CuLH_{-3}]^-$ complexes have been observed and recognized through isotopic pattern analysis (Fig. S11, Supplementary Information). Interestingly, a signal attributable to the transient species $[CuLH_{-1}]^+$ was also recorded in the ESI-MS experiments, while the formation of this complex is too small to be observed in potentiometry. It is worth of note that the experimental m/z ratio of the ion $[CuLH_{-3}]^-$ supports the loss of a proton by the ligand and rules out the formation of a hydroxo-species. Furthermore, we also exclude the deprotonation and coordination of a third amidic nitrogen of the backbone on the basis of UV–visible and CD spectroscopic data (see below).

UV–visible and CD spectroscopic results are in agreement with the coordination hypotheses described above. Vis-absorption spectra (Fig. 3 and Fig. S12, Supplementary Information) show only one band centred at λ_{max} = 526 nm, compatible with the hypothesis of a 4N coordination and in particular with a $[N_{NH2}, N_{Im}, 2N^-]$ (expected λ_{max} = 531 nm) [46]. Such absorption band is already observable at pH 4: initially the intensity increases with pH and then remains unchanged under the most alkaline conditions. Only at pH 4 a second (weak) band is also present in the Vis spectrum, around 800 nm, due the presence of non-bound Cu(II) ions.

A spectrophotometric titration of AAHAWG-NH_2 with Cu(II) performed at pH 7.4 is shown in Fig. 4a. Increasing the Cu(II) concentration in the peptide solution from copper/ligand ratio 0 to 1, we can observe that the absorbance at 526 nm steadily and almost linearly increases, following the formation of the complex $[CuLH_{-2}]$. In the presence of copper in excess the absorbance does not change anymore, confirming that only mono-nuclear complexes of stoichiometry 1:1 are formed in solution. Identical behaviors occurred repeating the same experiments at pH = 9.0 (Fig. S13a, Supplementary Information), in full agreement with the distribution diagram shown in Fig. 2. Further confirmation of the exclusive Cu(II):peptide 1:1 binding stoichiometry has been obtained through spectrofluorimetric titrations performed in the same conditions described above: in this case, the emission intensity decreases with the formation of the complex (Fig. 4b and Fig. S13b, Supplementary Information) [46] until the Cu(II) concentration becomes equimolar to that of AAHAWG-NH_2.

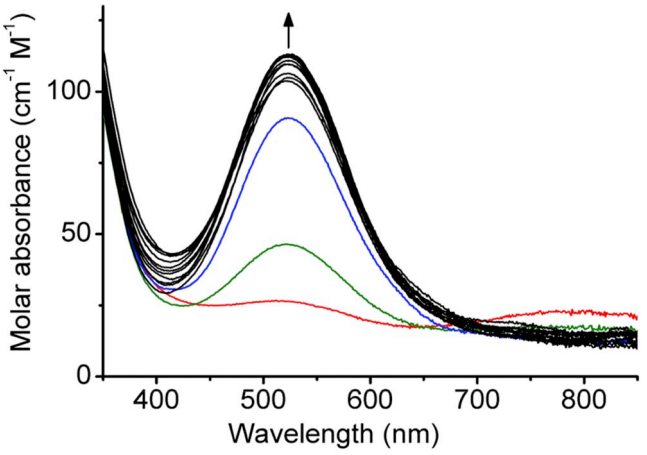

Fig. 3. Vis absorption spectra at variable pH of a Cu(II)/AAHAWG-NH_2 solution, at T = 25 °C and I = 0.1 M (KCl). C_{Cu} = 0.5 mM; Cu: L = 1:1.2. Dashed line: spectrum at pH 4.0; dotted line: spectrum at pH 4.3; dashed-dotted line: spectrum at pH 4.6; full black lines: spectra at pH 4.7-12.

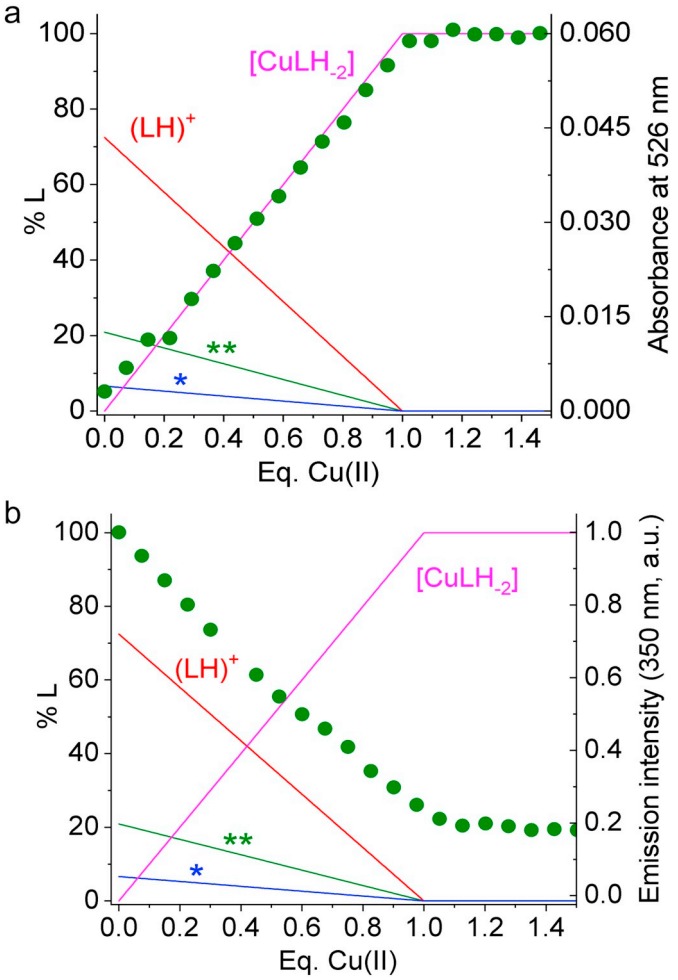

Fig. 4. Spectrophotometric (a) and spectrofluorimetric (b) titrations of AAHAWG-NH_2 with Cu(II) at pH 7.4 (aqueous HEPES buffer 25 mM). Dots represent: a) absorbance values at 526 nm (C_L = 0.70 mM); b) fluorescence emission data at 350 nm (λ_{exc} = 280 nm; C_L = 48 μM). Scale is reported on the right axes. Lines represent the speciation diagrams for the titration experiments (scale on the left axes). * = H_2L^{2+}; ** = L.

The quenching of the Trp fluorescence due to the formation of copper complexes has also been evidenced by means of a further spectrofluorimetric titration of a diluted Cu(II)/AAHAWG-NH_2 solution at fixed Cu(II)/L ratio and varying the pH value from 3.5 to 11.5 (Fig. S14, Supplementary Information). The emission intensity at 350 nm decreases until pH 5.5 where the formation of the complex $[CuLH_{-2}]$ is complete and then it remains stable until pH approximatively 10, when the species $[CuLH_{-3}]^-$ starts to form.

CD spectra recorded for Cu(II)/AAHAWG-NH_2 solutions in the pH range 4–12 (Fig. 5) are almost identical, confirming that the complex geometry remains unchanged when pH is varied. This observation, together with the absence of λ_{max} changes, confirm that in this pH range the coordination environment of Cu(II) is almost the same for both $[CuLH_{-2}]$ and $[CuLH_{-3}]^-$. Above pH 10, deprotonation/coordination of an amide should give rise to an important change in the complex geometry and, consequently, in the CD spectra. This is not observed and, as previously discussed, we suggest the deprotonation of the pyrrole-type nitrogen of the imidazole ring of His. In the UV range of the CD spectra two main bands have been observed, one negative at 274 nm and one positive at 310 nm. The former can be attributed to an intra-ligand transition due to the indole group; the latter is the well-known charge transfer band due to the coordination of amide nitrogens

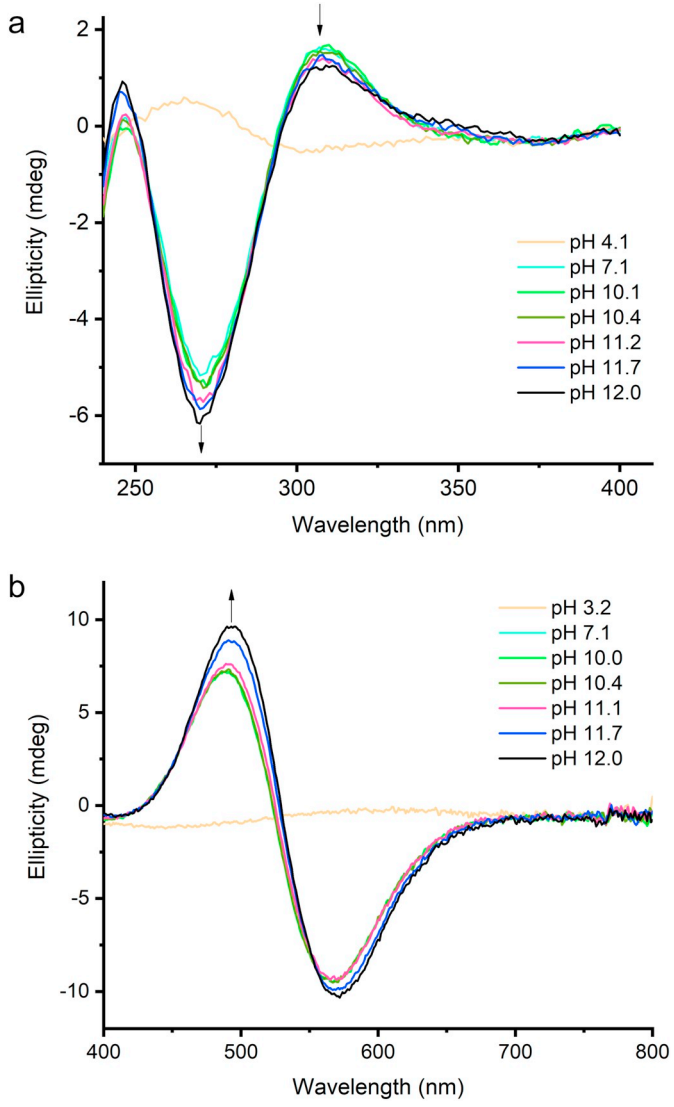

Fig. 5. a) UV and b) visible circular dichroism spectra at variable pH of a Cu (II)/AAHAWG-NH_2 solution, at T = 25 °C and I = 0.1 M (KCl). UV spectra C_{Cu} = 52 μM; Vis spectra: C_{Cu} = 0.52 mM; Cu:L = 1:2.

to the copper ion [46,47]. In the Vis region, the double band centred around 520 nm corresponds to the typical metal d-d transitions of a Cu (II) complex with ATCUN peptides [47,48]. It is worth of note that the CD spectra of the Cu(II)/AAHAWG-NH_2 system are almost perfectly superimposable to that reported for the Cu(II) binding to human serum albumin (Fig. S15, Supplementary Information) [22].

3.4. Cu(II) complexes with HAWG-NH_2 and HAWGC(SMe)-NH_2

Potentiometric analyses of the Cu(II)/HAWG-NH_2 and Cu(II)/HAWGC(SMe)-NH_2 systems were performed in the presence of an excess of either the ligands (Cu/L ratio = 1:1.2; 1:2.2) or the metal (Cu/L ratio = 1.3:1), in the pH range 3–11. No precipitation was observed with the employed conditions. Seven mono- and di-nuclear complexes have been revealed in these systems, as reported in Table 3 and in Figs. 6 and S16 (Supplementary Information). All the species detected by potentiometry for the system Cu(II)/HAWG-NH_2 have been observed by ESI-MS, as shown in Fig. S17 and Fig. S18 (Supplementary Information). At pH = 7.0 the signals corresponding to the $[CuL]^{2+}$ and $[CuL_2]^{2+}$ species can be recognized (at m/z = 265.58 and 499.83, respectively) along with those of the dimers $[Cu_2L_2H_{-2}]^{2+}$ (m/z = 531.25) and $[Cu_2L_2H_{-3}]^{+}$ (m/z = 1061.00). At pH = 9.0 the deprotonated complexes $[CuLH_{-2}]$ and $[CuLH_{-3}]^{-}$ were observed as K^+ adducts in the positive ion mode and alone (the latter) in the negative ion mode. The obtained speciation models of Table 3 are very similar considering both the stoichiometry and the stability of the formed complexes, thus suggesting again that the Cys(SMe) residue has a minor influence on the complex-formation behavior, as already mentioned for AAHAWC(SMe)G-NH_2. Therefore, only the Cu(II)/AAHAWG-NH_2 equilibria are examined in the following paragraphs.

Table 3
Cumulative complex-formation constants (β) and acid dissociation constants (K_a) of Cu(II) complexes with HAWG-NH_2 and HAWGC(SMe)-NH_2, at T = 298.2 K and I = 0.1 M (KCl). Standard deviations on the last figure in parentheses.

Ligand	Species	logβ	pK_a	Coordination mode
HAWG-NH_2	$[CuL]^{2+}$	8.24(1)	7.5	$[N_{NH2},N_{Im}]$
	$[CuLH_{-1}]^{+}$	0.7(3)	8.0	$[N_{NH2}/N_{Im},N^-]$
	$[CuLH_{-2}]$	−7.3(1)	7.7	$[N_{NH2}/N_{Im},2N^-]$
	$[CuLH_{-3}]^{-}$	−15.04(3)	–	$[N_{NH2}/N_{Im},3N^-]$
	$[CuL_2]^{2+}$	14.26(3)	–	$[2(N_{NH2},N_{Im})]$
	$[Cu_2L_2H_{-2}]^{2+}$	5.5(1)	7.8	
	$[Cu_2L_2H_{-3}]^{+}$	−2.3(1)	–	
HAWGC(SMe)-NH_2	$[CuL]^{2+}$	8.21(1)	7.4	$[N_{NH2},N_{Im}]$
	$[CuLH_{-1}]^{+}$	0.8(4)	7.6	$[N_{NH2}/N_{Im},N^-]$
	$[CuLH_{-2}]$	−6.8(1)	7.8	$[N_{NH2}/N_{Im},2N^-]$
	$[CuLH_{-3}]^{-}$	−14.57(4)	–	$[N_{NH2}/N_{Im},3N^-]$
	$[CuL_2]^{2+}$	14.63(4)	–	$[2(N_{NH2},N_{Im})]$
	$[Cu_2L_2H_{-2}]^{2+}$	5.9(1)	7.4	
	$[Cu_2L_2H_{-3}]^{+}$	−1.5(1)	–	

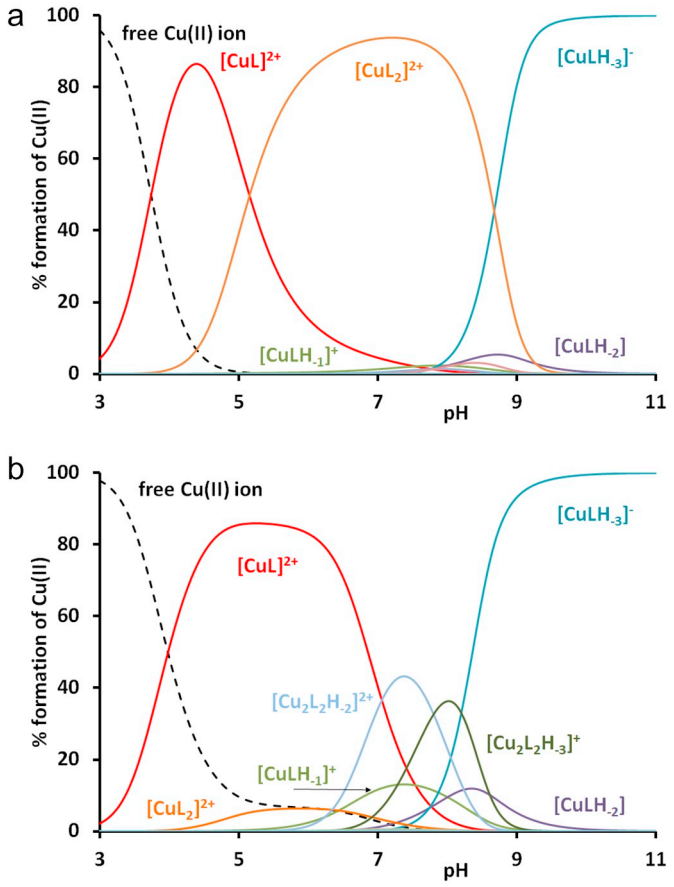

Fig. 6. Representative distribution diagrams for complex-formation of HAWG-NH_2 with Cu(II), at T = 25 °C and I = 0.1 M (KCl). C_{Cu} = 1 mM; a) Cu:L = 1:2; b) Cu:L = 1:1.

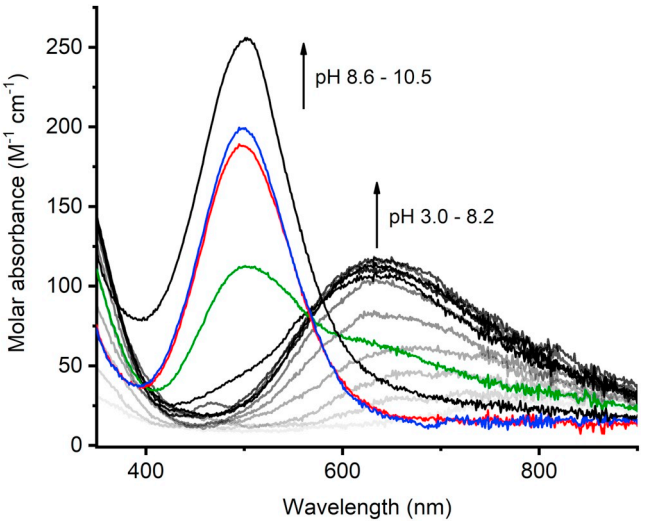

Fig. 7. Vis absorption spectra at variable pH for the binary solutions of HAWG-NH_2 with Cu(II), at T = 25 °C and I = 0.1 M (KCl). C_{Cu} = 0.556 mM; Cu/L = 1:2.2.

The peptide HAWG-NH_2 is characterized by the presence of His in the first position (amino-terminus), that can chelate the Cu(II) ion in the very effective *histamine-like* mode (Scheme 2). In fact, under the most acidic conditions, the first formed species is $[CuL]^{2+}$; its stoichiometry suggests that both the terminal amine and the side imidazole ring are unprotonated and bound to the metal ion, most likely in the equatorial plane of a distorted octahedral complex where the remaining positions are occupied by water molecules. The predicted wavelength of maximum absorption for this type of Cu(II) coordination is 675 nm [46], in very good agreement with the Vis absorption spectrum registered at pH 4.45 (λ_{max} = 676 nm), where this species is by far the most abundant in solution (Fig. 7).

In the presence of excess of peptide (Fig. 6a), at neutral or slightly alkaline pH, a second ligand binds the Cu(II) ion, leading to the formation of the $[CuL_2]^{2+}$ species, practically the only complex in solution in the pH range 6–8. Vis absorption spectra show a clear blue-shift and the wavelength of maximum absorption lowers approximately to 634 nm, suggesting the substitution of the coordinated water molecules with nitrogen donors. However, the blue-shift is too little to suggest that the second ligand also chelates copper in the *histamine-like* mode. In fact, in the case of four nitrogens bound to Cu(II) in the equatorial plane, the predicted wavelength of the absorption band would be 559 nm [46]. On the other hand, the stoichiometry of the complex reveals that both the nitrogens of the second ligand are unprotonated. The alternative structural hypothesis for the bis-complex is that the second ligand is bound to copper in the so-called *glycine-like* mode, i.e. through its terminal amino group and the neighboring carbonyl oxygen (Scheme 2c). By admitting the presence of both coordination modes, the predicted maximum of absorption is 607–617 nm [46]. The second amino group likely binds Cu(II) in axial position, and is responsible of the small red-shift of the band, from the expected 607–617 to the observed 634 nm [46]. The "plasticity" of the Cu(II) ion makes impossible to establish which of the two nitrogens is equatorial or axial: most likely, a mixture of species with slightly different geometry is present in solution. It is worth noting that when pH is raised from 4 to 7, CD spectra in the Vis region change only in their intensity but not in their shape (Fig. 8), suggesting that the donor atom set remains the same.

Starting from pH 8.5, both Vis absorption and CD spectra undergo an abrupt change, exactly in correspondence to the formation of the species $[CuLH_{-3}]^-$ which dominates in the alkaline pH range. It is clear that an important transformation of the complex takes place and this can be attributed to a change in the donor atom set due to the

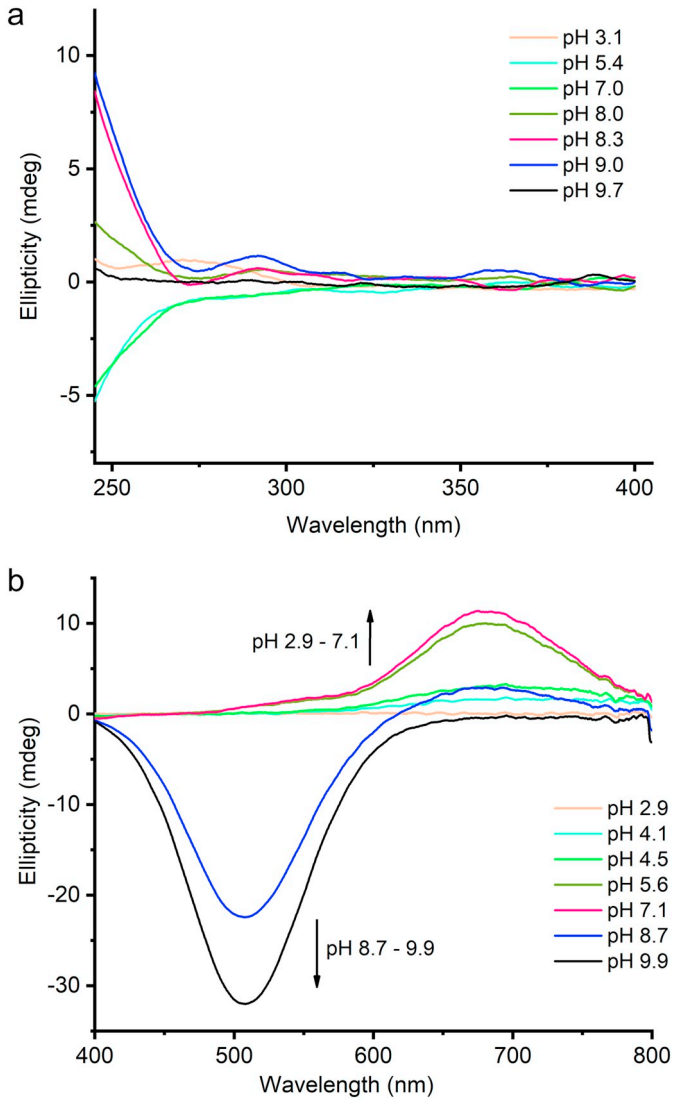

Fig. 8. a) UV and b) visible circular dichroism spectra at variable pH of a Cu(II)/HAWG-NH_2 solution, at T = 25 °C and I = 0.1 M (KCl). UV spectra: C_{Cu} = 50 μM; Vis spectra: C_{Cu} = 0.52 mM; Cu/L molar ratio = 1:2.

availability of deprotonated amide nitrogens of the backbone. Bis-complexes are no longer present in solution, most likely because the ligand wraps completely the metal and binds it in equatorial position with three amide nitrogens and the imidazole (or the terminal amine). The predicted absorption band for these [N_{im}, $3N^-$] or [N_{NH2}, $3N^-$] coordination modes should be located at 522 or 515 respectively [46]. The experimental value (500 nm) is in reasonable agreement with this prediction. Further proof of these coordination hypotheses comes from spectrophotometric titrations of HAWG-NH_2 with Cu(II) at fixed pH = 7 and 9. The absorption values at the registered λ_{max}, i.e. 630 nm at pH = 7.0 and 500 nm at pH = 9.0 (Fig. 9) were monitored. At pH 7.0 the intensity of the absorption band almost linearly increases until the molar amount of copper in solution is about half of that of HAWG-NH_2, thus confirming the prevalence in solution of a complex with Cu/L stoichiometry 1:2. Conversely at pH 9.0 (Fig. 9b) the plateau corresponding to the maximum absorption intensity is obtained for the equimolar Cu/L solution, thus confirming the presence of a dominant species with stoichiometry 1:1 (i.e. the complex $[CuLH_{-3}]^-$, see Fig. 6).

Spectrofluorimetric titrations were performed at pH 7.0 and 9.0 showing that the emission intensity decreases when the Cu(II) concentration increases in solution, as already observed for the ligand

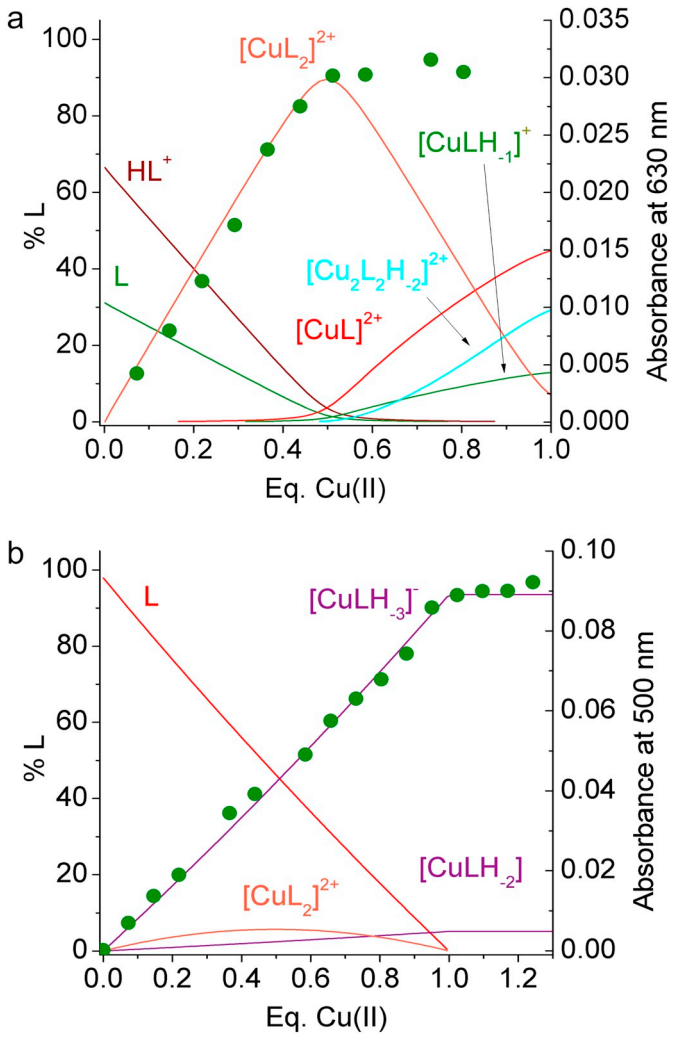

Fig. 9. Spectrophotometric titrations of HAWG-NH_2 with Cu(II) at pH 7.0 (a) and at pH 9.0 (b). C_L = 0.70 mM, aqueous HEPES or CHES buffer 25 mM for pH 7.0 and 9.0, respectively. Dots represent absorbance values. Scale is reported on the right axes. Lines represent the speciation diagrams for the titration experiments (scale on the left axes).

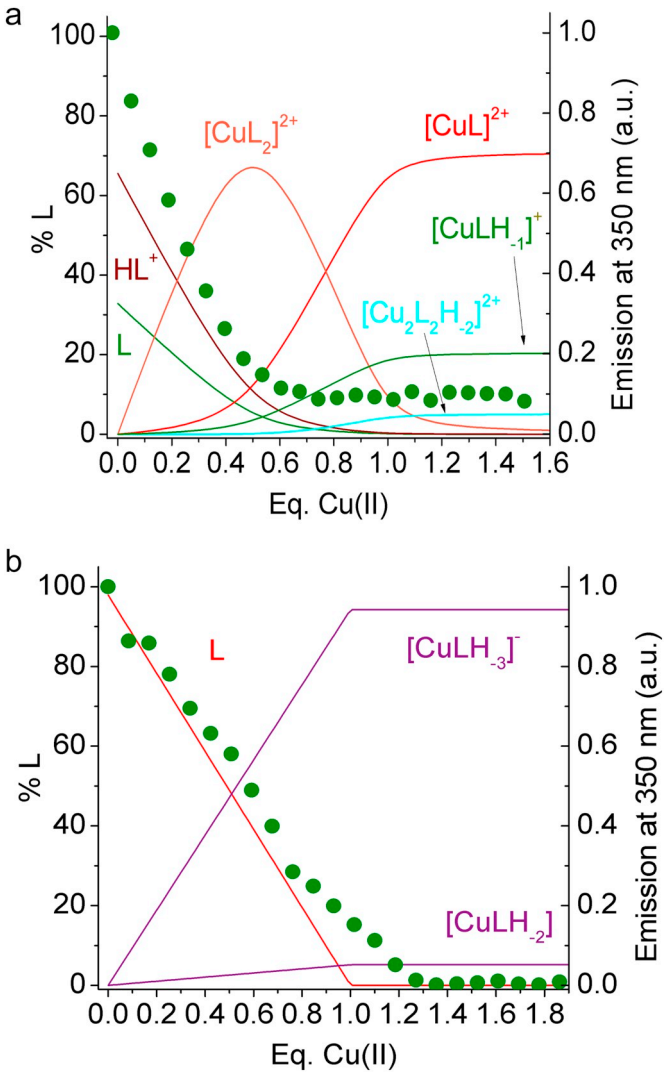

Fig. 10. Spectrofluorimetric titrations of HAWG-NH_2 with Cu(II) at pH 7.0 (a) and at pH 9.0 (b). C_L = 48 μM, aqueous HEPES or CHES buffer 25 mM for pH 7.0 and 9.0, respectively). Dots represent emission values at 350 nm (λ_{exc} = 280 nm). Scale is reported on the right axes. Lines represent the speciation diagrams for the titration experiments (scale on the left axes).

AAHAWG-NH_2. Data reported in Fig. 10 are in reasonable agreement with the UV–visible titrations and support the hypothesis of complexes with stoichiometry 1:2 at neutral pH and 1:1 under alkaline conditions.

It is worth noting that the interpretation of the spectral data is not so straightforward when the Cu/L ratio is close to 1:1. In this case, the dinuclear complexes observed in the ESI-MS spectra reach relevant concentrations (up to 40% of total copper, see Fig. 6b) and they can be detected also by potentiometry. Spectroscopic results for Cu(II)/HAWG-NH_2 and Cu(II)/HAWGC(SMe)-NH_2 with Cu/L ratio = 1: 1.2 also confirm the possible existence of these species in the pH range 6–8 (Figs. S19 and S20, Supplementary Information), where the UV–Vis spectra slightly change compared to the Cu/L = 1:2 solution. A hydroxo-bridged nature of these dinuclear complexes can be foreseen, consistently with literature data for similar systems [48,49].

3.5. Cu(II) complexes with $(AAHAWG)_4$-PWT2

With the speciation of the single-chain peptides in our hands, we studied the interaction of Cu(II) with the two tetramers built on the cyclam scaffold through spectroscopic and spectrometric techniques at fixed pH.

The mass spectrum at pH 4.9 of the ligand $(AAHAWG)_4$-**PWT2** (Fig. S21a, Supplementary Information), exhibits an excellent protonation pattern: all the species from LH_2^{2+} to LH_8^{8+} have been detected, accompanied by one or more additional signals at +60/z, attributable to adducts [$Na^+ + K^+ - 2H^+$] (23 + 39–2 = 60), with the same charge of the purely protonated ions. In the presence of a four-fold excess of Cu (II), both at pH 7.2 and 9.8, the only two recognizable complexes are the species $[Cu_4LH_{-8}]K_4^{4+}$ (m/z = 1029.4) and $[Cu_4LH_{-8}]K_3^{3+}$ (m/z = 1359.7), suggesting that each branch of the tetramer behaves exactly like the monomer and independently binds one Cu(II) ion (Fig. S21b, Supplementary Information). This hypothesis is confirmed by spectrophotometric and spectrofluorimetric titrations performed at pH 7.4 (Fig. 11). Actually, at pH 7.4 the absorbance increases and the fluorescence intensity decreases during the addition of Cu(II), reaching a plateau when the metal ion is equimolar to the peptide branches, i.e. when the concentration of copper is four times that of $(AAHAWG)_4$-**PWT2**. Accordingly, the CD spectra recorded at pH 7.4 in the presence of increasing amounts of Cu(II) have the same shape of those recorded for the system Cu(II)/AAHAWG-NH_2, confirming the same coordination behavior (Fig. S22, Supplementary Information). Similar spectrofluorimetric data were obtained at pH 9.0, while spectrophotometric and CD data could be collected only up to 1 eq. of Cu(II) due to

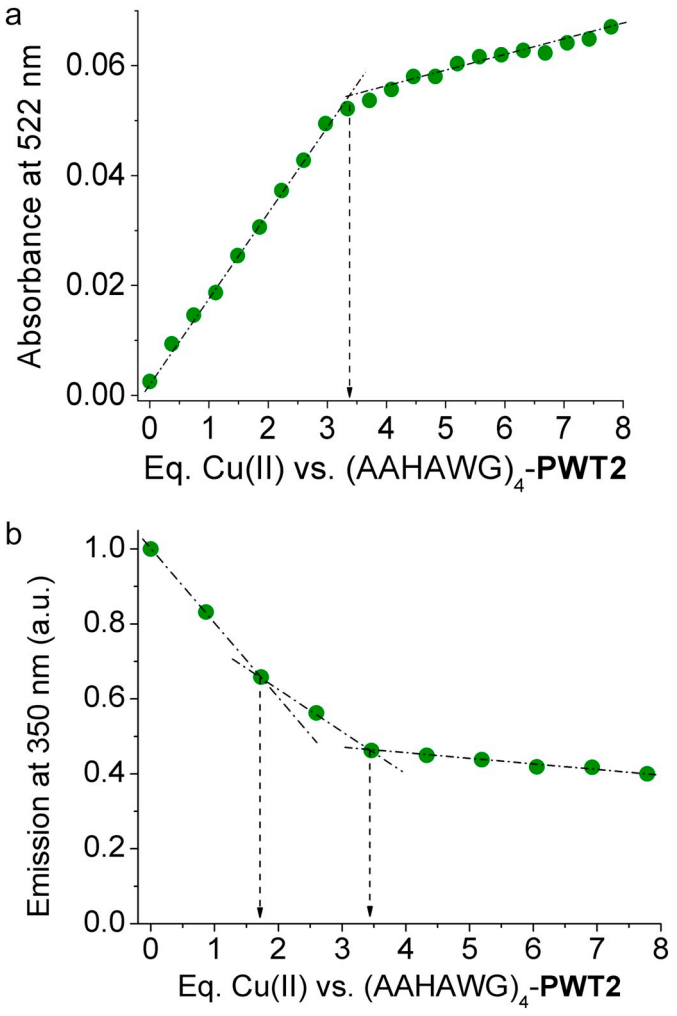

Fig. 11. a) Spectrophotometric (absorbance at 522 nm, C_L = 0.17 mM) and b) spectrofluorimetric (λ_{exc} = 280 nm; λ_{emis} = 350 nm, C_L = 48 μM) titrations for a solution of $(AAHAWG)_4$-**PWT2** with Cu(II) at pH 7.4 (aqueous HEPES buffer 25 mM).

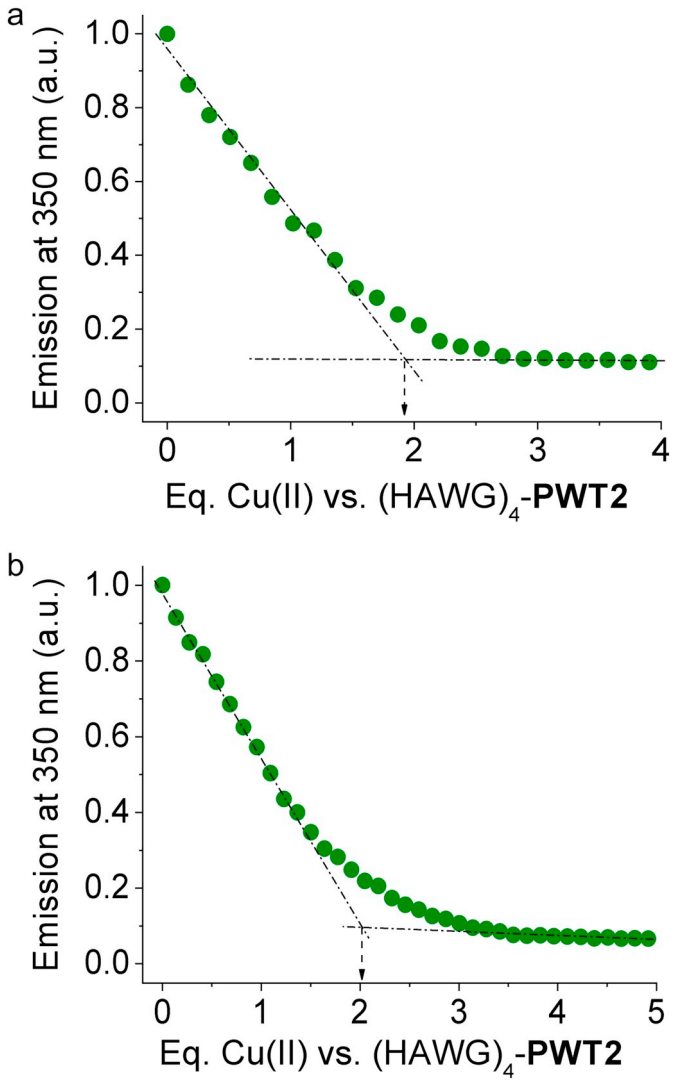

Fig. 12. Spectrofluorimetric titrations for a solution of $(HAWG)_4$-**PWT2** with Cu(II) at a) pH = 7.0 (HEPES buffer 25 mM) and b) pH = 9.0 (CHES buffer 25 mM). λ_{exc} = 280 nm; λ_{emis} = 350 nm, C_L = 48 μM.

appearance of opalescence in the solution (Figs. S23 and S24, Supplementary Information). The λ_{max} at 500–515 nm in the absorption spectra, together with CD information, reveals that also at this pH the ATCUN nature of the copper coordination systems at both pH values examined.

3.6. Cu(II) complexes with $(HAWG)_4$-PWT2

The mass spectrum recorded at pH 3.7 for the ligand $(HAWG)_4$-**PWT2**, in the absence of metal ions, contains all the protonated species, from LH_2^{2+} to LH_5^{5+}; the presence of Na^+ or K^+ adducts is negligible (Fig. S25, Supplementary Information). In the presence of a 2:1 excess of Cu(II), the solution was light-blue colored, both at neutral and alkaline pH. The mass spectra show the signals of both mono- and binuclear species, variously protonated (Fig. S26, Supplementary Information). Deprotonated and hydroxylated species, respectively $[Cu_2LH_{-1}]^{3+}$ (m/z = 1091.1) and $[Cu_2L(OH)]^{3+}$ (m/z = 1097.1), can be observed at pH = 9.1. On the other hand, when Cu(II) was present in a four-fold excess, the solution was pink and not perfectly clear at pH higher than 6.7. The signals of both three- and tetra-nuclear complexes are present in the MS spectrum (Fig. S27, Supplementary Information).

The spectrofluorimetric titration curve in Fig. 12a shows that, at pH 7, the tryptophan emission steadily decreases until the Cu(II)/$(HAWG)_4$-**PWT2** ratio reaches the value of 2 and it remains constant at higher values. This behavior suggests that Cu(II), at neutral pH, forms bis-complexes with the HAWG chains (and then two copper atoms for each **PWT2**), exactly the same behavior described above for the free HAWG-NH_2 peptide. At pH 9 (Fig. 12b) the emission decrease continues beyond the ratio Cu(II)/$(HAWG)_4$-**PWT2** = 2 until M/L ratio ca. 4. Perhaps most importantly, the equivalence point obtained from the analysis of the binding isotherm is 2 equivalents of Cu(II) per ligand $(HAWG)_4$-**PWT2**. These data suggest that at pH 9.0 the ligand $(HAWG)_4$-**PWT2** preferentially binds 2 equivalents of copper(II), in conditions where 4 Cu(II) ions are instead expected to bind, one per HAWG arm. On the other hand, the binding of four Cu(II) is promoted by the presence of an excess of Cu(II), as suggested by ESI-MS data (Fig. S27, Supplementary Information) and by fluorescence data which reach a plateau only for 4 eq. of copper added.

To further support the hypothesis of formation of Cu(II)/ligand 2:1 species both at pH 7.0 and at pH 9.0 we carried out absorption and CD studies. Complete spectrophotometric titrations of the ligand with Cu (II) was possible only at pH 7.0, since at pH 9.0 a marked drift in the baseline followed by turbidity appeared already at Cu(II):ligand of 0.3. The spectra are reported in Fig. 13. Only at pH 7.0 the visible CD spectra for addition of Cu(II) up to 4 eq. vs. ligand could be collected (Fig. S28, Supplementary Information). At pH 7.0 the maximum of

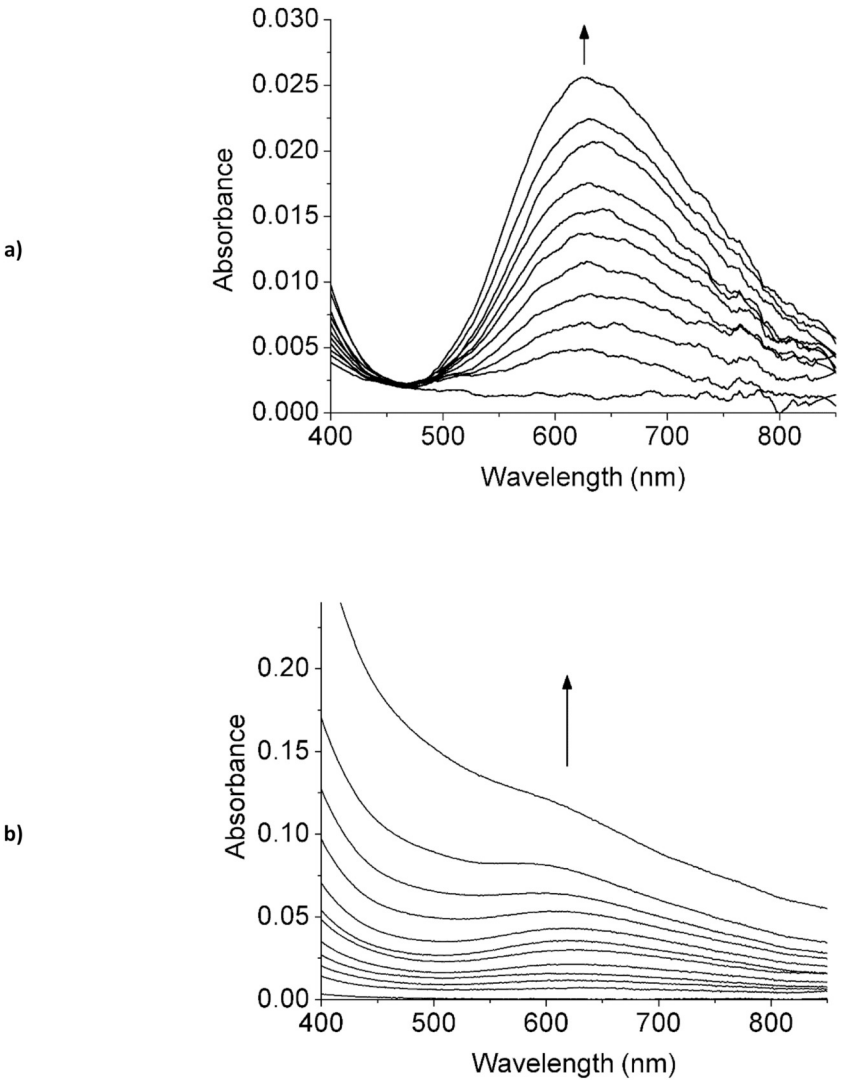

Fig. 13. Visible spectrophotometric titrations for a solution of $(HAWG)_4$-**PWT2** with Cu(II) at a) pH = 7.0 (HEPES buffer 25 mM) and b) pH = 9.0 (CHES buffer 25 mM). C_L = 0.20 mM. The spectra at highest Cu(II) content corresponds to 4 (pH 7.0) and 0.6 eq. (pH 9.0) of Cu(II) vs. ligand, respectively.

absorbance upon addition of Cu(II) is 630 nm, the same found for the system Cu(II)/HAWG-NH_2 at the same pH. Also, the corresponding CD spectrum exhibits a positive Cotton effect at 685 nm, again in agreement with the behavior of the single-chain HAWG-NH_2 peptide (Fig. S28, Supplementary Information). These results confirm that the complexation mode of $(HAWG)_4$-**PWT2** towards the Cu(II) ion, at neutral pH, is similar to that of the HAWG-NH_2 monomer, as already suggested by emission spectra described above.

Most importantly, also the spectra at pH 9.0 also present a maximum of absorption around 630 nm. That maximum corresponds to the observed at pH 7.0 for both $(HAWG)_4$-**PWT2** and HAWG-NH_2, but not of the latter at pH 9.0 (500 nm). Overall these spectroscopic data suggest that, at least in the presence of up to 2 eq. of copper, $(HAWG)_4$-**PWT2** may form 1:2 Cu: peptide complexes. This observation is fully consistent with spectrometric data (Fig. S25 and S26, Supplementary Information). Also, these results suggest that, in that species the coordination environment of copper is similar to that observed for $(HAWG)_4$-**PWT2** and HAWG-NH_2 at pH 7.0 (*histamine-like* and *glycine-like* coordinated peptide arms).

4. Discussion

In this study we present the complex-formation behavior of the two short peptides AAHAWG-NH_2 and HAWG-NH_2 along with that of their homo-tetramers $(AAHAWG)_4$-**PWT2** and $(HAWG)_4$-**PWT2**, mounted on a cyclam scaffold. Absorption and CD spectrophotometric and mass spectrometric characterization of the Cu(II) complexes with all ligands has been performed, together with the potentiometric study of the single-chain peptides speciation.

In the case of AAHAWG-NH_2, all the experimental data agree with the hypothesis of an ATCUN-type coordination for the complex $[CuLH_{-2}]$, the most abundant species in a large pH range around neutrality. Here, the chelation to the metal is carried out by the terminal amino nitrogen, the side imidazole and two deprotonated amide nitrogen atoms (Fig. 14).

The coordination behavior of the peptide HAWG-NH_2 is more complex, since two main coordination geometries are adopted, according to the pH conditions. At pH 7.0 and in the presence of an excess of ligand, the main species in solution is the complex $[CuL_2]^{2+}$, while in the alkaline pH range the species $[CuLH_{-3}]^{-}$ is predominant. It is interesting to note that these two species do not differ only in their stoichiometry but also in their coordination geometry. In fact, in the case of $[CuL_2]^{2+}$, one ligand chelates Cu(II) in the *histamine-like* mode while the other is bound to copper in the *glycine-like* mode, as suggested by visible absorption spectra. The coordination environment of Cu(II) mainly involves (3N, O) in the equatorial plane, with a possible

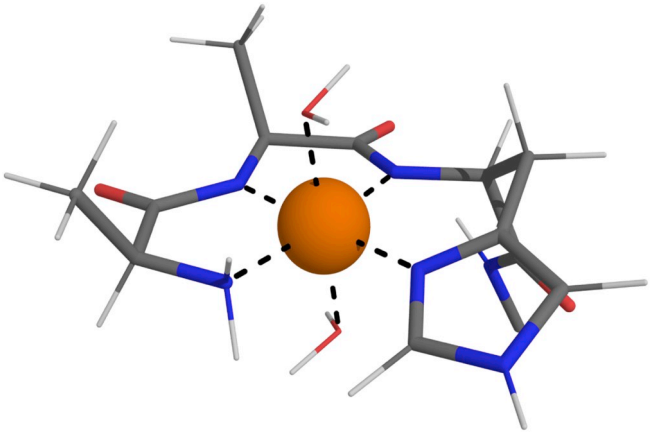

Fig. 14. Structural hypothesis for the complex [Cu(II)(AAHAWG-NH_2)H_{-2}]. Color code: orange = copper, blue = nitrogen, red = oxygen, light grey = hydrogen, grey = carbon.

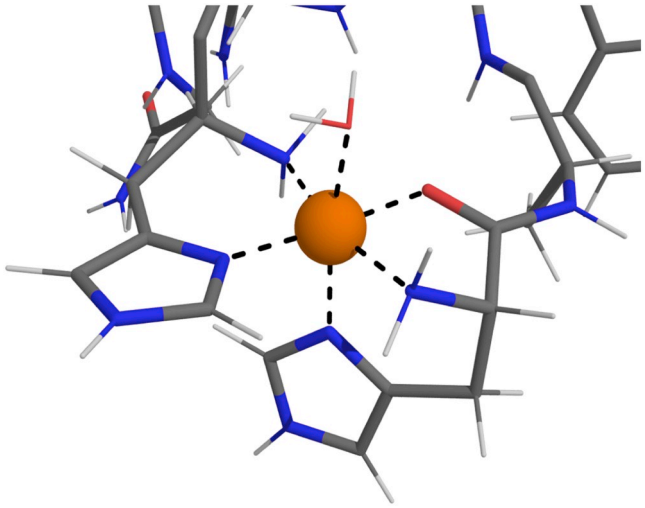

Fig. 15. Structural hypothesis for the complex $[Cu(II)(HAWG\text{-}NH_2)_2]^{2+}$. Color code: orange = copper, blue = nitrogen, red = oxygen, light grey = hydrogen, grey = carbon.

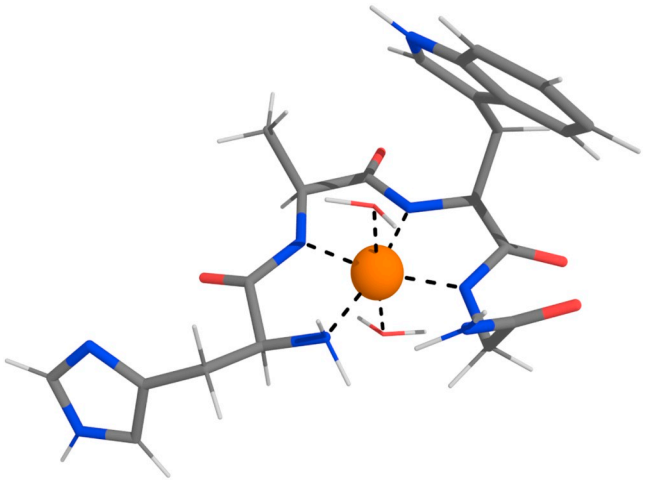

Fig. 16. Structural hypothesis for the complex $[Cu(II)(HAWG\text{-}NH_2)H_{-3}]^{-}$. Color code: orange = copper, blue = nitrogen, red = oxygen, light grey = hydrogen, grey = carbon.

interaction in the axial position with the imidazole nitrogen, as suggested by spectroscopic data (Fig. 15). Conversely, in the alkaline pH range the deprotonation of three amide nitrogen atoms of the peptide backbone occurs and the ligand wraps around the metal, with the participation of the terminal amine, in a (4N) coordination mode (Fig. 16). Bimetallic species, with different protonation degrees, were also detected in this system by potentiometric data analysis. These are however minor species if compared to monometallic ones, and their characterization was not carried out in further detail.

The data collected for the $(AAHAWG)_4$-**PWT2** system showed that the coordination behavior of each peptide branch parallels that of the AAHAWG-NH_2 peptide in solution. Thanks to spectroscopic measurements at fixed pH, it was possible to state that the metal forms a complex with 1:1 stoichiometry with each one of the four peptide arms anchored to the scaffold. An accurate observation of spectroscopic data for this system reveals two main features. The binding isotherm from fluorescence titration (Fig. 11) presents different slopes, with a change at 2–3 eq, and indicates that binding of Cu(II) ends at 3.5 equivalents of metal added to $(AAHAWG)_4$-**PWT2**. These aspects reveal that the binding of the first two metal ions is most likely non-cooperative (independent binding sites). However, after the first two-three Cu(II) eq. have been added, the coordination of further metal equivalents becomes de facto unfavoured either as an effect of high cations concentration or because some unidentified negative cooperative effects arise.

The behavior of $(HAWG)_4$-**PWT2** in solution was rather difficult to characterize due to insolubility problems, and nevertheless the spectroscopic data strongly suggest that 2:1 Cu/L species are formed at both pH 7.0 and 9.0, although the formation of solely 4:1 species were expected at the highest pH values. Based on fluorescence measurements at pH 7.0, we suggest the formation of a species where each metal ion is bound to two peptide arms, according to the species $[CuL_2]^{2+}$ observed for the single peptide. This means that $(HAWG)_4$-**PWT2** is saturated with two equivalents of Cu(II) *per* molecule. This hypothesis is confirmed by the Vis absorption spectra, since we observed a d-d band at 630 nm, which is very close to the λ_{max} of $[CuL_2]^{2+}$ complex of HAWG-NH_2. Moreover, CD spectra are perfectly superimposable to those recorded for the system Cu(II)/HAWG-NH_2, at neutral pH and in excess of ligand. At neutral pH, therefore, the four HAWG chains mounted on the cyclam scaffold behave exactly like the single-chain peptides.

The same behavior has been found at pH 9.0, which deviates from what could be hypothesized from the study of Cu(II)/HAWG-NH_2 system. As predicted from our design, through $(HAWG)_4$-**PWT2** we could stabilize the formation of Cu:peptide 1:2 species, in the presence of < 2 eq. of Cu(II). The fluorescence binding isotherm at pH 9.0 (Fig. 12b) shows that the emission intensity of the tryptophan residue is quenched very rapidly with Cu(II) addition, with an equivalence point corresponding to 2 copper ions per ligand. In these conditions the hypothesis of the formation of a 2:1 Cu:L complex (each Cu(II) coordinated by two peptide arms) is in full agreement with visible absorption data that, although affected by a marked drift of the baseline, clearly reveal that the absorption maximum of the Cu(II) adduct at this pH is above 600 nm. On the other hand, this information completely rules out the occurrence of the $[N_{NH2}, 3N^{-}]$ copper coordination found for the single-chain HAWG-NH_2 at alkaline pH. Rather, the absorption maximum is consistent with a $[2N_{NH2}, N_{Imidazole}, O]$ coordination that we associated to the $[CuL_2]$ species of the single-chain HAWG-NH_2 at neutral pH, as discussed.

The four arms of $(HAWG)_4$-**PWT2** are certainly different systems with respect to the free linear HAWG-NH_2 peptide. However, the spacer between the cyclam scaffold and the peptide moiety looks long enough (see below for discussion) to offer a quite high degree of freedom to the terminal peptide chain. Within the limit of the approximation of considering almost independent the four arms, as suggested by our structural models, we attempted to find an explanation for the different behavior of $(HAWG)_4$-**PWT2**, with respect to the HAWG-NH_2 simple

peptide, in the stoichiometry of the species formed at high pH. Therefore, the dependence of the solution composition for the system Cu(II)/HAWG-NH_2 on the overall metal and peptide concentrations, at fixed metal/ligand ratio (1:2), has been examined. It is possible for this system due to the availability of the complete speciation model of Table 3. The main result, for Cu(II) concentrations ranging from 0.1 mM to 0.1 M, is summarized in the distribution diagram reported in Fig. S29 (Supporting Information). The diagram refers to fixed pH 9.0, for a simultaneous increasing of both the Cu(II) and peptide concentrations, at fixed Cu(II)/L = 1:2. The diagram shows that the formation of 1:2 adducts ($[CuL_2]^{2+}$ species) is predominant when the total Cu(II) concentration is above 10 mM ($\log C_{Cu(II)} > -2.0$), while for lower concentrations the $[CuLH_{-3}]^{-}$ species predominates. As stated above, we can cautiously transfer this information to the Cu(II)/$(HAWG)_4$-**PWT2**. Since in our experiments the $(HAWG)_4$-**PWT2** concentration is 0.20 mM (corresponding to a formal concentration of the peptide branches of 0.80 mM), our data suggest that through $(HAWG)_4$-**PWT2** we could achieve an increase of the peptide "local concentration" [50] of 2–3 orders of magnitude compared to the same conditions using the single-chain analog. No direct experimental support is presently available for this hypothesis, due to the solubility problems of the branched peptides. An extension of the present research to more soluble peptides could give the required experimental demonstration.

Finally, we have taken into account, in evaluating our data, the presence in solution of different conformers or atropoisomers of $(HAWG)_4$-**PWT2** that surely exist as a consequence of the synthesis process (four branches are mounted on the scaffold). In this respect, conformational studies on the metal-free cyclam scaffolds reported in the literature [51], together with X ray structural data [52], suggest that N-functionalized cyclam molecules have a quite high degree of fluxionality. Under these circumstances N-linked functional groups may point away from the center of the cycle as schematically represented in Scheme 1. We analyzed the molecule with the software HyperChem 8.0 taking into account that $(CH_2)_2$N-C_{acyl} groups are coplanar with the C=O group since it is an amidic function. A large number of conformers have been generated in silico, and two different atropoisomers are represented in Fig. S30 (Supporting Information). The result of the isomers analysis showed that the four branches (peptide plus spacer) have an adequate length and a sufficient degree of flexibility to place the N-termini of the peptides close to each other, allowing the formation of *histamine-like* [Cu(peptide)$_2$] adducts.

5. Conclusions

In this paper we reported the synthesis of four single-chain short peptides, and two branched peptides which are template-mounted on a cyclam scaffold. All the peptides bear one histidine residue, and therefore an imidazole donor group, and a Trp residue as a spectroscopic tag. Single-chain peptides can be grouped into two couples possessing an Xxx-Xxx-His-N-terminus or a His-N-terminus, respectively. For each couple of peptides, the difference stands in the presence at the C-terminus of a Cys(S-Me) residue. This moiety simulates the thioether function present in the branched peptides as a consequence of the thio-Michael reaction used to mount the peptides on the cyclam scaffold.

Our results demonstrated that Cu(II) is bound to both the single-chain and the branched peptides preferentially at the N-termini, as previewed by our design. The ATCUN terminus in AAHAWG-NH_2 gave rise to mononuclear complexes of high stability with a [N_{NH2}, $2N^-$, N_{Im}] coordination. On the other hand HAWG-NH_2 formed 1:2 copper:peptide adducts at pH 7 (mixed *histamine-like* and *glycine-like* coordination), and 1:1 adducts at pH 9 where deprotonation of amidic nitrogen atoms occurred. Therefore, the major difference between the two peptides is that the ATCUN coordination mode for AAHAWG-NH_2 is stable in a wide pH range (4–10), while for HAWG-NH_2 there is a profound change of Cu(II) coordination from pH 7 to pH 9.

When mounted on the cyclam scaffold, the AAHAWG peptide retained the property to form ATCUN-type adducts with copper, as demonstrated by spectroscopic features. However, the affinity of the four chelating groups is not exactly the same, as qualitatively evidence by the spectroscopic analysis, with a decrease in chelation capacity for an increasing amount of Cu(II) bound to the ligand.

With the ligand HAWG-NH_2 we were able to qualitatively obtain what we expected from our design. On one hand, the nature of the scaffold and the length of the spacer allowed a large degree of freedom of the peptides which, at pH 7, can form 1:2 adducts with copper, adopting the mixed *histamine-like* and *glycine-like* coordination, as the single-chain peptide does. Most importantly, the latter coordination mode is predominant also at pH 9, unlike what occurs with free HAWG-NH_2. This behavior (i.e. avoiding peptide nitrogen deprotonation) is unachievable at pH 9 for the single chain-peptides unless its concentration is in the molar range. This is not only an extraordinarily high concentration for model peptides, but it is also out of the solubility range for the vast majority of proteins. Therefore, with our branched peptides we were able to shift up the effective molar concentration of the chelating groups (N-termini) of 2 to 3 orders of magnitude by mounting 4 equivalent peptides on a cyclam scaffold.

We expect that avoiding peptide nitrogen deprotonation and coordination will have, for instance, a noticeable effect on the Cu(I)/Cu(II) redox potential, since amide nitrogen coordination stabilizes Cu(II). Along with this consideration we preview that the development of these branched peptides will get into the development of copper bioinspired catalysts based on stable coordination environments at pH conditions unachievable with the use of single-chain peptides.

Declaration of competing interest

The authors declare that they have no known competing financial interests or personal relationships that could have appeared to influence the work reported in this paper.

Acknowledgements

This work has benefited from the equipment and framework of the COMP-HUB Initiative (University of Parma), funded by the 'Departments of Excellence' program of the Italian Ministry of Education, University and Research (MIUR, 2018-2022). The financial support of University of Ferrara (FAR 2018) and CIRCMSB (Consorzio Interuniversitario di Ricerca in Chimica dei Metalli nei Sistemi Biologici, Bari, Italy) is gratefully acknowledged.

Appendix A. Supplementary data

Supplementary data to this article can be found online at https://doi.org/10.1016/j.jinorgbio.2019.110980.

References

[1] H. Jiang, X.-Y. Hu, S. Mosel, S.K. Knauer, C. Hirschhäuser, C. Schmuck, ChemBioChem 20 (2019) 1410–1416.
[2] T.J. Thomas, T. Thomas, Int. J. Biol. Macromol. 109 (2018) 36–48.
[3] M. Zhao, R. Weissleder, Med. Res. Rev. 24 (2004) 1–12.
[4] R. Sawant, V. Torchilin, Mol. BioSyst. 6 (2010) 628–640.
[5] R. Khandia, A. Munjal, A. Kumar, G. Singh, K. Karthik, K. Dhama, Int. J. Pharm. 13 (2017) 677–689.
[6] M.A. Scorciapino, I. Serra, G. Manzo, A.C. Rinaldi, Int. J. Mol. Sci. 18 (2017) 542.
[7] J.-L. Reymond, T. Darbre, CHIMIA 67 (2013) 864–867.
[8] R. Hennig, A. Veser, S. Kirchhof, A. Goepferich, Mol. Pharm. 12 (2015) 3292–3302.
[9] A.R. Borges, C.L. Schengrund, Curr. Drug Targets Infect. Disord. 5 (2005) 247–254.
[10] T. Yi-Hsuan, H. Adela Ya-Ting, C. Po-Yu, C. Hui-Ting, K. Chai-Lin, Curr. Pharm. Des. 17 (2011) 2308–2330.
[11] Ł. Szyrwiel, Ł. Szczukowski, J.S. Pap, B. Setner, Z. Szewczuk, W. Malinka, Inorg. Chem. 53 (2014) 7951–7959.
[12] Ł. Szyrwiel, J.S. Pap, Ł. Szczukowski, Z. Kerner, J. Brasuń, B. Setner, Z. Szewczuk, W. Malinka, RSC Adv. 5 (2015) 56922–56931.
[13] J.S. Pap, Ł. Szyrwiel, D. Srankó, Z. Kerner, B. Setner, Z. Szewczuk, W. Malinka,

Chem. Commun. 51 (2015) 6322–6324.
[14] E. Farkas, D. Srankó, Z. Kerner, B. Setner, Z. Szewczuk, W. Malinka, R. Horvath, Ł. Szyrwiel, J.S. Pap, Chem. Sci. 7 (2016) 5249–5259.
[15] K. Jensen, De novo design of proteins, in: K. Jensen (Ed.), Peptide and Protein Design for Biopharmaceutical Applications, John Wiley and Sons Ltd, Chirchester, UK, 2009, pp. 207–248.
[16] A.G. Tebo, V.L. Pecoraro, Curr. Opin. Chem. Biol. 25 (2015) 65–70.
[17] M. Tegoni, Eur. J. Inorg. Chem. 2014 (2014) 2177–2193.
[18] Y.C. Chen, J.D. Eisner, M.M. Kattar, S.L. Rassoulian-Barrett, K. LaFe, S.L. Yarfitz, A.P. Limaye, B.T. Cookson, J. Clin. Microbiol. 38 (2000) 2302–2310.
[19] M. Mutter, G. Tuchscherer, Cell. Mol. Life Sci. 53 (1997) 851–863.
[20] G. Calo, A. Rizzi, C. Ruzza, F. Ferrari, S. Pacifico, E.C. Gavioli, S. Salvadori, R. Guerrini, Peptides 99 (2018) 195–204.
[21] Á. Dancs, N.V. May, K. Selmeczi, Z. Darula, A. Szorcsik, F. Matyuska, T. Páli, T. Gajda, New J. Chem. 41 (2017) 808–823.
[22] C. Harford, B. Sarkar, Acc. Chem. Res. 30 (1997) 123–130.
[23] L.W. Donaldson, N.R. Skrynnikov, W.-Y. Choy, D.R. Muhandiram, B. Sarkar, J.D. Forman-Kay, L.E. Kay, J. Am. Chem. Soc. 123 (2001) 9843–9847.
[24] J.P. Laussac, B. Sarkar, J. Biol. Chem. 255 (1980) 7563–7568.
[25] R.-P. Martin, L. Mosoni, B. Sarkar, J. Biol. Chem. 246 (1971) 5944–5951.
[26] T. Szabó-Plánka, A. Rockenbauer, L. Korecz, D. Nagy, Polyhedron 19 (2000) 1123–1131.
[27] Y. Altun, F. Köseoğlu, J. Solut. Chem. 34 (2005) 213–231.
[28] P.M.H. Kroneck, V. Vortisch, P. Hemmerich, Eur. J. Biochem. 109 (1980) 603–612.
[29] E.W. Wilson, M.H. Kasperian, R.B. Martin, J. Am. Chem. Soc. 92 (1970) 5365–5372.
[30] N.L. Benoiton, Chemistry of Peptide Synthesis, Taylor & Francis, 2005.
[31] N.A. Sole, G. Barany, J. Organomet. Chem. 57 (1992) 5399–5403.
[32] R. Guerrini, E. Marzola, C. Trapella, M. Pela, S. Molinari, M.C. Cerlesi, D. Malfacini, A. Rizzi, S. Salvadori, G. Calo, Bioorg. Med. Chem. 22 (2014) 3703–3712.
[33] M. Quaretti, M. Porchia, F. Tisato, A. Trapananti, G. Aquilanti, M. Damjanović, L. Marchiò, M. Giorgetti, M. Tegoni, J. Inorg. Biochem. 188 (2018) 50–61.
[34] P. Gans, A. Sabatini, A. Vacca, Talanta 43 (1996) 1739–1753.
[35] L. Alderighi, P. Gans, A. Ienco, D. Peters, A. Sabatini, A. Vacca, Coord. Chem. Rev. 184 (1999) 311–318.
[36] H.E. Gottlieb, V. Kotlyar, A. Nudelman, J. Organomet. Chem. 62 (1997) 7512–7515.
[37] L.D. Pettit, H.K.J. Powell, The IUPAC Stability Constants Database, Royal Society of Chemistry, London, 1992-2000.
[38] I.D.A. Swan, J. Mol. Biol. 65 (1972) 59–62.
[39] M. Shinttzky, R. Goldman, Eur. J. Biochem. 3 (1967) 139–144.
[40] D. Witkowska, S. Bielinska, W. Kamysz, H. Kozlowski, J. Inorg. Biochem. 105 (2011) 208–214.
[41] W. Bal, M. Jeżowska-Bojczuk, K.S. Kasprzak, Chem. Res. Toxicol. 10 (1997) 906–914.
[42] P. Mlynarz, D. Valensin, K. Kociolek, J. Zabrocki, J. Olejnik, H. Kozlowski, New J. Chem. 26 (2002) 264–268.
[43] C. Conato, H. Kozłowski, P. Młynarz, F. Pulidori, M. Remelli, Polyhedron 21 (2002) 1469–1474.
[44] K. Ősz, K. Várnagy, H. Süli-Vargha, A. Csámpay, D. Sanna, G. Micera, I. Sóvágó, J. Inorg. Biochem. 98 (2004) 24–32.
[45] R.B. Martin, J.T. Edsall, J. Am. Chem. Soc. 82 (1960) 1107–1111.
[46] H. Sigel, R.B. Martin, Chem. Rev. 82 (1982) 385–426.
[47] J.M. Tsangaris, R.B. Martin, J. Am. Chem. Soc. 92 (1970) 4255–4260.
[48] H. Kozłowski, W. Bal, M. Dyba, T. Kowalik-Jankowska, Coord. Chem. Rev. 184 (1999) 319–346.
[49] R.P. Agarwal, D.D. Perrin, J. Chem. Soc. Dalton Trans. (1975) 268–272.
[50] S. Oehler, B. Müller-Hill, J. Mol. Biol. 395 (2010) 242–253.
[51] M. Meyer, V. Dahaoui-Gindrey, C. Lecomte, R. Guilard, Coord. Chem. Rev. 178-180 (1998) 1313–1405.
[52] C.R. Groom, I.J. Bruno, M.P. Lightfoot, S.C. Ward, Acta Crystallogr. B 72 (2016) 171–179.